
Geophysical Monograph Series

Including
IUGG Volumes
Maurice Ewing Volumes
Mineral Physics Volumes

Geophysical Monograph Series

- 147 **Earth's Climate: The Ocean–Atmosphere Interaction** Chunzai Wang, Shang-Ping Xie, and James A. Carton (Eds.)
- 148 **Mid-Ocean Ridges: Hydrothermal Interactions Between the Lithosphere and Oceans** Christopher R. German, Jian Lin, and Lindsay M. Parson (Eds.)
- 149 **Continent-Ocean Interactions Within East Asian Marginal Seas** Peter Clift, Wolfgang Kuhnt, Pinxian Wang, and Dennis Hayes (Eds.)
- 150 **The State of the Planet: Frontiers and Challenges in Geophysics** Robert Stephen John Sparks, and Christopher John Hawkesworth (Eds.)
- 151 **The Cenozoic Southern Ocean: Tectonics, Sedimentation, and Climate Change Between Australia and Antarctica** Neville Exon, James P. Kennett and Mitchell Malone (Eds.)
- 152 **Sea Salt Aerosol Production: Mechanisms, Methods, Measurements, and Models** Ernie R. Lewis and Stephen E. Schwartz
- 153 **Ecosystems and Land Use Change** Ruth S. DeFries, Gregory P. Asner, and Richard A. Houghton (Eds.)
- 154 **The Rocky Mountain Region—An Evolving Lithosphere: Tectonics, Geochemistry, and Geophysics** Karl E. Karlstrom and G. Randy Keller (Eds.)
- 155 **The Inner Magnetosphere: Physics and Modeling** Tuija I. Pulkkinen, Nikolai A. Tsyganenko, and Reiner H. W. Friedel (Eds.)
- 156 **Particle Acceleration in Astrophysical Plasmas: Geospace and Beyond** Dennis Gallagher, James Horwitz, Joseph Perez, Robert Preece, and John Quenby (Eds.)
- 157 **Seismic Earth: Array Analysis of Broadband Seismograms** Alan Levander and Guust Nolet (Eds.)
- 158 **The Nordic Seas: An Integrated Perspective** Helge Drange, Trond Dokken, Tore Furevik, Rüdiger Gerdes, and Wolfgang Berger (Eds.)
- 159 **Inner Magnetosphere Interactions: New Perspectives From Imaging** James Burch, Michael Schulz, and Harlan Spence (Eds.)
- 160 **Earth's Deep Mantle: Structure, Composition, and Evolution** Robert D. van der Hilst, Jay D. Bass, Jan Matas, and Jeannot Trampert (Eds.)
- 161 **Circulation in the Gulf of Mexico: Observations and Models** Wilton Sturges and Alexis Lugo-Fernandez (Eds.)
- 162 **Dynamics of Fluids and Transport Through Fractured Rock** Boris Faybishenko, Paul A. Witherspoon, and John Gale (Eds.)
- 163 **Remote Sensing of Northern Hydrology: Measuring Environmental Change** Claude R. Duguay and Alain Pietroniro (Eds.)
- 164 **Archean Geodynamics and Environments** Keith Benn, Jean-Claude Mareschal, and Kent C. Condie (Eds.)
- 165 **Solar Eruptions and Energetic Particles** Natchimuthukonar Gopalswamy, Richard Mewaldt, and Jarmo Torsti (Eds.)
- 166 **Back-Arc Spreading Systems: Geological, Biological, Chemical, and Physical Interactions** David M. Christie, Charles Fisher, Sang-Mook Lee, and Sharon Givens (Eds.)
- 167 **Recurrent Magnetic Storms: Corotating Solar Wind Streams** Bruce Tsurutani, Robert McPherron, Walter Gonzalez, Gang Lu, José H. A. Sobral, and Natchimuthukonar Gopalswamy (Eds.)
- 168 **Earth's Deep Water Cycle** Steven D. Jacobsen and Suzan van der Lee (Eds.)
- 169 **Magnetospheric ULF Waves: Synthesis and New Directions** Kazue Takahashi, Peter J. Chi, Richard E. Denton, and Robert L. Lysal (Eds.)
- 170 **Earthquakes: Radiated Energy and the Physics of Faulting** Rachel Abercrombie, Art McGarr, Hiroo Kanamori, and Giulio Di Toro (Eds.)
- 171 **Subsurface Hydrology: Data Integration for Properties and Processes** David W. Hyndman, Frederick D. Day-Lewis, and Kamini Singha (Eds.)
- 172 **Volcanism and Subduction: The Kamchatka Region** John Eichelberger, Evgenii Gordeev, Minoru Kasahara, Pavel Izbekov, and Johnathan Lees (Eds.)
- 173 **Ocean Circulation: Mechanisms and Impacts—Past and Future Changes of Meridional Overturning** Andreas Schmittner, John C. H. Chiang, and Sidney R. Hemming (Eds.)
- 174 **Post-Perovskite: The Last Mantle Phase Transition** Kei Hirose, John Brodholt, Thorne Lay, and David Yuen (Eds.)
- 175 **A Continental Plate Boundary: Tectonics at South Island, New Zealand** David Okaya, Tim Stem, and Fred Davey (Eds.)
- 176 **Exploring Venus as a Terrestrial Planet** Larry W. Esposito, Ellen R. Stofan, and Thomas E. Cravens (Eds.)
- 177 **Ocean Modeling in an Eddying Regime** Matthew Hecht and Hiroyasu Hasumi (Eds.)
- 178 **Magma to Microbe: Modeling Hydrothermal Processes at Oceanic Spreading Centers** Robert P. Lowell, Jeffrey S. Seewald, Anna Metaxas, and Michael R. Perfit (Eds.)
- 179 **Active Tectonics and Seismic Potential of Alaska** Jeffrey T. Freymueller, Peter J. Haeussler, Robert L. Wesson, and Göran Ekström (Eds.)
- 180 **Arctic Sea Ice Decline: Observations, Projections, Mechanisms, and Implications** Eric T. DeWeaver, Cecilia M. Bitz, and L.-Bruno Tremblay (Eds.)
- 181 **Midlatitude Ionospheric Dynamics and Disturbances** Paul M. Kintner, Jr., Anthea J. Coster, Tim Fuller-Rowell, Anthony J. Mannucci, Michael Mendillo, and Roderick Heelis (Eds.)

Geophysical Monograph 182

The Stromboli Volcano:
An Integrated Study
of the 2002–2003 Eruption

Sonia Calvari

Salvatore Inguaggiato

Giuseppe Puglisi

Maurizio Ripepe

Mauro Rosi

Editors



American Geophysical Union
Washington, DC

Published under the aegis of the AGU Books Board

Kenneth R. Minschwaner, Chair; Gray E. Bebout, Joseph E. Borovsky, Kenneth H. Brink, Ralf R. Haese, Robert B. Jackson, W. Berry Lyons, Thomas Nicholson, Andrew Nyblade, Nancy N. Rabalais, A. Surjalal Sharma, Darrell Strobel, Chunzai Wang, and Paul David Williams, members.

Library of Congress Cataloging-in-Publication Data

The Stromboli Volcano : an integrated study of the 2002-2003 eruption / Sonia Calvari ... [et al.], editors.

p. cm. — (Geophysical monograph ; 182)

Includes bibliographical references and index.

ISBN 978-0-87590-447-4

1. Stromboli (Italy)—Eruption, 2002. 2. Stromboli (Italy)—Eruption, 2003. 3. Volcanism—Italy—Stromboli. I. Calvari, Sonia, 1962-

QE523.S9S77 2008

551.210945'811—dc22

2008047928

ISBN: 978-0-87590-447-4

ISSN: 0065-8448

Cover Photo: Landslides after the tsunami of 30 December 2002 (courtesy of Istituto Nazionale di Geofisica e Vulcanologia, sezione di Catania (INGV-CT)).

Copyright 2008 by the American Geophysical Union
2000 Florida Avenue, N.W.
Washington, DC 20009

Figures, tables and short excerpts may be reprinted in scientific books and journals if the source is properly cited.

Authorization to photocopy items for internal or personal use, or the internal or personal use of specific clients, is granted by the American Geophysical Union for libraries and other users registered with the Copyright Clearance Center (CCC) Transactional Reporting Service, provided that the base fee of \$1.50 per copy plus \$0.35 per page is paid directly to CCC, 222 Rosewood Dr., Danvers, MA 01923. 0065-8448/08/\$01.50+0.35.

This consent does not extend to other kinds of copying, such as copying for creating new collective works or for resale. The reproduction of multiple copies and the use of full articles or the use of extracts, including figures and tables, for commercial purposes requires permission from the American Geophysical Union.

Printed in the United States of America.

CONTENTS

Preface

Sonia Calvari, Salvatore Inguaggiato, Giuseppe Puglisi, Maurizio Ripepe, and Mauro Rosi ix

The Stromboli Volcano: An Integrated Study of the 2002–2003 Eruption—Introduction

Sonia Calvari, Salvatore Inguaggiato, Giuseppe Puglisi, Maurizio Ripepe, and Mauro Rosi 1

Section I: The Volcanic System of Stromboli

Geological–Structural Framework of Stromboli Volcano, Past Collapses, and the Possible Influence on the Events of the 2002–2003 Crisis

Alessandro Tibaldi, Claudia Corazzato, Tiziana Apuani, Federico A. Pasquaré, and Luigina Vezzoli 5

Volcanology and Magma Geochemistry of the Present-Day Activity: Constraints on the Feeding System

Antonella Bertagnini, Nicole Métrich, Lorella Francalanci, Patrizia Landi, Simone Tommasini, and Sandro Conticelli 19

Dynamics of Strombolian Activity

Maurizio Ripepe, Dario Delle Donne, Andrew Harris, Emanuele Marchetti, and Giacomo Ulivieri 39

Fluid Geochemistry of Stromboli

Fausto Grassa, Salvatore Inguaggiato, and Marcello Liotta 49

Crater Gas Emissions and the Magma Feeding System of Stromboli Volcano

Patrick Allard, Alessandro Aiuppa, Mike Burton, Tommaso Caltabiano, Cinzia Federico, Giuseppe Salerno, and Alessandro La Spina 65

Upper Conduit Structure and Explosion Dynamics at Stromboli

Bernard Chouet, Phillip Dawson, and Marcello Martini 81

Section II: Eruption Onset

Volcanic and Seismic Activity at Stromboli Preceding the 2002–2003 Flank Eruption

M. Burton, S. Calvari, L. Spampinato, L. Lodato, N. A. Pino, E. Marchetti, and F. Muré 93

The Eruptive Activity of 28 and 29 December 2002

Laura Pioli, Mauro Rosi, Sonia Calvari, Letizia Spampinato, Alberto Renzulli, and Alessio Di Roberto 105

Geochemical Prediction of the 2002–2003 Stromboli Eruption From Variations in CO₂ and Rn Emissions and in Helium and Carbon Isotopes

C. Federico, L. Brusca, M. L. Carapezza, C. Cigolini, S. Inguaggiato, A. Rizzo, and D. Rouwet 117

Section III: Landslides, Tsunami, and the Sciara del Fuoco Instability

Slope Failures Induced by the December 2002 Eruption at Stromboli Volcano

Paolo Tommasi, Paolo Baldi, Francesco Latino Chiocci, Mauro Coltelli, Maria Marsella, and Claudia Romagnoli 129

The Double Landslide-Induced Tsunami	
<i>S. Tinti, A. Armigliato, A. Manucci, G. Pagnoni, R. Tonini, F. Zaniboni, A. Maramai, and L. Graziani.....</i>	147
Deep-Sea Deposits of the Stromboli 30 December 2002 Landslide	
<i>Michael P. Marani, Fabiano Gamberi, Mauro Rosi, Antonella Bertagnini, and Alessio Di Roberto.....</i>	157
Integrated Subaerial–Submarine Morphological Evolution of the Sciara del Fuoco After the 2002 Landslide	
<i>Paolo Baldi, Alessandro Bosman, Francesco Latino Chiocci, Maria Marsella, Claudia Romagnoli, and Alberico Sonnessa.....</i>	171
Movements of the Sciara del Fuoco	
<i>A. Bonforte, M. Aloisi, G. Antonello, N. Casagli, J. Fortuny-Guash, L. Guerri, G. Nunnari, G. Puglisi, A. Spata, and D. Tarchi</i>	183

Section IV: The Lava Flow Emission on the Sciara Del Fuoco

Evolution of the Lava Flow Field by Daily Thermal and Visible Airborne Surveys	
<i>Letizia Spampinato, Sonia Calvari, Andrew J. L. Harris, and Jonathan Dehn.....</i>	201
Textural and Compositional Characteristics of Lavas Emitted During the December 2002 to July 2003 Stromboli Eruption (Italy): Inferences on Magma Dynamics	
<i>P. Landi, L. Francalanci, R. A. Corsaro, C. M. Petrone, A. Fornaciai, M. R. Carroll, I. Nardini, and L. Miraglia</i>	213
2002–2003 Lava Flow Eruption of Stromboli: A Contribution to Understanding Lava Discharge Mechanisms Using Periodic Digital Photogrammetry Surveys	
<i>Maria Marsella, Mauro Coltelli, Cristina Proietti, Stefano Branca, and Roberto Monticelli</i>	229
Ground Deformations Related to the Effusive Eruptions of Stromboli: The 2002–2003 Case	
<i>M. Aloisi, A. Bonforte, M. Mattia, and G. Puglisi</i>	247
Gas Flux Rate and Migration of the Magma Column	
<i>Emanuele Marchetti, Maurizio Ripepe, Giacomo Olivieri, Michael R. Burton, Tommaso Caltabiano, and Giuseppe Salerno</i>	259
Variations of Soil Temperature, CO₂ Flux, and Meteorological Parameters	
<i>Paolo Madonia, Lorenzo Brusca, Salvatore Inguaggiato, Manfredi Longo, and Sabina Morici.....</i>	269
Seismological Insights on the Shallow Magma System	
<i>M. Martini, L. D'Auria, T. Caputo, F. Giudicepietro, R. Peluso, A. Caputo, W. De Cesare, A. M. Esposito, M. Orazi, and G. Scarpato</i>	279
Fluid Circulation and Permeability Changes in the Summit Area of Stromboli Volcano	
<i>Anthony Finizola and Francesco Sortino.....</i>	287

Section V: The 5th April Paroxysmal Explosive Event

The 5 April 2003 Explosion of Stromboli: Timing of Eruption Dynamics Using Thermal Data	
<i>Andrew J. L. Harris, Maurizio Ripepe, Sonia Calvari, Luigi Lodato, and Letizia Spampinato</i>	305

The Paroxysmal Event and Its Deposits

Marco Pistolesi, Mauro Rosi, Laura Pioli, Alberto Renzulli, Antonella Bertagnini, and Daniele Andronico 317

Mineralogical, Geochemical, and Isotopic Characteristics of the Ejecta From the 5 April 2003 Paroxysm at Stromboli, Italy: Inferences on the Preeruptive Magma Dynamics

Lorella Francalanci, Antonella Bertagnini, Nicole Métrich, Alberto Renzulli, Riccardo Vannucci, Patrizia Landi, Stefano Del Moro, Michele Menna, Chiara Maria Petrone, and Isabella Nardini 331

The 5 April 2003 Paroxysm at Stromboli: A Review of Geochemical Observations

A. Rizzo, A. Aiuppa, G. Capasso, F. Grassa, S. Inguaggiato, M. Longo, and M. L. Carapezza 347

Ground Deformation From Ground-Based SAR Interferometry

Dario Tarchi, Nicola Casagli, Joaquim Fortuny-Guasch, Letizia Guerri, Giuseppe Antonello, and Davide Leva 359

Section VI: Risk Management**Stromboli (2002–2003) Crisis Management and Risk Mitigation Actions**

Guido Bertolaso, Bernardo De Bernardinis, Chiara Cardaci, Antonella Scalzo, and Mauro Rosi 373

Scientific Community and Civil Protection Synergy During the Stromboli 2002–2003 Eruption

G. Bertolaso, A. Bonaccorso, and E. Boschi 387

Index 399

PREFACE

Stromboli is recognized among volcanologists to have been characterized by a persistent, mild explosive (strombolian) activity for at least 1500 years, with gas, ash, and bombs ejected up to heights of 50–300 m in explosive events, typically at a rate of ~10 times an hour. Because of its persistent activity and the easy access to its summit craters, Stromboli has always been considered a volcano laboratory by volcanologists who have used it to investigate eruptive and degassing processes, organize experiments and test new techniques of volcano monitoring.

In addition to eruptive processes, Stromboli is also an important site for the study of volcano flank instability problems, as its NW flank (Sciara del Fuoco) has produced at least four major catastrophic collapses during the past 10,000 years. Flank instability on volcanic islands is one of the main sources of tsunami waves and thus represents a volcanic hazard with a major impact on society.

Between December 2002 and July 2003, an effusive eruption occurred at this volcano and involved a number of processes (such as lava flow output, explosive activity, flank instability, submarine and subaerial landslides, tsunami, paroxysmal explosive events). It activated the entire spectrum of hazards related to a volcano, making the monitoring of this volcano a real challenge. To face this eruptive crisis, and estimate the potential hazard, a number of novel multidisciplinary techniques have been applied to this volcano.

Volcanic risk climaxed on December 30th, when landslides triggered tsunami waves that hit the settled areas of Stromboli and of other Aeolian Islands, reaching the Sicilian and Calabrian coasts. Had the tsunami occurred during

the tourist season, the number of victims and economic loss could have been enormous. The volcanic crisis was a challenge for the national Civil Protection and for the volcanological community that was called on to give scientific support to manage the crisis.

The scientific community was required to rapidly (within weeks) upgrade the already existing monitoring system on Stromboli. Thus, a large number of instruments, some of which were used for the first time in a volcanic context, were deployed, providing an unprecedented documentation on eruptive phenomena at Stromboli. In the meantime, a new observatory was set up on the island, collecting in one place all data coming from different institutions and monitoring networks. The observatory also acted as the headquarters, facilitating the interaction between the scientific community and the Civil Protection. Indeed, a valuable result of this experience was the daily, multi-disciplinary scientific approach to the evaluation of the hazard, with continuous exchanges concerning the results from the multi-disciplinary networks among the scientists involved.

We believe that the multi-disciplinary monitoring systems applied to this volcano and the resulting interpretative theoretical models obtained by the analysis of data collected during this eruptive crisis, discussed during a number of meetings, can be used as examples for monitoring other active volcanoes.

The volume derives from presentations and discussions at several informal meetings devoted to comparing results and understanding the volcanic processes occurring during the 2002–03 volcanic crisis. To further enhance the project, several other researchers, who had long-time experience with the monitoring of Stromboli, were asked to join the project, and many agreed.

As editors, we are very grateful to all authors, who worked hard to meet the deadline and did everything they could to make this project a success. We appreciate the help, patience, and expertise of AGU staff, who worked diligently to publish the book. We are grateful to the reviewers who devoted so much of their time and effort helping to improve the volume, and especially to Stephen Conway for having improved the English in all the papers from INGV Catania. We would like to thank the technical staff of the geochemical laboratories of INGV Palermo. These colleagues made a great effort to

acquire a solid and unique geochemical data set, which allowed improving our knowledge of the Stromboli plumbing system.

Sonia Calvari

*Istituto Nazionale di Geofisica e Vulcanologia
Sezione di Catania, Catania, Italy*

Salvatore Inguaggiato

*Istituto Nazionale di Geofisica e Vulcanologia
Sezione di Palermo, Palermo, Italy*

Giuseppe Puglisi

*Istituto Nazionale di Geofisica e Vulcanologia
Sezione di Catania, Catania, Italy*

Maurizio Ripepe

University of Firenze, Firenze, Italy

Mauro Rosi

University of Pisa, Pisa, Italy

The Stromboli Volcano: An Integrated Study of the 2002–2003 Eruption—Introduction

Sonia Calvari,¹ Salvatore Inguaggiato,² Giuseppe Puglisi,¹ Maurizio Ripepe,³ and Mauro Rosi⁴

On 28 December 2002, after 17 years of steady strombolian activity, following a gradual increase in the frequency of explosions and in the magma level within the summit craters, a 300-m-long eruptive fissure opened on the upper NE flank of Stromboli volcano. As a result, low energy explosive activity from a lateral vent fed hot avalanches that flowed down the Sciara del Fuoco (SDF) to the sea. The avalanche activity was followed, minutes later, by an intense emission of lava spilled from the NE crater that fed a very fast lava flow. Eruptive activity stopped a few hours later and resumed early morning on 29 December with a new small lava flow from the lowermost tip of the fissure.

On 30 December, fractures formed along the SDF, causing the failure of two large portions of this already unstable flank of the volcano. The landslides triggered two tsunami waves extending over 100 m inland, that caused extensive damage to buildings and boats along the east coast of the island, and minor injuries to a few people. Large waves also struck the town of Milazzo on the northern coast of Sicily, 60 km south of Stromboli. Starting from 30 December, the national Department of Civil Protection, operating under the direct authority of the Prime Minister, took responsibility for the management of the emergency. The first action consisted in providing lodging and full assistance to residents who spontaneously decided to leave the island. The temporarily

evacuated residents returned to the island at the beginning of February. A significant effort of the scientific community has since been devoted to monitoring the movement of the SDF and the summit craters, with different kinds of novel techniques employed at this volcano for the first time.

The major landslide of 30 December was accompanied by intrusion of lava into the fracture, and a new effusive vent formed within the largest landslide scar. Explosive activity ceased at the summit craters of Stromboli following the start of the flank eruption. Persistent effusive activity became concentrated within the 30 December landslide scar on the SDF, resulting in a perched, compound lava flow field.

While lava was still erupting on the upper SDF, an extremely powerful explosive event began on 5 April 2003 at the summit craters, which had been inactive since the onset of the flank eruption. This event was the strongest recorded at Stromboli during the last century, and its timing has been reconstructed on the basis of photos and thermal images taken during a helicopter survey over the volcano before, during and after the paroxysm. The paroxysm lasted about 9 min, with bombs up to 4 m wide falling on the village of Ginostra, on the west flank of the island, and destroying two houses. This event signaled the start of the declining phase of the effusive eruption. Around 20 June, a resumption of strombolian explosions at the summit craters and a corresponding declining phase in the lava output, were observed. After 10 July, lava flows had become confined to the upper, proximal lava field, and there was a total cessation of effusive activity between 21 and 22 July.

This book examines the December 2002–July 2003 eruptive crisis at Stromboli which involved a variety of processes. We present the experience gained from a multi-disciplinary, integrated approach to the monitoring of the eruptive activity, including an overview and synthesis of the over 60 papers published in selective international journals, as well as new results.

The book is organized in six sections. The first section is an overview of the volcanic system of Stromboli gained over the last two decades. The second, third, fourth, fifth sections

¹Istituto Nazionale di Geofisica e Vulcanologia, sezione di Catania, Catania, Italy.

²Istituto Nazionale di Geofisica e Vulcanologia, sezione di Palermo, Palermo, Italy.

³University of Florence, Florence, Italy.

⁴University of Pisa, Pisa, Italy.

2 THE STROMBOLI VOLCANO: INTRODUCTION

describe special phases of the eruption: the eruption onset, the landslide on the SDF and its related tsunami and slope instability, the effusive phase, the 5 April paroxysmal event, respectively. The last section describes the Civil Protection management of the crisis and its synergy with the scientific community. Each chapter contains multi-disciplinary, integrated contributions from the scientists who have contributed to the monitoring of the eruption. Most of the papers are reviews of previously published data, and present integrated models and interpretations of the phenomena that took place during the crisis. However, the book is also a record of all the relevant original information that has been collected but had not yet been published in scientific papers.

Major advances in the fields of structural geology, dynamics of strombolian activity, degassing processes, and petrology of the active plumbing system of the volcano have been made in the last two decades. Flank instability processes and caldera collapses were recognized to play a fundamental role in controlling the Holocene and late Pleistocene evolution of the volcano. The paper by *Tibaldi et al.* offers a review of work published on these topics, discussing this process in the light of the mechanical properties of materials of the volcanic cone and flank stability models. One of the outstanding discoveries made on the plumbing system of the volcano was the identification of a gas-rich, crystal-poor magma erupted during highly energetic explosive events (paroxysms). *Bertagnini et al.* discuss the origin of the most energetic phases in relationship to the rapid rise of gas-rich magma pockets through the resident crystal-rich volatile poor magma. The dynamics of the persistent strombolian activity has been extensively investigated over the past two decades with the aid of geophysical tools. The papers by *Ripepe et al.* and *Chouet et al.* provide complementary aspects regarding the mechanism of generation, ascent and explosion of gas slugs in the upper conduit.

An accurate description of the geochemical system is outlined by *Grassa et al.* based on a review of the main scientific results obtained during the past decade. *Allard et al.* complete the picture showing the primary control of the magmatic gas phase on the eruptive regime of the volcano.

The second section presents several integrated and multi-parametric data illustrating the conditions of the volcano before and during the initial stages of the flank eruption. On the basis of thermal mapping, gas measurements and geophysical monitoring, *Burton et al.* present an integrated analysis of the events that preceded the onset of the flank eruption, suggesting a gradual increase in the magma level within the upper conduit. *Pioli et al.* describe small-scale instability processes occurring during the opening of the eruptive fissure on the uppermost SDF through eyewitness reports, geophysical monitoring, field and laboratory studies of the erupted products, and daily temperature measurements using a handheld thermal camera. A geochemical surveillance program started at

Stromboli in 1999 focused on identifying signals that might predict impending energetic explosive events. *Federico et al.* present the main geochemical signals occurring before the 2002 eruption, with the significant anomalies recorded prior to the eruption both in the coastal aquifer and in the summit area, indicative of a new gas-rich magma batch.

The instability of the SDF was one of the distinctive features of the 2002-03 eruption. The contributions of the third section focus on investigating the origin, effects and evolution of the December 2002 landslides, as well as their relationships with the eruption and with the current dynamics of this flank of the volcano. *Tinti et al.* propose a critical reconstruction of the two tsunamis based on field observations, eyewitness statements and results from numerical simulations. Aerophotogrammetric and bathymetric surveys carried out before and after the eruption were fundamental for assessing the flank dynamics of the SDF as well as the geometry and evolutions of the lava flow field. By integrating these data together with field observations and with the geotechnical behavior of the volcanics, *Tommasi et al.* set out a reconstruction of the sequence of landslides that occurred soon after the eruption onset. *Baldi et al.* monitored the continuous morphological changes on the subaerial and submarine flank of the SDF during the whole eruption, estimating the volume involved. *Marani et al.* estimated the volume of sediments deposited on the offshore from the SDF landslide from multi-beam bathymetry, side-scan sonar data and seabed visual observations. Heritage of the 2002-03 eruption was the integrated multi-parametric system for monitoring ground deformations on the SDF, which comprises a ground-based linear synthetic aperture radar (GB-InSAR), and an automated topographic monitoring system (named THEODOROS). *Bonforte et al.* described the design and set up of this system, initially based on periodic geodetic surveys and an innovative real-time GPS network, both destroyed during the eruption, and of its evolution during and after the 2003.

The fourth section deals with the emplacement of the lava flow field on the SDF. It describes the monitoring techniques used to analyze and quantify flow field growth in terms of structure, effusion rate, volume erupted, composition, deformation caused by the emplaced mass, gas released through the magma column and the ground surrounding the craters, and associated seismic activity. *Spampinato et al.* show the lava flow field growth monitored with a thermal camera from land and helicopter, describing its structure and relationship with the measured parameters. Periodic lava sampling carried out during the entire duration of the effusive eruption, and a fairly homogeneous composition of the lava, allowed *Landi et al.* to rule out important changes in the dynamics of the plumbing system shortly before the eruption. *Marsella et al.* studied the filling of the subaerial and submarine landslide scars by lava flows and debris, using a quantitative

analysis of the photogrammetric surveys carried out during the effusive eruption. Integrated with field observations, this showed that at the end of the eruption the scar left by the December 2002 landslide was only partially filled.

Aloisi et al. describe the newly installed ground deformation systems necessary to monitor the effusive phases. This supported the Civil Protection in making decisions related to hazards from landslide movements and volcanic activity, and allowed the authors to make some hypotheses on the dynamics of the craters. The transition from effusive to explosive activity was investigated by *Marchetti et al.* through the analysis of VLP seismic activity, delay times between infrasonic and thermal onsets of explosions, and SO₂ flux recorded during a one-year period. The synergy of these multiple geophysical observations pointed to a migration of the magma column.

Continuous monitoring of CO₂ flux from soil performed by *Madonia et al.* and integrated by daily field observations, showed that CO₂ flux and soil temperature are closely related to volcanic events. The seismological data set used by *Martini et al.* covers most of the effusive phase and the subsequent recovery of the explosive activity, and shows that the shallow magmatic system has not undergone significant changes during this period. Fluid flow mapping and profiles carried out by *Finizola and Sortino* with self-potential, temperature, and soil gas measurements since 1994 in the summit area, show the importance of old structural boundaries in the opening of part of the 2002-03 fracture field.

The fifth section describes many aspects of the 5 April paroxysm, and opens with a paper from *Harris et al.* presenting a new and updated revision of the timing and dynamics of this episode on the basis of thermal and visual images recorded during the explosion from helicopter, and from a fixed thermal sensor 450 m away. *Pistolesi et al.* present detailed mapping through field and laboratory description of the explosive deposits that allowed to calculate the volume, assess the eruptive mechanism, and calculate the peak discharge rate (eruptive intensity) of the event. Mineralogical, geochemical and isotopic compositions of the juvenile and fresh subvolcanic ejecta have been carried out by *Françalanci et al.*, indicating moderate pressure conditions for the mechanisms triggering this episode.

Thanks to a wide review of the published geochemical variations observed during the eruption, *Rizzo et al.* characterized the variations in chemical composition of ground waters and summit fumaroles before the paroxysm, identifying the progressive pressurization of the basal thermal aquifer due to the degassing of a new arrival of volatile-rich magma at depth. An in-depth analysis of the images acquired by the ground-based InSAR system installed before the 5 April explosion, allowed *Tarchi et al.* to detect the precursory signals of the explosion related to ground deformation and the occurrence

of an elastic deformation which affected the volcanic edifice progressively from the craters down to the SDF depression.

The sixth section comprises two papers dealing with the emergency management. The first paper by *Bertolaso et al.* illustrates the role, responsibilities and activities of the Civil Protection Italian Department during the crisis. The different actions undertaken to mitigate the volcanic risk are also described and discussed in the frame of other volcanic crises management around the world. The second paper, again by *Bertolaso et al.*, shows the multi-disciplinary cooperation and synergy between the Istituto Nazionale di Geofisica e Vulcanologia (INGV) and the Italian Civil Protection Department (DPC) during the Stromboli eruption, and describes the enormous effort made to complete and upgrade the observation network during the eruption. In addition, the vision of the system of civil protection envisaged by Italian law, in which DPC promotes and coordinates the administrations of the State during emergencies, and INGV supplies scientific support, has proved valid and functional.

A very useful addition to the monograph is the annexed DVD, which includes photos, videos and data dealing with several aspects of the eruption. Many of these electronic materials are related with, and complete, the written contributions of the book, but others are exclusive documents relevant to the most significant episodes of the eruption. For instance, this is the case of the images related to the 5 April paroxysm, which represent an incomparable and valuable collection of visible photos and SAR images describing, second by second, the evolution of such a phenomenon. Furthermore, videos filmed and edited by scientists involved in the eruption monitoring, included in the DVD, are not only useful to learn about the field operation, but also an authentic way to share the experience of those involved in the days of the eruption.

Acknowledgment. We wish to thank Stephen Conway for checking and improving the English.

S. Calvari, Istituto Nazionale di Geofisica e Vulcanologia, sezione di Catania, Piazza Roma 2, 95123 Catania, Italy. (calvari@ct.ingv.it)

S. Inguaggiato, Istituto Nazionale di Geofisica e Vulcanologia, sezione di Palermo, Via Ugo La Malfa, 153, 90146 Palermo, Italy. (s.inguaggiato@pa.ingv.it)

G. Puglisi, Istituto Nazionale di Geofisica e Vulcanologia, sezione di Catania, Piazza Roma 2, 95123 Catania, Italy. (puglisi-g@ct.ingv.it)

M. Ripepe, Dipartimento di Scienze della Terra, Università di Firenze, Via La Pira 4, 50121 Firenze, Italy. (maurizio.ripepe@unifi.it)

M. Rosi, Dipartimento di Scienze della Terra, Università di Pisa, Pisa, Italy. (rosi@dst.unipi.it)

Geological–Structural Framework of Stromboli Volcano, Past Collapses, and the Possible Influence on the Events of the 2002–2003 Crisis

Alessandro Tibaldi and Claudia Corazzato

Dipartimento di Scienze Geologiche e Geotecnologie, Università di Milano-Bicocca, Milan, Italy

Tiziana Apuani

Dipartimento di Scienze della Terra “Ardito Desio,” Università di Milano, Milan, Italy

Federico A. Pasquaré and Luigina Vezzoli

Dipartimento di Scienze Chimiche e Ambientali, Università dell’Insubria, Como, Italy

We delineate the geological–structural framework of Stromboli volcano through the description of the deposits and structures that developed during the various phases of buildup and morphostructural reorganization of the edifice. Piling of lava and minor pyroclastic deposits was repeatedly interrupted by summit caldera collapses during the late Pleistocene and by nested flank and sector collapses towards the NW in the Holocene. Field data suggest a strong instability of this volcano flank, and numerical modeling contributes to describing the process. In the Holocene, fissuring and dyking along a main NE-trending weakness zone crossing the island interacted with other magma paths with a horseshoe-shaped geometry in plan view. A brief discussion is aimed at deciphering the possible influence of the previous geological–structural history of the volcano on the location and type of events which occurred during the 2002–2003 crisis.

1. INTRODUCTION

Stromboli is a volcanic complex located in the southern Tyrrhenian Sea, Italy (Figure 1a). It is composed of two main joint cones: the northern one testified by the Strombolicchio

islet neck and the other one forming the Stromboli Island (Figure 1b). This complex has a SW–NE elongation parallel to the main tectonic structures recognized in the eastern sector of the Aeolian archipelago. This sector is characterized by extensional dynamics related to the rapidly extending Marsili oceanic basin and the southwestward migration of the Calabrian arc (Figure 1a) [De Astis *et al.*, 2003; Goes *et al.*, 2004; Billi *et al.*, 2006]. Focal mechanisms in this part of the southern Tyrrhenian basin show NNE- and NE-striking normal faulting [Falsaperla *et al.*, 1999; Neri *et al.*, 2003]. Contractual and transcurrent deformations have been found farther west [Ventura *et al.*, 1999; Argnani *et al.*, 2007].

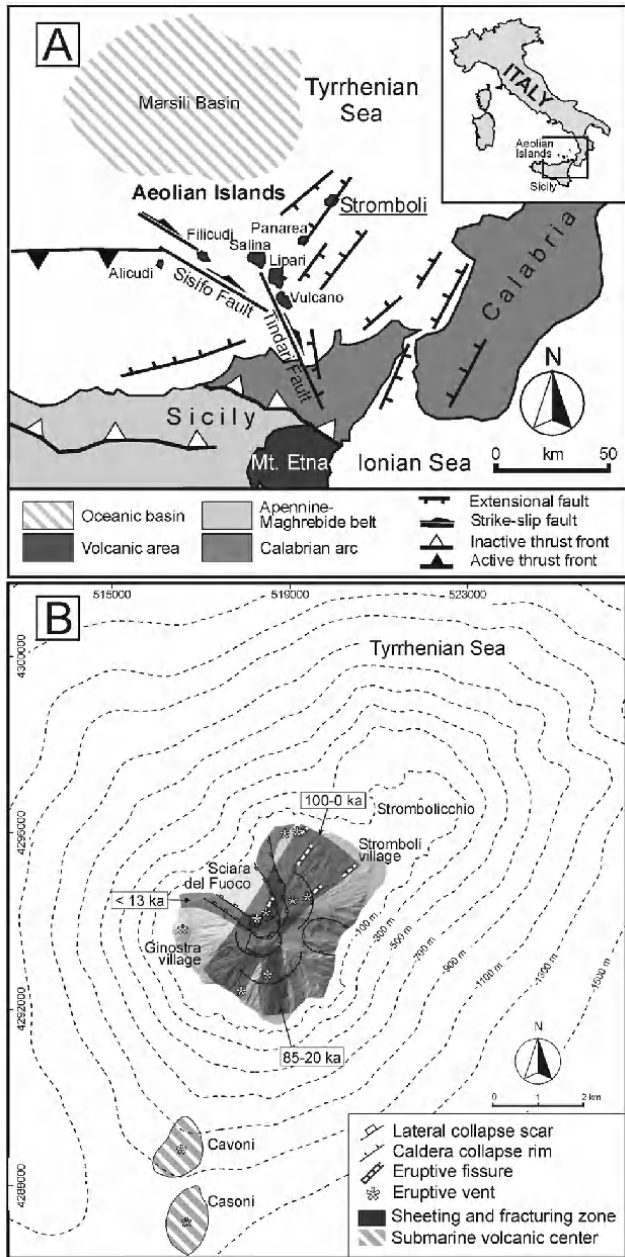


Figure 1. (a) Location of Stromboli volcano with respect to the structure of the Aeolian archipelago in the southern Tyrrhenian Sea and main tectonic features of the area (adapted from Neri *et al.* [2003], Goes *et al.* [2004], and Billi *et al.* [2006]). (b) Stromboli Island, Strombolicchio islet and the submerged morphology of the volcanic complex. Digital elevation model data of the emerged portion courtesy of M. Marsella and coworkers, Università di Roma. Bathymetric data (simplified) from Gabbianelli *et al.* [1993].

After the cessation of activity at Strombolicchio, dated 204 ± 25 ka B.P. [Gillot and Keller, 1993], the last 100-ka growth of Stromboli was interrupted by at least eight main collapses, through caldera formation or lateral failure events [Tibaldi, 2001]. Repetition of such events is thus well established in the geological record of this volcano, and its history can help unravel the present situation. However, it is necessary to take into account the morphological, structural, and lithological variations of the volcano, which can influence magma-feeding paths and the edifice lateral instability [Tibaldi, 2003]. Therefore, the present review will provide a brief summary of the lithostratigraphic, structural, and morphological evolution of the cone, with special emphasis on the Holocene reorganization of the volcanic system and its influence on the present behavior and the 2002–2003 events, and will present the state of the art of the knowledge about lateral instability.

2. GEOLOGICAL AND STRUCTURAL EVOLUTION OF THE ISLAND

The geology and stratigraphy of Stromboli were described and reported in geological maps by Magnani [1939], Rosi [1980], Keller *et al.* [1993], and Hornig-Kjarsgaard *et al.* [1993]. More recently, the stratigraphic study and geological mapping based on the reconnaissance of unconformity-bounded stratigraphic units were performed by Tibaldi [2008]. A simplified version of this map and a comparison with the previous stratigraphic studies are provided in Figure 2 and in the cross sections of Figure 3. The volcanic history of Stromboli is characterized by a series of caldera-type collapses, and one lateral collapse toward the southeast during the older period of activity and lateral collapses after ~ 13 ka ago [Pasquarè *et al.*, 1993; Tibaldi *et al.*, 1994; Tibaldi, 2001]. In the map by Rosi [1980], one of these caldera collapses was already recognized; in Keller *et al.*'s [1993] map, three caldera collapses and one lateral collapse are portrayed, although in the explanatory notes, one more sector collapse is suggested [Hornig-Kjarsgaard *et al.*, 1993; Tibaldi [2001, 2008], which recognized the occurrence of four lateral collapses in the Holocene (Figure 3).

One of the peculiar characteristics of Stromboli is the frequent coincidence between structural modifications and changes in magma composition [Francalanci *et al.*, 1988, 1989, 1993; Hornig-Kjarsgaard *et al.*, 1993] that ranges from calc-alkaline (CA) to potassic (KS), high-K calc-alkaline (HKCA), and shoshonitic (SHO). On the basis of structural unconformities and rock composition, the volcanic sequence of the subaerial cone has been subdivided into six periods of activity (Figures 2 and 3): (1) Paleostromboli I (Cavoni synthem), (2) Paleostromboli II, (3) Paleostrom-

boli III (Gramigna synthem), (4) Lower, Middle, and Upper Vancori (Frontone and Vancori synthems), (5) Neostromboli (Fossetta synthem), and (6) Recent Stromboli (Pizzo, Fili di Baraona, and Sciara synthems).

2.1. Late Pleistocene History

The stratigraphically lowermost rocks of Stromboli, cropping out along the eastern coast of the island (Lava A informal unit; Figure 2) are represented by lavas and breccias. Lavas and pyroclastic fall, flow, and lahar deposits with HKCA basaltic-andesite and andesite compositions were emplaced during the Paleostromboli I period (Cavoni synthem; Lower and Upper Paleostromboli I lavas; Figures 2 and 3). These rocks crop out in the Petrazza, Malopasso, and Cavoni areas and are dated to <100 and 85.3 ± 2 ka B.P. [Gillot and Keller, 1993]. In the upper part of the Cavoni canyon, the rim of the first caldera collapse cuts the Paleostromboli I volcanic sequence (caldera collapse 1; Figure 2).

During the Paleostromboli II period (Gramigna synthem, Rina subsynthem; Figures 2 and 3), prevalent lava flows and subordinate scoria fall deposits, with CA basaltic-andesite composition, filled up and overlapped the caldera 1 depression (Figure 2). The oldest lavas of Paleostromboli II, cropping out at the base of Vallone di Rina (Lower Rina lavas; Figure 2), are dated at 61 ± 12 ka B.P. [Condomines and Allègre, 1980] and are characterized by a boundary composition between the CA and HKCA series. The successive activity led to the emplacement of a thick lava sequence dated at 64.3 ± 4.9 and 54.8 ± 9.1 ka B.P. [Gillot and Keller, 1993] from Vallone di Rina to La Petrazza (Omo lavas; Figure 2), followed by red scoria agglomerates.

During the Paleostromboli III period (Gramigna synthem, Aghiastro subsynthem; Figures 2 and 3), the Stromboli cone was built up by lavas and pyroclastic rocks with HKCA and weakly SHO compositions. Pyroclastic deposits, mainly composed of lapilli fall and some lahars, are interbedded with HK basalt to HK andesite and shoshonite lavas. The Paleostromboli III rocks mainly crop out in the southern part of the island up to a height of about 700 m above sea level (asl). The Middle Rina lavas (dated at 35 ± 6 ka B.P. [Condomines and Allègre, 1980; Gillot and Keller, 1993]) and Upper Rina lavas crop out from Vallone di Rina to Vallone del Monaco, whereas the uppermost Aghiastro lava unit is found above Malo Passo (Figure 2). The Paleostromboli III activity ended with the caldera collapse 3 (Figure 2), whose rim is marked by a clear unconformity.

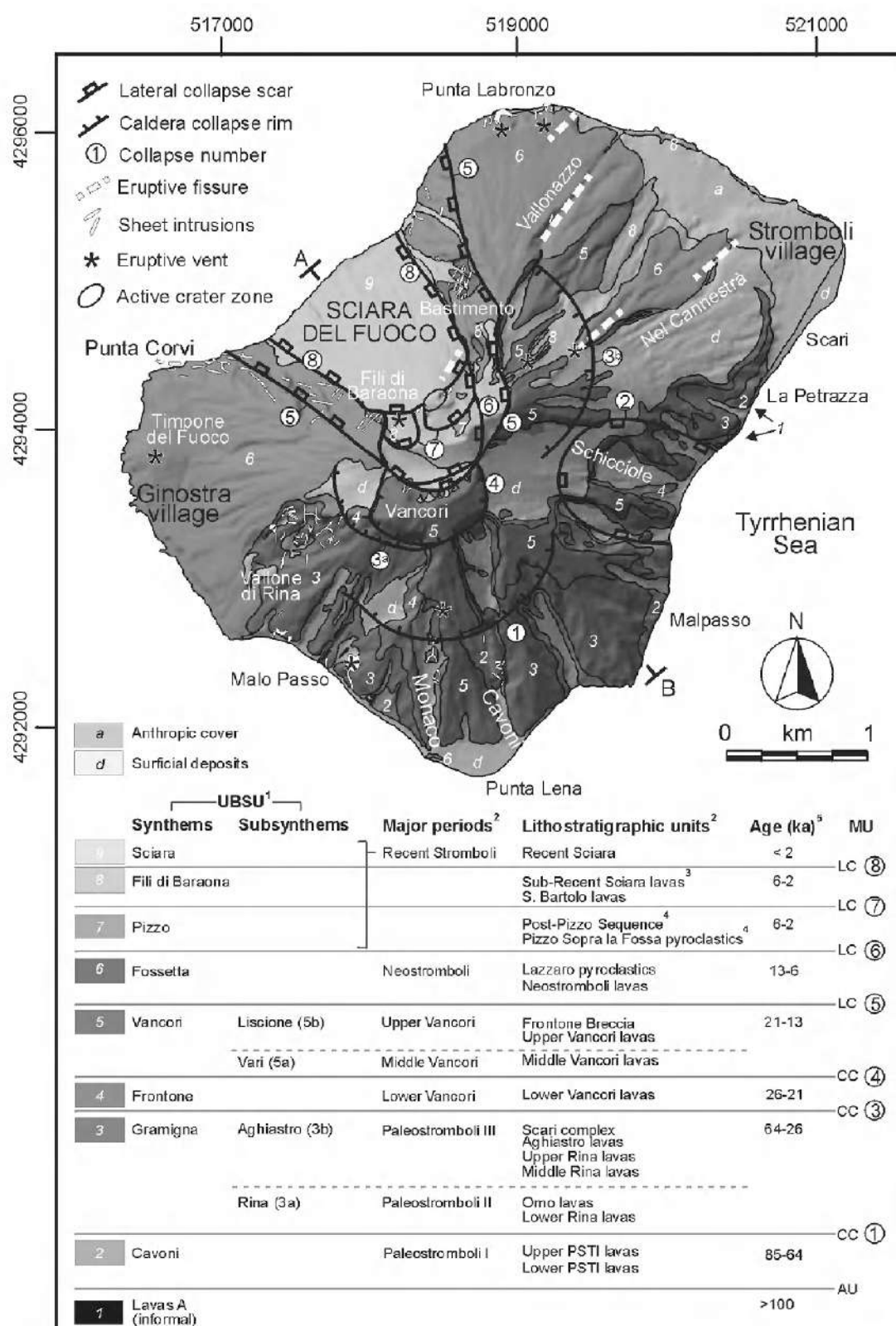
The Scari complex, found at the Scari and La Petrazza localities above Paleostromboli I and II products, is considered to be coeval with the Paleostromboli III products, having an age of 34.6 ± 3 ka B.P. [Gillot and Keller, 1993]. It mainly

consists of pyroclastic fall deposits and one lava flow ranging between HK and SHO basalts to shoshonites and latites. A lateral collapse towards SE (2 in Figure 2) occurred after the emplacement of the Scari complex.

The Vancori period, characterized by a prevalent effusive SHO activity which led to the emplacement of the topmost rocks of the island (Figures 2 and 3), has been subdivided into three subperiods (Lower, Middle, and Upper Vancori) on the basis of structural unconformities, volcanological criteria, and magma composition. The Lower Vancori lavas (Frontone synthem in Figure 2), ranging from SHO basalts to shoshonites (26.2 ± 3.2 ka B.P.; Gillot and Keller [1993]), filled the depression and overflowed the rim of the caldera 3, reaching the sea level in the S–SE part of the island. This activity was followed by the caldera collapse 4, whose depression was filled by the shoshonitic lavas of Middle Vancori (Vancori synthem, Vari subsynthem in Figure 2), with an age of 21 ± 6 ka B.P. [Gillot and Keller, 1993]. The Upper Vancori period (Vancori synthem, Liscione subsynthem in Figure 2) began with a pyroclastic series and is characterized by a more evolved magma composition ranging from shoshonites to trachytes, through latites. The lava sequence, dated 13 ± 1.9 ka B.P. [Gillot and Keller, 1993], is closed by an explosion breccia (Frontone breccia) cropping out in the summit area and representing a hybrid magma between the evolved Upper Vancori magmas and the leucite-bearing shoshonitic magmas erupted soon after [Hornig-Kjarsgaard et al., 1993]. The Middle and Upper Vancori sequences were widespread on the eastern sector of the volcano from the summit to the sea level, although their outcrops to the NW are now rare. The Vancori edifice was affected by the first lateral collapse of the volcano towards NW (lateral collapse 5 in Figure 2) that involved a larger area than the present Sciara del Fuoco (SdF) [Tibaldi, 2001].

2.2. Holocene History

During the Neostromboli period (Fossetta synthem; Figure 2), volcanic activity was mainly concentrated in the NW part of the volcano, producing thin and scoriaceous lava flows characterized by high potassium contents (KS series) associated with prevalent basic to intermediate compositions (leucite-bearing trachybasalts and shoshonites). These lavas were erupted either from central craters/fractures sited at about 750 m asl in the previously NW collapsed area, or from eccentric vents and eruptive fissures, such as the Timpone del Fuoco, Punta Labronzo, Vallonazzo, and Nel Cannestrà (Figure 2). A lava flow emitted from the central crater gave an age of 13.8 ± 1.9 ka [Gillot, 1984; Gillot and Keller, 1993], whereas an age of 5.6 ± 3.3 ka [Gillot, 1984; Gillot and Keller, 1993] was obtained on a lava sample from the



Punta Labronzo eccentric vent. The NW sector of the Neostromboli edifice failed during the lateral collapse 6. This collapse surface was nested in the collapse 5 depression [Tibaldi *et al.*, 2003; Apuani *et al.*, 2005a]. The phreatomagmatic explosive event of the Lazzaro pyroclastic deposits [Bertagnini and Landi, 1996], found all over the island in small outcrops above the Neostromboli lavas, seems to be the last eruptive event of this period and was probably triggered by the decompression of the shallow subvolcanic system during lateral collapse 6 [Renzulli and Santi, 1997].

The Recent Stromboli period (Pizzo, Fili di Baraona, and Sciara synthems; Figure 2) refers to the volcanic activity following the Neostromboli period, including the present-day Strombolian activity. The products are lavas and pyroclastic deposits with HK and SHO basaltic compositions, and some ages were recently obtained with archeomagnetic dating in the work of Arrighi *et al.* [2004] and Speranza *et al.* [2004] to better constrain this period of activity. The Pizzo Sopra la Fossa pyroclastic cone [Pizzo synthem; Figure 2] was built up to an elevation of 918 m asl from a central crater inside the depression of the lateral collapse 6. It was cut by the northwestward lateral collapse 7 and was followed by explosive activity which emplaced alternating ash tuff layers and scoriaceous spatters (Post-Pizzo Sequence, Petrone *et al.* [2006]). The sub-Recent Sciara lavas (Fili di Baraona synthem; Figure 2) dated 1350 ± 60 A.D. [Arrighi *et al.*, 2004]) lateral collapse 7. These lavas were in turn involved in the final lateral collapse 8, which led to the formation of the SdF depression in its present shape. The HK basalts of San Bartolo lavas (Fili di Baraona synthem; Figure 2), with an age of 2 ka B.P. [Arrighi *et al.*, 2004], were erupted outside the central crater area from an eccentric vent sited at 600 m asl in the NE part of the island [Laiolo and Cigolini, 2006]. They formed a quite large lava delta at sea level where the Stromboli village was partially built up. The Recent Sciara deposits (Sciara synthem; Figure 2) have been erupted by the present-day Strombolian activity which occurs inside the SdF depression from vents sited in a crater terrace at 750 m asl (usually three active craters). Blocks, scoriaceous bombs, lapilli, and ash are the products of the moderately explosive,

normal Strombolian activity, whereas light pumice and lava flows are erupted during paroxysms and effusive activity, respectively (e.g., eruptive crisis of 2002–2003 and 2007 [Landi *et al.*, 2006, and reference therein]).

Three magma feeding zones, testified by the alignment of the active summit vents, eruptive fissures, and sheet swarms, were recognized at Stromboli [Tibaldi, 1996; Tibaldi, 2003; Tibaldi *et al.*, 2003; Corazzato *et al.*, 2008]: (1) the NE-trending zone passing through the volcano summit, characterized by a gradual migration of dyking from SW to NE throughout the history of the volcano and geometrically controlled by the active NW-trending regional tectonic extension; (2) the north-trending zone affecting the southern part of the island; and (3) the zone located parallel and close to the shoulders of the northwestward collapse zone; it developed from 13 ka B.P. interacting with fissuring and dyking along the main NE-trending weakness zone (Figure 2).

3. LATERAL INSTABILITY

The first paper dedicated to the numerical modeling of the mechanical stability of Stromboli is the one by Russo *et al.* [1996], dealing with an elastic model and considering the influence of the regional stresses and magma reservoir. The geological history of lateral collapses alternated to building phases has been simulated by finite difference numerical modeling by Apuani *et al.* [2005a] with FLAC 4.0 code (Itasca), in terms of stress-strain evolution. This simulation revealed that (1) the gravitational forces alone are not sufficient to generate the hypothesized past collapses as single mechanisms, while magma pressure in dykes can represent a destabilizing factor; (2) deformations and superficial landslides mark the beginning of, and contribute to, the retrogressive plasticization and perhaps to the deepening of the failure surface; (3) shallow submarine landslides represent a possible triggering mechanism. The landslide events of 30 December 2002 fit the simulated evolution.

The numerical code has proved to be a useful tool for modeling such a complex system and investigating the cause-effect relationships in deep-seated instability phenomena,

Figure 2. (Opposite) Simplified geological map of Stromboli Island showing the main stratigraphic units (unconformity-bounded stratigraphic units, based on the study of Tibaldi [2008]), with indication of caldera and sector collapse traces (modified after Tibaldi [2001]), sheet intrusions (partially from Tibaldi [2003], Corazzato *et al.* [2008], and unpublished data), eruptive fissures and vents. The map is draped over a shaded view of the island (digital elevation model data courtesy of M. Marsella and coworkers, Rome University) (universal time meridian coordinates in meters). UBSU, unconformity bounded stratigraphic units; PSTI, Paleostromboli I; MU, main unconformities with number as referred in the text; LC, lateral collapse; CC, caldera collapse; AU, angular unconformity. 1, After Tibaldi [2008]; 2, major periods and informal lithostratigraphic units, after Keller *et al.* [1993] if not differently indicated; 3 after Hornig-Kjarsgaard *et al.* [1993]; 4, after Petrone *et al.* [2006]; 5, ages from Condomines and Allegre [1980] and Gillot and Keller [1993]. a–b is the subaerial trace for model cross section of Figure 4.

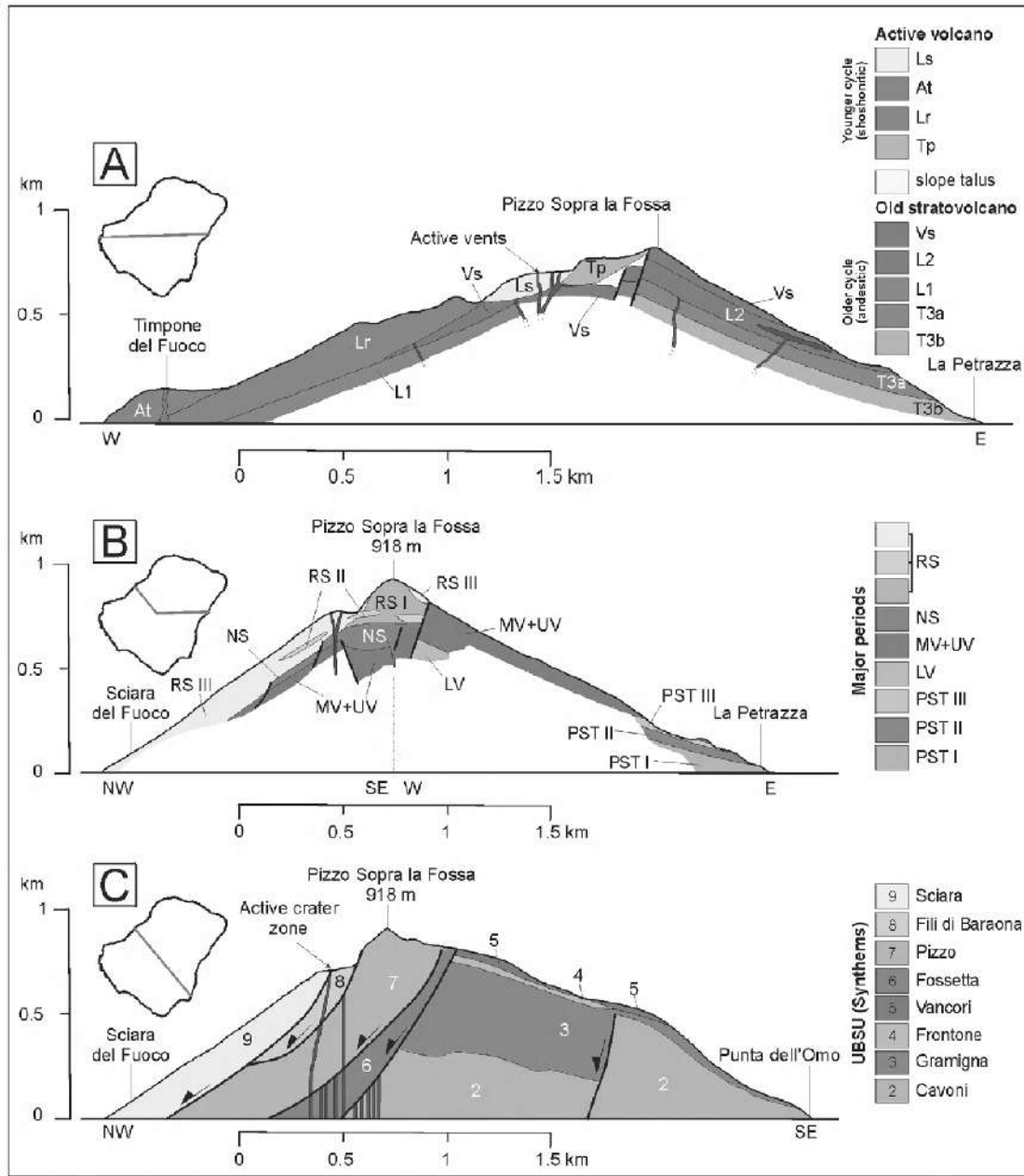


Figure 3. Geological cross sections of the subaerial portion of the Stromboli volcano. (a) After Rosi [1980]. T3, Older pyroclastic formation; L1, L2, Lava flows complex covering the older pyroclastic formation; Vs, Upper Vancori complex; Tp, Pizzo Sopra la Fossa tuffs; Lr, lava flows of stratovolcano near the SdF; At, Timpone del Fuoco parasitic cone; Ls, SdF lava flows and scoriae. (b) After Keller *et al.* [1993]. PST, Paleostromboli; SC, Scari unit; LV, MV and UV, Lower, Middle and Upper Vancori; NS, Neostromboli; RS, Recent Stromboli; (c) after Tibaldi [2008]. UBSU, Unconformity Bounded Stratigraphic Units.

allowing calibrating the response of the geotechnical model and testing the validity of the assumptions.

Actually, to support the stability analyses, it is necessary to define a geological–technical model of the volcano, based on an adequate knowledge of the geotechnical properties of the involved materials, as well as on stratigraphical, lithological, and structural data. Only recently have studies begun to quantify volcanic material properties [Watters *et al.*, 2000; Thomas *et al.*, 2004; Apuani *et al.*, 2005b; Moon *et al.*, 2005; Tommasi *et al.*, 2005; Malheiro and Nunes, 2007]. Apuani *et al.* [2005b] provided a dataset of the physical–mechanical properties of the Stromboli volcanic rock masses by integrating: (1) laboratory geotechnical and geomechanical tests on intact rocks; (2) rock-mass structural and geomechanical characterization [ISRM, 1981]; (3) evaluation of rock-mass strength and elastic parameters according to Hoek–Brown nonlinear strength law [Hoek *et al.*, 2002], for property scaling to rock-mass scale. These authors then defined four lithotechnical units, considering the relative percentage of the breccia fraction vs. lava deposits. Tommasi *et al.* [2005] focused on characterizing the volcaniclastic material of the SdF slope.

Slope instability phenomena are represented not only by (1) giant deep-seated gravitational slope deformations as those recognized in the past history of Stromboli, with mobilized volumes $>10 \text{ Mm}^3$, but also by (2) shallower, large, and more frequent landslides, such as the one which occurred in December 2002–January 2003, involving loose deposits and rock masses and mobilizing volumes $<10 \text{ Mm}^3$, and (3) very surficial landslides, involving loose or weakly consolidated deposits, that also represent a natural hazard and threaten residents and tourists, with mobilized volumes in the order of $100,000 \text{ m}^3$.

The researches published up to now were focused on stability analyses and numerical modeling concerning these different typologies of slope instability, and the effect of different instability factors and external forces, such as magma pressure and seismicity, initially explored by limit equilibrium analyses [Apuani *et al.*, 2005a].

Considering deep-seated gravitational slope deformations (1) and large landslides (2), Apuani and Corazzato [2008] dealt with the Stromboli NW flank instability, focusing on the effects of magma pressure in the feeding system. A two-dimensional numerical model was developed by the finite difference FLAC code, considering a cross section of the entire volcano, orthogonal to the SdF, and including both subaerial and submerged slopes (Figure 4, steps 1–3). The stability of the volcano was analyzed under gravity alone and by introducing the magma pressure effect, including magmatic static and overpressure components (Figure 4, step 4). The results indicate that gravity alone is not sufficient to affect

the stability of the volcano slopes, nor is the magmatic static pressure component. If a magma overpressure is introduced, instability is produced in accordance with field evidence and recent slope dynamics.

Another crucial issue to be analyzed in evaluating the stability of a volcanic edifice is represented by the effect of seismicity, related to tectonic activity or due to magma migration mechanisms. Apuani *et al.* [2007a] analyzed, by the FLAC code, the effects of seismic events associated to magma migration mechanisms on the stability of the volcano flanks, coupling the dynamic analysis with the effects of the magma pressure in the feeding conduits. The dynamic input was applied on both sides of the conduit, extended vertically below the active crater zone. Based on geophysical data [Chouet *et al.*, 2003], the dynamic source was located between 300 and 700 m deep (Figure 4, step 5). The effects of the dynamic perturbation were analyzed in terms of displacements vectors, strain increments, and pore pressure variations. The model showed that seismic activity alone is not a sufficient cause of deep-seated instability, but when coupled with magma overpressure during feeding processes, critical deep surfaces can develop. Their geometry and continuity is controlled by the entity and distribution of magma pressure and depth of the dynamic source. Consequently, the modality of a possible instability process and the involved volumes are strongly dependent on the stress concentration resulting from the applied triggering factors.

Concerning the development of minor very surface landslides (3), these can involve potentially unstable masses of loose or weakly cemented deposits that can be mobilized evolving in granular flow moving down the SdF into the sea, eventually forming small tsunami waves. Apuani *et al.* [2005c, 2007b] analyzed the surface local stability of the SdF recent volcanic debris, using the particle-based code PFC2D (Itasca) and building up a conceptual model (Figure 5a) made of a close-packed assembly of bonded or unbonded particles, interacting according to their specific particle contact properties. After the necessary calibration of the numerical model [Apuani *et al.*, 2005c], based on the comparison with experimental geotechnical data and aimed at finding particle micromechanical parameters that better represent the rheology of the volcanic debris, the analysis performed by Apuani *et al.* [2007b] could investigate the effect on local slope stability of some possible triggering factors such as the impact of large ejected boulders, like the ones emitted during major eruptions or paroxysmal events, which in any case affect only small areas, or the accumulation of lava (Figure 5b), which instead can be responsible for the development of superficial landslides at the front of the lava flow.

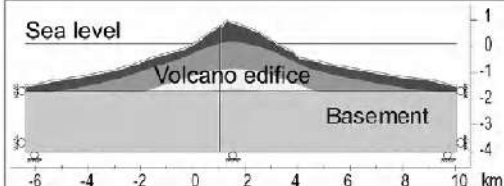
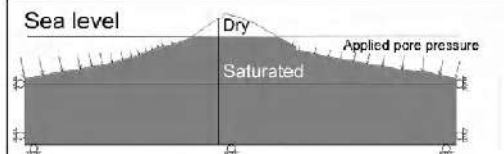
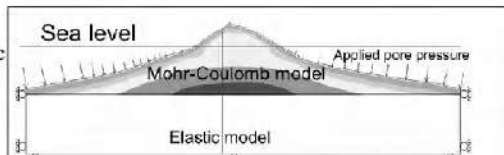
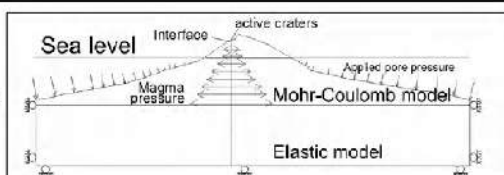
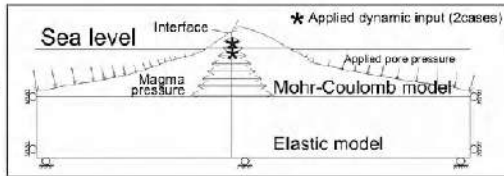
Step	Idealization of the model: properties and acting forces	Results
Step 1: elastic model, dry conditions		Volcano edifice: density and porosity vary with depth; elastic properties. Basement: elastic homogeneous body. Boundary conditions and gravitational forces are imposed. Stress field in dry conditions is determined.
Step 2: elastic model, saturated conditions		Flow boundary conditions are introduced. The sea level and its hydrostatic load are imposed to saturate the submerged edifice. Model is cycled setting mechanical analysis off. Pore pressure and effective stresses are calculated according to the new hydrological conditions.
Step 3: elasto-plastic model (Mohr - Coulomb analysis)		Mohr-Coulomb equivalent strength properties are introduced, applying the Hoek-Brown criterion. Cohesion and friction are a stress function. The stability condition under the effect of gravity alone is determined.
Step 4: introduction of magma pressure		Magma pressure is applied. Two different cases are implemented varying magma pressure and interface properties. The effect of magma pressure acting along the dyke is evaluated. Conditions of critical instability related to magma pressure are detected.
Step 5: introduction of dynamic inputs		Dynamic perturbations are applied at different depth, as armonic horizontal acceleration wave. The effects of Dyn input on the volcano stability are checked. Stress concentration regions, plasticization and effect on pore pressure are determined.

Figure 4. Conceptual steps of the numerical modelling: idealization of the model, applied forces, and results (after Apuani *et al.* [2007a]).

4. SUBMERGED STRUCTURES

The 1988–1990 oceanographic surveys around Stromboli documented [Gabbianelli *et al.*, 1993] that the subaerial portion of the volcano represents only about 1/25 of the area occupied by the whole volcanic complex. The entire edifice slopes gradually to both sides of a 18-km long, NE–SW trending axis [Romagnoli *et al.*, 1993]. Normal faults with the same orientation have been documented by Gabbianelli *et al.* [1993]. The island is bordered to the NE and SW by submerged abrasion platforms [Gabbianelli *et al.*, 1993; Romagnoli *et al.*, 1993; Favalli *et al.*, 2005], which are missing

offshore the SE and the NW portion of the island, the latter dominated by the SdF (Figure 2b). The submarine extension of this major collapse scar has been identified prolonging to 700 m below sea level [Gabbianelli *et al.*, 1993; Romagnoli *et al.*, 1993; Kokelaar and Romagnoli, 1995]. Two seamounts are located southwest of Stromboli Island, at a depth of 700 and 1000 m, respectively (Figure 2b). The shallower one, named Casoni, was already documented [Gabbianelli *et al.*, 1993]; the deeper one was recently described and informally named Casoni seamount [Gamberi *et al.*, 2006]. The collection of fresh lavas and scoriae from the Casoni seamount showed that the Stromboli plumbing system

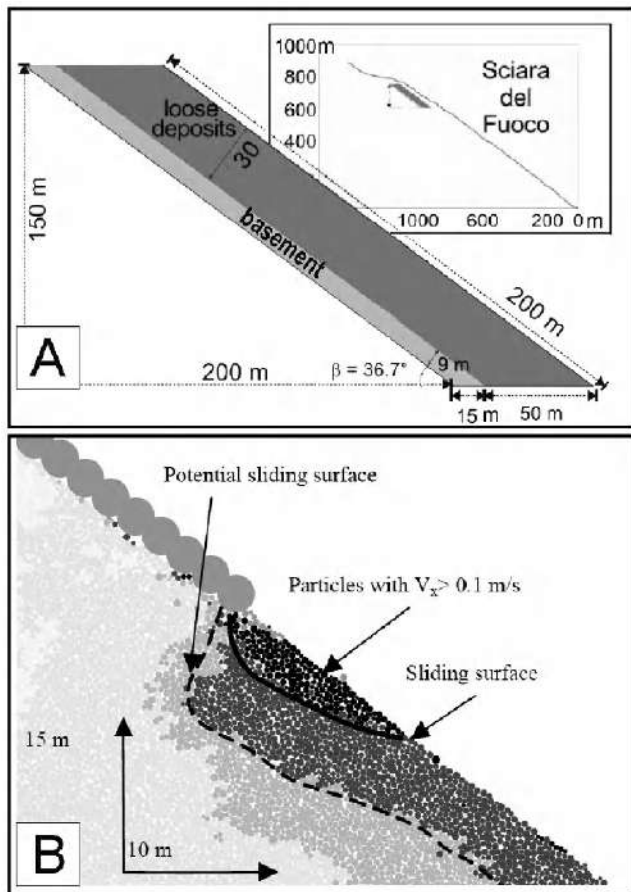


Figure 5. (a) Position of the modelled slope along the SdF. (b) Particle horizontal displacement at the lava front (after Apuan et al. [2007a]).

feeds also submarine activity, both effusive and explosive [Gamberi et al., 2006]. The Stromboli edifice is circled to the west and to the north by the Stromboli valley, a main morphologic feature originating on the slopes of the Sicilian margin and crossing the Aeolian volcanic arc between Stromboli and the Lametini seamounts [Kidd et al., 1998; Gamberi and Marani, 2007].

5. DISCUSSION AND CONCLUSIONS

This review of Stromboli delineates an evolution, in the last 100 ka, characterized by a series of phases of buildup of the edifice via dominant lava flows, interrupted by phases of destruction of part of the cone, ranging from slow slope erosion to rapid removal of huge masses. Different interpretations focus on the number (i.e., frequency) and type of large mass collapse. Hornig-Kjarsgaard et al. [1993] recognized

three calderas and two sector collapses, whereas Pasquarel et al. [1993] and Tibaldi [1996, 2001] distinguished another flank collapse to the SE plus other two sector collapses to the NW. The latter reconstruction shows the dominant occurrence of summit caldera collapse in the Pleistocene and lateral collapses in the Holocene, and several recent papers now agree that the NW flank of Stromboli has been a zone of high-gravity instability, although technical difficulties are still present in precisely dating the Holocene collapses. This series of lateral collapses is consistent with the lack of the submarine abrasion platform along the northwestern side of Stromboli, which was most likely removed by the failures. Similarly, flank failures towards SE (at least one documented by Tibaldi [1996, 2001]) and accelerated erosion rate can account for the lack of the same platform also on the opposite southeastern side. In any case, since landslides interact with the sea producing tsunami, the hazard posed by these unstable areas is considerably high.

Another, still open issue is to assess whether each lateral collapse occurred in a single major event, or through the occurrence of several, closely spaced in time, minor pulses. The relationship between causes and modalities of such events is one of the most interesting topics addressed and is worth being further investigated.

The fact is that the active part of Stromboli is growing into a lateral collapse depression, and in this case, geometries and locations of the magma rising into the uppermost part of the cone are subject to the concomitant conditions imposed by both the regional tectonic and local gravitational and magmatic stresses. This has been demonstrated at several other active multiple-collapsed volcanoes by field data [e.g., Tibaldi et al., 2005; Vezzoli et al., 2008, and references therein] and by analogue experiments [Walter and Troll, 2003]. The possible “draining” effect exerted by the debuttressed zone of the SdF depression on the magma rising into the cone was recently recognized [Tibaldi, 2004; Acocella and Tibaldi, 2005], a process which, in turn, has the feedback effect of further enhancing slope instability. The Holocene geological history of the volcano indicates that after a sector collapse develops, sheets tend to intrude preferentially along the shoulders of the amphitheater depression or within it. These intrusions, in turn, can deform the infilling of the collapse depression producing smaller landslides capable, however, of triggering tsunamis. This occurred in the past and could also be an explanation for the 2002–2003 events.

The geological–structural history of Stromboli also indicates that, in the Pleistocene, magma was mostly injected along the main NE-trending weakness zone, with single dykes striking from NNE to E-W. In the Holocene, sheet intrusions into the NW cone flank have been accompanied by frequent dyking also along the NE weakness zone, where

single dykes and fissure eruptions had a dominant NE strike and concentrated in the zone between the summit crater and the present location of the Stromboli village. This suggests a shift of the magma paths towards NE along the main weakness zone.

Volcanoes are prone to undergo phases of lateral instability mostly when magma intrudes the cone [Voight and Elsworth, 1997; Donnadieu *et al.*, 2001] and when the piling of lava and pyroclastic deposits reach a critical height [Borgia *et al.*, 1992]. The numerical modeling performed for Stromboli shows that magma overpressure during feeding processes is the dominant cause in generating deep-seated lateral collapses and/or large landslides, in agreement with the evidence of historical collapses. Even minor instability phenomena, which certainly represent the most frequent hazard scenario, can be controlled by dyke propagation and effusive events as those which occurred in 2002–2003, in agreement with the cited stability analyses. Concerning the mobilization of loose deposits, it has been demonstrated that the accumulation of lava on the slope can be responsible for the development of superficial landslides which develop at the front of the lava layer.

Pyroclastic rocks and loose deposits infilling the SdF are characterized by very poor physical properties, and this can account for the higher propensity of the present northwest volcano flank to lateral instability. We believe that this sector is prone to gravity instability also without intervening magma intrusions at a high level in the cone, as testified also by the acceleration of seaward displacement of a portion of the SdF during 2000–2001, with the development of a series of dry fissures [Tibaldi *et al.*, 2003] in a time interval without major volcanic events. This lateral instability can promote intrusions into the northwestern volcano flank, which, in turn, are capable of further destabilizing this sector with the possible development of landslides.

With special reference to the structural dynamics of the 2002–2003 event, different views have been suggested. According to Bonaccorso *et al.* [2003], the two vents which opened in the SdF at 500 and 600 m of altitude on 29–30 December were not located along a new eruptive fissure, but they formed at the intersection between the steps caused by the initial detachment of the SdF wall and the shallow feeding system of the volcano. Calvari *et al.* [2005] suggested that the three vents, opened on 28, 29, and 30 December, were due to lava tubes protruded by the main magma conduit at different levels. Acocella and Tibaldi [2005] and Acocella *et al.* [2006] claimed that these vents might be the expression of a NW–SE dyke protruded from the main conduit zone. Based on the available geophysical data [Chouet *et al.*, 2003] that indicate the presence, below the crater, of an active dyke dipping 60° to the NW, and considering

that the SdF slope dips 40° to the NW, the removal of the SdF deposit with a maximum thickness of 70 m [Baldi *et al.*, 2005], due to the 2002 landslides, might not have been large enough to intercept that dyke. Hence, we conclude that during this event, some intrusive sheets propagated from the main magma conduit to reach the surface at the new vents; however, to fully understand the local detailed geometry of these intrusions, further analyses are needed. We believe the important matter is that the entire geological and structural history of Stromboli indicates that subsurface intrusions did occur in the form of sheets. In the Holocene, at morphological stages of the volcano evolution when a lateral collapse depression was present, the propagation of the sheets was concentrated along the uppermost sides of the depression, within it or across the summit active crater zone along a NE–SW axis [Corazzato *et al.*, 2008]; therefore, there is no reason to rule out the possibility that these geometries and locations could occur again in the future.

Acknowledgments. The work was financed by Italian Dipartimento della Protezione Civile (DPC)–Istituto Nazionale di Geofisica e Vulcanologia Project V2 (02 A. Tibaldi, 17 T. Apuan) and DPC Stromboli Emergency Project V1. Maria Marsella is acknowledged for supplying subaerial topographic data for Figure 2 and Barbara Aldighieri for DEM processing. This study was performed in the framework of ILP-Task Force II, Project “New Tectonic Causes of Volcano Failure and Possible Premonitory Signals” (leader, A. Tibaldi) and of UNESCO-IUGS-IGCP Project 508 “Volcano Collapse and Fault Activity” (co-leader, C. Corazzato).

REFERENCES

- Acocella, V., and A. Tibaldi (2005), Dike propagation driven by volcano collapse: A general model tested at Stromboli, Italy. *Geophys. Res. Lett.*, 32, L08308, doi:10.1029/2004GL022248.
- Acocella, V., M. Neri, and P. Scarlato (2006), Shallow magma emplacement during the 2002–2003 Stromboli (Italy) eruption, *Geophys. Res. Lett.*, 33, L17310, doi:10.1029/2006GL026862.
- Apuan, T., and C. Corazzato (2008), Numerical model of the Stromboli volcano (Italy) including the effect of magma pressure in the dyke system, *Rock Mech. Rock Eng.*, doi:10.1007/s0060300801631.
- Apuan, T., C. Corazzato, A. Cancelli, and A. Tibaldi (2005a), Stability of a collapsing volcano (Stromboli-Italy): Limit equilibrium analysis and numerical modelling, in *The Tectonics and Physics of Volcanoes*, edited by A. Gudmundsson and V. Acocella, *J. Volcanol. Geotherm. Res. Spec. Publ.*, 144(1–4), 191–210.
- Apuan, T., C. Corazzato, A. Cancelli, and A. Tibaldi (2005b), Physical and mechanical properties of rock masses at Stromboli: A dataset for flank instability evaluation, *Bull. Eng. Geol. Environ.*, 64(4), 419–432.
- Apuan, T., M. Masetti, A. Uttini, L. Vezzoli, and C. Corazzato (2005c), Caratterizzazione geotecnica e modellazione numerica

- ad elementi distinti dei depositi della Sciara del Fuoco (Stromboli, Italia), *G. Geol. Appl.*, 2, 265–270.
- Apuani, T., A. Merri, and M. Masetti (2007a), Effects of volcanic seismic events on the Stromboli stability by finite difference numerical modelling, in *Volcanic Rocks. Proceedings of the International Workshop on Volcanic Rocks*, Workshop W2-11th Congress ISRM, Ponta Delgada, Azores, Portugal, 14–15 July 2007, edited by A.M. Malheiro and J.C. Nunes, pp. 101–109 Taylor and Francis, Philadelphia, Pa.
- Apuani, T., M. Masetti, and A. Uttini (2007b), Debris slope stability analysis in an active volcano area, in *Volcanic Rocks. Proceedings of the International workshop on volcanic rocks*, Workshop W2-11th Congress ISRM, Ponta Delgada, Azores, Portugal, 14–15 July 2007, edited by A.M. Malheiro and J.C. Nunes, pp. 141–146, Taylor and Francis, Philadelphia, Pa.
- Argnani, A., E. Serpelloni, and C. Bonazzi (2007), Pattern of deformation around the central Aeolian Islands: Evidence from multichannel seismics and GPS data, *Terra Nova*, 19, 317–323.
- Arrighi, S., M. Rosi, J.-C. Tanguy, and V. Courtillott (2004), Recent eruptive history of Stromboli (Aeolian Islands, Italy) determined from high-accuracy archeomagnetic dating, *Geophys. Res. Lett.*, 32, L19603, doi:10.1029/2004GL020627.
- Baldi P., M. Fabris, M. Marsella, and T. R. Monticelli (2005), Monitoring the morphological evolution of the Sciara del Fuoco during the 2002–2003 Stromboli eruption using multi-temporal photogrammetry, *ISPRS J. Photogramm. Remote Sens.*, 59, 199–211.
- Bertagnini, A., and P. Landi (1996), The Secche di Lazzaro pyroclastics of Stromboli volcano: A phreatomagmatic eruption related to Sciara del Fuoco Sector collapse, *Bull. Volcanol.*, 58, 239–245.
- Billi, A., G. Barberi, C. Faccenna, G. Neri, F. Pepe, and A. Sulli (2006), Tectonics and seismicity of the Tindari Fault System, southern Italy: Crustal deformations at the transition between ongoing contractional and extensional domains located above the edge of a subducting slab, *Tectonics*, 25, TC2006, doi:10.1029/2004TC001763.
- Bonaccorso A., S. Calvari, G. Garfi, L. Lodato, and D. Patanè (2003), Dynamics of the December 2002 flank failure and tsunami at Stromboli volcano inferred by volcanological and geophysical observations, *Geophys. Res. Lett.*, 30(18), 1941, doi:10.1029/2003GL017702.
- Borgia, A., L. Ferrari, G. and Pasquarè (1992), Importance of gravitational spreading in the tectonic and volcanic evolution of Mount Etna, *Nature*, 357, 231–235.
- Calvari, S., L. Spampinato, L. Lodato, A. J. L. Harris, M. R. Patrick, J. Dehn, M. R. Burton, and D. Andronico (2005), Chronology and complex volcanic processes during the 2002–2003 flank eruption at Stromboli volcano (Italy) reconstructed from direct observations and surveys with a handheld thermal camera, *J. Geophys. Res.*, 110, B02201, doi:10.1029/2004JB003129.
- Chouet, B., P. Dawson, T. Ohminato, M. Martini, G. Saccorotti, F. Giudicepietro, G. De Luca, G. Milana, and R. Scarpa (2003), Source mechanisms of explosions at Stromboli Volcano, Italy, determined from moment-tensor inversions of very-long-period data, *J. Geophys. Res.*, 108(B1), 2019, doi:10.1029/2002JB001919.
- Condomines, M., and C. J. Allègre (1980), Age and magmatic evolution of Stromboli volcano from $^{230}\text{Th}/^{238}\text{U}$ disequilibrium data, *Nature*, 288, 354–357.
- Corazzato, C., L. Francalanci, M. Menna, C. Petrone, A. Renzulli, A. Tibaldi, and L. Vezzoli (2008), What controls sheet intrusion in volcanoes? Petrological and structural characters of the Stromboli sheet complex, Italy, *J. Volcanol. Geotherm. Res.*, 173, 26–54, doi:10.1016/j.jvolgeores.2008.01.006.
- De Astis, G., G. Ventura, and G. Vilardo (2003), Geodynamic significance of the Aeolian volcanism (Southern Tyrrhenian Sea, Italy) in light of structural, seismological, and geochemical data, *Tectonics*, 22(4), 1040, doi:10.1029/2003TC001506.
- Donnadieu, F., O. Merle, and J.-C. Besson (2001), Volcanic edifice stability during cryptodome intrusion, *Bull. Volcanol.*, 63, 61–72.
- Falsaperla, S., G. Lanzafame, V. Longo, and S. Spampinato (1999), Regional stress field data in the area of Stromboli (Italy): Insight into structural data and crustal tectonic earthquakes, *J. Volcanol. Geotherm. Res.*, 88, 147–166.
- Favalli, M., D. Karàtson, R. Mazzuoli, M. T. Pareschi, and G. Ventura (2005), Volcanic geomorphology and tectonics of the Aeolian archipelago (southern Italy) based on integrated DEM data, *Bull. Volcanol.*, 68, 157–170.
- Francalanci, L., M. Barbieri, P. Manetti, A. Peccerillo, and L. Tolomeo (1988), Sr-isotopic systematics in volcanic rocks from the island of Stromboli (Aeolian arc), *Chem. Geol.*, 73, 164–180.
- Francalanci, L., P. Manetti, and A. Peccerillo (1989), Volcanological and magmatological evolution of Stromboli volcano (Aeolian islands): The roles of fractional crystallization, magma mixing, crustal contamination and source heterogeneity, *Bull. Volcanol.*, 51, 355–378.
- Francalanci, L., P. Manetti, A. Peccerillo, and J. Keller (1993), Magmatological evolution of the Stromboli volcano (Aeolian Arc, Italy): Inferences from major and trace element and Sr-isotopic composition of lavas and pyroclastic rocks, *Acta Vulcanol.*, 3, 127–151.
- Gabbianelli, G., C. Romagnoli, P. L. Rossi, and N. Calanchi (1993), Marine geology of the Panarea–Stromboli area (Aeolian archipelago, southeastern Tyrrhenian sea), *Acta Vulcanol.*, 3, 11–20.
- Gamberi, F., and M. Marani (2007), Downstream evolution of the Stromboli slope valley (southeastern Tyrrhenian Sea), *Mar. Geol.*, 243, 180–199.
- Gamberi, F., M. Marani, V. Landuzzi, A. Magagnoli, D. Penitenti, M. Rosi, A. Bertagnini, and A. Di Roberto (2006), Sedimentologic and volcanologic investigation of the deep Tyrrhenian Sea: Preliminary results of cruise VST02, *Ann. Geophys.*, 49(2–3), 767–781.
- Gillot, P. Y. (1984), Datation por la méthode K/Ar des roches volcaniques récentes (pléistocenes et holocenes), thesis, 225 pp., Paris XI-Orsay.
- Gillot, P. Y., and J. Keller (1993), Radiochronological dating of Stromboli, *Acta Vulcanol.*, 3, 11–20.
- Goes, S., D. Giardini, S. Jenny, C. Hollenstein, H.-G. Kahle, and A. Geiger (2004), A recent tectonic reorganization in the south-central Mediterranean, *Earth Planet. Sci. Lett.*, 226, 335–345.

- Hoek, E., C. T. Carranza-Torres, and B. Corkum (2002), Hoek-Brown failure criterion—2002 edition, *Proc. North American Rock Mechanics Society-TAC Conference*, Toronto, Canada, July 2002, vol. 1, 267–273.
- Hornig-Kjarsgaard, I., J. Keller, U. Koberski, E. Stadlbauer, L. Francalanci, and R. Lenhart (1993), Geology, stratigraphy and volcanological evolution of the island of Stromboli, Aeolian arc, Italy, *Acta Vulcanol.*, 3, 21–68.
- ISRM (1981), *Rock Characterization, Testing and Monitoring—International Society for Rock Mechanics Suggested Methods*, Elsevier, London.
- Keller, J., I. Hornig-Kjarsgaard, U. Koberski, E. Stadlbauer, and R. Lenhart (1993), Geological map of the island of Stromboli—scale 1:10,000, *Acta Vulcanol.*, 3, appendix.
- Kidd, R. B., R. G. Lucchi, M. Gee, and J. M. Woodside (1998), Sedimentary processes in the Stromboli Canyon and Marsili Basin, SE Tyrrhenian Sea: Results from side-scan sonar surveys, *Geo Mar. Lett.*, 18, 146–154.
- Kokelaar, P., and C. Romagnoli (1995), Sector collapse, sedimentation and clast population evolution at an active island-arc volcano: Stromboli, Italy, *Bull. Volcanol.*, 57, 240–262.
- Laiolo, M., and C. Cigolini (2006), Mafic and ultramafic xenoliths in San Bartolo lava field: New insights on the ascent and storage of Stromboli magmas, *Bull. Volcanol.*, 68, 653–670.
- Landi, P., L. Francalanci, M. Pompilio, M. Rosi, M. A. Corsaro, C. M. Petrone, I. Cardini, and L. Miraglia (2006), The December 2002–July 2003 effusive event at Stromboli volcano, Italy: Insights into the shallow plumbing system by petrochemical studies, *J. Volcanol. Geotherm. Res.*, 155, 263–284, doi:10.1016/j.jvolgeores.2006.03.032.
- Magnani, M. 1939, Osservazioni geologiche e morfologiche sull’isola di Stromboli, *L’Universo*, 18, 1–63.
- Malheiro, A. M., and J. C. Nunes (Eds.) (2007), *Volcanic rocks. Proceedings of the International Workshop on Volcanic Rocks*, Workshop W2-11th Congress ISRM, Ponta Delgada, Azores, Portugal, 14–15 July 2007, edited by A.M. Malheiro and J.C. Nunes, pp. 141–146, Taylor and Francis, Philadelphia, Pa.
- Moon, V., J. Bradshaw, R. Smith, and W. de Lange (2005), Geotechnical characterisation of stratocone crater wall sequences, White Island Volcano, New Zealand, *Eng. Geol.*, 81, 146–178.
- Neri, G., G. Barberi, B. Orecchio, and A. Mostaccio (2003), Seismic strain and seismogenic stress regimes in the crust of the southern Tyrrhenian region, *Earth Planet. Sci. Lett.*, 213, 97–112.
- Pasquarè, G., L. Francalanci, V. H. Garduno, and A. Tibaldi (1993), Structure and geological evolution of the Stromboli volcano, Aeolian islands, Italy, *Acta Vulcanol.*, 3, 79–89.
- Petrone, C. M., F. Olmi, E. Braschi, and L. Francalanci (2006), Mineral chemistry profile: A valuable approach to unravel magma mixing processes in the recent volcanic activity of Stromboli, Italy, *Per. Mineral.*, 75, 277–292.
- Renzulli, A., and P. Santi (1997), Subvolcanic crystallization at Stromboli (Aeolian Islands, southern Italy) preceding the Sciara del Fuoco sector collapse: Evidence from monzonite lithic suite, *Bull. Volcanol.*, 59, 10–20.
- Romagnoli, C., P. Kokelaar, P. L. Rossi, and A. Sodi (1993), The submarine extension of Sciara del Fuoco feature (Stromboli Isl.): Morphologic characterization, *Acta Vulcanol.*, 3, 91–98.
- Rosi, M. (1980), The Island of Stromboli. *Rend. Soc. Ital. Mineral. Petrol.*, 36, 345–368.
- Russo, G., G. Giberti, and G. Sartoris (1996), The influence of regional stresses on the mechanical stability of volcanoes: Stromboli (Italy), in *Volcano Instability on the Earth and Other Planets*, edited by W. McGuire, A.P. Jones, and J. Neuberg, *Geol. Soc. Spec. Publ.*, 110, 65–75.
- Speranza, F., M. Pompilio, L. and D. Sagnotti (2004), Paleomagnetism of spatter lavas from Stromboli volcano (Aeolian Islands, Italy): Implications for the age of paroxysmal eruptions, *Geophys. Res. Lett.*, 31, L02607, doi:10.1029/2003GL018944.
- Thomas, M. E., N. Petford, and E. N. Bromhead (2004), Volcanic rock-mass properties from Snowdonia and Tenerife: Implication for volcano edifice strength, *J. Geol. Soc.*, 161, 939–946.
- Tibaldi, A. (1996), Mutual influence of diking and collapses at Stromboli volcano, Aeolian Arc, Italy, in *Volcano Instability on the Earth and Other Planets*, edited by W. McGuire, A.P. Jones, and J. Neuberg, *Geol. Soc. Spec. Publ.*, 110, 55–63.
- Tibaldi, A. (2001), Multiple sector collapses at Stromboli volcano, Italy: How they work, *Bull. Volcanol.*, 63(2–3), 112–125.
- Tibaldi, A. (2003), Influence of volcanic cone morphology on dikes, Stromboli, Italy, *J. Volcanol. Geotherm. Res.*, 126, 79–95.
- Tibaldi, A. (2004), Major changes in volcano behaviour after a sector collapse: Insights from Stromboli, Italy, *Terra Nova*, 16, 2–8.
- Tibaldi, A. (2008), A new geological map of Stromboli volcano (Tyrrhenian Sea, Italy) based on application of lithostratigraphic and UBS units, in *Stratigraphy and Geology in Volcanic Areas*, edited by G. Groppelli and L. Viereck-Goette, *Geol. Soc. of Am. Spec. Publ.*, in press.
- Tibaldi, A., G. Pasquaré, L. Francalanci, and H. Garduño (1994), Collapse type and recurrence at Stromboli volcano, associated volcanic activity, and sea level changes, Accademia dei Lincei, *Atti Conv. Lincei*, 112, 143–151.
- Tibaldi, A., C. Corazzato, T. Apuani, and A. Cancelli (2003), Deformation at Stromboli volcano (Italy) revealed by rock mechanics and structural geology, *Tectonophysics*, 361, 187–204.
- Tibaldi, A., A. M. F. Lagmay, and V. Ponomareva (2005), Effects of basement structural and stratigraphic heritages on volcano behaviour and implications for human activities. *Episodes*, 28(3), 158–170.
- Tommasi, P., D. Boldini, and T. Rotonda (2005), Preliminary characterization of the volcanoclastic material involved in the 2002 landslides at Stromboli, in *Proceedings of the International Conference on Problematic Soils GEOPROB 2005, Famagusta, Northern Cyprus*, edited by H. Bilsel and Z. Nalbantoglu, vol. 3, pp. 1093–1101.
- Ventura, G., G. Vilardo, G. Milano, and N. A. Pino (1999), Relationships among crustal structure, volcanism and strike-slip

- tectonics in the Lipari–Vulcano Volcanic Complex, Aeolian Islands, Southern Tyrrhenian Sea, Italy, *Phys. Earth Planet. Int.*, **116**, 31–52.
- Vezzoli, L., A. Tibaldi, A. Renzulli, M. Menna, and S. Flude (2008), Faulting-assisted lateral collapses and influence on shallow magma feeding system at Ollagüe volcano (Central Volcanic Zone, Chile-Bolivia Andes). *J. Volcanol. Geotherm. Res.*, **171**(1–2), 137–159.
- Voight, B., and D. Elsworth (1997), Failure of volcano slopes, *Geotechnique*, **47**(1), 1–31.
- Walter, T. R., and V. R. Troll (2003), Experiments on rift zone evolution in unstable volcanic edifices, *J. Volcanol. Geotherm. Res.*, **127**, 107–120.
- Watters, R. J., D. R. Zimbelman, S. D. Bowman, and J. K. Crowley (2000), Rock mass strength assessment and significance to edifice stability, Mount Rainier and Mount Hood, Cascade Range volcanoes, *Pure Appl. Geophys.*, **157**, 957–976.
-
- T. Apuani, Dipartimento di Scienze della Terra “Ardito Desio,” Università di Milano, Via Mangiagalli 34, 20133 Milan, Italy. (tiziana.apuani@unimi.it)
- C. Corazzato and A. Tibaldi, Dipartimento di Scienze Geologiche e Geotecnologie, Università di Milano-Bicocca, Piazza della Scienza 4, 20126 Milan, Italy. (claudia.corazzato@unimib.it; alessandro.tibaldi@unimib.it)
- F. A. Pasquare and L. Vezzoli, Dipartimento di Scienze Chimiche e Ambientali, Università dell’Insubria, Via Valleggio 11, 22100 Como, Italy. (federico.pasquare@unimib.it; vezzoli@uninsubria.it)

Volcanology and Magma Geochemistry of the Present-Day Activity: Constraints on the Feeding System

Antonella Bertagnini,¹ Nicole Métrich,^{1,2} Lorella Francalanci,³ Patrizia Landi,¹
Simone Tommasini,³ and Sandro Conticelli³

Stromboli volcano is famous in the scientific literature for its persistent state of activity, which began about 1500 years ago and consists of continuous degassing and mild intermittent explosions (normal Strombolian activity). Rare lava emissions and sporadic more violent explosive episodes (paroxysms) also occur. Since its formation, the present-day activity has been dominated by the emission of two basaltic magmas, differing chiefly in their crystal and volatile contents, whose characteristics have remained constant until now. The normal Strombolian activity and lava effusions are fed by a crystal-rich, degassed magma, stored within the uppermost part of the plumbing system, whereas highly vesicular, crystal-poor light-colored pumices are produced during paroxysms testifying to the ascent of volatile-rich magma batches from deeper portions of the magmatic system. Mineralogical, geochemical, and isotopic data, together with data on the volatile contents of magmas, are presented here with the aim of discussing (1) the relationships between the different magma batches erupted at Stromboli, (2) the mechanisms of their crystallization and transfer, (3) the plumbing system and triggering mechanisms of Strombolian eruptions.

1. INTRODUCTION

For a long time, the volcanic island of Stromboli in the Aeolian arc (Southern Italy) has been attracting scientists and travelers because of its persistent state of mild explosive activity, usually visible for several kilometers.

The subaerial part of the volcano was built in the last 100 ka, through six main periods of effusive and explosive activity (Paleostromboli I, II, and III, Vancori, Neostromboli, and Recent Stromboli; Hornig-Kjarsgaard *et al.* [1993]). Transitions between each period are marked by significant structural modifications of the edifice (caldera collapses during the early evolution and sector collapses after the Vancori period [Tibaldi *et al.*, this volume] and by significant changes in the magma composition from calc-alkaline to shoshonitic, through high-K calc-alkaline [Francalanci *et al.*, 1988, 1989; Hornig-Kjarsgaard *et al.*, 1993].

The activity of the volcano, its eruptive features, its recurrent eruptive phenomena, and the morphological evolution of the crater area have been widely described in reports and scientific works since the end of the 17th century [Barberi *et al.*, 1993 and references therein]. The oldest unequivocal account of the Stromboli activity dates back to the 10th century A.D., whereas the earlier, rare historical sources are from the 4th century B.C. These historical records, however, do not

¹Istituto Nazionale di Geofisica e Vulcanologia, Sezione di Pisa, Pisa, Italy.

²Laboratoire Pierre Sue, CEA-CNRS, CE-Saclay, Gif/Yvette, France.

³Dipartimento di Scienze della Terra, Università degli Studi di Firenze, Firenze, Italy.

allow the exact recognition of the beginning of the persistent state of activity [Rosi *et al.*, 2000 and references therein].

Chronostratigraphic studies suggested that the present-day eruptive behavior began after a period of dormancy, nearly 1500 years ago and since then has continued without significant breaks or changes in eruptive style [Rosi *et al.*, 2000].

In the previous centuries, at least until the 4th century B.C., activity was dominated by repeated episodes of sustained fire fountains, separated by either quiescence or periods of mild Strombolian activity. In this time span, lava effusions also occurred from an adventive vent, on the north-eastern flank of the volcano, pouring out the San Bartolo lava flow, which is dated between 360 B.C. and 100 A.D. by paleomagnetic and archeomagnetic methods [Speranza *et al.*, 2008; Arrighi *et al.*, 2004] (Figure 1). Magmas feeding this period of activity were fairly porphyritic (20–25 vol % of phenocrysts) high-K (HK) basaltic andesites [Rosi *et al.*, 2000; Petrone *et al.*, 2006].

The present-day activity takes place at three main craters located in a flattish area (the Crater Terrace) at 750 m above sea level (asl) within the Sciara del Fuoco (SdF), a deep horseshoe scar in the NW sector of the island, likely resulting from at least four sector collapses [Tibaldi *et al.*, this volume] (Figure 1). Since the early observations, the position of active craters has remained almost unchanged, whereas their morphology has been repeatedly modified [Washington, 1917]. As an example, pictures of the Crater

Terrace taken in a time interval of 2 years are shown in Figure 2.

The persistent activity consists of continuous streaming of gas from the crater area [Allard *et al.*, 1994; this volume], mild intermittent explosions (normal Strombolian activity), rare lava emissions and sporadic more violent explosive episodes (paroxysms) [Barberi *et al.*, 1993]. Normal Strombolian activity and lava flows do not represent seriously hazardous phenomena. On the contrary, paroxysms due to their violent character and sudden occurrence are a major threat to people either visiting the volcano summit or living in the settled areas. In the last two centuries, large-scale paroxysms have produced damage to the villages of Stromboli and Ginostra, located along the coast at distances of 2–3 km from the craters.

Volcanological studies highlighted that normal Strombolian activity is characterized by the emission of highly porphyritic black scoriae (hereafter HP scoria or HP magma). In contrast, the paroxysms recorded in the last century and previous large-scale paroxysms (hereafter the historical paroxysms) produced low porphyritic golden pumices (hereafter LP pumice or LP magma) in addition to black HP scoriae identical to those of the normal Strombolian activity.

In this paper, we present a review of the most recent data with the aim of elucidating the main volcanological characteristics of the present-day activity; chemical, isotopic, and mineralogical data together with those regarding the volatile content of magmas. They are used to discuss the petrological evolution of the volcanic systems and put constraints on the Stromboli plumbing system(s).

2. VOLCANOLOGICAL CHARACTERISTICS OF THE PRESENT-DAY ACTIVITY

2.1. Normal Strombolian Activity

Normal activity consists of rhythmic, mild to moderate events lasting a few seconds, which take place at different vents every 10–20 min, and eject gas, scoriae, ash, bombs, and blocks that are thrown up to heights of several hundred meters. The proportion between different types of ejecta is variable with a prevalence of coarse ballistic ejecta or ash-charged plumes or both [Chouet *et al.*, 1999; Patrick *et al.*, 2007]. The fallout of the coarsest ejecta is usually limited to a few hundred meters from the source vent. Typical products of the normal activity are highly porphyritic (HP) black scoriae and spatter clasts. Vesicle number and texture are variable in scoria reflecting different intensity and style of the Strombolian explosions and/or a different melt rheology in the shallow conduit [Lautze and Houghton, 2005, 2007; Burton *et al.*, 2007b] (Plates 1a and 1b).

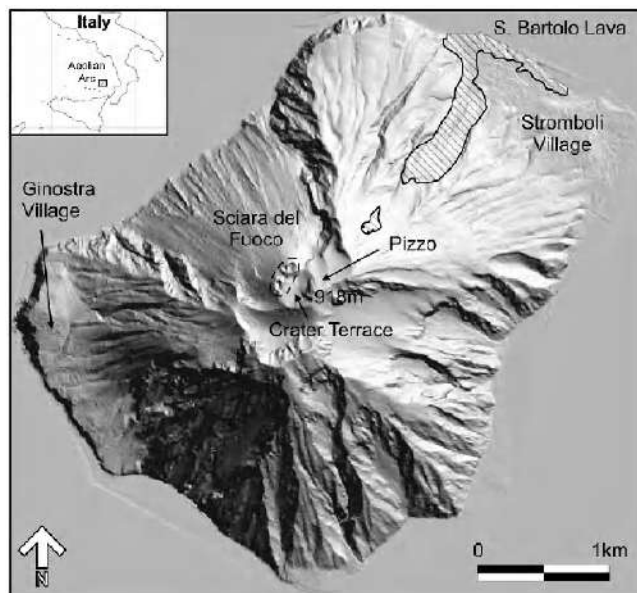


Figure 1. Map of the island of Stromboli. The position of San Bartolo lava is from Hornig-Kjarsgaard *et al.* [1993].

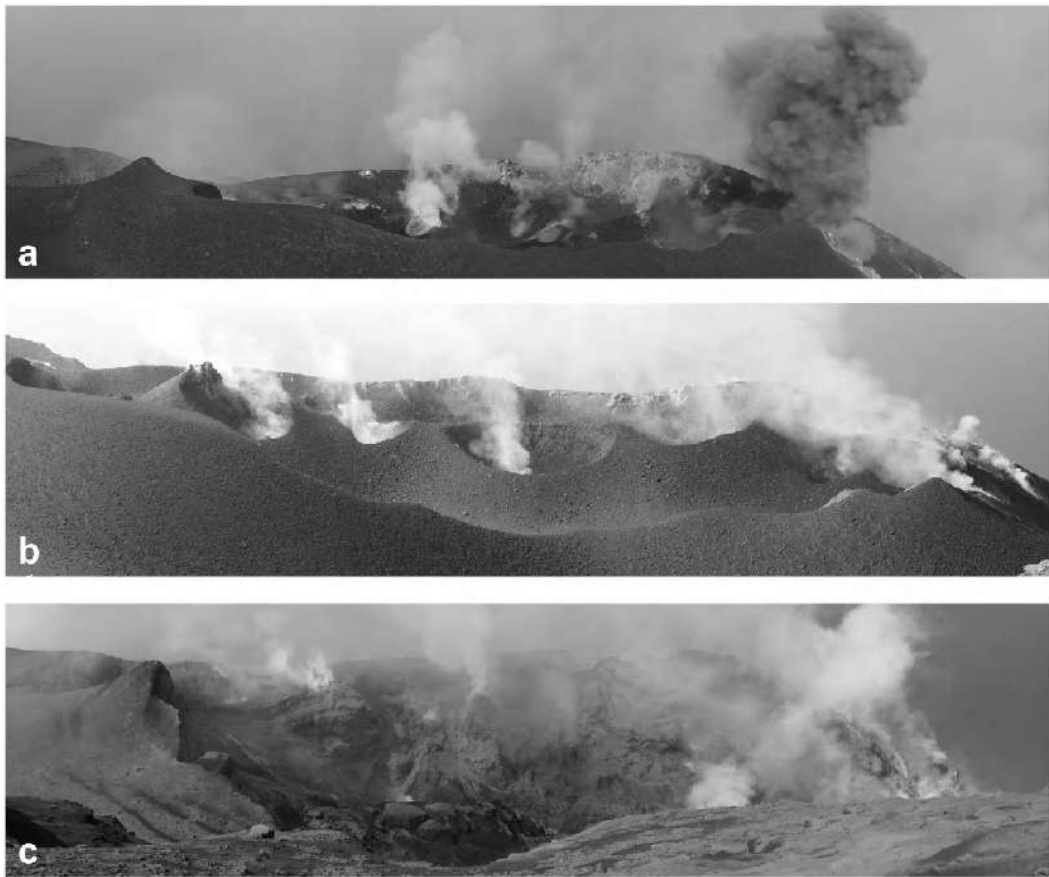


Figure 2. The Crater Terrace seen from Pizzo; (a) 2 June 2005; (b) 1 October 2006; (c) 11 April 2007.

2.2. Lava Flow Emission

Lava flows are usually produced by overflows from the summit craters or by vents opened inside the SdF, a few hundred meters below the Crater Terrace. The opening of a vent at shoreline level was reported to have occurred in 1955 [Abbruzzese and Cavallaro, 1956]. No evidence of vent opening outside the SdF exists in the present period of activity. Twenty-six episodes of lava emission occurred between 1888 and 2002, with duration varying from some days to 11 months. The last significant lava effusion preceding the 2002–2003 crisis lasted 141 d (from December 1985 to April 1986) and produced a lava volume of $5\text{--}6 \times 10^6 \text{ m}^3$ [De Fino et al., 1988]. Two small overflows from the summit craters occurred in May 1993 during a period of vigorous Strombolian activity [Bonaccorso et al., 1996]. During the lava emission, Strombolian activity at the central craters is usually reported. Only scarce information is available on the state of the activity in the period preceding effusive episodes. A significant rising of the magma level in the conduits

was reported 15–20 d before the beginning of the 1915 lava effusion that lasted 6 months [Perret, 1916]. Lava flows associated with paroxysms are also reported (see below). A short explosive phase was reported at the beginning of the 1954, 1975, and 1985 effusive episodes [Nappi, 1976; De Fino et al., 1988]. Magma emitted during lava flow activity is a crystal-rich magma, identical to that commonly sustaining normal Strombolian activity.

2.3. Paroxysms

More energetic explosive episodes, so called Strombolian paroxysms [Mercalli, 1907] occur sporadically.

They usually consist of a sequence of explosive events from different craters (Plate 2a) lasting from a few minutes to days, even weeks as reported in November 1882 [Mercalli, 1884] and April 1907 [Platania, 1910]. Strong detonations, described by eyewitnesses as single or repeated cannon shots, and window-breaking pressure waves [Riccò and Mercalli, 1892; De Fiore, 1923] are accompanied by the

impulsive emission of hundred-meters-high jets of gas, ash, and incandescent materials rapidly evolving into convective plumes, up to 10 km high [Barberi *et al.*, 1993]. Barberi *et al.* [1993] classified the explosive events more energetic than those of the normal Strombolian activity on the basis of their hazard implications: “paroxysms” being the events affecting the settled areas and “major explosions” only the upper part of the volcano. However, a real limit in terms of intensity and magnitude does not correspond to these two categories. For this reason, hereafter, we refer to these episodes with the general term of “paroxysms.”

During small-scale paroxysms, decimeter-sized ballistic blocks and bombs are ejected within a distance of several hundred meters from the Crater Terrace. Ash and scattered light-lapilli fallout are restricted to the volcano slopes as what typically occurred in August 1998 or August 1999 (Plate 2b). During the paroxysm of 11 July 1959, which can be considered as an intermediate-scale event, the fallout of ash, lapilli, and scattered juvenile bombs on the volcano slopes was more intense (Plate 2d), and the proximal pumice deposit reached a thickness of 40–60 cm [Cavallaro, 1962]. During the large-scale paroxysms, meter-sized clasts fall on the volcano slopes up to a few kilometers (Plate 2c). Heavy rain of meter-sized spatter clasts, decimeter-sized bombs, lapilli, and ash covers the volcano as described in 1930 [Rittmann, 1931]. Likewise, red ash covering the sea, floating pumice for several miles around the island and “pumice banks” were reported during large-scale paroxysms of the 19th century [Mercalli, 1881, 1883, 1884]. Lapilli fallout issued from the large-scale events led to the accumulation of alternating discrete layers of pumice and ash on the downwind slopes up to low elevations. They are usually associated with incipiently welded deposits mainly formed by decimeter-sized fluidal spatter clasts cropping out on the SdF flanks down to elevations of about 200 m asl. In some cases, the rapid accumulation of incandescent clasts on the upper sandy slopes triggered hot avalanches that reached the sea (1930, 1944).

Tsunami waves also occurred in association with some past paroxysms such as in 1879, 1916, 1919, 1930, 1944, and 1954 [Mercalli, 1881; Rittmann, 1931; Maramai *et al.*, 2005]. According to eyewitnesses’ accounts, Maramai *et al.* [2005] suggested that most of these events could be related to submarine failure of the SdF. Paroxysms produced also deep changes in the crater area as in 1930 when the crater terrace lowered by about 70 m [Rittmann, 1931] or in 1936 when a large collapse crater formed [Abbruzzese, 1937].

The volume of products is always low. A rough estimate of the volume of the juvenile component gives maximum values of 10^3 – 10^5 m 3 . The total volume of the emitted products, both juvenile and lithic clasts, is probably less than 10 6 m 3 in the largest events [Bertagnini *et al.*, 2003].

The reported state of the volcano before paroxysmal episodes is highly variable. No variations in the normal state of activity were reported before the 1930 and 1936 large-scale paroxysms, February 1993, February and October 1996 small-scale paroxysms. In contrast, the explosive activity increased for days and months before the paroxysms of 1907, 1912, 1916, 1919, 1959; overflows or lava flows occurred immediately before and during the paroxysmal crisis of 1916, 1919, 1930, 1936, and 1941. Two paroxysms took place during a 6-month-long effusive crisis with lava flows inside the SdF and mild explosive activity at the craters in 1915 [Platania, 1910; Riccò, 1917; De Fiore, 1915, 1923; Ponte, 1919, 1921; Rittmann, 1931; Abbruzzese, 1937; Ponte, 1948; Cavallaro, 1957, 1962; Bonaccorso *et al.*, 1996; Coltellini *et al.*, 2000]. The last two paroxysms (5 April 2003 and 15 March 2007) occurred during effusive episodes, after 3 months (in the 2003 event) and 15 d (in the 2007 event, see <http://www.ct.ingv.it/>) of intense lava effusion.

In the last 15 years, about 24 well-documented paroxysms were reported [Barberi *et al.*, 1993; Bonaccorso *et al.*, 1996; Coltellini *et al.*, 2000; <http://www.ct.ingv.it/>; <http://www.volcano.si.edu/>]. They can be classified as small-scale events except the last episodes in 5 April 2003 and 15 March 2007. It is necessary to go back about 50 years, in 1959, to find a similar event. However, they are less energetic than the 1930-type paroxysm. According to Barberi *et al.* [1993], in the last two centuries, about 25 large-scale paroxysms occurred, but assessing their number and frequency from the beginning of the present-day activity is not an easy task.

Recent paleomagnetic data on lava spatter deposits cropping out along the SdF rims suggest that the largest, spatter-forming paroxysms occurred in two distinct clusters, respectively, between 1400 and 1600 A.D. and in the 20th century [Speranza *et al.*, 2004]. Arrighi *et al.* [2004], by using archeomagnetic method, date spatter deposits cropping out on the northern flank of the volcano to the 20th century and point out the occurrence of a large paroxysmal eruption in 550 AD (± 50), possibly related to the beginning of the present activity.

The unquestionable signature of Strombolian paroxysms is the production of highly vesicular, crystal-poor, light-colored (“golden”) pumices. These are variably expanded and show various textures (Plate 1). Pumices result from the eruption of LP magma, wrapping HP scoria lamps and even mingled with the HP magma feeding the normal Strombolian activity and lava flows. The extent of mingling is highly variable among clasts issued from one single event and from different paroxysms (Plate 1). Unmingled HP products, identical to those emitted by the normal Strombolian activity, are present as well.

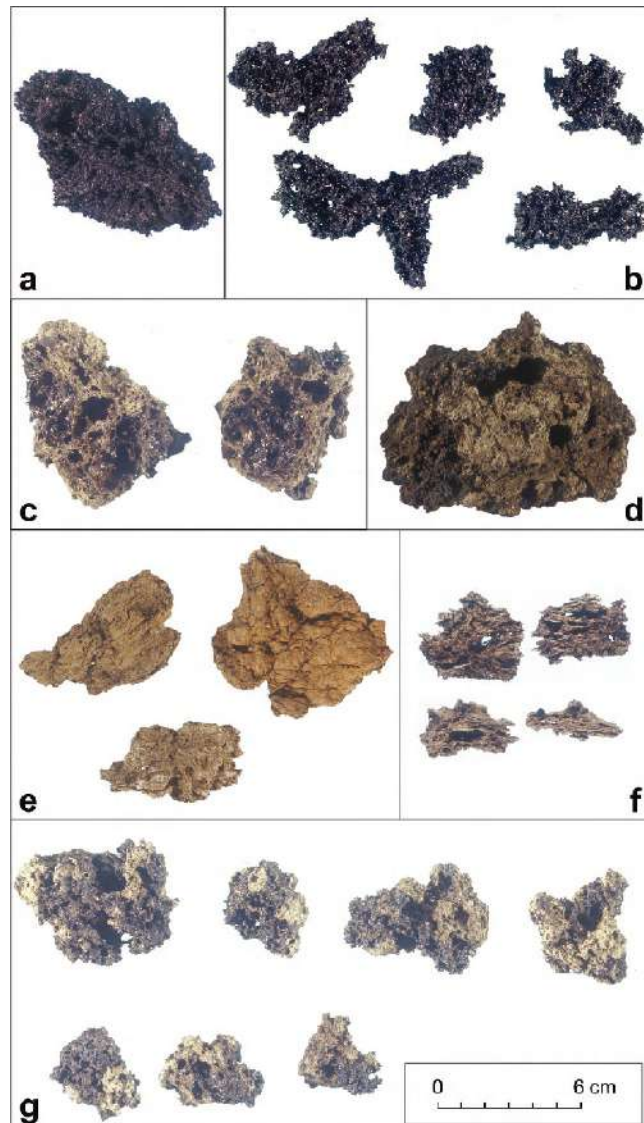


Plate 1. Highly porphyritic (HP) and low porphyritic (LP) juvenile clasts. Black HP scoriae with variable vesicularity (a) and (b); LP pumice showing an external light colored (golden) surface and a black luster interior with large coalescent bubbles (c) or with an only cavity (d); platy LP clasts with smooth microvesicular golden surface (e); highly vesicular fibrous LP clasts (f); mingled HP (dark colored)/LP (light colored part) clasts (g).

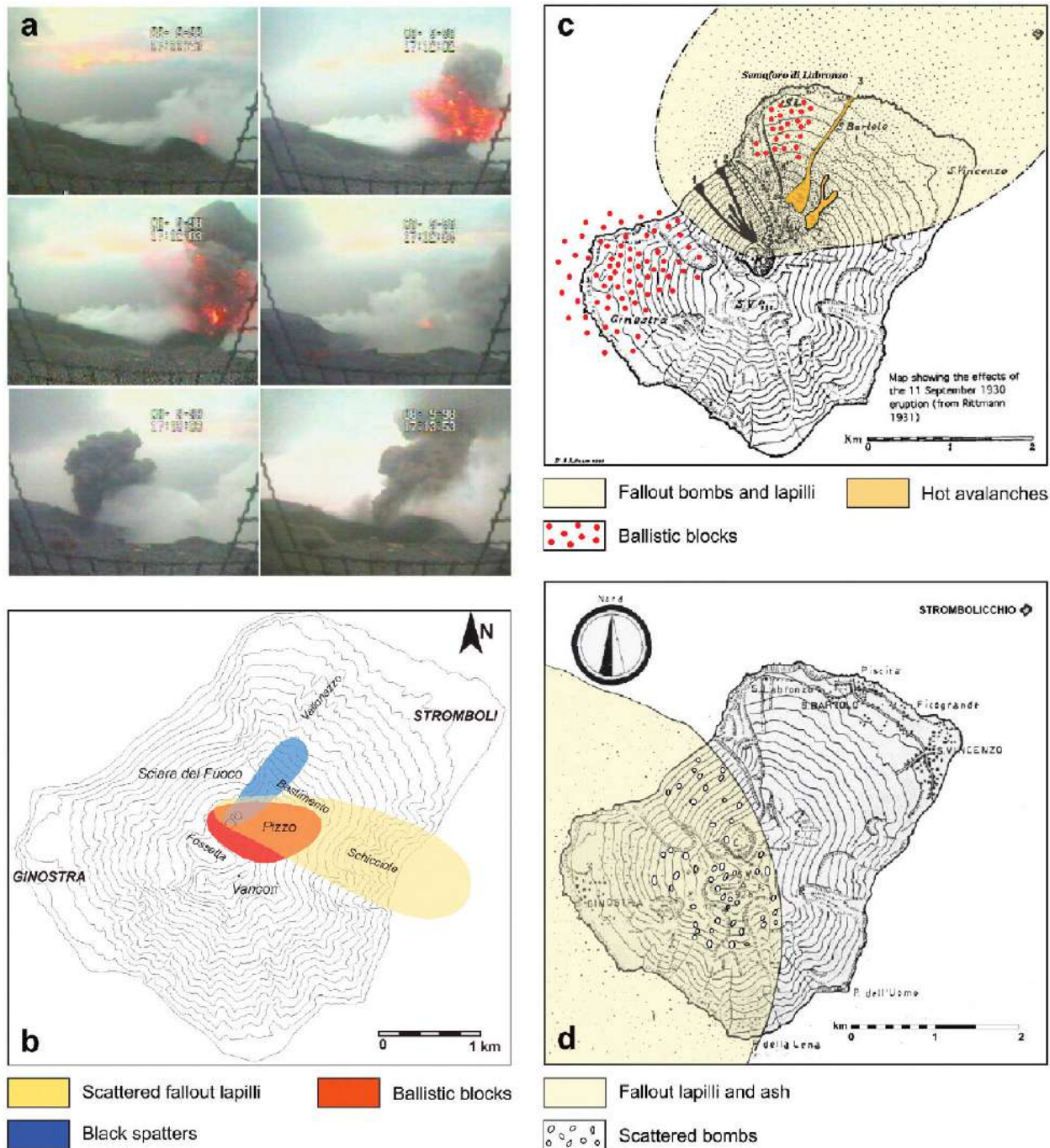


Plate 2. (a) Explosive sequence of a small-scale paroxysm (8 September 1998) as recorded by the surveillance camera at Pizzo, located about 250 m from the Crater Terrace [from Bertagnini *et al.*, 1999]. Product dispersal during: (b) small-scale paroxysm (23 August 1998, modified from Bertagnini *et al.* [1999]), (c) large-scale paroxysm (11 September 1930, modified from Rittmann [1931]), (d) intermediate-scale paroxysm (9 July 1959, modified from Cavallaro [1962]).

The presence of golden pumices characterizes all the large-scale paroxysms and most of the smaller ones [Barberi et al., 1993; Bonaccorso et al., 1996; Bertagnini et al., 1999, 2003; Coltellini et al., 1999; Francalanci et al., 1999, 2004; Rosi et al., 2000; Métrich et al., 2001; Bertagnini et al., 2003]. In some small-scale events (e.g., 8 September 1998; 20 October 2001; 23 January 2002 [Bertagnini et al., 1999; Calvari et al., 2002], only black crystal-rich scoria and/or lithic clasts were emitted without any evidence of pumices. Lithic clasts are represented both by scoria and lava with hydrothermal and fumarolic alteration and fresh lava fragments [Ponte, 1921; Rittmann, 1931].

3. MINERALOGICAL, CHEMICAL, AND ISOTOPIC CHARACTERISTICS OF PRODUCTS FROM THE PRESENT-DAY ACTIVITY

Over a period of about 1500 years, the eruptive products of Stromboli show a net bimodality in the characteristics of the erupted magmas as testified by the emission of crystal-rich/volatile poor [highly porphyritic (HP)] magmas erupted as scoria and lava and crystal-poor/volatile-rich [low porphyritic (LP)] magmas erupted as pumice. The LP pumice/HP scoria pairs have fairly similar bulk major element compositions, but distinctive textures, crystal, and volatile contents, matrix glass, and Sr isotope compositions [Métrich et al., 2001; Bertagnini et al., 2003; Francalanci et al., 1999, 2004; Landi et al., 2004; Francalanci et al., 2005].

3.1. Highly Porphyritic (HP) Magma

The HP magma feeding the normal Strombolian activity and the effusive events is a HK/shoshonitic basalt (in wt %: $48.5 < \text{SiO}_2 < 51.5$; $1.9 < \text{K}_2\text{O} < 2.5$; $\text{CaO}/\text{Al}_2\text{O}_3 = 0.59\text{--}0.62$) (Figure 3), containing 45–55 vol % of euhedral crystals including plagioclase (0.1–2.5 mm), clinopyroxene (0.5–5 mm), and olivine (0.1–4 mm).

Plagioclase is the most abundant phase (33 vol % on average) with a compositional mode at An_{68} (Figure 4a). They show concentric zoning with alternating layers of (1) labradoritic plagioclase ($\text{An}_{60}\text{--}\text{An}_{70}$) and (2) sieved textured, patchy zoned plagioclase ($\text{An}_{70}\text{--}\text{An}_{90}$) rich in melt inclusions and voids which commonly grow on dissolution surfaces. These characteristics are related to repeated episodes of resorption and growth events under high undercooling, [Landi et al., 2004]. Their outer rims, which are in textural equilibrium with the groundmass have labradoritic composition ($\text{An}_{64\text{--}70}$). The clinopyroxene represents ~12% volume. Its composition ranges from Fs_5 to Fs_{18} [$\text{Wo}_{38\text{--}48}$, magnesium number, $\text{Mg} \# = \text{Mg}/(\text{Mg} + \text{Fe}^{2+})$ 0.91–0.69], showing two distinct modes at $\text{Fs}_{12\text{--}15}$ and $\text{Fs}_{6\text{--}9}$ (Figure 4b). The MgO-rich

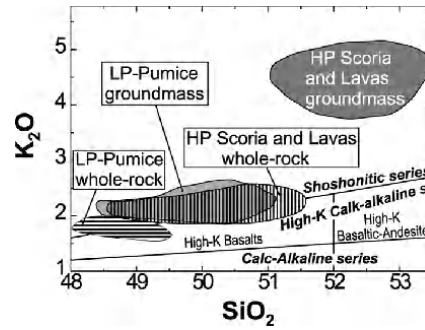
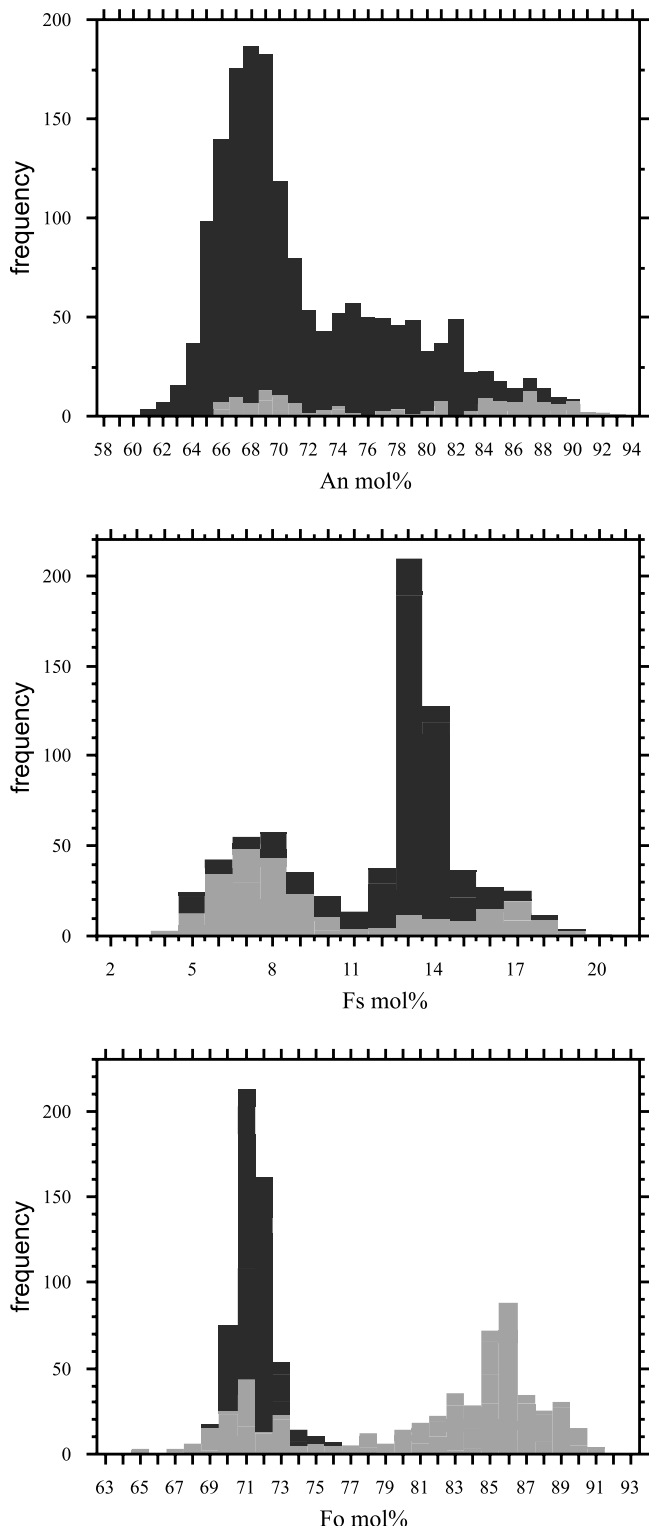


Figure 3. Compositional fields, reported in the K_2O versus silica classification diagram [Peccerillo and Taylor, 1976] for the whole rocks and the glassy groundmasses of products erupted in the period 1900–2002. HP, highly porphyritic; LP, low porphyritic. Data are plotted on water-free bases. Data are from Métrich et al. [2001], Francalanci et al. [2004, 2005] and Landi et al. [2004].

component ($\text{Fs}_{5\text{--}10}$) is subordinate and occurs only as rounded cores and/or intermediate thin layers with rounded surfaces. Fe-rich clinopyroxene ($\text{Fs} > 15$, $\text{Wo} < 40$ mol %) is also present as rare corroded cores. The two clinopyroxene groups (Figure 4b) are also distinguished on the basis of minor element contents. The group at lower Fs contents shows higher Cr content, lower Mn and Ti abundances, and well-defined correlations of Mg # with Al_{tot} , Mn, Ti, and Cr. This characteristic suggests different mineral/liquid equilibrium [Francalanci et al., 2004]. Olivine (~5 vol %) generally shows a restricted compositional range between $\text{Fo}_{70\text{--}73}$. Resorbed crystals with $<10 \mu\text{m}$ rims of $\text{Fo}_{74\text{--}75}$ are sporadically found. Finally, glomeroporphyritic aggregates up to 6–7 mm in diameter are common. They are made up of the same mineral phases sometimes associated to small interstitial plagioclase. The compositional ranges of plagioclase, clinopyroxene, and olivine do not show systematic variations with time since the beginning of the 20th century [Francalanci et al., 2004; Landi et al., 2004].

Crystal size distribution (CSD) of scoria and lavas emitted over the last 20 years [Armienti et al., 2007] shows a linear dependence from the crystal size with quite constant slopes and intercepts, revealing a system that is close to the equilibrium from a kinetic point of view. The linear crystal size distribution, particularly for plagioclase, is reached through recurrent episodes of growth and resorption.

In summary, the systematic mineralogical study of scoriae and lavas, produced since the beginning of the present-day activity, testifies to the systematic prevalent crystallization of plagioclase An_{68} , in equilibrium with olivine $\text{Fo}_{71\text{--}73}$, clinopyroxene $\text{Fs}_{12\text{--}15}$, and the shoshonitic residual melt. Compositions of glassy to hypocrystalline groundmasses



are shoshonitic basalts and shoshonites (Figure 3). Extensive analyses of the glassy matrices erupted over the last 100 years prove their chemical homogeneity [Landi *et al.*, 2004; Lautze and Houghton 2005].

Detailed geochemical analyses on products emitted during the 19th century suggest a slight increase of the mafic character of the HP magma between 1906 and 1930 (e.g., MgO: 5 to 6.5 wt %, Ni: 28 to 58 ppm; Table 1; Figure 5a), and then a decrease after 1965 [Francalanci *et al.*, 2004]. A different behavior is observed for the incompatible trace element contents (especially for Ba, Sr, Rb, Nb, and light REE), which are more enriched after 1930 (e.g., Ba > 900 ppm, Sr > 650 ppm, Nb > 18 ppm; Table 1; Figure 5b). This increase of incompatible trace element contents was attributed to a compositional variation in the replenishing LP magma [Francalanci *et al.*, 2004].

Sr isotope ratios in scoria and lavas from the beginning of the 20th century to around 1980–1985 are constant with an average of 0.70626 ($\pm 2, 2\sigma$), then start to smoothly decrease down to a value of 0.70616 in June 2002 scoria. This time variation was used to calculate a short residence time ($\approx 19 \pm 12$ years) of the HP magma feeding the present-day activity (Figure 5c). Nd isotope ratios since 1996 are more homogeneous (0.51255–0.51256) than $^{87}\text{Sr}/^{86}\text{Sr}$ variation [Francalanci *et al.*, 1999, 2004].

3.2. Low Porphyritic (LP) Magma

The LP magma is erupted as pumice during paroxysms. The bulk pumices are HK-basalts (in wt%: $48 < \text{SiO}_2 < 0$; $1.6 < \text{K}_2\text{O} < 2.2$; Table 1, Figure 3), carrying about 10 to 30 vol % crystals composed of plagioclase An_{64-90} , clinopyroxene Fs_{5-17} , Wo_{48-38} and olivine Fo_{65-91} . These crystals are in large proportion xenocrysts whose textures indicate negligible to extensive and repeated interactions with volatile-rich melts.

Most of the xenocrysts (plagioclase, clinopyroxene, and olivine) are entrained from HP magma body during its syn-eruptive mingling with the ascending LP magma. They represent the majority of the crystals in grain-sizes > 1 mm and also occur in smaller grain-sizes [Bertagnini *et al.*, 1999; Métrich *et al.*, 2001]. Crystals ultimately entrained at time of eruption are rimmed by the typical shoshonitic residual glass or by thin reaction and growth rims. In contrast, other crystals show extensive reverse and/or oscillatory zon-

Figure 4. (Opposite) Cumulative compositional distribution of (a) plagioclase (in An mol %), (b) clinopyroxene (in Fs mol %), and (c) olivine (in Fo mol %). Black bars: crystal-rich scoria and lavas (HP); gray bars: crystal-poor pumice (LP) [data from Métrich *et al.*, 2001; Francalanci *et al.*, 2004; Landi *et al.*, 2004; Bertagnini *et al.*, 2003; Métrich *et al.*, 2005; Landi *et al.*, 2006].

Table 1. Whole Rock Compositions of Selected Scoria, Lava and Pumice Representative of the Magma Feeding the Present Activity of Stromboli

Table 1. (continued)

Sample Date	HP								LP								
	STR9/ ST89.0 ^b 1989		STR9/ Str93-1 ^e 10/2/93		STR9/ 95c ^f 27/9/95		STR9/ 96e ^f 4/9/96		ST133s ^{a,*} 23/8/98	ST182 ^g 26/8/99	ST82p ^h Hist.	ST79p ^h Hist.	ST81p ^h Hist.	STR9-2 ^e 10/2/93	STR9/ 96d ^f 4/9/96	ST140p ^{a,*} 23/8/98	ST178 ^h 26/8/99
	Scoria	Scoria	Scoria	Scoria	Scoria	Scoria	Scoria	Scoria	Scoria	Scoria	Pumice	Pumice	Pumice	Pumice	Pumice	Pumice	
SiO ₂	50.63	49.91	49.30	49.52	49.89	50.40	50.87	51.51	51.61	49.13	48.59	49.05	49.05	50.01			
TiO ₂	0.87	0.99	0.97	0.96	0.98	0.95	0.9	0.87	0.87	1.02	0.99	0.97	0.97	0.97			
Al ₂ O ₃	17.29	17.77	17.93	18.07	18.05	17.83	16.56	16.67	16.22	17.08	16.31	17.14	17.14				
Fe ₂ O ₃	2.89	1.82	2.58	2.87	3.86	2.48	3.46	3.01	3.01	4.18	3.60	4.6	2.56				
FeO	5.17	6.63	6.08	6.00	4.9	5.88	5.11	5.10	5.4	5.09	5.75	4.4	6.16				
MnO	0.16	0.16	0.16	0.17	0.16	0.16	0.16	0.15	0.16	0.17	0.18	0.16	0.16				
MgO	6.22	6.30	6.57	6.08	5.97	6.27	6.66	6.34	6.64	6.25	7.84	6.93	6.37				
CaO	11.05	10.87	11.17	11.21	10.78	10.73	10.91	10.34	10.61	12.21	12.21	11.59	11.24				
Na ₂ O	2.54	2.51	2.47	2.49	2.6	2.52	2.39	2.75	2.45	2.30	2.05	2.38	2.51				
K ₂ O	2.16	2.07	2.04	2.08	2.07	1.97	1.82	2.21	1.87	1.65	1.68	1.62	1.75				
P ₂ O ₅	0.47	0.45	0.38	0.38	0.45	0.44	0.4	0.39	0.38	0.45	0.37	0.42	0.46				
H ₂ O	0.31	0.52	0.34	0.17	0.28	0.33	0.77	0.66	0.79	0.48	0.43	0.73	0.60				
Sc			33.2	32.2	30						35.9						
V	258		269	280	264	264	270	249	247		287	278	259				
Cr	90	49	76	62	49	55	116	132	98	38	54	51	36				
Co			35	32	33	31	34	31	32		36.6	34	33				
Ni	44	35	35	36	41	34	51	49	44	37	46	46	37				
Rb	63	67	78	82	66	65	62	73	63		66	52	55				
Sr	682	707	753	757	734	708	742	756	728	720	748	701	721				
Y			24	28	27	25	24	25	24		27	26	25				
Zr	175		174	161	152	153	148	164	146		142	132	141				
Nb		25	20	21	19	18	18	20	18	18	19	16	15				
Cs				4.9	4.2	4.6	5.5	4.4			3.7	3.5					
Ba	938		971	998	956	912	901	982	954		818	816	848				
La			50	50	45	44	45	47	49		42	39	42				
Ce		98	97	91	89	88	92	96			87	81	84				
Pr				10.8	10.8	10.5	10.6	11.3			9.8	9.9					
Nd		38	39	42	43	40	42	42			34	39	39				
Sm		9.4	9.0	8.1	8.5	7.5	8.2	8.5			8.2	7.8	7.9				
Eu		2.26	2.22	2.0	2.2	2.0	2.1	2.2			2.10	2.0	2.2				
Gd				7.0	6.7	6.3	6.3	6.2			6.7	6.4					
Tb		1.10	0.95	0.98	0.93	0.84	0.84	0.90			0.93	0.95	0.92				
Dy				5.30	4.94	4.56	4.63	4.72				4.90	4.88				
Ho				0.98	0.97	0.87	0.83	0.88				0.92	0.88				
Er				2.65	2.25	2.19	2.24	2.45				2.44	2.21				
Tm				0.38	0.35	0.32	0.34	0.31				0.36	0.3				
Yb		2.8	2.4	2.26	2.28	2.11	2.07	2.36			2.4	2.10	2.19				
Lu		0.46	0.5	0.33	0.34	0.29	0.31	0.35			0.48	0.31	0.31				
Hf		3.7	3.7	3.6	3.7	3.1	3.4	3.5			3.2	3.2	3.2				
Ta		1.7	1.5	1.09	1.20	1.07	1.22	1.22			1.14	0.90	1.03				
Pb		27	23	17	17	16	18	18			20	14	14				
Th	9	17	17	14.4	14.3	15.6	18.2	15.0	7	13	11.4	11.9					
U				3.70	3.78	3.45	4.13	3.91				2.88	2.96				
⁸⁷ Sr/ ⁸⁶ Sr	0.706248		0.706162	0.706165	0.706160						0.706105	0.706107					
¹⁴³ Nd/ ¹⁴⁴ Nd			0.512556	0.512551							0.512570	0.512564					

(Hist) historical activity from (a) Métrich *et al.* [2001]; (b) Hornig-Kjarsgaard *et al.* [1993]; (e) Bonaccorso *et al.* [1996]; (f) Francalanci *et al.* [2004]; (g) Landi *et al.* [2004]; (h) Bertagnini *et al.* [2003]. (*) isotopic compositions from Francalanci *et al.* [2004].

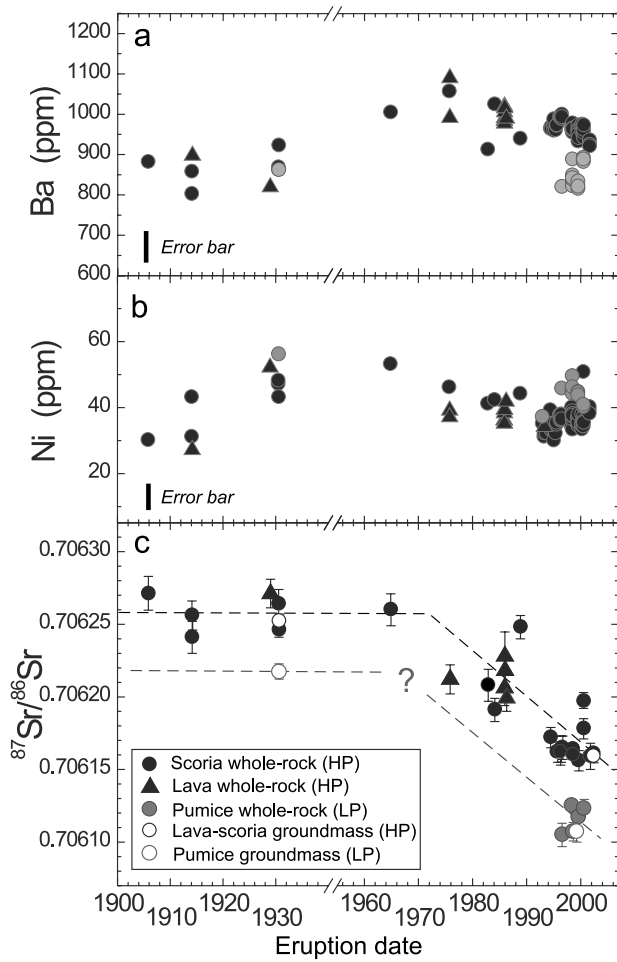


Figure 5. Compositional variations with time for the products erupted in the period 1906–2002. (a) and (b) Ni and Ba variations reported as representative of compatible and incompatible trace elements, respectively. Error bars are generally referred to errors of ~5% for Ba and ~10% for Ni calculated at the average composition of the studied rocks [data from *Francalanci et al.*, 2004 with reference therein and unpublished]; (c) Sr isotope ratio variations with reported 2σ errors [data from *Francalanci et al.*, 1999, 2004, 2005] HP and LP indicate highly porphyritic and low porphyritic products, respectively.

ing, dissolution surfaces, successive reequilibration events and growth rims of variable thickness (Figures 6a and 6b). Similar features are also observed in clinopyroxene. Crystals that record extensive disequilibria dominate in pumice erupted during small-scale paroxysms as what occurred in August 1998 and 1999 [*Métrich et al.*, 2001; *Bertagnini et al.*, 2003].

Actually, the mineral paragenesis of pumice consists in small (<1 mm) and scarce (<5 vol %) diopside (Fs_{8-5} , Wo_{48-45})

and skeletal or euhedral homogeneous olivine (Fo_{82} to Fo_{87}), with numerous irregular melt inclusions (Figure 6c). Skeletal Ca-rich plagioclase (An_{80-92}) is frequently found as reaction and growth rims surrounding xenocrystic relicts and results from the final stages of crystallization. In addition, pumices of the large-scale paroxysms systematically contain MgO-rich olivine (Fo_{88-91}) as homogeneous, normally or reversely zoned, skeletal or composite crystals (Figure 6d). Their composition and association with Cr-spinel (Cr # 64–67, Mg # 59–67) testify to their derivation from more primitive melts. Systematic chemical profiles in reversely zoned olivine crystals indicate variable times of crystal–magma interaction that is of the order of a few hours to weeks before the eruption [*Bertagnini et al.*, 2003].

The pumice samples display bulk rock compositions quite similar to those of scoriae and lavas erupted in the same period, with only slightly lower incompatible and higher compatible element contents (Table 1, Figures 5a and 5b). In contrast, the pumice matrix glasses are HK/SHO-basalts with distinctive less evolved compositions than those of the HP scoria and lavas [*Métrich et al.*, 2001; *Francalanci et al.*, 2004].

Although the LP pumices emitted in the 20th century have major and trace element contents similar to those of the coeval HP scoria, they show significantly lower Sr isotope ratios than scoriae. In addition, a significant variation of Sr isotope ratios has been also found in LP pumices. More, specifically, the LP pumices emitted in 1930 have $^{87}\text{Sr}/^{86}\text{Sr}$ values higher than the younger pumices (since 1984 onward). These data suggest a variation with time similar to that of HP magmas (Figure 5c). The $^{143}\text{Nd}/^{144}\text{Nd}$ values of LP pumices erupted since 1996 do not significantly differ from those of coeval HP magmas, showing only slightly higher values (0.51256–0.51257) [*Francalanci et al.*, 1999, 2004, 2005].

4. CONTRIBUTIONS FROM MICROANALYTICAL Sr ISOTOPE DATA

Detailed microanalytical Sr isotope analyses were performed by microdrilling techniques on largely zoned plagioclase and clinopyroxene and groundmasses on four samples (an HP scoria erupted in 1984, a lava sample of the 1985–1986 event, HP scoria and LP pumice of the 1996 small-scale paroxysm) [*Francalanci et al.*, 2005].

Large and comparable Sr isotope variations have been detected in plagioclase and clinopyroxene. The resorbed cores of crystals from HP magmas show high $^{87}\text{Sr}/^{86}\text{Sr}$ (0.70635–0.70630) or low $^{87}\text{Sr}/^{86}\text{Sr}$ (0.70614–0.70608), with the latter values similar to the values of the outer cores. Mineral rims and glassy groundmasses generally have intermediate $^{87}\text{Sr}/^{86}\text{Sr}$ (0.70628–0.70613; Figure 7). Three groups of $^{87}\text{Sr}/^{86}\text{Sr}$

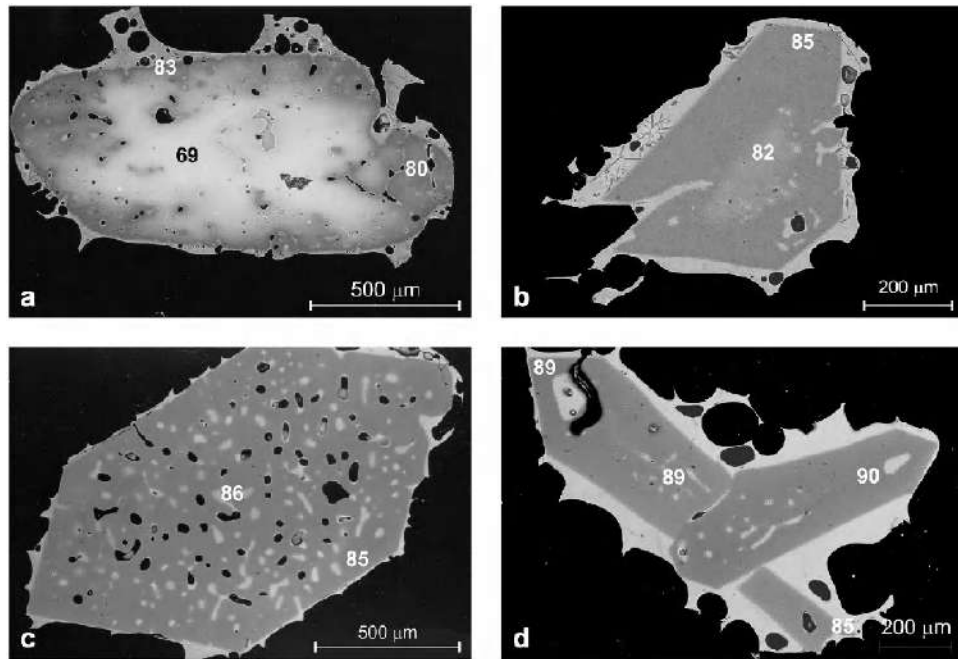


Figure 6. Back-scattered electron micrographs of olivines from LP pumice. (a) Fe-rich resorbed core surrounded by a heterogeneous mottled zone rich in MI (large-scale historical paroxysm, St79 sample); (b) reverse zoned crystal with a large and homogeneous growth rim and skeletal shape (small-scale paroxysm of 23 August 1998, St130 sample); (c) homogeneous euhedral olivine showing high density of irregular elongated melt inclusions (large-scale historical paroxysm, St82 sample); (d) skeletal crystals of Mg-rich olivine (large-scale historical paroxysm, St82 sample).

values also characterize the mineral growth zones from the LP magmas, but the lowest values are present in the mineral rims and groundmass glass. In minerals of scoria/pumice pair from 1996 paroxysm, the low Sr-isotope values are comparable, and in HP magmas, Sr isotope ratios increase toward the external zones of phenocrysts (with the intermediate isotope values) starting from the lowest $^{87}\text{Sr}/^{86}\text{Sr}$ ratios of cores and/or outer cores. Furthermore, the crystal zones with the lowest and intermediate Sr isotope ratios have the main compositions typical of minerals in equilibrium with LP magmas and HP magmas, respectively (Figure 7). This clearly indicates that the external zones of plagioclase and clinopyroxene from scoria and lavas crystallized concurrently with, or after, mingling/mixing between the LP and HP magmas.

Finally, the usually resorbed, mineral cores with high $^{87}\text{Sr}/^{86}\text{Sr}$ values have been considered to represent a third component in the plumbing system, such as a cumulus crystal-mush zone, situated just below the shallow magma reservoir and associated with the more Sr-radiogenic feeding system of the preceding volcanic activity. It is proposed that the cumulus phases are incorporated by the LP magma ascending

from depth and transported into the shallow reservoir [Francalanci *et al.*, 2005].

The micro-Sr isotope data have also suggested a rapid decrease of $^{87}\text{Sr}/^{86}\text{Sr}$ in the replenishing LP magma before the eruption of the 1985 lava flow, associated with an increased volume of LP magma into the shallow magma reservoir [Francalanci *et al.*, 2005].

5. CONTRIBUTIONS FROM MELT INCLUSIONS

5.1. Textural Aspects

Specific attention has been paid to olivine-hosted melt inclusions from scoria and pumice that show a large spectrum in morphology and composition. As a result, a large chemical data set on melt inclusions and their host crystals was published in Métrich *et al.* [2001] and Bertagnini *et al.* [2003]. Melt inclusions in clinopyroxene are often crystallized, and only a few major element compositions have been published [Clocchiatti, 1981]. Rapid growth of plagioclase and its recurrent dissolution prevent reliable analysis of their entrapped glasses [Landi *et al.*, 2004].

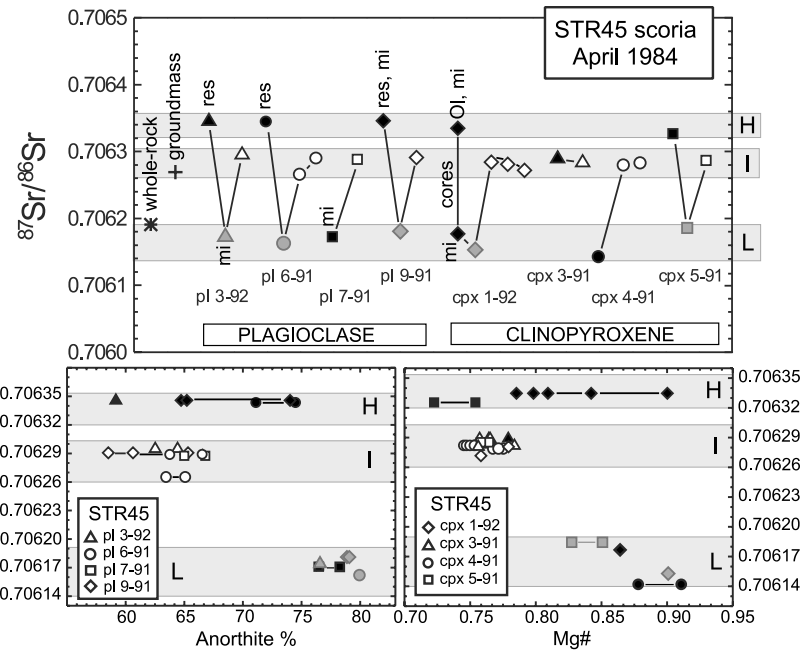


Figure 7. Sr isotope data of HP scoria (erupted by normal Strombolian activity on 28 April 1984) measured in whole-rock, glassy groundmass and core-rim traverses of plagioclase and clinopyroxene. Each mineral is reported with a different symbol. From left to right of each mineral of the above diagram: from core (filled symbol), to outer core (grey symbol), up to outer rim (open symbol). The two diagrams below show that the high Sr-radiogenic crystal zones (H) have variable composition, the low Sr-radiogenic crystal zones (L) always have high anorthite contents or magnesium number [Mg # = Mg/(Mg + Fe²⁺)], whereas the zones with intermediate Sr isotope ratios (I) usually have intermediate anorthite contents or Mg #. Res, resorbed; mi, melt inclusions. The 2 σ error corresponds with the symbol size. Modified after Francalanci *et al.* [2005].

Scoriae of normal Strombolian activity contain euhedral Fe-rich olivine with melt inclusions that are regularly distributed along the crystal growth boundaries. Melt inclusions rarely exceed 25–30 μm in size. They contain at most one shrinkage bubble; few of them contain tiny, Cu–Fe sulfide globules.

The large-scale historical paroxysms bring to surface a range of olivine crystals and melt inclusions whose morphology indicates successive dissolution–crystallization events, multistage crystallization, dynamic mixing upon magma ascent [Bertagnini *et al.*, 2003]. One can observe morphological evolution from typical isolated, two-phase inclusions in the Mg-rich olivines (Fo_{88-90}) toward irregular elongated and interconnected melt inclusions in more Fe-rich olivine (Fo_{82-87} ; Figure 6c). The high density of trapped glass, without any preferential orientation, together with variable proportions between bubble and glass often attest to very rapid growth rates of the host from a heterogeneous gas–melt mixture.

5.2. Major Element and Volatile Compositions and Optical Thermometry

Melt inclusions and matrix glasses define a compositional trend that is far wider than that of the whole rocks (Figures 8a and 8b). More specifically, in scoriae, olivine-hosted melt inclusions are evolved ($\text{CaO}/\text{Al}_2\text{O}_3 = 0.6–0.4$) and are closely comparable in composition to the shoshonitic matrix glass. Their decreasing $\text{K}_2\text{O}/\text{Na}_2\text{O}$ ratio and Al_2O_3 content testify to plagioclase crystallization in accordance with their low water content. Melt inclusions in olivine (Fo_{71-73}) contain 0.05–0.6 wt % H_2O [Métrich *et al.*, 2001] although water loss through olivine network cannot be totally excluded. As a whole, the volatile content in melt inclusions from scoriae is low ($\text{CO}_2 < 100$ ppm; $\text{dl} > \text{S} < 1300$ ppm; $\text{Cl} = 1000–2600$ ppm), except fluorine (1000–1300 ppm; Métrich *et al.* [2001]). Finally, the temperature of crystallization of the HP magma was determined at $1115 \pm 10^\circ\text{C}$ from optical thermometry measurements in melt inclusions

in clinopyroxene and olivine [Clocchiatti, 1981; Métrich *et al.*, 2001].

In pumice, olivine-hosted melt inclusions recorded a compositional range extending from HK-basalt akin to those of pumice bulk rocks and glassy matrices to Ca-rich compositions (Figure 8a; Table 2). The latter, recorded as melt in-

clusions in Fo_{88-90} that are entrained during the large-scale paroxysms, are regarded as representative of the possible parental melts ($\text{CaO}/\text{Al}_2\text{O}_3 \sim 1$) of the magma batches ($\text{CaO}/\text{Al}_2\text{O}_3 \sim 0.65$) feeding the present activity. They have slightly variable K_2O content. Accordingly, the bulk pumice compositions were explained by the removal of nearly 24% solid, made up of clinopyroxene and minor olivine, from the parental Ca-rich melt(s) [Bertagnini *et al.*, 2003]. The temperature of crystallization of the Stromboli LP magma ranges from 1200° to $1135 \pm 10^\circ\text{C}$ as estimated using MELTS code [Bertagnini *et al.*, 2003] and microthermometry measurements on melt inclusions [Métrich *et al.*, 2001], respectively.

Melts trapped in heterogeneous olivine that recorded dissolution–crystallization events were systematically identified, but never considered as representative of the magma system and never reported in diagrams showing the typical trend of magma evolution at Stromboli. This type of melt inclusion and olivine dominates (>95% of crystals from the 0.5- to 1-mm grain-size fractions; regardless of crystals entrained from the HP magma) in pumice produced by small-scale paroxysms (e.g., eruptions of August 1998 and August 1999).

Melt inclusions in olivine Fo_{82-90} yield high volatile content (in wt %: $\text{H}_2\text{O} = 1.8\text{--}3.4$, $\text{CO}_2 = 890\text{--}1890$ ppm, $\text{S} = 1660\text{--}2250$ ppm, $\text{Cl} = 1660\text{--}2030$ ppm; $\text{F} = 640\text{--}680$ ppm; Métrich *et al.* [2001] and Bertagnini *et al.* [2003]) (Table 3). Prior to significant degassing, basaltic magma(s) at Stromboli are characterized by a S/Cl ratio of 1.1 ± 0.1 (Figure 8c) and a F/Cl ratio of between 2.5 ± 0.2 on average. The high water content in pumice-forming melts inhibits plagioclase crystallization in agreement with experimental phase equilibria [Di Carlo *et al.*, 2006]. Plagioclases often observed in pumice are inherited from the HP magma and/or have

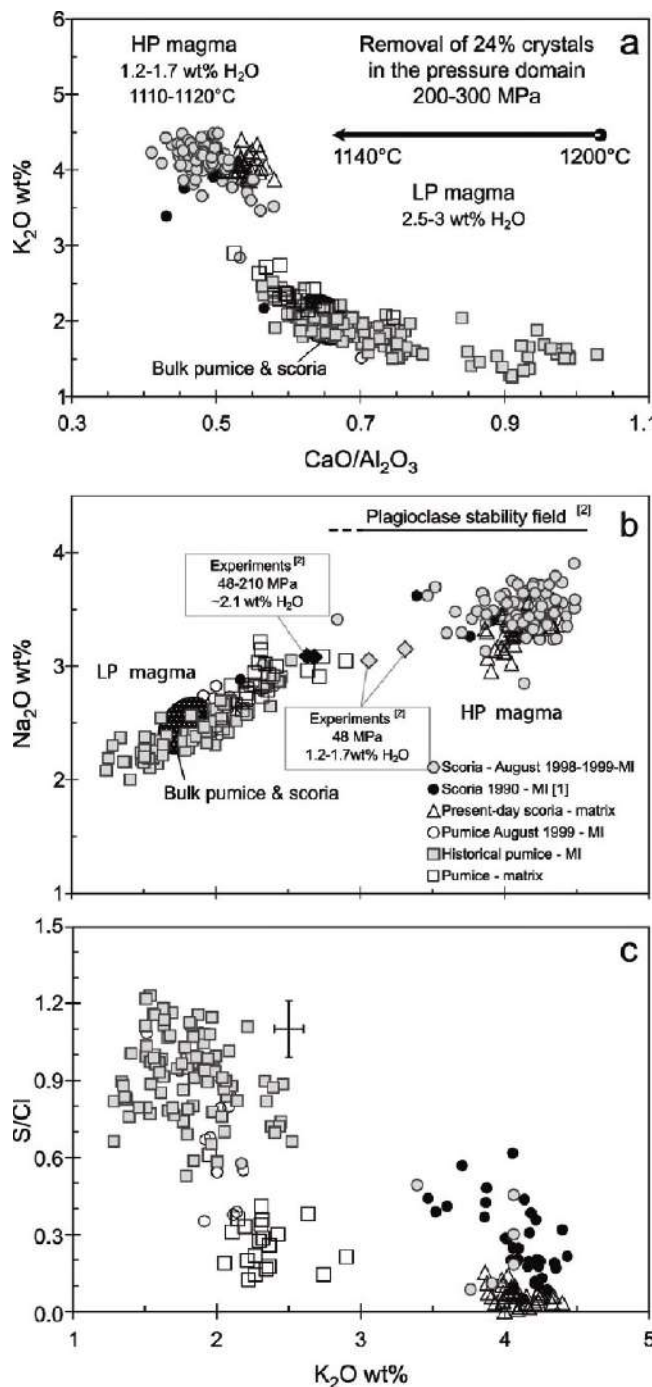


Figure 8. (Opposite) (a) Synthetic diagram [modified from Bertagnini *et al.*, 2003] showing the evolution of $\text{CaO}/\text{Al}_2\text{O}_3$ versus K_2O , with pressure and temperature of olivine-hosted melt inclusions and of matrix glasses in pumices (samples ST81, 82, 79, 207) emitted during large-scale historical paroxysms and of pumices and scoriae produced during the 1998–1999 small-scale paroxysms. The compositions of the whole rocks (scoria and pumice) and of experimental melts are reported for comparison (see text for details). The temperatures of crystallization are either determined by microthermometry on melt inclusions [Métrich *et al.*, 2001] or calculated using MELTS code [Ghiorso and Sack, 1995]. The pressures are derived from the H_2O and CO_2 dissolved content of melt inclusions using Volatilecalc (see text); (b) variation of K_2O versus Na_2O and (c) evolution of the S/Cl ratio versus K_2O in olivine-hosted melt inclusions and matrix glasses of Stromboli pumice and scoria. [1] and [2] are from Allard *et al.* [1994] and Di Carlo *et al.* [2006], respectively.

Table 2. Selected Analyses of Melt Inclusions in Olivine of Pumice and Scoria

Sample Inclusion No. of analysis	St81 ^a Ol 11 Mean (20)	St207 ^a Ol a5 MI 1 (3)	St82p ^b Ol 11 Mean (14)	St79p ^b Ol n30 Mean (12)	St81 ^a Oln10 Mean (12)	St81 ^a Ol 8 MI 1 (3)	St82p ^b Ol n50 MI a (3)	St79s ^b Ol n14 MI a,b,c (4)	St82s ^b Ol n2 MI 2 (2)	St133s ^b Ol 10 MI 2 (2)
SiO ₂ (wt%)	47.66	47.74	47.73	47.31	48.47	48.33	49.29	49.36	52.85	51.47
TiO ₂	0.89	0.91	0.83	0.86	0.82	0.83	0.87	0.83	1.45	1.48
Al ₂ O ₃	14.23	14.92	15.64	14.84	15.88	16.60	15.54	16.92	15.16	15.17
FeO _{tot}	7.28	6.19	7.71	6.73	7.22	7.63	8.53	7.42	9.60	11.25
MnO	0.12	0.11	0.14	0.12	0.08	0.23	0.18	0.12	0.18	0.28
MgO	7.64	6.51	7.30	6.89	6.60	6.67	6.03	4.79	3.43	3.92
CaO	14.05	13.84	12.18	14.36	11.48	11.25	10.02	10.01	6.91	6.82
Na ₂ O	2.27	2.16	2.24	2.28	2.35	2.57	2.44	2.86	3.53	3.40
K ₂ O	1.58	1.36	1.58	1.61	1.88	1.82	1.97	2.44	3.84	4.10
P ₂ O ₅	0.54	0.54	0.54	0.54	0.50	0.52	0.59	0.59	0.76	1.06
S	0.235	0.150	0.162	0.225	0.175	0.168	0.121	0.129	0.074	0.069
Cl	0.198	0.180	0.169	0.203	0.173	0.174	0.155	0.175	0.226	0.180
Total	96.43	94.34	96.10	95.72	95.63	96.79	95.74	95.64	98.00	98.52
Olivine Fo mol%	88.4	88.7	87.5	88.0	87.0	86.5	83.7	82.3	72.7	72.0
% PEC	0.08	0.05	0.03	0.06	0.07	0.05	0.04	0.07	0.01	0.02
CaO/Al ₂ O ₃	0.98	0.93	0.78	0.97	0.72	0.68	0.64	0.59	0.46	0.52
K ₂ O/Na ₂ O	0.70	0.63	0.70	0.71	0.80	0.71	0.81	0.85	1.09	1.18
S/Cl	1.18	0.83	0.96	1.11	1.02	0.96	0.77	0.74	0.33	0.35

Major and volatile elements are corrected for olivine postentrainment crystallization (% PEC). Fo mol% = [100 × Mg/(Fe + Mg)]. ^a From Bertagnini et al. [2003]. Analytical techniques in Métrich et al. [2001]. ^b From Métrich et al. [2001].

crystallized in response to late water degassing at time of eruption.

The dissolved H₂O and CO₂ contents of melt inclusions were used to assess the total fluid ($P_{\text{CO}_2} + P_{\text{H}_2\text{O}}$) pressures us-

ing the model of Papale [1999] and Volatilecalc code [Newman and Lowenstern 2002]. The models resulted in different pressure estimates because of the paucity of experimental data of CO₂ solubility in water-rich basalts, as discussed

Table 3. Water and Carbon Concentrations in Selected Melt Inclusions in Olivine of Pumice

Sample	Fo, ^a mol%	K ₂ O, ^b wt%	S, ^b wt%	Cl, ^b wt%	CaO/Al ₂ O ₃	H ₂ O, ^b wt%	CO ₂ , ^b ppm
St81^c							
Oln12-MI1	84.4	1.79	0.169	0.171	0.71	2.0	799
Oln8-MI1	86.1	1.83	0.165	0.167	0.64	2.7	1098
Oln8-MI2	86.3	1.92	0.166	0.170	0.69	2.1	1887
Oln10-MI2	86.7	1.78	0.180	0.175	0.75	2.3	792
Oln10-MI3	86.6	1.82	0.197	0.176	0.76	2.7	1204
Oln10-MI1	86.9	1.84	0.183	0.171	0.73	2.6	1003
Oln10-MI7	87.1	1.94	0.174	0.176	0.73	2.6	762
Oln10-MI6	85.9	1.86	0.170	0.172	0.70	2.5	1008
Oln14-MI1	83.5	2.05	0.148	0.168	0.61	3.2	1117
Oln14-MI2	83.2	2.10	0.152	0.173	0.60	2.8	867
Oln14-MI3	83.7	2.07	0.142	0.170	0.60	2.4	716
St79p^d							
Oln30	88.0	1.61	0.225	0.203	0.97	2.3	1107
St82p^d							
Oln52a	84.6	1.73	0.170	0.179	0.73	2.7	1087
Oln50	83.7	1.97	0.121	0.155	0.64	2.7	894

^a Fo is the host olivine composition as [100 × Mg/(Mg + Fe)]. ^b Concentrations corrected for the post-entrainment crystallisation of olivine.

^c From Bertagnini et al. [2003]. ^d From Métrich et al. [2001].

in *Bertagnini et al.* [2003]. In order to take into account the influence of magma composition and dissolved water amount on the CO₂ solubility [Botcharnikov *et al.*, 2005], the best pressure estimates were calculated by Volatilecalc program whose SiO₂ contents are derived from the Π coefficient defined by Dixon [1997] to be 48 wt %. Hence, the olivine-hosted melt inclusions from large-scale paroxysms were trapped at a total fluid pressure of between 200 and 300 MPa [Métrich *et al.*, 2005]. A similar conclusion was reached more recently by *Di Carlo et al.* [2006]. This lithostatic pressure would correspond to a depth of 7.5–11 km assuming an average rock density of Stromboli basement of 2700 kg m⁻³.

6. CONSTRAINTS ON THE FEEDING SYSTEM AND DYNAMICS OF THE PRESENT-DAY ACTIVITY

Since its beginning, about 1500 years ago, the persistent activity at Stromboli has been dominated by the interplay between magmas having contrasting density and viscosity: the shallow, crystal-rich, partially degassed magma (HP magma) and the nearly aphyric, volatile-rich, ascending, magma batches of deeper derivation (LP magma). Textural, mineralogical, geochemical, and isotopic data of the emitted products were combined with detailed microanalyses of melt inclusions and minerals to provide a reference data set on the magma-dissolved volatile contents, the path and pressure (depth) of magma crystallization, and its dynamics of ascent.

One of the most outstanding characteristics of the Stromboli magmas is the closely comparable basaltic composition of the scoria/pumice pairs, in spite of a marked difference in their crystal and volatile contents that makes Stromboli a classic example of crystallization driven by water loss [Métrich *et al.*, 2001]. However, slight chemical differences between scoria and pumice were attributed to crystal fractionation [Landi *et al.*, 2004]. The magma batches (occasionally erupted as pumice) have a high initial water content (2.5–3.0 wt %), regardless of the paroxysm scale or its age [Métrich *et al.*, 2001; Bertagnini *et al.*, 2003]. Actually, their dissolved water content remains high enough to prevent plagioclase crystallization, except at the ultimate stage(s) of their transfer to the surface when the water loss associated with the lower pressure, drives the melt composition toward the stability field of plagioclase. In contrast, plagioclase is the dominant mineral phase of the shallow degassed magma where it crystallizes in equilibrium with clinopyroxene and olivine, in melts having water content ≤1.2–1.7 wt % [Landi *et al.*, 2004; *Di Carlo et al.*, 2006].

Minerals in scoria record strong chemical, isotopic, and textural heterogeneity at the micrometer scale. These recur-

rent disequilibria provide evidence of repeated and discrete arrivals of water-rich, less radiogenic ⁸⁷Sr/⁸⁶Sr melts in the shallow system promoting efficient and dynamic water degassing, magma crystallization, and magma mixing [Francalanci *et al.*, 1999, 2004, 2005; Métrich *et al.*, 2001; Landi *et al.*, 2004]. In contrast, their chemistry and crystal size distribution suggest that the shallow crystal-rich body operates as a steady-state system close to the kinetic equilibrium [Armienti *et al.*, 2007]. All these features are reconciled when considering convective motions at different scales in space and time promoting interactions and mixing between magmas initially containing variable volatile contents and isotopic ratios [Francalanci *et al.*, 1999; Landi *et al.*, 2004]. Such ideas are fully consistent with previous findings of convection associated with intrusive degassing, degassed magma sinking [Allard *et al.*, 1994, Harris and Stevenson, 1997; Allard *et al.*, this volume], and differential transfer of gas bubble and slug rise through the crystal-rich shallow body [Burton *et al.*, 2007a, 2007b].

The refilling magma batches ultimately derive from their volatile-rich parental melt(s), via crystal fractionation, at a lithostatic pressure of 200–300 MPa as what were derived from the H₂O and CO₂ dissolved content of melt inclusions [Métrich *et al.*, 2001; Bertagnini *et al.*, 2003]. The volume of the crystal-mush associated with deep fractional crystallization processes over the last 1500 years was assessed on the order of 3.5–7 km³ [Bertagnini *et al.*, 2003]. According to these authors, the magma ponding zone is located at ~7.5–11 km depth. In this model, the chemical evolution of magma is driven by crystal fractionation in this range of lithostatic depths, whereas crystallization driven by water loss prevails in the shallow reservoir that sustains normal Strombolian activity. Such processes clearly involve mixing between magmas having similar major and trace element bulk composition but different temperature, volatile content, and Sr-isotopic ratios. Actually, the dynamics of water loss and crystallization accounts for the absence of a transition between the crystal-poor and the crystal-rich magma. The evidence of their interaction only survives in mineral zoning and their Sr isotopic ratios.

A model of a polybaric multireservoir plumbing system at Stromboli has been proposed by Francalanci *et al.* [1999, 2004, 2005] and Vaggelli *et al.* [2003] on the basis of extensive results on trace elements and in situ Sr-isotope measurements in crystals and bulk rocks of the 1906–1998 period. It consists of (1) a LP magma reservoir at ~10 km depth, periodically replenished by a mafic magma with relatively low Sr isotope ratios (0.70608) that agrees with the magma ponding zone at ~7.5–11 km depth proposed by Bertagnini *et al.* [2003], (2) an intermediate reservoir at ~3 km depth, which could be a remnant of the old Stromboli struc-

ture according to *Vaggelli et al.* [2003], where LP and HP magmas mix together and continuously crystallize olivine, pyroxene, and plagioclase, (3) an intermediate older crystal-mush body where plagioclase and pyroxene record highly variable and high Sr-isotope signature of the previous magmas, and (4) the uppermost part of the system deduced from the seismic data [*Chouet et al.*, 2003]. During the periodic magma recharge events, LP magma passes through the cumulus reservoir sampling minerals and transporting them into the shallower reservoir. The overall decrease of Sr isotope ratios with time in the HP magmas (1980–1985) was due to the nearly coeval decrease of $^{87}\text{Sr}/^{86}\text{Sr}$ values in the replenishing LP magmas. This isotopic time variation in the HP magmas (Figure 5c) was used to calculate a short residence time ($\approx 19 \pm 12$ years) at intermediate level (above reservoir 2) for the magma feeding present-day activity, although this model does not take into account the presence of many xenocrysts having widely variable Sr isotopic ratios [*Francalanci et al.*, 1999, 2004, 2005]. A lower resident time (<520 d) for the HP magmas was calculated by *Gauthier and Condomines* [1999], on the basis of $^{210}\text{Pb}/^{226}\text{Ra}$ activity ratios, linked to the degassing process in the very shallow magma body (above reservoir 4). The different calculated residence time probably are referred to the different depths of magma rest.

Finally, we show that the large (1930-type eruption) and small-scale (August 1998-type eruption) paroxysmal eruptions can be discriminated on the basis of their mineralogy [*Métrich et al.*, 2001; *Bertagnini et al.*, 2003]. Besides their widespread deposits, the large paroxysms reveal the deep input(s) of volatile-rich, primitive magma batches, weeks or days before the eruption which are identifiable by the presence of high pressure olivine and clinopyroxene (with high Mg/Fe ratios) in the resulting pumices. In contrast, pumices issued from small-scale paroxysms do not have such minerals. They carry xenocrysts showing successive dissolution-crystallization characteristics, whereas crystals in equilibrium with their carrier magma are rare [*Bertagnini et al.*, 2003]. Hence, it has been proposed that the large-scale paroxysms of Stromboli are generated by the rapid uprise, from 7.5 to 11 km, of a fast-moving blob of low-density magmatic foam with no gas/liquid decoupling during its ascent [*Métrich et al.*, 2001; *Bertagnini et al.*, 2003]. The respective role of magma and gas in triggering the paroxysmal eruptions was recently questioned by Allard [2004, 2007] who proposed catastrophic uprise of CO₂-rich gas pockets generated by intermittent gas accumulation in the subvolcanic plumbing system. Accordingly, gas bubbles would be able to carry up primitive melts and crystals in their envelope and bring them rapidly to surface. Whether or not there is gas-accumulation in the plumbing system at a depth of

7.5–11 km is still under debate. The paroxysmal eruption that occurred on April 5, 2003 brought additional data and constraints on the eruption-triggering mechanism.

Acknowledgments. The critical revisions by M.A. Menzies and an anonymous reviewer are greatly acknowledged. Special thanks to P. Pantani for graphic assistance, O. Belhadj for her help in sample preparation, M. Ulivi for helping with isotope analyses in Firenze, and our colleagues for fruitful discussions: A. Aiuppa, P. Allard, M. Burton, P. Papale, M. Pichavant, and B. Scaillet.

REFERENCES

- Abbruzzese, D. (1937), Attività dello Stromboli dal 1934 al 1936, *Boll. Vulcanol.*, 2, 70–76.
- Abbruzzese, D., and C. Cavallaro (1956), L’eruzione sottomarina dello Stromboli del 28 febbraio 1955, *Riv. Stromboli*, 4, 25–29.
- Allard, P. (2004), Stromboli, an erupting system powered by steady and catastrophic gas transfer. *INGV workshop: ‘L’eruzione di Stromboli (28 Dicembre 2002–20 Luglio 2003)*, 21–24 May 2004, Catania, Italy, Abstract, p. 7.
- Allard, P. (2007), A CO₂-rich gas trigger of explosive paroxysms at Stromboli volcano (Italy). EGU General Assembly, *Geophys. Res. Abstr.*, 9, EGU2007-A-08044.
- Allard, P., J. Carbonnelle, N. Métrich, H. Loyer, and P. Zettwoog (1994), Sulphur output and magma degassing budget of Stromboli volcano, *Nature*, 368, 326–330.
- Armenti, P., L. Francalanci, and P. Landi, (2007), Textural effects of steady state behaviour of the Stromboli feeding system, *J. Volcanol. Geotherm. Res.*, 160, 86–98.
- Arrighi, S., M. Rosi, J.-C. Tanguy, and V. Courtillot (2004), Recent eruptive history of Stromboli (Aeolian Islands, Italy) determined from high-accuracy archeomagnetic dating, *Geophys. Res. Lett.*, 31, L19603, doi:10.1029/2004GL020627.
- Barberi, F., M. Rosi, and A. Sodi (1993), Volcanic hazard assessment at Stromboli based on review of historical data, *Acta Vulcanol.*, 3, 173–187.
- Bertagnini, A., M. Coltellini, P. Landi, M. Pompilio, and M. Rosi (1999), Violent explosions yield new insights into dynamics of Stromboli volcano, *Eos Trans. AGU*, 80(52), 633–636.
- Bertagnini A., N. Métrich, P. Landi, and M. Rosi (2003), Stromboli volcano (Aeolian Archipelago, Italy): An open window on the deep-feeding system of a steady state basaltic volcano, *J. Geophys. Res.*, 108(B7), 2336, doi:10.1029/2002JB002146.
- Bonaccorso, A., C. Cardaci, M. Coltellini, P. Del Carlo, S. Falsaperra, S. Panucci, M. Pompilio, and L. Villari (1996), Annual report of the world volcanic eruptions in 1993, Stromboli, *Suppl. Bull. Volc. Eruptions*, 35, 8–14.
- Botcharnikov, R., M. Freise, F. Holtz, and H. Berhens (2005), Solubility of C–O–H mixtures in natural melts: New experimental data and application range of recent models. *Ann. Geophys.*, 48(4–5), 633–646.
- Burton, M. R., P. Allard, F. Muré, and A. La Spina (2007a), Magmatic gas composition reveals the source depth of slug-driven Strombolian explosive activity, *Science*, 37, 227–230.

- Burton, M. R., H. M. Mader, and M. Polacci (2007b), The role of gas percolation in quiescent degassing of persistently active basaltic volcanoes, *Earth Planet. Sci. Lett.*, doi:10.1016/j.epsl.2007.08.028.
- Calvari, S., M. Pompilio, and D. Andronico (2002), Preliminary report on the eruptive activity occurred at Stromboli volcano on 23 January 2002, *INGV-CT report*, SrvSt20020124. <http://www.ct.ingv.it/>.
- Cavallaro, C. (1957), L'attivita' dello Stromboli dal 1940 al 1953. *Boll. Acc. Gioenia Sci. Nat. Catania Ser. IV, III, 10*, 526–531.
- Cavallaro, C. (1962), L'esplosione dello Stromboli dell'11 luglio 1959. *Riv. Stromboli*, 8, 11–14.
- Chouet, B., G. Saccorotti, P. Dawson, M. Martini, R. Scarpa, G. De Luca, G. Milana, and M. Cattaneo (1999), Broadband measurements of the sources of explosions at Stromboli Volcano, Italy. *Geophys. Res. Lett.*, 26, 1937–1940.
- Clocchiatti, R. (1981), La transition augite-diopside et les liquides silicates intra-cristallins dans les pyroclastes de l'activité actuelle du Stromboli: témoignages de la réinjection et du mélange magmatiques. *Bull. Volcanol.*, 44, 339–357.
- Coltellini, M., S. Falsaperla, P. Del Carlo, M. Pompilio, and A. Bonaccorso (1999), Volcanic, seismic, and ground deformation data concerning the Stromboli volcano in 1995, *Suppl. Bull. Volc. Eruptions*, 35, 8–14.
- Coltellini, M., P. Del Carlo, and M. Pompilio (2000), Vulcano and Stromboli 1. Eruptive activity (Stromboli). *Acta Vulcanol.*, 12(1–2), 93–95.
- De Fino, M., L. La Volpe, S. Falsaperla, G. Fazzetta, G. Neri, L. Francalanci, M. Rosi, and A. Sbrana (1988), The Stromboli eruption of December 6, 1985–April 25, 1986: Volcanological, petrological and seismological data, *Rend. Soc. Ital. Mineral. Petrol.*, 43, 1021–1038.
- De Fiore, O. (1915), I fenomeni eruttivi avvenuti allo Stromboli dal 1909 al 1914 ed il loro meccanismo, *Zeit. f. Vulk.*, 1, 225–246.
- De Fiore, O. (1923), I fenomeni eruttivi avvenuti allo Stromboli dal 1914 al 1916, *Boll. Soc. Sismol. Ital.*, 24, 9–66.
- Di Carlo, I., M. Pichavant, S. Rotolo, and B. Scaillet (2006), Experimental crystallization of a high-K arc basalt: The golden pumice, Stromboli Volcano (Italy), *J. Petrol.*, 1–27, doi:10.1093/petrology/egl011.
- Dixon, J. B. (1997), Degassing of alkalic basalts, *Am. Mineral.*, 82, 368–378.
- Francalanci, L., M. Barbieri, P. Manetti, A. Peccerillo, and L. Tolomeo (1988), Sr-isotopic systematics in volcanic rocks from the island of Stromboli (Aeolian arc), *Chem. Geol.*, 73, 164–180.
- Francalanci, L., P. Manetti, and A. Peccerillo (1989), Volcanological and magmatological evolution of Stromboli volcano (Aeolian islands): The roles of fractional crystallisation, magma mixing, crustal contamination and source heterogeneity, *Bull. Volcanol.*, 51, 355–378.
- Francalanci, L., S. Tommasini, S. Conticelli, and G. R. Davies (1999), Sr isotope evidence for short magma residence time for the 20th century activity at Stromboli volcano, Italy, *Earth Planet. Sci. Lett.*, 167, 61–69.
- Francalanci, L., S. Tommasini, and S. Conticelli (2004), The volcanic activity of Stromboli in the 1906–1998 period: Mineralogical, geochemical and isotope data relevant to the understanding of Strombolian activity, *J. Volcanol. Geotherm. Res.*, 131, 179–211.
- Francalanci, L., G. R. Davies, W. Lustenhouwer, S. Tommasini, P. R. D. Mason and S. Conticelli (2005), Old crystal re-cycle and multiple magma reservoirs in the plumbing system of the present day activity at Stromboli volcano, South Italy: Sr-isotope in situ microanalyses, *J. Petrol.*, 46, 1997–2021, doi:10.1093/petrology/egl045.
- Gauthier, P. J., and M. Condomines (1999), 210Pb/226Ra radioactive disequilibria in recent lavas and radon degassing: inferences on the magma chamber dynamics at Stromboli and Merapi volcanoes, *Earth Planet. Sci. Lett.*, 172, 111–126.
- Ghiorso, M. S., and R. O. Sack (1995), Chemical transfer in magmatic processes IV, *Contrib. Mineral. Petrol.*, 119, 197–212.
- Global Volcanism Program at <http://www.volcano.si.edu/>.
- Hornig-Kjarsgaard, I., J. Keller, U. Koberski, E. Stadlbauer, L. Francalanci, and R. Lenhart (1993), Geology, stratigraphy and volcanological evolution of the island of Stromboli, Aeolian arc, Italy. *Acta Vulcanol.*, 3, 21–68.
- Istituto Nazionale di Geofisica e Vulcanologia, sezione di Catania at <http://www.ct.ingv.it/>.
- Landi, P., N. Métrich, A. Bertagnini, and M. Rosi (2004), Dynamics of magma mixing and degassing recorded in plagioclase at Stromboli (Aeolian Archipelago, Italy), *Contrib. Mineral. Petrol.*, 147, 213–237.
- Landi, P., L. Francalanci, M. Pompilio, M. Rosi, R. A. Corsaro, C. M. Petrone, I. Nardini, and L. Miraglia (2006), The December 2002–July 2003 effusive event at Stromboli volcano, Italy: Insights into the shallow plumbing system by petrochemical studies, *J. Volcanol. Geotherm. Res.*, 155, 263–284.
- Lautze, N. C., and B. F. Houghton (2005), Physical mingling of magma and complex eruption dynamics in the shallow conduit at Stromboli volcano, Italy, *Geology*, 33, 425–428.
- Lautze, N. C., and B. F. Houghton (2007), Linking variable explosion style and magma textures during 2002 at Stromboli volcano, Italy, *Bull. Volcanol.*, 69, 445–460, doi:10.1007/s00445-006-0086-1.
- Maramai, A., L. Graziani, and S. Tinti (2005), Tsunamis in the Aeolian Islands (southern Italy): A review, *Mar. Geol.*, 215, 11–21.
- Mercalli, G. (1881), Natura delle eruzioni dello Stromboli ed in generale dell'attività sismo-vulcanica delle Isole Eolie, *Atti Soc. Ital. Sci. Nat.*, 24, 105–135.
- Mercalli, G. (1883), *Vulcani e fenomeni vulcanici in Italia*, 374, A. Forni, Sala Bolognese, Italy.
- Mercalli, G. (1884), Notizie sullo stato attuale dei Vulcani attivi italiani, *Atti Soc. Ital. Sci. Nat.*, 27, 184–199.
- Mercalli, G. (1907), *I Vulcani Attivi della Terra*, Hoepli, Milan, Italy.
- Métrich, N., A. Bertagnini, P. Landi, and M. Rosi (2001), Crystallisation driven by decompression and water loss at Stromboli volcano (Aeolian Islands), *J. Petrol.*, 42, 1471–1490.
- Métrich, N., A. Bertagnini, P. Landi, M. Rosi and O. Belhadj (2005) Triggering mechanism at the origin of paroxysms at Stromboli (Aeolian Archipelago, Italy): The 5 April 2003 eruption, *Geophys. Res. Lett.*, 32, L10305, doi:10.1029/2004GL022257.

- Nappi, G. (1976) L'eruzione dello Stromboli del novembre 1975, *Boll. Soc. Geol. It.*, 95, 1975, 991–1008.
- Newman, S., and J. B. Lowenstern (2002), VOLATILECALC: A silicate melt-H₂O-CO₂ solution model written in visual basic excel, *Comput. Geosci.*, 28, 597–604.
- Papale, P. (1999), Modelling of the solubility of two-component H₂O-CO₂ fluid in silicate liquids, *Am. Mineral.*, 84, 477–492.
- Patrick, M., A. J. L. Harris, M. Ripepe, J. Dehn, D. A. Rothery, and S. Calvari (2007), Strombolian explosive styles and source conditions: insights from thermal (FLIR) video, *Bull. Volcanol.*, 69, 769–784, doi:10.1007/s00445-006-0107-0.
- Peccerillo, A. and S. R. Taylor (1976), Geochemistry of Eocene calc-alkaline volcanic rocks from the Kastamonu area, Northern Turkey, *Contrib. Mineral. Petrol.*, 58, 63–81.
- Perret, F. A. (1916), The lava eruption of Stromboli summer–autumn, 1915, *Am. J. Sci.*, 42, 436–457.
- Petrone, C. M., F. Olmi, E. Braschi, and L. Francalanci (2006), Mineral chemistry profile: A valuable approach to unravel magma mixing processes in the recent volcanic activity of Stromboli, Italy, *Per. Min.*, 75(2–3), 277–292.
- Platania, G. (1910), I fenomeni eruttivi dello Stromboli nella primavera del 1907, *Ann. Uff. Cent. Meteor. Geodinam. It.*, 30, 1–27.
- Ponte, G. (1919), La catastrofica esplosione dello Stromboli, *R. Accad. Naz. Lincei*, 28, 89–94.
- Ponte, G. (1921), La formidabile esplosione dello Stromboli del 1916, *Mem. R. Com. Geol. It.*, 7, 1–34.
- Ponte, G. (1948), Attività straordinaria dello Stromboli, *Ann. Geofis.*, 1, 200–202.
- Riccò, A. (1917), Parossismo dello Stromboli del 1915, *Att. Accad. Naz. Lincei*, 25, 251–259.
- Riccò, A., and G. Mercalli (1892), Sopra il periodo eruttivo dello Stromboli cominciato il 24 giugno 1891, *Ann. Uff. Cent. Meteor. Geodinam. It.*, 11, 189–221.
- Rittmann, A. (1931), Der Ausbruch des Stromboli am 11 September 1930, *Zeits. Vulkanol.*, 14, 47–77.
- Rosi, M., A. Bertagnini, and P. Landi (2000), Onset of the persistent activity at Stromboli volcano (Italy), *Bull. Volcanol.*, 62, 294–300.
- Speranza, F., M. Pompilio, and L. Sagnotti (2004), Paleomagnetism of spatter lavas from Stromboli volcano (Aeolian Islands, Italy): Implications for the age of paroxysmal eruptions, *Geophys. Res. Lett.*, 31, L02607, doi:10.1029/2003GL018944.
- Speranza, F., M. Pompilio, F. D'Ajello Caracciolo, and L. Sagnotti (2008), Holocene eruptive history of the Stromboli volcano: Constraints from paleomagnetic dating, *J. Geophys. Res.*, 113, B09101, doi:10.1029/2007JB005139.
- Vaggelli, G., L. Francalanci, G. Ruggieri, and S. Testi (2003), Persistent polybaric rests of calc-alkaline magmas at Stromboli volcano, Italy: Pressure data from fluid inclusions in restitic quartzite nodules, *Bull. Volcanol.*, 65, 385–404.
- Washington, H. S. (1917), Persistence of vents at Stromboli and its bearing on volcanic mechanism, *Bull. Geol. Soc. Am.*, 28, 249–278.
-
- A. Bertagnini, P. Landi, and N. Métrich, Istituto Nazionale di Geofisica e Vulcanologia, Sezione di Pisa, Via della Faggiola 32, 56126 Pisa, Italy. (bertagnini@pi.ingv.it)
- S. Conticelli, L. Francalanci, and S. Tommasini, Dipartimento di Scienze della Terra, Università degli Studi di Firenze, Via La Pira 4, 50121 Firenze, Italy.
- N. Métrich, Laboratoire Pierre Sue, CNRS-CEA, CE-Saclay, 91191 Gif/Yvette, Italy.

Dynamics of Strombolian Activity

Maurizio Ripepe and Dario Delle Donne

Dipartimento Scienze della Terra, Università di Firenze, Firenze, Italy

Andrew Harris

HIGP/SOEST, University of Hawai'i, Honolulu, Hawaii, USA

Emanuele Marchetti and Giacomo Olivieri

Dipartimento Scienze della Terra, Università di Firenze, Firenze, Italy

The persistent mild explosive activity of Stromboli is explained in terms of the dynamics of large gas slugs that ascend the magma conduit to burst at the free surface. This simple physical model has now strong evidence from both geophysical and geochemical viewpoints. In recent years, combined analyses of geophysical data, such as infrasound and thermal, integrated with seismological information, have improved constraint on conduit dynamics. We now know that gas expansion, preceding the explosion onset by 2 to 20 s, occurs at a depth of ~260 m within the conduit. Explosions repeat at a typical rate of ~13 events/h with gas jet velocities of 10–130 m/s. The time delay between the infrasound and thermal onset indicates a depth of <120 m below the vent. Infrasonic pressure and thermal transient amplitudes increases as the time delay of their onsets increases. We show how coupled fluctuations in these parameters are compatible with the migration of the magma column in response to increased gas flux. Infrasound and thermal data reveal that activity is also characterized by a persistent bursting of small gas bubbles, occurring every 1–2 s. This activity (puffing) releases more gas (~100 t/d) than “normal” Strombolian explosions (~35 t/d) and represents a major aspect of the volcano dynamics. Explosions and puffing show significant short-term variability. This can be explained in terms of changing gas supply to the shallow feeding system.

1. CURRENT EXPLOSIVE ACTIVITY AT STROMBOLI

Stromboli's summit region is characterized by three craters at an elevation of ~750 m, each with a distinctive explosive

The Stromboli Volcano: An Integrated Study of the 2002–2003 Eruption
Geophysical Monograph Series 182
Copyright 2008 by the American Geophysical Union.
10.1029/182GM05

behavior and activity history. The three craters (Plate 1a) span a distance of ~300 m and are aligned along a NE–SW structurally controlled line [Rosi, 1980; Tibaldi *et al.*, this volume]. Explosive activity is generally persistent at each of the three craters, and their location is generally stable with a variable number (typically 5–15) of active vents [Harris and Ripepe, 2007]. Normal Strombolian activity is interrupted once or twice a year by major explosions [Bertagnini *et al.*, 1999] or, more rarely, by paroxysms [Harris *et al.*, this vol-

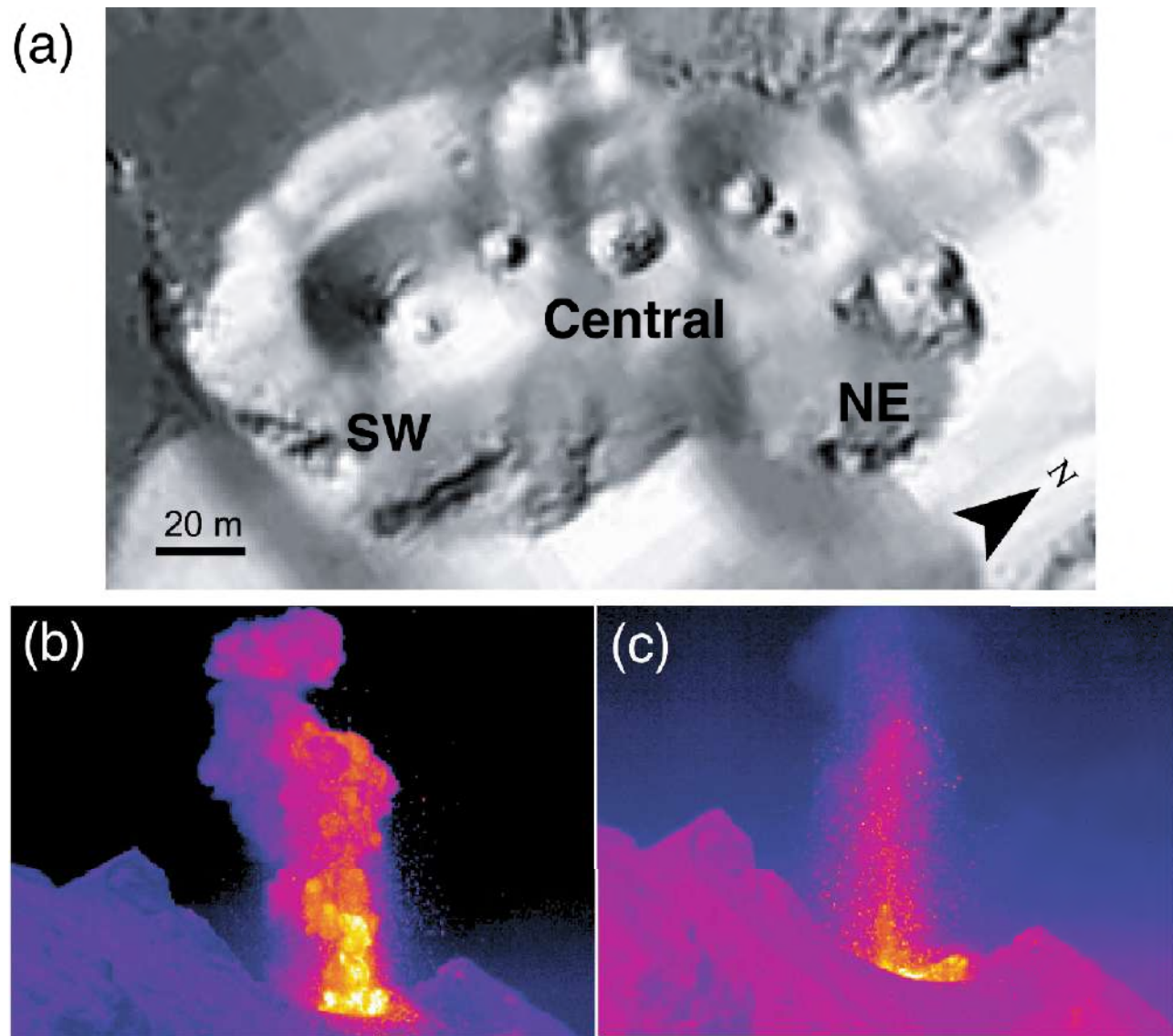


Plate 1. (a) Shaded relief map of Stromboli's crater terrace in 2006 with position of the vents in the SW, Central, and NE craters. Examples of thermal images [Patrick *et al.*, 2007b] showing (b) an ash-rich explosion and (c) a fragment-rich explosion.

ume] and effusive phases. The analysis of recent stratigraphy leads to the conclusion that this activity has been persistent without a significant break since sometime between the 3rd and 7th centuries A.D. [Rosi *et al.*, 2000].

Although Stromboli's activity is persistent, it would be wrong to view it as steady in time. Instead, it is highly variable even over the time scale of hours and days. The repose time between two Strombolian events can be highly variable with a typical recurrence time of 270 s. Eruption frequencies can range between 7 and 17 events/h with a typical frequency of ~13 events/h [Delle Donne *et al.*, 2006] or one explosion every 4.5 min (Figure 1a). Emission duration ranges from 4 to 30 s (Figure 1b), with a mean duration for the gas thrust phase of ~8 s [Hort *et al.*, 2003; Patrick *et al.*, 2007; Delle Donne *et al.*, 2006]. While some emissions barely rise a few

tens of meters (50–150 m) above the vents, others can attain heights of hundreds of meters (250–400 m), typically higher than Pizzo sopra la Fossa [Patrick *et al.*, 2007].

Ejected material thrown out during Strombolian explosions exhibits a range of densities [Lautze and Houghton, 2005], which indicates that the top of the magma column has undergone a range of degassing histories. The ejected mass of solid fragments ranges from 0 kg, for eruptions involving gas only, to ~6000 kg [Ripepe *et al.*, 1993; Patrick, 2005]. Given a mean density of ~900 kg/m³ [Lautze and Houghton, 2005], this converts to a maximum erupted volume of ~7 m³, with a range of 0.5–2.4 m³ [Harris and Ripepe, 2007]. Considering a mean eruption duration of ~8 s and 312 explosions per day (13 events/h), this value converts in a mean erupted mass flux of fragments of 0.2–0.9 kg/s with a maximum value of 2.7 kg/s. Using measurements made between 1980 and 1993, Allard *et al.* [1994] found that gas emission during Strombolian explosions peaked at 6–19 kg/s, with a mean of 14 kg/s. This indicates that the erupted mass of gas is larger than the ejecta, with a fragments-to-gas ratio ranging between 0.01 and 0.15.

Ejection velocities have been measured by using photo ballistic methods [Blackburn *et al.*, 1976; Chouet *et al.*, 1974; Ripepe *et al.*, 1993], thermal images [Patrick *et al.*, 2007; Delle Donne *et al.*, 2006], sound Doppler radar (SODAR) [Weill *et al.*, 1992], and Doppler radar [Seyfried and Hort, 1999] measured velocity range between 10 and 130 m/s (Figure 1c). Typically, particle sizes measured by Doppler radar [Hort *et al.*, 2003] and by photoballistic method [Chouet *et al.*, 1974] range between 0.3 and 2.5 cm with most of the emissions being vertically oriented.

Detailed analysis of the explosive dynamics by infrared images [Ripepe *et al.*, 1993], thermal imagery [Patrick, 2007; Patrick *et al.*, 2007], and Doppler radar [Urbanski *et al.*, 2002; Hort *et al.*, 2003] reveal that Strombolian activity can range between two distinct styles (Plates 1b and 1c): (1) relatively long-lasting (10–20 s) ash-rich eruptions, generally associated with the SW crater and (2) shorter (5–10 s) explosions rich in incandescent scoria and bombs typically associated with the NE crater activity. The different explosion styles is consistent with the different seismic, infrasonic, and thermal waveforms that characterize the activity at the two craters [e.g., Ripepe *et al.*, 1993; Neuberg *et al.*, 1994; Ripepe, 1996; Chouet *et al.*, 1999; Ripepe and Marchetti, 2002; Marchetti and Ripepe, 2005; Patrick *et al.*, 2007].

Short eruptions associated with the NE crater are seismically characterized by a high-frequency content (>0.1 Hz) and a duration of ~10 s (Figure 2a). Infrasound is represented by short (3–5 s) high-amplitude (20–80 Pa at 350 m from the vent) pressure waves [Ripepe and Marchetti, 2002]. The thermal signal is also short, usually showing a single low amplitude

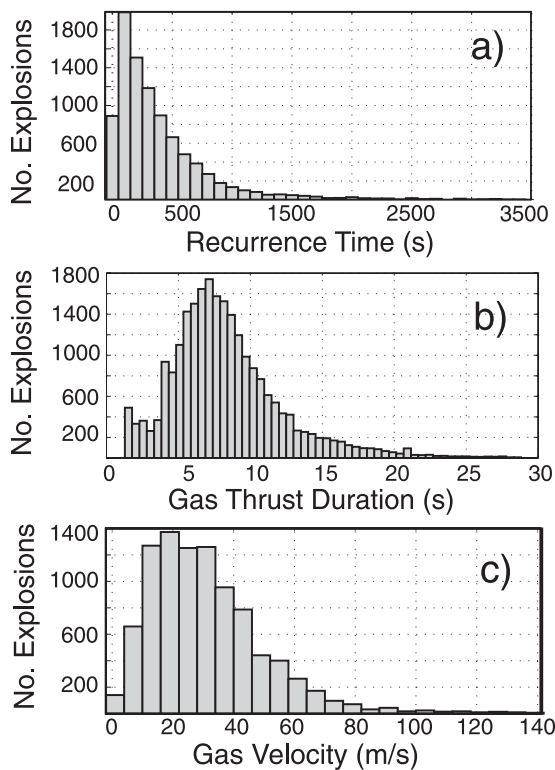


Figure 1. Parameters derived from 1 year (2006) of data on Strombolian activity defined by real-time thermal image processing based on 32,979 events [Delle Donne *et al.*, 2006]. (a) Poissonian distribution of time interval between consecutive explosions. This has a mean value of 270 s (4.5 min) equivalent to a mean rate of ~13 explosions per hour. (b) Duration of explosive events detected by the thermal camera ranges from 1.2 to 30 s, with a mean duration of 7 s. The small bimodal distribution at 1.2 s reflects puffing activity. (c) Poissonian distribution of gas jet velocities ranges from 10 to 130 m/s, with a mean of 40 m/s.

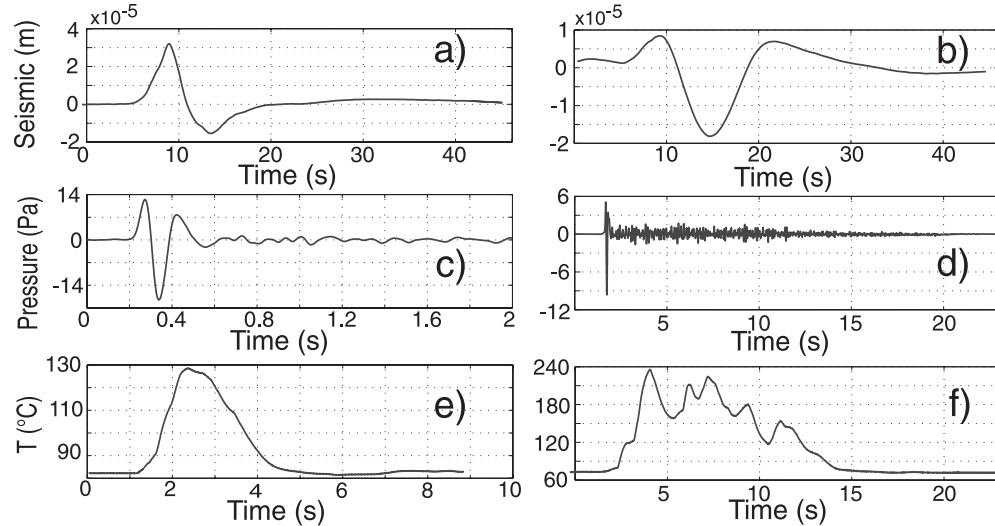


Figure 2. (a, b) Seismic, (c, d) acoustic, and (e, f) thermal waveforms generated by the stacking of several tens of signals obtained for the (a, c, e) fragment-rich explosions at the NE crater and (b, d, f) ash-rich explosions at the SW crater. Vertical component of the ground displacement in the seismic very long period band is (a) larger and impulsive at the NE crater and (b) smaller and longer at the SW crater. Acoustic signals produced by the explosions are also shorter and more energetic (c) at the NE crater than (d) at the SW crater, where the longer duration of the acoustic signal indicates a longer mass discharge process. Thermal signal is consistent with this picture where explosions (e) at the NE crater are shorter, thermally less intense, and comprise less burst of material (as revealed by the number of peaks) than (f) explosions at the SW crater.

(~150°C) thermal oscillation, with a sharp onset and a long tail (Figures 2c and 2e). These characteristics are consistent with an explosive event driven by a single bubble burst.

Longer and more complex eruptions characterized by ash-rich events are generally associated with the SW crater. Infrasound has a longer (>10 s) coda with lower acoustic pressure, 10–30 Pa at 350 m from the vent [Ripepe and Marchetti, 2002] (Figure 2d). The thermal signal has larger amplitude (~250°C) and is longer lasting, with a complex waveform with multiple peaks (Figure 2f). These characteristics are consistent with a more complex explosive event driven by a sustained gas flow regime generating several eruptive bursts or a pulsed emission.

In both cases, all observations are consistent with an unsteady mass discharge regime, which varies between low volumes of mass released in short, single-shot events, and higher volumes released during longer, fluctuating events [Ripepe et al., 1993]. Based on infrasonic data, explosion dynamics have been quantified in terms of gas overpressure of $\sim 2 \times 10^5$ Pa and gas volumes of ~ 20 and 35 m^3 for eruptions from the NE and SW craters, respectively [Ripepe and Marchetti, 2002; Vergniolle and Brandies, 1996]. Amplitude of the thermal signal, as recorded by thermal radiometers, is proportional to erupted mass [Ripepe et al., 2005; Harris and Ripepe, 2007; Scharff et al., 2008] and is consistent

with explosions at the NE crater (Figure 2e) being of lower-thermal amplitude (less material) than explosions at the SW crater (Figure 2f).

2. SHALLOW CONDUIT PROCESSES

The persistent explosive activity at Stromboli is inferred to be the evidence for efficient conduit convection [Allard et al., 1994; Kazahaya et al., 1994; Stevenson and Blake, 1998], in which gas-rich magma ascends, degasses, and sinks within the conduit at a rate of 300–1300 kg/s either as discrete batches or as a continuous cycle [Harris and Stevenson, 1997].

Geophysical data show that explosive activity at the SW, Central, and NE craters are linked to a common, shallow source [Harris et al., 1996; Settle and McGetchin, 1980; Ripepe et al., 2005]. Statistical analysis of the explosion rate [Settle and McGetchin, 1980] showed that the number of explosions at the SW and central craters increased when the repose time at the NE crater increased. A shallow linkage is apparent also in continuous thermal measurements at the three craters, where the activity at the central crater decreases during eruptions at the other two craters [Harris et al., 1996]. Moreover, the amplitude of thermal radiation, which can be related to the mass of ejecta

during explosive events shows systematic temporal variations indicating that the crater system is linked at a shallow level (150–650 m below the surface) to a common feeding system.

The presence of a shallow magma reservoir, or dyke, to which all conduits are linked is also supported by modeling of the long-term thermal equilibrium of the explosive system [Giberti *et al.*, 1992], which can only be explained if a small magma reservoir is active ~250 m below the crater system. This is in agreement with the location of the very long period (VLP) seismic wavefield. This has an equally shallow (220–300 m below the craters) source location in a zone offset from the crater complex by ~160 m in the NW direction [Neuberg *et al.*, 1994; Kirkdorfen, 1999; Chouet *et al.*, 1999, 2003; Marchetti and Ripepe, 2005]. This applies to both the VLP signals associated with the NE and SW craters.

3. DYNAMICS OF THE GAS SLUG

Strombolian explosions are generally explained in terms of generation, ascent, and bursting of a large gas slug [Blackburn *et al.*, 1976]. Seismic records support this model. A small volumetric expansion followed by a large downward single force represents the source process, which explains the origin of the VLP (~10 s) seismic events. This VLP seismic activity is associated with the explosive events at the surface and is located at 220–300 m below the craters [e.g., Chouet *et al.*, this volume]. The large downward force (~10⁸ N) indicates a conduit decompression before the explosion and is assumed to be generated by the magma flowing downward around an expanding gas slug. The bubble expanding in the conduit will decrease the magmastic pressure proportionally to the magma displaced during expansion.

Two models can explain the origin of the gas slug: a rise speed-dependent model [Parfitt, 2004] and a collapsing foam model [Jaupart and Vergniolle, 1988].

In the collapsing foam model, accumulation of gas bubbles within the magma chamber gives rise to foam. Upon reaching a critical thickness, the foam collapses to generate the gas slug. This enters and ascends the conduit to burst at the free surface [Jaupart and Vergniolle, 1988, 1989].

In the rise speed-dependent model, the rise rate of the melt is relatively slow (<0.01 m/s) such that bubbles have time to grow and coalesce to generate the slug. When the small gas bubble forms at depth, it slowly grows mainly by diffusion, and the size of the bubble remains as small as 1 cm. Only approaching the surface (100–200 m) does the decompression effect exceed diffusion effects [Spark, 1978], and the bubble reaches a larger size. If the rise speed of the magma is relatively slow, then the bubbles have sufficient time to

coalesce [Wilson, 1980; Parfitt and Wilson, 1995]. In this case, coalescence is achieved by clouds of small gas bubbles ascending the conduit without the need for a geometrical gas trap. In both models, the time between two explosions is controlled by the gas flux in the rheology and/or geometry of the magma system.

Recent Fourier transform infrared (FTIR) measurements at Stromboli have revealed that this phenomenon can be active at greater depth [Burton *et al.*, 2007a]. From the composition of gas released during a single explosive event, Burton *et al.* [2007a] have calculated that the equilibrium pressure for the gas is at ~70 MPa, which corresponds to a magmatic depth of ~3 km. This seems to indicate that the gas slug is already formed when it reaches the uppermost portion of the conduit.

If the slug has already formed, then a change in the geometrical structure at a depth of 220–300 m (the depth of the VLP source) of the shallow feeding system, such as an inclined dyke, could also promote a change in flow regime, with the VLP being generated at the point of transition [James *et al.*, 2004]. This structural control on the seismic source process seems to be confirmed by the quite stable position of the VLP seismicity [Auger *et al.*, 2006]. However, during the 2002–2003 effusive eruption, the inclination of the seismic polarization vector indicated a small but steady upward migration of the VLP source. This would argue against a structural control on the VLP source process suggesting a more active control of the position of the magma level on the source process [Marchetti and Ripepe, 2005; Marchetti *et al.*, this volume].

However, whether the gas slug is already formed or not, seismic data indicate that a large pressure drop is induced by the gas bubble flowing within the terminal part of the conduit. In this case, the pressure time history will depend on the bubble growth rate, and the time between two successive bubbles will reflect the rate at which they form within the conduit.

4. POSITION OF THE MAGMA LEVEL

The bubble burst generates an infrasonic signal and drives the upward motion of a hot cloud of gas and fragments (Plates 1b and 1c). As soon as the cloud reaches the vent, the infrared thermometer pointed at the vent detects the explosion as a sudden transient in the thermal signal. The time delay between the infrasonic and thermal onset [Ripepe *et al.*, 2001, 2002] can be used to constrain the depth of the explosive fragmentation and the emission ascent velocity. Assuming that the infrasonic wave and thermal signal are generated at the same depth and at the same origin time, we can define the thermo-acoustic time delay (Δt_c) by:

$$\Delta t_e = h_c \left(\frac{C_{\text{conduit}} - U_{\text{jet}}}{U_{\text{jet}} C_{\text{conduit}}} \right) - \left(\frac{\Delta x}{C_{\text{air}}} \right) \quad (1)$$

where h_c is the depth of the explosion in the conduit below the vent, C_{conduit} is the sound speed inside the conduit (708 m/s; Weill *et al.* [1994]), Δx is the distance between the sensor and the vent (250 m), and C_{air} is the sound speed in the atmosphere (340 m/s). Equation (1) can be used to infer changes in the depth of the explosive surface (h_c) and/or the gas jet velocity (U_{jet}). Given an explosion at the ground surface ($h_c = 0$), the infrasonic signal should arrive at a distance (Δx) of 250 m approximately 0.73 s after the thermal signal. Therefore, time delays greater than -0.73 s indicate that (1) the source of the infrasound must be within the conduit and (2) the velocity of gas jet must be subsonic ($U_{\text{jet}} < C_{\text{conduit}}$).

Following equation (1) and assuming a range of velocities U_{jet} for the gas from 10 to 130 m/s [Weill *et al.*, 1994; Hort and Seyfried, 1998; Ripepe *et al.*, 2001; Patrick *et al.*, 2007; Delle Donne *et al.*, 2006], it is possible to constrain the position of the explosions in the conduit from the measured time delay (Δt_e), which ranges from -0.45 to $+4$ s (Figure 3). From Figure 3, it is clear that for positions (h_c) of the explosive level >60 m, U_{jet} assumes values outside the velocity range measured at Stromboli. This allows us to conclude that the depth of explosive surface has quite a narrow range of variability within the conduit and does not exceed a depth of tens of meters during normal stage of the Strombolian activity.

5. GAS FLUX CONTROL

Variations in the thermal–infrasonic time delay (Δt_e) can be related to fluctuations in the position of the explosive source and/or to changes in the gas jet velocity (Figure 4). It is likely that both parameters change together responding to fluctuations in the gas flux.

When the position of the explosive fragmentation is shallow, h_c will be small, and the time delay Δt_e will also be small. However, when the gas flux increases, the magma column will become shallower and the gas slug volume will be larger. Assuming that gas expansion during the first instant of the explosion is isothermal, gas overpressure (P_g) can be related to the gas jet velocity using the Bernoulli modified equation [Self *et al.*, 1979]:

$$U_{\text{jet}}^2 = 2 \left[\frac{nRT}{m} \ln \left(\frac{P_g}{P_{\text{atm}}} \right) + \frac{1-n}{\rho_{\text{magma}}} (P_g - P_{\text{atm}}) \right] \quad (2)$$

where P_{atm} is the external atmospheric pressure (1.1×10^5 Pa); R , m , and T are the universal gas constant (8.314 J/mol

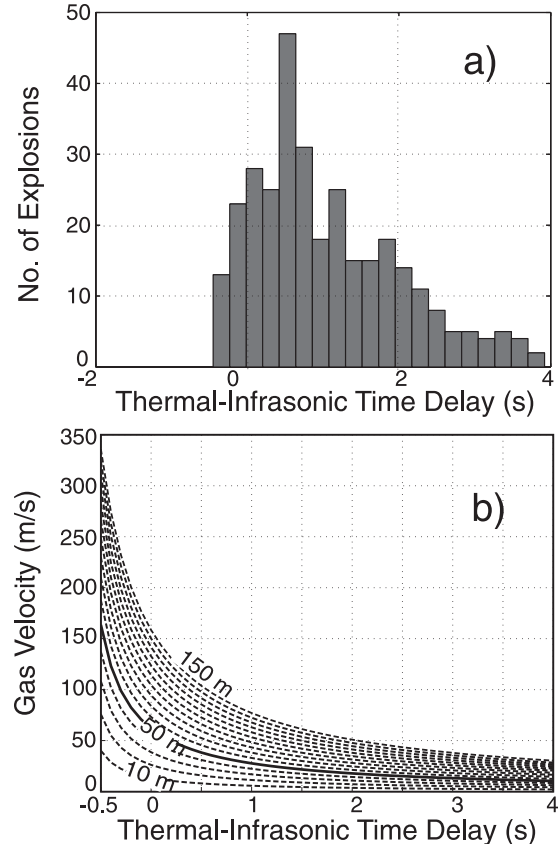


Figure 3. (a) Distribution of the time delays between acoustic and thermal onsets for explosions recorded during 3 days of Strombolian activity during 2001. Onset ranges from -0.45 to ~ 4 s and indicates that acoustic waves are traveling faster than the gas–fragment mixture during the explosions. (b) Gas jet velocity plotted as a function of the measured infrasonic and thermal time delays following equation (1). Considering that the position of the explosive fragmentation is stable, at least for short time intervals (a few days), then the observed time delays (-0.45 to 4 s) and the measured gas jet velocity are consistent with a magma level no deeper than 60 m.

K), gas molecular mass, and gas temperature (1270 K), respectively; n is the gas mass fraction; and ρ_{magma} is the magma density (2500 kg/m^3). From this relation, it is evident that gas jet velocity will increase both when gas overpressure or gas mass fraction in the melt increases.

In addition, an increase in the gas mass fraction will result in more gas/fragment-rich explosions detected by the thermal sensor as high amplitude thermal transients. The variations in the measured parameters: excess pressure, thermal radiation, and thermal–infrasonic time delay (Figure 5) seem to support this model where changes in the gas flux controls

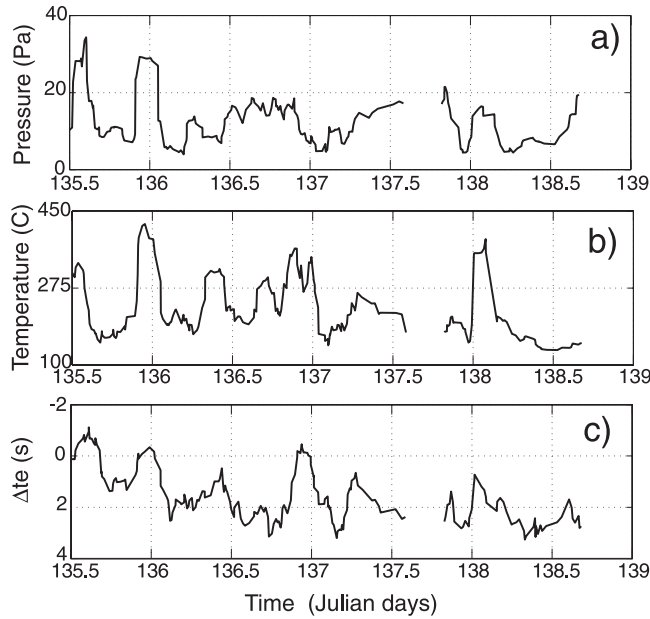


Figure 4. (a) Acoustic pressure, (b) thermal amplitude, and (c) infrasonic–thermal time delay Δt_e recorded during 3 days in 2001 for explosions at the NE crater. Each parameter shows synchronous temporal variations indicating a common link to the explosive dynamics. While acoustic pressure and time delay are both controlled by the gas overpressure, which is directly responsible for the gas jet velocity, thermal amplitude is more representative for the quantity of gas and fragments ejected during the explosive event. The relationship indicates that gas overpressure and gas volume are both changing in time as a consequence of temporal changes in the gas flux.

the position of the magma level and the explosivity of the volcanic system, so that all three parameters rise and fall together.

6. DEGASSING MAGMA COLUMN

Strombolian activity can thus be very sensitive to changes in gas flux. Degassing of a magmatic system is generally understood as a “passive” mechanism due to the slow exsolution process of the gas from the melt. This allows the gas to build no overpressure. However, if gas bubbles, moving with a higher velocity than the melt, have insufficient time to equilibrate their pressure, they will reach the uppermost portion of the conduit with an overpressure and will explode. At Stromboli, infrasonic records reveal that overpressurized gas is released not only during Strombolian explosions but also during discrete small gas bursts that feeds continuous puffing. This activity generates small ($<10^4$ Pa at 1 m from the vent) infrasonic pulses [Ripepe et al., 1996; 2007] every 1–2

s and a series of gas puffs detected as discrete thermals with a short gas thrust phase at the same rate [Ripepe et al., 2002; Harris and Ripepe, 2007]. This overpressurized condition of the magma degassing is generally called “puffing” and represents the “active” expression of continuous degassing of the magma column.

Each gas burst involves emission of $40\text{--}150\text{ m}^3$ of gas, equivalent to a mass of $10\text{--}30\text{ kg}$. Gas bursting is extremely stable, with very little variation in the rate, duration, and volume of emission over years [Harris and Ripepe, 2007]. Infrasonic and thermal location of puffing activity indicates that this process is active only at one vent at once and is typically located within the central crater or on the central crater side of the NE crater [Harris and Ripepe, 2007; Ripepe et al., 2007]. Location of the puffing is stable in a single vent over hour-to-day periods, or it can swap from vent to vent without any apparent evidence of trigger mechanisms.

This gas bubble behavior seems to be consistent with experimental and numerical studies on the partitioning of particles and drops at pipe bifurcations, whereas small particles and bubbles tend to favor the high-flow branch of bifurcations [Ditchfield and Olbricht, 1996; Manga, 1996]. Overpressurized gas bursting thus not only reflects the high gas flux regime in the conduit but also indicates where the gas flux is localized within the feeder system.

This gas burst activity is typically responsible for the emission of $\sim 100\text{ t/d}$ of SO_2 [Harris and Ripepe, 2007] much more than the total SO_2 contribution of $\sim 35\text{ t/d}$ [Allard et al., 1994; Burton et al., 2007a] due to normal Strombolian activity. Considering that the average SO_2 flux measured at Stromboli during steady-state degassing is of $\sim 200\text{ t/d}$ [Burton et al., 2007b], puffing activity contributes $\sim 50\%$ to Stromboli’s total gas flux. Puffing can thus be considered a characteristic feature of the persistent activity at Stromboli, and any variation in puffing activity both in terms of rate,

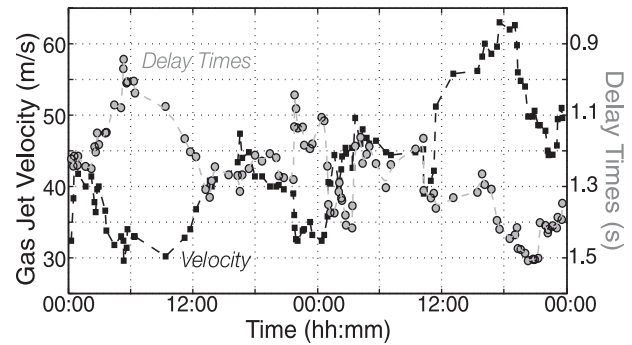


Figure 5. Gas jet velocity and infrasonic–thermal time delays measured at the NE crater during 2 days in 2006.

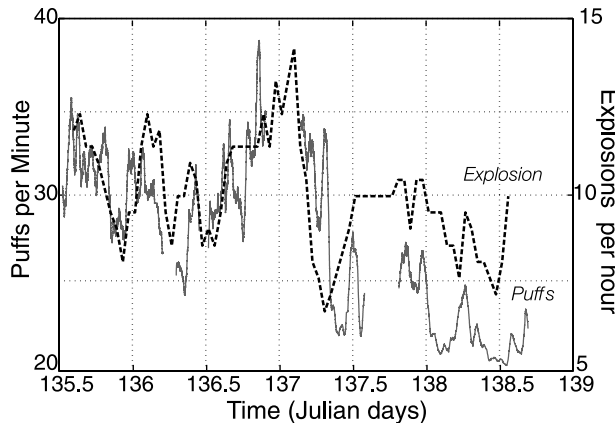


Figure 6. Gas puffing rate (puffs per minute) and number of explosions per hour measured during a period of 3 days in 2002. Number of explosions changes from 6 to 14 events/h. This change in explosive activity is matched by a change in the number of puffs per minute. The link between these two independent parameters reveals the influence of gas flux on the explosive and bursting activity.

amplitude, and location will indicate a change in the gas flux regime within the magmatic feeding system.

This appears to be confirmed by the correlation between gas puffing and number of Strombolian events (Figure 6). An increase in the puffing rate implies an increase in gas flux. In turn, the increase in the gas flux would generate a more frequent gas bubble formation both as number of explosions and as puffing rate (Figure 6). Changes in the frequency and amplitude of puffing and of the explosive activity can be thus associated with cycles of high and low levels of magma degassing.

7. CONCLUSIONS

Strombolian dynamics is one of the best investigated explosive phenomena. In recent years, a large number of geophysical and geochemical experiments have improved enormously our knowledge of Stromboli's explosive system. In particular, integration of infrasonic, thermal, and seismic data has provided crucial constraints on the shallow system geometry. These data show that, although eruptions at Stromboli can be roughly grouped into two characteristic styles, activity shows significant short-term variability in many of the monitored geophysical parameters. Thermal energy of explosions shows that, in spite of the different dynamics at the different craters, the feeding system is shallow and common to all the vents. Seismic VLP indicates that most likely this common feeding system is located at 450–550 m above sea level, a location where gas expansion

occurs a few seconds before each explosion. Acoustic and thermal onsets constrain the depth of explosive fragmentation at 40–150 m below the vent. This level is not stable, but changes in time with pressure and thermal amplitude of the explosive activity increases as the source depth decreases. This relationship can be explained in terms of changes in the gas flux rate in the shallow feeding system.

In addition, infrasonic and thermal data reveal that Strombolian activity is characterized by persistent bursting of small gas bubbles, which occur at only one vent at once and at a rate of one burst every 1–2 s. This overpressurized style of degassing is not stable in time, but its rate and amplitude changes according to changes in explosion rate. This correlation between the two phenomena is interpreted as also resulting from variability in the gas flux within the conduit.

The next level of data integration is to consider other geophysical data sets, such as gas flux, gas chemistry, and ground deformation, as well as physical volcanology data, such as bubble and crystal contents of the erupted products. With full constraint of the shallow system behavior and dynamics, modeling and experimental approaches can be applied to fit the full range of data to produce robust models and possibly predict the behavior of Stromboli volcano.

Acknowledgments. We thank Takeshi Nishimura and Matthew Patrick for their comments and suggestions, which have greatly helped to improve the manuscript.

REFERENCES

- Allard, P., J. Carbonnelle, N. Metrich, H. Loyer, and P. Zettwoog (1994), Sulfur output and magma degassing budget of Stromboli volcano, *Nature*, 368, 326–330.
- Auger, E., L. D'Auria, M. Martini, B. Chouet, and P. Dawson (2006), Real-time monitoring and massive inversion of source parameters of very long period seismic signals: An application to Stromboli Volcano, Italy, *Geophys. Res. Lett.*, 33, L04301, doi:10.1029/2005GL024703.
- Blackburn, E. A., L. Wilson, and R. S. J. Sparks (1976), Mechanisms and dynamics of Strombolian activity, *J. Geol. Soc. London*, 132, 429–440.
- Burton, M. R., P. Allard, F. Muré, and A. La Spina (2007a), Magmatic gas composition reveals the source depth of slug-driven Strombolian explosive activity, *Science*, 317, 227–230.
- Burton, M. R., H. M. Mader, and M. Polacci (2007b), The role of gas percolation in quiescent degassing of persistently active basaltic volcanoes, *Earth Planet. Sci. Lett.*, 264, 46–60.
- Chouet, B., N. Hamisevicz, and T. R. McGetchin (1974), Photoballistics of volcanic jet activity at Stromboli, Italy, *J. Geophys. Res.*, 79, 4961–4976.
- Chouet, B., G. Saccorotti, P. Dawson, M. Martini, R. Scarpa, G. De Luca, G. Milana, and M. Cattaneo (1999), Broadband measure-

- ments of the sources of explosions at Stromboli Volcano, Italy, *Geophys. Res. Lett.*, 26, 1937–1940.
- Chouet, B., P. Dawson, T. Ohminato, M. Martini, G. Saccorotti, F. Giudicepietro, G. De Luca, G. Milana, and R. Scarpa (2003), Source mechanisms of explosions at Stromboli Volcano, Italy, determined from moment-tensor inversions of very-long-period data, *J. Geophys. Res.*, 108(B1), 2019, doi:10.1029/2002JB001919.
- Delle Donne, D., E. Marchetti, M. Ripepe, G. Ulivieri, and G. Lanza (2006), Monitoring explosive volcanic activity using thermal images, Stromboli volcano, Italy, *Eos Trans. AGU*, 79, 1795.
- Ditchfield, R., and W. L. Olbricht (1996), Effects of particle concentration on the partitioning of suspensions at small divergent bifurcations, *J. Biomech. Eng.*, 118(3), 287–294.
- Giberti, G., C. Jaupart, and G. Sartoris (1992), Steady-state operation of Stromboli volcano, Italy: Constraints on the feeding system, *Bull. Volcanol.*, 54, 535–541.
- Harris, A., and M. Ripepe (2007), Temperature and dynamics of degassing at Stromboli, *J. Geophys. Res.*, 112, B03205, doi:10.1029/2006JB004393.
- Harris, A. J. L., and D. S. Stevenson (1997), Thermal observations of degassing open conduits and fumaroles at Stromboli and Vulcano using remotely sensed data, *J. Volcanol. Geotherm. Res.*, 76, 175–198.
- Harris, A. J. L., N. F. Stevens, A. J. H. Maciejewski, and P. J. Röllin (1996), Thermal evidence for linked vents at Stromboli, *Acta Vulcanol.*, 8, 57–62.
- Hort, M., and R. Seyfried (1998), Volcanic eruption velocities measured with a micro radar, *Geophys. Res. Lett.*, 25, 113–116.
- Hort, M., R. Seyfried, and M. Voge (2003), Radar Doppler velocimetry of volcanic eruptions: Theoretical considerations and quantitative documentation of changes in eruptive behaviour at Stromboli volcano, Italy, *Geophys. J. Int.*, 154, 515–532.
- James, M. R., S. J. Lane, B. Chouet, and J. S. Gilbert (2004), Pressure changes associated with the ascent and bursting of gas slugs in liquid-filled vertical and inclined conduits, *J. Volcanol. Geotherm. Res.*, 129, 61–82.
- Jaupart, C., and S. Vergniolle (1989), The generation and collapse of a foam layer at the roof of a basaltic magma chamber, *J. Fluid Mech.*, 203, 347–380.
- Jaupart, C., and S. Vergniolle (1998), Laboratory models of Hawaiian and Strombolian eruptions, *Nature*, 331, 58–60.
- Kirchdorfer, M. (1999), Analysis and quasistatic FE modeling of long period impulsive events associated with explosions at Stromboli Volcano (Italy), *Ann. Geofis.*, 42, 379–390.
- Lautze, N. C., and B. F. Houghton (2005), Physical mingling of magma and complex eruption dynamics in the shallow conduit at Stromboli volcano, Italy, *Geology*, 33(5), 425–428.
- Manga, M. (1996), Dynamics of drops in branched tubes, *J. Fluid Mech.*, 189, 105–117.
- Marchetti, E., and M. Ripepe (2005), Stability of the seismic source during effusive and explosive activity at Stromboli Volcano, *Geophys. Res. Lett.*, 32, L03307, doi:10.1029/2004GL021406.
- Marchetti, E., M. Ripepe, G. Ulivieri, M. R. Burton, T. Caltabiano, and G. Salerno (2008), Gas flux rate and migration of the magma column, this volume.
- Neuberg J., R. Luckett, M. Ripepe, and T. Braun (1994), Highlights from a seismic broadband array on Stromboli volcano, *Geophys. Res. Lett.*, 21, 749–752.
- Parfitt, E. A. (2004), A discussion of the mechanisms of explosive basaltic eruptions, *J. Volcanol. Geotherm. Res.*, 134, 77–107.
- Parfitt, E. A., and L. Wilson (1995), Explosive volcanic eruptions: IX. The transition between Hawaiian-style lava fountaining and Strombolian explosive activity, *Geophys. J. Int.*, 121, 226–232.
- Patrick, M. R. (2005), Strombolian eruption dynamics from thermal (FLIR) video imagery, Ph.D. dissertation, 281 pp., Department of Geology and Geophysics, Univ. of Hawaii.
- Patrick, M. R. (2007), Dynamics of Strombolian ash plumes from thermal video: Motion, morphology, and air entrainment, *J. Geophys. Res.*, 112, B06202, doi:10.1029/2006JB004387.
- Patrick, M. R., A. J. L. Harris, M. Ripepe, J. Dehn, D. A. Rothery, and S. Calvari (2007), Strombolian explosive styles and source conditions: Insights from thermal (FLIR) video, *Bull. Volcanol.*, 69, 769–784, doi:10.1007/s00445-006-0107-0.
- Ripepe, M. (1996), Evidence for gas influence on seismic signals recorded at Stromboli, *J. Volcanol. Geotherm. Res.*, 70, 221–233.
- Ripepe, M., and E. Marchetti (2002), Array tracking of infrasonic sources at Stromboli volcano, *Geophys. Res. Lett.*, 29(22), 2076, doi:10.1029/2002GL015452.
- Ripepe, M., M. Rossi, and G. Saccorotti (1993), Image processing of explosive activity at Stromboli, *J. Volcanol. Geotherm. Res.*, 54, 335–351.
- Ripepe, M., P. Poggi, T. Braun, and E. Gordeev (1996), Infrasonic waves and volcanic tremor at Stromboli, *Geophys. Res. Lett.*, 23(2), 181–184.
- Ripepe, M., S. Ciliberto, and M. Della Schiava (2001), Time constraints for modeling source dynamics of volcanic explosions at Stromboli, *J. Geophys. Res.*, 106(B5), 8713–8727.
- Ripepe, M., A. J. L. Harris, and R. Carniel (2002), Thermal, seismic and infrasonic insights into conduit process at Stromboli volcano, *J. Volcanol. Geotherm. Res.*, 118, 285–307.
- Ripepe, M., A. J. L. Harris, and E. Marchetti (2005), Coupled thermal oscillations in explosive activity at different craters of Stromboli volcano, *Geophys. Res. Lett.*, 32, L17302, doi:10.1029/2005GL022711.
- Ripepe, M., E. Marchetti, and G. Ulivieri (2007), Infrasonic monitoring at Stromboli volcano during the 2003 effusive eruption: Insights on the explosive and degassing process of an open conduit system, *J. Geophys. Res.*, 112, B09207, doi:10.1029/2006JB004613.
- Rosi, M. (1980), The island of Stromboli. *Rend. Soc. Ital. Mineral. Petrol.*, 36, 345–368.
- Rosi, M., A. Bertagnini, and P. Landi (2000), Onset of the persistent activity at Stromboli Volcano (Italy), *Bull. Vulcanol.*, 62, 294–300.
- Scharff, L., M. Hort, A. J. L. Harris, M. Ripepe, J. M. Lees, and R. Seyfried (2008), Eruption dynamics of the SW crater of Stromboli volcano, Italy—An interdisciplinary approach, *J. Volcanol. Geotherm. Res.*, 118, 285–207.
- Self, S., L. Wilson, and I. A. Nairn (1979), Vulcanian eruption mechanisms, *Nature*, 277, 440.

- Settle, M., and T. R. McGetchin (1980), Statistical analysis of persistent explosive activity at Stromboli, 1971: Implications for eruption prediction, *J. Volcanol. Geotherm. Res.*, **8**, 45–58.
- Seyfried, R., and M. Hort (1999), Continuous monitoring of volcanic eruption dynamics: A review of various techniques and new results from a frequency-modulated radar Doppler system, *Bull. Volcanol.*, **60**, 627–639.
- Steinberg, G. S., and J. I. Babenko (1978), Gas velocity and density determination by filming gas discharges, *J. Volcanol. Geotherm. Res.*, **3**, 89–98.
- Urbanski, N.-A., M. Voge, R. Seyfried, L. Rupke, T. Petersen, T. Hanebuth, and M. Hort (2002), Fifteen days of continuous activity survey at Stromboli volcano, Italy, in late September 2000: Doppler radar, seismicity, infrared, soil humidity, and mapping of the crater region, *Int. J. Earth Sci.*, **91**, 712–721.
- Vergniolle, S., and G. Brandeis (1994), Origin of sound generated by Strombolian explosions, *Geophys. Res. Lett.*, **21**, 1959–1962.
- Vergniolle, S., and G. Brandeis (1996), Strombolian explosions: 1. A large bubble breaking the surface of a lava column as a source of sound, *J. Geophys. Res.*, **101**(B9), 20,433–20,447.
- Vergniolle, S., G. Brandeis, and J.-C. Mareschal (1996), Strombolian explosions 2. Eruption dynamics determined from acoustic measurements, *J. Geophys. Res.*, **101**(B9), 20,449–20,466.
- Weill, A., G. Brandeis, S. Vergniolle, F. Baudin, J. Bilbille, J.-F. Fevre, B. Piron, and X. Hill (1992), Acoustic sounder measurements of the vertical velocity of volcanic jets at Stromboli volcano, *Geophys. Res. Lett.*, **19**, 2357–2360.
- Wilson, L. (1980), Relationships between pressure, volatile content and ejecta velocity in three types of volcanic explosion, *J. Volcanol. Geotherm. Res.*, **8**, 297–313.

D. Delle Donne, E. Marchetti, M. Ripepe, and G. Olivieri, Dipartimento Scienze della Terra, Università di Firenze, V. La Pira 4, 50121 Firenze, Italy. (maurizio.ripepe@unifi.it)

A. Harris, HIGP/SOEST, University of Hawai'i, 1680 East-West Road, Honolulu, HI 96822, USA.

Fluid Geochemistry of Stromboli

Fausto Grassa, Salvatore Inguaggiato, and Marcello Liotta

Istituto Nazionale di Geofisica e Vulcanologia, Sezione di Palermo, Palermo, Italy

An accurate description of the geochemical system is presented here based on a review of scientific work performed during the past decade. The surface manifestations of the volcanic system of Stromboli have been investigated using several measuring techniques. Studying the chemical composition of the volcanic plume and of fumarolic emissions has provided information on magma degassing processes. The total fluxes of the emitted gases from both the plume and the soil were found to vary with changes in volcanic activity (from normal Strombolian activity to effusive and/or paroxysmal activity). Thermal water results from the interaction between volcanic gases, host rock, seawater, and meteoric water and temporal changes observed in the chemical and the isotopic composition of the gases dissolved into thermal waters highlighted the rising of new magma batches. Combining modeling of gas–water–rock interactions with an understanding of the volcanic system allowed identifying preferential sampling sites and parameters for the geochemical monitoring of volcanic activity at Stromboli Island.

1. INTRODUCTION

Geochemical monitoring of active volcanoes provides a useful tool for hazard mitigation. Evaluation of geochemical signals requires a good knowledge of volcanic systems and the formulation of accurate models.

The features of a volcanic system can be defined by its structural and morphological settings, style of volcanic activity, and by the type and the amount of magmatic and/or shallow fluids (e.g., seawater, meteoric water). This geochemical approach can be used to model the interaction processes between the involved fluid phases.

Analyses of volcanic gas, being the most mobile phase in magma, yield useful information on the feeding system. Each volcano presents different degassing styles depending on its origin and evolution. In open-conduit volcanoes, such as Stromboli, most gas is released from the summit vent. Never-

theless, fumarolic fields and diffuse soil degassing represent other important modes of gas release [Giammanco *et al.*, 1998; Carapezza and Federico, 2000; Varley and Armienta, 2001; Aiuppa *et al.*, 2004; Brusca *et al.*, 2004]. Gases escaping from the magma along high-permeability pathways interact with groundwater and with the host rocks. Dissolution of acidic gases in water quickly lowers the pH which facilitates water–rock interactions. In areas with high gas fluxes, groundwater rapidly becomes saturated with gas and so any further addition of volatiles results in the deep gas-phase flow through the aquifer without significant interactions. In such volcanic systems, gas–water–rock interactions govern the chemical and isotopic compositions of the circulating fluids.

Rising steam and gas that has separated from magma at depth, may interact with shallow aquifers. Released fluids may condense and/or dissolve into the liquid phase, manifesting as hydrothermal systems and/or mineral waters.

The contribution of magmatic fluids to the hydrothermal systems can be hidden by mixing processes with other non-magmatic fluid components (e.g., meteoric waters, seawater, air, crustal and biogenic gas) or by the chemical and isotopic fractionation occurring during water–gas interactions. Nonetheless, many studies have demonstrated that thermal

waters associated with the most important active volcanic systems such as Etna, Vulcano, Vesuvius, Ischia Island, Popocatepetl, and El Chichón, tend to maintain the geochemical information of the deep magmatic source [Allard *et al.*, 1997; Capasso *et al.*, 2001; Federico *et al.*, 2004; Inguaggiato *et al.*, 2000, 2005; Taran *et al.*, 1998]. Therefore, thermal discharges represent interesting sites for surface investigations that may provide significant, additional, and sometimes complementary information about deep degassing dynamics.

The occurrence of thermal waters depends on the aquifer geometry, the geological and stratigraphic setting, the hydraulic properties such as transmissivity and porosity, and the recharge and discharge mechanisms. Therefore, the knowledge of the hydrogeological setting is critical to understanding interactions between deep and shallow fluids.

This paper is a review of the most relevant published papers on the fluid geochemistry at Stromboli Island, focusing its main attention on the geochemistry of thermal waters. Based on the data collected since 1999 within the framework of the geochemical volcano monitoring, this paper provides an overview of the most relevant results including a conceptual model of fluid circulation for the volcanic system of Stromboli.

2. VOLATILE BUDGET AT STROMBOLI ISLAND

Magmatic volatiles are released during magma migration toward the surface. Decreasing pressure induced by magma batches rising within the conduit and/or by fracturation of the volcanic edifice results in exsolving of fluids whose chemical composition is strongly dependent on the relative solubility of each volatile component in the magma. Generally, volatiles exsolved from magma can be released via the following three main degassing processes:

1. *Open-conduit degassing*. Fluids rising along the conduit reach the top of the magmatic column to form the so-called volcanic plume;

2. *Fumaroles and diffused soil degassing*. Gas and steam are dispersed through the soil as they migrate along high permeability zones;

3. *Degassing associated with geothermal waters*. During their rising, steam and gas may condense and/or dissolve in shallow fluids such as groundwater giving origin to hydrothermal aquifers.

In terms of mass balance, the relative contribution of each degassing process is mainly dependent on the type of volcanism and the level of volcanic activity.

2.1. Open-Conduit Degassing

Stromboli is an open-conduit basaltic volcano characterized by persistent degassing and frequent mild explosions

(Strombolian activity). Both quiescent degassing and explosive events contribute to feed a volcanic plume which in the past was discontinuously measured. It has been estimated that the largest fraction of the gas output occurs from the plume, whose total output of gas has been estimated approximately at $3 \times 10^6 \text{ Mg year}^{-1}$ [Allard *et al.*, 1994, this volume]. During persistent passive degassing, the plume chemistry is mainly made of a water-rich gas phase with CO_2/SO_2 and SO_2/HCl molar ratios close to 8 and 0.7, respectively [Allard *et al.*, 1994].

Comparison between CO_2 efflux from the craters and soil in the crater rim area [Carapezza and Federico, 2000] revealed that more than 90% of the gas is released from the open-conduit degassing system.

The mass output of specific gases in crater plume emissions as well as the plume chemistry are continuously measured within the framework of geochemical monitoring of the volcanic activity since this information has provided insights into the plumbing system. For example, the daily SO_2 flux at Stromboli is highly variable with strong increases being evident during 2002–2003 eruption as well as during intense phases of Strombolian activity [Allard *et al.*, this volume]. The plume chemistry is monitored by remote measurements of halogens, sulfur, and carbon compounds [Oppenheimer, 2003]. Within the framework of the geochemical monitoring of volcanic activity at Stromboli 2 d before the 5 April 2003 paroxysm, Aiuppa and Federico [2004], using diffusive tubes, recorded a peak in the SO_2/HCl ratio four to eight times higher than those observed during passive degassing (SO_2/HCl ratio ~ 1 , Allard *et al.* [1994]). These authors interpreted this change in the plume chemistry as an evidence of a S-rich magma rising within the volcanic conduit toward the surface which was probably later involved in the paroxysm.

Therefore, the changes in plume composition are useful indicators of the stage of the degassing process and could be used as potential geochemical precursors of high energetic explosions [Aiuppa and Federico, 2004; Rizzo *et al.*, this volume; Allard *et al.*, this volume].

2.2. Fumaroles and Diffused Soil Degassing

Uprising hot fluids migrating through highly permeable zones such as porous layers and volcano-tectonic structural discontinuities give rise to hydrothermal activity at the summit area. Finizola *et al.* [2002, 2003, this volume] correlated in situ self-potential measurements with temperature and CO_2 anomalies in several profiles across the entire island. From their results, they proposed a new structural model that includes three perched hydrothermal zones below the summit. These systems, whose structural limits approximately coincide with the local volcano-tectonic structures

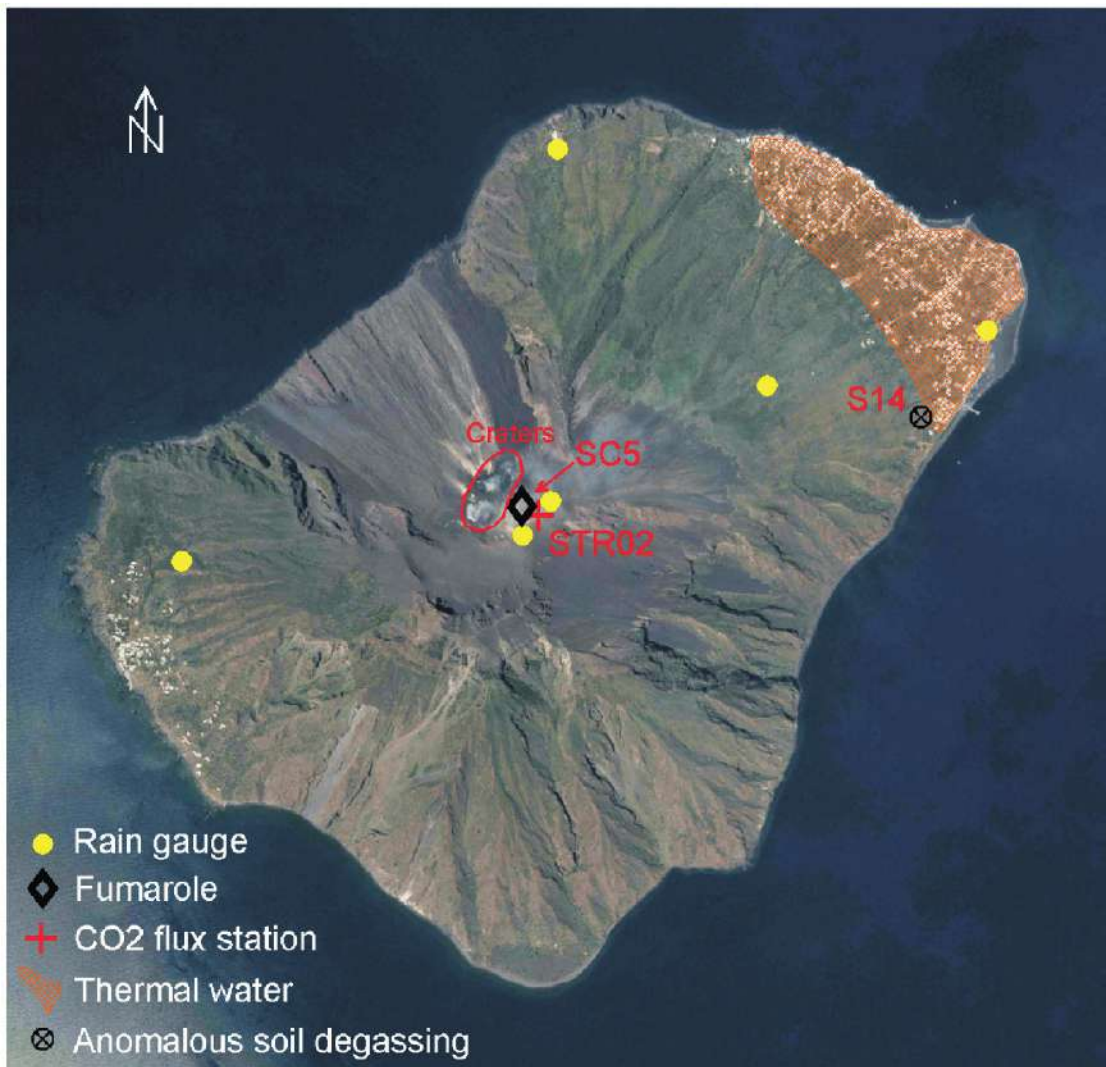


Plate 1. Base map and sampling sites of natural fluids on Stromboli Island. Filled yellow circles indicate the site of rain gauges; Crater fumaroles (site SC5) as well as low-elevation anomalous soil degassing zones (site S14) are also showed. Site STR 02 is the location of the automatic station installed in July 1999 for continuous monitoring of CO₂ flux from soil (see text). Red grid indicates the northeastern corner of the island where thermal waters were found.

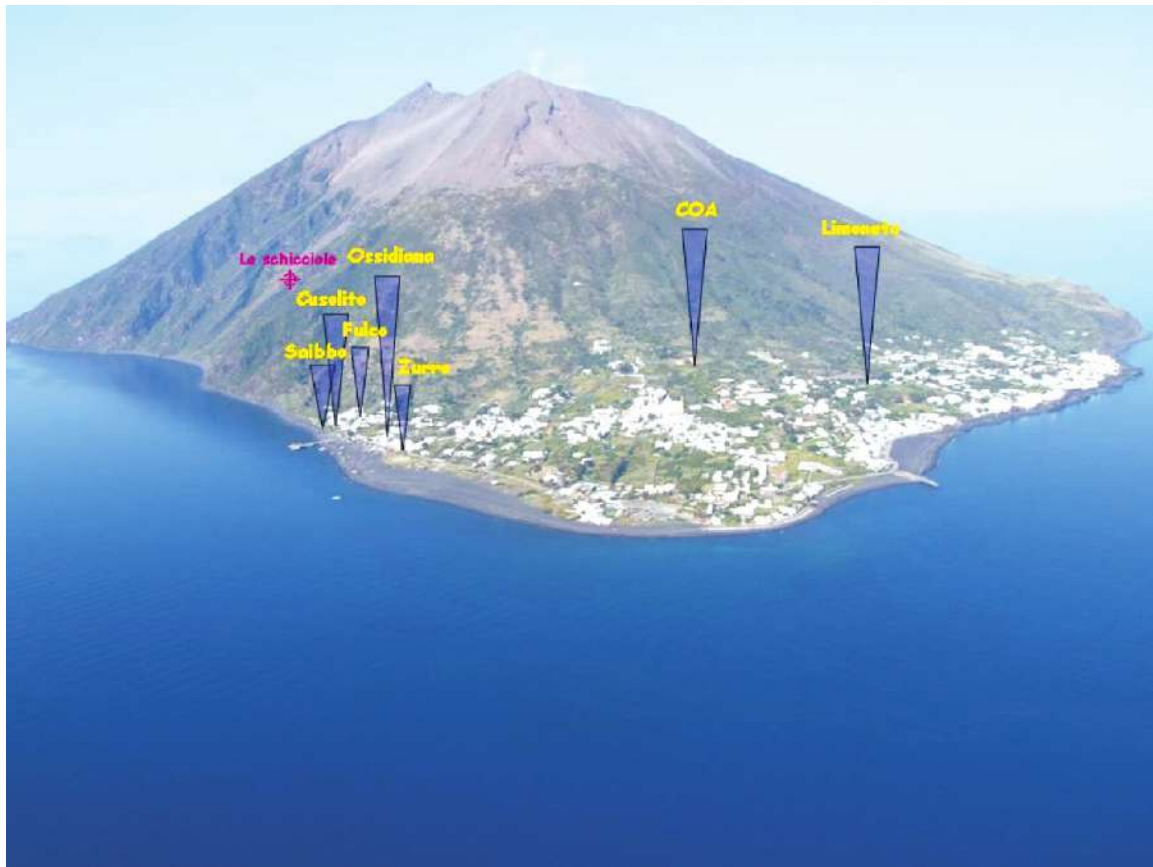


Plate 2. Aerial view of Stromboli (taken from northeast) showing the location of thermal wells and Le Schicciola cold spring.

such as dikes, calderas and regional faults [Finizola *et al.*, 2002, this volume], appear to feed both crateric fumaroles and widespread anomalous diffuse degassing zones at the summit area. Fumaroles are clustered into two zones: (1) in the Fossa area around the eastern flank of the active craters and (2) in the Pizzo area. High-temperature fumaroles (up to 410°C) located in the Fossa area [Martini *et al.*, 1991; Finizola and Sortino, 2003] are sampled only occasionally because this area is highly hazardous due to its high instability and its vicinity to the active vents. In contrast, fumaroles in the Pizzo area are more easily accessible and safe, but they exhibit only low-flux and low-temperature emissions. Carapezza and Federico [2000], Finizola *et al.* [2003], and Capasso *et al.* [2005] found that the maximum temperature was 95°C which is approximately the boiling temperature of water at an elevation of 900 m above sea level (asl).

The data from the most representative fumarole (site SC5, see Plate 1) are listed in Table 1. Despite their low temperature, the chemical and isotope composition of the Pizzo area fumaroles revealed a clear magmatic origin of the gases. CO₂ is the dominant gas phase (up to 93%) having δ¹³C_{CO₂} values ranging between -3.2 and -0.7 ‰ versus Vienna PeeDee belemnite (VPDB). Helium, up to 20 ppmvol, shows a marked mantle-derived signature with the ³He/⁴He ratios (corrected for air contamination) being in the range between 2.3 and 3.6 R/Ra, where Ra is the ³He/⁴He ratio in the atmosphere (1.39×10^{-6}). The carbon and helium isotope compositions of fumarolic gases at SC5 revealed their precursory character of the 2002–2003 eruption [Capasso *et al.*, 2005; Rizzo *et al.*, this volume; Federico *et al.*, this volume]. A unique field survey at the summit allowed the total output of diffuse CO₂ emissions to be estimated in the range between 200 and 250 t d⁻¹ [Carapezza and Federico, 2000].

The CO₂ soil efflux in the Pizzo area was monitored by an automatic station (site STR02 see Plate 1) that was installed in July 1999 at a high flux site was considered rep-

resentative of the entire area. The average measured output at this site was a few thousands of grams per square meters per day. Soil gas emissions increased concomitantly with intense explosive activity as well as during preeruptive periods. For instance, the highest soil CO₂ effluxes of about 10⁵ g m⁻² d⁻¹ were reached a few days before the 2002–2003 eruption [Carapezza *et al.*, 2004; Federico *et al.*, this volume].

Apart from the summit area, CO₂ soil efflux anomalies were also recognized mainly along the northern flank of the edifice where fractures and faults as well as porous layers allow the rising of deep fluids [Finizola *et al.*, 2002] both at intermediate altitudes (Nel Cannestrà and Rina Grande areas) and in the peripheral areas at lower elevations (Pizzillo and San Bartolo). Such anomalous CO₂ soil emissions could be directly related to a deep degassing source (through structural discontinuities), or they may represent a fluid phase separated from thermal reservoirs. Finizola *et al.* [2002] suggested that such anomalous gas emissions are decoupled from the volcanic structures but are linked to two major faults: (1) the N41° structural trend (Pizzillo-Rina Grande alignment) that coincides closely both with a recent dyke intrusion [Bonaccorso, 1998] and a regional fault [Falsaperla *et al.*, 1999] and (2) N64° structural trend (Nel Cannestrà-San Bartolo alignment) that corresponds to a well-known direction of structural weakness zone [Zanchi and Francalanci, 1989].

2.3. Thermal Water at Stromboli

Water-well drilling that began in the 1980s first revealed a very shallow hydrothermal system (at a depth of 5–10 m) at nearby Scari village. In this area, there are favorable conditions for the development of an aquifer. The presence of permeable structural elements and porous layers that characterize the entire northern flank [Finizola *et al.*, 2002, this volume] enhances rainwater infiltration. In contrast, the other flanks of the volcano are mainly comprised of scarcely

Table 1. Chemical and Isotope Compositions of Low-Temperature (<95°C) Fumaroles at the Summit (Mean, Max, and Min Values)^a

Sample	He	H ₂	O ₂	N ₂	CO	CH ₄	CO ₂	δ ¹³ C _{CO₂}	³ He/ ⁴ He	He/Ne	³ He/ ⁴ He _c
SC5	Mean	8.9	178.0	4.0	19.6	4.8	15.4	76.5	-2.1	2.3	1.40
	SD	3.5	173.5	3.6	13.5	7.8	40.7	17.5	0.5	0.4	0.69
	Max	20.3	770.1	19.0	76.2	45.9	189.3	93.5	-0.7	3.1	3.46
	Min	4.4	6.2	0.3	6.5	1.1	0.9	2.1	-3.2	1.1	0.45
	n	38	50	51	51	42	40	51	43	70	64
Air		5.2	n.d.	20.8	78	n.d.	n.d.	0.0	-8	1	0.32

^aSD, standard deviation; n, number of samples; n.d., no data. He, H₂, CO, and CH₄ contents are expressed in ppmVol, while O₂, N₂, and CO₂ in volumetric percentages. Helium isotope ratios (³He/⁴He) are expressed as R/Ra. ³He/⁴He_c is the helium isotope ratio corrected for air contamination [Sano *et al.*, 1993]. Air composition is also given for reference.

Table 2. Physicochemical Parameters, Chemical and Isotope Composition of Thermal Waters Collected at Stromboli^a

Sample	EC, mS																
	T, °C	pH	cm ⁻¹	Eh, mv	Na	K	Mg	Ca	F	Cl	Br	NO ₃	SO ₄	HCO ₃	δ ¹⁸ O	δD	
Zurro	Mean	35.4	6.97	43.3	-38.4	10,704	513	1,200	542	46	19,300	66	72	2,475	315	0.1	1
	SD	1.1	0.21	7.3	85.6	1,250	87	201	116	145	2,329	14	53	298	41	0.9	4
	Max	37.5	7.78	55.0	272.3	12,104	842	1,467	856	661	22,351	120	203	2,926	470	0.9	6
	Min	32.3	6.61	23.3	-236.0	6,030	292	145	181	1	9,974	22	3	1,394	229	-2.0	-9
	n	125	127	88	98	94	94	94	94	20	94	93	32	94	112	43	32
Fulco	Mean	41.1	6.41	18.0	21.0	3,373	263	465	302	5	6,053	20	32	938	791	-4.2	-22
	SD	1.2	0.11	8.4	85.4	1,844	85	194	92	5	3,450	11	22	376	133	1.1	6
	Max	43.1	6.98	39.9	242.0	7,980	484	966	572	18	14,881	71	103	1,929	1,104	-2.0	-10
	Min	37.6	6.19	-13.7	-266.0	782	123	190	121	1	11	3	5	360	458	-5.8	-34
	n	116	113	110	103	101	101	101	101	100	101	101	99	101	109	53	42
Saibbo	Mean	39.9	6.31	30.5	86.3	7,134	428	880	523	n.d.	13,267	44	n.d.	1,717	474	-2.0	-11
	SD	2.5	0.11	5.6	84.7	1,122	51	132	65	-	2,132	7	-	293	47	0.6	3
	Max	42.6	6.55	37.8	237.0	9,579	555	1,125	668	-	17,698	62	-	2,315	528	-0.8	-5
	Min	29.9	6.02	7.9	-80.0	5,596	377	683	425	-	10,539	35	-	1,311	305	-2.9	-15
	n	26	26	26	21	17	17	17	17	-	17	17	-	17	25	12	12
Limoneto	Mean	41.0	6.66	29.9	11.7	6,537	459	871	439	n.d.	12,263	39	n.d.	1,591	650	-2.9	-16
	SD	1.1	0.07	6.4	105.7	1,538	61	154	70	-	2,766	10	-	351	114	1.0	5
	Max	42.8	6.8	38.8	283.5	9,509	582	1,206	603	-	17,902	58	-	2,295	885	-0.7	-10
	Min	38.6	6.53	17.6	-129.0	3,626	343	593	313	-	7,040	19	-	963	464	-4.8	-24
	n	32	32	29	26	37	37	37	37	-	37	37	-	37	42	23	19
COA	Mean	40.5	6.52	27.6	30.5	5,944	369	770	431	n.d.	11,011	36	n.d.	1,393	448	-2.2	-12
	SD	2.1	0.08	4.9	70.1	1,821	125	224	79	-	3,254	10	-	412	151	-	-
	Max	42.1	6.62	31.5	78.0	7,231	458	929	487	-	13,313	43	-	1,684	555	-	-
	Min	38.1	6.47	22.1	-50.0	4,656	281	612	376	-	8,710	29	-	1,101	342	-	-
	n	3	3	3	3	2	2	2	2	-	2	2	-	2	2	1	1
Cusolito	Mean	42.3	6.68	33.7	-77.1	7,682	448	883	484	11	14,023	47	56	1,792	494	-2.0	-12
	SD	1.4	0.18	5.8	45.9	1,745	90	208	114	11	3,326	13	53	374	73	0.7	4
	Max	46.9	7.18	45.4	32.0	10,776	605	1,209	724	42	19,969	76	228	2,410	708	-0.6	-8
	Min	38.9	6.27	17.0	-205.8	3,198	284	473	264	1	5,994	14	1	770	305	-3.6	-20
	n	62	62	61	57	65	65	65	65	11	65	65	26	65	65	23	11
Ossidiana	Mean	35.8	6.97	36.0	-88.9	9,106	416	943	457	2	16,026	54	26	2,068	604	n.d.	n.d.
	SD	1.8	0.14	20.7	97.3	4,491	131	385	113	1	7,685	26	5	965	196	-	-
	Max	38.3	7.7	61.5	169.9	12,822	559	1,270	617	4	22,013	83	32	3,041	772	-	-
	Min	31.9	6.78	9.8	-264.0	1,858	209	325	276	1	3,572	9	20	611	302	-	-
	n	73	70	41	34	20	20	20	20	20	20	20	4	20	46	-	-
Le Schiccihole	17/04/03	15.9	6.62	1.1	n.m.	63	30	30	159	7	119	n.d.	n.d.	403	403	-6.2	-34
Seawater	23/05/07	21.1	8.14	42.9	98.0	11,648	415	1,477	487	n.d.	21,798	76	n.d.	171	171	0.6	6

^aAll data are reported in terms of Min, Max, and Mean values. SD, standard deviation; n, number of samples; n.d., data. Data relative to the Le Schiccihole cold spring sample and a seawater sample collected in proximity of the coast of Stromboli Island are also given for comparison. Ion concentrations are expressed in mg kg⁻¹. Isotope values are expressed in parts per thousand (‰) with respect to the Vienna standard mean ocean water (VSMOW) international reference.

permeable deposits or sealed altered lavas that result in low infiltration rates. For these reasons, exploration drilling aimed at finding thermal waters in the remnant part of the island was unproductive.

Nowadays, there are about 10 thermal wells clustered in a limited area on the northeastern corner of Stromboli (Plate 2), two of which were drilled for scientific purposes in 2004 (Saibbo well) and 2005 (COA well). Thermal wells are lo-

cated at elevations between 5 and 70 m asl. Their respective phreatic levels are reasonably constant and slightly lower than the seawater level. This suggests the occurrence of unconfined or partially confined aquifers hosted within a spatially homogeneous porous media (i.e., pyroclastic deposits) that are hydraulically isolated from seawater probably due to the presence of impermeable layers such as altered lava flows.

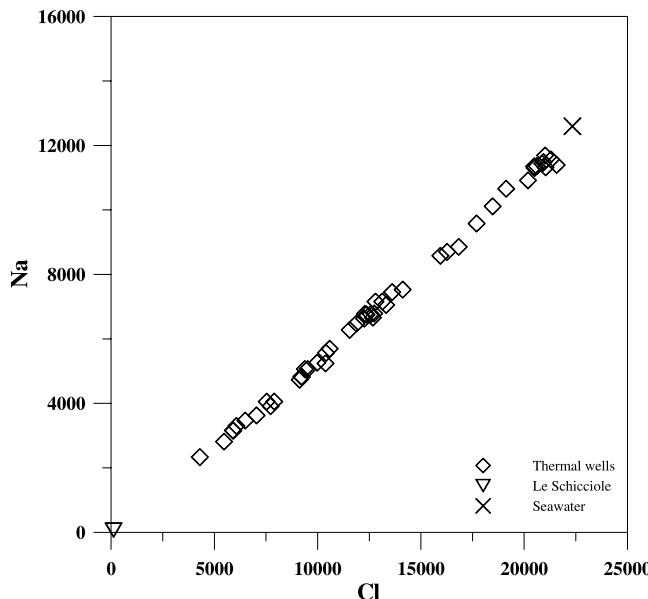


Figure 1. Binary diagram showing Na versus Cl contents in the groundwater of Stromboli. All the samples fall along the seawater ratio line. Concentrations are expressed in mg kg^{-1} . Selected data from the INGV-PA internal database.

3.1. Water Geochemistry

Physico-chemical parameters and the chemical and the isotope composition of waters collected from five selected thermal wells (Fulco, Limoneto, Saibbo, COA, and Zurro) are listed in Table 2. This table also lists analytical data relative to the Le Schicciore (LS) cold spring sample (temperature = 15.9°C) and are also shown together with a seawater sample collected near the beach of Punta Lena. Data are extracted from the INGV-PA internal database but those from 1999 to 2000 and from 2002 to 2003 which were published by Carapezza and Inguaggiato [2001] and Capasso *et al.* [2005], respectively.

The water temperature which was almost constant over time, ranged from 35.5°C (Zurro) to 42.8°C (Fulco). The pH was nearly neutral or slightly acidic ranging between 6.3 (Saibbo well) and 6.9 (Zurro well). The water chemistry was dominated by NaCl with an almost constant Na/Cl ratio over time and that was close to that of the seawater (Figure 1). The total dissolved solids (TDS) content varied from 7.1 g l^{-1} (Fulco) to about 40 g l^{-1} (Zurro).

In the Cl– HCO_3 – SO_4 ternary diagram in Figure 2, all the collected waters show a trend from seawater composition toward the composition of the Le Schicciore sample. The latter sample

3. GEOCHEMICAL INVESTIGATIONS ON THERMAL WATERS

In this section is reported an overview of the most relevant results concerning a pluriannual geochemical monitoring of thermal waters at Stromboli. The thermal waters are periodically sampled to assess the magmatic contribution of fluids and heat to the thermal aquifers and to model the gas–water–rock interactions in the thermal aquifers of Stromboli. Seawater and freshwater from the only one cold discharge at Stromboli island (Le Schicciore cold spring) were also collected. The concentration of the major and some of the minor dissolved elements and the chemical composition of the main dissolved gas phase were determined in the collected groundwater. Moreover, a rain gauge network consisting of six stations was installed to collect suitable samples for chemical and isotope analyses (Plate 1). Precipitation was sampled approximately bimonthly between October 2003 and October 2005 [Liotta *et al.*, 2006]. Finally, the dD and $d^{18}\text{O}$ values of waters, $d^{13}\text{C}_{\text{CO}_2}$ values and $^3\text{He}/^4\text{He}$ ratios in the gas phase dissolved in thermal waters have also been measured [Carapezza and Federico, 2000; Capasso *et al.*, 2005, unpublished data from INGV-PA internal database].

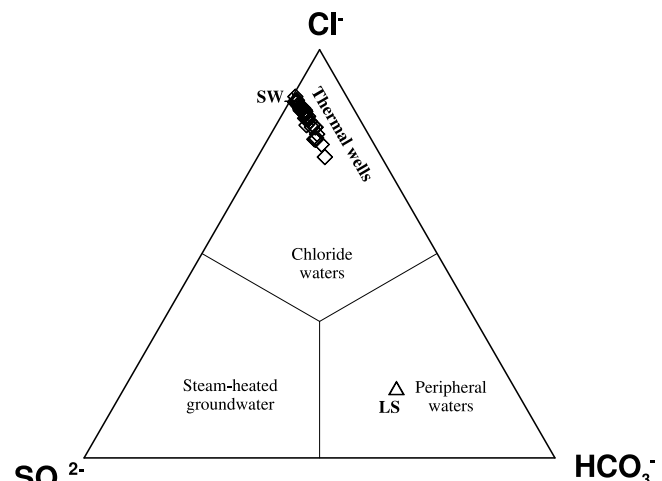


Figure 2. Cl– SO_4 – HCO_3 ternary diagram. All the collected waters show a trend from seawater composition toward that of Le Schicciore sample. In volcanic areas, the HCO_3 -rich end-member has been related to peripheral waters [Giggenbach, 1991] resulting from the interaction between groundwater and magmatic CO_2 . Selected data from the INGV-PA internal database.

falls within the “peripheral waters” field typical for waters that reflect the dissolution of CO₂-rich magmatic fluids into meteoric waters [Giggenbach, 1991]. Due to its relatively low salinity, it is a sample representative of a low degree of gas–water interaction, as better described in the following subsection.

Stable isotope data of collected waters are plotted on a δD–δ¹⁸O diagram (Figure 3), which also includes the Mediterranean meteoric water reference line (MMWL δD = 8 × δ¹⁸O + 22, *Gat and Carmi* [1970]) and the local meteoric water line (LMWL, δD = 6.5 × δ¹⁸O + 6.7, *Liotta et al.* [2006]). δD and δ¹⁸O values range from −34‰ (Fulco) to +6‰ (Zurro) and from −5.8‰ (Fulco) to +0.9‰ (Zurro), respectively. All the sample points appear on a mixing line between the seawater composition (δD = 6‰ and δ¹⁸O = 0.6‰) and the composition of mean annual weighted precipitation (δD ≈ −40‰ and δ¹⁸O ≈ −7.2‰) at Stromboli [*Liotta et al.*, 2006], thus suggesting that the thermal waters result from mixing in different proportions between these two end-members. This process is also indicated by the strong correlation between δ¹⁸O and Cl contents (Figure 4).

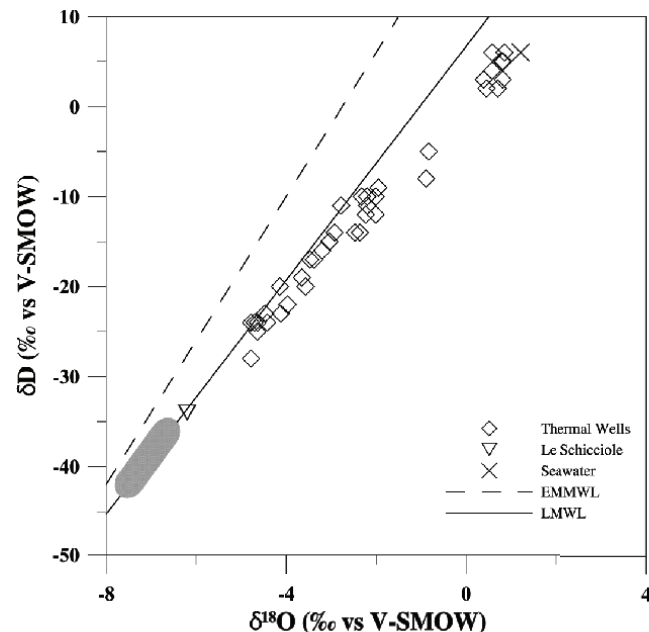


Figure 3. Diagram showing δD versus δ¹⁸O in the groundwater of Stromboli. Open symbols indicate thermal (squares) and shallow (diamonds) groundwater samples. The dotted area encloses the meteoric recharge composition [*Liotta et al.*, 2006]. The solid line is the local meteoric water line (LMWL, *Liotta et al.* [2006]), and the dashed line is the Eastern Mediterranean meteoric water line (EMMWL [*Gat and Carmi*, 1970]). Selected data from the INGV-PA internal database.

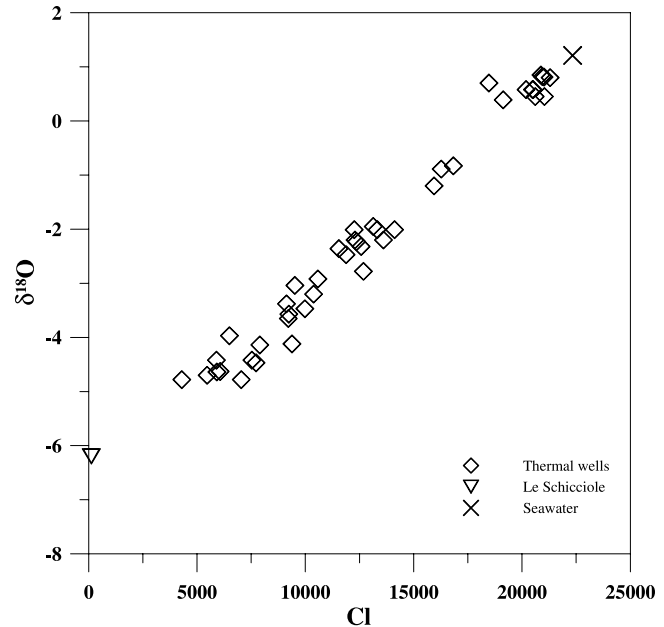


Figure 4. Correlation plot of δ¹⁸O versus Cl. All samples fall between two end-members: seawater and shallow groundwater. Concentrations are expressed in mg kg^{−1}, and isotope values are reported in δ values versus Vienna standard mean ocean water (VSMOW).

3.2. Water–Rock Interaction Processes

Figure 5 plots the SO₄, Ca, K, DIC (i.e., dissolved inorganic carbon), Mg, and Br contents in the sampled waters against the Cl content. Although the thermal waters of Stromboli are characterized by a wide range of Cl concentrations and therefore also of salinity, the compositional ratios vary only slightly among the wells. Therefore, thermal waters seem to result from a simple mixing between meteoric-like waters and the saline waters, where the former is similar to seawater.

By assuming that all dissolved Cl has a marine origin and that it behaves conservatively, meaning that this element is not involved in other geochemical processes, the hydrothermal saline end-member should have a Cl content equal to seawater (i.e., 22,300 mg kg^{−1}). Following the approach used by *Taran et al.* [2002], the total chemical composition of the hydrothermal saline end-member was extrapolated to a Cl concentration of 22,300 mg kg^{−1}. The obtained chemical composition was characterized by a slightly lower SO₄ concentrations but much higher Ca, K, and DIC contents than those of seawater with Na, Mg, and Br contents being comparable to those of seawater.

This indicates that the pristine seawater composition is chemically modified by leaching high-K calcalkaline to shoshonitic volcanic rocks of the aquifer and weathering of

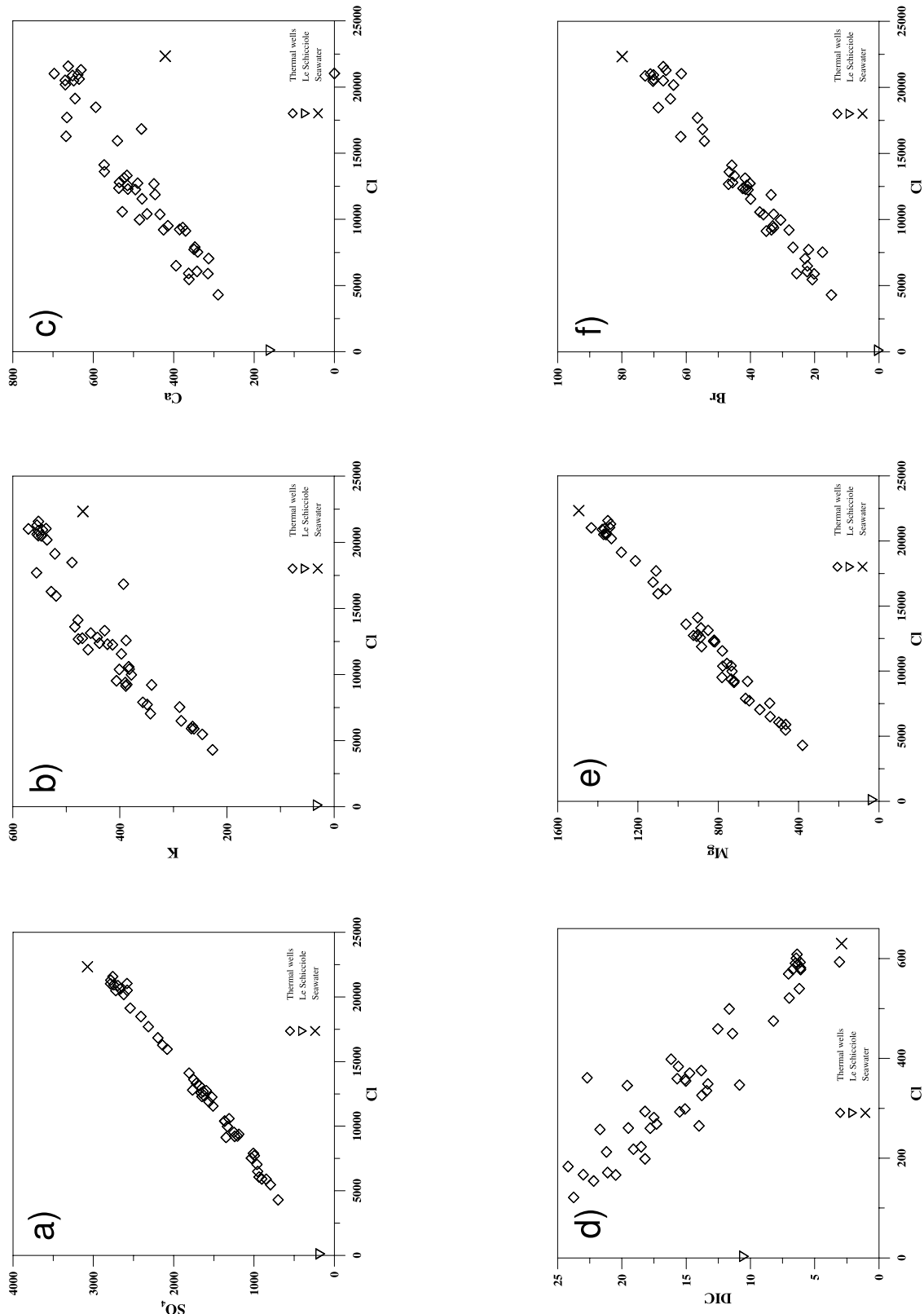


Figure 5. Major and minor ions plotted versus Cl contents in Strombolian groundwater. Mg/Cl (e), DIC/Cl (d), and Br/Cl (f) reflect a seawater composition, whereas K/Cl (b), Ca/Cl (c), and DIC/Cl (d) differ significantly from the seawater ratio being enriched in K , Ca , and DIC . The $\text{SO}_4^{2-}/\text{Cl}$ ratio (a) is slightly lower than that of seawaters. Concentrations are expressed in mg kg^{-1} , except for panel (d) which is in mmol l^{-1} . Selected data from the INGV-PA internal database.

plagioclase that in Strombolian rocks have 45 to 90% anorthite content [Francalanci, 1993]. On the contrary, SO_4 may be involved in reduction reactions favored by the prevailing reduction condition in the thermal aquifer.

Similarly, we have also estimated the chemical composition of the diluted end-member. In this case, we extrapolated to a Cl content of 117 mg kg^{-1} which is the average Cl content in the rainwater collected at the summit crater [Liotta *et al.*, 2006]. The obtained composition roughly coincides with that of the Le Schicciola cold spring. The most relevant differences between the inferred and the measured Le Schic-

ciole compositions are in the depletion both in DIC and in K contents. These differences could be due to a lower degree of interaction between meteoric recharge and CO_2 -rich deep fluids leading to reduced leaching of rocks as well.

3.3. Dissolved Gas Geochemistry

Table 3 reports the concentrations of dissolved gaseous species expressed in cubic centimeters per liter (cc l^{-1}) of water at standard temperature and pressure (STP) condition together with the concentration of dissolved gases in a water

Table 3. Chemical and Isotope Compositions of Gas Dissolved in Thermal Wells Reported in Terms of Mean, Max, and Min Values^a

Sample		He	H_2	O_2	N_2	CO	CH_4	CO_2	$\delta^{13}\text{C}_{\text{TDIC}}$	${}^3\text{He}/{}^4\text{He}$
Zurro	Mean	7.62E-04	1.01E-02	0.6	15.0	2.22E-04	6.44E-03	20.3	-0.8	4.16
	SD	8.34E-04	2.87E-02	0.7	3.4	2.27E-04	9.67E-03	19.3	1.9	0.14
	Max	6.47E-03	2.04E-01	3.2	29.1	1.18E-03	8.34E-02	140.9	4.5	4.41
	Min	1.48E-04	3.39E-04	0.1	3.6	7.94E-06	1.83E-04	1.8	-5.8	3.74
	n	61	64	109	127	68	121	127	108	91
Fulco	Mean	8.58E-04	7.22E-03	0.9	11.5	4.21E-04	4.44E-03	159.6	1.3	4.16
	SD	1.93E-03	1.86E-02	0.6	2.7	4.23E-04	4.22E-03	35.0	0.9	0.16
	Max	1.58E-02	1.02E-01	3.0	19.2	2.28E-03	3.51E-02	292.3	1.6	4.49
	Min	1.73E-04	2.19E-04	0.1	5.6	1.89E-05	9.06E-05	76.1	-0.6	3.46
	n	64	55	122	129	53	112	129	123	88
Saibbo	Mean	7.36E-04	7.14E-03	0.6	12.3	3.19E-04	4.95E-03	129.4	0.3	4.24
	SD	2.39E-04	1.49E-02	2.2	1.5	3.71E-04	1.14E-03	23.7	0.6	0.09
	Max	1.38E-03	5.90E-02	13.8	16.6	1.71E-03	6.46E-03	183.5	2.0	4.44
	Min	2.56E-04	3.05E-04	0.0	8.6	2.54E-05	1.28E-03	62.8	-0.8	4.06
	n	39	25	39	39	37	39	39	32	40
Limoneto	Mean	1.27E-03	8.15E-03	0.6	13.6	1.26E-04	7.67E-03	66.4	0.8	4.22
	SD	5.47E-04	1.24E-02	0.4	2.1	2.00E-04	4.76E-03	17.2	0.7	0.08
	Max	2.90E-03	4.15E-02	1.3	20.2	8.81E-04	2.24E-02	94.5	2.2	4.43
	Min	6.04E-04	4.05E-04	0.0	6.4	8.73E-06	1.93E-03	8.1	-1.0	4.07
	n	39	25	37	38	17	39	39	41	40
COA	Mean	1.13E-03	4.09E-03	0.1	14.6	5.00E-05	1.87E-02	83.5	-0.4	4.24
	SD	1.65E-04	5.10E-03	0.1	1.5	6.80E-05	1.28E-02	12.0	0.3	0.07
	Max	1.35E-03	1.56E-02	0.5	17.0	1.87E-04	4.00E-02	104.4	0.3	4.37
	Min	8.30E-04	3.94E-04	0.0	12.7	7.14E-06	7.01E-03	66.8	-0.8	4.08
	n	11	9	11	11	6	11	11	7	14
Cusolito	Mean	9.95E-04	1.86E-02	0.8	14.7	2.10E-04	4.65E-03	58.3	1.2	4.16
	SD	1.59E-03	5.26E-02	0.6	3.0	1.55E-04	6.33E-03	30.1	1.2	0.16
	Max	8.56E-03	2.83E-01	3.1	25.9	7.12E-04	4.09E-02	219.1	4.9	4.50
	Min	1.99E-04	1.29E-04	0.1	8.0	4.23E-05	2.39E-04	22.9	-0.4	3.73
	n	26	35	73	75	26	74	75	73	49
Ossidiana	Mean	1.15E-03	7.09E-03	1.7	13.6	1.98E-04	2.95E+00	45.6	1.3	n.d.
	SD	6.37E-04	1.45E-02	1.1	4.4	2.78E-04	9.38E+00	26.8	1.1	n.d.
	Max	2.33E-03	6.79E-02	3.6	27.9	1.12E-03	3.43E+01	86.7	2.7	n.d.
	Min	3.06E-04	3.58E-04	0.1	6.5	2.27E-05	1.30E-04	0.5	-0.1	n.d.
	n	10	22	31	33	26	32	33	16	n.d.
ASW		4.81E-05	n.d.	6.4	12	n.d.	n.d.	0.3	0	1

^aSD, standard deviation; n, number of samples; n.d., no data. He, H_2 , CO, and CH_4 contents are expressed in ppmVol, while O_2 , N_2 , and CO_2 in volumetric percentages. $\delta^{13}\text{C}_{\text{TDIC}}$ values are given in parts per thousand (‰) with respect to the Vienna PeeDee belemnite (VPDB). Helium isotope ratios (${}^3\text{He}/{}^4\text{He}$) are expressed as R/Ra. Air saturated water (ASW) composition is also given for reference.

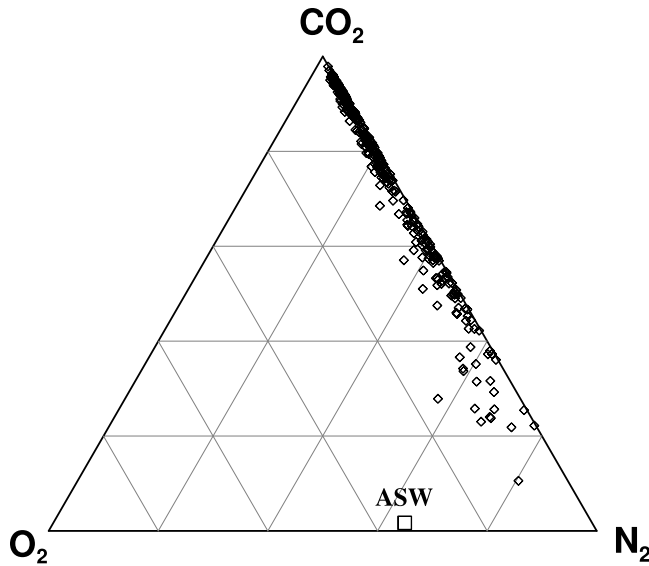


Figure 6. $\text{O}_2\text{--N}_2\text{--CO}_2$ ternary diagram. All the samples are characterized by an O_2/N_2 ratio lower than that of air saturated water (ASW) due to oxygen consumption associated with reduction reactions.

sample equilibrated with air [air saturated water (ASW)]. This table also lists the carbon isotope composition of the total dissolved inorganic carbon ($\delta^{13}\text{C}_{\text{TDIC}}$) as well as the helium isotope ratios.

O_2/N_2 ratios lower than that of ASW (Figure 6) are probably due to the oxygen consumption associated to reduction processes [Capasso et al., 2005], while high CH_4 contents, as high as $1.1 \times 10^{-2} \text{ cc l}^{-1}$ STP [Capasso et al., 2005] are produced within the hydrothermal systems itself rather than derived from a magmatic source.

The dissolved helium shows contents exceeding that of ASW by at least one order of magnitude (He_{ASW} at $25^\circ\text{C} = 4.5 \times 10^{-5} \text{ cc l}^{-1}$ STP). The dissolved CO_2 contents are quite high between 20 and 30 cc l^{-1} STP (Zurro) and 200 cc l^{-1} STP (Fulco; Figure 7), mainly due to its high solubility in water (β_{CO_2} at $25^\circ\text{C} = 862 \text{ cc l}^{-1}$ STP, Whitfield [1978]).

The $\delta^{13}\text{C}_{\text{TDIC}}$ values range between -5.8 and $+4.5\text{\textperthousand}$ versus PDB. This geochemical parameter represents the average of the isotopic composition of the dissolved inorganic carbon species (CO_{2g} , HCO_3^- , and CO_3^{2-}) weighted on their respective content.

When the $\delta^{13}\text{C}_{\text{TDIC}}$ values as well as the concentration of each dissolved inorganic carbon species are known, the isotopic composition of the free CO_2 in equilibrium with thermal waters of Stromboli was computed [Capasso et al., 2005] for an equilibrium temperature of 40°C which corresponds to the mean sampling temperature.

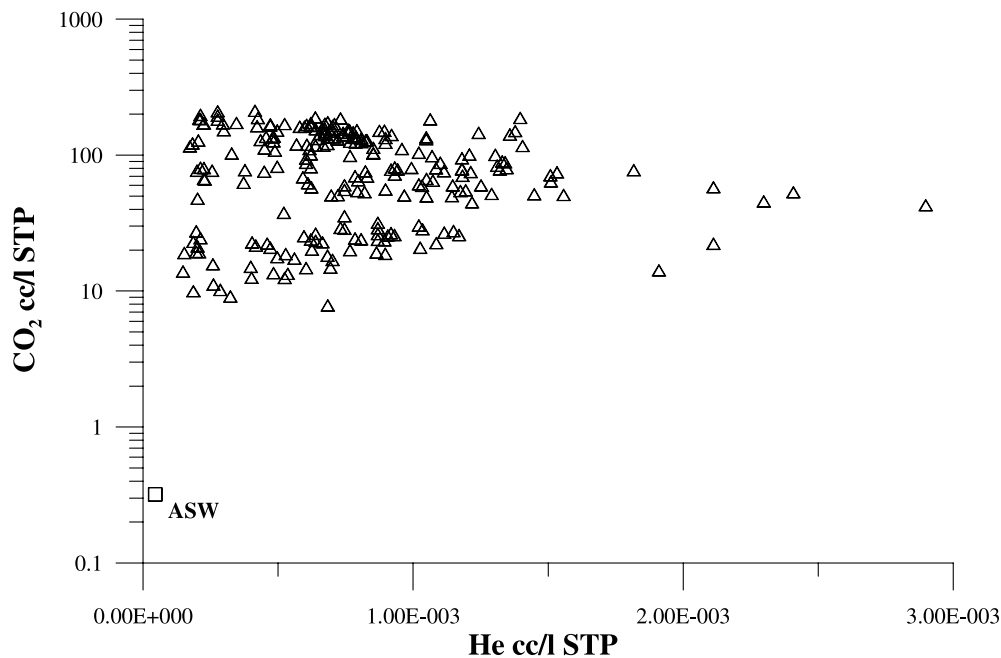


Figure 7. Correlation plot of He versus CO_2 . Dissolved carbon dioxide and helium contents exceed those of ASW by up to three and up to two orders of magnitude, respectively. Both gases have a clear magmatic origin (see text).

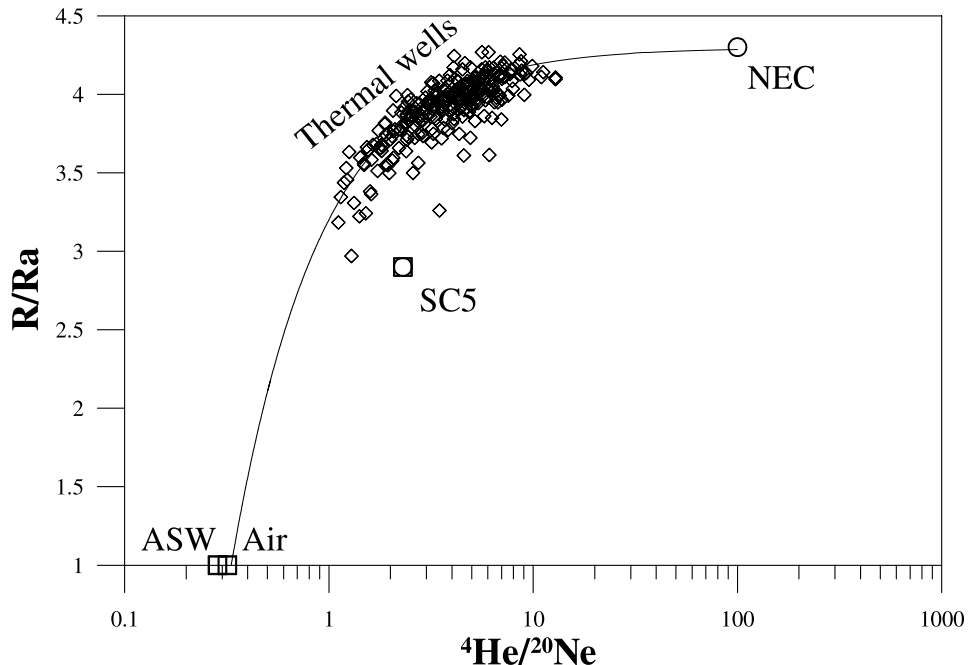


Figure 8. Plot of R/Ra versus He/Ne molar ratios. All the samples lie on a theoretical mixing curve between an atmospheric component (air or ASW) and the most representative magmatic end-member (NEC sample, *Finizola and Sortino* [2003]). The mean composition at site SC5 is also shown.

The obtained $\delta^{13}\text{C}_{\text{CO}_2}$ values ranged between $-4.4\text{\textperthousand}$ and $-1.1\text{\textperthousand}$ versus VPDB. These values are slightly more negative than the carbon isotope composition of the SC5 fumarole, with this difference being attributed to isotope fractionation processes between deep and shallow fluids.

The isotope ratios of helium dissolved in the thermal waters at Stromboli, after correcting for air contamination using the method proposed by *Sano et al.* [1993], range between 3.4 and 4.5 Ra [*Inguaggiato and Rizzo*, 2004; *Capasso et al.*, 2005]. The measured values are very close to those found by *Finizola and Sortino* [2003] in the high-temperature fumarole near the northeast crater formed during the 2003 eruption, whose average value (4.3 Ra) was considered as the magmatic end-member for Stromboli (Figure 8).

On the basis of the He/CO₂ ratios and the calculated $\delta^{13}\text{C}_{\text{CO}_2}$ values in equilibrium with thermal waters, *Capasso et al.* [2005] proposed a geochemical model for the origin of fluids dissolved in the Stromboli thermal aquifer. A vapor phase is partially separated from a boiling aquifer heated by magmatic fluids at a temperature of about 130°C and a pres-

sure of 2.5 bars. Rising fluids that separate from the boiling aquifer condense in the shallow aquifer at about 40°C.

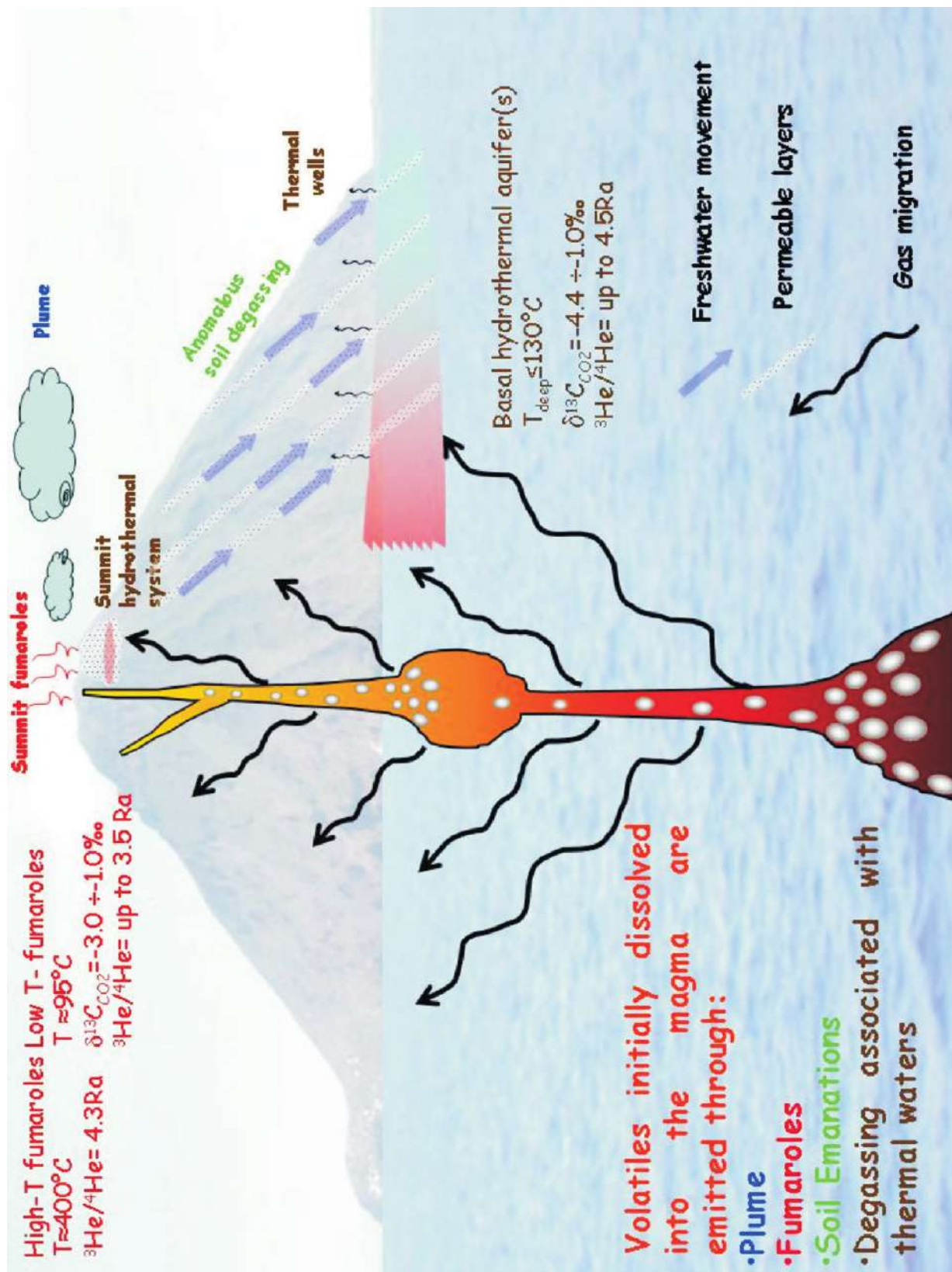
Therefore, gas phase dissolved in thermal waters of Stromboli derived from magmatic volatiles and helium isotope ratios in the dissolved gas provide the same geochemical information as the high-temperature crater fumaroles.

Temporal variations observed in the helium isotope ratios dissolved in the thermal waters of Stromboli, revealed a clear uprising of new batches of ³He-rich magma, a few months preceding the 2002–2003 eruption [*Capasso et al.*, 2005].

4. CONCLUDING REMARKS

Chemical and isotopic data on fluids discharged from the Stromboli volcano allow the main geochemical processes affecting the deep fluids during their rise toward the surface to be identified. Moreover, the composition of the end-members feeding the geothermal system has been calculated. Plate 3 shows the formulated geochemical model explaining the fluid circulation. This proposed model considers Strom-

Plate 3. (Opposite) Representative scheme of fluid circulation at Stromboli. Most of the volatiles (around 90% of the total mass) are released through the open-conduit degassing, with a gas output of approximately of $3 \times 10^6 \text{ Mg year}^{-1}$ [*Allard et al.*, 1994; *Allard et al.*, this volume]. Rising fluids give origin to high-temperature fumaroles (up to 410°C), located close to active craters, low-temperature fumaroles (as the SC5 site) located in the Pizzo area, and anomalous CO₂ fluxes from soil at the summit.



boli volcano as a natural system where the totality of energy and mass of deep fluids coming from the magmatic chamber is discharged at the surface following different pathways. The volatiles initially dissolved into the magma are emitted via the plume, fumaroles, soil emanations, and as fluids associated with thermal waters.

More than 90% of the gas is released from the open-conduit degassing system. The total output of gas emitted from the plume was estimated to be of the order of $10^6 \text{ Mg year}^{-1}$ [Allard *et al.*, 1994; Allard *et al.*, this volume].

Gas emitted both from high-temperature fumaroles (up to 410°C) and from low-temperature fumaroles located at the summit showed chemical and isotope signatures of an undoubtedly magmatic origin.

Anomalous CO_2 fluxes from soil were recognized both at the summit and in peripheral areas. Summit zones are characterized by extremely high fluxes due to gases being released laterally from the conduit (primary degassing). Diffusive gas emissions at low altitude probably derive from volatiles separated from boiling and/or degassing thermal aquifers (secondary degassing).

Thermal water originates from mixing between seawater and meteoric waters. The chemical composition of both of these end-members is modified from their pristine ones by leaching of host rocks and the dissolution of the CO_2 -rich gas phase as well.

Based on their chemical composition and the isotopic signature, volatile species dissolved in the thermal waters of Stromboli are clearly of magmatic origin and reveal intense gas–water interaction processes. Dissolved He and CO_2 contents, as well as the helium isotope ratios highlighted significant variations over time related to volcanic activity.

Such features highlight the scientific relevance of these peripheral manifestations, as suitable sites for monitoring the volcanic activity of Stromboli, especially during periods of intense Strombolian activity when summit areas are inaccessible.

REFERENCES

- Aiuppa, A., and C. Federico (2004), Anomalous magmatic degassing prior to the 5th April 2003 paroxysm on Stromboli, *Geophys. Res. Lett.*, 31, L14607, doi:10.1029/2004GL020458.
- Aiuppa, A., A. Allard, W. D'Alessandro, S. Giammanco, F. Parella, and M. Valenza (2004), Magmatic gas leakage at Mount Etna (Sicily, Italy): Relationships with the volcanic-tectonic structures, the hydrological pattern and the eruptive activity, in *Mt. Etna: Volcano Laboratory, Geophys. Monogr. Ser.*, vol. 143, edited by A. Bonaccorso *et al.*, pp. 129–145, AGU, Washington, D. C.
- Allard, P., J. Carbonnelle, N. Metric, H. Loyer, and P. Zettwoog (1994), Sulfur output and magma degassing budget of Stromboli volcano, *Nature*, 368, 326–330.
- Allard, P., P. Jean-Baptiste, W. D'Alessandro, F. Parella, B. Parisi, and C. Flehoc (1997), Mantle-derived helium and carbon in groundwaters and gases of Mount Etna, Italy, *Earth Planet. Sci. Lett.*, 148, 501–516.
- Allard P., M. Burton, A. Aiuppa, T. Caltabiano, C. Federico, A. La Spina, C. Oppenheimer, and G. Salerno (2008), Gas emissions and plumbing system, this volume.
- Bonaccorso, A. (1998), Evidence of a dyke-sheet intrusion at Stromboli volcano inferred through continuous tilt, *Geophys. Res. Lett.*, 25, 4225–4228.
- Brusca, L., S. Inguaggiato, M. Longo, P. Madonia, and R. Maugeri (2004), The 2002–2003 eruption of Stromboli (Italy): Evaluation of the volcanic activity by means of continuous monitoring of soil temperature, CO_2 flux, and meteorological parameters, *Geochem. Geophys. Geosyst.*, 5, Q12001, doi:10.1029/2004GC000732.
- Capasso, G., and S. Inguaggiato (1998), A simple method for the determination of dissolved gases in natural waters. An application to thermal waters from Vulcano Island, *Appl. Geochem.*, 13, 631–642.
- Capasso G., W. D'Alessandro, R. Favara, S. Inguaggiato, and F. Parella (2001), Interaction between the deep fluids and the shallow groundwaters on Vulcano island (Italy), *J. Volcanol. Geotherm. Res.*, 108, 187–198.
- Capasso, G., M. L. Carapezza, C. Federico, S. Inguaggiato and A. Rizzo (2005), Geochemical variations in fluids from Stromboli volcano (Italy): Early evidences of magma ascent during 2002–2003 eruption, *Bull. Volcanol.*, 68, 118–134, doi:10.1007/s00445-005-0427-5.
- Carapezza, M. L., and C. Federico (2000), The contribution of fluid geochemistry to the volcano monitoring of Stromboli, *J. Volcanol. Geotherm. Res.*, 95, 227–245.
- Carapezza, M. L., and S. Inguaggiato (2001), Interaction between thermal waters and CO_2 -rich fluids at Stromboli, in *Proceedings of the Tenth International Symposium on Water-Rock Interaction*, vol. 2, edited by R. Cidu, pp. 791–794, A. A. Balkema, Rotterdam, Netherlands.
- Carapezza, M. L., S. Inguaggiato, L. Brusca, and M. Longo (2004), Geochemical precursors of the activity of an open-conduit volcano: The Stromboli 2002–2003 eruptive events, *Geophys. Res. Lett.*, 31, L07620, doi:10.1029/2004GL019614.
- Deines, P., D. Langmuir, and R. S. Harmon (1974), Stable carbon isotope ratios and the existence of a gas phase in the evolution of carbonate groundwaters, *Geochim. Cosmochim. Acta*, 38, 1147–1164.
- Falsaperla, S., G. Lanzafame, V. Longo, and S. Spampinato (1999), Regional stress field in the area of Stromboli (Italy): Insights into structural data and crustal tectonic earthquakes, *J. Volcanol. Geotherm. Res.*, 88, 147–166.
- Federico, C., A. Aiuppa, R. Favara, S. Gurrieri, and M. Valenza (2004), Geochemical monitoring of groundwaters (1998–2001) at Vesuvius volcano (Italy), *J. Volcanol. Geotherm. Res.*, 133, 81–104.
- Federico, C., L. Brusca, M. L. Carapezza, G. Cigolini, S. Inguaggiato, A. Rizzo, and D. Rouwet (2008), Geochemical variations before the eruption onset, this volume.
- Finizola, A., and F. Sortino (2003), Preliminary model of fluid circulation at Stromboli volcano inferred by water and gas

- geochemistry, paper presented at 7th International conference on gas geochemistry, Freiberg, Germany, 22–26 Sept.
- Finizola, A., F. Sortino, J.-F. Lénat, and M. Valenza (2002), Fluid circulation at Stromboli volcano (Aeolian Islands, Italy) from self-potential and soil gas surveys, *J. Volcanol. Geotherm. Res.*, 116(1–2), 1–18.
- Finizola, A., F. Sortino, J. F. Lénat, M. Aubert, M. Ripepe, and M. Valenza (2003), The summit hydrothermal system of Stromboli. New insights from self-potential, temperature, CO₂ and fumarolic fluid measurements, with structural and monitoring implications, *Bull. Volcanol.*, 65, 486–504.
- Finizola, A., A. Revil, and F. Sortino (2008), Fluid circulation, and permeability changes in the summit area, this volume.
- Francalanci, L. (1993) Mineral chemistry of Stromboli volcanics as indicator of magmatic processes, *Acta Vulcanol.*, 3, 99–113.
- Gat, J. R., and I. Carmi (1970), Evolution of the isotopic composition of atmospheric waters in the Mediterranean Sea area, *J. Geophys. Res.*, 75, 3039–3048.
- Giammanco, S., S. Inguaggiato, M. Valenza (1998), Soil and fumarole gases of Mount Etna: Geochemistry and relations with volcanic activity, *J. Volcanol. Geotherm. Res.*, 81, 297–310.
- Giggenbach, W. F. (1991), Chemical techniques in geothermal exploration, in *Application of Geochemistry in Geothermal Reservoir Development*, F. D'amore coordinator, pp. 119–144, UNITAR/UNDP, Rome, Italy.
- Inguaggiato, S., and A. Rizzo (2004), Dissolved helium isotope ratios in ground-waters: A new technique based on gas–water re-equilibration and its application to a volcanic area, *Appl. Geochim.*, 19, 665–673.
- Inguaggiato, S., G. Pecoraino, and F. D'Amore (2000), Chemical and isotopical characterisation of fluid manifestations of Ischia Island (Italy), *J. Volcanol. Geotherm. Res.*, 99, 151–178.
- Inguaggiato S., A. L. Martin-Del Pozzo, A. Aguayo, G. Capasso, and R. Favara (2005), Isotopic, chemical and dissolved gas constraints on spring water from Popocatepetl (Mexico): Evidence of gas–water interaction magmatic component and shallow fluids, *J. Volcanol. Geotherm. Res.*, 141, 91–108.
- Liotta, M., L. Brusca, F. Grassa, S. Inguaggiato, M. Longo, and P. Madonia (2006), Geochemistry of rainfall at Stromboli volcano (Aeolian Islands): Isotopic composition and plume–rain interaction, *Geochem. Geophys. Geosyst.*, 7, Q07006, doi:10.1029/2006GC001288.
- Martni, M. (1991), Stromboli, report activity, *Bull. Global Volcanism Network*, 16, 20–21.
- Oppenheimer, C. (2003), Volcanic degassing, in *Treatise on Geochemistry*, vol. 3, edited by H. D. Holland and K. K. Turekian, pp. 123–166, Elsevier-Pergamon, Oxford, U.K.
- Rizzo A., A. Aiuppa, G. Capasso, M. L. Carapezza, F. Grassa, S. Inguaggiato, and M. Longo (2008), The 5th April 2003 paroxysm at Stromboli: A review of the geochemical observations, this volume.
- Sano, Y., N. Takahata, Y. Mahara, and S. Yasuike (1993), Precise measurement of helium isotopes in groundwater, *J. Sci. Hiroshima Univ., Ser. C*, 9, 603–610.
- Taran, Y., T. P. Fischer, B. Pokrosky, Y. Sano, M. A. Armienta, and J. L. Macias (1998), Geochemistry of the volcano–hydrothermal system of El Chichón Volcano, Chiapas, Mexico, *Bull. Volcanol.*, 59, 436–449.
- Taran, Y. A., S. Inguaggiato, M. Marin, and L. M. Yurova (2002), Geochemistry of fluids from submarine hot springs at Punta de Mita, Nayarit, Mexico, *J. Volcanol. Geotherm. Res.*, 115, 329–338.
- Varley, N. R., and A. Armienta (2001), The absence of diffuse degassing at Popocatepetl volcano (Mexico), *Chem. Geol.*, 177, 157–173.
- Whitfield M. (1978), Activity coefficients in natural waters, in *Activity Coefficients in Electrolyte Solutions*, vol. II, edited by R. M. Pytkowicz, pp. 153–300, CRC Press, Boca Raton, Fla.
- Zanchi, A., and L. Francalanci (1989), Analisi geologico-strutturale dell’isola di Stromboli: Alcune considerazioni preliminari, *Boll. GNV*, 5, 1027–1044.

F. Grassa, S. Inguaggiato, and M. Liotta, Istituto Nazionale di Geofisica e Vulcanologia, Sezione di Palermo, Via Ugo La Malfa, 153-90146 Palermo, Italy. (f.grassa@pa.ingv.it)

Crater Gas Emissions and the Magma Feeding System of Stromboli Volcano

Patrick Allard,^{1,2} Alessandro Aiuppa,³ Mike Burton,¹ Tommaso Caltabiano,¹ Cinzia Federico,⁴
Giuseppe Salerno,^{1,5} and Alessandro La Spina^{1,3}

Quiescent and explosive magma degassing at Stromboli volcano sustains high-temperature crater gas venting and a permanent volcanic plume which constitute key sources of information on the magma supply and dynamics, the physical processes controlling the explosive activity and, more broadly, the volcano feeding system. The chemical composition and the mass output of these crater emissions (gases, trace metals, radioactive isotopes) were measured using different methodologies: within-plume airborne measurements, ground-based plume filtering, and/or in situ analysis, remote UV and open-path Fourier transform infrared absorption spectroscopy. The results obtained, summarized in this paper, demonstrate a primary control of the magmatic gas phase on the eruptive regime and the budget of the volcano. The large excess gas discharge, compared with the lava extrusion rate, and the source depth of slug-driven Strombolian explosions evidence extensive separate gas transfer across the volcano conduits, promoted by the high gas content (vesicularity) and then permeability of the shallow basaltic magma. Combined with data for volatiles dissolved in olivine-hosted melt inclusions, the results provide updated constraints for the magma supply rate ($\sim 0.3 \text{ m}^3 \text{ s}^{-1}$ on average), the ratio of intrusive versus extrusive magma degassing (~ 15), and the amount of unerupted degassed magma that should be convectively cycled back in conduits and accumulated beneath the volcano over time ($\sim 0.25 \text{ km}^3$ in the last three decades). The results also provide insight into the possible triggering mechanism of intermittent paroxysmal explosions and the geochemical signals that might allow forecasting these events in the future.

¹Istituto Nazionale di Geofisica e Vulcanologia, Sezione di Catania, Catania, Italy.

²Groupe des Sciences de la Terre, Laboratoire Pierre Sue, CNRS-CEA, Gif sur Yvette, France.

³Università di Palermo, CFTA, Palermo, Italy.

⁴Istituto Nazionale di Geofisica e Vulcanologia, Sezione di Palermo, Palermo, Italy.

⁵Department of Geography, Cambridge University, Cambridge, United Kingdom.

The Stromboli Volcano: An Integrated Study of the 2002–2003 Eruption
Geophysical Monograph Series 182
Copyright 2008 by the American Geophysical Union.
10.1029/182GM07

1. INTRODUCTION

It is now well established that the expanding gas phase (bubbles) that forms during magma decompression, by gradual exsolution of the dissolved volatile components (H_2O , CO_2 , S, Cl, F, etc.), exerts a key control on the dynamics of magma ascent and volcanic eruptions [Anderson, 1975; Giggenbach, 1996; Sparks, 2003]. Moreover, this gas phase has two main properties that make it a sensitive vector of information for volcano monitoring: (1) it is highly mobile, as gas bubbles can migrate differentially across magmas with sufficiently low viscosity (e.g., basalts), and (2) its chemical composition gradually evolves upon ascent, from CO_2 -rich

at great depth to water-halogen-rich at shallow depth, due to the differing solubility behavior of volatile components in function of pressure [e.g., *Anderson*, 1975; *Giggenbach*, 1996]. Therefore, the study of both dissolved volatiles in magmas and gas emissions from volcanoes unquestionably constitutes a key approach for improved understanding and forecasting of how volcanoes work.

Stromboli volcano, in the Aeolian island arc, provides a school-case illustration of those key properties and role of the magmatic gas phase. Stromboli is a very active ~2.5–3-km-high stratovolcano, with overall volume ~250 km³ [*Allard et al.*, 1994], whose only small upper part (~5 km³, 924 m above sea level [asl]) emerges from the Tyrrhenian Sea (Plate 1a). It is fed by a volatile-rich high-potassium (HK) arc basalt (Section 1.2) whose continuous degassing through open conduits (Plate 1b) sustains a permanent volcanic plume. But the most remarkable feature of Stromboli is the rhythmic explosive activity that has persisted at its crater vents (750 m asl) over the past 1400 years [*Rosi et al.*, 2000]. Every ~10 min on average, sudden jets or explosions lasting a few (5–10) seconds propel molten lava blocks, scoriae, and ash to 100–200 m above the vents (Plate 1c). These explosions have long been closely watched by thousands of tourists each year. They tap the crystal-rich (40–50%) magma column filling the upper volcano conduits, but are typically driven by the bursting of gas pockets, or slugs, that form by coalescence of smaller bubbles at greater depth and rise across the conduits [e.g., *Chouet et al.*, 1974; *Jaupart and Vergniolle*, 1989; *Burton et al.*, 2007a].

This long-lived standard activity of Stromboli, plus the quite monotonous chemical composition and mineralogy of its erupted products—at least over the last century [e.g., *Capaldi et al.*, 1978; *Francalanci et al.*, 1993, 2004; *Landi et al.*, 2006], point to remarkably steady-state conditions of magma supply, degassing, and differentiation in a plumbing system of broadly constant geometry. Temporary departures from that steady-state regime, however, occur on shorter time scales as manifested by temporal fluctuations in the frequency of Strombolian explosions and the magma level in conduits, but also by the intermittent occurrence (approximately two per year) of much more violent discrete explosions (thereafter termed as paroxysms) and more episodic (every 5–10 years) lava effusions [*Barberi et al.*, 1993]. Such variations in the eruptive activity imply dynamic changes in the feeding system, whose actual causes are not yet well understood. As a matter of fact, the insular position of Stromboli, most of which stands below sea water, has long hampered deep geophysical sounding of its feeding system. Hence, studying and monitoring its crater gas emissions is of peculiar interest since, according to the arguments introduced above, it can provide deep insight into the magmatic processes.

In this paper, we present an overview of our current knowledge of Stromboli's crater gas emissions and their implications for the magma dynamics and the volcano feeding system. The continuous degassing and steady explosive rhythm of this volcano make it a unique test site for gas studies, which attracted the interest of physicists and geochemists since volcano research began. Because direct access to the crater vents is prevented by hazard from the explosions, different types of airborne and ground-based measurements, using either in situ and/or remote sensing methodologies, have successively been tested and applied for analyzing Stromboli's crater gas emissions. Combined with recent data for volatiles dissolved in the magma (Section 1.2), the results obtained allow us to provide an updated assessment of the magmatic processes controlling the eruptive behavior of that remarkable volcano.

2. METHODOLOGIES FOR CRATER GAS STUDIES

The first volcanic fluids investigated on Stromboli were the crater rim fumaroles (200°–400°C). Initiated in the mid-1960s [*Tazieff and Tonani*, 1963; *Chaigneau*, 1965; *Tazieff*, 1970; Figure 1], their study was subsequently carried out through discrete sampling and analysis [*Allard et al.*, 1994, and references therein; *Carapezza and Federico*, 2000; *Finizola et al.*, 2003]. These fumaroles were found to contain magma-derived gas species, such as CO₂ and ³He-enriched mantle-derived helium [*Carapezza and Federico*, 2000], even though they are strongly diluted by meteoric steam from the shallow hydrothermal system that is centered on the upper volcanic conduits [*Finizola et al.*, 2003]. Interestingly, fast variations of the fumarolic gas concentrations were early observed in coincidence with the Strombolian explosions [*Tazieff and Tonani*, 1963; *Tazieff*, 1970]. This evidences a remote but true physical connection of these fluids with the conduit processes, as also later demonstrated for the CO₂-rich gas emanations which affect volcanic soils at the crater rim [*Carapezza et al.*, 2004].

Because the volcanic plume emissions are more directly linked to the degassing magma than fumaroles and of safer access than the hot magmatic gases, they became the target of repeated airborne measurements for about two decades since 1980 [*Allard et al.*, 1994, 1999, 2000]. The measurements included UV (correlation spectrometer [COSPEC]) remote sensing of the SO₂ plume flux (Figure 2), onboard analysis of within-plume gas concentrations (SO₂, CO₂, and H₂O), and sampling of the plume particulate matter (cascade impactor and filter-packs) for subsequent analysis of trace elements in laboratory (using neutron activation and inductively coupled plasma–mass spectrometry). However, airborne measurements are highly expensive and, therefore, were



Plate 1. Photos of (a) the subaerial cone of Stromboli volcano with its permanent gas plume, (b) the quiescent crater gas venting, and (c) explosive degassing during a Strombolian-type explosion. From P. Allard and T. Pfeiffer.



Figure 1. Geochemists (Franco Tonani and Yvan Elskens) with heavy protection studying Stromboli's crater rim fumaroles in the mid-1960s. Photo from H. Tazieff.

subsequently complemented then replaced by ground-based plume investigations with filter packs [Allard *et al.*, 2000; Aiuppa and Federico, 2004] and multigas sensors [Aiuppa *et al.*, 2005, 2007]. Moreover, after having been measured intermittently in the period 1980–2004 using COSPEC [Allard *et al.*, 1994, and references therein; Allard *et al.*, 1999, 2000; Ripepe *et al.*, 2005; Burton *et al.*, this volume], then differential optical absorption spectroscopy (DOAS) [Edner *et al.*, 1994; McGonigle *et al.*, 2003], the SO₂ plume flux is now continuously monitored with a network of UV (mini-DOAS) sensors (Burton *et al.*, unpublished data).

It is much more recently that real-time remote sensing of the hot crater gas compositions could be realized for the first time on Stromboli, thanks to the advent of compact open-path Fourier transform infrared (OP-FTIR) spectroscopy [e.g., Francis *et al.*, 1998; Burton *et al.*, 2000; Allard *et al.*, 2005]. OP-FTIR measurements were repeatedly performed in 2000–2002, at slanting distances of 220–240 m from the crater vents (Pizzo Sopra la Fossa; Plate 2), using the hot crater walls and/or molten lava ejecta as IR radiation sources. FTIR absorption spectra obtained from interferograms collected every 1 to 4 s have provided a unique data set for the complete chemical composition (H₂O, CO₂, SO₂, HCl, CO, and COS) of the magmatic gases issuing from the crater

during both quiescent and explosive degassing [Burton *et al.*, 2001, 2007a].

Thereafter, we describe and discuss the main information gathered from these different types of measurement.

3. QUIESCENT MAGMA DEGASSING

One fundamental but often overlooked aspect of Stromboli's activity is that its most prominent manifestation, in terms of mass budget and long-term behavior, is not its explosive activity: it is instead the continuous crater gas venting that occurs *between* the explosions. This quiescent gas venting, sustained by open-conduit bubbly degassing of the basaltic magma, actually accounts for 98% of the volcanic activity—the explosions, with an average frequency of six per hour and a duration \leq 10 s each, represent only 2%—and contributes most of the gas output [Allard *et al.*, 1994]. Knowing its chemical composition and mass budget is thus of prime importance.

3.1. Chemical Composition of Quiescent Emissions

Chemical investigations of quiescent crater gas venting on Stromboli, by the means of different methods, have revealed the following main features:

1. These emissions have a well-defined time-averaged chemical composition, despite short-term oscillations that are due to dynamic variations of the degassing from quite fuming to more energetic gas puffing (Plate 3). They are prevalently composed of water vapor [Allard *et al.*, 1999], averaging \sim 80 mol % [Burton *et al.*, 2007a], followed by CO₂, SO₂, and HCl in decreasing order of abundance (Table 1). HF was occasionally detected in the volcanic plume [Allard *et al.*, 2000; Aiuppa and Federico, 2004] but appears to be an order of magnitude less abundant than HCl. Among trace elements, bromine and highly volatile metalloids and metals with sulfur affinity (such as Se, Cd, Bi, In, and As) are the most enriched [Allard *et al.*, 2000]. These elements typically occur in the finest ($<1\ \mu\text{m}$) aerosol particles produced by condensation of the magmatic gas phase in the atmosphere [Allard *et al.*, 2000].

2. The CO/CO₂ ratio of quiescent emissions, measured with OP-FTIR spectroscopy, indicates their last equilibration at temperatures of about 700°C [Burton *et al.*, 2007a], much lower than the subsurface melt temperature (\sim 1100°C). The quiescent gas phase thus extensively cools prior to emission by interacting with the colder upper cap of the lava column then by expansion and air dilution in the open upper part of the conduits.

3. SO₂ represents by far the main sulfur species: SO₂/H₂S molar ratios range from 14 to 17 [Aiuppa *et al.*, 2005] and

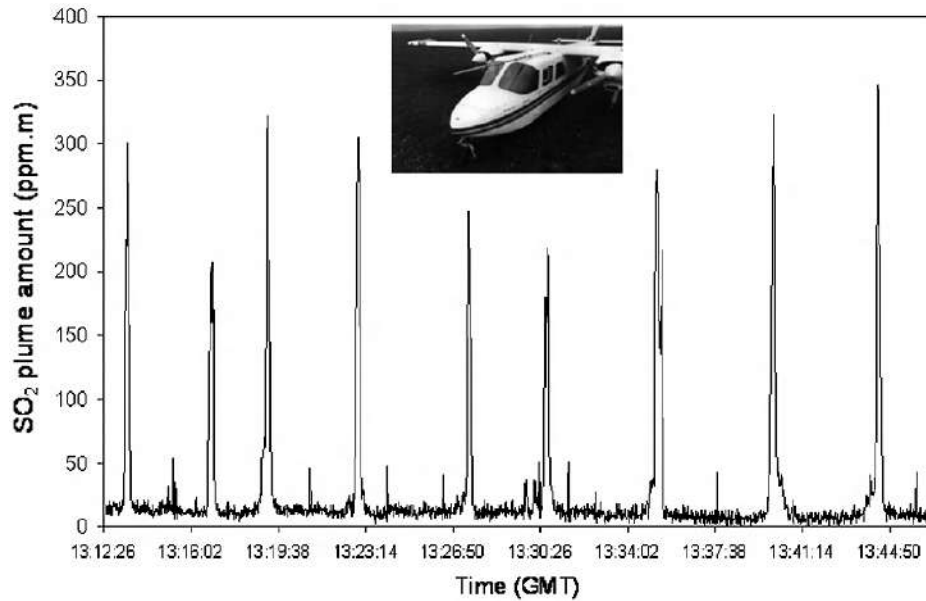


Figure 2. Example of successive airborne COSPEC traverses for measuring the SO₂ plume flux of Stromboli, June 1997 [Allard et al., 1999] (volcanic SO₂ column amounts in ppm m).

particulate sulfur accounts for $\leq 5\%$ of total sulfur [Allard et al., 2000]. Therefore, the SO₂ plume flux is well representative of the emission rate of bulk elemental sulfur from the magma and can be directly used to compute the amount of degassing magma (see below).

4. The SO₂/HCl ratio, repetitively determined both in the volcanic plume using filter packs [Allard et al., 1994, 2000] or diffusive tubes [Aiuppa and Federico, 2004] and in the hot crater gases using OP-FTIR spectroscopy [Burton et al., 2007a], displays molar values from 0.3 to 3.1, with a cluster at 1.0–1.5 (Figure 3). This latter mean value closely matches that (~ 1.5) expected for a bulk degassing of the magma, based on data for melt inclusions and matrix glasses [Métrich et al., 2001; Bertagnini et al., 2003]. A remarkable exception is the anomalous SO₂/HCl ratio observed shortly before the 5 April 2003 paroxysm, as will be discussed in Section 5.

5. The CO₂/SO₂ molar ratio oscillates between 5 and 12, in relationship to the degassing intensity, but maintains a time-averaged value of about 8 ± 1 [Allard et al., 1999; Allard, 2007; Burton et al., 2007a; Aiuppa et al., 2007]. With such a ratio, Stromboli's magmatic gases plot within the CO₂-rich upper range for persistently degassing basaltic volcanoes (Figure 4). This provides evidence for a high CO₂ content in the feeding magma [Allard, 2004, 2007], as well as for a persistent supply of deeply derived CO₂-rich gas bubbles to the shallow plumbing system (see Section 5).

6. Finally, the proportions of short-lived radioactive daughters of radon-222 (^{210}Po , ^{210}Bi , and ^{210}Pb) in the quiescent

gas emissions point to a rather fast transfer (a few hours) of gas bubbles between the magma degassing cell and the surface [Gauthier et al., 2000].

3.2. Gas Output and Magma Degassing Budget

The mass output of emitted gas provides key quantitative constraints on the dynamics of Stromboli. Airborne measurements of the SO₂ plume flux have revealed that the quiescent emissions contribute on average $\geq 95\%$ of the bulk discharge of SO₂ [Allard et al., 1994] and by extension of other major and minor gas species (H₂O, CO₂, HCl, etc.). Although they release more concentrated amounts of gas, the Strombolian explosions usually contribute little of the bulk gas discharge, owing to their brevity. However, significant variations of the bulk SO₂ emission rate were actually measured in relationship with the level of volcanic activity (Figure 5): from as low as ~ 150 t/d during periods of weak activity to as high as 800–1600 t/d during periods of more intense explosive activity [Stoiber et al., 1988; Allard et al., 1994, and references therein; Edner et al., 1994; Allard et al., 1999, 2000; McGonigle et al., 2003] or recent lava flow eruptions [Ripepe et al., 2005; Burton et al., this volume]. Such variations clearly track temporal changes in the supply rate of magma, its gas content, and dynamics of degassing and/or the degree of aperture of the shallow conduits.

The time-averaged SO₂ emission rate representative for medium volcanic activity was inferred as about 300–350 t/d



Plate 2. OP-FTIR spectroscopic measurement of hot crater gas compositions from the top of Stromboli (Pizzo Sopra la Fossa). Photo from F. Muré.

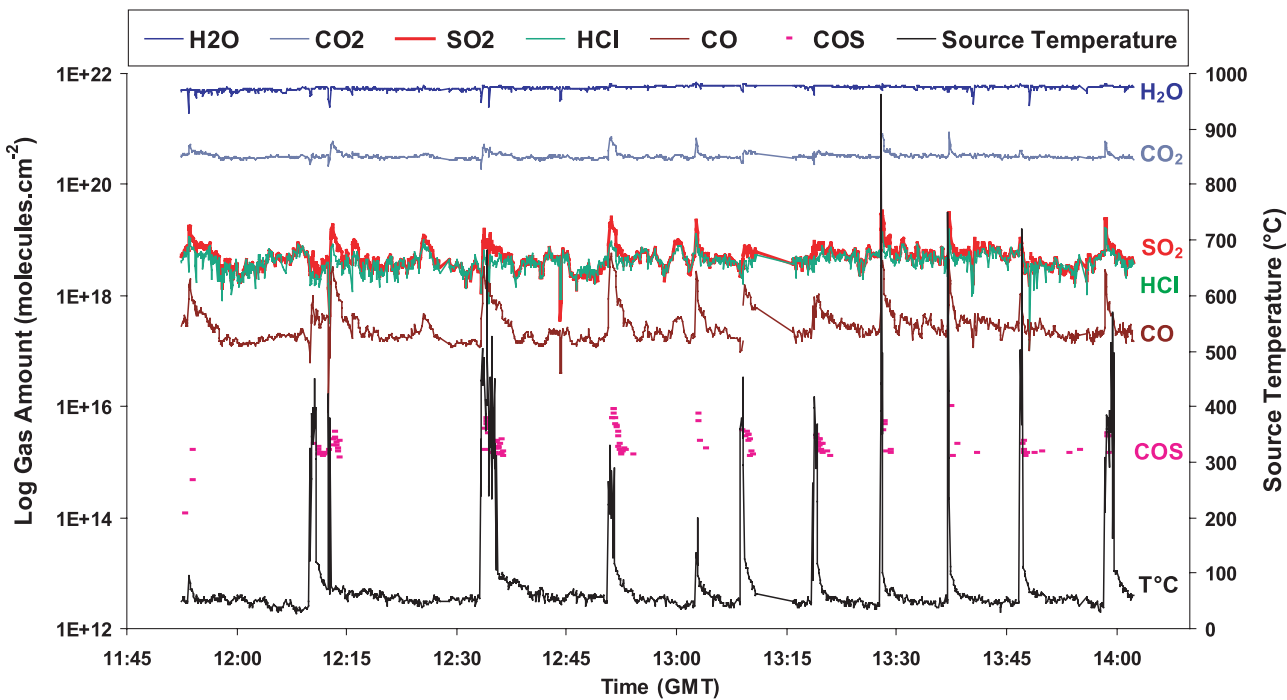


Plate 3. Variations of chemical composition of Stromboli's hot crater gases during quiescent and explosive degassing, as measured with OP-FTIR spectroscopy [Burton *et al.*, 2007a]. Spectral data sampled at ~4-s frequency, on 9 May 2001. The quiescent gas emissions have a well-defined composition, although with short-term oscillations controlled by temporal variations from quite fuming to more energetic gas puffing. Each explosion is marked by very sharp peak increases of the emitted gas concentrations and the radiation source temperature (reflecting the amount of molten lava blocks crossing the field of view of the spectrometer). The gas ratios demonstrate that the explosive gas phase (slugs) markedly differs in composition from the quiescent emissions and originates from greater depth (see text and Plate 4).

Table 1. Chemical Composition of Magmatic Gases Emitted During Quiescent and Explosive Crater Degassing at Stromboli (Modified From Burton *et al.* [2007a])

Gas Features	Quiescent Degassing	Typical Explosions ^a	Smaller Explosions ^b	Gas Output ^c , kg/s
H ₂ O, %	82.9	64.4	79.3	41.1
CO ₂ , %	13.6	33.1	19.0	16.5
SO ₂ , %	1.7	1.8	1.15	3.0
HCl, %	1.7	0.33	0.43	1.7
CO, %	0.03	0.44	0.15	0.023
COS, %	b.d.	0.008	b.d.	
H ₂ O/CO ₂	6.1	2.3 ± 0.8	4.5 ± 2.3	
CO ₂ /S	7.8	20.7 ± 2.1	16.8 ± 1.9	
S/Cl	1.0–5	4.7 ± 0.8	2.5 ± 0.8	
CO/SO ₂ , 10 ⁻²	1.8	24 ± 4	14.6 ± 0.4	
CO/CO ₂ , 10 ⁻²	0.21	1.14 ± 0.09	0.9 ± 0.08	
Equilibrium temperature, ^d °C	700	1020–1130	1000–1040	
Source pressure, ^e MPa	≤0.3–4	~70–80	~20–50	

^a Representative molar composition for one single explosion and average molar ratios for standard Strombolian explosions.

^b Representative molar composition and chemical ratios for smaller explosions.

^c Computed for the time-averaged SO₂ flux of 3 kg/s and the mean chemical composition of quiescent emissions, which provide most of the bulk gas discharge [Allard *et al.*, 1994].

^d Computed from the CO/CO₂ ratio of the gas phases and thermodynamic data for the equilibrium reaction CO₂ = CO + O₂ under redox conditions buffered by the basaltic melt.

^e Inferred from the measured gas compositions and pressure-related modeling of Stromboli basalt degassing (see text and Burton *et al.* [2007a]).

from the 1980–1997 airborne measurements [Figure 5; Allard *et al.*, 2000]. A lower background limit of ~200 t/d, typical for weaker fuming, was estimated from ground-based monitoring in 2006 [Burton *et al.*, 2007b]. Considering an intermediate average SO₂ emission rate of 250 ± 50 t/d (or 3.0 ± 0.5 kg/s), the mean composition of the quiescent magmatic emissions (Table 1) constrains a total gas discharge of 5400 ± 860 t/d (62 ± 10 kg/s) from the volcano (Table 2), in the lower range of initial estimates [Allard *et al.*, 1994]. With such a gas discharge, Stromboli is a much (10–20 times) weaker volcanic source than nearby Mount Etna [Allard *et al.*, 1991; Caltabiano *et al.*, 2004], but is a typical arc emitter contributing 1–2% of the estimated global volcanic yield of sulfur, halogens, and trace metals to the atmosphere [Allard *et al.*, 2000].

More importantly, Stromboli was recognized early to release much more gas than can be produced from the erupted magma [Chouet *et al.*, 1974; Allard *et al.*, 1994, 2000]. The SO₂ flux alone is comparable to the average solid output from Strombolian explosions [~150–260 t/d; Ripepe *et al.*, 1993], and the total gas discharge exceeds the latter by one order of magnitude. Hence, during its standard activity, the volcano produces much more gas than lava *by mass*, approaching the behavior of a lava lake [Allard *et al.*, 1994].

However, the prevalent mode of magma extrusion on Stromboli is through the occasional lava flow eruptions. Estimates for all such eruptions in the 20th century [Capaldi *et al.*, 1978; De Fino *et al.*, 1988] suggested a time-averaged lava flow contribution of ~420 t/d [Allard *et al.*, 1994]. But this figure is likely underestimated: it is strongly determined by one single eruption in 1985–1986 [De Fino *et al.*, 1988], which casts some doubt on lava flow estimates for many former eruptions. A more reliable estimate is provided by data for the recent period 1975–2005, during which three well-studied eruptions (including the 2002–2003 one) happened, and the SO₂ plume flux became measured (Figure 5). The magma extrusion rate as lava flows in this period averages about 4 × 10³ t/d and, therefore, represents ≥94% of the overall magma output from both explosive and effusive activities (the contribution of intermittent explosive paroxysms is poorly known, but is likely modest or minor when time-averaged: for illustration, the 10⁸ kg of dense magma extruded during the paroxysmal explosion on 5 April 2003 [Rosi *et al.*, 2006] represents a trivial component, 9 t/d, over the same period). Nevertheless, the mean values for the total gas discharge and the magma extrusion rate show that on the scale of three decades, Stromboli has emitted as much gas as lava *by mass*, which still implies a large excess gas release.

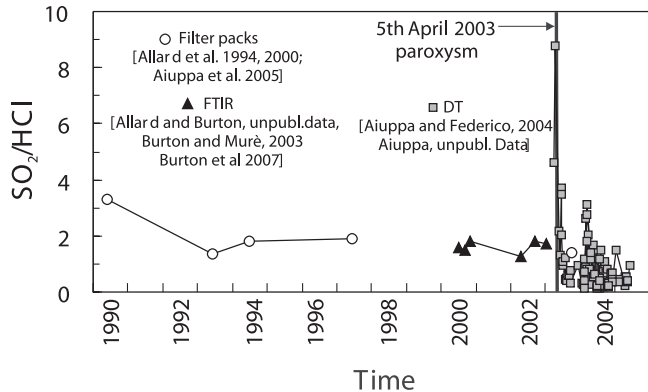


Figure 3. SO_2/HCl (or S/Cl) molar ratio in Stromboli's crater gas emissions during the period 1990–2005, as measured in either the volcanic plume (airborne and ground-based filtering) or the hot crater gases (OP-FTIR spectroscopy). The background gas emissions are characterized by an average molar ratio of 1.0–1.5. The sharp peak anomaly, with a ratio of about 9, detected a few days before the 5 April 2003 paroxysmal explosion [Aiuppa and Federico, 2004] may represent a true geochemical precursor of that paroxysm, indicating the upstream of deeply derived gas (see text).

This excess gas release can be quantified by comparing the magma extrusion rate in 1975–2005 ($0.018 \text{ m}^3/\text{s}$, for an erupted magma density of 2700 kg/m^3 ; Métrich *et al.* [2001]) with the supply rate of volatile-rich aphyric basalt ($\sim 2500 \text{ kg/m}^3$) needed to sustain the gas discharge. Scaling the mean SO_2 output to the initial sulfur content of Stromboli magma [$\sim 0.2 \text{ wt } \%$; Métrich *et al.*, 2001; Bertagnini *et al.*, 2003; N. Métrich, personal communication, 2006]—the bulk of which is outgassed as SO_2 at the surface—constrains a mean basalt supply rate of $0.3 \pm 0.05 \text{ m}^3/\text{s}$. This is 15 ± 4 times greater than the magma extrusion rate (Table 2). Therefore, only a small fraction ($\sim 7 \pm 2 \%$) of the feeding and degassing HK-basalt is eventually erupted at the surface, $\sim 93\%$ of it remaining unerupted! Such a strong disequilibrium between magma supply (degassing) and magma eruption at Stromboli requires that extensive gas-melt separation and differential gas transfer occur across the volcano conduits [Allard *et al.*, 1994, 2000; Burton *et al.*, 2007b]. Moreover, the unextrusion of 93% of the supplied magma bears important implications for the feeding system, as will be discussed in Section 5.

4. EXPLOSIVE MAGMA DEGASSING

4.1. Strombolian Explosions

The gas slugs driving the Strombolian explosions have estimated sizes between 40 and 200 m^3 [Allard *et al.*, 1994;

Vergniolle *et al.*, 1996; Chouet *et al.*, 2003] but, as already mentioned, contribute little of the bulk gas output. In contrast, their chemical composition provides key insight into the magmatic processes controlling the Strombolian explosive activity. The first measurements of Strombolian explosive degassing, made by flying with an aircraft through the ash-laden explosion clouds just above the crater, revealed higher CO_2/SO_2 molar ratios (15–25) than during quiescent gas venting [Allard *et al.*, 1999], suggesting a deeper (CO_2 -enriched) origin of the gas slugs. OP-FTIR spectroscopic measurements performed since then [Burton *et al.*, 2001, 2007a] have spectacularly verified this initial observation and revealed the following main features: (1) The occurrence of sharp increases of the gas concentrations during each explosion, associated with peak increases of both the gas temperature and that of the radiating source (molten lava blocks) used for IR absorption spectroscopy (Plate 3). (2) Compared with quiescent emissions, the bursting gas slugs have a distinct chemical composition: the slugs are less hydrated, richer in CO_2 , SO_2 , CO , and COS , and moreover display higher CO_2/SO_2 ($\times 2$ – 3), SO_2/HCl ($\times 2$ – 4), and CO/CO_2 ($\times 10$) molar ratios (Table 1). Their exit temperature ($\sim 1000^\circ\text{C}$), inferred from spectral data, and their equilibrium temperature (1000° – 1140°C), computed from their mean CO/CO_2 ratio, are not only much higher than those inferred for the quiescent emissions, but fit each other and with the temperature of the magma. This demonstrates that the explosive gas phase remains in thermodynamic equilibrium with the melt until the surface and, hence, suffers little

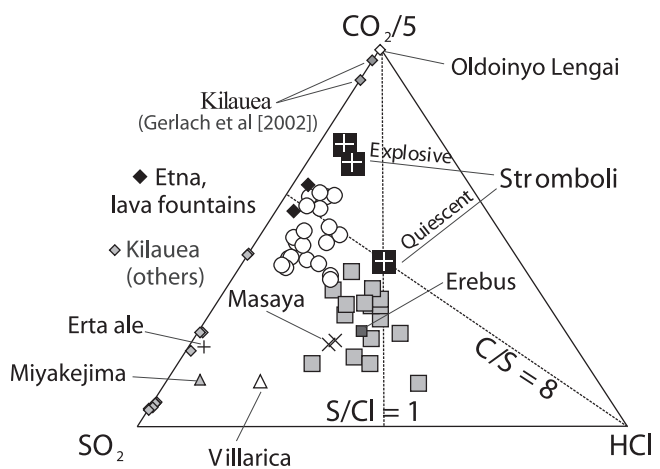


Figure 4. CO_2 – SO_2 – HCl triangular diagram showing the CO_2 -rich composition of basaltic gases from Stromboli compared with gas compositions from other basaltic or alkaline volcanoes in various tectonic settings: Etna (Italy), Kilauea (Hawaii), Erta'Ale (Ethiopia), Villarica (Chile), Miyakejima (Japan), and Oldonyo Lengai (Tanzania). Modified from Aiuppa *et al.* [2006].

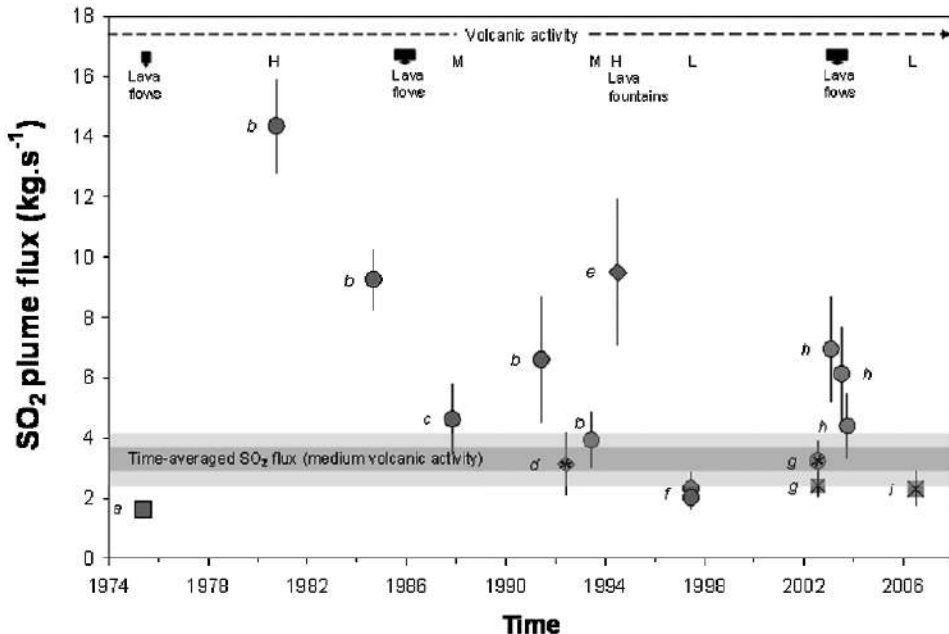


Figure 5. SO₂ plume flux (kg/s) from Stromboli volcano in 1975–2006 as a function of eruptive activity. Symbols refer to the different types of UV remote sensing measurements (squares, ground-based; circles, aircraft- or helicopter-borne; diamonds, sea-based), using either correlation spectrometry (COSPEC) or differential optical absorption spectroscopy (DOAS, symbols filled with a cross). Vertical bars give the standard deviation on the mean flux value at respective date or period. Letters indicate data source. The relative level of contemporaneous explosive activity is described as low (L), medium (M), and high (H), and lava flow eruptions by dark rectangles. A time-averaged SO₂ flux of 3.0–3.5 kg/s corresponds to medium volcanic activity. Data sources, with number of measurements: (a) Stoiber *et al.* [1978], 3; (b) Allard *et al.* [1994], 75; (c) Caltabiano and Romano [1988], 2; (d) Edner *et al.* [1994], 6; (e) Allard *et al.* [1994, unpublished data], 13; (f) Allard *et al.* [1999, 2000], 35; (g) McGonigle *et al.* [2003], 19; (h) Ripepe *et al.* [2005], and INGV-Catania Reports, average values from daily measurements during 2002–2003 eruption; (i) Burton *et al.* [2007b], continuous survey.

cooling upon ascent (adiabatic cooling due to gas expansion being likely counteracted by continuous and fast heat exchange with the melt). (3) The existence of compositional gas differences between the main explosions, separated by standard repose intervals (10–20 mn) and smaller explosions succeeding more closely. The latter tend to display lower CO₂/SO₂ and SO₂/HCl ratios and higher H₂O/CO₂ ratios than the former (Table 1), suggesting a shallower gas derivation. Alternatively, smaller and hence slower slugs powering the smaller explosions might be more affected by mixing with CO₂-poor, Cl-rich gas bubbles forming at shallower depth in the conduits [Burton *et al.*, 2007a, 2007b].

These chemical observations were interpreted in light of a degassing model for Stromboli basalt [Burton *et al.*, 2007a], constrained by the abundance of dissolved volatiles in the magma (Section 1.2) and by VolatilCalc computations [Newman and Lowenstern, 2002] of the pressure-related exsolution of H₂O and CO₂ during decompression of the basalt

from ~10 km depth to the surface. This modeling has revealed that to preserve their composition at the surface, the gas slugs should rise separately across the magma from as deep as 3 km (standard explosions) to at least ~1 km (small explosions). Such a depth interval corresponds to the submarine part of the volcanic pile, comprised between its metamorphic basement and the Tyrrhenian Sea level (Plate 4). Within these lower two thirds of the volcano conduits, slug generation could result from two main processes: (1) the periodic collapse of bubble foams accumulating at sill-like discontinuities (the model of Jaupart and Vergniolle [1989]), such as the volcano–crust interface, and/or (2) the dynamic coalescence of bubbles rising in conduits [Parfitt and Wilson, 1995]. This second mechanism is favored in inclined conduits, where bubbles tend to concentrate and coalesce on upper walls [James *et al.*, 2004] and may thus prevail in the 40° southeast-dipping feeder dyke that was imaged seismically within the volcano [Chouet *et al.*, 2003; Chouet *et al.*,

Table 2. Updated Average Estimate for the Magma Degassing Budget of Stromboli Volcano (See Text and Quoted References Therein)

Parameter	Average Estimate
SO ₂ output 1975–2006, kg/s	3.0 ± 0.5
Total gas discharge, kg/s	62 ± 10
Magma supply rate, m ³ /s	0.3 ± 0.5
Magma extrusion rate 1975–2005, m ³ /s	~0.018
Intrusive/extrusive magma ratio	15 ± 4
% supplied magma erupted	~7
% supplied magma unerupted	~93
Stored degassed magma 1975–2005, km ³	~0.25
Stored degassed magma in 1400 years, km ³	~11.5

2008]. Whatever the actual mechanism of slug genesis, the chemical composition of gas slugs driving the Strombolian explosive activity demonstrates that this latter has much deeper roots [Burton *et al.*, 2007a] than previously believed from the source depth (~250–300 m) of seismic and acoustic signals associated with most of the explosions [Chouet *et al.*, 2003; Ripepe *et al.*, 2002; Vergniolle *et al.*, 1996]. Instead, these geophysical signals most likely track a permanent geometrical discontinuity at the bottom of the shallow eruptive conduits, where deeper-derived gas slugs undergo an abrupt change in their flow pattern [James *et al.*, 2006; Burton *et al.*, 2007a; Chouet *et al.*, 2008].

4.2. Explosive Paroxysms

Rarer but much more violent degassing occurs during the explosive paroxysms that intermittently hit Stromboli volcano (approximately two to three per year). The dynamics of these events, where eruptive speeds can reach 300 m/s [Rosi *et al.*, 2006], implies their driving by overpressurized gas. But their most singular feature is the direct extrusion of the crystal-poor (aphyric), gas-rich feeding basalt as highly vesicular blond pumice, mingled with the common crystal-rich shallow magma [Métrich *et al.*, 2001, 2005; Bertagnini *et al.*, 2003; Landi *et al.*, 2004]. Two possible triggering mechanisms were then proposed for these violent events: (1) the fast uprise of gas-rich primitive magma blobs from great depth [Bertagnini *et al.*, 2003; Métrich *et al.*, 2005; Rosi *et al.*, 2006], or (2) the fast ascent of CO₂-rich gas pockets generated by bubble foam accumulation and collapse at deep feeder discontinuities, which promotes partial extrusion of co-entrained aphyric melt [Allard, 2004, 2007; P. Allard, A CO₂-rich gas trigger of explosive paroxysms on Stromboli volcano, *Earth and Planetary Science Letters*, 2008, herein-after referred to as Allard, submitted manuscript].

No datum has yet been obtained for the gas phase emitted during an explosive paroxysm, which might permit to

discriminate between these two triggering mechanisms. However, it is worthy to note that the very first possible precursor to a paroxysm was actually detected in crater gas emissions. A few days before the 5 April 2003 explosion, Aiuppa and Federico [2004] measured an exceptional peak anomaly in the SO₂/HCl plume ratio [≈ 9 , Figure 3; see also Rizzo *et al.*, this volume], which they interpreted as a hint for the pre-eruptive degassing of a S-rich primitive magma, later erupted as pumice during the explosion [Métrich *et al.*, 2005]. A SO₂/HCl ratio of ≈ 9 is indeed consistent with the equilibrium composition of the vapor phase exsolving from the deep aphyric magma (S/Cl ~ 1.2 ; Bertagnini *et al.* [2003]), assuming a factor ~ 10 solubility contrast between S and Cl, as is typical of basaltic magmas at moderate to low pressures [Aiuppa *et al.*, 2004]. However, this interpretation would require that the extruded aphyric magma was injected and residing for a few (2–3) days in the shallow plumbing system prior to the 5 April 2003 event, in contradiction with petrologic evidence of its very fast ascent without preeruptive ponding [Métrich *et al.*, 2005]. Instead, in the model proposed by Allard [2004, 2007], the aphyric melt plays a marginal role in the genesis of explosive paroxysms, CO₂-rich gas pockets being the main driving agent and actual trigger of these events. According to the degassing model described in Section 4.1, the SO₂/HCl peak anomaly measured shortly before the 5 April 2003 paroxysmal explosion could have tracked the precursory leakage of a bubble foam layer accumulated at a minimal depth of 6 km below the crater (Allard, submitted manuscript). Since carbon dioxide highly predominates in the magmatic gas phase at such a depth [Allard, 2007], then enhanced CO₂ release should have accompanied this S/Cl anomaly and should herald the paroxysms in general [Allard, 2004, 2007, also submitted manuscript]. A remarkable support to this interpretation is provided by recent observations [Aiuppa *et al.*, 2007] of a prominent increase of both CO₂/SO₂ ratio and the CO₂ flux in crater plume emissions prior to a further paroxysm on the 15 of March 2007.

5. IMPLICATIONS FOR THE MAGMA FEEDING SYSTEM

Our current understanding of Stromboli's feeding system is still partial but has strongly been improved in the recent years thanks to enhanced multidisciplinary investigations. Combining the information presented here for the crater gas emissions with other data types allows us to emphasize a few main features that are now reasonably well established:

1. Stromboli stands on a locally 15-km thick metamorphic arc crust [Panza *et al.*, 2006], at the base of which magma ponding (underplating?) has been detected seismically

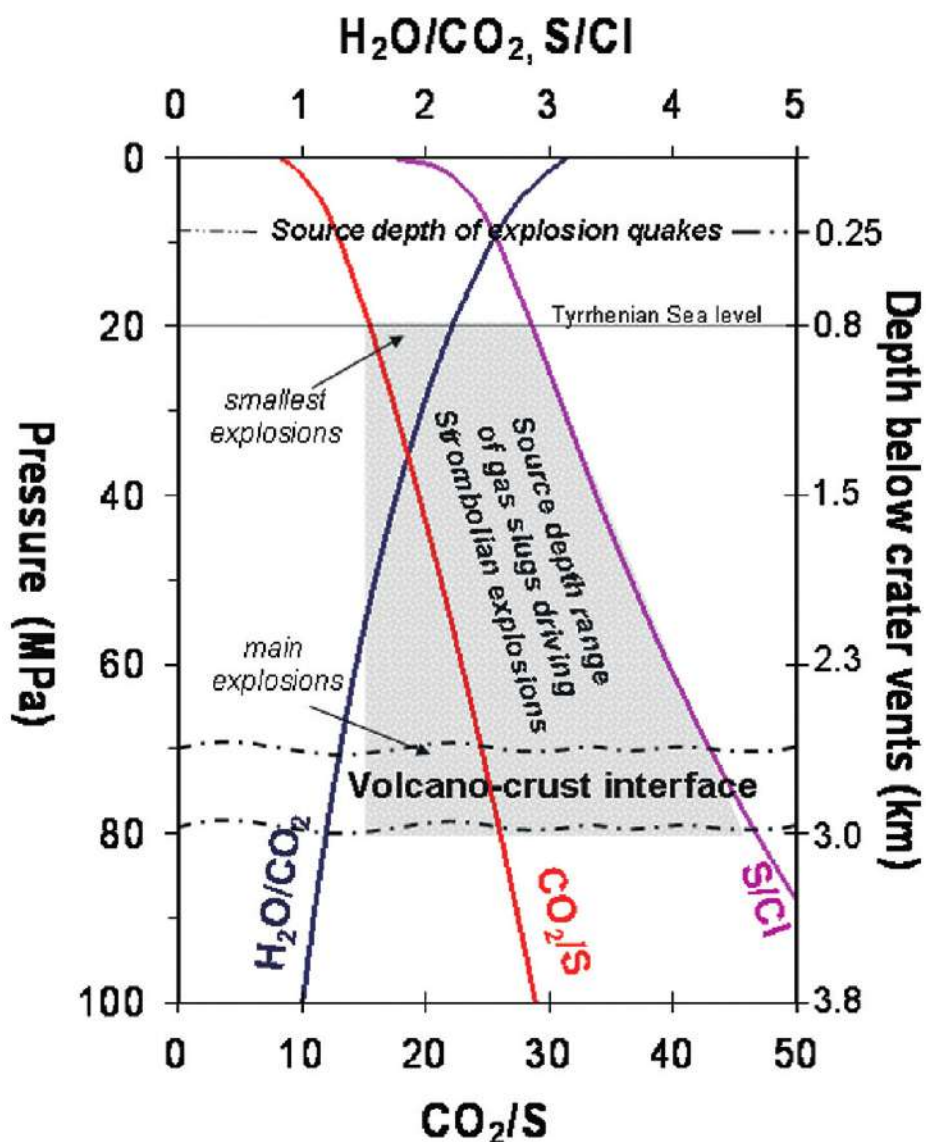


Plate 4. Source depth of the gas slugs driving Strombolian explosions, as inferred from their measured chemical composition and pressure-related modeling of Stromboli basalt degassing. Modified from Burton *et al.* [2007a]. Gas slugs driving standard explosions (every 10–20 mn) originate from as deep as the volcano–crust interface (2.5–3 km below the crater vents), while smaller explosions succeeding at shorter intervals are driven by slugs with intermediate to shallower source depth (~1 km, i.e., close to the Tyrrhenian Sea level). Gas data thus reveal that the Strombolian explosive activity has much deeper roots than previously thought (~250–300 m) from seismic signals associated with the explosions (see text).

[Capaldi *et al.*, 1978; Barberi *et al.*, 2007]. The CaO-rich parental magmas that rise from that Moho depth are very rich in water, sulfur, and chlorine [Bertagnini *et al.*, 2003; Francalanci *et al.*, 1993]. From their initial sulfur content and the mean CO₂/SO₂ ratio of the crater plume emissions, it was inferred that they may originally contain as much as 2.4 wt % of carbon dioxide, whose exsolution should begin at mantle depth [Allard, 2007]. These feeding melts thus co-exist early with a CO₂-rich gas phase.

2. Upon ascent, the CaO-rich parental magmas differentiate by crystal fractionation (~25%) into the shoshonitic HK-basalt that feeds the volcano and is eventually erupted [Bertagnini *et al.*, 2003]. Pressure estimates derived from the dissolved H₂O–CO₂ contents of melt inclusions in magmatic olivines [Métrich *et al.*, 2001; Bertagnini *et al.*, 2003], fluid inclusions in crustal xenoliths [Vagelli *et al.*, 2003], and petrologic experiments [Di Carlo *et al.*, 2006] suggest that this differentiation may occur in the pressure range 300–250 MPa, i.e., at lithostatic depths of order 10 km below the crater vents (~7 km in the crust). A differentiating magma reservoir or ponding zone may thus exist at that level [see also Capaldi *et al.*, 1978; Francalanci *et al.*, 2004].

3. Gas modeling [Allard, 2007; Burton *et al.*, 2007a, 2007b] shows that the uprising HK-basalt suffers little crystallization and degassing (except for CO₂ and partly for H₂O) prior to reaching the base of the volcanic pile. The aphyric basalt, supplied at a mean rate of ~0.3 m³/s (Section 3.2) and occasionally erupted as blond pumice during the explosive paroxysms, thus replenishes the plumbing system up to a very shallow depth. Its subsequent decompression within the volcano conduits would provoke extensive water exsolution and then a rapid increase of both its vesicularity (from ~0.35 at 3 km to 0.5 at ~2 km depth [Allard, 2007; Burton *et al.*, 2007b]) and crystallization rate [Métrich *et al.*, 2001; Landi *et al.*, 2004]. During this process, the basalt progressively transforms into the crystal-rich magma that is erupted, and its increasing permeability promotes gas percolation and pure open system degassing [Burton *et al.*, 2005; Burton *et al.*, 2007b]. This open degassing then becomes the main source of quiescent crater gas emissions and is responsible for the large excess gas discharge measured at the surface (Section 3.2). Because gas-melt separation is also at the origin of periodic slug flow that drives the Strombolian explosions (Section 4.1), the volatiles emitted during both quiescent and explosive degassing essentially escape freely from the basaltic magma filling the volcano conduit system.

4. Most (~93%) of the degassed magma does not erupt (Section 3.2) and, thus, remains within the shallow plumbing system. Now, because this magma is sterile to further gas release, it must be replaced more or less constantly by some equivalent amount of the undegassed feeding basalt in

order to maintain the time-averaged gas discharge and eruptive activity (otherwise, the volcano would gradually stop erupting). This requires that efficient convective overturn should occur in the volcano conduit system where magma degassing and crystallization prevalently take place [Allard *et al.*, 1994; Burton *et al.*, 2007b]. The strong density contrast between the two magmas (about 10³ kg/m) will promote downward recycling of the crystal-rich (2700 kg/m) degassed magma and upward ascent of the lighter aphyric and bubbly melt (1670 kg/m for a 35% vesicularity at 3 km depth). Turbulent ascent of the buoyant melt and periodic slug flow driving the Strombolian explosions should additionally favor this convective overturn. The reality of that convection process is supported by heat flow computations [Harris and Stevenson, 1997; Stevenson and Blake, 1998], as well as by crystal zoning oscillations and resorptions [Clocchiatti, 1981; Landi *et al.*, 2004], the chemistry of melt inclusions [e.g., Métrich *et al.*, 2001; Landi *et al.*, 2004], and detailed ⁸⁷Sr/⁸⁶Sr profiles in minerals [Francalanci *et al.*, 2004], all of which indicate that the degassed magma repeatedly interacts, mingles, and occasionally mixes with the uprising aphyric melt.

5. The volcano–crust interface, at ~2.5–3 km depth below the vents, is certainly a key structural and geological transition in Stromboli's feeding system. As shown in Section 4.1, it corresponds to the deepest source level of gas slugs driving the Strombolian explosions (Plate 4), where slugs may periodically form through bubble accumulation and bubble foam collapse [Jaupart and Vergniolle, 1989; Menand and Phillips, 2006; Burton *et al.*, 2007a]. Furthermore, it is a discontinuity at and/or below which the crystal-rich degassed magma convectively recycled back from the volcano conduits may accumulate in a shallow “reservoir.” The presence of a sill-like magma reservoir under the volcanic pile was suggested from early gas flux and crystal melt inclusion data [Allard *et al.*, 1994; Allard and Métrich, 2001], geobarometers in crustal xenoliths [Vagelli *et al.*, 2003], ⁸⁷Sr/⁸⁶Sr variations in recent lavas [Francalanci *et al.*, 1999], and magma degassing modeling [Menand and Phillips, 2006]. Based on ⁸⁷Sr mixing trends in recent lavas, Francalanci *et al.* [1999] assessed a possible size between 0.04 and 0.3 km³ for that shallow reservoir, in which Stromboli magma might reside for 19 ± 12 years. However, besides its large uncertainty, this estimate could be biased if, as was verified, the magma interacts with host material having heterogeneous ⁸⁷Sr/⁸⁶Sr ratio [Francalanci *et al.*, 2004].

Here we provide quantitative numbers for the amount of purely degassed magma that could be stored in a shallow reservoir underlying the volcano. According to the mean rates of basalt supply and extrusion quoted above (Table 2), 0.26 km³ of unerupted degassed magma would have accumulated

in the shallow plumbing system of Stromboli over the last three decades (1975–2005). Such an amount most likely exceeds the storage capacity of the volcano conduit system alone. The latter is unknown, but can be estimated from the magma supply rate of $0.3 \text{ m}^3/\text{s}$ and the maximum magma residence time in the degassing cell that sustains the crater gas emissions. An upper magma residence time of $\sim 215 \text{ d}$ was assessed from the ratios of short-lived radioactive daughters ($^{210}\text{Po}/^{210}\text{Bi}/^{210}\text{Pb}$) of radon-222 in crater plume emissions, measured during a period (May 1985) of “normal” volcanic activity [Gauthier *et al.*, 2000]. Using this value, and taking account of the high vesicularity of the uprising basalt (from ~ 35 to 65% between 3 and 1 km depth), we infer a degassing cell with size $\sim 1.2(\pm 0.3) \times 10^7 \text{ m}^3$. If the overall volcano conduit system contains equivalent volumetric proportions of degassed magma and aphyric basalt on average, then its bulk storage capacity could be twice that value. Note that such an estimate is only two to four times greater than the amount of magma outpoured during recent lava flow eruptions in 1985–1986 [De Fino *et al.*, 1986] and 2002–2003 [De Fino *et al.*, this volume], implying substantial emptying (and renewal) of the conduit system during such events. More importantly, despite its uncertainties, our above estimate for the conduit capacity demonstrates that most ($\sim 95\%$) of the 0.26 km^3 of magma that degassed without erupting in 1975–2005 should have been cycled back and stored *beneath* the volcano (even allowing for solidification of a fraction of it as dyke intrusions within the volcanic pile). One can extend this reasoning to a longer time scale. Taking the modern rates of basalt supply and extrusion as representative for the past 1400 years of similar activity at Stromboli, as much as 11.5 km^3 of unerupted degassed magma could have accumulated beneath the volcano over that time. This is equivalent to 5% of the bulk volume of the volcanic pile. If, moreover, a high intrusive/extrusive ratio has often characterized the growth of the volcano since 0.2 Ma, then huge quantities of unerupted degassed magma may have progressively solidify in its crustal basement, in the same way as inferred beneath Mount Etna [Allard, 1997].

Our above calculations are intended to show that a sill-like “reservoir” containing large amounts of dense degassed magma (as liquid blobs, crystal mush, and solid blocks) may plausibly be emplaced in the shallow metamorphic arc crust beneath Stromboli volcanic pile. In that “reservoir,” whose geophysical detection might be hampered by small density contrasts with the host rocks, fewer amounts of the aphyric HK-basalt rising from depth could extensively interact and mingle with the more abundant, colder degassed magma. We emphasize two potential consequences of that framework: (1) A much more rapid degassing and crystallization of the uprising HK-basalt than is currently expected from simple

decompression models, owing to accelerated feedback between cooling, water exsolution, and basalt crystallization [Métrich *et al.*, 2001]; and (2) a possible triggering of some explosive paroxysms by intermittent gravitational instability in the shallow reservoir. As a matter of fact, the actual depth and dynamics of the transition zone between the aphyric and the crystal-rich magma end-members are key parameters to be known for a better understanding of Stromboli’s eruptive activity. Whether this transition is gradual or, instead, extremely chaotic, depending on the rate and dynamics of conduit magma recycling, still remains an enigma. Future investigations are badly required to resolve this important question.

6. CONCLUSIONS

The results so far obtained for Stromboli’s crater gas emissions (fumaroles, the volcanic plume, and the hot magmatic gas phases), combined data for dissolved volatiles in crystal melt inclusions, provide key information on the magma degassing processes, the magma supply rate, the source depth of Strombolian explosions and, more broadly, the dynamics of the volcano feeding system. In particular, they provide insight into deep processes that are still undetected or hardly detectable with geophysical methods, owing to the submarine position of the volcano. Therefore, continuous monitoring of the crater gas emissions with automated in situ sensors and/or remote sensing tools must be ranked among the highest priorities for a better understanding and forecasting of the eruptive manifestations of Stromboli. In addition to continuous survey of the SO_2 flux [M. Burton *et al.*, unpublished data] and the main gas ratios [Aiuppa *et al.*, 2007] in plume emissions, which were initiated recently, continuous OP-FTIR survey of the hot crater gas compositions should reveal extremely powerful, as outlined by Burton *et al.* [2007a] and again in this paper. In particular, one can expect that a permanent gas survey with these different tools will not only permit us to better understand the triggering mechanism of explosive paroxysms, but also to detect precursory geochemical signals of these events that constitute the greatest hazard to tourists, volcanologists and, occasionally, the inhabitants of Stromboli island.

Acknowledgments. The overview presented in this paper has benefited from fruitful discussions with various scientific colleagues, especially N. Métrich, A. Bertagnini, P. Landi, M. Pompilio, M. Ripepe, B. Chouet, S. Falsaperla, C. Jaupart, S. Vergniolle, and M. Martini. Gas studies performed on Stromboli by the authors have benefited from key logistical support from the Italian Civil Defense (Protezione Civile) and, since as early as 1980, from funding supports from CNRS and CEA (France), GNV, INGV and Palermo University (Italy), and the Europe (EC research contracts EV5V-

CT92-177 and ENV4-CT96-288). Thorough reviews of our manuscript by B. Chouet and N. Métrich are greatly appreciated.

REFERENCES

- Aiuppa, A., and C. Federico (2004), Anomalous magmatic degassing prior to the 5th April 2003 paroxysm on Stromboli, *Geophys. Res. Lett.*, 31, L14607, doi:10.1029/2004GL020458.
- Aiuppa, A., C. Federico, G. Giudice, S. Gurrieri, A. Paonita, and M. Valenza (2004), Plume chemistry provides insights into the mechanisms of sulfur and halogen degassing at basaltic volcanoes, *Earth Planet. Sci. Lett.*, 222, 469–483.
- Aiuppa, A., S. Inguaggiato, A. J. S. McGonigle, M. O'Dwyer, C. Oppenheimer, M. J. Padgett, D. Rouwet, and M. Valenza (2005), H₂S fluxes from Mt. Etna, Stromboli, and Vulcano (Italy) and implications for the sulfur budget at volcanoes, *Geochim. Cosmochim. Acta*, 69(7), 1861–1871.
- Aiuppa, A., C. Federico, G. Giudice, S. Gurrieri, M. Liuzzo, H. Shinohara, R. Favara, and M. Valenza (2006), Rates of carbon dioxide plume degassing from Mount Etna volcano, *J. Geophys. Res.*, 111(B9), B09207, doi:10.1029/2006JB004307.
- Aiuppa, A., et al. (2007), Measurements of plume CO₂ and SO₂ flux during the 2007 Stromboli eruption, paper presented at IUGG 2007 Assembly, Perugia, Italy, July 2007.
- Allard, P. (1997), Endogenous magma degassing and storage at Mount Etna, *Geophys. Res. Lett.*, 24, 2219–2222.
- Allard, P. (2004), Stromboli: An erupting system powered by steady and catastrophic gas transfer, paper (extended Abstract) presented at INGV Meeting, *The 2002–2003 Stromboli eruption*, Catania, Italy, 24–25 May 2004.
- Allard, P. (2007), A CO₂-rich gas trigger of explosive paroxysms at Stromboli volcano, Italy, paper presented at EGU Assembly, Vienna, Austria, *Geophys. Res. Abstr.*, 9, 08044, April 2007.
- Allard, P., and Métrich N. (2001), The magma feeding system of Stromboli: Constraints from crystal melt inclusions and volatile fluxes, paper (extended Abstract) presented at Stromboli GNV Workshop, Stromboli, Italy, June 2001.
- Allard, P., et al. (1991), Eruptive and diffuse emissions of CO₂ from Mount Etna, *Nature*, 351, 387–391.
- Allard, P., J. Carbonnelle, N. Métrich, H. Loyer, and P. Zettwoog (1994), Sulphur output and magma degassing budget of Stromboli volcano, *Nature*, 368, 326–330.
- Allard, P., A. Aiuppa, and H. Loyer (1999), Airborne determinations of gas and trace-metal fluxes in volcanic plumes of Mt. Etna and Stromboli, in *Monitoring Volcanic Risks by Remote Sensing*, CEE Research Contract ENV4-CT96-288, Final Report, 55 pp., Bruxelles, Belgium.
- Allard, P., A. Aiuppa, H. Loyer, F. Carrot, A. Gaudry, G. Pinte, A. Michel, and G. Dongarra (2000), Acid gas and metal emission rates during long-lived basalt degassing at Stromboli volcano, *Geophys. Res. Lett.*, 27(8), 1207–1210.
- Allard, P., M. Burton, and F. Muré (2005), Spectroscopic evidence for a lava fountain driven by previously accumulated magmatic gas, *Nature*, 433, 407–410.
- Anderson, A.T. (1975), Some basaltic and andesitic gases, *Rev. Geophys. Space Phys.*, 13, 37–55.
- Barberi, F., M. Rosi, and A. Sodi (1993), Volcanic hazard assessment at Stromboli based on review of historical data, *Acta Vulcanol.*, 3, 173–187.
- Barberi, G., et al. (2007), Crustal evidence of a low velocity Vp and Vs volume beneath Stromboli volcano, Italy, paper presented at EGU Assembly, Vienna, Austria, *Geophys. Res. Abstr.*, 9, 02621, April 2007.
- Bertagnini, A., N. Métrich, P. Landi, and M. Rosi (2003), Stromboli volcano (Aeolian Archipelago, Italy): An open window on the deep-feeding system of a steady state basaltic volcano, *J. Geophys. Res.*, 10(B7), 2336, doi:10.1029/2002JB002146.
- Burton, M., P. Allard, and F. Murè (2001), High temporal resolution measurements of volcanic gas composition using FTIR on Stromboli volcano, Italy, paper presented at AGU Fall Meeting, San Francisco, Calif., USA, December 2001.
- Burton, M., H. Mader, M. Polacci, and P. Allard (2005), Constraints on the dynamics of degassing in basaltic systems, *Eos Trans. AGU*, 86, Fall Meet. Suppl., 52, Abstract V13G-01.
- Burton, M., P. Allard, A. La Spina, and F. Murè (2007a), Magmatic gas composition reveals the source depth of slug-driven Strombolian explosive activity, *Science*, 317, 227, doi:10.1126/science.1141900.
- Burton, M., S. Calvari, L. Spampinato, L. Lodato, N. A. Pino, E. Marchetti, and F. Murè (2008), Volcanic and seismic activity at Stromboli preceding the 2002–2003 flank eruption, this volume.
- Burton, M. R., C. Oppenheimer, L. Horrocks, and P. W. Francis (2000), Remote sensing of CO₂ and H₂O emission rates from Masaya volcano, Nicaragua, *Geology*, 28(10), 915–918.
- Burton, M. R., H. M. Mader, and M. Polacci (2007b), The role of gas percolation in quiescent degassing of persistently active basaltic volcanoes, *Earth Planet. Sci. Lett.*, 264, 46–60.
- Caltabiano, T., and R. Romano (1988), *Rep. Boll. Grup. Naz. Vulcan. Italy*, 4, 133–145.
- Caltabiano, T., M. Burton, S. Giammanco, P. Allard, N. Bruno, F. Murè, and R. Romano (2004), Volcanic gas emissions from the summit craters and flanks of Mt. Etna, 1987–2000, in *Mt. Etna: Volcano Laboratory*, *Geophys. Monogr. Ser.*, vol. 143, edited by S. Bonaccorso et al., pp. 111–128, AGU, Washington, D. C.
- Capaldi, G., et al. (1978), Stromboli and its 1975 eruption, *Bull. Volcanol.*, 41(3), 259–285.
- Carapezza, M. L., and C. Federico (2000), The contribution of fluid geochemistry to the volcano monitoring of Stromboli, *J. Volcanol. Geotherm. Res.*, 95, 227–245.
- Carapezza, M. L., S. Inguaggiato, L. Brusca, and M. Longo (2004), Geochemical precursors of the activity of an open-conduit volcano: The Stromboli 2002–2003 eruptive events, *Geophys. Res. Lett.*, L07620, doi:10.1029/2004GL019614.
- Chaigneau, M. (1965), Sur les gaz volcaniques de Stromboli (Îles Eoliennes), *C. R. Acad. Sci. Paris*, 261(11), 2241–2244.
- Chouet, B., N. Hamisevicz, and T. R. McGetchin (1974), Photoballistics of volcanic jet activity at Stromboli, Italy, *J. Geophys. Res.*, 79, 4961–4976.

- Chouet, B., et al. (2003), Source mechanisms of explosions at Stromboli Volcano, Italy, determination from moment-tensor inversion of very-long-period data, *J. Geophys. Res.*, 108(B1), 2019.
- Chouet, B., P. Dawson, and M. Martini (2008), Shallow-conduit dynamics at Stromboli Volcano, Italy, imaged from waveform inversions, in *Fluid Motion in Volcanic Conduits: A Source of Seismic and Acoustic Signals*, *Geol. Soc. Spec. Publ.*, edited by S. J. Lane, and J. S. Gilbert, Geological Society, London, in press.
- Clocchiatti, R. (1981), La transition augite-diopside et les liquides silicatés intra-cristallins dans les pyroclastes de l'activité actuelle du Stromboli: Témoignages de la ré-injection et du mélange magmatiques, *Bull. Volcanol.*, 44, 339–357.
- De Fino, M., et al. (1988), The Stromboli eruption of 6 December 1985–25 April 1986: Volcanological, petrological and seismological data, *Rend. Soc. Ital. Mineral. Petrol.*, 43, 1021–1038.
- Di Carlo, I., M. Pichavant, S. G. Rotolo, and B. Scaillet (2006), Experimental crystallization of a high-K arc basalt: The golden pumice, Stromboli volcano, Italy, *J. Petrol.*, 47(7), 1317–1343, doi:10.1093/petrology/egl011.
- Edner, H., P. Ragnarson, S. Svanberg, E. Wallinder, R. Ferrara, R. Cioni, B. Raco, and G. Taddeucci (1994), Total fluxes of sulfur dioxide from the Italian volcanoes Etna, Stromboli and Vulcano measured by differential adsorption lidar and passive differential optical adsorption spectroscopy, *J. Geophys. Res.*, 99, 18,827–18,838.
- Finizola, A., S. Sortino, J.-F. Lénat, M. Aubert, M. Ripepe, and M. Valenza (2003), The summit hydrothermal system of Stromboli: New insights from self-potential, temperature, CO₂ and fumarolic fluid measurements—Structural and monitoring implications, *Bull. Volcanol.*, 65, 486–504, doi:10.1007/s004450030276z.
- Francalanci, L., P. Manetti, A. Peccerillo, and J. Keller (1993), Magmatological evolution of the Stromboli volcano (Aeolian arc, Italy): Inferences from major and trace element and Sr-isotopic composition of lavas and pyroclastic rocks, *Acta Vulcanol.*, 3, 217–151.
- Francalanci, L., S. Tommasini, S. Conticelli, and G. R. Davies (1999), Sr isotopic evidence for short magma residence time for the 20th century activity at Stromboli volcano, Italy, *Earth Planet. Sci. Lett.*, 167, 61–69.
- Francalanci, L., S. Tommasini, and S. Conticelli (2004), The volcanic activity of Stromboli in the 1906–1998 AD period: Mineralogical, geochemical and isotope data relevant to the understanding of the plumbing system, *J. Volcanol. Geotherm. Res.*, 131, 179–211.
- Francis, P. W., M. Burton, and C. Oppenheimer (1998), Remote measurements of volcanic gas compositions by solar FTIR spectroscopy, *Nature*, 396, 567–570.
- Gauthier P.-J., M.-F. Le Cloarec, and M. Condomines (2000), Degassing processes at Stromboli volcano inferred from short-lived disequilibria (²¹⁰Pb–²¹⁰Bi–²¹⁰Po) in volcanic gases, *J. Volcanol. Geotherm. Res.*, 102(1/2), 1–19.
- Giggenbach, W. F. (1996), Chemical composition of volcanic gases, in *Monitoring and Mitigation of Volcano Hazards*, edited by R. Scarpa, and R. I. Tilling, pp. 221–256, Springer-Verlag, Berlin.
- Harris, A. J. L., and D. S. Stevenson (1997), Magma budgets and steady-state activity of Vulcano and Stromboli, *Geophys. Res. Lett.*, 24, 1043–1046.
- James, M. R., S. J. Lane, B. A. Chouet, and J. S. Gilbert (2004), Pressure changes associated with the ascent and bursting of gas slugs in liquid-filled vertical and inclined conduits, *J. Volcanol. Geotherm. Res.*, 129, 61–82.
- James, M. R., S. J. Lane, and B. A. Chouet (2006), Gas slug ascent through changes in conduit diameter: Laboratory insights into a volcano-seismic source process in low-viscosity magmas, *J. Geophys. Res.*, 111(B5), B05201, doi:10.1029/2005JB003718.
- Jaupart, C., and S. Vergniolle (1989), The generation and collapse of a foam layer at the roof of a basaltic magma chamber, *J. Fluid Mech.*, 203, 347–380.
- Landi, P., N. Métrich, A. Bertagnini, and M. Rosi (2004), Dynamics of magma mixing and degassing recorded in plagioclase at Stromboli (Aeolian Archipelago, Italy), *Contrib. Mineral. Petrol.*, 147, 213–227, doi:10.1007/s00400-0405555.
- Landi, P., et al. (2006), The December 2002–July 2003 effusive event at Stromboli volcano, Italy: Insights into the shallow plumbing system by petrochemical studies, *J. Volcanol. Geotherm. Res.*, 155, 263–284.
- McGonigle A. J. S., C. Oppenheimer, B. Galle, M. Edmonds, T. Caltabiano, G. Salerno, M. Burton, and T. A. Mather (2003), Volcanic sulphur dioxide flux measurements at Etna, Vulcano and Stromboli obtained using an automated scanning static ultraviolet spectrometer, *J. Geophys. Res.*, 108, doi:10.1029/2002JB002261.
- Menand, T., and J. C. Phillips (2007), Gas segregation in dykes and sills, *J. Volcanol. Geotherm. Res.*, 159, 393–408.
- Métrich, N., A. Bertagnini, P. Landi, and M. Rosi (2001), Crystallization driven by decompression and water loss at Stromboli volcano (Aeolian Islands, Italy), *J. Petrol.*, 42, 1471–1490.
- Métrich, N., A. Bertagnini, P. Landi, M. Rosi, and O. Belhadj (2005), Triggering mechanism at the origin of paroxysms at Stromboli (Aeolian Archipelago, Italy): The 5 April 2003 eruption, *Geophys. Res. Lett.*, 32, doi:10.1029/2004GL022257.
- Newman, S., and J. B. Lowenstern (2002), V_{OLATILE}C_{ALC}: A silicate melt–H₂O–CO₂ solution model written in Visual Basic Excel, *Comput. Geosci.*, 28(5), 597–604, doi:10.1016/s0098-3004(01)000814.
- Panza, G. F., A. Peccerillo, K. Aoudia, and B. Farina (2006), Geophysical and petrological modelling of the structure and composition of the crust and upper mantle in complex geodynamic settings: The Tyrrhenian sea and surroundings, *Earth Sci. Rev.*, 80, 1–46.
- Parfitt, E. A., and L. Wilson (1995), Explosive volcanic eruptions: IX. The transition between Hawaiian-style lava fountaining and Strombolian explosive activity, *Geophys. J. Int.*, 121, 226–232.
- Ripepe, M., A. J. L. Harris, and R. Carniel (2002), Thermal, seismic and infrasonic insights into conduit process at Stromboli volcano, *J. Volcanol. Geotherm. Res.*, 118, 285–297.
- Ripepe, M., E. Marchetti, G. Olivieri, A. Harris, J. Dehn, M. Burton, T. Caltabiano, and G. Salerno (2005), Effusive to explosive transition during the 2003 eruption of Stromboli volcano, *Geology*, 33(4), 273–276, doi:10.1130/G211731.

- Rizzo, A., A. Aiuppa, G. Capasso, F. Grassa, S. Inguaggiato, M. Longo, and M. L. Carapezza (2008), The 5 April 2003 paroxysm at Stromboli: A review of geochemical observations, this volume.
- Rosi, M., A. Bertagnini, and P. Landi (2000), Onset of the persistent activity at Stromboli volcano (Italy), *Bull. Volcanol.*, 62, 294–300.
- Rosi, M., A. Bertagnini, A. J. L. Harris, L. Pioli, M. Pistolesi, and M. Ripepe (2006), A case history of paroxysmal explosion at Stromboli: Timing and dynamics of the April 5, 2003 event, *Earth Planet. Sci. Lett.*, 243, 594–606.
- Sparks, R. S. J. (2003), Dynamics of magma degassing, in *Volcanic Degassing, Geol. Soc. Spec. Publ.*, vol. 123, edited by C. Oppenheimer et al., pp. 5–22, Geological Society, London.
- Stevenson, D. S., and S. Blake (1998), Modelling the dynamics and thermodynamics of volcanic degassing, *Bull. Volcanol.*, 60, 307–317.
- Stoiber, R. E., G. B. Malone, and G. P. Bratton (1978), Volcanic emission of SO₂ at Italian and Central American volcanoes (abstract), *Geol. Soc. Am. Abstr. Programs*, 10, 148.
- Tazieff, H. (1970), New investigations on eruptive gases, *Bull. Volcanol.*, B34, 421–438.
- Tazieff, H., and F. Tonani (1963), Fluctuations rapides et importantes de la phase gazeuses éruptive, *C. R. Acad. Sci. Paris*, 257, 3985–3987.
- Vagelli, G., L. Francalanci, G. Ruggieri, and S. Testi (2003), Persistent polybaric rests of calc-alkaline magmas at Stromboli volcano, Italy: Pressure data from fluid inclusions in restitic quartzite nodules, *Bull. Volcanol.*, 65, 385–404.
- Vergniolle, S., G. Brandeis, and J.-C. Maréchal (1996), Strombolian explosions 2: Eruption dynamics determined from acoustic measurements, *J. Geophys. Res.*, 101(B9), 20,449–20,466.

A. Aiuppa, Università di Palermo, CFTA, Via Archirafi 36, 90123 Palermo, Italy.

P. Allard, Groupe des Sciences de la Terre, Laboratoire Pierre Sue, CNRS-CEA, Saclay, 91191 Gif sur Yvette, France. (patrick.allard@cea.fr)

M. Burton, T. Caltabiano, A. La Spina, and G. Salerno, Istituto Nazionale di Geofisica e Vulcanologia, Sezione di Catania, Catania, Piazza Roma 2, 95123 Catania, Italy.

C. Federico, Istituto Nazionale di Geofisica e Vulcanologia, Sezione di Palermo, Via Ugo La Malfa 153, I-90146 Palermo, Italy.

Upper Conduit Structure and Explosion Dynamics at Stromboli

Bernard Chouet and Phillip Dawson

U.S. Geological Survey, Menlo Park, California, USA

Marcello Martini

Osservatorio Vesuviano, Naples, Italy

Modeling of very long period seismic data recorded during explosive activity at Stromboli in 1997 provides an image of the uppermost 1 km of its volcanic plumbing system. Two distinct dike-like conduit structures are identified, each representative of explosive eruptions from two different vents located near the northern and southern perimeters of the summit crater. Inferred volumetric changes in the dikes are viewed as the result of a piston-like action of the magma associated with the disruption of a gas slug transiting through discontinuities in the dike apertures. Accompanying these volumetric source components are single vertical forces resulting from an exchange of linear momentum between the source and the Earth. In the dike system underlying the northern vent, a primary disruption site is inferred at an elevation near 440 m where a bifurcation in the conduit occurs. At a depth of 80 m below sea level (bsl), a sharp corner in the conduit marks another location where the elastic response of the solid to the action of the upper source induces pressure and momentum changes in the magma. In the conduit underlying the southern vent, the junction of two inclined dikes with a subvertical dike at 520 m of elevation is a primary site of gas slug disruption, and another conduit corner 280 m bsl represents a coupling location between the elastic response of the solid and fluid motion.

1. INTRODUCTION

Eruptive behavior at Stromboli is characterized by mild, intermittent explosive activity, during which well-collimated jets of gases laden with molten lava fragments burst in short eruptions commonly lasting 5–15 s and occurring at a typical rate of three to ten events per hour [Chouet *et al.*, 1974]. This explosive activity is interrupted by occasional episodes of

more vigorous activity accompanied by lava flows as seen in 1975 [Capaldi *et al.*, 1978], 1985, and more recently in 2002–2003 [Calvari *et al.*, 2005] and 2007 [Dipartimento Della Protezione Civile, Rischio Vulcanico, Stromboli, Descrizione dell'Eruzione 2007, <http://www.protezionecivile.it>].

Persistent eruptive activity and ease of access make this volcano an ideal laboratory for detailed measurements of the seismic wave fields radiated by Strombolian activity, and much effort has been extended over the past 15 years to gain a better understanding of the origin of these wavefields [see Chouet *et al.*, 2003, for a review of these studies]. To further improve our understanding of the seismic source mechanisms of Strombolian explosions, detailed measurements were carried out at Stromboli in September of 1997 by

Chouet et al. [2003] using a network of 21 three-component broadband (0.02–60 s) seismometers (Figure 1). This network remained in operation for one week. Eruptive activity during this experiment was limited to two distinct vents located near the northern and southern perimeters of the crater, and two characteristic types of waveforms representative of eruptions from these vents were observed. The signals associated with eruptions at the northern vent were subsequently named type 1 events, and those related to eruptions at the southern vent were named type 2 events [*Chouet et al.*, 2003]. In their analyses, *Chouet et al.* [2003] focused their attention on data from the top two rings of sensors where the largest signal amplitudes were recorded. Using these data, they carried out systematic inversions of eruption signals band-pass-filtered in the 2- to 20-s band for the type 1 event, or the 2- to 30-s band for the type 2 event. Two-point sources associated with eruptions from the two vents were imaged at elevations of 520 m (type 1) and 480 m (type 2), roughly 160 m NW of the vents [*Chouet et al.*, 2003]. A source mechanism represented by a volumetric component involving the

expansion and compression of a steeply NW-dipping dike, coupled with a dominantly vertical force attributed to mass advection in the dike, was found to consistently yield optimum variance reduction in the waveform matches obtained for the two types of events.

In January 2003, the INGV-Osservatorio Vesuviano began the installation of a permanent broadband seismic network on Stromboli. A paroxysmal eruption on 5 April 2003 provided a unique opportunity to gain insights into shallow conduit processes underlying such violent but relatively rare event at Stromboli. Unfortunately, this eruption destroyed two receivers and further impaired the function of three sensors, in the eight-station network in operation at the time, thus allowing only rough qualitative analyses of the usable portions of the broadband data recorded [*D'Auria et al.*, 2006]. Although the limited coverage provided by the few remaining receivers precluded a robust determination of the source mechanism for this event, the results obtained by *D'Auria et al.* [2006] point to a picture that is generally consistent with the earlier findings of *Chouet et al.* [2003].

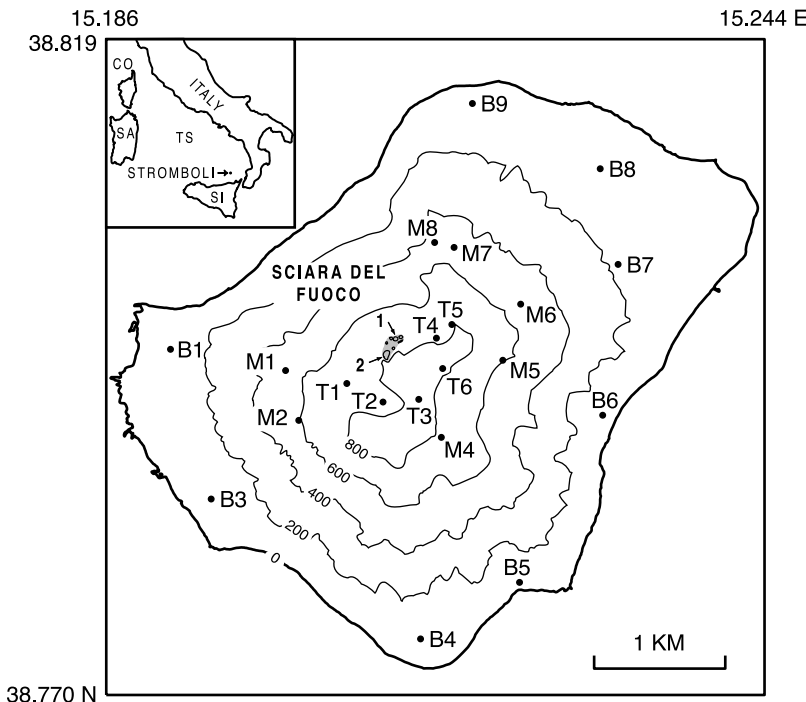


Figure 1. Map of Stromboli volcano showing locations of three-component broadband stations deployed during the seismic experiment in 1997 (solid dots). Stations prefixed by “T” denote those of the “T” ring of sensors, “M,” those of the “M” ring, and “B,” those of the “B” ring, located at the crater level, midlevel, and base of the volcano, respectively. The crater is marked by the shaded area, which encompasses distinct vents. The arrows point to two eruptive vents that were active at the time. Contour lines represent 200 m contour intervals. The inset shows the location of Stromboli in the Tyrrhenian Sea (TS) in relation to Italy, Sicily (SI), Sardegna (SA), and Corsica (CO).

Following the work of *Chouet et al.* [2003], further analyses of the waveforms recorded in September 1997 were subsequently carried out by *Chouet et al.* [2008] using data from the entire available network (see Figure 1). This more detailed investigation illuminates the subterranean processes driving eruptions and clearly points to the key role played by the conduit geometry in controlling fluid motion and resultant processes.

In this paper, we review the most recent model of the shallow conduit structure at Stromboli obtained by *Chouet et al.* [2008] from analyses of very long period (VLP) data in the 2- to 30-s band. Although the study by *Chouet et al.* [2008] provides only a momentary glimpse of Strombolian activity in September 1997, another recent study by *Auger et al.* [2006], based on data from the 13-station network currently operating at Stromboli, underscores the great stability of the seismic sources underlying eruptive activity at this volcano. As the operative source processes are essentially stationary with time within the bandwidth of the VLP data, an analysis of representative events is adequate to fully describe the overall source dynamics.

2. CONDUIT STRUCTURE IMAGED FROM WAVEFORM INVERSION

Modeling of VLP seismic data recorded during explosive activity in 1997 has imaged two distinct dike structures representative of explosive eruptions from two different vents located near the northern and southern perimeters of the summit crater [*Chouet et al.*, 2003, 2008]. Plates 1 and 3a show two representations of the conduit geometry underlying the northern vent area. Plate 1 shows the seismic source mechanisms obtained from inversion of VLP waveforms; the mechanisms include two-point sources, each of which marks a flow disruption site along the conduit. The upper point source (Plate 1a) is located 440 m above sea level (asl) and represents a bifurcation in the conduit; this is the main flow disruption site for gas slugs ascending toward the northern vent. The lower point source (Plate 1b), located 520 m below the upper source, features a sharp corner in the conduit and represents a secondary flow disruption site. Both upper and lower sources feature a dominant component in the form of a crack (dike) sustaining the largest volume change (colored red) and a subdominant crack (another dike segment) undergoing a smaller volume change (shaded gray). Both cracks in the upper source (Plate 1a) display a similar sequence of inflation–deflation–inflation. The dominant crack in the lower source displays a volumetric response similar to that seen in the dominant crack at the upper source, but delayed by about 1.1 s with respect to the upper source. This implies a propagation speed of roughly 490 m/s between the two sources,

consistent with the slow speed expected for the crack wave propagating at the interface between fluid and solid [*Chouet, 1986; Ferrazzini and Aki, 1987; Chouet, 1988*].

Plate 3a shows a picture of the conduit geometry derived from the seismic source mechanisms imaged in Plate 1. The conduit is comprised of four dike segments, whose strikes and dips are given in Plate 1. The closely matching dips of the two dominant cracks in Plate 1 point to a conduit that extends essentially straight from 80 m below sea level (bsl) to the crater floor, 760 m asl. At a depth of 80 m bsl, the conduit features a sharp corner leading into a dike segment dipping 40° to the southeast. The upper dominant dike segment and deep segment below the lower abrupt corner both strike NE–SW along a direction parallel to the elongation of the volcanic edifice and a prominent zone of structural weakness, as expressed by lineaments, dikes, and brittle structures. The surface trace of the upper dominant dike segment trends through the northern vent area, while the surface trace of the upper subdominant segment extends NW–SE in rough alignment with several vents active in the NW quadrant of Stromboli in 2002–2003 [*Acocella et al., 2006*]; the upper subdominant dike trace intersects the main dike trace ~170 m north of the northern vent area.

A striking aspect of the mechanisms imaged at the two sources in Plate 1 is the presence of dominantly vertical single-force components with common-looking time histories, except for a polarity reversal in one source compared with the other. The upper source (Plate 1a) displays an initially downward force followed by an upward force, while an upward force followed by a downward force is manifest in the lower source (Plate 1b). These force components compensate each other so that the total momentum in the overall source volume is conserved. In contrast to the delay of ~1.1 s in the volumetric components noted above, no significant delay is noted in the onsets of the vertical forces at the two sources, suggesting that transmission of the force between the two sources occurs via the faster speed (3.5 km/s [*Chouet et al., 2003*]) of the compressional wave in the rock matrix.

A similar analysis carried out for eruptions at the southern vent images an uppermost conduit geometry composed of a NE-striking dike dipping 51°NW, intersecting a west-striking dike dipping 58°N (Plates 2a and 3b). At 520 m of elevation, the two dikes merge into a subvertical dike striking NE, and at a depth of 280 m bsl, the conduit features a second, more abrupt corner leading into a fracture dipping 50°S (Plates 2b and 3b). The upper and lower sources again feature a dominant crack sustaining the largest volume change (colored red) and subdominant crack undergoing a smaller volumetric variation (shaded gray; Plates 2a and 2b). The volume change in the upper dominant dike (Plate 2a) starts with an initial deflation of the dike, followed by a sequence of

inflation–deflation–inflation similar to that seen in Plate 1a. Assuming a straight conduit and distance of 818 m between the upper and lower sources, the delay of about 4.4 s in the peak amplitude of volume change in the dominant subvertical dike at the lower source compared to the dominant dike at the upper source yields a propagation speed of ~ 186 m/s, 2.6 times slower than the speed of propagation of the volumetric disturbance inferred from the volume changes in Plate 1. The slower speed in this event is compatible with a slower wave speed of the crack wave for the longer period of the signal observed in this event compared to the event in Plate 1.

Plate 2 shows that a dominantly vertical force accompanies the volumetric source components in both sources. The two forces share similar waveforms with opposite polarities, in accord with a conservation of linear momentum in the overall source volume. The synchronicity of these forces is again consistent with a propagation path in the rock. Unlike the vertical force components in Plate 1, however, the vertical forces in Plate 2 start with a clear upward polarity in the upper and downward polarity in the lower source.

Plate 3c illustrates the two conduit structures imaged beneath the Sciara del Fuoco (SdF). These two structures are distinct within the uppermost 1 km of the edifice, although the conduits come to within 100 m of each other 250 m below the crater floor. The geometries of the topmost segments of the two conduits are both suggestive of the activation of a funnel-like flow disturbance induced by the transit of a gas slug through the shallow conduit bifurcation imaged near this location.

Laboratory simulations carried out by *James et al.* [2006] provide insights into the origin of the initial pressurization and downward force observed at the upper source in Plate 1a. These experiments investigate the ascent of a slug of gas in a vertical liquid-filled tube featuring a flare that sharply doubles the cross-sectional area. The tube is instrumented with pressure transducers mounted flush with the inner tube wall, and one accelerometer mounted on the exterior of the tube, and the whole assembly is free to move in the vertical direction. Detailed measurements of the flow transients obtained by *James et al.* [2006] show that the transit of a gas slug through the tube flare involves complex changes in flow pattern (Figure 2). A characteristic pinching of the slug tail (Figure 2a) is observed to occur synchronously with strong pressure and acceleration transients at the time the slug clears the flare (Figure 2b), a picture consistent with the downward and inward motion of a liquid piston formed by the thickening film of liquid falling past the slug expanding in the wider tube. The sudden deceleration of the liquid annulus as it impinges the narrower inlet to the lower tube segment generates a pressure pulse in the liquid below the flare and also induces a downward force on the apparatus

(Figure 2b). These observations are consistent with the pressurization phase and initial downward force imaged for the upper source (Plate 1a), and a similar funneling mechanism was inferred by *Chouet et al.* [2008] to be operative there. The repeatability of recorded pressure data and dependence of the magnitude of the pressure transient on slug size seen in the experiments of *James et al.* [2006] are also in harmony with the observed spatio-temporal properties of VLP signals at Stromboli [*Chouet et al.*, 2003; 2008].

At the lower source imaged in Plate 1b, the start of the vertical force signal is synchronous with the onset of deflation of the subdominant dike segment (see arrows in Plate 1b, left). As the amplitude of the upward force increases, the subdominant dike segment continuously deflates. During the same interval, the dominant dike (red-colored volumetric trace in Plate 1b) remains in a slightly deflated state. The subdominant dike reaches maximum deflation at the time the dominant dike segment goes through a transition from weak contraction to expansion, and the upward force reaches its peak amplitude ~ 0.5 s later. This picture is consistent with a compression of the subdominant dike synchronous with a downward acceleration of the liquid mass, both of which are suggestive of increasing external pressure on the conduit wall resulting from the downward vertical force acting at the upper source. Compression of the subdominant dike segment proceeds unimpeded until this process is overprinted by the arrival of the much slower volumetric expansion signal from the upper source.

A similar slug disruption mechanism was inferred in the dike system underlying the southern vent [*Chouet et al.*, 2008], although the details of the funneling process are obviously different (compare Plates 1a and 2a). *Chouet et al.* [2008] ascribed these distinct characteristics to differences in the combination of downward force due to viscous drag applied to the conduit wall by the falling liquid, and upward force resulting from the initial downward acceleration of the slumping liquid. The net force generated in this manner is much smaller than the force generated once the liquid piston forms [*James et al.*, 2006]. In one case (Plate 1a), these two force components compensate each other so that only the force induced by the deceleration of the liquid in the narrow neck of the conduit remains. In the other case (Plate 2a) the force due to initial downward acceleration of the liquid mass prevails over the drag force, and a weak upward force is seen to precede the downward force associated with the liquid piston. The initial conduit deflation synchronous with the upward force in Plate 2a may be attributed to the pressure decrease caused by a dynamical removal of mass associated with this downward acceleration of the liquid magma.

In both conduit systems, the early response of the lower source relative to the volumetric disturbance arriving from

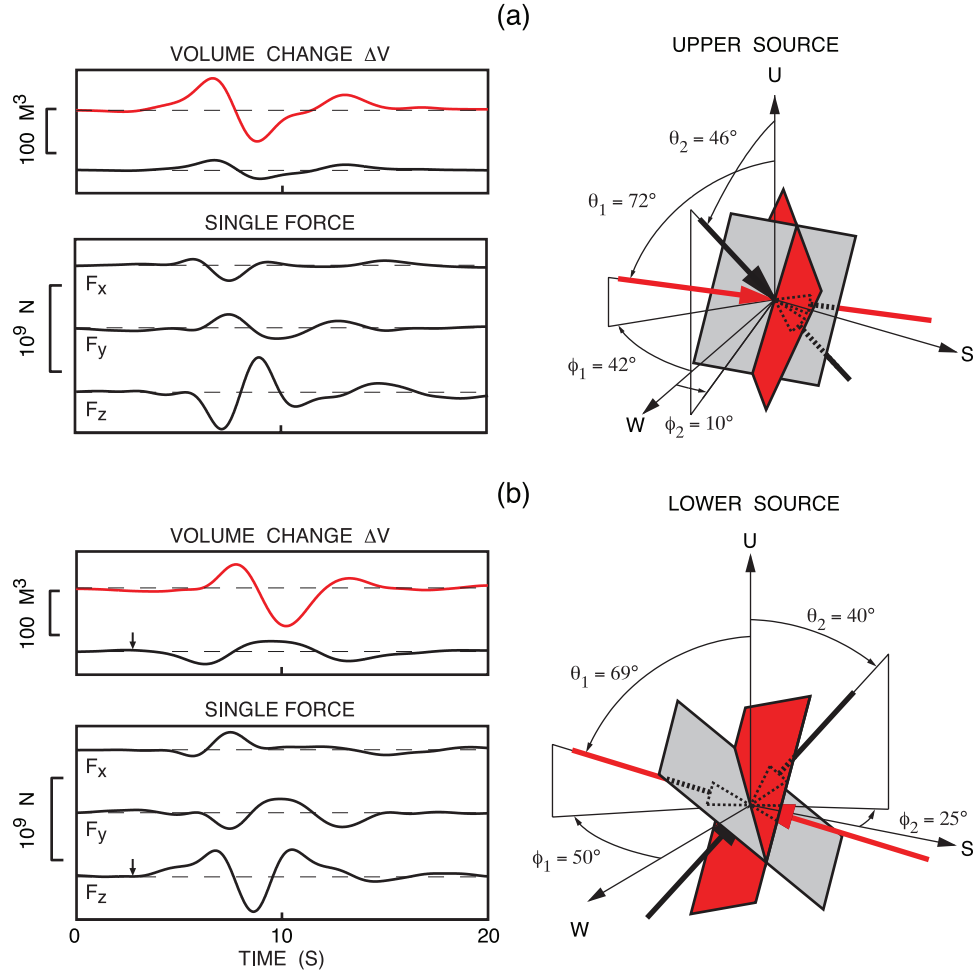


Plate 1. Sources of the type 1 event associated with eruptions from the northern vent area of Stromboli Volcano [after Chouet et al., 2008]. The two point sources are positioned at different depths in the edifice (see text for details), and each source consists of two intersecting cracks and three single-force components: F_x (east), F_y (north), and F_z (up). The source-time histories of volume change and force components are resolved over the 2- to 20-s band. Volume changes are color-coded with the color of the crack they represent in each point source. The orientation of each crack is defined by the normal to the crack plane, shown as a colored bold arrow whose direction reflects the main deflation phase of the crack. (a) Upper source. (b) Lower source. Arrows in the left panels mark the onset of deflation in the lower dike (gray dike in the right panel) and synchronous start of the upward force.

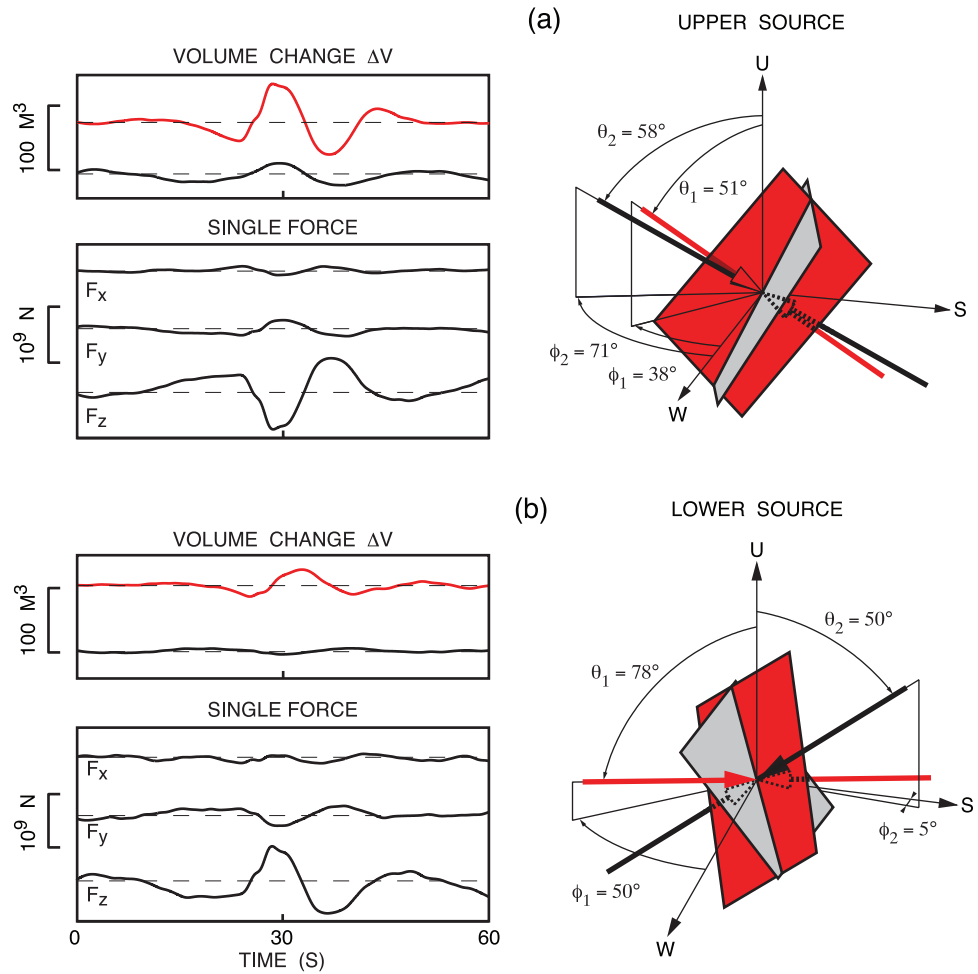


Plate 2. Same as Plate 1 but here for the type 2 event associated with eruptions from the southern vent [after Chouet *et al.*, 2008]. Note the different time scales. The source-time histories are resolved over the 2- to 30-s band. (a) Upper source. (b) Lower source.

the upper source may be interpreted as the passive response of the liquid to the movement of the conduit wall induced by elastic radiation from the force acting at the upper source. The picture emerging from these dynamics is that of an upper source representing an active fluid phase and passive solid phase, and a lower source representing an active solid phase and passive fluid phase. The overall seismic source process associated with eruptions at Stromboli may then be summarized as follows. A slug of gas formed in the deeper reaches of conduit [Burton *et al.*, 2007] rises through the lower conduit corner (the lower seismic source). At this point, the slug is most likely a few meters long and traverses this corner aseismically; past this corner, the slug expands on its way to the upper conduit bifurcation (the upper seismic source). The transit time from the lower to the upper seismic source is probably in the range of 5–15 min [James *et al.*, 2006]; hence, related changes in magmatic head are well beyond the capability of broadband seismometers to detect and are not apparent within the VLP band imaged in Plates 1 and 2. As it traverses the upper seismic source, the slug length has expanded to tens of meters, and the slug is by then seismically noisy. Gravitational slumping of the liquid occurs as the slug expands through a flare in the conduit at this location. The slumping liquid rapidly decelerates in the narrowing dike neck, increasing the liquid pressure and inducing a volume expansion in the main conduit and its subsidiary branch. The rapid deceleration and associated pressurization of the liquid couples to the conduit wall via the flare shoulders and induces a downward vertical force on the Earth. The volumetric signal propagates along the conduit at the slow speed of the crack wave, while the force signal itself propagates in the solid at the much higher speed of the compressional wave in the rock matrix, arriving at the lower conduit corner well before the crack wave. At this corner, the downward displacement of the rock induced by the force acting at the upper source impinges the bottom dike and squeezes this segment of conduit; this segment essentially acts like a spring that absorbs the downward motion of the rock. This scenario is consistent with both the small volume change of the lower dike segment, as well as its early response. The subsequent conduit response then reflects the combined effects of volumetric and mass oscillations of this liquid/gas/solid system, which are damped and eventually terminated by changing flow conditions.

3. DISCUSSION AND CONCLUSIONS

The surface traces of the upper dike segments in the two conduit systems are shown in map view in Plate 4. Gray swaths represent the uncertainty in position of the surface traces of individual segments. These swaths span a range of waveform fits that are essentially indistinguishable from

each other, and the corresponding source-time histories of volumetric and force components are virtually identical to those illustrated in Plates 1 and 2. Interestingly, the dominant dike traces in the two conduits intersect roughly 300 m NE of the northern perimeter of the summit crater. The relative positions of these two dikes in the crater area, and their intersection to the north, are in general agreement with the collapse features that developed during the effusive eruptions in 2003 and 2007. The secondary dike segment associated with the northern vent extends NW and lines up well with temporary vents active in 2003, while the secondary segment associated with the southern vent closely parallels the collapse scarps flanking the Sciara Del Fuoco to the west.

The dominant and subdominant dike traces in the conduit feeding the southern vent (red and blue traces labeled T2 in Plate 4) define an arcuate path whose apex is offset 50–100 m east of the line of vents along the main crater axis. The close proximity to this path of the three orifices NE of the southern vent suggests these may all be part of the same feeder system. The apparent overshoot of the best model of the upper conduit geometry with the vent positions along the main crater axis may easily be resolved if one assumes that the conduit becomes steeper near the surface. Although near-surface conduit curvature cannot be assessed with the data used by Chouet *et al.* [2008], it appears to be consistent with the idea of a magma pathway following the steepening dip of a preexisting sliding surface activated during a past sector collapse in the Sciara Del Fuoco [Tibaldi, 2001]. Analogue models of volcano collapse certainly seem to support this idea [see Acocella, 2005, Figure 4c].

The simple point source solutions obtained by Chouet *et al.* [2008] do not provide any constraints on the lateral extents of the dike elements shown in Plates 3 and 4, and the dimensions depicted in these plates are shown here purely for illustrative purpose. In that respect, the bifurcation imaged 320 m below the northern vent area is of particular interest. This bifurcation represents the intersection of the main dike with a dike remnant inclined 46° from the horizontal (Plate 1a). This subsidiary dike appears to be a permanent feature of the upper conduit, initially in the form of a buried segment (at the time of observations in 1997), which was momentarily forced open to the surface as a result of overpressurization during the vigorous activity of 2002–2003. This surface breakout was marked by the presence of several vents lined up along the trace of this dike during this activity [Acocella *et al.*, 2006]. The subsidiary dike is roughly orthogonal to the main dike, and its orientation follows the anticipated trajectories of the maximum gravitational stress in the upper reaches of the edifice [Gudmundsson, 2002; Acocella and Tibaldi, 2005]. The main dike itself appears to have developed along an en echelon fracture subparallel

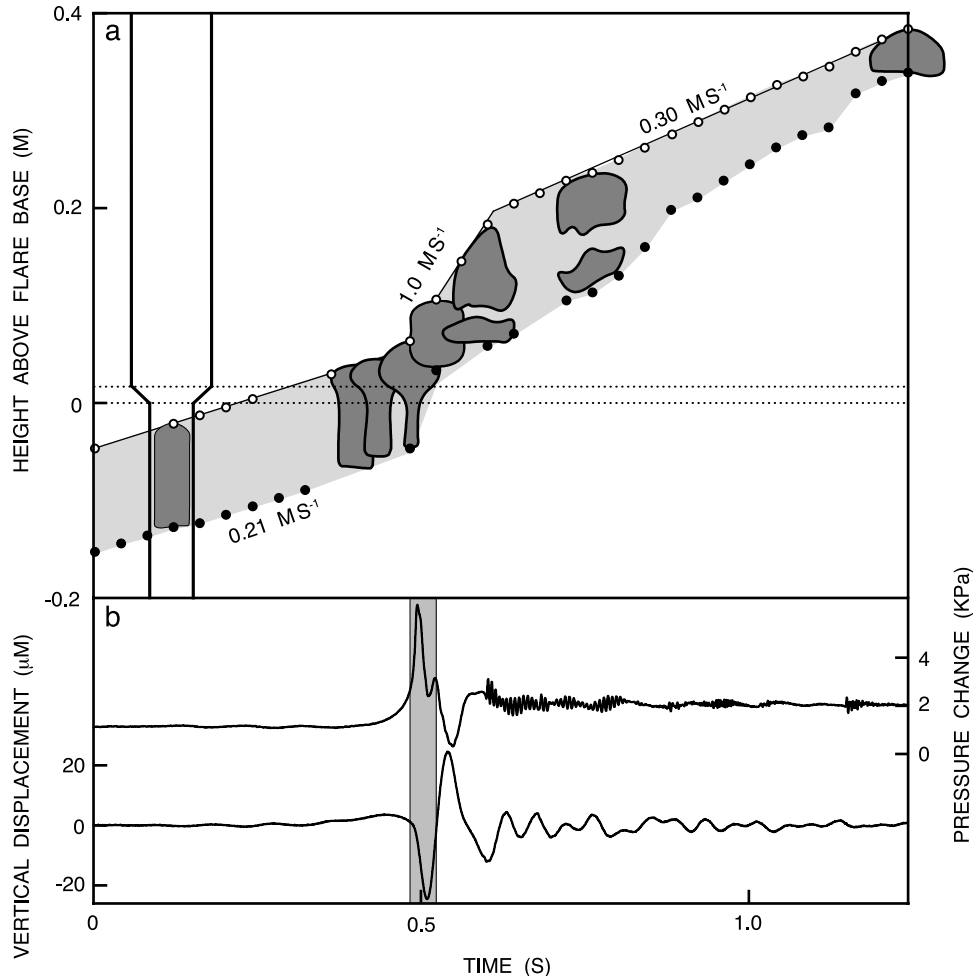


Figure 2. Slug ascent from small to large diameter tube in the laboratory experiments of James *et al.* [2006]. (a) Sketches of bubble at different positions in the tube shown at the left (diameter drawn to scale, but only short vertical segment of tube illustrated). The bubble is shown by the outline filled with dark gray. Circles and solid dots, respectively, mark the positions of the nose and tail of the bubble obtained from video data. Dotted lines mark the inlet and outlet of the flare. The slug is disrupted by turbulence shortly after entering the larger tube, with resulting daughter bubbles rapidly coalescing. (b) Pressure change (upper trace) measured at the base of the apparatus, and vertical displacement (lower trace) of the apparatus. The gray stripe represents the interval between video frames during which the slug tail passed through the flare. Note the increase of pressure synchronous with the downward displacement (downward acceleration) of the tube. The higher frequency signal starting near 0.6 s in the pressure trace probably results from the turbulence responsible for the disruption and break up of the bubble. The fluid used is a 0.1-Pa s sugar solution. Slug outlines and positions modified from James *et al.* [2006, Figure 5b]; pressure and displacement data supplied by Mike James (see James *et al.* [2006] for details).

to the dominant fracture in the conduit system feeding the southern vent.

To estimate actual dike dimensions, inversions of the eruption signals at shorter periods are necessary. Our present ability to resolve the lateral extent of the conduit is limited by our lack of knowledge of the detailed three-dimensional velocity structure of the edifice. Preliminary

inversions performed over the period range 0.5–2 s, for which the approximation of a homogeneous velocity structure is reasonable, suggest lateral dike extents of ~200 m, roughly comparable with the main dimension of the summit crater. These inversions indicate that the dominant source of radiation in this band originates in fluid oscillations in the uppermost 250 m of conduit, consistent with the idea of

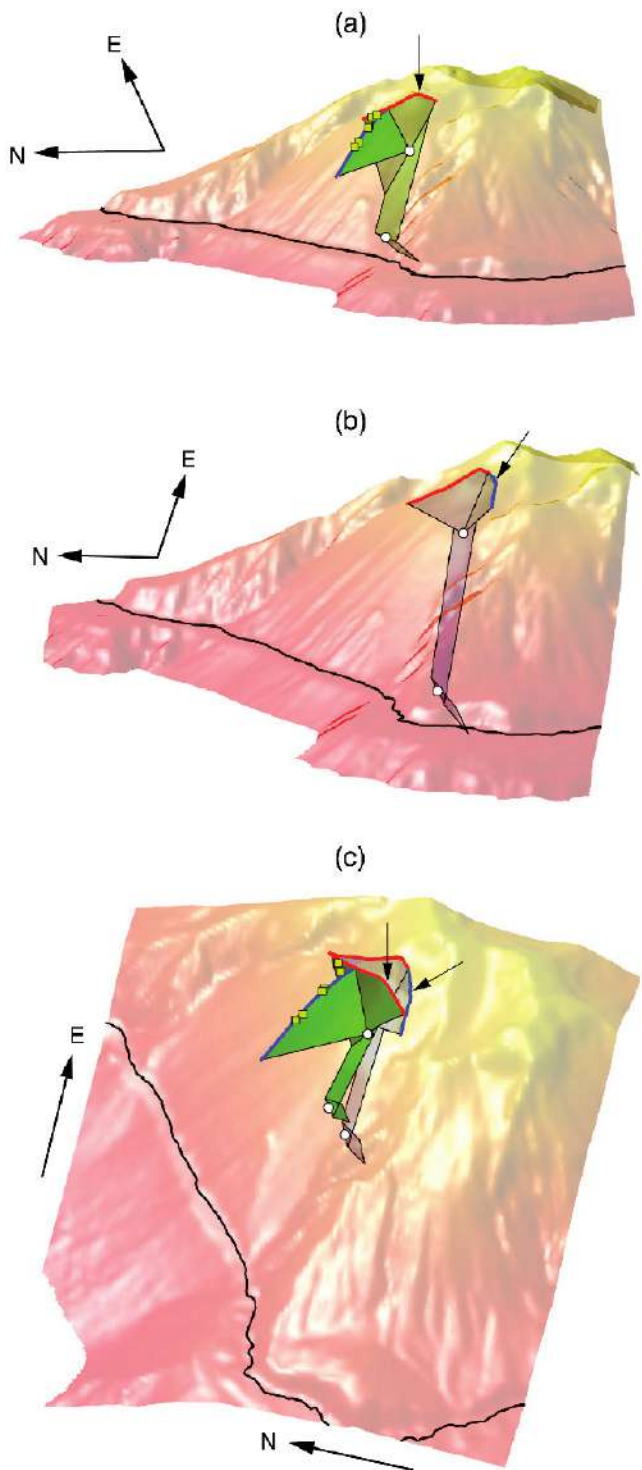


Plate 3. (a) Geometry of the uppermost 1 km of conduit underlying the northern vent area of Stromboli. A semitransparent view of the northwest quadrant of the edifice including the sector graben of the Sciara Del Fuoco, provides the reference for the location and geometry of the conduit, which is derived from the seismic source mechanisms obtained from inversions of VLP signals associated with explosions. A black line indicates sea level. The summit of the volcano is 924 m above sea level (no vertical exaggeration). The two flow disruption sites that are sources of VLP elastic radiation are indicated by small circles. The irregular red and blue lines, respectively, mark the surface traces of the dominant and is subdominant dike segments constituting the shallowest portions of the conduit system. The eruptive vent is marked by vertical arrow, and temporary vents that were active during the flank eruption in 2002–2003 are indicated by green squares. The lateral extents of individual dike segments are unknown and are shown for illustrative purpose only. (b) Same as Plate 3a for conduit underlying the southern vent area. A slanted arrows points to the southern vent. (c) Plunging view of the Sciara Del Fuoco showing the two dike systems underlying the summit crater. The conduit structure underlying the northern vent (marked by a vertical arrow) ia shaded green, and that underlying the southern vent (marked by a slanted arrow) is colored blue (see Plate 3a for details).

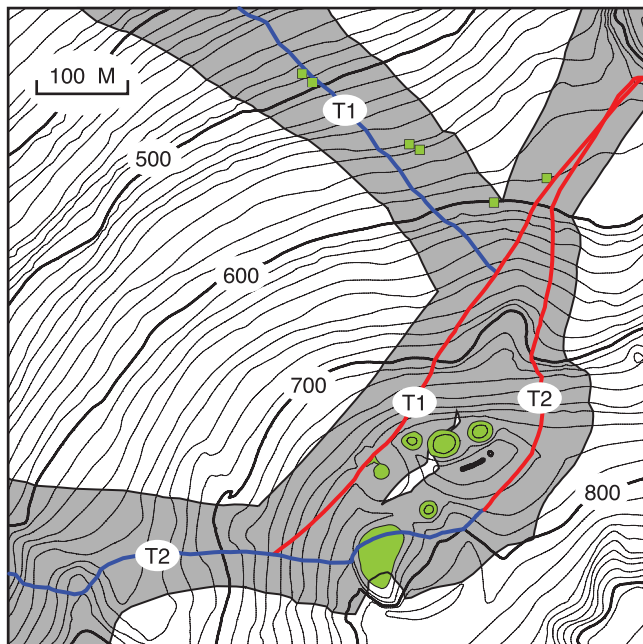


Plate 4. Map view of the upper northwest quadrant of Stromboli showing the traces of individual dike segments (colored lines and associated gray swaths) composing each of the uppermost segments of the dike systems underlying the summit crater of Stromboli. The summit vents are shown by contours filled in with green, and green squares marks the position of vents that were active in the Sciara Del Fuoco during the flank eruption in 2002–2003 [after Acocella *et al.*, 2006]. The irregular red and blue lines, respectively, mark the surface traces of the dominant and subdominant dike segments imaged for the models producing the minimum residual error between data and model (T1 refers to the dike system underlying the northern vent area, and T2 refers to the dike system underlying the southern vent). The gray swaths show the ranges of solutions producing residual errors in fitted VLP waveforms that are within 0.5% of the minimum residual error. Thin contour lines represent 10-m contour intervals and bold contours mark 100-m contour intervals.

a disruption of the magma column induced by the action of a liquid piston.

The conduit structures illustrated in Plate 3 are consistent with results from earlier analyses by Chouet 1997. Using array measurements carried out over the band 0.2–2.5 s, Chouet 1997 demonstrated that a combination of source and path effects can explain the complexities observed in the short-period components of the seismic wave fields of tremor and explosions at Stromboli. Their results clearly indicate that the sources of these shorter-wave components originate at depths shallower than 200 m beneath the summit crater, with occasional bursts of energy originating from deeper sources extending to depths as great as 3 km. This dominance of shallow source components in the short-period wavefields is in agreement with the results of waveform inversions obtained in the 0.5- to 2-s band (see above). Interestingly, the array results of Chouet 1997 are also suggestive of a NW dip in the upper conduit [see Chouet *et al.*, 1997, Figure 11], although this could not be independently confirmed at the time. These array data, however, are now found to be in harmony with the northwestern dip of the uppermost reaches of the conduit system imaged in Plate 3. A shallow NW-dipping source region under the crater was also inferred by La Rocca *et al.* [2004] based on probabilistic analyses of dual-array data.

The analyses carried out by Chouet *et al.* [2008] clearly point to the key role played by the conduit geometry in controlling fluid motion and resultant processes. Each discontinuity in the conduit provides a site where pressure and momentum changes resulting from flow processes associated with the transit of a gas slug through the discontinuity are coupled to the Earth or where the elastic response of the conduit can couple back into pressure and momentum changes in the fluid. The resulting processes are naturally oscillatory and feature rich dynamics that reflect the complex physicochemical behavior of the volcanic system from the surface downward. As our ability to image the volcanic conduit response to flow processes improves, a major challenge facing us is the development of our quantitative description of the fluid dynamics underlying the observed seismic source mechanisms. Refined understanding of these processes will require a multidisciplinary research effort involving detailed field measurements, laboratory experiments, and numerical modeling. This research is fundamental to monitoring and interpreting the underground migration of magma, and thus enhances our ability to forecast hazardous volcanic activity.

Acknowledgments. We are indebted to David Hill, Willie Lee, and two anonymous reviewers for helpful suggestions. We are grateful to Mike James and Stephen Lane for the compilation and elaboration of Figure 2. This research was supported in part through

a grant from the Consiglio Nazionale delle Ricerche, Gruppo Nazionale di Vulcanologia. The laboratory work was funded by the Royal Society and the Leverhulme Trust.

REFERENCES

- Acocella, V. (2005), Modes of sector collapse of volcanic cones: Insights from analogue experiments, *J. Geophys. Res.*, **110**, B02205, doi:10.1029/2004JB003166.
- Acocella, V., and A. Tibaldi (2005), Dike propagation driven by volcano collapse: A general model tested at Stromboli, Italy, *Geophys. Res. Lett.*, **32**, L08308, doi:10.1020/2004GL022248.
- Acocella, V., M. Neri, and P. Scarlato (2006), Understanding shallow magma emplacement at volcanoes: Orthogonal feeder dykes during the 2002–2003 Stromboli (Italy) eruption, *Geophys. Res. Lett.*, **33**, L17310, doi:10.1029/2006GL026862.
- Auger, E., L. D'Auria, M. Martini, B. Chouet, and P. Dawson (2006), Real-time monitoring and massive inversion of source parameters of very long period seismic signals: An application to Stromboli volcano, Italy, *Geophys. Res. Lett.*, **33**, L04301, doi:10.1029/2005GL024703.
- Burton, M., P. Allard, F. Muré, and A. La Spina (2007), Magmatic gas composition reveals the source depth of slug-driven Strombolian explosive activity, *Science*, **317**, 5835, 227–230.
- Calvari, S., L. Spampinato, L. Lodato, A. J. L. Harris, M. R. Patrick, J. Dehn, M. R. Burton, and D. Andronico (2005), Chronology and complex volcanic processes during the 2002–2003 flank eruption of Stromboli volcano (Italy) reconstructed from direct observations and surveys with a handheld thermal camera, *J. Geophys. Res.*, **110**, B02201, doi:10.1029/2004JB003129.
- Capaldi, G., et al. (1978), Stromboli and its 1975 eruption, *Bull. Volcanol.*, **41**, 1–27.
- Chouet, B. (1986), Dynamics of a fluid-driven crack in three dimensions by the finite difference method, *J. Geophys. Res.*, **91**, 13,967–13,992.
- Chouet, B. (1988), Resonance of a fluid-driven crack: Radiation properties and implications for the source of long-period events and harmonic tremor, *J. Geophys. Res.*, **93**, 4375–4400.
- Chouet, B., N. Hamisevicz, and T. R. McGetchin (1974), Photoballistics of volcanic jet activity at Stromboli, Italy, *J. Geophys. Res.*, **79**, 4961–4976.
- Chouet, B., G. Saccorotti, M. Martini, P. Dawson, G. De Luca, G. Milana, and R. Scarpa (1997), Source and path effects in the wave fields of tremor and explosions at Stromboli Volcano, Italy, *J. Geophys. Res.*, **102**, 15,129–15,150.
- Chouet, B., P. Dawson, T. Ohminato, M. Martini, G. Saccorotti, F. Giudicepietro, G. De Luca, G. Milana, and R. Scarpa (2003), Source mechanisms of explosions at Stromboli Volcano, Italy, determined from moment-tensor inversions of very-long-period data, *J. Geophys. Res.*, **108(B1)**, 2019, doi:10.1029/2002JB001919.
- Chouet, B., P. Dawson, and M. Martini (2008), Shallow conduit dynamics at Stromboli volcano, Italy, imaged from waveform inversions, in *Fluid Motions in Volcanic Conduits: A Source of*

- Seismic and Acoustic Signals*, edited by S. J. Lane, and J. S. Gilbert, *J. Geol. Soc. London Spec. Publ.*, 307, 57–84.
- D'Auria, L., F. Giudicepietro, M. Martini, and R. Peluso (2006), Seismological insight into the kinematics of the 5 April 2003 Vulcanian explosion at Stromboli Volcano (southern Italy), *Geophys. Res. Lett.*, 33, L08308, doi:10.1029/2006GL026018.
- Ferrazzini, V., and K. Aki (1987), Slow waves trapped in a fluid-filled infinite crack: Implication for volcanic tremor, *J. Geophys. Res.*, 92, 9215–9223.
- Gudmundsson, A. (2002), Emplacement and arrest of sheets and dykes in central volcanoes, *J. Volcanol. Geotherm. Res.*, 116, 279–298.
- James, M. R., S. J. Lane, and B. A. Chouet (2006), Gas slug ascent through changes in conduit diameter: Laboratory insights into a volcano-seismic source process in low-viscosity magmas, *J. Geophys. Res.*, 111, B05201, doi:10.1029/2005JB003718.
- La Rocca, M., G. Saccorotti, E. Del Pezzo, and J. Ibanez (2004), Probabilistic source location of explosion quakes at Stromboli Volcano estimated with double array data, *J. Volcanol. Geotherm. Res.*, 131, 123–142.
- Tibaldi, A. (2001), Multiple sector collapses at Stromboli volcano, Italy: How they work, *Bull. Volcanol.*, 63, 112–125.
-
- B. Chouet and P. Dawson, US Geological Survey, 345 Middlefield Road, MS 910, Menlo Park, CA 94025, USA. (chouet@usgs.gov).
- M. Martini, Osservatorio Vesuviano, 328 Via Diocleziano, I-80124, Naples, Italy.

Volcanic and Seismic Activity at Stromboli Preceding the 2002–2003 Flank Eruption

M. Burton,¹ S. Calvari,¹ L. Spampinato,¹ L. Lodato,¹ N. A. Pino,² E. Marchetti,³ and F. Murè¹

Regular surveys with a thermal camera from both ground- and helicopter-based surveys have been carried out on Stromboli since October 2001. This data set allowed us to detect morphological changes in Stromboli's summit craters produced by major explosions and to track an increase in volcanic activity associated with a heightened magma level within the main conduit that preceded the 2002–2003 effusive eruption. Together with thermal measurements, geophysical surveys performed in May and September/October 2002 highlighted clear increases in the amplitude of very long period (VLP) events, consistent with the ascent of the magma column above the VLP source region. The increased magma level was probably induced by elevated pressure in the deep feeding system, controlled by regional tectonic stress. This, in turn, pressurized the uppermost part of the crater terrace, producing greater soil permeability and soil degassing. Eventually, the magma loading caused the NW flank of the summit craters to fracture, allowing lava to flood out at high effusion rates on 28 December 2002, starting an approximately 6-month-long effusive eruption.

1. INTRODUCTION

Stromboli volcano is the easternmost island in the Aeolian archipelago, Italy (Figure 1). It has been almost continuously active for the least 13 centuries [Rosi *et al.*, 2000], producing mild explosive activity interspersed with rare effusive and major explosive events [Barberi *et al.*, 1993]. Typical explosions send small volumes of ejecta ~50–300 m above the summit craters every 5–10 min producing a wide range of styles of activity [Patrick *et al.*, 2007] described in general as Strombolian activity. Explosion products are typically ~50%

crystallized, 30–60% vesiculated black scoria sourced from the superficial part of Stromboli's plumbing system [Landi *et al.*, 2004; Lautze and Houghton, 2005, 2007; Polacci *et al.*, 2006]. Continuous quiescent degassing occurs between explosive events, and this process accounts for the majority of gas release from the volcano [Allard *et al.*, 1994; Burton *et al.*, 2007; Harris and Ripepe, 2007a]. Mild Strombolian activity is interrupted roughly twice a year by larger explosions that can eject magma fragments hundreds of meters above the craters, representing a hazard for any nearby volcano observers. Such explosions have been termed “major” explosions by Barberi *et al.* [1993], to distinguish from the more powerful, and rarer, “paroxysmal” explosions that can produce bombs that land on populated areas around the coast of Stromboli; these latter incidents have occurred in 1930, 1944, and 2003. Major explosions and paroxysms erupt crystallized resident magma mixed with “golden pumice,” a glassy and gas-rich magma rising from several kilometers’ depth [Bertagnini *et al.*, 1999, 2003].

Lava effusions are observed on Stromboli every 5–20 years [Barberi *et al.*, 1993]. The most recent effusive eruptions

¹ Istituto Nazionale di Geofisica e Vulcanologia, Catania, Italy.

² Istituto Nazionale di Geofisica e Vulcanologia, Napoli, Italy.

³ Dipartimento Scienze della Terra, Università di Firenze, Firenze, Italy.

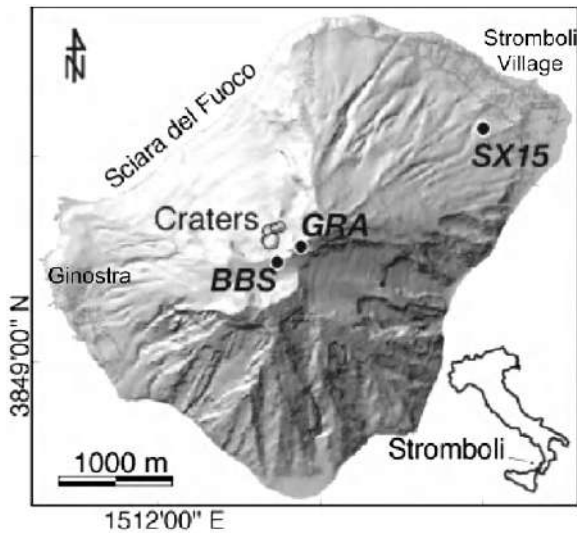


Figure 1. Digital elevation model of Stromboli volcano showing the location of the Island (right low corner), Stromboli village, the summit craters, Sciarra del Fuoco, the flank affected by lava effusion, PSF (indicated by the GRA seismic station) from which we collected thermal images in ground-based mode, and the position of seismic stations deployed during the temporary experiments before the 2002–2003 flank eruption.

occurred in 1975 [Capaldi et al., 1978], 1985 [De Fino et al., 1988], 2002–2003 [Bonaccorso et al., 2003; Calvari et al., 2005; Lodato et al., 2007], and 2007 (S. Calvari, et al., Comparison between the 2002–03 and 2007 flank eruptions at Stromboli Volcano: Basis for predicting future volcanic events, submitted to Geophysical Research Letters, 2007). The 2002–2003 event was of particular significance since on 30 December, 2 days after eruption onset, a minor collapse of the NW flank of the volcano occurred (Sciarra del Fuoco in Figure 1) [Bonaccorso et al., 2003; Pino et al., 2004; Tinti et al., 2004], inducing a tsunami wave that inundated the coast of Stromboli, and mildly damaged coastlines of other islands in the archipelago as well as the port of Milazzo, Sicily (Figure 1). The landslide was followed by an approximately 6-month-long effusion of lava from the Sciarra del Fuoco [Calvari et al., 2005].

In this paper, we present and interpret thermal imagery and seismic data collected at Stromboli before the 2002–2003 eruption, highlighting coupled volcanological and seismic eruption precursors as well as morphological changes in the summit craters associated with larger explosions. We use this evidence to examine the likely causes of the 2002–2003 eruption, and to assess likely precursors to further effusive eruptions.

2. METHODS

2.1. Thermal Imaging on Stromboli

In recent years, Stromboli has been used as a laboratory for the development of thermal imaging techniques applied to volcanology, with use of the forward-looking infrared (FLIR; www.flir.com) cameras being particularly prevalent. This work has allowed detailed descriptions to be made of the emission dynamics during normal Strombolian activity [Patrick et al., 2007] as well as during gas puffing [Harris and Ripepe, 2007a]. It has also been used to measure and track volcanic activity during the 2002–2003 effusive eruption [Calvari et al., 2005], and paroxysmal events [Harris et al., this volume].

Thermal measurements presented in this work were carried out using a FLIR TM 695 thermal. The instrument detector consists of an uncooled focal plane array of microbolometers with sensitivity in the midinfrared between 7.5 and 13 μm . It has a $24^\circ \times 18^\circ$ field-of-view (FOV) producing an effective 1.3 mrad FOV for each pixel in the 320×240 detector array. Images were collected from both the ground at a fixed position [at Pizzo Sopra la Fossa (PSF); see Plate 1 and 2] and from airborne surveys using a helicopter provided by the Italian Department of Civil Protection (Plate 1). The TM695 required significant exposure times on the order of tenths of a second, producing a challenge for airborne data collection as the velocity of the helicopter tended to produce blurred imagery. This problem was overcome by collecting imagery while hovering.

Thermal imagery is information-rich, and provides insights on the morphology of the active structures within Stromboli's summit craters and qualitative temperature variations therein; however, quantitative determination of surface temperatures is a challenge for several reasons: absorption of infrared radiation by the atmosphere, volcanic gases, and aerosols [Sawyer and Burton, 2006]; non-Lambertian emission of radiation from the highly structured emitting surface; nonperpendicular viewing angles; subpixel temperature variations [Wright and Flynn, 2003; Ball and Pinkerton, 2006; Patrick et al., 2007]. The sum of these effects tends to result in an underestimate of the true source temperature by ~10–20%. Data presented here have been carefully selected to minimize the effect of plume attenuation; however, the fact that the source of degassing is coincident with the volcanic structures that we observe means that it is impossible to completely exclude this effect. All images were collected within a 1-km distance from the summit craters and from similar viewing angles; minor corrections due to attenuation from atmospheric water vapor were taken into account using the built-in correction algorithm of the thermal camera, using 60% relative humidity and distances estimated for each survey. The effects of non-Lambertian

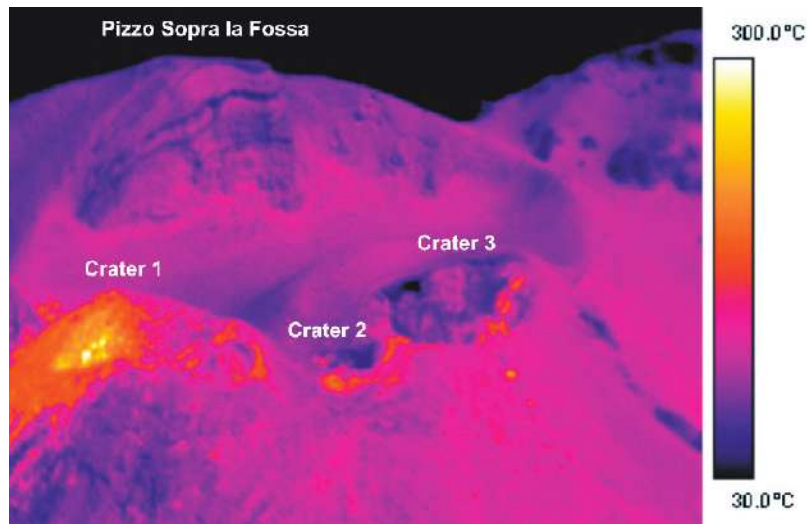


Plate 1. Thermal image of the summit craters of Stromboli and PSF collected on 23 July 2002 from Civil Protection helicopter. View is from the northwest. The craters are aligned over a distance of ~250 m in a NE–SW orientation, and the PSF is ~150 m above the crater terrace.



Plate 2. Composite thermal image of the summit terrace of Stromboli on 20 October 2001, as seen from PSF, SE of the craters. The field of view covers a horizontal distance of ~300m. Crater 1 (or CR1) is also known as the northeast crater (NEC) and crater 3 (CR3) as the southwest crater (SWC). Hot spots in the foreground between crater 2 and crater 1 are probably the result of the major explosion that occurred on 20 October 2001 at 0032. The larger hot spots within craters 2 and 3 are active vents.

radiation emission have been ignored in this analysis, but we believe that this effect is minor compared with plume attenuation. Temperature underestimates due to imagery distortion were attenuated by selecting mainly zenith images pointing within the summit crater vents.

In summary, determining errors on the measured temperature of the summit craters of Stromboli is a challenge; however, we estimate that our quantitative measurements may underestimate the true source temperature by up to $\sim 100^{\circ}\text{C}$. Considering that the order of magnitude of observed temperatures is significantly larger than this underestimation, clear trends of temperature variation are still detectable.

2.2. Seismic Measurements

Explosive activity at Stromboli volcano has been investigated and monitored for the past 30 years with permanent geophysical instruments and temporary experiments (see *Harris and Ripepe* [2007b] for a review) and contributed greatly to the understanding of the dynamics driving explosive activity at open-conduit basaltic volcanoes. Data presented here were collected during two temporary seismic broadband–acoustic–thermal experiments (Figure 1) on 14–27 May, and 29 September–2 October 2002 on the summit area of the volcano [*Marchetti and Ripepe*, 2005]. The broad frequency content of the instrument deployed during the experiment and the short source-to-receiver distance, allow precise observations of very long period (VLP) seismic activity during the typical explosive activity at Stromboli. During May 2002, two seismic–acoustic stations (BBS, GRA) were deployed on the summit of Stromboli volcano at distances of 250–300 m from the summit craters (Figure 1). Four months later, between 29 September and 2 October 2002, a seismoacoustic station was deployed again at one of the two sites investigated during the previous experiment (GRA). In both experiments, each station consisted of a five-channel, 16-bit analog-to-digital converter digitizing signals from a Guralp CMG-40T broadband seismometer, with sensitivity of $800 \text{ V m}^{-1} \text{ s}^{-1}$ and 30-s Eigen period, and a Monacor preamplified electret microphone with sensitivity of 46 mV Pa . Time synchronization was achieved with a radiocode receiver. Despite the short deployment of the seismic–acoustic stations the two temporary experiments are of particular interest, because they represent the only close-range geophysical observations of the active craters in the 7 months preceding the eruption onset.

3. VOLCANIC ACTIVITY AT STROMBOLI PRIOR TO THE 2002–2003 ERUPTION

Before the 2002–2003 eruption, field and thermal surveys were carried out immediately after three major explosions:

on 20 October 2001, 23 January 2002, and 25 July 2002. On 23 January 2002, some morphologic changes at the summit craters were detected by comparison with a previous survey, as well as mapping of the fallout and characterization of the erupted products [*Calvari and Pompilio*, 2001a; *Calvari et al.*, 2002]. Thermal surveys were also carried out on 11 March, 16 May, and 22 June 2002 [*Burton and Murè*, 2002a, 2002b].

The major explosion on 20 October 2001 at 0032 GMT led to the death of one tourist who had been sleeping in the summit area. A thermal camera survey of the craters was performed a few hours after the explosion with the TM695 (see Plate 2). Ejecta from the explosion were widely dispersed around the craters. The central part of the crater terrace between crater 1 and crater 3 contained three closely spaced vents in the middle portion, and three hornitos oriented approximately NE–SW to the northern margin. Crater 2 showed three hot spots with maximum temperatures of $\sim 200^{\circ}\text{C}$. Strombolian activity was observed at a single vent located on the northern margin of crater 3, and from two vents within crater 2. During ~ 1 hour of observation, ~ 10 explosions were recorded from crater 1, throwing jets of lava ~ 100 m above the crater rim (Plate 3a). Crater 3 instead exhibited gas venting, with rare Strombolian explosions producing jets 20–30 m in height (Plate 3b). In general, during 2002 crater 2 exhibited high temperature gas venting with rare but violent Strombolian explosions.

On 23 January 2002 at 2054 (local time), another major explosion occurred at Stromboli. The noise from the explosion was audible from the villages at the base of the island, and was accompanied by ash fallout that lasted several minutes. The following morning a survey of the summit area of the volcano was performed to verify the dispersal of the erupted products and their nature [*Calvari et al.*, 2002]. The area around the summit craters was covered with ash and blocks, composed of lithic material up to 60 cm in size, with minor amounts of spatter up to 1.7 m in length. No low porphyritic products were found. The greatest density of lithic deposits was observed in a belt about 200 m wide between the craters and PSF. Spatter was more heavily deposited NE of PSF. Fine-grained material covered the crater zone and the NE flank of the volcano up to the village of Stromboli. Fallout material formed an almost continuous carpet at PSF, in the areas where usually many tourists typically observe the eruptive activity. During the 2.5 h of field survey, only five weak explosions from crater 1 were recorded, and none at all from craters 2 and 3. This activity was therefore much weaker compared with that observed after the major explosion of 20 October 2001 (Plate 4). The survey also revealed profound morphological and temperature changes at crater 2 compared with October 2001, which had widened by ~ 16

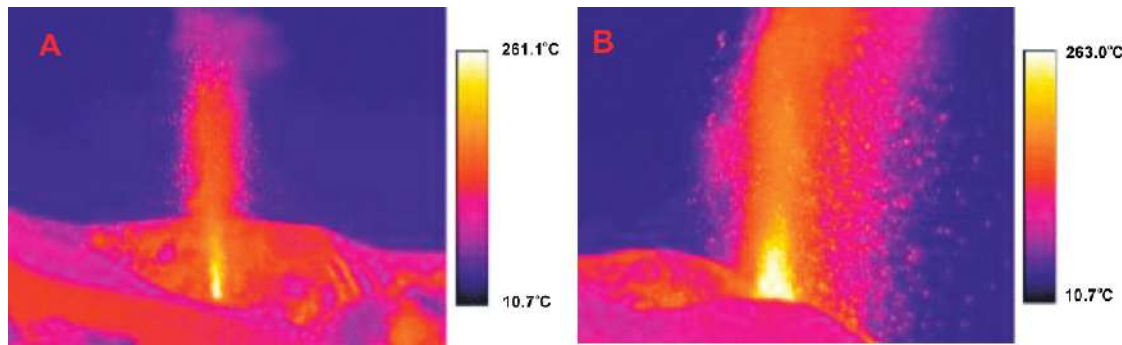


Plate 3. Thermal images recorded on 20 October 2001 from PSF, showing explosive activity at (a) crater 3 and (b) crater 1 [Calvari and Pompilio, 2001b]. The temperature scale does not show the peak values, which exceeded 500°C.

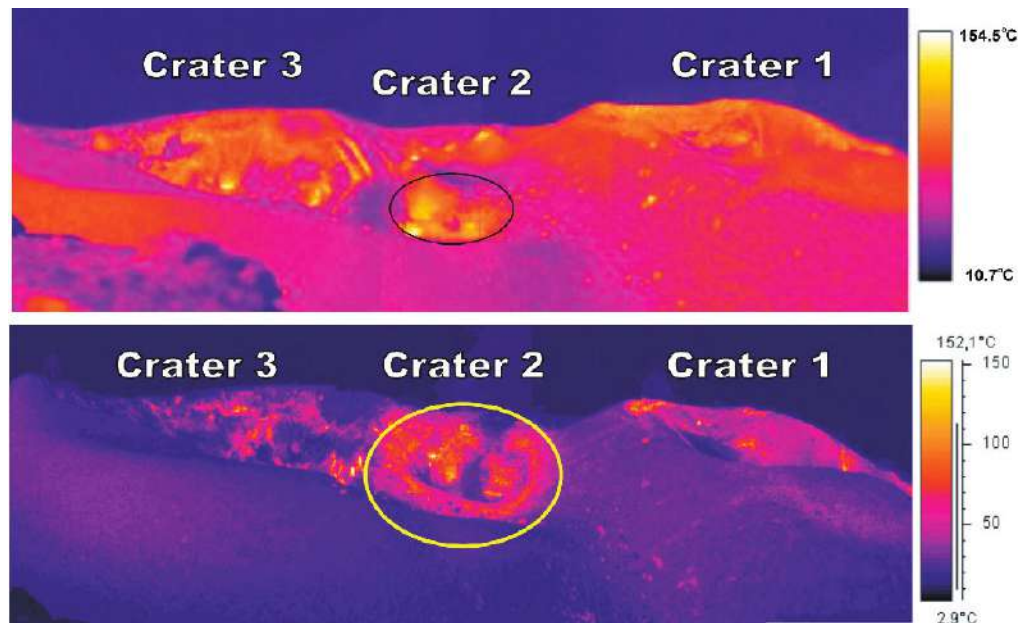


Plate 4. Comparison of two thermal images collected from PSF on 20 October 2001 (top) and 24 January 2001 (bottom), respectively. The second was recorded ~10 h after the major explosion of 23 January. Hot spots above crater 2 are hornitos, whereas those on the flanks of crater 1 are spatter from the explosive event. The black circle around crater 2 in the upper figure indicates the area affected during the explosion, and the yellow circle in the lower plot highlights the new morphology of crater 2 after the explosion.

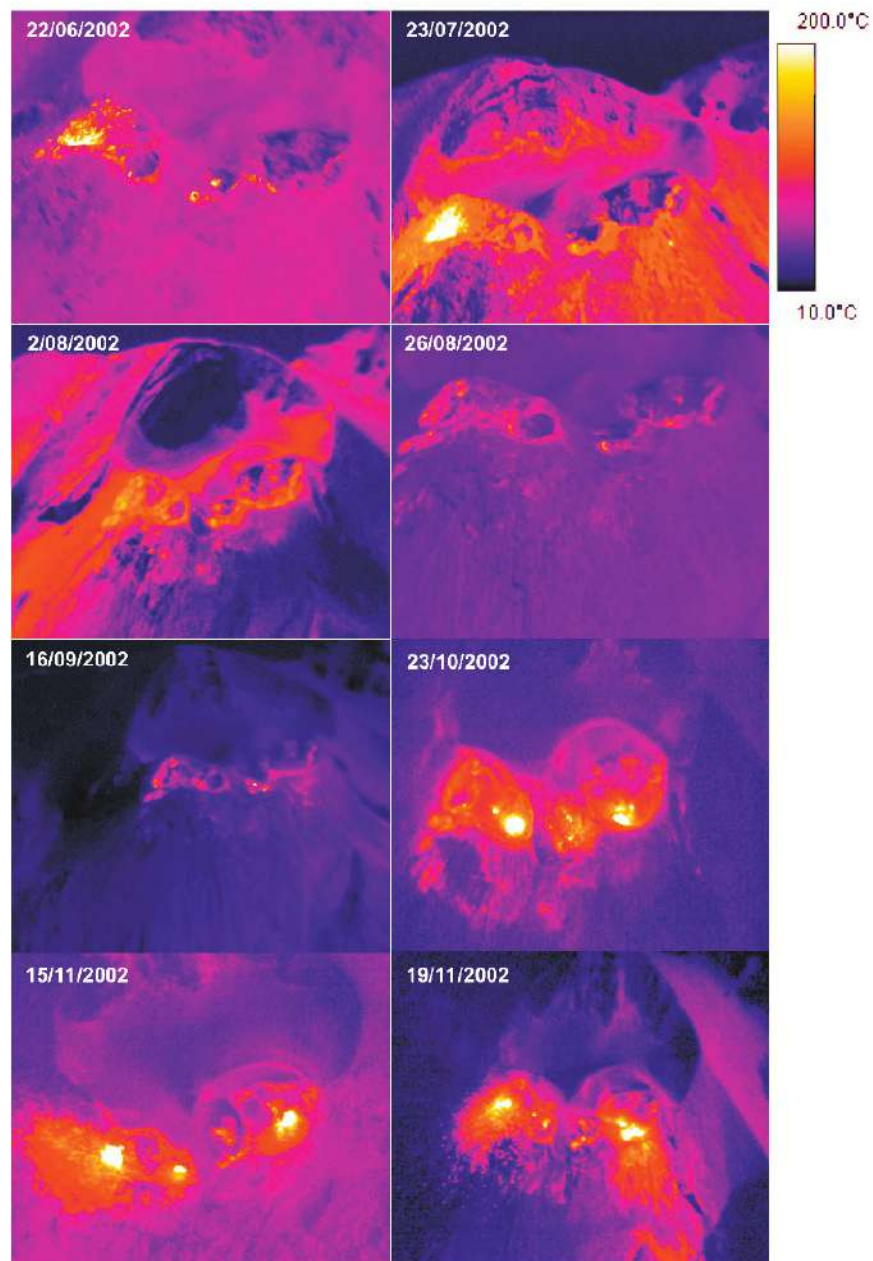


Plate 5. Thermal images collected from August to November 2002 from NW. The same temperature scale was used in all images. All images collected from a ~NW direction, showing craters 1, 2, and 3 from left to right. Note the marked increase in thermal emission at the summit craters from September 2002.

m (to 26 m diameter from ~10 m) and warmed by 120°C (to 320°C from ~200°C) [see also *Harris and Ripepe*, 2007a]. The high temperature of the inner walls of crater 2 was probably the result of morphological changes and possibly residual heating from near-surface magma. The combined observations led *Calvari et al.* [2002] to conclude that the eruptive event of 23 January 2002 could have been caused by obstruction of crater 2 overpressuring the system and triggering an explosion. After this major explosion, some concern arose regarding the lack of explosive activity at crater 3, suggesting a potential obstruction, which might have been followed by a new violent episode similar to that of 23 January 2002. A total of nine further field surveys were conducted with the FLIR thermal camera on Stromboli from April 2002 until the eruption onset on 28 December 2002 (see Plate 5). Below, we highlight the main volcanological observations made during these surveys.

On 16 May 2002, FLIR measurements were carried out at PSF from 10.14 to 1235 GMT (all following times are GMT). Activity at the summit was primarily located at crater 1 and consisted of relatively weak explosions, expelling smaller amounts of pyroclasts than had been detected in the preceding months. On 22 June 2002, measurements were performed again from PSF, from 0942 to 1150. Activity at the summit was still sited at crater 1 and consisted of explosions that propelled scoriae up to ~250 m in height above the craters. Occasionally, ash emissions were observed from craters 1 and 3. The activity was of significantly greater intensity compared with that observed in May.

On 23 July 2002, thermal imaging was carried out at PSF using a helicopter of the National Civil Protection. During the period of observation (1012–1357) activity at the summit craters was characterized by 50- to 300-m-high explosions of incandescent material from crater 1 that fell primarily on the N flank of the crater. Jets of ash and scoria from crater 3 powered convecting clouds of ash to maximum heights of ~500 m above the craters. Explosions occurred approximately every 10 min from crater 1 and every 20 min from crater 3. Continuous quiescent gas emissions were observed at the other craters. The presence of large (1–2 m), incandescent scoria ejected from crater 1 suggested that this crater was open, allowing magma to easily be expelled. High-pressure jets of ash from crater 3 indicated that its conduit was still partially obstructed. The level of volcanic activity was significantly higher compared with that observed in the preceding surveys.

On 25 July 2002, in response to a major explosion that occurred on 24 July during poor weather, an overflight of the summit craters of Stromboli was performed. Low cloud prevented landing at the summit, and thermal images and digital photographs were collected from the helicopter (Plate

6). No clear morphological changes had taken place within the summit craters; however, a clear NE-trending thermal anomaly was visible within the crater terrace and on the N flank of crater 1. On 1 and 2 August 2002, sequences of thermal imagery were collected from PSF and from helicopter, respectively. The intensity of explosive activity was relatively low on both days, leaving few hot deposits on the crater floor. On 26 August 2002, further observations from PSF showed a higher frequency of explosions from both craters 1 and 3 compared with that observed in August. The northernmost sector of crater 1 showed almost continuous mild strombolian activity during 5 min of a 1-h observation. Helicopter-borne measurements showed modest temperatures at the base of the summit craters. This observation represents the minimum level of activity observed before the 2002–2003 eruption.

Measurements on 16 September showed the first signs of an increasing trend in volcanic activity at the summit craters of Stromboli; explosions were of greater intensity from both craters 1 and 3, with scoria landing outside the crater rim. Crater 2 showed an intermittent, passively released, high-temperature gas emission. This trend continued in October, when observations performed on 23 October 2002 from the helicopter showed higher temperatures than those previously seen for all three craters. Craters 1 and 3 had large thermal anomalies at their base associated with recently deposited pyroclasts from explosive activity. A vent in crater 2 displayed continuous gas venting, at an inclined angle relative to vertical. Overall, in October the observations showed notable increase in thermal energy release compared with the previous observations of 2001 and 2002. A thermal survey carried out on 15 November showed exceptionally high temperatures (Plate 7) and the presence of two small lava flows sourced from overflowing magma from vents within craters 1 and 2. Intense explosive activity and increasingly shallow magma level had filled the summit craters with scoria. Superficial magma was clearly visible in digital photographs.

In summary, the thermal imagery collected during 2001–2002 allowed us to qualitatively track a distinct increasing trend in volcanic activity that had begun since August 2002, after a sharp reduction in activity after the major explosion of 24 July 2002. These trends are shown quantitatively in Plate 8, where we plot the maximum observed temperatures from comparable images during each survey. We distinguish between temperatures measured during quiescent degassing (circles) and during explosions (crosses). As discussed above, we estimate that these temperatures are underestimated by about 100°C due to attenuation effects.

Detailed temperature variations in each crater are complex, due to a combination measurement error and real activity changes. Crater 2 showed the clearest temperature trends,

increasing sharply in March 2002 before reducing to a minimum in July and August and rising again from September. Craters 1 and 3 showed rapid temperature increases in June, which decreased before the major explosion of 25 July. These craters, such as crater 2, demonstrated a clear increasing trend from September 2002 until the eruption onset. The increased thermal emission from September followed by minor lava overflows from craters 1 and 2 in November and the eruption itself on 28 December suggests that a significant increase in the magma level within the conduit occurred during this period. In the following section, we present seismic data that allows further investigation of the inferred changes in magma level preceding the 2002–2003 eruption.

4. SEISMIC INVESTIGATIONS ON STROMBOLI DURING 2002

The two seismic investigation conducted during 2002 were carried out during periods when the intensity of volcanic activity varied greatly. As described above, in May 2002 the level of explosive activity was relatively low, with infrequent, weak explosions observed at crater 1 and crater 3, and sustained quiescent degassing from the crater 2. On the contrary, in September 2002 the explosive activity was more intense with frequent explosions from crater 1s and 3. There was also a variation in volcanic activity during the 4-day September campaign, with increased energy of explosions from crater 3 starting from 30 September, when bombs and fragments were ejected up to ~ 300 m above the summit vents. We were therefore able to investigate the coupling between seismic and volcanic activity for a range of explosive intensities during two distinct periods and during the course of the September campaign.

The change in the intensity of volcanic activity during the May and September 2002 experiment was clearly reflected by the amplitude of VLP events (Plate 9) recorded at the summit of Stromboli volcano. The amplitude of VLP events was quite stable during May 2002, with a mean value of 5×10^{-6} m, and increased to $\sim 10^{-5}$ m during the September–October experiment (Plate 9). Furthermore, the amplitude of VLP events appeared to be coupled with the observed increase in explosive activity during the September experiment, with a rapid increase of VLP amplitude (from 6×10^{-6} to 1.5×10^{-5} m) on 30 September 2002, together with an observed increase in the heights of erupted products during explosions.

5. DISCUSSION

Magma level within Stromboli's conduits exercises a fundamental control on the nature of eruptive activity. The fact that mild explosive activity has been maintained almost

continuously for hundreds of years at Stromboli [Rosi *et al.*, 2000] suggests that the magma level must have varied relatively little over that timescale. The observation of an increasing thermal emission and increasing volcanic activity from August to December 2002, was a clear perturbation to this steady-state behavior. The lava overflows that preceded the 2002–2003 eruption indicate that the level of magma within the conduit was higher than usual, and suggests that the main cause of the increase in thermal/volcanic activity had been a steadily increasing level of magma at Stromboli. It also appears likely that the increased pressure exerted by the magma-filled conduits contributed to the eventual failure of the conduit system on 28 December, the rapid outflow of resident lava and therefore the start of the 2002–2003 eruption.

Laboratory experiments [Ripepe *et al.*, 2001; James *et al.*, 2004] and moment tensor inversion of seismic records [Chouet *et al.*, 2003] suggest that VLP seismic transients may be produced by rapid transfer and expansion of gas volumes within volcanic conduits, and therefore their frequency should reflect the rate of formation of gas slugs within magma columns. The amplitude of VLP events is instead controlled by both volume and gas overpressure within gas slugs. Accordingly, VLP seismicity is a direct expression of both gas dynamics and magma level at Stromboli volcano, and the increased amplitude recorded in September 2002 may be the result of an increased gas overpressure due to the heightened magma-free surface within the summit crater conduits, as evidenced by thermal data and direct observations.

Since an increasing magma level appears to be the fundamental physical process that produced the observed variations in the volcanological, thermal, and seismic data presented here, it is useful to assess what controls the magma level within Stromboli's conduit system. In the simplest of interpretations, the pressure within a feeding reservoir at several kilometers depth beneath the summit craters supports the weight of the magma column. There are therefore two main ways in which magma level may be perturbed: a change in the density of magma or a change in the pressure of the feeding reservoir. Although there is little evidence for a change in magma density from September 2002, there is ample evidence for a heightened magnitude of regional tectonic stress in late 2002. In September 2002, a large magnitude earthquake occurred off the coast of Palermo [Cigolini *et al.*, 2007], causing fractures to open in the countryside near the northern coast of Sicily; and late in October 2002, a major dike-driven eruption began on Mt. Etna [Andronico *et al.*, 2005]. Cigolini *et al.* [2005] hypothesized that the increased levels of Radon degassing at Stromboli observed leading up to the 2002–2003 eruption may have been induced by the regional tectonic stress. Our observations are

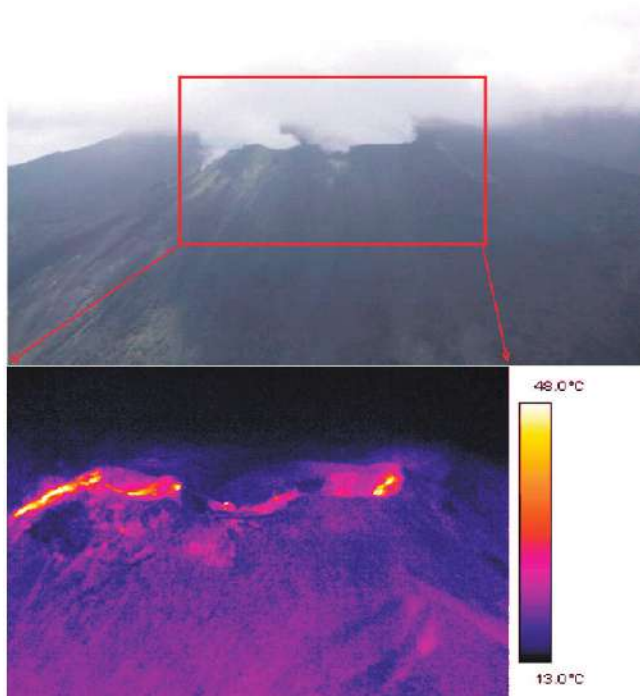


Plate 6. The upper image is an aerial photograph of the summit craters of Stromboli recorded on 25 July 2002 from NW. Red box indicates approximate field of view shown in the thermal image (below).



Plate 7. Visible image of the summit craters of Stromboli on 15 November. Lava overflows from crater 2 are highlighted with a yellow line. Note the presence of superficial magma in the northern sector of crater 1. The craters are filled with pyroclastic deposits, compare with figure 2.

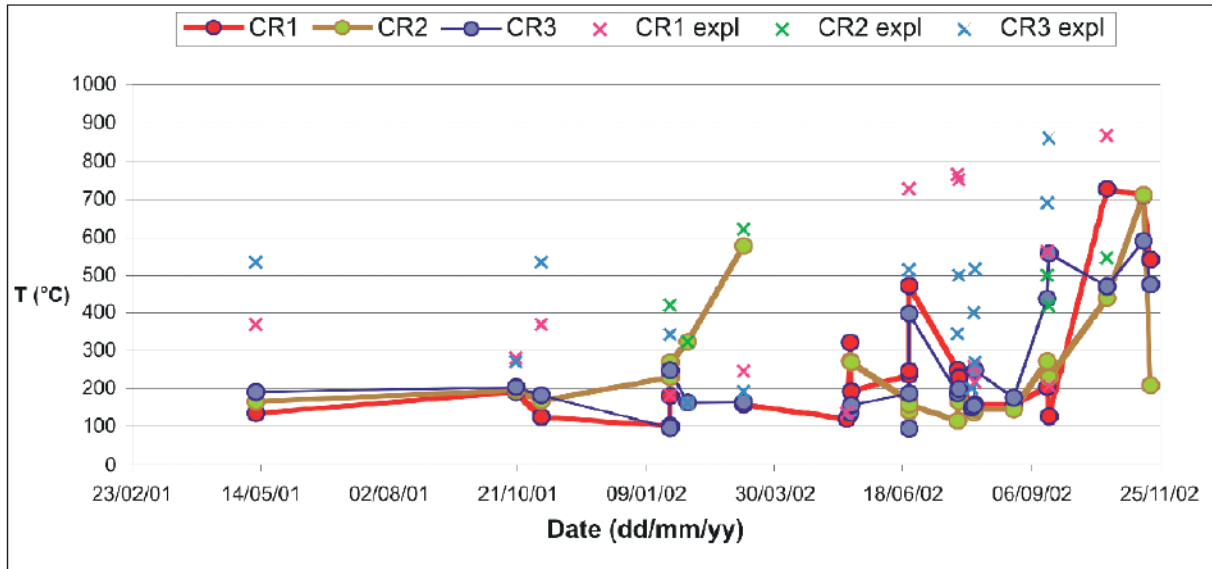


Plate 8. Time series of maximum apparent temperatures observed at the summit craters of Stromboli from 11 May 2001 to 19 November 2002. Circles show the peak temperatures at each crater during quiescent degassing; crosses show peak temperatures measured at each crater during explosions.

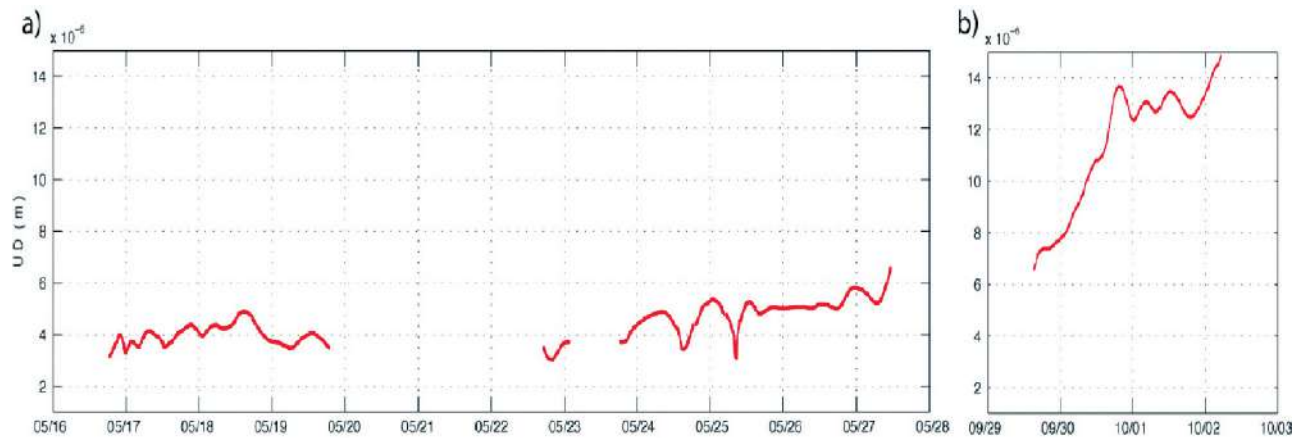


Plate 9. Amplitude of VLP seismic transients recorded at station GRA deployed on the summit of Stromboli volcano during temporary experiments carried out in (a) May and (b) September 2002.

consistent with a hypothesis that such a stress could have heightened magma level within Stromboli's conduit triggering (1) increase in thermal energy released at the surface; (2) higher overpressure in VLP events; and (3) eventual rupturing of the northern flank of crater 1, producing an effusive eruption. Increased magma levels could have also induced changes in permeability of gas flow through structural weaknesses of the volcano summit area, as the stress exerted by the high magma level produces strain in the surrounding superficial rocks. Such strain could have produced the observed increases in CO₂ [Carapezza et al., 2002] and Radon [Cigolini et al., 2007] degassing measured before the 2002–2003 eruption.

6. CONCLUSIONS

Regular surveys with a handheld or tripod-mounted thermal camera from both ground and helicopter allowed us to detect changes in the morphology of the summit craters produced by major explosions, detect thermal anomalies, discriminate between different styles of activity at different vents, investigate vent obstructions, and, most importantly, track the increasing level of magma within the conduits of Stromboli that preceded and led to the 2002–2003 effusive flank eruption. The integration of thermal imaging data, direct observations, and seismic surveys provide us with a clear observation of increasing magma levels within the conduit system of Stromboli before the 2002–2003 eruption. In the future, careful monitoring of infrared radiation from the summit areas of Stromboli, integrated with other geophysical and geochemical observations, will allow variations in magma level to be carefully tracked, and thereby improve hazard assessments for this volcano.

Acknowledgments. We wish to thank the Italian Civil Protection and its pilots for the helicopter surveys of the volcano, and Alessandro Bonaccorso and Enzo Boschi for their support to this work. Constructive reviews by Andy Harris and an anonymous reviewer improved this work significantly.

REFERENCES

- Allard, P., J. Carbonelle, N. Métrich, H. Loyer, and P. Zettwoog (1994), Sulphur output and magma degassing budget of Stromboli volcano, *Nature*, **368**, 326–330.
- Andronico, D., et al. (2005), A multi-disciplinary study of the 2002–03 Etna eruption: Insights into a complex plumbing system, *Bull. Volcanol.*, **67**, 314–330.
- Ball, M., and H. Pinkerton (2006), Factors affecting the accuracy of thermal imaging cameras in volcanology, *J. Geophys. Res.*, **111**, B11203, doi:10.1029/2005JB003829.
- Barberi, F., M. Rosi, and A. Sodi (1993), Volcanic hazard assessment at Stromboli based on review of historical data, *Acta Vulcanol.*, **3**, 173–187.
- Bertagnini, A., M. Coltell, P. Landi, M. Pompilio, and M. Rosi (1999), Violent explosions yield new insights into dynamics of Stromboli volcano, *Eos Trans. AGU*, **80**(52), 633–636.
- Bertagnini, A., N. Métrich, P. Landi, and M. Rosi (2003), Stromboli volcano (Aeolian Archipelago, Italy): An open window on the deep-feeding system of a steady state basaltic volcano, *J. Geophys. Res.*, **108**(B7), 2336, doi:10.1029/2002JB002146.
- Bonaccorso, A., S. Calvari, G. Garfi, L. Lodato, and D. Patané (2003), Dynamics of the December 2002 flank failure and tsunami at Stromboli volcano inferred by volcanological and geophysical observations, *Geophys. Res. Lett.*, **30**(18), 1941, doi:10.1029/2003GL017702.
- Burton, M. R., and F. Muré (2001), Report on visual observation made at Stromboli summit 21/8/2001, internal report, 2 pp., Ist. Naz. di Geofis. e Vulcanol., sez. di Catania, Catania, Italy.
- Burton, M. R., and F. Muré (2002a), Report on visual observation made at Stromboli summit 16/5/2002, internal report, 4 pp., Ist. Naz. di Geofis. e Vulcanol., sez. di Catania, Catania, Italy.
- Burton, M. R., and F. Muré (2002b), Report on visual observation made at Stromboli summit 22/6/2002, internal report, 3 pp., Ist. Naz. di Geofis. e Vulcanol., sez. di Catania, Catania, Italy.
- Burton, M. R., H. M. Mader, and M. Polacci (2007), The role of gas percolation in quiescent degassing of persistently active basaltic volcanoes, *Earth Planet. Sci. Lett.*, **70**(9), 1023–1029, doi:10.1016/j.epsl.2007.08.028.
- Calvari, S., and M. Pompilio (2001a), Rapporto del sopralluogo a Stromboli del 5 novembre 2001, internal report, 5 pp., Ist. Naz. di Geofis. e Vulcanol., sez. di Catania, Catania, Italy.
- Calvari, S., and M. Pompilio (2001b), Rapporto del sopralluogo a Stromboli del 20 ottobre 2001, internal report, 4 pp., Ist. Naz. di Geofis. e Vulcanol., sez. di Catania, Catania, Italy.
- Calvari, S., M. Pompilio, and D. Andronico (2002), Stromboli (Italy) Fallout from 23 January explosion carpets popular tourist area, *Bull. Global Volc. Network*, **27**(1), 14–15.
- Calvari, S., L. Spampinato, L. Lodato, A. J. L. Harris, M. R. Patrick, J. Dehn, M. R. Burton, and D. Andronico (2005), Chronology and complex volcanic processes during the 2002–2003 flank eruption at Stromboli volcano (Italy) reconstructed from direct observations and surveys with a hand-held thermal camera, *J. Geophys. Res.*, **110**, B02201, doi:10.1029/2004JB003129.
- Capaldi, G., et al. (1978), Stromboli and its 1975 Eruption, *Bull. Volcanol.*, **41**(3), 259–285.
- Carapezza, M. L., S. Ingaggiato, L. Brusca, and M. Longo (2004), Geochemical precursors of the activity of an open-conduit volcano: The Stromboli 2002–2003 eruptive events, *Geophys. Res. Lett.*, **31**, L07620, doi:10.1029/2004GL019614.
- Chouet, B., P. Dawson, T. Ohminato, M. Martini, G. Saccorotti, F. Giudicepietro, G. De Luca, G. Milana, and R. Scarpa (2003), Source mechanisms of explosions at Stromboli Volcano, Italy, determined from moment-tensor inversions of very-long-period data, *J. Geophys. Res.*, **108**(B1), 2019, doi:10.1029/2002JB001919.
- Cigolini, C., G. Gervino, R. Bonetti, F. Conte, M. Laiolo, D. Coppolo, and A. Manzoni (2005), Tracking precursors and degassing

- by radon monitoring during major eruptions at Stromboli Volcano (Aeolian Islands, Italy), *Geophys. Res. Lett.*, 32, L12308, doi:10.1029/2005GL022606.
- Cigolini, C., M. Laiolo, and D. Coppola (2007), Earthquake–volcano interactions detected from radon degassing at Stromboli (Italy), *Earth Planet. Sci. Lett.*, 257(3), 511–525.
- De Fino, M., L. La Volpe, S. Falsaperla, G. Fazzetta, G. Neri, L. Francalanci, M. Rosi, and A. Sbrana (1988), The Stromboli eruption of December 6, 1985–April 25, 1986: Volcanological, petrological and seismological data, *Rend. Soc. Ital. Mineral. Petrol.*, 43, 1021–1038.
- Harris, A., and M. Ripepe (2007a), Temperature and dynamics of degassing at Stromboli, *J. Geophys. Res.*, 112, B03205, doi:10.1029/2006JB004393.
- Harris, A. J. L., and M. Ripepe (2007b), Synergy of multiple geophysical approaches to unravel explosive eruptions conduit and source dynamics—A case study from Stromboli, *Chem. Erde*, 67, 1–35.
- James, M. R., S. J. Lane, B. Chouet, and J. S. Gilbert (2004), Pressure changes associated with the ascent and bursting of gas slug in liquid-filled vertical and inclined conduits, *J. Volcanol. Geotherm. Res.*, 129, 61–82.
- Landi, L., N. Métrich, A. Bertagnini, and M. Rosi (2004), Dynamics of magma mixing and degassing recorded in plagioclase at Stromboli (Aeolian Archipelago, Italy), *Contrib. Mineral. Petrol.*, 147, 213–227.
- Lautze, N. C., and B. F. Houghton (2005), Physical mingling of magma and complex eruption dynamics in the shallow conduit at Stromboli volcano, Italy, *Geology*, 33, 425–428.
- Lautze, N. C., and B. F. Houghton (2007), Linking variable explosion style and magma textures during 2002 at Stromboli volcano, Italy, *Bull. Volcanol.*, 69, 445–460.
- Lodato, L., L. Spampinato, A. Harris, S. Calvari, J. Dehn, and M. Patrick (2007), The morphology and evolution of the Stromboli 2002–2003 lava flow field: An example of a basaltic flow field emplaced on a steep slope, *Bull. Volcanol.*, 69, 661–679, doi:10.1007/s00445-006-0101-6.
- Marchetti, E., and M. Ripepe (2005), Stability of the seismic source during effusive and explosive activity at Stromboli Volcano, *Geophys. Res. Lett.*, 32, L03307, doi:10.1029/2004GL021406.
- Patrick, M. R., A. J. L. Harris, M. Ripepe, J. Dehn, D. A. Rothery, and S. Calvari (2007), Strombolian explosive styles and source conditions: Insights from thermal (FLIR) video, *Bull. Volcanol.*, 69, 769–784, doi:10.1007/s00445-006-0107-0.
- Pino, N. A., M. Ripepe, and G. B. Cimini (2004), The Stromboli Volcano landslides of December 2002: A seismological description, *Geophys. Res. Lett.*, 31, L02605, doi:10.1021/2003GL018385.
- Polacci, M., D. R. Baker, L. Mancini, G. Tromba, and F. Zanini (2006), Three-dimensional investigation of volcanic textures by X-ray computed microtomography and implications for conduit processes, *Geophys. Res. Lett.*, 33, L13312, doi:10.1029/2006GL026241.
- Ripepe, M., S. Ciliberto, and M. Della Schiava (2001), Time constraints for modeling source dynamics of volcanic explosions at Stromboli, *J. Geophys. Res.*, 106(B5), 8713–8727.
- Rosi, M., A. Bertagnini, and P. Landi (2000), Onset of the persistent activity at Stromboli Volcano (Italy), *Bull. Volcanol.*, 62, 294–300.
- Sawyer, G. M., and M. R. Burton (2006), Effects of a volcanic plume on thermal imaging data, *Geophys. Res. Lett.*, 33, L14311, doi:10.1029/2005GL025320.
- Tinti, S., A. Armigliato, G. Pagnoni, A. Manucci, R. Tonini, and F. Zaniboni (2004), Analysis of landslides and tsunamis of the 30th December 2002 in Stromboli, Italy, paper presented at L'eruzione di Stromboli (28 dicembre 2002–20 luglio 2003), Istituto Nazionale di Geofisica e Vulcanologia, Catania, Italy, 20–21 May 2004.
- Wright, R., and L. P. Flynn (2003), On the retrieval of lava-flow surface temperatures from infrared satellite data, *Geology*, 31(10), 893–896, doi:10.1130/G19645.1.

M. Burton, S. Calvari, L. Lodato, F. Murè, and L. Spampinato, Istituto Nazionale di Geofisica e Vulcanologia, Piazza Roma, I-95123 Catania, Italy. (burton@ct.ingv.it)

E. Marchetti, Dipartimento Scienze della Terra, Università di Firenze, I-50121 Firenze, Italy.

N. A. Pino, Istituto Nazionale di Geofisica e Vulcanologia, I-80124 Napoli, Italy.

The Eruptive Activity of 28 and 29 December 2002

Laura Pioli,¹ Mauro Rosi,² Sonia Calvari,³ Letizia Spampinato,³ Alberto Renzulli,⁴ and Alessio Di Roberto⁵

At 1820 UT of 28 December 2002, an eruptive vent opened on the NE flank of the Sciara del Fuoco (SdF) at 600 m above sea level, marking the onset of the 2002–2003 eruptive crisis of Stromboli volcano. The first eruptive hours were characterized by mild spattering and effusive activity from the new vent and the summit vent at crater 1. Gravitational instability processes also determined the partial collapse of NE walls of the summit cone (crater 1). Pyroclastic material partly accumulated on the NE part of the SdF and partly flowed downslope and reached the sea at Spiaggia dei Gabbiani, forming a ~4-m-thick, reddish avalanche, that was soon covered by a lava flow emitted in the following hours. In this paper, we describe the first hours of activity through eyewitnesses' reports, geophysical monitoring, field and laboratory studies, of the erupted pyroclastic material and lava flows. Daily temperature measurements were carried out on the avalanche deposit formed by the flow of scoria along the SdF, using a handheld thermal camera mainly during helicopter surveys. A fast cooling rate was typical of the deposit surface, and a slow cooling rate was representative of its inner portion.

1. INTRODUCTION

The Stromboli eruptive crisis of 2002–2003 started on the early evening of 28 December 2002, interrupting high-frequency and energetic Strombolian explosions at the summit vents [Bonaccorso *et al.*, 2003; Tommasi *et al.*, 2004;

Burton et al., this volume]. The eruptive phenomena were not preceded by significant geophysical precursors and were witnessed by local people. No direct information about fracture formation, deformation, and failure phenomena is available for these early phases; the Istituto Nazionale di Geofisica e Vulcanologia (INGV) optical cameras located on the Pizzo and pointing the summit craters only partially monitored the onset of the crisis, suggesting that at least part of the eruptive phenomena occurred below the crater terrace. The INGV permanent GPS network did not record any significant changes in benchmark position before and during the eruption [Bonaccorso *et al.*, 2003].

The very initial phenomena included the proximal accumulation of a spatter and lithic agglutinate and the emission, from the NE crater, of an unusually fast-moving lava flow, which lined the agglutinate deposit and covered the hot avalanche apron, and the formation of a hot avalanche, which reached the sea in the northern corner of the Sciara del Fuoco (SdF, the unstable NW flank of the volcano, Figure 1). In this work, we present accounts of witnesses, field observation of the deposits carried out during early January 2003, grain size, component, petrography, and chemistry of

¹Department of Geological Sciences, University of Oregon, Eugene, Oregon, USA.

²Dipartimento di Scienze della Terra, Università di Pisa, Pisa, Italy.

³Istituto Nazionale di Geofisica e Vulcanologia, Sezione di Catania, Catania, Italy.

⁴Istituto di Scienze della Terra, Università di Urbino, Urbino, Italy.

⁵Istituto Nazionale di Geofisica e Vulcanologia, Sezione di Pisa, Pisa, Italy.

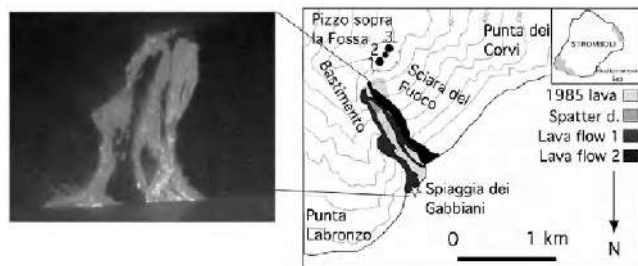


Figure 1. Map of the deposit erupted on 28 and 29 December 2002 compared with thermal image taken during a survey made in the morning of 29 December: (1) 1985 lava flow, (2) lava flow 1, (3) lava flow 2, and (4) spatter agglutinate. Numbers on the map indicate the summit craters. The star indicates the outcrop of the hot avalanche deposit.

the material emitted in the initial phase of the eruption. The data are used to assess eruptive dynamics, and timing of the phenomena occurred on 28 and 29 December.

2. METHODS

Eyewitnesses' observations were collected and cross-checked during interviews conducted in the month of January 2003. Images collected by the INGV video camera from 1600 to 2025 UT of 28 December were also analyzed. The first scientific direct observations (comprising visual and thermal inspection) of the eruption were conducted during a helicopter survey, on the morning of 29 December 2002. Several field surveys were conducted before the deposits were completely covered by lava flows in the upper SdF sector and completely eroded at the coast exposures. Proximal deposits produced during the first hours of the eruption were observed in the days following the onset of the eruption starting from 2 January 2003 during several field inspections conducted inside the SdF. Part of the deposits was displaced from its original position seaward, by slope movements of the northeasternmost sector of the SdF, which also formed a scarp that truncated the 28 December late afternoon deposits. The deposits above and below the scarp, eventually survived the major landslide event of 30 December, which instead affected the sector of the SdF located further west.

Samples of the lava flows and pyroclastic fragments were collected from 600 m above sea level (asl) outcrops and the coast area and further analyzed for chemical composition, componetry, grain size, and texture. Grain size analyses were performed partly in the field (for the fraction coarser than 5ϕ) and partly in the laboratory with standard dry half sieving techniques. Chemical whole-rock analyses were performed at the Actlabs Laboratory Ltd (Ontario, Canada) by induc-

tively coupled plasma-optical emission spectroscopy (ICP-OES) for major elements and ICP-mass spectrometry (MS) for trace elements after crushing and powdering the samples in an agate mortar to avoid contamination. Samples for the ICP-OES-MS methods were mixed with a flux of lithium metaborate and lithium tetraborate and fused in an induction furnace. The molten melts were poured into a solution of 5% nitric acid containing an internal standard and mixed continuously until completely dissolved. Errors are $\leq 1\%$ for major oxides and $\leq 3\%$ for trace elements. Phenocryst contents were obtained through comparative charts for estimating volume percent of minerals in thin sections.

Thermal monitoring was carried out using a TM 695 forward-looking infrared (FLIR) thermal camera. This is capable of acquiring a 320×240 -pixel image every 2 s, and the $24^\circ \times 18^\circ$ field of view of the lens equates to a $0.075^\circ \times 0.1^\circ$ pixel. Over the typical 1–2 km line of sight distances considered in this study, the pixel size is 1.3–2.6 m. This thermal camera can record images according to three temperature ranges: -40° to 120°C ; 0° to 500°C ; 350° to 1500°C . To investigate the thermal behavior of the 28 December deposit, we generally used the middle range, taking care to avoid sun reflection or direct solar irradiation that increases apparent temperatures of several tens of Celsius degrees [Calvari and Pinkerton, 2004]. FLIR thermal cameras can automatically calibrate; in fact, if path length, air temperature and relative humidity, and emissivity are input, temperatures corrected for atmospheric and emissivity effects are output. For these purposes, distances were corrected on the basis of observed dimensions of the summit craters, measured during field surveys with a Leica range finder.

3. RESULTS

3.1. INGV Camera Images

Timing of the crisis onset was also inferred from the images collected by the INGV video camera, which was installed on the Pizzo Sopra la Fossa area (Figure 1), and was pointing directly toward the summit craters. The wind was blowing to the NE, and any gas plume was rapidly drifted to the same direction. The images revealed that just before the crisis onset, intermittent Strombolian explosions were visible above crater 3 vents, alternating with lower fountaining from craters 2 and 1 (Figure 2). Starting from 1720 UT, diffuse red glowing was visible from an area located below the craters' rim, east of crater 1, rapidly increasing in intensity. Glowing intensity reached a climax from 1800 to 1900 UT, suggesting that, at least occasionally, the eruptive activity occurred very close to the field of view of the camera. At least four main glowing periods alternated to short pauses

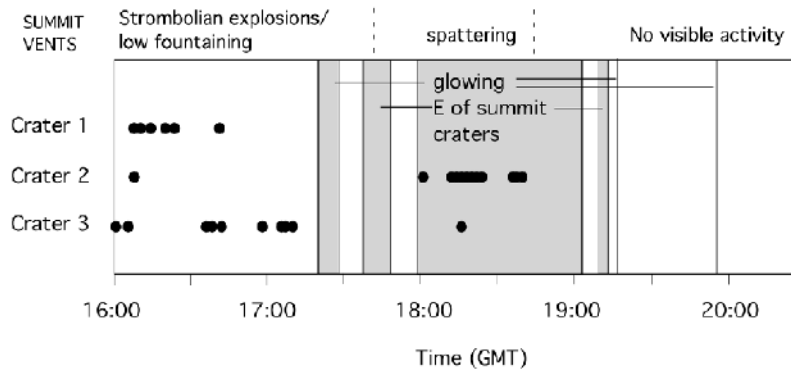


Figure 2. Sequence of Strombolian explosion that occurred at the summit craters from 1500 to 1700 UT (1600–1800 LT) on 28 December 2002. Dots indicate explosions.

(~10–15 min) of no visible activity. After the onset of the eruption, the activity at the summit craters consisted of low fountaining mainly visible above the crater 2 area. After 1910 UT, only occasional, low-intensity, red glowing was visible from the main area. A very bright flash resembling lightning was visible in the sky at 1923 UT. Throughout all the observation period, degassing plumes were visible above the crater terrace, flowing to the east of the field of view.

3.2. Eyewitnesses' Reports

Several residents of Stromboli and Ginostra villages witnessed the early phenomena, which started late afternoon of 28 December 2002, making valuable observations on their timing. Description and timing reported by the different witnesses were fairly consistent and provided very useful and valuable information, which complement those started by the scientific personnel of the INGV in the morning of 29 December. Among the interviewed people were Pino Restuccia, Mario Pruitt, and Carlo Lanza. They all have good knowledge of the mountain and made observations from different spots on the SdF borders in the first 4 h after the onset of the eruption. People in both Stromboli and Ginostra villages noticed an intense, persistent glowing at the summit of the mountain between 1700 and 1800 UT. The onset of the glowing was followed minutes later by the raising of a white steam column from a location close to the SdF shoreline. For the residents of Stromboli village, this was immediately perceived as indicating that hot, fast-moving material had reached the sea. Pruitt reached the viewpoint of Punta dei Corvi on the west side of the SdF between 1730 and 1800 UT and observed two distinct fans of hot water originating from two points on the coastline of the SdF. Restuccia refers that, after the onset of the phenomena, he was hearing for

sometime a sound like “a river of stone” from the SdF and that the sound was accompanied by the vertical rising of ash-laden clouds from the whole northeastern side of the SdF. While reaching Punta Labronzo, he was engulfed in a dense ash cloud and hit by a shower of lapilli and sand. Because the wind was blowing from NW, the only possible source of the lapilli was from explosions that originated at the Spiaggia dei Gabbiani where the first hot material had reached the seashore. Between 1800 and 1900 UT, two lavas descending the SdF had also reached the sea. The one flowing along the northeastern border of the SdF was extremely fast and reached the Spiaggia dei Gabbiani between 1745 and 1800 UT, with an estimated speed of 4–9 km/h [Lodato et al., 2007]. As soon as the lava entered the sea, it produced a large mass of vapor carrying droplets of salty water. The westernmost one was slower and reached the sea a little later but within the same time interval. Between 1800 and 1830 GMT, Lanza, from a spot at 700 m asl, observed that the fast-moving lava flow originated by an overflow from the northeastern crater. Later on, between 1830 and 1900 UT, from this same place, Restuccia reported that the overflow was over, the NE cone was still intact, but two lava vents were active at the foot of the cone. One was located where the hornitos of May–June 2003 would have later formed; the other one was located more inside the SdF at higher elevation. The eruptive scene was clearly visible due to the glowing of the active lava flows. At about 1900 UT, when he was on his way back between 700 and 400 m asl along the pathway, he heard a loud sound. A few minutes later, he observed a flow moving at high speed along the SdF slope; it was “getting bigger as it advanced.” According to the witnesses who reached Punta Labronzo later between 2000 and 2100 UT, the lava flow activity had either substantially decreased or ceased.

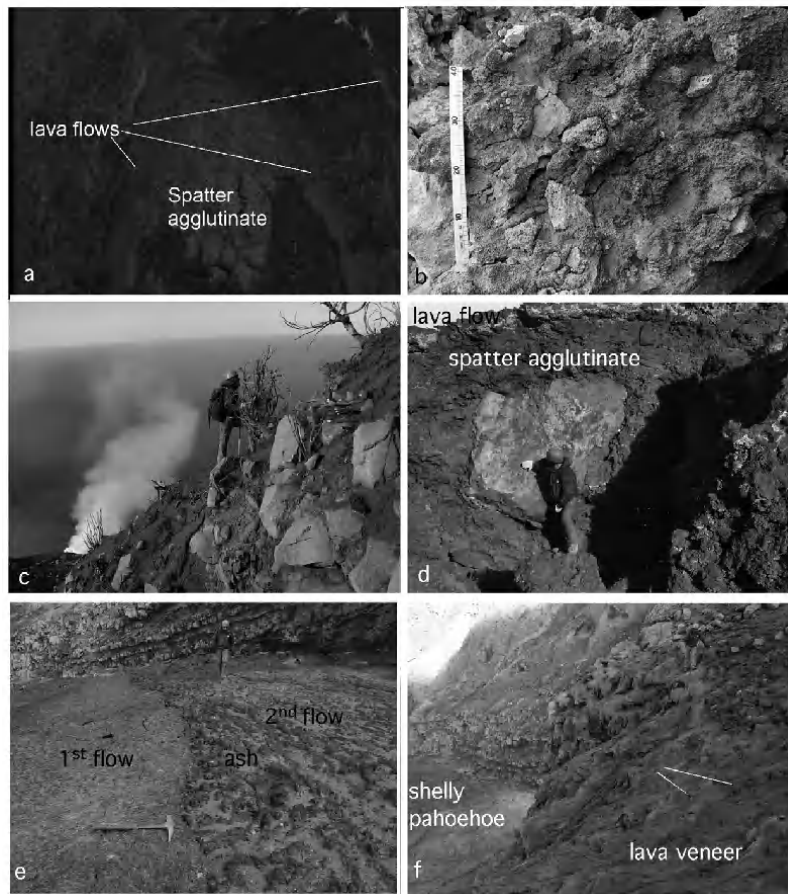


Figure 3. (a) Aerial picture of the proximal deposits, (b) spatter agglutinate, (c) burnt vegetation on the hot avalanche path, (d) large lava block embedded in the spatter agglutinate in very proximal location, (e) lava flow 1, and (f) lava flows 1 and 2. A thin ash pyroclastic layer is separating the two flows.

3.3. Field Observations

Products of the activity of December 28 and 29 consisted of pyroclastic deposits overlain by lava flows (Figures 1, 3a, and 3b). Pyroclastic deposits consisted of a spatter agglutinate (high portion of the SdF) and pyroclastic flow breccia (coast area, Spiaggia dei Gabbiani). Three lava flows, which originated from distinct vents in the high portion of the SdF and extending to the sea, were also visible from thermal images collected on the mornings of 29 and 30 December 2002 [Calvari *et al.*, 2005, Figures 1 and 3]. A notch was visible on the east rim of crater 1, due to a collapse event.

3.3.1. Pyroclastic deposits. The spatter agglutinate was dispersed over an area of about $2-3 \times 10^4 \text{ m}^2$ and was partly covered by the overlying lava flows. A maximum thickness of 7 m was observed in cracks, but the total thickness

in proximal areas was probably greater than 10–20 m. Downslope, it consisted of tens of meters wide and hundreds of meters of long slab spatter deposit bearing up to 2-m-diameter fresh lava blocks (Figure 3d). The deposit was roughly stratified, consisting from base to top of a loose breccia and spatter bed (1–2 m) overlain by moderately agglutinated spatter and lithic bed (2 m) followed upward by another bed of loose breccia and spatter. A cross section of the deposits was still visible on the Bastimento scarp in the first months of 2003. On higher areas on the east SdF rim, burnt vegetation and a thin ash layer likely marked the pyroclastic flow path (Figure 3c).

Along the coast, progressive erosion of the lava flow uncovered a pyroclastic breccia apron, with maximum lateral extension of about 30 m and maximum thickness of about 5 m (Figure 4a). The deposit was marked by a sharp contact with the substrate, constituted by loose debris from old vol-

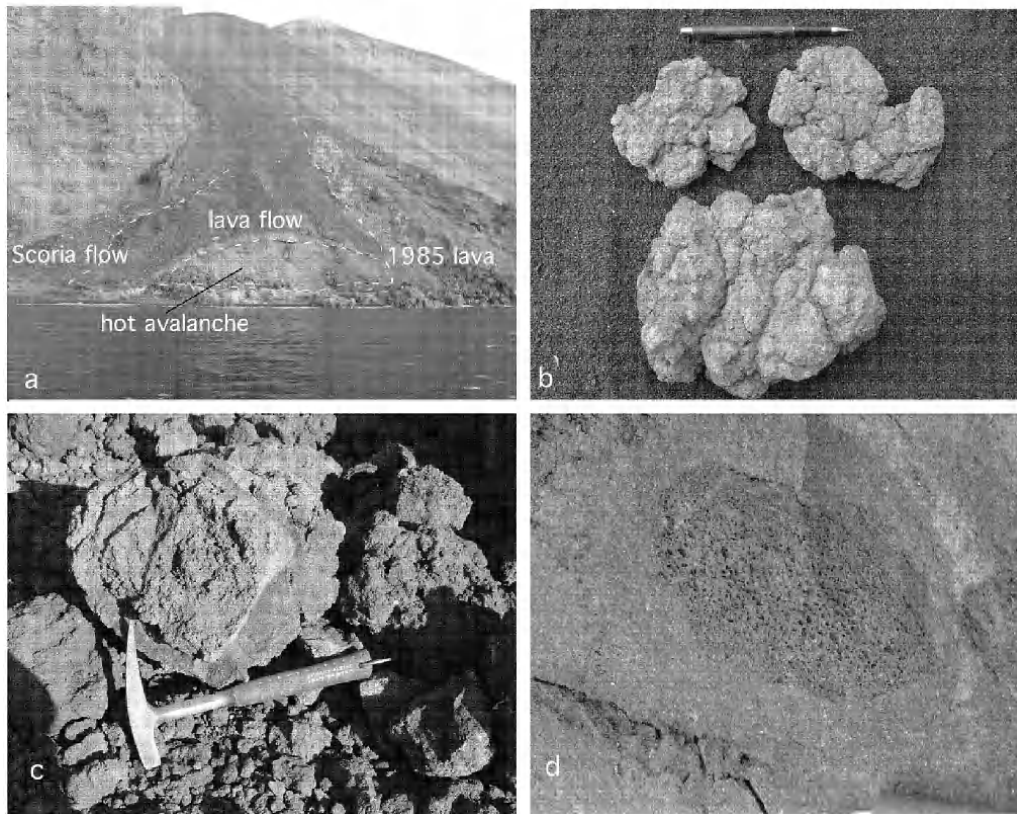


Figure 4. (a) Hot avalanche deposit at the Spiaggia dei Gabbiani. (b) Breadcrust bombs. (c) Cored bomb. (d) Xenolith fragment on lava flow overlying the hot avalanche.

canics. The deposit consisted of two units: a lower, reddish breccia and an upper, finer grained, light-colored, discontinuous layer up to 1.5 m thick. The lower breccia was massive, except for the occurrence of discontinuous, meter-sized clast-supported lenses occurring at different stratigraphic heights. It had a bimodal grain size distribution, with two main modes at +2 and -5/-6 ϕ . The upper layer is finer with a coarse mode at -4 and a fine mode at +1 ϕ (A. Solano, Interazione tra fenomeni eruttivi e gravitativi di versante durante la crisi del 28–30 Dicembre 2002 a Stromboli, Università di Pisa, unpublished thesis, 2005; hereinafter referred to as Solano, unpublished thesis, 2005); sorting is very poor ranging from 3.1 to 3.7 in the lower layer and from 2.7 to 2.8 in the upper one. Juvenile clasts constitute 36–71 wt % of the deposit and consist of poorly vesicular, contorted to bent, or stretched spatter, with cauliflower structure (Figure 4d; Solano, unpublished thesis, 2005). The fragments are porphyritic, with phenocryst assemblage closely matching that of the overlying lava flow. Groundmass is generally cryptocrystalline except the external, millimeter-thick rim that

is glassy and unaltered. Olivine phenocrysts show deuteritic alteration comparable to crystals in the overlying lava flow. Glassy (tachylite) fragments occur in the finer fraction (≤ 8 mm). Their concentration is maximum at the very base of the deposit (where glassy fragments > 1 mm constitute 8 wt % of the bulk material) and is variable in the remaining samples (the same fraction constitutes from 0 to 0.5 wt % of the bulk sample). Some of the larger clasts have cored structure. The core consists of lithic, altered scoria fragments with diameters of between 10 and 3 cm (Figure 4c).

Density of juvenile fragments with a diameter ranging from 6.4 to 1.1 cm was measured over a population of 162 specimens collected from nine different areas in the outcrop. Average density is 2360 ± 132 kg/m³, corresponding to a vesicularity of $18\% \pm 4\%$ (for measured DRE density = 2880 kg/m³; Solano, unpublished thesis, 2005).

Representative lithic blocks within the hot avalanche deposit show two distinct lavas composition: (1) basalts and (2) trachytes. The basaltic lithic blocks consist of highly porphyritic (35%–45%) lavas with seriate texture and pheno-

crysts of plagioclase > clinopyroxene (up to 4 mm) \geq olivine (Figure 5b); groundmass is mainly microcryptocrystalline, and accessory phases are represented by abundant opaque microlite grains. Olivine can be partially replaced by iddingsite, and all plagioclases phenocrysts show a strong sieve texture. Trachytes are characterized by a porphyritic index between 10% and 15%, with phenocrysts and microphenocrysts represented by plagioclase (up to 7 mm) > clinopy-

roxene > biotite \geq amphibole, set in a microcryptocrystalline groundmass (Figure 5a) with some pilotassitic domains. Quenched microlite laths of feldspar (swallow-tailed habitus) are abundant. Accessory phases consist of apatite and opaque minerals, whereas olivine xenocrysts and glomerophyres of plagioclase + clinopyroxene \pm biotite \pm opaque minerals. Modal mineralogy and textures of the basalt and trachyte lithic blocks closely match those of the lavas erupted during (1) recent to present-day Stromboli and (2) Upper Vancori volcanostratigraphic periods [Hornig-Kjarsgaard *et al.*, 1993], respectively. Major and trace element compositions (Table 1 and Figure 6) further support the provenance of the lithic lavas mainly from the above volcanostratigraphic periods of Stromboli.

A scoria flow deposit was also identified on the west of the lava/pyroclastic apron. The deposit was formed by centimeter- to decimeter-sized, stretched to twisted scoria fragments, in all similar to the juvenile components of the lower breccia. The flow was up to 15 m wide and comprised lateral levees up to 50 cm high.

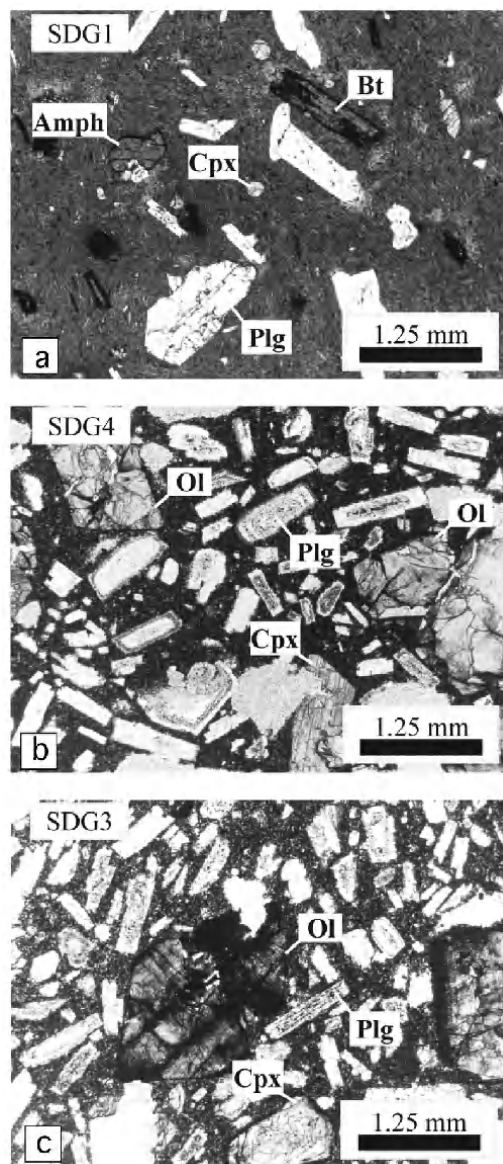


Figure 5. Thin-section petrography of representative lithic lavas in the hot avalanche, (a) SDG1 and (b) SDG4, and the 28 December thin lava flow, (c) SDG3, were taken at the Spiaggia dei Gabbiani outcrops.

3.3.2. Lava flows. Three lava flows were visible on the morning of 29 December (Figure 1); they fed two aprons located east and west of the old 1985 lava flow on the Spiaggia dei Gabbiani. These flows were not active on December 29 [Calvari *et al.*, 2005]. The same flows were later covered above 450 m asl by further lava emission, which occurred during the eruptive crisis; by the end of which only the distal portion east of the 1985 lava apron was still preserved. Where overlapping, the two flows were separated by a few-millimeters-thick ash layer (Figure 3e). Lava flows consisted of pahoehoe and subordinate a'a lavas either overlying preeruption material or the spatter and breccia deposits. Exceptionally smooth and horizontal lava surface formed close to the sidewall of the SdF where the lava pond due to the former presence of a local counter slope left by the 1985 lavas. With the exception of limited amount of a'a lavas formed in the inner part of small valleys, the pahoehoe lava formed a fairly large sheetlike lava leaving, on very inclined slopes, only a decimeter-thick lava veneer (Figure 3f). It is worth noticing, however, that the topography had limited control on the flow, suggesting very high thickness of the flow and thus high mass flow rate. The high mass flow rate had to be combined with an exceptionally low kinematic viscosity as the lava deposit showed features consistent with turbulent flow, determining the formation of spatter on the side of the channel.

The lava consists of approximately 26% plagioclase, 8% olivine, and 6% clinopyroxene with a seriate texture and microcryptocrystalline to cryptocrystalline groundmass. Accessory phases are mainly represented by opaque minerals. Chemical

Table 1. Major and Trace Element Compositions of the Lithic Fragments Within the Hot Avalanche (SDG1, 2, 4, and 5) and the Thin Lava Flow (SDG3), Erupted on 29 December 2002

Sample	SDG1	SDG2	SDG4	SDG5	SDG3
<i>Major Elements (ICP-OES)</i>					
SiO ₂	60.63	62.36	50.27	50.42	50.41
Al ₂ O ₃	16.87	17.12	17.05	17.54	17.17
Fe ₂ O ₃	5.24	4.97	8.58	8.61	8.62
MnO	0.11	0.15	0.15	0.15	0.16
MgO	2.09	1.46	6.31	6.05	6.31
CaO	4.6	3.85	11.19	11.02	11.19
Na ₂ O	4.08	4.35	2.47	2.56	2.48
K ₂ O	4.08	4.27	2.16	2.26	2.19
TiO ₂	0.61	0.58	0.92	0.93	0.92
P ₂ O ₅	0.35	0.31	0.55	0.57	0.55
L.O.I.	0.61	0.13	-0.12	-0.14	-0.01
Total	99.26	99.55	99.52	99.95	99.9
<i>Trace Elements (ICP-MS)</i>					
V	81	64	260	236	238
Cr	<20	<20	57	51	55
Co	8.8	6.5	27.4	26.8	26.7
Ni	26	<20	42	41	39
Rb	123	131	67	67	64
Sr	531	519	761	755	714
Y	30	31	25	24	24
Zr	284	293	158	157	151
Nb	30	31	21	21	20
Ba	1380	1460	1070	1060	1010
La	63	68	45	46	44
Ce	128	138	98	100	96
Pr	12.7	13.4	10.2	10.4	10.2
Nd	47	49	41	42	41
Sm	8.4	8.8	8.3	8.2	8.2
Eu	2.0	2.0	2.2	2.2	2.1
Gd	6.5	6.3	6.6	6.6	6.5
Tb	1.01	1.04	1.02	1.02	0.94
Dy	5.7	5.9	5.3	5.1	5.2
Ho	1.09	1.14	0.94	0.95	0.95
Er	3.3	3.5	2.7	2.7	2.6
Tm	0.49	0.51	0.36	0.37	0.36
Yb	3.2	3.4	2.3	2.3	2.3
Lu	0.49	0.52	0.33	0.34	0.33
Hf	6.7	6.9	3.9	3.9	3.8
Ta	1.7	1.8	1.1	1.1	1.1
Tl	0.16	0.25	<0.1	<0.1	<0.1
Pb	21	15	14	14	17
Th	28	30	16	16	16
U	7.1	7.6	4.1	4.1	4.0

composition (Table 1; Figure 6) is similar to the present-day Stromboli basalts. Texture, glass composition, and mineral chemistry [Landi *et al.*, 2006; Bertagnini *et al.*, this volume] of the 28 December lava flow do not show variations with

respect to those of both the porphyritic basaltic scoria normally erupted during the mild explosions of past decades and the following effusive products of the whole 2002–2003 eruptive crisis. Also, Sr–Nd isotopic compositions of the 28 December lava flow [Landi *et al.*, 2006] is in the range of the crystal-rich magmas of the present-day activity. Rounded, centimeter- to decimeter-size xenolithic fragments are dispersed in the massive portion of the lava flow (Figure 4d). They are reddish, macrovesicular scoria, similar to those usually ejected by the normal Strombolian activity. It is worth to note that olivine phenocrysts in the thin lava flow at Spiaggia dei Gabbiani shows a severe alteration under oxidizing conditions. They are mostly replaced by iddingsite and large pervasive Fe–Ti oxides only in this outcrop, where the thin lava flows covered the hot avalanche. By contrast, in the shelly pahoehoe lava in the upper flank of the volcano, olivine crystals are fresh. Olivine with reddish to opaque mineral patches in the lava outcrop of Spiaggia dei Gabbiani is therefore the result of deuterian intermediate temperature alteration [Baker and Haggerty, 1967] to subsolidus high-temperature reheating [Haggerty and Baker, 1967]. Due to thickness of 1–2 m, the lava flow underwent a rapid cooling but the underlying hot avalanche could have continued to release hot fluid for days, and therefore, continuous subsolidus reheating of the olivine in the overlying thin lava flows can be inferred.

Northward, the lavas and underlying breccia and agglutinated deposits were truncated by seaward slope displacement that occurred in the late evening and night of 28 December. The same movements were likely responsible for the fracturing of the agglutinate downslope of the eruptive vent.

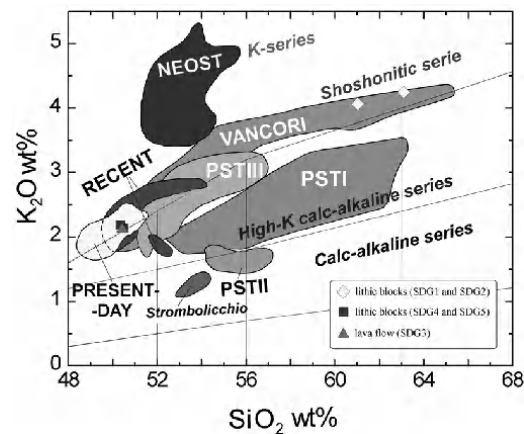


Figure 6. K₂O–SiO₂ diagram (whole-rock analyses) of the lithic lavas found in the hot avalanche of the 28 December 2002 and the superimposed thin lava flow.

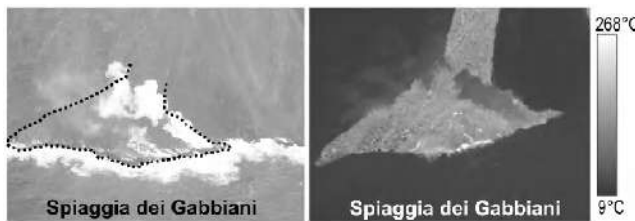


Figure 7. Photo on the left and thermal image on the right, both collected on 29 December 2002, of the hot avalanche that emplaced on Spiaggia dei Gabbiani on 28 December. The dotted line in the photo bounds the portion of the avalanche imaged on the right.

3.4. Thermal Surveys

Thermal images of the 28 December hot avalanche (Figure 7) were regularly performed from 29 December 2002 to 29 September 2003 [Calvari *et al.*, 2005]. After this date, the deposit was no longer visible because it was covered by the upper lava flow. In particular, between 29 December and the first half of February, thermal imaging was extremely useful in detecting the daily maximum apparent temperatures of the avalanche [Figure 8a; Calvari *et al.*, 2005]. From the end of February, thermal measurements were irregular. On 29 December, after a day from the emplacement, the deposit had maximum apparent temperature of 368°C (Figure 8a). Through time, temperature showed a general declining trend characterized by a number of sudden, unexpected peaks. These anomalies were recorded on 2, 8, and 9 January, 6 and 14 February, 13 March, and 2 June 2003. In Figure 8a, these anomalies are represented with red dots numbered from 1 to 8, respectively. Dots 1, 2, and 7 in Figure 8a are

not real temperature increases; they are simply associated with shorter path lengths from which thermal images were taken with respect to the other day measurements. Peaks 3 to 7 in Figure 8a were due instead to real increases of apparent temperatures produced by the occurrence of local collapses of the deposit front exposing hot deposit core (Figure 8b). The frequent exposures of the avalanche section allowed the clear discrimination between the cold external skin (crust) of the deposit, the crust, and the hot inner portion (core) of the deposit interior. Assuming that the temperature of 29 December (368°C) corresponded to the initial temperature of the deposit emplacement, it was possible to discriminate between the mean cooling trend of the external crust and that of the deposit core. In the period observed, crust apparent temperatures decreased from 368°C on 29 December 2002 to 25°C on 29 September 2003, whereas the lowest maximum apparent temperature recorded at the inner portion (96°C) was associated with the 13 March 2003 front collapse (dot 7 in Figure 8a). The lower temperature recorded on 13 January (dot 5 in Figure 8a) with respect to 14 February (dot 6 in Figure 8a) could be explained taking into account the width of the hot area exposed at the surface or/and to external features (e.g., presence of ash, steam, weather conditions) attenuating the radiance detected by the camera.

4. DATA INTERPRETATION

4.1. Eruptive Dynamics

The 2002–2003 eruptive crisis of Stromboli volcano was preceded by several months of high intensity activity, related to a very high magma level in the shallow main summit con-

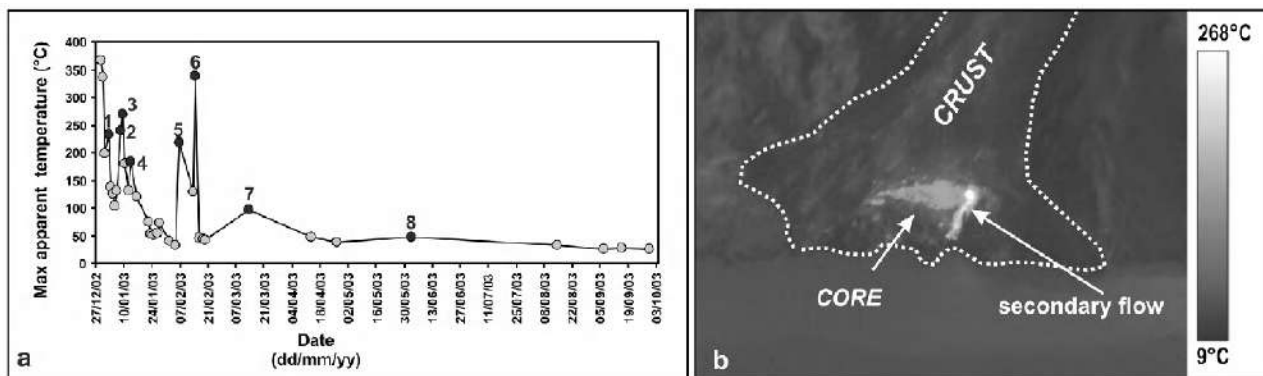


Figure 8. (a) Graph showing the variability of the maximum apparent temperatures recorded at the avalanche deposit surface between 29 December 2002 and 29 September 2003. The black dots indicate thermal anomalies interrupting the gradual decreasing cooling trend. (b) Thermal image collected on 14 February 2003 showing the high temperature of the avalanche core (lighter colors), exposed to the surface by sea erosion, contrasting the cold avalanche crust (darker colors). The dotted line represents the new shape of the deposit foot as a result of the sea erosion processes and collapses.

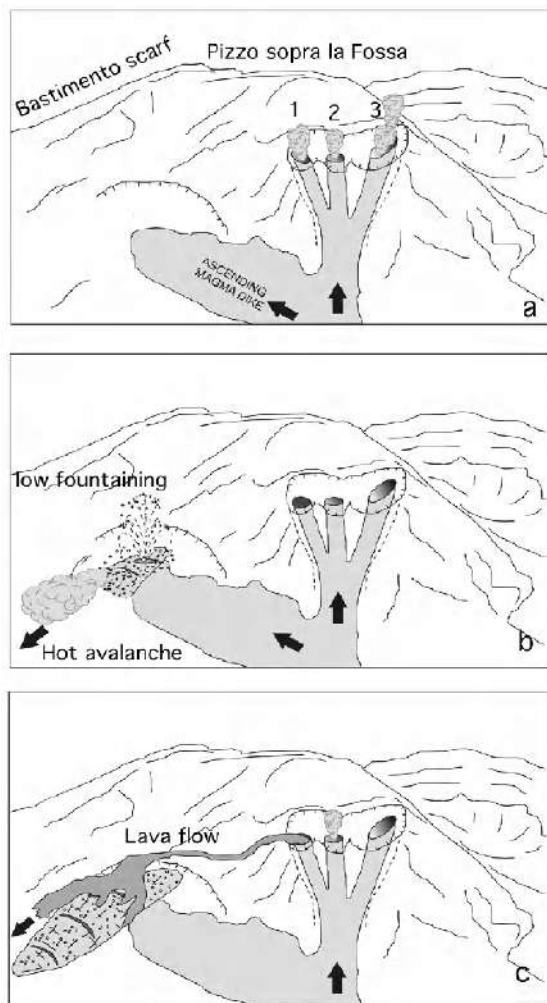


Figure 9. Main phases of the eruption: (a) magma intrusion along a shallow dike, (b) vent opening and onset of low fountaining, and (c) lava output from vent at crater 1.

duit system, which culminated in the onset of the 2002–2003 effusive crisis on 28 December 2002 [Bonaccorso *et al.*, 2003; Calvari *et al.*, 2005; Burton *et al.*, this volume].

Eyewitnesses' observations and the INGV video camera (although not directly monitoring the eruptive activity) suggest that the crisis started around 1720 UT with the opening of an eruptive vent NE of the summit craters and that the first eruptive phase lasted approximately 3 h. Repeated glowing, as shown by the INGV camera and layering of the main welded deposit could be related to repeated eruptive pulses. The onset of a lateral eruption did not immediately "shut off" the main summit conduits system, but the activity at the summit vents strongly decreased in intensity; spattering and

degassing were still occurring up to 1840 UT, likely during the spatter fountaining or flowing of the first lava.

The crisis that started with an explosive event depositing a lithic-rich spatter agglutinate on the SdF and the hot avalanche are related to mild explosive activity and vent opening on the SdF (Figure 9). We interpret the unusual high lithic content of the deposit (Figure 3b) as related to explosive incorporation of wall rocks during the vent opening. Lateral thickness and grain size variations indicate that the source area for the spatter deposit was likely located close to the Bastimento scarf. Stratigraphic relationship and component also suggest that the hot avalanche on the Spiaggia dei Gabiani was likely deposited by a secondary pyroclastic flow formed by gravitational instability of the peripheral portion of spatter deposit accumulating over the SdF. Another possibility for the formation of the agglutinate is through low fountaining at crater 1 associated to lava emission and collapse of the north cone walls, as suggested by Calvari *et al.* [2005]. However, abundant occurrence of fresh lava blocks up to several meters wide in the spatter agglutinate (Figure 3d) and in the hot avalanche deposits, likely originating from the fragmentation of old lavas preserved in the shallow portion of the volcano, but not part of the summit cone structure, better accord with the first hypothesis (i.e., initial vent at ~650 m at the east rim of SdF). The nature of these lithic clasts also differs from the xenoliths in the lower lava flow, exclusively constituted by rounded, highly vesicular, basaltic scoria fragments, eventually picked up by the lava while flowing out of the crater 1. Lava emission started after the emplacement of the hot avalanche; Calvari *et al.* [2005], using thermal monitoring data, also estimated the maximum lava flow rate (~280 m³/s). These flows likely determined significant drainage of magma from the summit conduits system, lowering of the magma level, ending the summit explosive activity. After this short-lived flow, an eruptive pause (likely marked by small phreatic explosions, covering the lava flow surface with lithic ash, as shown in Figure 3e) occurred. On the NW side, the uppermost lavas were sharply truncated by the scar formed on the NE flank of cone 1 making it difficult to unequivocally assess in the field from which vent they had been erupted. Some authors [Bonaccorso *et al.*, 2003; Calvari *et al.*, 2005; Acocella *et al.*, 2006] suggest that they originated from an eruptive fracture extending from the rim of cone 1 to the NE, determined by a shallow dike intrusion and accompanied by partial collapse of the cone itself on the north side. Pompilio [2003] and Tommasi *et al.* [2004] suggested that the explosive activity occurred from a vent located at 650 m asl, at the east rim of the SdF [Tommasi *et al.*, 2004, Figure 9, vent 1]; for the same authors, this vent also fed the first lava flow. A second lava flow issued from a vent located at 550 m asl in the SdF. This flow covered

the western branch of the first lava flow at the Spiaggia dei Gabbiani.

4.2. Thermal Surveys

Daily thermal measurements enabled us the study of the thermal behavior of the 28 December hot avalanche. The range of maximum temperatures found for this deposit (250° – 350° C, Figure 8a), a few hours after the emplacement, fitted within the range obtained with the thermal remnant magnetization technique on different types of pyroclastic density currents from the A.D. 79 eruption of Vesuvius [Cioni *et al.*, 2004] and within the range of temperature for derived pyroclastic flows at Montserrat, measured within 72 h of deposit emplacement [Calder *et al.*, 1999]. Between 29 December 2002 and 14 February 2003, regular daily measurements were carried out. The apparent temperatures recorded during this interval allowed us to estimate the cooling rate for the outer part of the deposit. This was significantly high, resulting in about 37.7° C/d. Conversely, although the exact timing of the front collapse of 14 February was unclear, the maximum apparent temperature recorded that day suggested a maximum cooling rate of 0.66° C/d for the inner portion of the deposit. Over a period of 9 months, this results in an estimated cooling rate of 1.25° C/d for the outer part. For the core, we could carry out this evaluation only until 13 March, resulting in a cooling rate of $\approx 0.31^{\circ}$ C/d. Collapses of the front of the deposit proved the existence of an inner portion of the deposit characterized by high temperatures and still relatively low density (poor clast cohesion), which showed decrease in apparent temperatures of only 30° C after 30 d. As for pyroclastic density current deposits, the fast cooling of the outer part was mainly due to external parameters, such as rainfalls and external waters, air ingestion, deposit transport processes, and emplacement [Martí *et al.* 1991; Cioni *et al.*, 2004]. The cooling of the inner portion might be strictly linked to the shape of the deposit, morphology, and thickness. On 14 February 2003, the combination of the still relatively high temperatures and the poor cohesion of the core, with the efficiency of sea erosion, allowed the drainage of an inner portion of the deposit with the formation of a small, short-lived secondary flow (Figure 8b).

5. CONCLUSIONS

We have reconstructed the first day of the eruption through eyewitnesses' observations, field studies, and thermal monitoring of the deposits. The onset was related to shallow lava intrusion in the SdF, eventually evolved in the opening of two vents located at 670 and 550 m asl. Intense fountaining

from the upper vent determined local accumulation of spatter and the formation of a pyroclastic flow, likely related to gravitational instability due to accumulation on the SdF slope.

We then propose this eruptive sequence for the 28 December 2002 events: (1) shallow-dike emplacement on the west SdF below the crater terrace, during energetic Strombolian activity and high magma level at the summit conduits; (2) opening of a vent at ~ 650 m asl (~ 1720 UT) and occurrence of repeated low fountaining events determining spatter agglutination in the proximal areas and formation of a hot avalanche due to gravitational instability of the deposit over steep slopes; (3) lava emission from a new vent; (4) lowering of magma level, end of lava flow; (5) cessation of eruptive activity at summit craters ~ 2000 UT; (6) collapse of the NE flank of cone 1 and formation of the crater notch; (7) opening of a new vent at 580 m asl and emission of a new lava flow.

Acknowledgments. The authors are grateful to A. Solano for extensive help in field and laboratory activities and L. Lodato collecting the thermal images used in this paper. They also thank E. Boschi, A. Bonaccorso, and all their colleagues in INGV from Catania, Palermo, Naples, Rome, and Milan for their support and contribution to the monitoring of the eruption; G. Bertolaso and the Italian Civil Protection for their substantial support of our activities; M. Zaia (Zazà), M. Pruiti, and the Alpine Guides of Stromboli for their field assistance; the helicopter pilots of Air Walser and of the Italian Civil Protection, whose great expertise and courage allowed us to collect a huge amount of data. This work was financially supported by INGV and the Dipartimento di Protezione Civile through the project "Monitoring and Research Activity at Stromboli and Panarea" (V2/10 for M.R. and V2/18 for A.R.). L.P. was partly founded by NSF EAR0510493.

REFERENCES

- Acocella, V., M. Neri, and P. Scarlato (2006), Understanding shallow magma emplacement at volcanoes: Orthogonal feeder dikes during the 2002–2003 Stromboli (Italy) eruption, *Geophys. Res. Lett.*, 33, L17310, doi:10.1029/2006GL026862.
- Baker, I., and S. E. Haggerty (1967), The alteration of olivine in basaltic and associated lavas. Part I. Intermediate and low temperature alteration, *Contrib. Mineral. Petrol.*, 16, 258–273.
- Bertagnini, A., L. Francalanci, P. Landi, N. Metrich, and M. Pomilio (2008), Volcanology and petrology of the present day activity, this volume.
- Bonaccorso, A., S. Calvari, G. Garfi, L. Lodato, and D. Patanè (2003), Dynamics of the December 2002 flank failure and tsunami at Stromboli volcano inferred by volcanological and geophysical observations, *Geophys. Res. Lett.*, 30(18), 1941, doi:10.1029/2003GL017702.
- Burton, M., S. Calvari, L. Lodato, L. Spampinato, S. Mangiagli, E. Pecora, N. A. Pino, E. Marchetti, and F. Muré (2008), The state of the volcano before the eruption onset, this volume.

- Calder, E. S., P. D. Cole, W. B. Dade, T. H. Druitt, R. P. Hoblitt, H. E. Huppert, L. Ritchie, R. S. J. Sparks, and S. R. Young (1999), Mobility of pyroclastic flows and surges at the Soufriere Hills Volcano, Montserrat, *Geophys. Res. Lett.*, **26**, 537–540.
- Calvari, S., and H. Pinkerton (2004), Birth, growth and morphologic evolution of the “Laghetto” cinder cone during the 2001 Etna eruption, *J. Volcanol. Geotherm. Res.*, **132**, 225–239.
- Calvari, S., L. Spampinato, L. Lodato, A. J. L. Harris, M. R. Patrick, J. Dehn, M. R. Burton, and D. Andronico (2005), Chronology and complex volcanic processes during the 2002–2003 flank eruption at Stromboli volcano (Italy) reconstructed from direct observations and surveys with a handheld thermal camera, *J. Geophys. Res.*, **110**, B02201, doi:10.1029/2004JB003129.
- Calvari, S., L. Spampinato, and L. Lodato (2006), The 5 April 2003 vulcanian paroxysmal explosion at Stromboli volcano (Italy) from field observations and thermal data, *J. Volcanol. Geotherm. Res.*, **149**, 160–175.
- Cioni, R., L. Gurioli, R. Lanza, and E. Zanella (2004), Temperatures of the A.D. 79 pyroclastic density current deposits (Vesuvius, Italy), *J. Geophys. Res.*, **109**, B02207, doi:10.1029/2002JB002251.
- Haggerty, S. E., and I. Baker (1967), The alteration of olivine in basaltic and associated lavas. Part I. High temperature alteration, *Contrib. Mineral. Petrol.*, **16**, 233–257.
- Harris, A., J. Dehn, M. Patrick, S. Calvari, M. Ripepe, and L. Lodato (2005), Lava effusion rates from hand-held thermal infrared imagery: An example from the June 2003 effusive activity at Stromboli, *Bull. Volcanol.*, **68**, 107–117.
- Hornig-Kjarsgaard, I., J. Keller, U. Koberski, E. Stadlbauer, L. Francalanci, and R. Lenhart (1993), Geology, stratigraphy and volcanological evolution of the island of Stromboli, Aeolian arc, Italy, *Acta Vulcanol.*, **3**, 21–68.
- Landi, P., L. Francalanci, M. Pompilio, M. Rosi, M. A. Corsaro, C. M. Petrone, I. Cardini, and L. Miraglia (2006), The December 2002–July 2003 effusive event at Stromboli volcano, Italy: Insights into the shallow plumbing system by petrochemical studies, *J. Volcanol. Geotherm. Res.*, **155**, 263–284.
- Lodato, L., L. Spampinato, A. J. L. Harris, S. Calvari, J. Dehn, and M. R. Patrick (2007), The morphology and evolution of the Stromboli 2002–03 lava flow field: An example of a basaltic flow field emplaced on a steep slope, *Bull. Volcanol.*, **69**, 661–679.
- Marti, J., J. L. Diez-Gil, and R. Ortiz (1991), Conduction model for the thermal influence of lithic clasts in mixtures of hot gases and ejecta, *J. Geophys. Res.*, **96**, 21,879–21,885.
- Pompilio, M. (2003), Cronologia dell’eruzione, localizzazione emigrazione delle bocche eruttive, *INGV Internal Report* (in Italian), 16 pp.
- Tinti, S., A. Mannucci, G. Pagnoni, A. Armigliato, and F. Zaniboni (2005), The 30 december 2002 landslide-induced tsunamis in Stromboli: Sequence of events reconstructed from the eyewitness accounts, *Nat. Hazards Earth Syst. Sci.*, **5**, 763–775.
- Tommasi P., F. Chiocci, M. Marsella, M. Coltellini, and M. Pompilio, Preliminary analysis of the December 2002 instability phenomena at Stromboli volcano. Proceedings of the Int Symp Flows, Sorrento, 15–16 May 2004.
-
- S. Calvari and L. Spampinato, Istituto Nazionale di Geofisica e Vulcanologia, Sezione di Catania, Catania, Piazza Roma 2, 95123 Catania, Italy.
- A. Di Roberto, Istituto Nazionale di Geofisica e Vulcanologia, Sezione di Pisa, Via della Faggiola 32, 56123 Pisa, Italy.
- L. Pioli, Department of Geological Sciences, University of Oregon, 1272 University of Oregon, Eugene, OR 97403, USA. (pioli@dst.unipi.it)
- A. Renzulli, Istituto di Scienze della Terra, Università di Urbino, Campus Scientifico, 61029 Urbino, Italy.
- M. Rosi, Dipartimento di Scienze della Terra, Università di Pisa, Via Santa Maria 53, 56126 Pisa, Italy.

Geochemical Prediction of the 2002–2003 Stromboli Eruption From Variations in CO₂ and Rn Emissions and in Helium and Carbon Isotopes

C. Federico,¹ L. Brusca,¹ M. L. Carapezza,² C. Cigolini,³ S. Inguaggiato,¹ A. Rizzo,¹ and D. Rouwet¹

Significant changes in both the chemistry of coastal thermal waters and the soil CO₂ and Rn emissions in the crater area were recorded at Stromboli prior to the eruption that began on 28 December 2002. The dissolved CO₂ contents and the δ¹³C and ³He/⁴He values were elevated in the thermal aquifer from July 2002. Synchronous variations in the same isotope ratios were recorded in the summit fumarolic gases, with both ³He/⁴He and δ¹³C values of gases released from a fumarole in the summit area increasing between May and November 2002. These variations are indicative of early degassing of a new gas-rich magma batch with a ¹³C- and ³He-rich signature. This magma recharge probably fed the intense Strombolian activity recorded during that period. The eruption began with a major explosion that produced a glowing avalanche, immediately followed by a fluid lava overflow from the NE crater and subsequent lava effusion from vents opened in the Sciara del Fuoco depression. Sharp increases in CO₂ soil flux and Rn emissions—to values never observed previously—were recorded in the summit crater area 10 d before the eruption onset. These CO₂ and Rn anomalies are indicative of a high gas-driven magma supply rate and gas overpressure within the conduit. The sudden depressurization of the magma filling the upper conduit probably caused the major explosion that occurred on 28 December, which heralded the effusive phase. These data demonstrate the importance of collecting a wide spectrum of geochemical data from different geological sites when monitoring a volcano.

1. INTRODUCTION

The importance of geochemical monitoring of volcanic fluids in forecasting volcanic events has increased in the past 20 years. The reliability and usefulness of fluid geo-

chemistry data obtained during volcano monitoring has been demonstrated for fumarole chemistry [Hirabayashi *et al.*, 1982; Hammouya *et al.*, 1998; Capasso *et al.*, 1999; Taran *et al.*, 2002], soil gas emissions [Badalamenti *et al.*, 1994; McGee *et al.*, 2000; Badalamenti *et al.*, 2004], plume chemistry [Casadevall *et al.*, 1994; Fischer *et al.*, 1994; Watson *et al.*, 2000; Aiuppa *et al.*, 2002, 2004; Gerlach *et al.*, 2002; Burton *et al.*, 2007], and isotope geochemistry [Caracausi *et al.*, 2003; Rizzo *et al.*, 2006].

A geochemical surveillance program started at Stromboli in 1999 based on the work of Capasso and Carapezza [1994] and Carapezza and Federico [2000] and was focused on identifying signals predictive of impending energetic explosive events. Indeed, the activity at Stromboli is characterized by typical Strombolian mild explosions consisting of gas jets charged of dark scoria and lava fragments, whose source lies in the upper part of the plumbing system that is filled by a

¹ Istituto Nazionale di Geofisica e Vulcanologia, Sezione di Palermo, Palermo, Italy.

² Istituto Nazionale di Geofisica e Vulcanologia, Sezione di Roma, Rome, Italy.

³ Dipartimento di Scienze Mineralogiche e Petrologiche, Università degli Studi di Torino, Turin, Italy.

partly degassed crystal-rich magma [Bertagnini *et al.*, 1999; Métrich *et al.*, 2001]. The shallow dikelike feeding system extends from the summit craters to about sea level [Chouet *et al.*, 2003; Mattia *et al.*, 2004]. The chemical composition of the gas emitted during Strombolian explosions suggests that it rises as discrete slugs separately from the magma from a depth between 2.7 and 0.8 km below the vents [Burton *et al.*, 2007]. The emitted products usually reach heights of tens or a few hundred meters and fall back to the surface in the proximity of the crater area. The same crystal-rich scoria is emitted during occasional lava eruptions, channeling onto the Sciara del Fuoco (SdF) depression. More energetic explosions (called major explosions and paroxysms) produce high eruptive columns and emit huge amounts of blocks, lapilli, and ash that cover a large portion of the summit area. Sometimes the most violent explosions threaten inhabitants as well as tourists visiting the crater area [Barberi *et al.*, 1993; Rosi *et al.*, 2006]. During such explosions, nearly aphyric volatile-rich magma, probably ascending from a depth of about 11 km, erupts together with the crystal-rich magma [Bertagnini *et al.*, 2003]. Both magmas have the same HK-basaltic or shoshonitic composition.

On 28 December 2002, Stromboli produced a new lava effusion that had been preceded since the previous summer by an increase in the Strombolian activity with magma at high levels in the conduit, several energetic explosions, and small lava overflows [Bonaccorso *et al.*, 2003; Landi *et al.*, 2006]. The eruption started with a major explosion (described as “mild” by Landi *et al.* [2006], but actually representing a major Stromboli explosion according to the classification of Barberi *et al.* [1993]) from a lateral vent near the summit that produced a glowing avalanche, followed soon after by the emission of an exceptionally fluid lava from the NE crater along a new fissure extending from 750 to 600 m above sea level (asl), followed by a less fluid lava from a vent at ~600 m asl [Calvari *et al.*, 2005; Landi *et al.*, 2006]. The lava rapidly channeled onto the SdF depression on the western flank of the volcano and quickly reached the sea [Bonaccorso *et al.*, 2003; Landi *et al.*, 2006]. On 30 December 2002, new lava flows were emitted in the SdF depression and from a new vent that had opened at 500 m asl, and the failure of a portion of the SdF depression caused a tsunami [Tinti *et al.*, 2003]. The eruption culminated on 5 April 2003 with a paroxysmal explosion, whose ejecta reached the lower flanks of the volcano [Rosi *et al.*, 2006]. The effusive activity ceased on 22 July 2003, and from early May 2003, the normal Strombolian activity gradually resumed at the summit craters [Calvari *et al.*, 2005; Landi *et al.*, 2006].

Here we show that geochemical monitoring is a valuable tool for predicting the ascent of gas-rich magma that heralds the onset of the eruption. Geochemical data were collected in

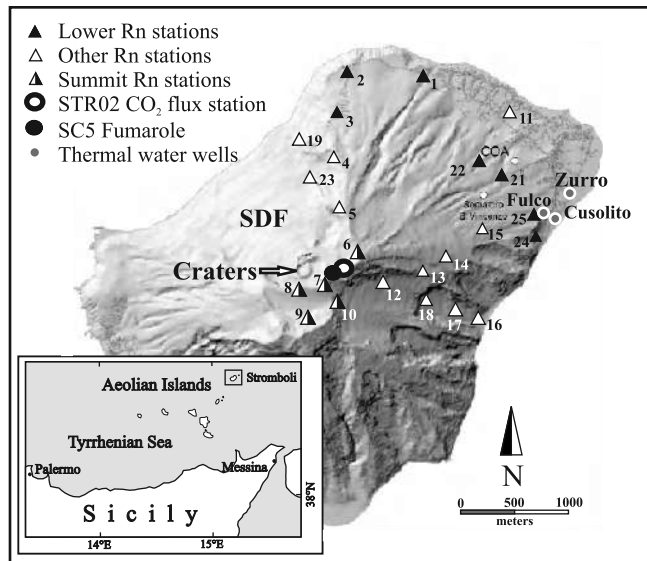


Figure 1. Sketch map of Stromboli island, showing locations of sampling and measurement points.

both the summit area and the northeastern coastal part of the island, including the Scari harbor area, where thermal waters and CO₂ soil degassing have been systematically monitored [Carapezza and Inguaggiato 2001; Carapezza *et al.*, 2004; Capasso *et al.*, 2005a]. In addition, Rn measurements were made at 25 sites located in the summit area and on the northeastern flank of the volcano [Cigolini *et al.*, 2005]. One station for the real-time monitoring of soil CO₂ flux and environmental parameters was operating in the summit area (Pizzo Sopra la Fossa, hereafter named Pizzo). The water of three thermal wells was collected monthly and analyzed for major ion chemistry, dissolved gases, and carbon and helium isotopes [Carapezza and Inguaggiato, 2001; Capasso *et al.*, 2005a]. The locations of the monitoring sites are shown in Figure 1.

This paper focuses on the geochemical changes related to the degassing of ascending magma batches that heralded the onset of the 2002–2003 eruption [Brusca *et al.*, 2004; Carapezza *et al.*, 2004, 2005a; Cigolini *et al.*, 2005].

2. DATA GATHERING: METHODOLOGY

2.1. Continuous Soil CO₂ Flux Measurements

The CO₂ diffuse soil flux from Stromboli was monitored using an accumulation chamber station (West Systems) equipped with an IR spectrometer (Dräger Polytron) in the range 0%–10% (with a precision of ±0.01%; see the stud-

ies of *Chiodini et al.* [1998] and *Carapezza and Granieri* [2004], for the methodology, and *Brusca et al.* [2004], for further details of the station). The CO₂-flux station (STR02) in the summit area has recorded data automatically every hour since August 2000 (Pizzo, Figure 1) [*Carapezza et al.*, 2002, 2004; *Brusca et al.*, 2004]. Monitored parameters were carbon dioxide flux, wind speed and direction, air temperature and relative humidity, soil temperature and water content, and atmospheric pressure. Data were transmitted to the Istituto Nazionale di Geofisica e Vulcanologia–Palermo geochemical monitoring center and to the COA (volcano observatory of the Department of Civil Protection) during the eruptive period.

2.2. Soil Rn Measurements

Twenty-five E-PERM® electrodes [*Kotrappa et al.*, 1993] and α -track-etch detectors were placed in the summit area and at various sites on the northern and eastern sectors of the volcano, ~60 cm below the soil surface and protected by 1-m-long and 12-cm-wide capped tubes [*Cigolini et al.*, 2005]. The E-PERM detectors were exposed for 1–4 d, thus increasing the possibility of correlating Rn emissions with changes in volcanic activity. Track etches (LR 115) were exposed for 1–6 weeks, which was long enough to smooth out fluctuations in radon emissions due to variations in atmospheric pressure, daily temperature, and microseismicity [*Cigolini et al.*, 2005].

2.3. Collection of Water and Gas Samples

Ground thermal waters have been collected monthly since 1999 from three wells (Fulco, Zurro, and Cusolito located near the NE coast of Stromboli Island Figure 1 [*Carapezza and Inguaggiato*, 2001]). The sampling frequency was increased after the onset of the 2002–2003 eruption from monthly to twice weekly. Temperature, pH, conductivity, and Eh (redox potential) were directly measured during sampling, once a month before the 2002–2003 eruption, and daily during the eruption.

The dissolved gas content and carbon and helium isotopes were measured in water samples collected in 121- to 242-mL glass bottles and sealed hermetically to prevent air contamination [*Capasso and Inguaggiato*, 1998; *Inguaggiato and Rizzo*, 2004]. All samples were analyzed within a few days after sampling [*Capasso et al.*, 2005a].

Free gas samples were collected from a fumarole near the STR02 station at Pizzo (SC5) approximately every month [*Capasso et al.*, 2005a]. The dry gas samples were collected in Pyrex® flasks through a 50-cm-long stainless steel probe inserted into the soil.

2.4. Analytical Methods

The chemical compositions of free and dissolved gases were measured by a chromatograph (Perkin Elmer 8500) equipped with both a thermal conductivity detector and a flame ionization detector associated with a methanizer, using Ar as a carrier gas and a 5-Å molecular sieve. The detection limits were 500 ppmv for O₂, 1000 ppmv for N₂, 20 ppmv for CO₂, and 1 ppmv for CH₄. Dissolved gases were analyzed after introducing a nonreactive host gas (Ar) and equilibration (>12 h), based on the principle of equilibrium partitioning of gases between liquid and gas phases [*Capasso and Inguaggiato*, 1998].

The carbon-isotope composition of CO₂ in free (SC5 fumarole) and dissolved gases in thermal waters was measured with a mass spectrometer (Finnigan Delta Plus). The carbon-isotope composition is classically reported as $\delta^{13}\text{C}$ in parts per thousand relative to V-PDB (the delta notation is

$$\delta^{13}\text{C} = \left(\frac{(^{13}\text{C}/^{12}\text{C})_s}{(^{13}\text{C}/^{12}\text{C})_{\text{std}}} - 1 \right) \cdot 1000$$

where $(^{13}\text{C}/^{12}\text{C})_s$ is the isotopic ratio in the sample and $(^{13}\text{C}/^{12}\text{C})_{\text{std}}$ is the isotope ratio in the belemnite from the PeeDee formation), with an accuracy of 0.15‰. Details on the analytical method used to gather $\delta^{13}\text{C}$ data is available in the works of *Favara et al.* [2002] and *Capasso et al.* [2005b].

The helium-isotope ratio, $^3\text{He}/^4\text{He}$, expressed as R/Ra (with Ra = $^3\text{He}/^4\text{He}$ in air = 1.39×10^{-6} [*Ozima and Podosek*, 1983]), together with the $^4\text{He}/^{20}\text{Ne}$ ratio in free (SC5 fumarole) and dissolved gases in thermal waters were measured using a static vacuum mass spectrometer (VG-5400TFT, VG Isotopes). The method used to measure $^3\text{He}/^4\text{He}$ ratios in dissolved gases is detailed in *Inguaggiato and Rizzo* [2004] and *Capasso et al.* [2005a]. The errors in determining $^3\text{He}/^4\text{He}$ ratios in ^3He -rich gases such as volcanic gases are lower than 0.1% and were corrected for atmospheric contamination as follows [*Sano and Wakita*, 1985]:

$$Rc = [(^3\text{He}/^4\text{He})_M - r]/(1 - r) \quad (1)$$

where $r = (^4\text{He}/^{20}\text{Ne})_{\text{air}}/(^4\text{He}/^{20}\text{Ne})_M$ and $(^4\text{He}/^{20}\text{Ne})_{\text{air}}$ and $(^4\text{He}/^{20}\text{Ne})_M$ are the atmospheric and measured $^4\text{He}/^{20}\text{Ne}$ ratios, respectively.

3. THE PIZZO SOPRA LA FOSSA AREA

The Fossa depression, which hosts the summit craters, is bordered by a 350-m-wide rim called Pizzo. Large portions of this rim are affected by a network of cracks and fractures,

which represent a preferential pathway for the ascending hot fluids (mostly water vapor and CO₂) circulating within the Fossa depression [Finizola *et al.*, 2003; Revil *et al.*, 2004]. Positive CO₂-flux anomalies are associated with a high temperature (due to the upward convection of water vapor and gas) [Carapezza and Federico, 2000]. A nearly constant temperature of ~96°C has been measured at a depth of 50 cm in a low-flux fumarole (SC5). The composition of the dry gas is essentially CO₂ (constituting from 66% to 93% by volume), variably diluted by air and containing traces of He (4–12 ppm), H₂ (up to 470 ppm), CH₄, and CO [Capasso and Carapezza, 1994; Carapezza and Federico, 2000; Capasso *et al.*, 2005a]. Helium-isotope ratios, expressed as R_{c/Ra} values, range from 2.7 to 3.4 and are slightly lower than those measured in the dissolved gases of the coastal thermal well waters [Capasso *et al.*, 2005a]. The continuous soil-flux monitoring station at Pizzo recorded background CO₂ values of 8000–10,000 g/m²/d with peaks up to 45,000 g/m²/d during the 2 years preceding the 2002–2003 eruption [Carapezza *et al.*, 2002]. Here we also report the data on radon emissions collected at five summit stations, two of which reached values well above 10,000 Bq/m³ in November 2002 and peaked above 27,000 Bq/m³ shortly before the onset of the eruption [Cigolini *et al.*, 2005].

4. THE BASAL THERMAL AQUIFER

Stromboli magmatic gases are often emitted from open crater vents [Allard *et al.*, 1994], but some fraction of them also escape diffusively through the volcanic soils or become partially trapped within the basal aquifers following fault-controlled pathways. The characteristics of the basal aquifers are described by Grassa *et al.* [this volume]. At the base of the volcano, the northeastern part of the island is affected by anomalous CO₂ degassing and temperature, and the composition and dissolved-gas content of the shallow aquifer are greatly modified by the input of hot acidic fluids [Carapezza and Inguaggiato, 2001; Capasso *et al.*, 2005a]. The water temperatures in this part of the island range from 25° to 42°C, with dissolved CO₂ contents ranging from 10 to 200 cm³/L at standard temperature and pressure (STP) conditions. The isotope signature of dissolved CO₂ ($\delta^{13}\text{C}$) is similar to that measured in the fumaroles of the summit crater area, indicating a magmatic gas input into the aquifer. This is also demonstrated by the helium content, ranging from 1.5×10^{-4} to 1×10^{-3} cm³/L STP, and the helium-isotope ratios [$3.39 < \text{R}_c/\text{Ra} < 4.56$; Capasso *et al.*, 2005a]. The presence of CH₄ in the range 3×10^{-4} to 1×10^{-2} cm³/L STP is indicative of a contribution of hydrothermal fluids, given the very low methane content in high-temperature magmatic gases [Giggenbach, 1996].

Magmatic gases reach the shallowest water levels after probable reequilibration in a deeper hydrothermal aquifer, as suggested by the significant CH₄ contents measured in shallow thermal waters [Capasso *et al.*, 2005a]. The vapor that separates from this aquifer may enter the shallower water levels. According to Capasso *et al.* [2005a], the deep magmatic gas should experience large modifications during ascent. Its chemical composition would probably be controlled by the local hydrothermal conditions (lower temperature and reducing redox conditions) and by steam loss during boiling of the aquifer. This would promote the preferential partitioning of the less-soluble gas species into the vapor phase (He and CH₄ with respect to CO₂) and ¹³C enrichment in boiled-off CO₂ (at a temperature of 120°–130°C, according to Mook *et al.* [1974]). This fractionation depends on the extent of steam separation that produces marked partitioning, particularly for small steam fractions. After separation from the hydrothermal aquifer, the vapor enters the shallower meteoric aquifer, which is variably contaminated by seawater [Carapezza and Inguaggiato, 2001; Grassa *et al.*, this volume]. This aquifer probably acts as a filter, where more soluble gas species (particularly CO₂) may dissolve, and ¹³C is enriched in dissolved carbon (CO₃²⁻ and HCO₃⁻ ions). The absorption of CO₂ should be favored by the contribution of seawater flowing into the shallow aquifer since this gas is rapidly hydrolyzed to form H₂CO₃, HCO₃⁻, and CO₃²⁻ at the relatively high pH of seawater (pH = 8.3). The final effect is an increase in dissolved carbon content along with pH, which is summarized as follows [Stumm and Morgan, 1996; see also Capasso *et al.*, 2005a]:

$$(R1) \quad [\text{H}_2\text{CO}_3] = \frac{\text{pCO}_2}{K_{\text{H}}}$$

$$(R2) \quad [\text{HCO}_3^-] = \frac{K_1}{[\text{H}^+]} \frac{\text{pCO}_2}{K_{\text{H}}},$$

and

$$(R3) \quad [\text{CO}_3^{2-}] = \frac{K_1 \cdot K_2 \text{ pCO}_2}{[\text{H}^+]^2 K_{\text{H}}},$$

where K_{H} , K_1 , and K_2 are Henry's constant and the first and second dissociation constants of carbonic acid, respectively. The apparent Henry's constant of CO₂ is therefore

$$(R4) \quad K_{\text{H}}^* = \frac{K_{\text{H}}}{\left(1 + \frac{K_1}{[\text{H}^+]} + \frac{K_1 K_2}{[\text{H}^+]^2}\right)}.$$

For carbon isotopes, a higher pH results in stronger partitioning of ¹³C in water due to the total fractionation factor $10^3 \ln \alpha_{\text{TDC-CO}_2}$ (the fractionation factor $10^3 \ln(\alpha_{1-2})$ is

roughly equal to the difference between the isotopic composition ($\delta^{13}\text{C}$) of species 1 and 2) being obtained by summing up the enrichment factors between each dissolved carbon species and CO_2 , weighted for their abundance with respect to total dissolved carbon:

(R5)

$$10^3 \ln \alpha_{\text{TDC}-\text{CO}_{2g}} = \frac{\varepsilon_{\text{HCO}_3^- - \text{CO}_{2g}} [\text{HCO}_3^-] + \varepsilon_{\text{CO}_3^{2-} - \text{CO}_{2g}} [\text{CO}_3^{2-}] + \varepsilon_{\text{H}_2\text{CO}_3 - \text{CO}_{2g}} [\text{H}_2\text{CO}_3]}{[\text{HCO}_3^-] + [\text{CO}_3^{2-}] + [\text{H}_2\text{CO}_3]}$$

The respective enrichment factors between dissolved carbon species and CO_2 at 40°C are $\varepsilon_{\text{HCO}_3^- - \text{CO}_{2g}} = 6.7\text{\textperthousand}$, $\varepsilon_{\text{H}_2\text{CO}_3 - \text{CO}_{2g}} = -0.84\text{\textperthousand}$, $\varepsilon_{\text{CO}_3^{2-} - \text{CO}_{2g}} = 5.5\text{\textperthousand}$ [Deines *et al.*, 1974]. Therefore, given the temperature–pH dependency of the chemical proportion of dissolved carbon species [reactions (1)–(3)], $10^3 \ln \alpha_{\text{TDC}-\text{CO}_{2g}}$ increases with the pH.

The above-described fractionation mechanisms result in the chemical and isotopic composition of the original volcanic gas changing during its ascent. The carbon–isotope composition is probably not modified by the addition of organic carbon on the assumption that the contribution of organic CO_2 is insignificant compared to the huge content of volcanic CO_2 in the sampled waters. As an example, the CO_2 content of water in contact with organic CO_2 in sample 47 of Mt. Vesuvius (a volcanic area at a similar latitude [Federico *et al.*, 2002]) is about $8 \text{ cm}^3/\text{L STP}$ ($\delta^{13}\text{C}_{\text{CO}_2}$ of $-21.7\text{\textperthousand}$), which is about 30 times lower than the CO_2 content measured in the Stromboli thermal aquifer. Assuming a nearly constant water flow into the aquifer, the effect of

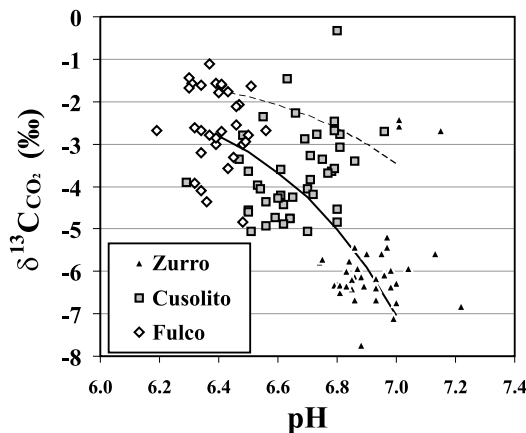


Figure 2. $\delta^{13}\text{C}$ of CO_2 versus pH measured in thermal waters. The dotted line represents a higher CO_2 /water mass ratio (0.4 mol of CO_2 interacting with 1 L of water) and therefore a higher CO_2 flux; the solid line represents a lower CO_2 /water mass ratio (0.2 mol of CO_2 interacting with 1 L of water).

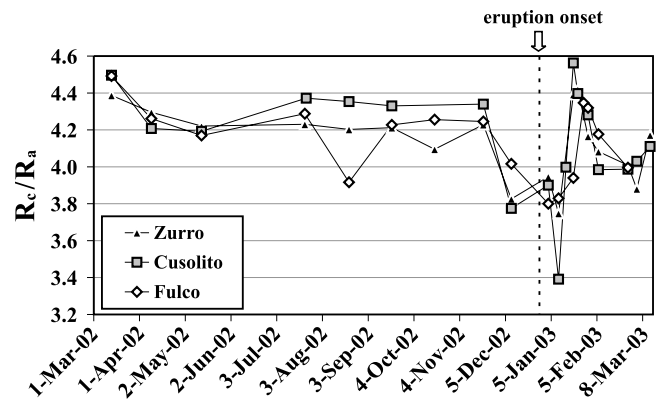


Figure 3. Temporal trends of R_c/R_a ratios measured in thermal waters.

this fractionation is also related to given amounts of CO_2 and water (which are, in turn, related to CO_2 fluxes). As indicated in Figure 2, the Fulco well is the least affected by fractionation and appears as the most representative of the original gas, whereas the Cusolito and Zurro wells appear to be strongly affected by fractionation, due to a higher contribution of seawater. The variability observed in Fulco data might be essentially related to gas flux from a deep source, which is consistent with the trends of the two curves shown in Figure 2 plotting the composition of the residual gas after exchange with waters with different pH values—lower CO_2 fluxes are associated with more negative isotopic compositions (at similar pH values).

The use of helium isotopes has the advantage of overcoming the possible influence of the aquifer since they are virtually unaffected by fractionation during boiling or dissolution into water [Benson and Krause, 1980]. He isotopes can actively fractionate only during gas separation from magma due to preferential partitioning of ${}^3\text{He}$ into gas bubbles, coupled with its concomitant depletion within the magma during degassing [Ozima and Podosek, 1983; Caracausi *et al.*, 2003].

The ratios of dissolved helium isotopes in Stromboli thermal waters range from 3.39 to 4.56 Ra (Figure 3), after correcting for air contamination, and are systematically higher than values measured at the SC5 fumarole in the Pizzo area [Carapezza and Federico, 2000; Inguaggiato and Rizzo, 2004; Capasso *et al.*, 2005a]. The gas emitted from this fumarole comes from the upper portion of the conduit, whereas gas dissolved in the thermal aquifer at the base of the volcano has a deeper source. The upper portions of the conduit are filled by largely degassed and crystallized magma [Bertagnini *et al.*, 1999; Métrich *et al.*, 2001; Landi *et al.*, 2004, 2006], probably depleted of ${}^3\text{He}$ with respect to deeper portions, whose gases probably feed the basal aquifer.

5. GEOCHEMICAL CHANGES BEFORE THE ERUPTION ONSET

At 6:30 LT on 28 December 2002, immediately after the emission of a glowing avalanche and fluid lava outflow from the NE crater, lava started to pour out from a fissure at the base of the NE crater that extended from 750 to 600 m asl [Calvari *et al.*, 2005; Landi *et al.*, 2006]. Other vents opened in the following days within the SdF depression at elevations of 670, 550, and 500 m asl. After the huge landslide that occurred on 30 December 2002, which generated a tsunami, the lava was emitted mostly from vents located at 500 and 550 m asl. The magma height within the upper conduits fluctuated until mid-February 2003, and the decrease in the effusion rate from the 500-m vent was frequently accompanied by enhanced effusion from the 670-m vent [Calvari *et al.*, 2005]. After the beginning of the eruption, Strombolian activity at the summit craters—which had been quite intense during June, July, and October 2002, with a major explosion in July 2002—completely ceased due to the lowering of the magma level in the conduit due to it draining from lateral eruptive fissures.

Some geochemical signals marked both the period of intense Strombolian activity at the craters, with a constantly high magma level within the conduits and the onset of the effusive phase. These signals were related to the degassing of deep magma after depressurization and ascent, and to fractionation processes, affecting helium and carbon isotopes, which occurred throughout this period.

The peaks in dissolved CO₂ contents measured in the basal thermal aquifer since July 2002 [Carapezza *et al.*, 2004; Capasso *et al.*, 2005a] suggest that pulses of gas-rich magma arrived in the shallow plumbing system and explain both the intense Strombolian activity observed at the summit craters and the magma ascending in the conduits. This is shown in Figure 4, which plots the temporal trends of dissolved CO₂ contents and carbon-isotope composition ($\delta^{13}\text{C}$) in Fulco and Zurro wells. The monthly rainfall amount is also plotted, which shows that the gas content is unaffected by the eventual dilution of the aquifer after high-rainfall events. As discussed in section 4, the gas sampled at the Fulco well is the least affected by secondary fractionation processes and, therefore, is the most representative of the original volcanic or hydrothermal gas. On the other hand, even larger peaks in dissolved CO₂ were measured in the Zurro well together with higher $\delta^{13}\text{C}$ ratios that were significantly above background values. Peaks in the dissolved CO₂ contents were measured in June, August, and November 2002. These were generally accompanied by higher $\delta^{13}\text{C}$ values and, as commented on above (see Figure 2), could reflect variable gas fluxes from a deep source (provided that the water flow into the aquifer re-

mained unchanged). High dissolved CO₂ contents and $\delta^{13}\text{C}$ values had also been observed in 2000, when normal Strombolian activity was interrupted by two violent explosions on June and September (see the 2000 monthly reports of the Global Volcanism Program at <http://www.volcano.si.edu>).

Helium and carbon isotopes provide further insights into magma ascent since they fractionate during bubble nucleation and growth. Indeed, magma is progressively depleted of both ³He and ¹³C during degassing [Javoy *et al.*, 1978; Ozima and Podosek, 1983; Trull *et al.*, 1991], and thus, high Rc/Ra and $\delta^{13}\text{C}$ values indicate replenishment of gas-rich magma from a deep source. Conversely, these parameters are lower for a gas released from a shallow and degassed magma column. In the basal thermal aquifer, the ratios of dissolved helium isotopes were constantly high (about 4.2 Ra) in 2002 until November, with samples from December 2002 exhibiting slightly lower Rc/Ra ratios (down to 3.8) and high values (4.30–4.56) only again being measured in late January 2003 at the thermal wells (Figure 3). Similar trends were observed even at the SC5 crater fumarole (Figure 5), with parallel variations in the helium (Rc/Ra) and carbon ($\delta^{13}\text{C}_{\text{CO}_2}$) isotopes and with higher values in October and November 2002. Based on the behavior of both He and C isotopes during magma degassing, the high values measured since summer 2002 can be ascribed to degassing of new gas-rich magma batches that entered the shallower and partially degassed magma column (see the interpretative model in Figure 6 [Tibaldi, 2001; Bertagnini *et al.*, 2003; Tibaldi *et al.*, 2003; Landi *et al.*, 2004]). This occurred until nearly 1 month before the eruption onset and is compatible with the observed increase in dissolved CO₂ contents and $\delta^{13}\text{C}$ values in the basal aquifer. Besides being typical of a gas unmodified by dissolution-driven secondary fractionation (see section 4), these values are consistent with a gas phase in equilibrium with a deep “primitive” magma that did not experience any extensive degassing.

The decrease in Rc/Ra and $\delta^{13}\text{C}_{\text{CO}_2}$ observed in the single December sampling (about 3 weeks before the eruption onset) and until March 2003 can be attributed to ³He and ¹³C depletion in magma due to fractionation of helium and carbon isotopes caused by progressive degassing [Capasso *et al.*, 2005a]. This suggests that there was no further input of gas-rich magma from the deeper into the shallower plumbing system after November 2002, as confirmed by petrological data [Landi *et al.*, 2006]. Ten days before the eruption onset, very high soil CO₂ fluxes (daily averages up to 76,000 g/m²/d) were recorded on the crater rim at the STRO2 station [Carapezza *et al.*, 2004] (Figure 7a). Unfortunately, no flux data are available for summer 2002 since the station had been severely damaged by volcanic ejecta, and it was not operational again until 18 December 2002 (Figure 7b). The

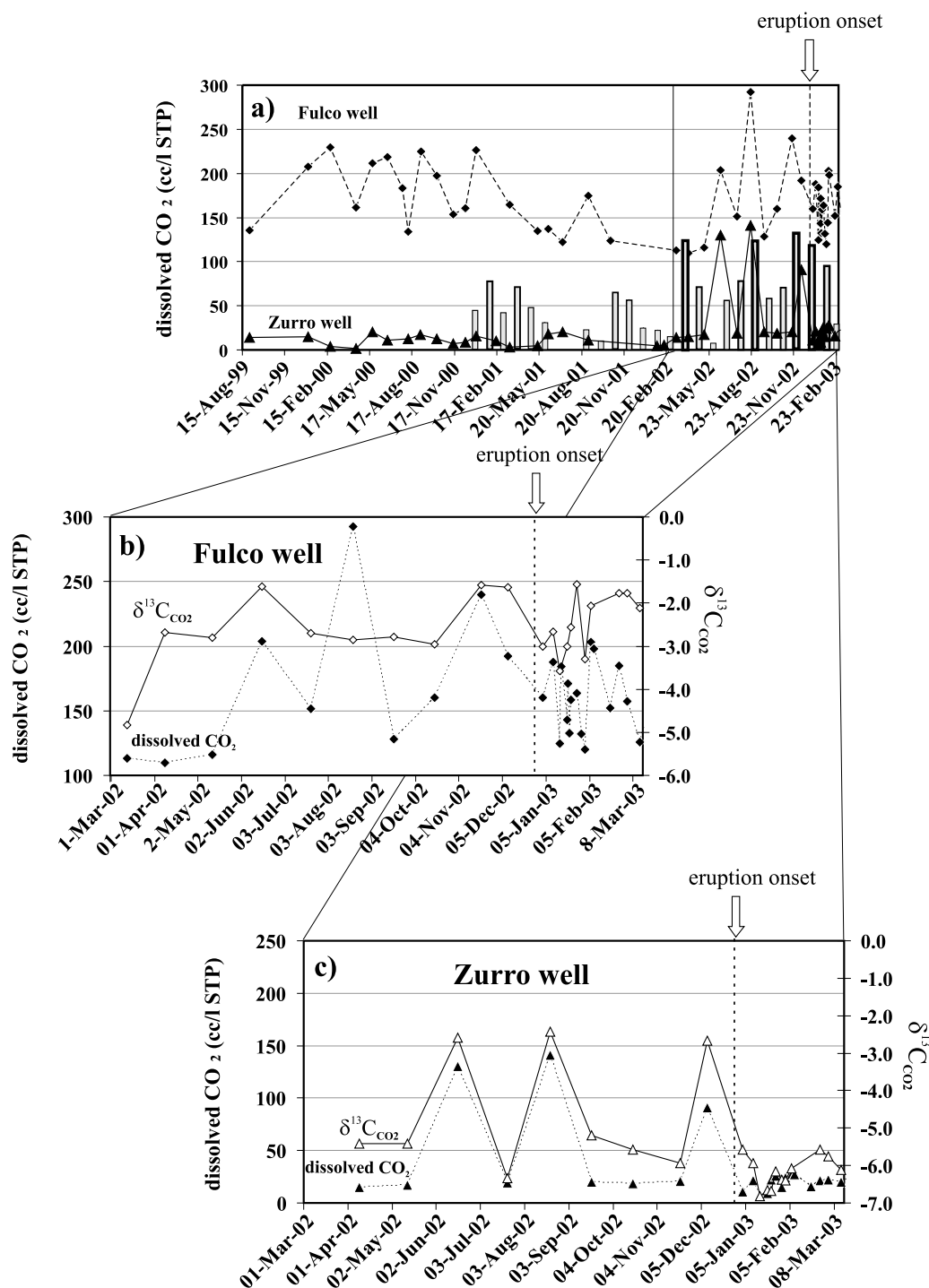


Figure 4. Temporal trends of dissolved CO_2 contents measured in (a) Fulco and Zurro well waters since 1999 and monthly rainfall (data available at <http://www.meteosicilia.it>, Messina station). Temporal trends of dissolved CO_2 contents and $\delta^{13}\text{C}$ of CO_2 values measured since March 2002 at the (b) Fulco and (c) Zurro wells.

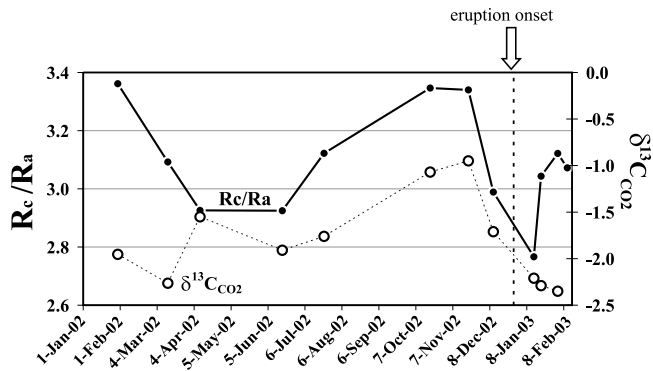


Figure 5. Temporal trends of R_c/R_a ratios and $\delta^{13}\text{C}$ of CO_2 measured at the SC5 fumarole (Pizzo).

increasing CO_2 fluxes were matched by high Rn concentrations in the soil measured at various sites in the summit area, as shown in Figure 7c. This indicates that trace gases (such as Rn) are efficiently transported by carrier gases (essentially CO_2 [e.g., Etiope and Martinelli, 2002, and references therein]). The very high soil CO_2 fluxes and Rn concentrations in the summit area (Pizzo) measured in the second

half of December 2002 strongly suggest a high gas-driven magma supply rate and/or a gas overpressure in the conduits, which would be responsible for the intense Strombolian activity that occurred during that period. Both gas fluxes and explosive activity peaked late in December, with finally the onset of the eruption on 28 December being marked by a major explosion from a lateral vent and a fluid lava emission from a fissure that opened on the northern rim of the NE crater [Landi *et al.*, 2006].

Following Ripepe *et al.* [2005], the transition from the explosive to the effusive phases at Stromboli is indicated by an increased magma supply rate and gas overpressure in the shallow conduits. According to their model, for a given threshold value of the supply rate ($>0.2 \text{ m}^3/\text{s}$), the Strombolian activity becomes unable to spread out the increased volume flux, and the resulting overpressure causes the brittle failure of the conduit and the onset of a lava flow [see also Calvari *et al.*, 2005; Landi *et al.*, 2006]. The sudden decrease in CO_2 fluxes and Rn concentrations measured after the opening of the eruptive fracture—when the magma level lowered in the conduit—are indicative of a decrease in gas overpressure due to drainage from lateral vents. The CO_2 fluxes showed an overall decreasing trend during Janu-

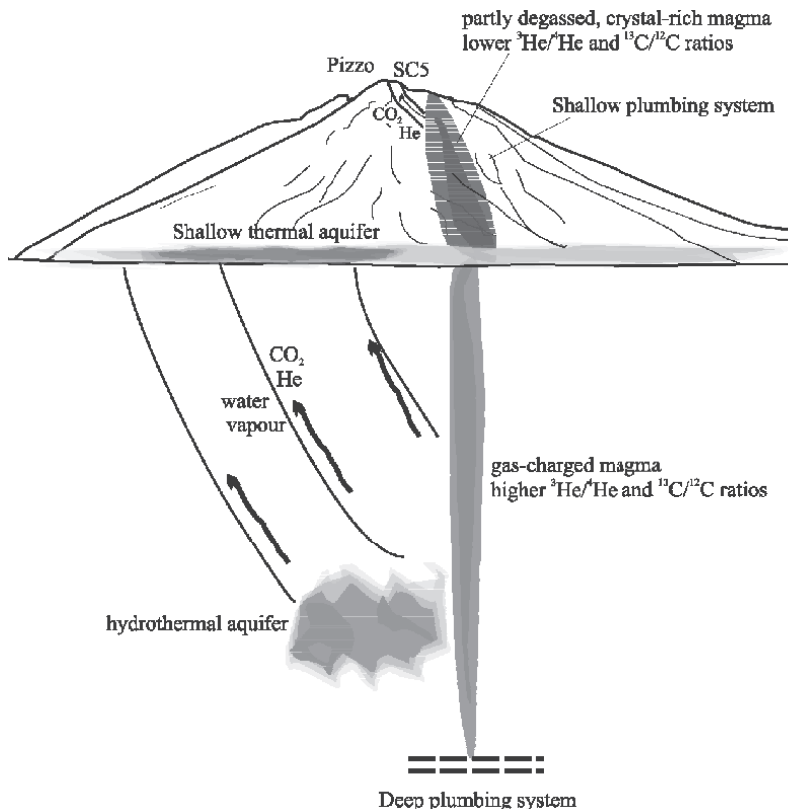


Figure 6. Schematic interpretative model of the gas feeding system at Stromboli. The vertical scale is arbitrary.

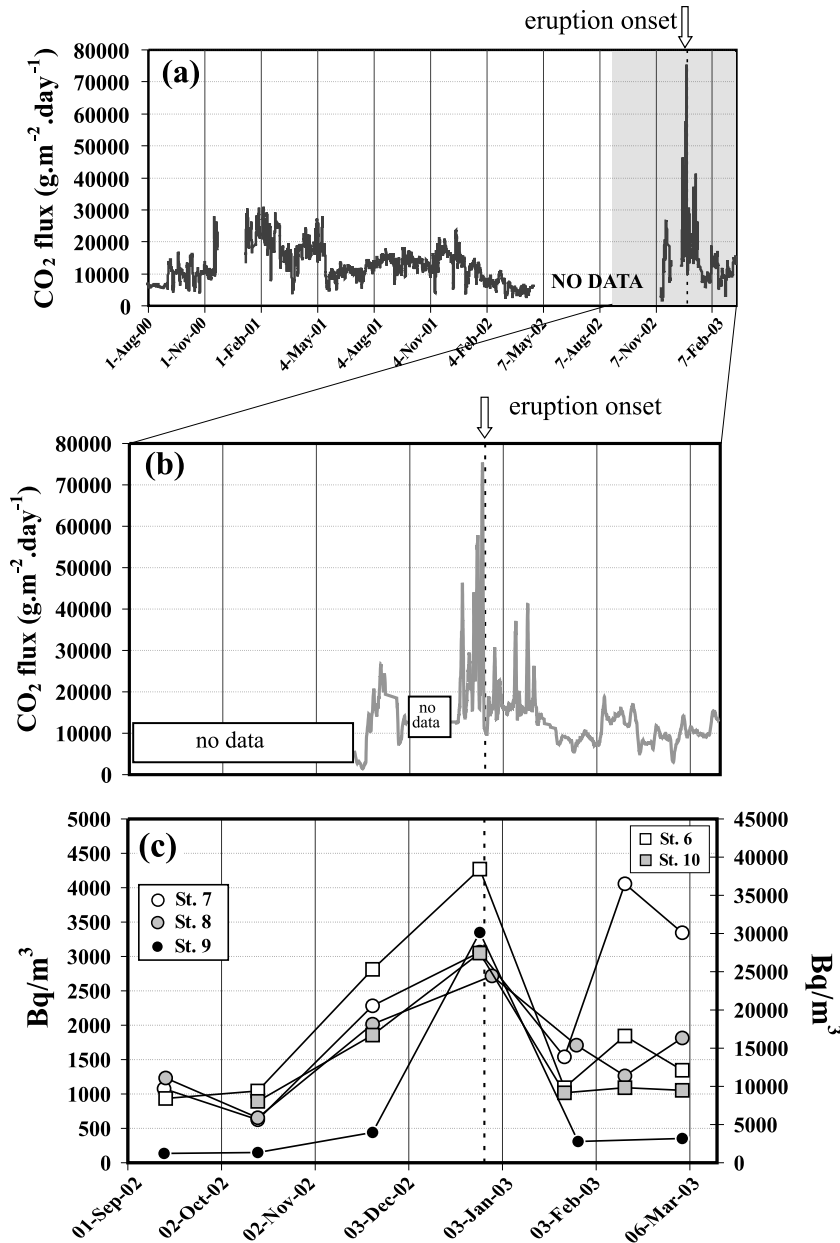


Figure 7. (a) Temporal trends of soil CO_2 fluxes (24-point running averages) measured at the summit STR02 station since 2000. Temporal trends from September 2002 to February 2003 of (b) soil CO_2 fluxes (24-point running averages) at the STR02 station and (c) α -track data of Rn emissions measured in the summit area. Data are the measured values integrated over the exposure time. The time coordinate of single points is the average time of exposure.

ary 2003 (Figure 7a), which was characterized by frequent closing and opening of the 500-m vent due to the periodic sealing of fractures during and after periods characterized by lower effusion rates [Calvari *et al.*, 2005]. Such periodic sealing of the eruptive fractures would have increased the gas overpressure in the conduits [Ripepe *et al.*, 2005] and would explain the several peaks evident in soil CO_2 fluxes

during the overall decreasing trend observed in January 2003 (Figure 7a).

A new small input of fresh magma into the shallow plumbing system probably occurred in March 2003, whose arrival was marked by increasing Rc/Ra ratios and $\delta^{13}\text{C}$ values in thermal wells and the resumption of normal Strombolian activity at the summit craters [Lodato *et al.*, 2007].

6. CONCLUSIONS

Geochemical data obtained from thermal waters, crater fumaroles, and soil gases at Stromboli allowed us to detect chemical and isotopic precursors of the 2002–2003 lava-flow eruption. Increasing CO₂ contents, δ¹³C of CO₂, and Rc/Ra ratios in thermal waters of the basal aquifer are consistent with the intrusion of fresh gas-rich magma into the upper part of the Stromboli plumbing system, which induced intense Strombolian activity at the summit crater several months before the eruption.

The Rc/Ra ratios also increased in gases at the summit area from July 2002, although relative to the values measured in the basal aquifer, they appear to be related to a magma that was partially degassed during its ascent within the conduits. This scenario is supported by the recorded variations in carbon isotopes. These geochemical variations coincided with a period of intense Strombolian activity at the summit craters, with a very high level of magma in the conduit and frequent small lava overflows from the NE crater rim. The last samples, collected nearly 20 d before the eruption, showed a decrease in ³He and ¹³C isotopes both in thermal waters and in the summit fumarolic gases, coupled with a lower average level of dissolved CO₂ in the thermal waters. Together with petrological data, this would indicate that there was no input of primitive magma batches into the shallow plumbing system shortly before the eruption onset. Anomalously high CO₂ fluxes and Rn concentrations were recorded in the summit area (Pizzo) from 10 d before the eruption, which lasted nearly 7 months. These anomalous CO₂ and Rn data, and the coeval intense Strombolian activity that culminated on 28 December, account for an enhanced gas-driven magma supply rate and gas overpressure within the conduits, which probably heralded the conduit failure and the onset of the effusive phase.

Results obtained from measurements made at Stromboli before and during the onset of the 2002–2003 eruption demonstrate the importance of collecting a wide spectrum of geochemical data from different geological sites when monitoring a volcano. Measurement points located both in the uppermost parts and at the subaerial base of the volcanic edifice represent accessible windows to the shallowest portions of the volcano and the deeper part of the feeding system, respectively. Geochemical variations of the gases emitted from the summit area are key to detecting any perturbation of the magma dynamics in the shallower plumbing system, since they reflect the balance between the supply rate and gas overpressure within the conduit. Similarly, the geochemical variations recorded in the basal aquifer more directly relate to gases exsolving from a more primitive magma at greater depth and can be used to predict modifications in the eruptive regime.

Acknowledgments. This study forms part of the GNV “Stromboli volcanic hazard” project and the volcano monitoring activities of INGV-Palermo.

REFERENCES

- Aiuppa, A., C. Federico, A. Paonita, G. Pecoraino, and M. Valenza (2002), S, Cl and F degassing as an indicator of volcanic dynamics: The 2001 eruption of Mount Etna, *Geophys. Res. Lett.*, 29(11), 1559, doi:10.1029/2002GL015032.
- Aiuppa, A., C. Federico, G. Giudice, S. Gurrieri, A. Paonita, and M. Valenza (2004), Plume chemistry provides insights into mechanisms of sulfur and halogen degassing in basaltic volcanoes, *Earth Planet. Sci. Lett.*, 222, 469–483.
- Allard, P., J. Carbonelle, N. Metrich, H. Loyer, and P. Zettwoog (1994), Sulphur output and magma degassing budget of Stromboli volcano, *Nature*, 368, 326–330.
- Badalamenti, B., et al. (1994), Soil gas investigations during the 1991–1993 Etna eruption, *Acta Vulcanol.*, 4, 135–141.
- Badalamenti, B., N. Bruno, T. Caltabiano, F. Di Gangi, S. Giannanco, and G. Salerno (2004), Continuous soil CO₂ and discrete plume SO₂ measurements at Mt. Etna (Italy) during 1997–2000: A contribution to volcano monitoring, *Bull. Volcanol.*, 66, 80–89, doi:10.1007/s004450030305y.
- Barberi, F., M. Rosi, and A. Sodi (1993), Volcanic hazard assessment at Stromboli based on review of historical data, *Acta Vulcanol.*, 3, 173–187.
- Benson, B., and D. Krause Jr. (1980), Isotope fractionation of helium during solution: A probe for the liquid state, *J. Solution Chem.*, 9, 895–909.
- Bertagnini, A., M. Coltelli, P. Landi, M. Pompilio, and M. Rosi (1999), Violent explosions yield new insights into dynamics of Stromboli volcano, *Eos Trans. AGU*, 80, 633–636.
- Bertagnini, A., N. Métrich, P. Landi, and M. Rosi (2003), Stromboli volcano (Aeolian Archipelago, Italy): An open window on the deep-feeding system of steady state basaltic volcano, *J. Geophys. Res.*, 108(B7), 2336, doi:10.1029/2002JB002146.
- Bonaccorso, A., S. Calvari, G. Garfi, L. Lodato, and D. Patanè (2003), Dynamics of the December 2002 flank failure and tsunami at Stromboli volcano inferred by volcanological and geophysical observations, *Geophys. Res. Lett.*, 30(18), 1941, doi:10.1029/2003GL017702.
- Brusca, L., S. Inguaggiato, M. Longo, P. Madonia, and R. Maugeri (2004), The 2002–2003 eruption of Stromboli (Italy): Evaluation of the volcanic activity by means of continuous monitoring of soil temperature, CO₂ flux, and meteorological parameters, *Geochem. Geophys. Geosys.*, 5(12), Q12001, doi:10.1029/2004GC000732.
- Burton, M., P. Allard, F. Muré, and A. La Spina (2007), Magmatic gas composition reveals the source depth of slug-driven Strombolian explosive activity, *Science*, 317, 227–230.
- Calvari, S., L. Spampinato, L. Lodato, A. J. L. Harris, M. R. Patrick, J. Dehn, M. R. Burton, and D. Andronico (2005), Chronology and complex volcanic processes during the 2002–2003 flank eruption at Stromboli volcano (Italy) reconstructed from

- direct observations and surveys with a handheld thermal camera, *J. Geophys. Res.*, 110, B02201, doi:10.1029/2004JB003129.
- Capasso, G., and M. L. Carapezza (1994), A geochemical survey of Stromboli, *Acta Vulcanol.*, 6, 52–53.
- Capasso, G., and S. Inguaggiato (1998), A simple method for the determination of dissolved gases in natural waters. An application to thermal waters from Vulcano Island, *Appl. Geochem.*, 13, 631–642.
- Capasso, G., M. L. Carapezza, C. Federico, S. Inguaggiato, and A. Rizzo (2005a), Geochemical monitoring of the 2002–2003 eruption at Stromboli volcano (Italy): Precursory changes in the carbon and helium isotopic composition of fumarole gases and thermal waters, *Bull. Volcanol.*, 68, 118–134, doi:10.1007/s0044500504275.
- Capasso, G., R. Favara, F. Grassia, S. Inguaggiato, and M. Longo (2005b), On-line technique for preparing and measuring stable carbon isotope of total dissolved inorganic carbon in water sample ($\delta^{13}\text{C}_{\text{DIC}}$), *Ann. Geophys.*, 48, 159–166.
- Caracausi, A., R. Favara, S. Giannanco, F. Italiano, P. M. Nuccio, A. Paonita, G. Pecoraino, and A. Rizzo (2003), Mount Etna: Geochemical signals of magma ascent and unusually extensive plumbing system, *Geophys. Res. Lett.*, 30(2), 1057, doi:10.1029/2002GL015463.
- Carapezza, M. L., and C. Federico (2000), The contribution of fluid geochemistry to the volcano monitoring of Stromboli, *J. Volcanol. Geotherm. Res.*, 95, 227–245.
- Carapezza, M. L., and D. Granieri (2004) CO₂ soil flux at Vulcano (Italy): Comparison between active and passive methods, *Appl. Geochem.*, 19, 73–88.
- Carapezza, M. L., and S. Inguaggiato (2001), Interaction between thermal waters and CO₂-rich fluids at Stromboli volcano (Italy), *Proc. WRI-10*, 2, pp. 791–794, Rotterdam, Balkema.
- Carapezza, M. L., S. Inguaggiato, L. Brusca, and M. Longo (2004), Geochemical precursors of the activity of an open-conduit volcano: The Stromboli 2002–2003 eruptive events, *Geophys. Res. Lett.*, 31, L07620, doi:10.1029/2004GL019614.
- Casadevall, T. J., M. P. Doukas, C. A. Neal, R. G. McGimsey, and C. A. Gardner (1994), Emission rates of sulfur dioxide and carbon dioxide from Redoubt Volcano, Alaska during 1989–1990 eruptions, *J. Volcanol. Geotherm. Res.*, 62, 519–530.
- Chioldini, G., R. Cioni, M., Guidi, L., Marini, and B. Raco (1998), Soil CO₂ flux measurements in volcanic and geothermal areas. *Appl. Geochem.*, 13, 543–552.
- Chouet, B., P. Dawson, T. Ohminato, M. Martini, G. Saccorotti, F. Giudicepietro, G. De Luca, G. Milana, and R. Scarpa (2003), Source mechanisms of explosions at Stromboli Volcano, Italy, determined from moment-tensor inversions of very-long-period data, *J. Geophys. Res.*, 108(B1), 2019, doi:10.1029/2002JB001919.
- Cigolini, C., G. Gervino, R. Bonetti, F. Conte, M. Laiolo, D. Coppolo, and A. Manzoni (2005), Tracking precursors and degassing by radon monitoring during major eruptions at Stromboli Volcano (Aeolian Islands, Italy), *Geophys. Res. Lett.*, 32, L12308, doi:10.1029/2005GL022606.
- Deines, P., D. Langmuir, and R. S. Harmon (1974), Stable carbon isotope ratios and the existence of a gas phase in the evolution of carbonate groundwaters, *Geochim. Cosmochim. Acta*, 38, 1147–1164.
- Etiope, G., and G. Martinelli (2002), Migration of carrier and trace gases in the geosphere: An overview, *Phys. Earth Planet. Inter.*, 129, 185–204.
- Favara, R., F. Grassia, S. Inguaggiato, G. Pecoraino, and G. Capasso (2002), A simple method to determine the $\delta^{13}\text{C}$ content of total dissolved inorganic carbon, *Geofis. Int.*, 41, 313–320.
- Federico, C., A. Aiuppa, P. Allard, S. Bellomo, P. Jean-Baptiste, F. Parello, and M. Valenza (2002), Magma-derived gas influx and water–rock interactions in the volcanic aquifer of Mt. Vesuvius, Italy, *Geochim. Cosmochim. Acta*, 66, 963–981.
- Finizola, A., F. Sortino, J.-F. Lénat, M. Aubert, M. Ripepe, and M. Valenza (2003), The summit hydrothermal system of Stromboli: New insights from self-potential, temperature, CO₂ and fumarolic fluids measurements, with structural and monitoring implications, *Bull. Volcanol.*, 65, 486–504, doi:10.1007/s004450030276-2.
- Fischer, T. P., M. M. Morrisey, M. L. Calvache, M. Diego Gomez, R. Torres, J. Stix, and S. N. Williams (1994), Correlations between SO₂ flux and long period seismicity at Galeras volcano, *Nature*, 368, 135–137.
- Gerlach, T. M., K. A. McGee, T. Elias, A. J. Sutton, and M. P. Doukas (2002), Carbon dioxide emission rate of Kīlauea Volcano: Implications for primary magma and the summit reservoir, *J. Geophys. Res.*, 107(B9), 2189, doi:10.1029/2001JB000407.
- Giggenbach, W. F. (1996), Chemical composition of volcanic gases, in *Monitoring and Mitigation of Volcanic Hazards*, edited by R. Scarpa, and R. I. Tilling, pp. 221–256, Springer, Berlin.
- Granieri, D., M. L. Carapezza, G. Chioldini, R. Avino, S. Caliro, M. Ranaldi, T. Ricci, and L. Tarchini (2006), Correlated increase in CO₂ fumarolic content and diffuse emission from La Fossa crater (Vulcano, Italy): Evidence of volcanic unrest or increasing gas release from a stationary deep magma body? *Geophys. Res. Lett.*, 33, L13316, doi:10.1029/2006GL026460.
- Grassia, F., S. Inguaggiato, and M. Liotta (2008), Fluid geochemistry of Stromboli, this volume.
- Hammouya, G., P. Allard, P. Jean-Baptiste, F. Parello, M. Semet, and S. Young (1998), Pre- and syn-eruptive geochemistry of volcanic gases from Soufrière Hills of Montserrat, West Indies, *Geophys. Res. Lett.*, 25, 3685–3688.
- Hirabayashi, J., J. Ossaka, and T. Ozawa (1982), Relationship between volcanic activity and chemical composition of volcanic gases—A case study on the Sakurajima volcano, *Geochem. J.*, 16, 11–21.
- Inguaggiato, S., and A. Rizzo (2004), Dissolved helium isotope ratios in ground-waters: A new technique based on gas-water re-equilibration and its application to a volcanic area, *Appl. Geochem.*, 19, 665–673.
- Javoy, M., F. Pineau, and I. Liyama (1978), Experimental determination of the isotopic fractionation between gaseous CO₂ and carbon dissolved in tholeiitic magma, *Contrib. Mineral. Petro.*, 67, 35–39.
- Kotrappa, P., J. C. Dempsey, and L. R. Stieff (1993), Recent advances in electret ion chamber technology, *Radiat. Prot. Dosim.*, 47, 461–464.
- Landi, P., N. Métrich, A. Bertagnini, and M. Rosi (2004), Dynamics of magma mixing and degassing recorded in plagioclase at

- Stromboli (Aeolian Archipelago, Italy), *Contrib. Mineral. Petrol.*, 147, 213–227, doi:10.1007/s0041000405555.
- Landi, P., L. Francalanci, M. Pompilio, M. Rosi, R. A. Corsaro, C. M. Petrone, I. Nardini, and L. Miraglia (2006), The December 2002–July 2003 effusive event at Stromboli volcano, Italy: An insight into the shallow plumbing system by petrochemical studies, *J. Volcanol. Geotherm. Res.*, 155, 263–284.
- Lodato, L., L. Spampinato, A. Harris, S. Calvari, J. Dehn, and M. Patrick (2007), The morphology and evolution of the Stromboli 2002–2003 lava flow field: An example of a basaltic flow field emplaced on a steep slope, *Bull. Volcanol.*, 69, 661–679, doi:10.1007/s0044500601016.
- McGee, K. A., T. M. Gerlach, R. Kessler, and M. P. Doukas (2000), Geochemical evidence for a magmatic CO₂ degassing event at Mammoth Mountain, California, September–December 1997, *J. Geophys. Res.*, 105(B4), 8447–8456, doi:10.1029/2000JB900009.
- Métrich, N., A. Bertagnini, P. Landi, and M. Rosi (2001), Crystallization driven by decompression and water loss at Stromboli volcano (Aeolian Islands, Italy), *J. Petrol.*, 42, 1471–490.
- Mook, W. G., J. C. Bommerson, and W. H. Staverman (1974), Carbon isotope fractionation between dissolved bicarbonate and gaseous carbon dioxide, *Earth Planet. Sci. Lett.*, 22/2, 169–76.
- Ozima, M., and F. A. Podosek (1983), *Noble Gas Geochemistry*, 344 pp., Cambridge Univ. Press, New York.
- Revil, A., A. Finizola, F. Sortino, and M. Ripepe (2004), Geophysical investigations at Stromboli volcano, Italy. Implications for ground water flow, *Geophys. J. Int.*, 157, 426–440.
- Ripepe, M., E. Marchetti, G. Olivieri, A. Harris, J. Dehn, M. Burton, T. Caltabiano, and G. Salerno (2005), Effusive to explosive transitio during the 2003 eruption of Stromboli volcano, *Geology*, 33, 341–344, doi:10.1130/G21173.1.
- Rizzo, A., A. Caracausi, R. Favara, M. Martelli, P. M. Nuccio, A. Paonita, A. Rosciglione, and M. Paternoster (2006), New insights into magma dynamics during last two eruptions of Mount Etna as inferred by geochemical monitoring from 2002 to 2005, *Geochem. Geophys. Geosyst.*, 7, Q06008, doi:10.1029/2005GC001175.
- Rosi, M., A. Bertagnini, A. J. L. Harris, L. Pioli, M. Pistoletti, and M. Ripepe (2006), A case history of paroxysmal explosion at Stromboli: Timing and dynamics of the April 5, 2003 event, *Earth Planet. Sci. Lett.*, 243, 594–606.
- Sano, Y., and H. Wakita (1985), Geographical distribution of ³He/⁴He in Japan: Implications for arc tectonics and incipient magmatism, *J. Geophys. Res.*, 90, 8729–8741.
- Stumm, W., and J. J. Morgan (1996), *Aquatic Chemistry: Chemical Equilibria and Rates in Natural Waters*, Wiley-Interscience, New York.
- Taran, Y., J. C. Gavilanes, and A. Cortes (2002), Chemical and isotopic composition of fumarolic gases and the SO₂ flux from Volcan de Colima, Mexico, between the 1994 and 1998 eruptions, *J. Volcanol. Geotherm. Res.*, 117, 105–119.
- Tibaldi, A. (2001), Multiple sector collapses at Stromboli volcano, Italy: How they work, *Bull. Volcanol.*, 63, 112–125, doi:10.1007/s004450100129.
- Tibaldi, A., C. Corazzato, T. Apuani, and A. Cancelli (2003), Deformation at Stromboli volcano (Italy) revealed by rock mechanics and structural geology, *Tectonophysics*, 361, 187–204.
- Tinti, S., G. Pagnoni, and F. Zaniboni (2003), Tsunami generation in Stromboli Island and impact on the south-east Tyrrhenian coasts, *Nat. Hazards Earth Syst. Sci.*, 3, 299–309.
- Trull, T., F. Pineau, Y. Bottinga, and M. Javoy (1991), Experimental study of CO₂ bubble growth and ¹³C/¹²C isotopic fractionation in tholeiitic melt. Paper presented at 4th Silicate Melt Workshop, Le Hohwald, France, 19–23 March.
- Watson, I. M., et al. (2000), The relationship between degassing and deformation at Soufrière Hills volcano, Montserrat, *J. Volcanol. Geotherm. Res.*, 98, 117–126.
-
- L. Brusca, C. Federico, S. Inguaggiato, A. Rizzo, and D. Rouwet, Istituto Nazionale di Geofisica e Vulcanologia, Sezione di Palermo, via Ugo La Malfa 153, 90146 Palermo, Italy. (c.federico@pa.ingv.it)
- M. L. Carapezza, Istituto Nazionale di Geofisica e Vulcanologia, Sezione di Roma 1, Via di Vigna Murata 605, 00143 Rome, Italy.
- C. Cigolini, Dipartimento di Scienze Mineralogiche e Petrologiche, Università degli Studi di Torino, Via Valperga Caluso 35-37, 10125 Turin, Italy.

Slope Failures Induced by the December 2002 Eruption at Stromboli Volcano

Paolo Tommasi,¹ Paolo Baldi,² Francesco Latino Chiocci,^{1,3} Mauro Coltelli,⁴
Maria Marsella,⁵ and Claudia Romagnoli⁶

We reconstruct the sequence of landslides that occurred soon after the beginning of the December 2002 eruption on the NW flank of Stromboli volcano. Landslides involved the northeastern part of the Sciara del Fuoco (SdF) slope, an old collapse scar filled by products of volcanic activity, producing tsunami waves that severely damaged the coast of the island of Stromboli. Volumes of the mass detached from the subaerial and submarine slope were quantified by comparing preslide and postslide slope surfaces obtained by aerophotogrammetric and bathymetric data, which also allowed, in conjunction with field observations and helicopter surveys, the reconstruction of geometry and kinematics of landslides. According to the reconstructed sequence, 2 days after the beginning of the eruption, the upper part of the NE sector of the SdF slope experienced major displacements (few tens of meters). Movements propagated downslope and affected the nearshore portion of the submerged slope without a rapid sliding of the displaced mass into the sea. The following hours were characterized by a progressive increase of deformations, localized along shear zones extending over two thirds of the subaerial slope. This phase proceeded until a submarine slide about 6×10^6 m³ in volume occurred, causing a first tsunami wave. The subaerial mass delimited by the shear zones and unbuttressed at its foot, then slipped into the sea producing a second tsunami wave. The main landslide event (and the minor slumps which followed) removed a volume of about 10×10^6 m³ of the infilling deposit, to a thickness of at least 65 m. Hypotheses were formulated on the mechanisms that controlled the different phases of the instability sequence. Since hydraulic and stress/strain conditions progressively changed during the slope evolution, the formulated mechanisms are also based on geotechnical analyses and considerations on the mechanical behavior of volcaniclastic materials. The process that led to the landslide events

¹Istituto di Geologia Ambientale e Geo-Ingegneria, National Research Council, Rome, Italy.

²Dipartimento di Fisica, Bologna University, Bologna, Italy.

The Stromboli Volcano: An Integrated Study of the 2002–2003 Eruption
Geophysical Monograph Series 182
Copyright 2008 by the American Geophysical Union.
10.1029/182GM12

³Dipartimento di Scienze della Terra, Sapienza University, Rome, Italy.

⁴Istituto Nazionale di Geofisica e Vulcanologia, Sezione di Catania, Catania, Italy.

⁵Dipartimento di Idraulica, Trasporti e Strade, Sapienza University, Rome, Italy.

⁶Dipartimento di Scienze della Terra e Geologico Ambientali, Bologna University, Bologna, Italy.

was initiated by forces exerted by magma intruded into the slope, while further steps of the evolution of slope stability conditions (especially the submarine failure) were controlled by the particular shear behavior of the volcaniclastic material, mainly influenced by grain crushability. In fact, strength progressively decreased as shear strains proceeded, and the intensely sheared saturated material forming the submarine slope may have become susceptible of failure when sudden strain/stress increments occurred.

1. INTRODUCTION

The island of Stromboli (930 m above sea level [asl]) is the subaerial portion of a large volcanic edifice belonging to the Aeolian volcanic arc in the South Tyrrhenian sea; it rises for a total height of some 3200 m above the sea floor (Figures 1 and 2). On 30 December 2002, 2 days after the beginning of a lava flow eruption [Bonaccorso *et al.*, 2003], tsunami waves hit the inhabited coastal areas of the Stromboli Island, damaged buildings, and threatened the population. At the first recognition of the NW volcano flank, where volcanic activity concentrates (Sciara del Fuoco, hereafter indicated as SdF), two large landslide scars were visible on the northeastern part

of the subaerial slope (Plate 1). The retreat of some 50–70 m of the SdF shoreline, the first sea withdrawal of the tsunami wave at Stromboli village and the witness of a sudden lowering of the sea level offshore the SdF [Tinti *et al.*, 2005] suggested that a large submarine landslide had occurred.

Photogrammetric and bathymetric surveys funded by the Department of Civil Protection were performed during the days following the landslide events. Preslide and postslide digital models were used for estimating volumes and morphological changes by Baldi *et al.* [2005, this volume] and by Chiocci *et al.* [2008].

In this paper, the morphology derived from aerial photogrammetry and bathymetric surveys is analyzed in conjunc-

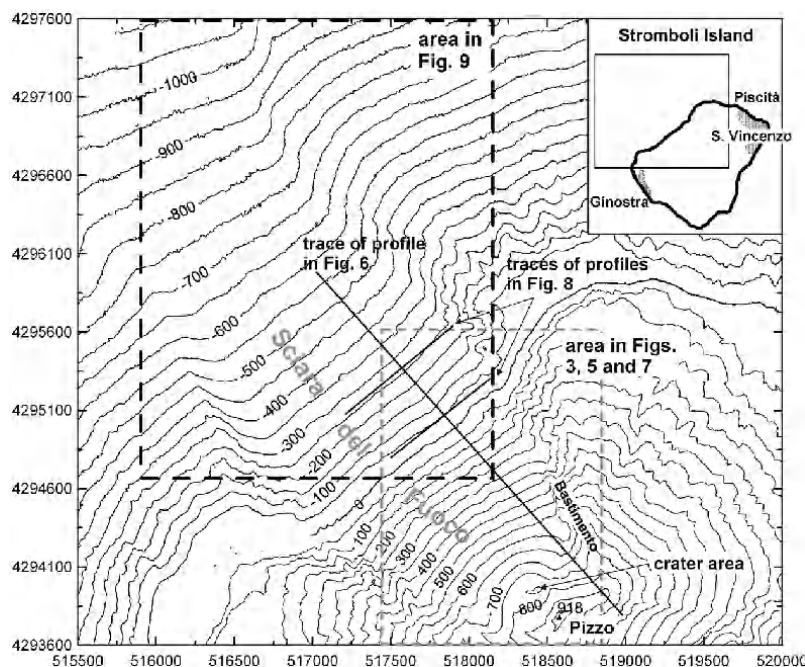


Figure 1. Integrated subaerial and submarine topography before the 2002 landslides showing areas depicted in the following figures (boxes) and trace of the longitudinal profiles in Figures 5 and 8.

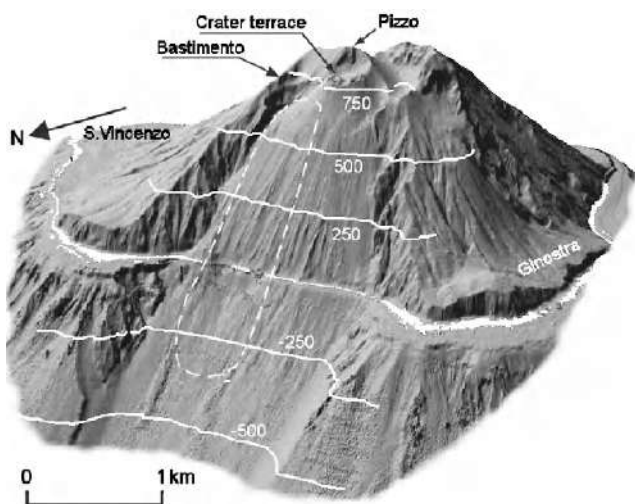


Figure 2. Shaded relief (oblique view) of the NW flank of Stromboli Island before the 2002 slides. The coalescence of debris fans and their continuity over the subaerial and submarine slope are to be noted. The white band is due to a lack of swath bathymetry in very shallow water.

tion with field observations and close-range photographs taken from helicopter before and after the slide, with the aim of reconstructing the complex succession of landslide events, their geometry, and kinematics. On the basis of this reconstruction, stability analyses and considerations on the shear behavior of volcaniclastic materials, hypotheses are formulated on the mechanisms that controlled the different phases of the instability sequence, which developed under hydraulic and stress/strain conditions that progressively changed as the evolution of the slope proceeded. Analysis of failure mechanisms is currently being refined by means of numerical models and laboratory investigations on the volcaniclastic materials. Preliminary results are described by *Boldini et al.* [2005] and *Tommasi et al.* [2007].

The chance to follow the evolution and quantify the geometry of the December 2002 events represented a rare opportunity to collect data and analyze mechanisms of slope failure phenomena having a relevant impact on the island and a significant frequency at man time scale. In fact, although signs of large landslides can be found on the morphology of SdF, no records exist in archives or historical sources concerning this type of slope failures. A better knowledge of mechanisms controlling large slides on the SdF slope is, therefore, important for risk assessment, as their volume and velocity are able to generate tsunami waves having remarkable consequences on the coast. In particular, submarine slides had never been proved so far to be a source of tsunami in

the area [a tsunami generated by a subaerial landslide had been recorded instead in the nearby Island of Vulcano, *Tinti et al.*, 1999].

The 2002 instability sequence was characterized by a specific evolution of stability conditions and had only minor similarities to lateral or sector collapses. In fact, flank collapses, which are the object of wide literature, involve much larger volumes and have different geometry and instability mechanisms (e.g., regarding forces applied by the intruding magma and pore fluid pressurization) at Stromboli [Tibaldi, 2001] like elsewhere [see, e.g., *Voight and Elsworth*, 1997].

2. GEOLOGIC FRAMEWORK

The subaerial part of the Stromboli volcanic edifice is a steep cone having slopes dipping up to 38° , which become gentler on the submerged portion. The structure of the present Stromboli edifice is the result of alternating periods of constructive volcanic activity and destructive summit and lateral collapses [*Hornig-Kjarsgaard et al.*, 1993; *Pasquare et al.*, 1993], which have left steep escarpments. The most recent collapses produced a large scar (Figures 1 and 2) extending over the subaerial and the submarine NW flank down to 700 m below sea level (bsl) [*Kokelaar and Romagnoli*, 1995]. The collapse scar, bounded on both sides by sharp escarpments up to 120 m high, has been partly filled by the products of the persistent volcanic activity creating the steep SdF slope.

The filling of the SdF collapse scar (Plate 2) consists of vertical and lateral alternations of layers of epiclastic volcanogenic sediments, lava flows, and pyroclastites produced by Strombolian activity and periodical lava effusions from craters (located at 750 m asl) and other ephemeral vents located at lower elevations.

Despite the lower frequency of effusive eruptions, from observations on the lateral scarps of the 2002 slides, it appears that lava materials represent the most voluminous primary product of recent volcanic activity on the SdF slope. They are deposited in the form of alternations of thin lava sheets and thick beds of loose blocks (typical of an emplacement on steep slopes) and of thick lava horizons in the flatter zones. Primary pyroclastic products are mainly layers of tephra, whose grain size ranges from that of spatter/bombs to that of lapilli.

Epiclastic sediments (debris) consist of reworked pyroclastic fall materials and small blocks of scoriaceous lava produced by failure of the quickly cooled lava flows. They roll and break along the steep SdF slope after primary deposition and during periodic remobilization by grain flows and small debris avalanches. These processes form a series of

irregular, mostly reverse-graded continuous layers formed by clasts that are finer, more sorted and rounded than the primary products [Kokelaar and Romagnoli, 1995].

SdF can be divided into an upper part (above 600 m asl) with a cinder cone shape, built up through the accumulation of fallout products, and a lower part representing a smooth scree slope without any significant break, having an average dip of 35°. Here grain flows and small avalanches dominate, producing large depositional fans. The transition between the two depositional environments is marked by a gradual change in dip (from 40°–42° to 33°–35°).

Offshore SdF develops again within a wide scar bounded above ~750 m by pronounced scarps, in continuity with the subaerial lateral escarpments (Figures 1 and 2). The SdF scar continues downslope in a broad canyon [Kokelaar and Romagnoli, 1995] where gravity flows transport into deeper water the volcaniclastic debris produced on the subaerial slope [Marani *et al.*, this volume].

The debris infilling of the SdF scar is arranged in small fans and chutes that extend with remarkable continuity from the lower subaerial slope to the upper submarine slope (Figure 2) and coalesce to form an apron down to ~350 m, created by the present-day depositional processes [Chiocci *et al.*, 2008]. Below such a depth, the seafloor dip gradually decreases basinward.

There is no information on the inner structure of the submarine apron, as reflection seismics do not penetrate the seafloor due to the steep slope, rough morphology, and coarse texture and inhomogeneity of the debris. However, side scan sonar imaging revealed that the lateral scarp of the 30 December submarine slide has a stepped surface, evidence that the apron is also made up of strata having different erodibility.

Seafloor sampling within the SdF scar recovered volcaniclastic gravel and sand extremely variable in grain size and roundness, even within very short distances and not dissimilar to the subaerial material. Fine sediment (silt and clay) was never sampled.

3. INVESTIGATIONS

3.1. Onshore

Onshore investigations included field and helicopter surveys with acquisition of oblique aerial photographs, carried out by the staff of Istituto Nazionale di Geofisica e Vulcanologia (INGV) and the Civil Protection Department and aerial photogrammetric surveys.

Protracted bad weather conditions largely reduced visibility of the slope during January 2003, especially over the upper part of the slope, whose deformation was instrumental for understanding landslide mechanisms. The first

photogrammetric surveys performed by the Italian Air Force (CIGA) on 5 January do not allow observing the upper portion of the slope, while on 27 January, good-quality images were collected.

Orthophotos and digital terrain models (DTMs) obtained from photogrammetric data were used to extract postlandslide topography, to measure landslide features, including volume estimates, and quantify morphological changes, thanks to the availability of a recent preeruption survey performed on May 2001 [Baldi *et al.*, 2005].

DTMs with 5 × 5-m grid size and accuracy of 1–2 m on both horizontal and vertical components were extracted. Due to the presence of a thick plume and difficult flight conditions, the extraction of accurate digital models over 700 m asl was not possible in the first month. Details about processing of photogrammetric data are reported by Baldi *et al.* [2005, this volume].

3.2. Offshore

Offshore investigations included multibeam surveys conducted a few days after the failure events, reflection seismics, and side scan sonar surveys, carried out at different times after the slide, and seafloor grab sampling [Chiocci *et al.*, 2008].

Preslide multibeam bathymetry (down to a depth of 1000 m bsl) collected in February 2002 represents the reference data for computing volumes involved in the submarine failure. The first survey following the instability events was carried out in 9 January, as soon as the meteorological conditions allowed it, aboard a small-sized Coast Guard vessel, using differential GPS and RTK (*Real Time Kinematics*) positioning. The resolution of the multibeam data decreases with depth, due to the fact that the footprint on the seafloor of each conical beam increases in size; in shallow water (i.e., above 200 m bsl), a DTM with 2 × 2-m grid spacing was constructed [see Chiocci *et al.*, 2008, for details].

3.3. Data Integration

By merging the three-dimensional data collected on the subaerial and the submerged portion of the SdF slope, a unified model of the slope surface was obtained. The integration requires the two data sets to be geometrically congruent and similarly sampled, at least in the proximity of the shoreline. Furthermore, a comparable accuracy of the two data sets is desirable in order to better reconstruct the continuity of morphology from the onshore to the offshore slope. The last requirement cannot always be satisfied because data spacing of onshore and offshore surveys depends on different factors. In order to refer data to the same system, surveys were conducted by adopting congruent GPS reference stations for

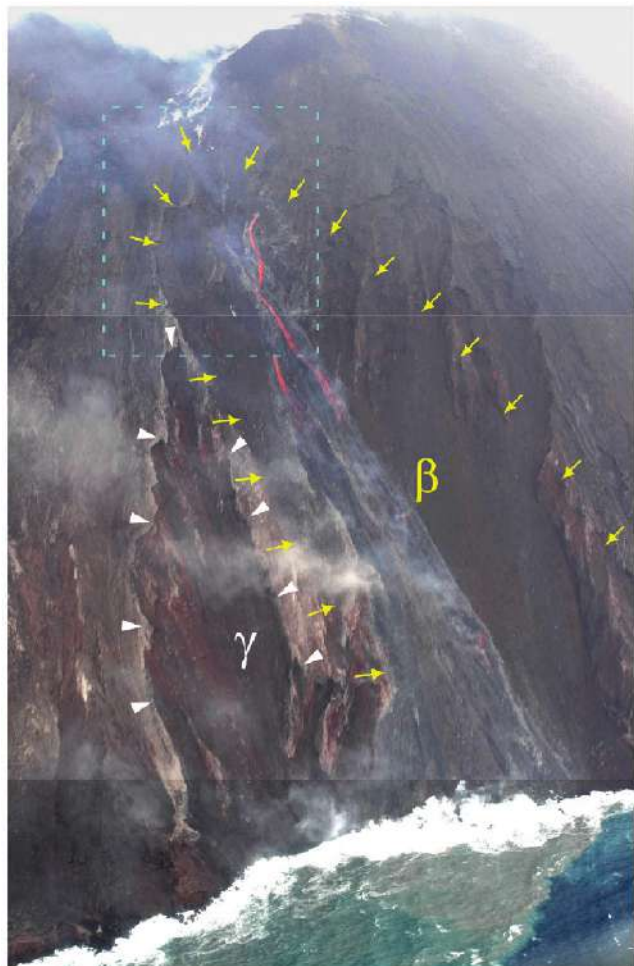


Plate 1. Aerial view of the SdF slope 2 days after the tsunamis. The scars of two subaerial slides, referred as β and γ in the text, are apparent and delimited by yellow arrows and white triangles, respectively. The box at the slope top refers to the zone depicted in Plate 2.

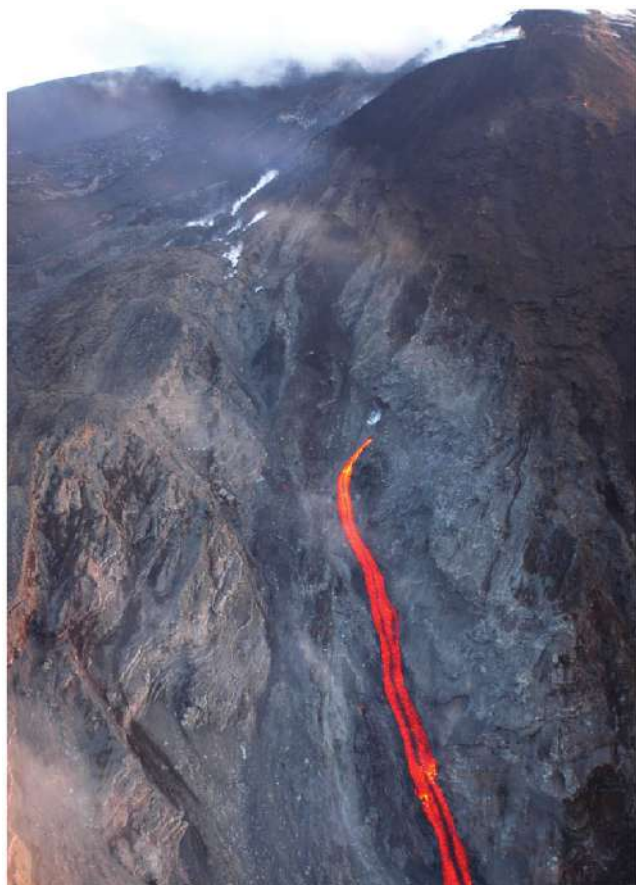


Plate 2. Aerial photo of the scar of the β slide occurred on 30 December (see Plate 1 for location) showing the inner structure of SdF infilling deposit (on the left) made up of alternations of loose volcaniclastic layers and thin lava flows. In the center, a lava flow outpours from the main scarp of the slide.

the photogrammetric control network and for the multibeam sensor navigation [Baldi *et al.*, this volume].

The subaerial and submarine DTM presented in this paper was obtained by merging photogrammetric and bathymetric surveys carried out in May 2001 and February 2002 for the preslide conditions and on 5 and 9 January 2003 for postslide morphology. In both cases, bathymetric data were acquired up to a minimum depth of 20 m, thus leaving a gap across the shoreline (the first very shallow water survey was possible only in February 2003).

4. THE 28–30 DECEMBER INSTABILITY SEQUENCE

Since nobody witnessed the failure events and continuous observations and surveys of the slope were not possible during the initial phases, the sequence of instabilities was reconstructed a posteriori utilizing investigations carried out before and after the slides.

The beginning of the eruption was marked by very energetic and frequent explosions from the northern crater which suddenly disappeared when the lava outpouring started. Reports from eyewitnesses and records of the INGV permanent video camera located at Pizzo indicate that the eruption started on 28 December at about 1730 UT, heralded by glowing on the summit area. Two lava flows and an *ash and block* deposit, which spread during the early stage of the eruption, were emitted from two vents (1 and 2 in Figure 3) in a few hours.

In the morning of 29 December, no active lava flows or evidence of deformations or failures on the lower two thirds of the slope were observed during the helicopter survey, while the upper part was not visible because it was covered by thick clouds. During the evening, effusive activity resumed.

4.1. 30 December Morning (Until 1000 UT)

The first photographs taken in barely sufficient visibility conditions during the morning of 30 December indicated that failures and deformations had also occurred in the upper part of the slope. A scarp extended from the SdF northern flank (Bastimento cliff) up to the base of the northern side of the crater, where a large breach had opened (Figures 3 and 4). Furthermore, a lateral scarp along the southern limit of the lava field had formed between elevations 500 and 650 m. Below the elevation 600 m, sharp steps, elongated parallel to the slope strike, were recognizable on the ground surface being probably the morphological expression of high-angle shear surfaces dipping seaward.

These morphological changes seem to be produced by relatively deep-seated deformations (*i.e.*, the α movement in

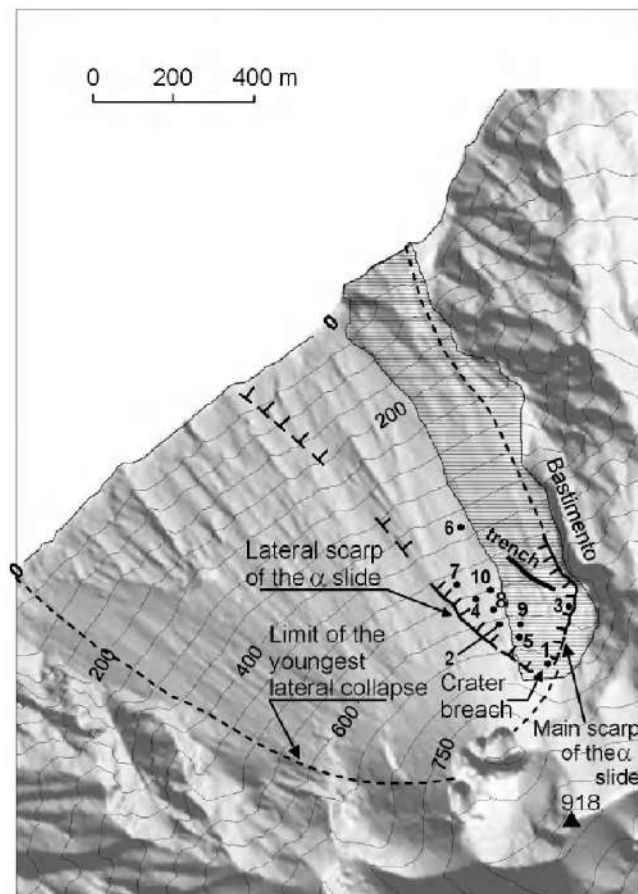


Figure 3. Preslide shaded relief with vent location (dot numbers are ordered according to vent formation) and main features of the early deep-seated α landslide (see text for details). Hatch indicates the area covered by the 1985 lava flows.

Figure 3) delimited by the main and lateral scarps mentioned above. This large landslide body suffered major displacements without sliding into the sea.

A lava tongue issuing from a vent located at 600 m asl was active (vent 5 in Figure 3), whereas two other flows that originated the day before at 570 m (underneath the Bastimento, vent 3) and at 550 m (vent 4) were inactive and cooling on the western side of the flow field.

4.2. 30 December After 1000 UT

Helicopter photographs show that the deformation process of the slope was still active. Two longitudinal shear bands (slightly diverging downhill) developed from 450 m asl down to some tens of meters above the shoreline (Plate 3). The southern shear zone (on the right in Plate 3) corresponds

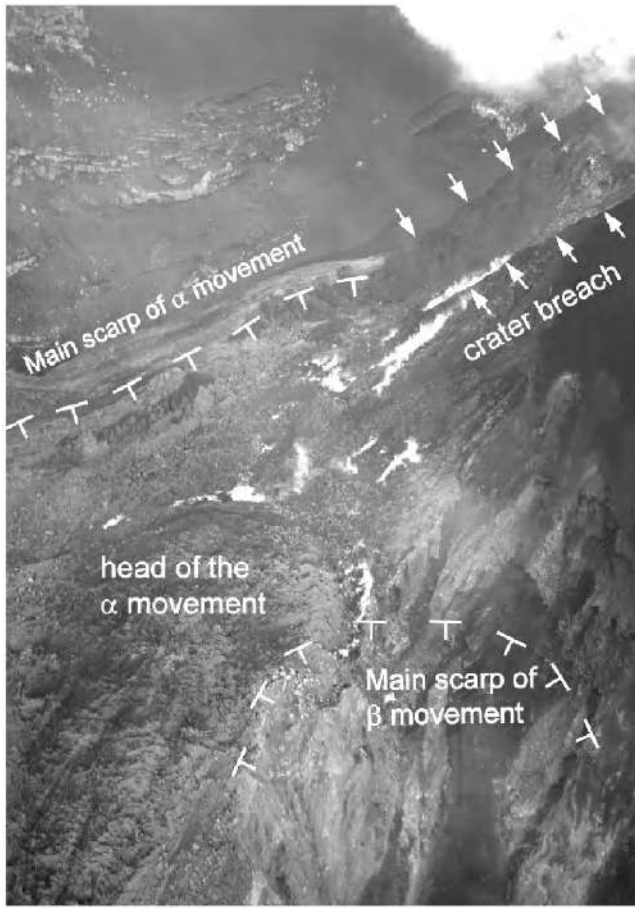


Figure 4. Aerial view of the slope top, taken the day after the slope failures, showing the continuity between the main scarp of the initial α movement and the breach opened through the northern side of the NE crater.

to the downhill extension of the southern lateral scarp of the deep-seated movement α . Along the northern shear discontinuity (on the left in Plate 3), the presence of steam and dust were attributed to ongoing shearing. The two lateral shear zones, together with a major intermediate scarp of the α movement, formed two thirds of the way down the slope (Plate 3), delimited a new slide body, here named slide β .

4.3. The 30 December Destructive Submarine and Subaerial Slides and Tsunami

At about 1215 UT, a video camera recording (by Massimo Pompilio, INGV) witnessed a rock avalanche entering the sea in the northern part of the SdF (we presume outside the β slide mass) at such a high velocity that could only be attained if the mass had detached from the upper part of the slope.

At about 1222 UT, a series of tsunami waves originating from the SdF hits the Stromboli coasts penetrating in land with a maximum run-up of more than 10 m [Tinti *et al.*, 2005]. A number of eyewitnesses reported that waves appeared with an initial retreat of the sea at the shoreline. In the near field, such behavior is common when tsunamis are generated by submarine slides [e.g., Watts, 2000]. In fact, a scar produced by a submarine failure was later detected by bathymetric surveys (hereafter indicated as τ slide).

A few hours after the tsunami, when visibility improved, two scars, separated by a thin ridge, were observed during the surveillance helicopter flight (Plate 1 and Figure 5a). The larger one (on the right in Plate 1) was produced by the sliding of the block isolated by the two longitudinal shear zones (indicated as β slide). A minor scar (on the left in Plate 1) was produced by a relatively shallow planar slide (indicated as γ slide).

On the basis of seismic signals recorded at Stromboli (seismic station SX15), Pino *et al.* [2004] and La Rocca *et al.* [2004] confirmed the occurrence of two large slide episodes that were related to a submarine slide and a subsequent subaerial failure.

5. RECONSTRUCTION OF THE GEOMETRY OF THE SLIDES

5.1. The Early Deep-Seated, Nondestructive α Event

The limits of the area involved in the initial α movement are shown in Plate 3 and Figure 5a, and its slip surface is schematically reconstructed in the cross section shown in Figure 6.

The head scarp and the southern lateral scarp were high and steep (Figure 4 and Plate 3). The vertical displacement at the main scarp estimated from pre-event and postevent photogrammetric surveys was at least 20 m. In the subaerial slope, the depth of the α movement should correspond at least to that of the successive β slide which involved the mass already displaced by the α movement. The depth of the β slide scar, estimated from elevation differences, was at least 75 m.

Major uncertainties concern the northern lateral limit and the toe of the area involved in the α movement. A lateral scarp running along the northern SdF limit was visible only in the upper part of the slope, underneath the Bastimento cliff (Figure 3 and Plate 4). The location of the toe of the displaced mass at the nearshore area can be only inferred from the extension of the southern lateral scarp (that reaches the shoreline well before the failure) and from the shape of the submarine scar, discussed in the next section.

The lack of continuity of the longitudinal structures delimiting the deforming mass and the presence of a sharp

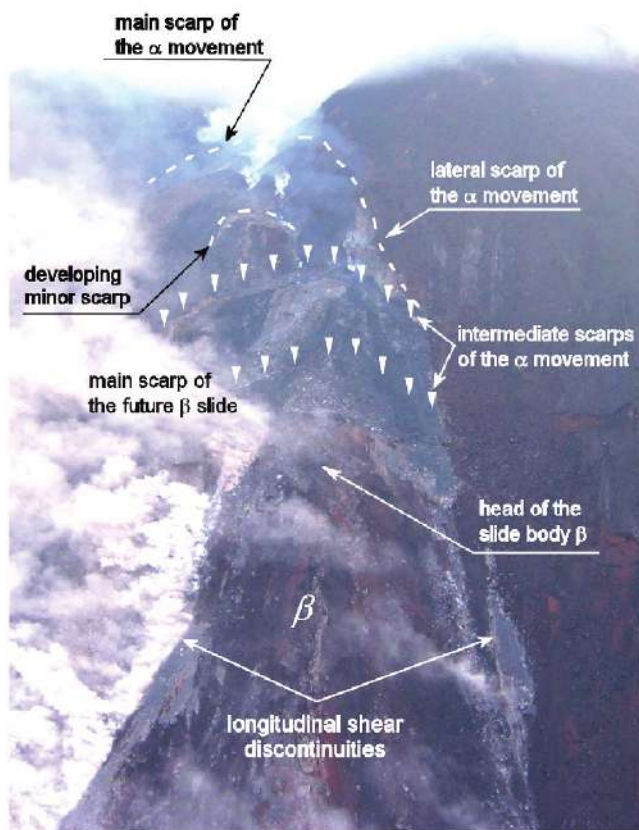


Plate 3. Oblique aerial view of the central and lower part of the SdF slope before the failures (between 1000 and 1030 UT). The body of the imminent β slide is completely isolated by an intermediate scarp of the early deep-seated α movement and by two lateral shear zones (photograph by S. Calvari, INGV).

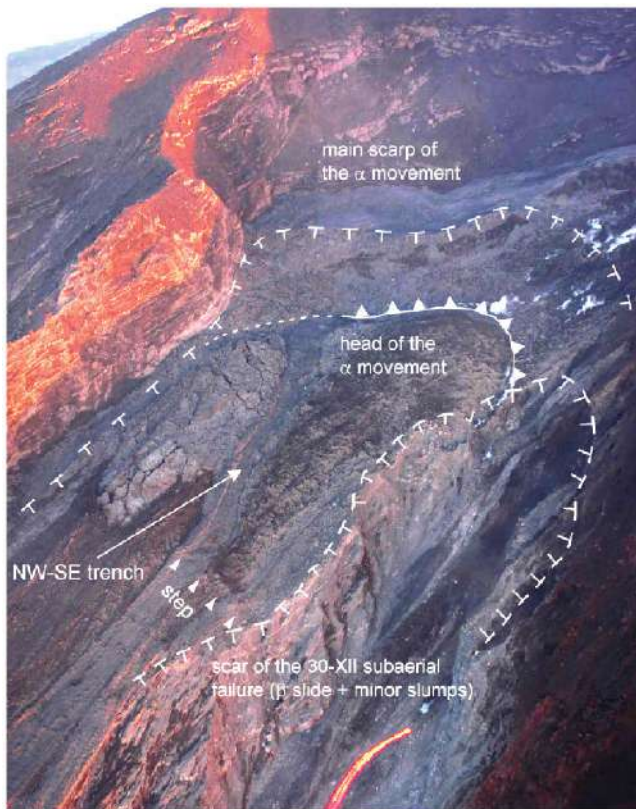


Plate 4. Oblique photograph of the upper part of the slope, taken 5 d after 30 December with morphological elements of the subaerial instabilities.

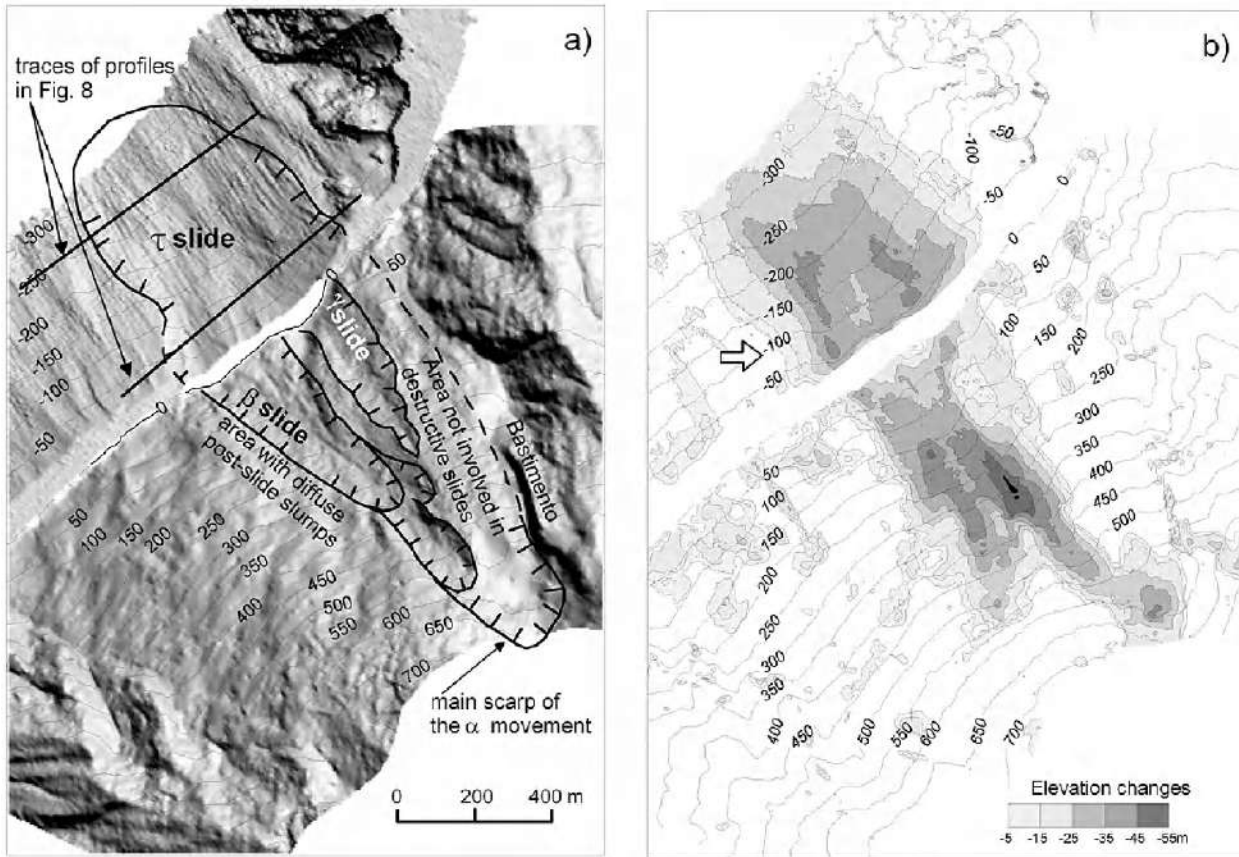


Figure 5. (a) Postslide shadow relief of the Sciara slope reporting limits of the major instability phenomena that occurred on 30 December and (b) elevation changes after the slides, obtained comparing preslide and postslide DTMs. The arrow in Figure 5b indicates the “bottleneck” of the submarine scarp. In Figure 5a, traces of profiles of Figure 8 are indicated.

transversal trench running NW–SE separating an intensely deformed part of the slope uphill from a smoother part downhill (Figure 3 and Plate 4) suggest a more complex scenario. The initial deep-seated movement involved an upper “block” (A in Figure 7) delimited by the steep slide scarps and by a discontinuity corresponding to the NW–SE trench, and a lower “block” (B in Figure 7) roughly corresponding to the β slide body. The area indicated with C in Figure 7 experienced only minor displacements.

5.2. The Submarine Failure

The volume and geometry of the submarine failure were defined by comparing preslide and postslide bathymetric surveys (Figures 5b and 8); depth changes up to 45 m were observed on the northern side of the submarine SdF slope. The postslide bathymetric contours (Figure 5a) suggest that the material was completely removed during the submarine failure. Subsequently, lava flows and slide debris from the

subaerial slope deposited during the 10 days following the failure (the first bathymetric surveys was carried out on 9 January).

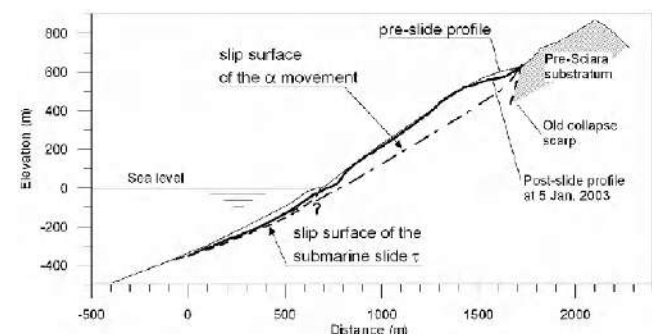


Figure 6. Cross section of the slope and reconstruction of the slip surfaces of the deep-seated α movement and of the submarine failure (trace of the profile is reported in Figure 1).

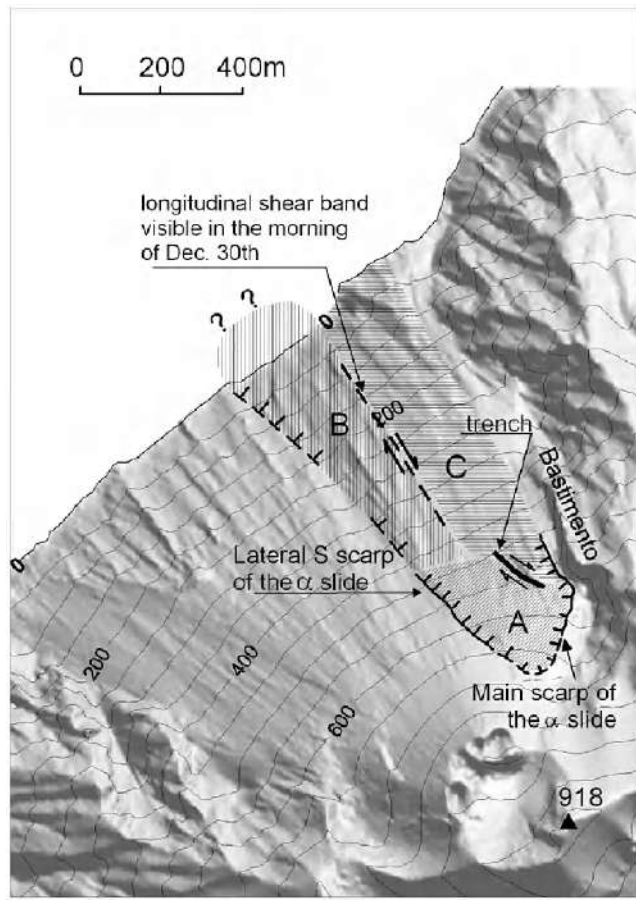


Figure 7. Zones characterized by different movements during the initial stage of the instability sequence.

The original scar geometry was reconstructed by extrapolating the morphology of the basal surface under the debris deposited between 30 December and the date of the first bathymetric survey (9 January). In plan view, the width of the submarine scar is larger than that of the subaerial one, especially to the north, where the lateral submarine escarpment approaches the NE SdF margin (Figure 5a). The scar morphology is evident down to a water depth of 300–350 m. Below this depth, the scar progressively vanishes and fringes into an area with diffuse shallow erosion (Figure 9) probably produced by the transit of gravity-driven debris [Chiocci *et al.*, 2008]. Within the whole area, from the coast down to some 1000 m bsl (i.e., where preslide and postslide data can be compared), no evidence of deposition is present.

As discussed in Section 5.1, at about 100–150 m bsl, the submarine scar is characterized by a bottleneck (Figure 5b), which could result from the overlapping of a roughly subcircular scar (extending between –100 and –350 m) produced by

an entirely submarine failure (τ slide) and the toe (in shallow water) of a mostly subaerial movement [Chiocci *et al.*, 2008].

The total volume removed from the submarine SdF slope down to 1000 m bsl, estimated from integration of the depth changes, is at least 20.5×10^6 m³; about half of that (10.9×10^6 m³) refers to the scar of the τ slide [from 0 to 350 m bsl; Baldi *et al.*, this volume], and the rest represents the volume excavated by the debris transit on the deeper seafloor [Chiocci *et al.*, 2008].

5.3. The Destructive Subaerial Failures

After the tsunami, two distinct scars were observed on the subaerial slope. The largest one (southern) results from the coalescence of the β slide with a couple of successive slumps that detached from the upper part of the slope (Plate 1 and Figure 5); its main scarp was present in the late morning of 30 December. The smaller one (γ slide) was much shallower and was likely produced by the unbuttressing that followed the submarine failure.

The material removed by the β landslide had an estimated maximum thickness of 60 m. The landslide exposed a large part of the main and southern lateral scarp of the α movement and exhibited an impressive subvertical northern lateral scarp up to 40 m high, where the internal structure of the SdF deposit was visible (Plates 2 and 4). By subtracting the post-slide DTM (5 January 2003) from the preslide DTM (May 2001), we observed a negative volume difference of about 9×10^6 m³. If we aim at estimating correctly the volume removed during the 30 December 2002 subaerial slide events

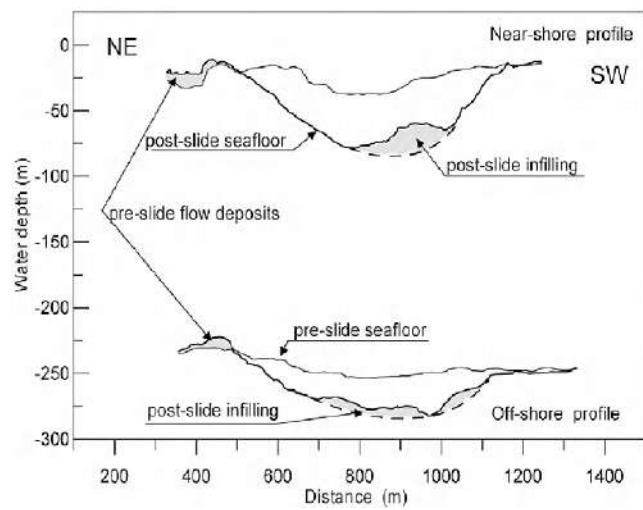


Figure 8. Bathymetric cross sections of the submarine slope, parallel to the coastline at two different distances from the coast; traces of cross sections are reported in Figures 1 and 5a.

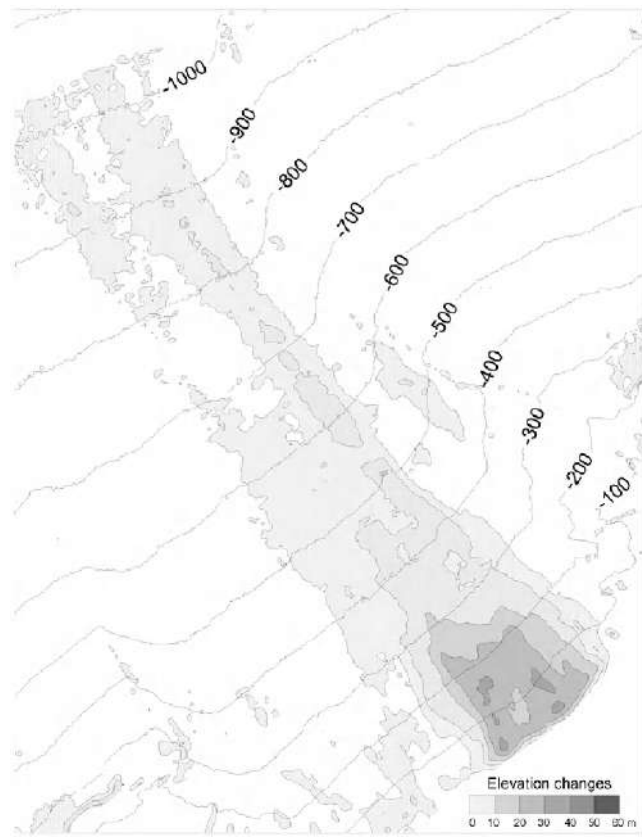


Figure 9. Depth differences calculated by subtracting preslide and postslide bathymetries down to about 1000 m bsl.

(β and γ slides), we should account for two processes that occurred between the two aerophotogrammetric surveys:

1. The original slide scars formed on 30 December successively propagated toward the crater area and the center of the SdF slope, by means of continuous slides and slumps that surely removed a significant amount of material from the slope.

2. In the time span 30 December 2002 to 5 January 2003, the slide scars were partially filled by lava flows and debris.

To address the uncertainties in the scar volume estimate resulting from the difficulty in quantifying the former processes, we reconstructed the surface geometry of β and γ slide scars and calculated their total volume again as a difference of the preslide and postslide DTMs, which turned out to be between 5.5×10^6 and $7 \times 10^6 \text{ m}^3$. To this value, we add the contribution of the infilling process, which for the whole NE SdF sector was estimated to be $3.3 \times 10^6 \text{ m}^3$. If we assume that lava flows and debris were deposited only within the β and γ scars, the maximum estimate of the volume of the material slide during the two events is $10.3 \times 10^6 \text{ m}^3$.

6. HYPOTHESES ON THE INSTABILITY MECHANISMS

6.1. Slope Movements Before the Destructive Landslides

The α movement is believed to have been induced by forces exerted by the magma, filling a nearly vertical blade-type dyke that intruded in the uppermost NE part of the SdF slope. The intrusion, which had a strike about N20°E as reconstructed from the alignment of the most active eruptive vents, should have utilized a preexisting discontinuity roughly corresponding to the contact between the SdF infilling deposit and the buried sector collapse escarpment.

Conversely, dynamic actions associated to low-energy seismic activity that occurred during the eruption were not sufficient to induce such a large failure. This is indirectly confirmed by the absence of even minor sliding on the occasion of a strong paroxysmal explosion that occurred a few months later (5 April), although the slope was weakened and partly formed by loose debris.

A back analysis of the α movement with the limit equilibrium method was conducted by means of the CLARA-W code (computer code for limit equilibrium slope stability analysis in two or three dimensions) [Hung, 1998] using the simplified Janbu method of slices in its two- and three-dimensional formulation [Hung *et al.*, 1989]. Three-dimensional analyses better account for the end effect on the sides of the sliding mass and for the geometry of the magma forces. The general three-dimensional slip surface was generated by interpolating two-dimensional slip surfaces reconstructed on a series of longitudinal sections of the slope by comparing preslide and postslide profiles. Two-dimensional analyses were also carried out on the reconstructed slip surfaces; the critical one is that reported in Figure 6. For computing the force exerted by the magma intrusion, the intruding dyke was modeled with a vertical plane striking parallel to the alignment of the vents and extending down to the extrapolated contact between the infilling deposit and the preexisting material. The scheme of magma pressure distribution used in stability analyses is depicted in Figure 10. Magma pressure at the dyke base was assumed to be hydrostatic, and a bulk density of 2.75 Mg/m^3 was adopted for the magma. A linear head loss is then assumed from the dyke base up to the intrusion outbreak (i.e., the main slide scarp). The general slip surface was limited at the back by the dyke and, on lateral sides, by the northern limit of the SdF and the southern lateral scarp (Figure 5a); the basal surface was reconstructed interpolating adjoining cross sections obtained from the comparison of preslide and postslide DTMs (e.g., Figure 6). The initial α movement occurred in dry conditions

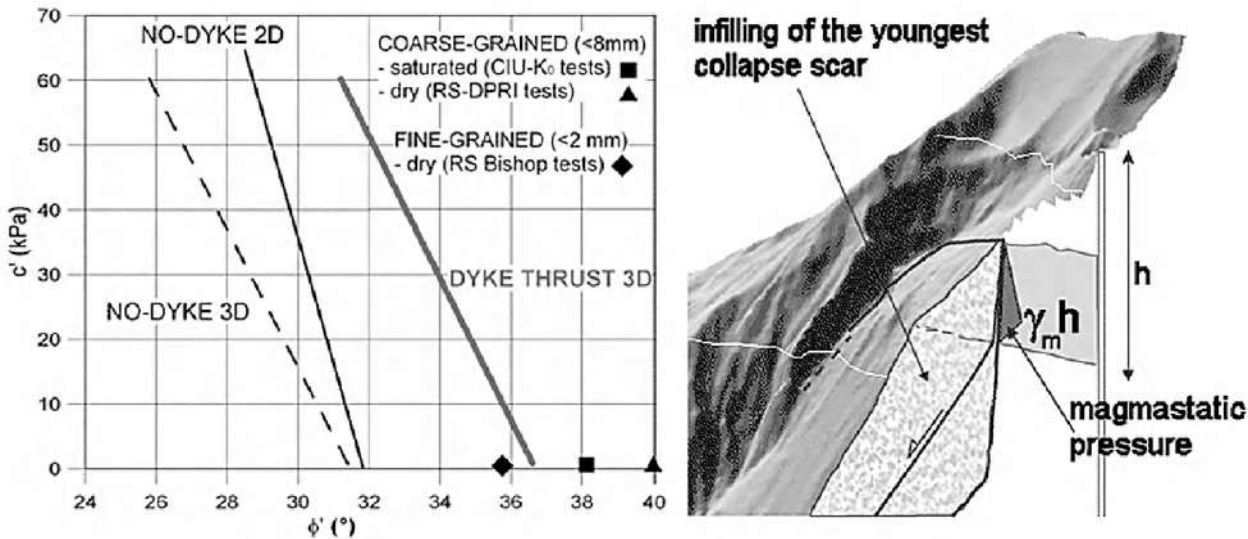


Figure 10. Mobilized strength parameters at $F_s = 1$ from back analyses of the α movement (solid lines) compared with experimental strength values of volcaniclastic materials. Large-sized CIU- K_0 triaxial tests and ring shear tests (RS-DPRI) were performed on the coarse grained material, while Bishop ring shear tests (RS Bishop) were performed on the finer fraction (<2 mm).

on the subaerial slope and likely in drained conditions on the submarine one. In other words, shear strain rate was so slow (compared with the permeability of the material) to allow dissipation of excess pore pressures generated within the saturated submarine deposit during shearing.

Values of cohesion (c') versus those of friction angle (ϕ') at limit equilibrium ($F_s = 1$) are plotted in Figure 10 together with peak shear strength parameters of SdF materials determined by Tommasi *et al.* [2007], i.e., the movement can be considered a “first-time” slide.

Back-calculated strength approaches the experimental data only if magma forces are taken into account. The triggering action of the dyke has been confirmed by Tommasi *et al.* [2007] on the basis of three-dimensional stress-strain analyses of the slope. Dyke intrusion has been considered by many authors as being a triggering factor for lateral collapses and “giant” landslides on volcano flanks [see, e.g., Voight and Elsworth, 1997; Hurlimann *et al.*, 2000] and also for large intracalderic landslides [Chadwick *et al.*, 1991].

With the assumed geometry and magnitude of magma pressure, values of mobilized strength suggest that shearing involved the weakest volcaniclastic materials. Alternatively, magma should have induced higher shear stresses. In particular, it cannot be excluded that while a basal shear surface was forming, magma intruded along it, applying uplifting forces to the displacing mass. The formation of a new vent at lower elevation (450 m asl) on the northern longitudinal shear surface visible in the morning of 30 December (Figure

3) could be indirect evidence that magma found a path along the slip surface.

6.2. The Continuous Sliding of the Subaerial Slope and the Submarine Failure

The insight in the mechanisms controlling this critical stage deserves some hints on the shear behavior of the volcaniclastic layers being given. The shear strength of the volcaniclastic material (even of the sandy fraction) in dry and in saturated drained conditions (i.e., when excess pore pressure generated during shearing can be dissipated) is relatively high, and the stress-strain behavior does not exhibit any significant drop in strength after peak [Tommasi *et al.*, 2007; Samuelsson *et al.*, 2008]. Undrained triaxial tests indicate that when deformations are relatively small, and hence grain size is not reduced by crushing, also undrained conditions (i.e., establishing if excess pore pressure cannot be dissipated) do not introduce significant changes in the shear behavior of the material [Tommasi *et al.*, 2007]. As the shearing process proceeds, the content in fines (sand size) within the shear zone progressively increases due to the comminution of the crushable volcanic grains, and the shear strength of the material slowly reduces without sudden drop and remains, however, higher or close to the shear stress acting in the slope. When undrained conditions establish in the intensely sheared material, failure (static liquefaction) is instead recognized [Boldini *et al.*, 2005; Tommasi *et al.*, 2007].

The submarine failure occurred while the deformation process on the subaerial slope was rapidly evolving, producing sharp modifications of the slope surface down to the shoreline. In this context, deformations were large and likely involved also the submarine slope. With reference to the experimental knowledge on the shear behavior of the volcaniclastic layers, failure should have necessarily been generated by the development of relevant excess pore pressures, which could not be promptly dissipated, induced by a load applied to the submarine deposit or by a rapid increase of the displacement rate of the submarine slope. Since permeability of submerged materials is relatively high even in case that failure starts along a finer volcaniclastic horizon, a sudden increase of stress/strain should have thus occurred.

Conversely, the time that elapsed between the rapid loading exerted on the seafloor by the avalanche deposit video recorded at 1215 UT and the tsunami was sufficient to allow dissipation of pore pressure due to loading. Furthermore, deposition on the submerged slope of material from lava flows emplaced before failure involved a limited area and occurred at a rate slow enough to allow dissipation of excess pore pressures generated by lava loading.

It appears more probable that during the progressive slipping of a partly submerged mass of volcaniclastic material, a sudden increase of slip rate may have occurred, due to some local failure. Although there are no measurements or qualitative description of displacement rates, seismic recordings from the Stromboli SX15 station of the SAPTEX array [Cimini et al., 2006] indicate that in the 6-h preceding the tsunami (since the early morning of 30 December), a large number of high-amplitude pulses were recorded (Figure 11), which could be interpreted as due to seismic energy released during localized fracturing/failure events.

Failure could have initiated by static liquefaction of part of the submerged sliding mass and rapidly extended to a larger portion of the submarine slope. On the basis of large-scale ring-shear tests on the Stromboli volcaniclastic materials, Boldini et al. [2005] point out that liquefaction can occur

both in fully undrained conditions and when drainage of pore water is allowed. In the latter case, however, local undrained conditions should necessarily establish locally.

As already discussed, liquefaction is favored by the high crushability of the grains of the Stromboli volcaniclastic material, which allows reduction of grain size (and hence of permeability) during shear and determines sudden grain collapse with drastic reduction of pore spaces.

Bathymetric surveys indicated that, after the submarine slide, the morphology of the slip surface was extremely smooth and that no remnants of the slide body were present. This evidence supports the hypothesis that failure was followed by a flow that completely removes the sliding mass.

6.3. Instability Propagation to the Subaerial Slope After the Submarine Failure

Once the large submarine slide had occurred, undermining the foot of the subaerial slope, the β mass could slide down and enter the sea where it was rapidly dispersed because of its intense loosening and high kinematic energy. The lesser thickness of the γ slide suggests that it was triggered by the sole foot removal (i.e., it was not necessarily loosened by previous movements). As described in Section 5.3, the geometry of the largest subaerial scar indicates that the failure of the β slide was followed by the detachment of minor slumps from upslope. This hypothesis is supported by the analysis of seismic signals [Pino et al., 2004; La Rocca et al., 2004], which include many low-frequency signals related to small slides following the main event.

7. CONCLUSIVE REMARKS

Authors are aware that some aspects of the sequence and geometry of instability events results from an a posteriori reconstruction and that they are not supported by direct monitoring/observation. Similarly, some analyses and considerations on mechanical aspects cannot rely, as it usually occurs, on subsurface geophysical and in situ geotechnical

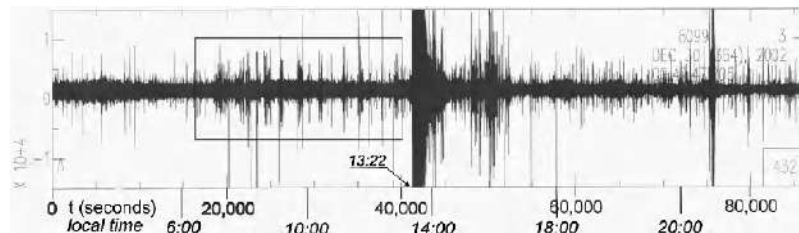


Figure 11. Seismic record of 29–30 December acquired at Stromboli SX15 station of the SAPTEX array [Cimini et al., 2006]. In the box, the sequence of pulses preceding the tsunami and the related landslide phenomena is reported (local time is 1 h ahead of GMT).

investigations, due to the dangerous and adverse environmental conditions existing all over the slope.

Furthermore, in order to minimize speculations, a simple distribution of magma pressures was introduced, and the unclear and not realistically quantifiable influence that some factors have on slope stability (i.e., thermal effects) was not discussed. Attention was concentrated on aspects that have a more consolidated geotechnical literature and can be supported by experimental results. Therefore, this study wishes to contribute to the comprehension of the evolution of slope stability conditions at Stromboli more than provide a thorough explanation of such a complex succession of failure events.

In this respect, the December 2002 instabilities required an updating of previous models on the evolution of the NW Stromboli flank (i.e., lateral/sector collapses were the only type of large failure that had been considered so far) and have changed the approach to risk assessment. In fact, rapid failures on the submarine and subaerial SdF slope can involve volumes that are large enough to generate tsunami waves, producing severe consequences on the inhabited coast of the island.

In this respect, aerial and bathymetric surveys promptly conducted on the subaerial and submerged slope not only allowed an estimate of the landslide masses, but also demonstrated to be a fundamental investigation tool in such a difficult and dangerous environment, providing data that are instrumental for any analysis and decision.

The reconstruction of the instability sequence culminating in the tsunamigenic slope failures indicates that they represented the final stage of a complex process of destabilization of the NW flank. Such a process consists of different stages that are all instrumental in creating conditions favoring failure and are controlled by three main factors: the stress changes induced by a dyke intrusion associated with a major eruption, the high percentage within the SdF infilling deposit of volcaniclastic layers (characterized by a particular mechanical behavior resulting from high-grain crushability), and the partial submersion of the volcanic edifice that entails a dependence of failure on pore pressure development in saturated material.

The evolution of stability conditions that led to the 2002 failures was peculiar, and no similar case has been reported so far in the literature regarding volcano flank instability. Nevertheless, the Stromboli case should be taken into account when managing risk assessment or back-analyzing past landslides in partially submerged volcano flank, formed by loose or slightly-bonded volcaniclastic/pyroclastic materials.

Acknowledgments. All activities have been funded by the Department for Civil Protection. Many interpretations and discus-

sions about the volcanological aspects of the prefailure stage were shared by the authors with M. Pompilio (INGV-Pisa). Acquisition and processing of the preslide and the first postslide data were carried out by R. Monticelli (DITS-Sapienza University, Rome) and M. Fabris (DIF, Bologna University) for aerial photogrammetry surveys. S. Castellini and L. Rosa (CNR-IGAG) performed slope stability analyses. A. Bosman (DST-Sapienza University, Rome) supervised all the phases of acquisition, processing, and volume computing of multibeam data; D. Casalbore, P. Abballe, and A. Fascati of DST-Sapienza University (Rome) and G. De Alteriis and R. Tonielli of CNR-IAMC also participated in bathymetric surveys. N. A. Pino of INGV-OV is acknowledged for the useful discussions on seismogram interpretation. E. Galanti and B. De Bernardinis of the Department for Civil Protection and the Scientific Committee for the Stromboli Emergency encouraged and supported the technical activities. A. Scalzo and C. Cardaci of the Department for Civil Defence provided continuous technical assistance to survey activities. The first bathymetric survey was carried out on board the Coast Guard unit CP-875, whose captain and crew are acknowledged. The staff of the CIGA (Italian Air Force) performed the aerial photogrammetric surveys. Volcanological guides provided assistance during field surveys; special thanks are due to Mario Zaia for his unfailing support. Finally, the authors wish to thank Barry Voight of Penn State University, who gave useful suggestions for investigations and data interpretation during the 2003 emergency activities, and the reviewers T. Walter and W. W. Chadwick for their thorough revision of the manuscript and general suggestions for its improvement. The TRANSFER project contributed to publication costs as part of geo-hazard data dissemination activity.

REFERENCES

- Baldi, P., M. Fabris, M. Marsella, and R. Monticelli (2005), Monitoring the morphological evolution of the Sciara del Fuoco during the 2002–2003 Stromboli eruption using multi-temporal photogrammetry, *ISPRS J. Photogramm. Remote Sens.*, 59(4), 199–211.
- Baldi, P., A. Bosman, F. L. Chiocci, M. Marsella, C. Romagnoli, and A. Sonnessa (2008), Integrated subaerial–submarine evolution of the Sciara del Fuoco after the 2002 landslide, this volume.
- Boldini, D., F. Wang, K. Sassa, and P. Tommasi (2005), Mechanism of landslide causing the December 2002 tsunami at Stromboli volcano (Italy), in *Landslide—Risk analysis and sustainable disaster management*, pp. 173–180, Springer, New York.
- Bonaccorso, A., S. Calvari, G. Garfi, L. Lodato, and D. Patanè (2003), Dynamics of the December 2002 flank failure and tsunami at Stromboli volcano inferred by volcanological and geophysical observations, *Geophys. Res. Letters*, 30(18), 1941, doi:10.1029/2003GL017702.
- Chadwick, W. W. Jr., T. De Roy, and A. Carrasco (1991), The September 1988 intra-caldera avalanche and eruption at Fernandina volcano, Galapagos Islands, *Bull. Volcanol.*, 53, 276–286.
- Chiocci, F. L., C. Romagnoli, P. Tommasi, and A. Bosman (2008), The Stromboli 2002 tsunamigenic submarine slide: Character-

- istics and possible failure mechanisms, *J. Geophys. Res.*, **113**, B10102, doi:10.1029/2007JB005172.
- Cimini, G. B., P. De Gori, and A. Frepoli (2006), Passive seismology in Southern Italy: The SAPTEX array, *Ann. Geofis.*, **49**(2/3), 825–840.
- Gabbianelli, G., C. Romagnoli, P. L. Rossi, and N. Calanchi (1993), Marine geology of the Panarea–Stromboli area (Aeolian Archipelago, southeastern Tyrrhenian sea), *Acta Vulcanol.*, **3**, 11–20.
- Hornig-Kjarsgaard, I., J. Keller, U. Koberski, E. Stadlbauer, L. Francalanci, and R. Lenhart (1993), Geology, stratigraphy and volcanological evolution of the island of Stromboli, Aeolian arc, Italy, *Acta Vulcanol.*, **3**, 21–68.
- Hungr, O. (1998), *CLARA-W*, O. Hungr Geotech. Res., Inc., West Vancouver, B. C., Canada.
- Hungr, O., F. M. Salgado, and P. M. Byrne (1989), Evaluation of a three-dimensional method of slope stability analysis, *Can. Geotech. J.*, **26**, 679–686.
- Hürlimann, M., J. O. Garcia-Piera, and A. Ledesma (2000), Causes and mobility of large volcanic landslides: Application to Tenerife, Canary Islands, *J. Volcanol. Geotherm. Res.*, **103**, 121–134.
- Kokelaar, P., and C. Romagnoli (1995), Sector collapse, sedimentation and clast population evolution at an active island–arc volcano—Stromboli, Italy, *Bull. Volcanol.*, **57**(4), 240–262.
- La Rocca, M., D. Galluzzo, G. Saccorotti, S. Tinti, G. B. Cimini, and E. Del Pezzo (2004), Seismic signals associated with landslides and with a tsunami at Stromboli volcano, Italy, *Bull. Seismol. Soc. Am.*, **94**, 1850–1867.
- Marani, M. P., F. Gamberi, M. Rosi, A. Bertagnini, and A. Di Roberto (2008), Deep-sea deposits of the Stromboli 30 December 2002 landslide, this volume.
- Pasquare, G., L. Francalanci, V. H. Garduño, and A. Tibaldi (1993), Structure and geologic evolution of the Stromboli volcano, Aeolian Islands, Italy, *Acta Vulcanol.*, **3**, 79–89.
- Pino, N. A., M. Ripepe, and G. B. Cimini (2004), The Stromboli Volcano landslides of December 2002: A seismological description, *Geophys. Res. Lett.*, **31**, L02605, doi:10.1029/2003GL018385.
- Samuelson, J., C. Marone, B. Voight, and D. Elsworth (2008), Laboratory investigation of the frictional behavior of granular volcanic material, *J. Volcanol. Geotherm. Res.*, **173**, 265–279, doi:10.1016/j.jvolgeores.2008.01.015.
- Tibaldi, A. (2001), Multiple sector collapses at Stromboli volcano, Italy: How they work, *Bull. Volcanol.*, **63**, 112–125.
- Tinti, S., E. Bortolucci, and A. Armigliato (1999), Numerical simulation of the landslide-induced tsunami of 1988 on Vulcano Island, Italy, *Bull. Volcanol.*, **61**, 127–137.
- Tinti, S., A. Manucci, G. Pagnoni, A. Armigliato, and F. Zaniboni (2005), The 30 december 2002 landslide-induced tsunamis in Stromboli: Sequence of events reconstructed from the eyewitness accounts, *Nat. Hazards Earth Syst. Sci.*, **5**, 763–775.
- Tommasi, P., F. Chiocci, M. Marsella, M. Coltell, and M. Pompilio (2004), Preliminary analysis of the December 2002 instability phenomena at Stromboli volcano, in *Occurrence and Mechanisms of Flows in Natural Slopes and Earth Fills, Proceedings of International Workshop, Sorrento, Patron, Bologna*, edited by L. Picarelli, pp. 297–306.
- Tommasi, P., D. Boldini, F. Cignitti, A. Graziani, A. Lombardi, and T. Rotonda (2007), Geomechanical analysis of the instability phenomena at Stromboli volcano, in *I Canadian–U.S. Rock Mechanics Symposium, Vancouver*, vol. 2, edited by E. Eberhardt, and D. Stead, pp. 933–941.
- Voight, B. (2003), Report on volcanic landslide–tsunami crisis, *Private Report for the Italian Dept. for Civil Defence*, Jan.
- Voight, B., and D. Elsworth (1997), Failure of volcano slopes, *Geotechnique*, **47**, 1–31.
- Watts, P. (2000), Tsunami features of solid block underwater landslides, *J. Waterw. Port Coastal Ocean Eng.*, **126**(3), 144–151.

P. Baldi, Dipartimento di Fisica, Bologna University, Viale C. Berti Pichat 8, I-40127 Bologna, Italy.

F. L. Chiocci, Dipartimento di Scienze della Terra, Sapienza University, Piazzale Aldo Moro 5, I-00185 Rome, Italy.

M. Coltell, Istituto Nazionale di Geofisica e Vulcanologia, Sezione di Catania, Piazza Roma 2, I-95125 Catania, Italy.

M. Marsella, Dipartimento di Idraulica, Trasporti e Strade, Sapienza University, Via Eudossiana 18, I-00184 Rome, Italy.

C. Romagnoli, Dipartimento di Scienze della Terra e Geologico Ambientali, Bologna University, Piazza Di Porta S. Donato 1, I-40126 Bologna, Italy.

P. Tommasi, Istituto di Geologia Ambientale e Geo-Ingegneria, National Research Council, Via Bolognola 7, I-00138 Rome, Italy, (paolo.tommasi@uniroma1.it)

The Double Landslide-Induced Tsunami

S. Tinti, A. Armigliato, A. Manucci, G. Pagnoni, R. Tonini, and F. Zaniboni

Department of Physics, University of Bologna, Bologna, Italy

A. Maramai and L. Graziani

Istituto Nazionale di Geofisica e Vulcanologia, Section Roma 2, Rome, Italy

The 2002 crisis of Stromboli culminated on December 30 in a series of mass failures detached from the Sciara del Fuoco, with two main landslides, one submarine followed about 7 min later by a second subaerial. These landslides caused two distinct tsunamis that were seen by most people in the island as a unique event. The double tsunami was strongly damaging, destroying several houses in the waterfront at Ficogrande, Punta Lena, and Scari localities in the northeastern coast of Stromboli. The waves affected also Panarea and were observed in the northern Sicily coast and even in Campania, but with minor effects. There are no direct instrumental records of these tsunamis. What we know resides on (1) observations and quantification of the impact of the waves on the coast, collected in a number of postevent field surveys; (2) interviews of eyewitnesses and a collection of tsunami images (photos and videos) taken by observers; and (3) on results of numerical simulations. In this paper, we propose a critical reconstruction of the events where all the available pieces of information are recomposed to form a coherent and consistent mosaic.

1. INTRODUCTION

On 30 December 2002, two tsunamis occurred a few minutes apart in the island of Stromboli, with waves exceeding 10 m in height in some locations, and only the lucky circumstance that they took place in winter, that is, a low tourist season, avoided the loss of human lives. A look at the catalogues of Italian tsunamis [Tinti *et al.*, 2004; Maramai *et al.*, 2005b] shows that tsunamis are not infrequent in the Aeolian islands, due to both seismic activity and instability of volcanic flanks, with significant events that occurred in 1930, in 1944, and in 2002. The most frequent source area is

the Sciara del Fuoco (SdF), the big scar on the northwestern coast of Stromboli, which starts just under the craters at 600 m above sea level (asl) and continues underwater for several kilometers down to at least 2000 m depth. Most of volcanic ejecta and lava flows accumulate here, attaining periodical conditions of gravitational instability, due also to seismic shaking and dike intrusion. For the Stromboli population that is concentrated in the northern and northeastern coasts of the island, with the exception of the small village of Ginostra on the south, the highest risk comes from the tsunamis that can be generated by the mass failures down the SdF. The tsunami wave ingressions is favored by some flat beaches crowning the northeastern part of the island.

In this paper, we provide a scientific recount of the two tsunamis of 30 December 2002, including the collection of eyewitness accounts [Tinti *et al.*, 2005b], the postevent field surveys [Tinti *et al.*, 2006a; Maramai *et al.*, 2005a], and

The Stromboli Volcano: An Integrated Study of the 2002–2003 Eruption
Geophysical Monograph Series 182
Copyright 2008 by the American Geophysical Union.
10.1029/182GM13

the numerical simulation of the waves [Tinti *et al.*, 2005a, 2006b].

2. INSTRUMENTAL DATA

In addition to eyewitness accounts and field surveys, other relevant data to reconstruct the cause and the dynamics of the events come from various instrumental measures summarized below.

2.1. Seismic Records

In 2002, the seismic network consisted of short-period, intermediate-period, and broadband stations, managed by different sections of INGV (i.e., INGV-CT, INGV-OV, and INGV-CNT). It recorded two distinct signals on 30 December 2002, which were attributed to a series of mass failures including two major landslides, the first one starting at 1314:05 LT and the second at 1322:38 LT [Bonacorso *et al.*, 2003; Pino *et al.*, 2004]. In addition, broadband records from three three-component temporary stations placed in the island of Panarea, 20 km southwest of Stromboli, recorded high-amplitude, low-frequency signals with onset time delayed by a few minutes. Since the delay was compatible with the tsunami travel time from Stromboli to Panarea, the signals were interpreted as due to the attack of tsunamis against the island coast, with an estimated period of 100–120 s [La Rocca *et al.*, 2004].

2.2. Tide Gauge

A temporary tide gauge, jointly operated by INGV-CNT (Rome) and by the Bologna section of the Istituto di Scienze Marine of the Comitato Nazionale delle Ricerche (ISMAR-CNR), was in operation in the Panarea main jetty to measure slow- and small-amplitude sea level changes with a 5-min sampling rate, which is inadequate for tsunami recording. From such records, one can deduce that the tsunami hit the Panarea harbor between 1319 and 1324 LT, and that at 1329 the sea level was 1 m over its normal value [Tinti *et al.*, 2005b]. Tsunami disturbances lasted for several hours.

2.3. Aerophotogrammetry

On the northern subaerial portion of the SdF, a large area of mass ablation, which was divided into two sectors and was probably connected to the second slide event, was clearly visible from pictures taken on 31 December [Bonacorso *et al.*, 2003]. Comparison between the 2001 and 2006 aerial photos allowed us to estimate that the subaerial missing mass was in the order of a few millions (7–9) of cubic meters [Baldi *et al.*, 2003].

2.4. Bathymetric Surveys

Numerous surveys were performed just after the events to explore the submerged part of the SdF. Comparing post-event with preevent data led surveyors to estimate a missing submarine volume of about 10–20 million m³, further showing that the two subaerial scars were merging into a unique submarine one [Chiocci *et al.*, 2003].

2.5. Video Recordings

These consist of digital movies from Dr. Pompilio (see next section).

3. EYEWITNESS ACCOUNTS

Since instrumental data on tsunamis and the causative landslides are not abundant, interviews of eyewitnesses have fundamental values. They were collected at the beginning of 2003. The main accounts on the landslides come from only two eyewitnesses who were observing the ongoing eruption, one from the northern side and one from the southern side of the SdF: Dr. Pompilio, a researcher of INGV-CT, and Mr. Grassi, living on the island. Dr. Pompilio was at the position denoted P₁ in Figure 1, and with a

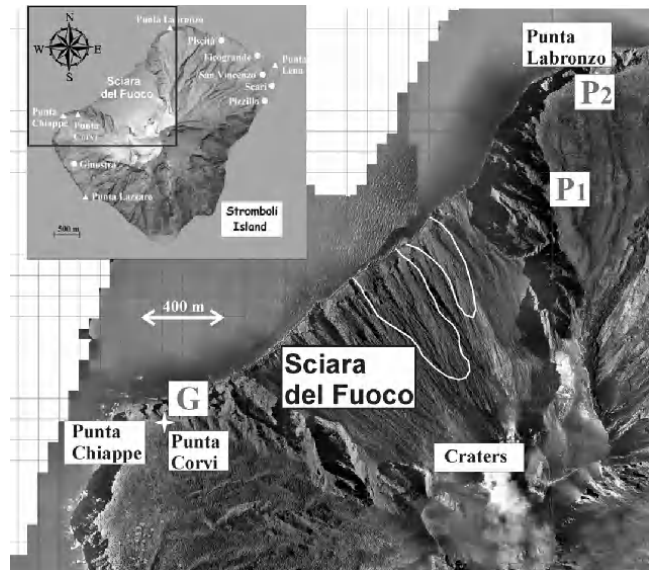


Figure 1. Orthophoto of the Sciara del Fuoco, provided by P. Baldi (University of Bologna). Dr. Pompilio was at point P₁ at the time of the precursor slide (1311 LT), then moved to point P₂, where he documented the second tsunami. Mr. Grassi was at Punta dei Corvi (G). The white lines border the two main bodies of the subaerial slide, causing the second tsunami.

digital video camera documented a surface sliding of light material along the SdF at 1311 LT, which was very fast and piled up on the sea surface, before sinking in the sea water. This was later interpreted as a precursor of the main process of mass failures.

Then, Dr. Pompilio ran to a safer place, that is, to the Punta Labronzo restaurant (point P₂ in Figure 1), resuming filming from that position more or less 10 min later. We know he missed the first tsunami, but he documented the impact of the second tsunami against Punta Labronzo rocks, where the seawater was already turbulent and muddy, as a consequence of the attack of the first tsunami. Mr. Grassi was sitting on a rock at Punta dei Corvi (point G in Figure 1), observing the eruption. He saw as well the 1311 LT event documented in Dr. Pompilio's movie. Then he describes the effect of the first submarine landslide: the sea opened some meters offshore, "a sort of vertical cut in the water that opened parallel to the coast not too fast." Mr. Grassi also gives details on the second subaerial slide: "the SdF collapsed down as a unique block, with loud noise and ground shaking, and a train of water waves impacted later the coast." The main conclusions coming from these eyewitnesses can be summarised as:

1. The cut in the water is the clear evidence of the first tsunami generated by the submarine landslide. The cut is the water withdrawal uncovering the sea floor that was produced by the mass movement. It is well known that underwater slides induce positive waves in the front and negative in the rear [Ward, 2001; Enet and Grilli, 2007]. The occurrence of the slide was confirmed by bathymetric surveys performed some days later that brought evidence of a submarine scarp, with strongest erosion concentrated near the coast. We associated this slide to the event recorded in the seismic records at 1314–1315 LT.

2. The submarine slide increased the instability of the upper subaerial part of SdF, causing also a sequence of small failures along the slope.

3. The subaerial slide seen by Mr. Grassi was responsible for the second tsunami (the one that was recorded by Dr. Pompilio), which is estimated to have occurred at 1322–1323 LT, based on seismic records.

The biggest part of the interviews concerns the tsunamis hitting the northern coast of Stromboli. In Piscità, some people observed water withdrawal by 30–40 m at most, which occurred three times, at an estimated interval of 30–40 s between waves. At the beach of Ficogrande, where the shore (30–40 m wide and 220–240 m long) is separated by a road from a row of restaurants, houses, shops, and hotels, the tsunami damage was most severe. Some eyewitnesses describe the wave coming obliquely from Piscità and manifesting with a sea retreat followed by an inundation. One person recognized the second tsunami and saw it to arrive more or less 5

min later. After Punta Lena Nord, the coast turns southward and is characterized by a long pebble beach, called Scari: there are several privately owned houses on the beach, and behind the street that runs parallel to the coast, there is an electric power plant (point E in Figure 2). A number of tourists who were walking close to the power plant escaped the flooding waves by running to higher places; one of them was able to observe two distinct trains of waves, the first more or less at 1315 LT and the second some minutes later.

Some relevant accounts were given by inhabitants from the little village of San Vincenzo, which dominates the northeast corner of the island (Figure 2, point U). From the main square, one has a panoramic view of a wide portion of the coast. Local people felt safe in this position, and from here, they looked at the tsunami attacking the coasts below. A series of pictures shot by Mr. Utano (Figure 2, right) show the second tsunami hitting Punta Lena in the form of a high breaking wave and flooding the coast stretch between Punta Lena and Scari. The sea excitation lasted for about 5–6 min.

In Panarea, SSW of Stromboli, the tsunami caused some damage in the harbor and in the first row of shops. Some witnesses report a 100-m sea withdrawal and 1-m wave height.

By combining all the eyewitness reports that have been summarized here, one has elements to reconstruct the sequence of events, although one has to cope with some contradictions that characterize individual accounts.

1. Only two eyewitnesses stated to have observed two distinct tsunamis: one in Ficogrande and one at the power plant site. Concerning the first tsunami, numerous accounts consistently describe a first withdrawal of the sea, which confirms the observation of Mr. Grassi on the initial cut of the sea surface and our conjecture that a submarine landslide occurred first. The difficulty of recognizing the second tsunami is easily explained by the fact that the arrival of a second train of waves was superposed to the queue of the first tsunami, and hence, most people perceived it as a unique tsunami attack.

2. The waves took less than 3–4 min to attack the northern coast of Stromboli from their source. Waves radiating from the SdF propagated with fronts circling around Stromboli: one front toward the north (clockwise seen on a geographic map) and one toward the south (anticlockwise). One interesting observation comes from the account of one eyewitness who reported that at Scari, she saw the waves to come from opposite directions and to meet slightly offshore. This has a known explanation from the theory of wave-front propagation around steep islands, since, as the result of strong refraction ray bending, edge waves tend to form along the coast with consequent energy trapping [see Tinti and Vannini, 1995; Tinti et al., 2000, 2003].

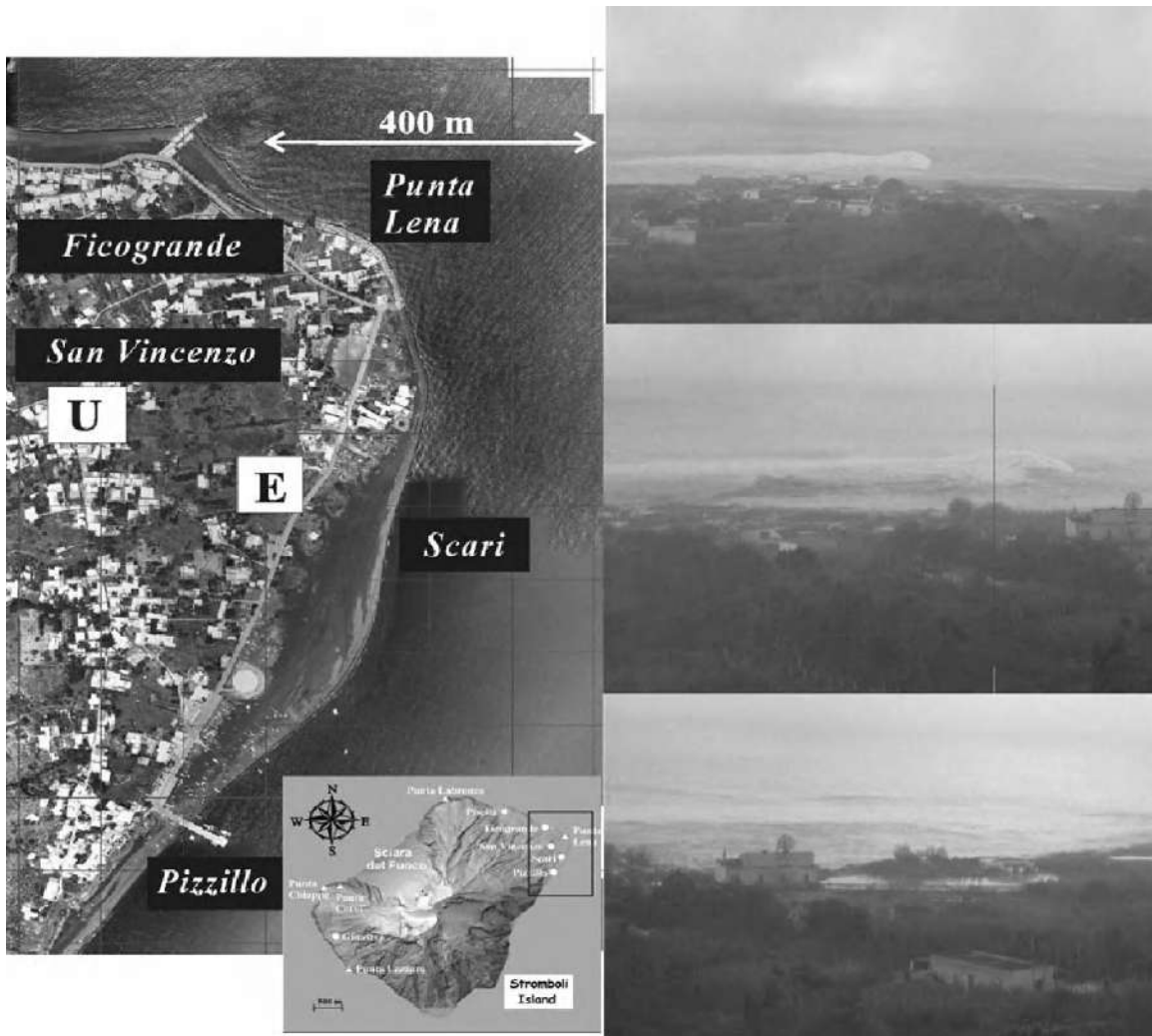


Figure 2. (left) Orthophoto of the northeastern corner of the island of Stromboli (Punta Lena Nord). U, the square of San Vincenzo; E, the electric power plant. (right) Three pictures taken by Mr. Utano from San Vincenzo square, showing the second tsunami attacking and flooding the portion of the coast in front of the power plant between Scari and Pizzillo (sequence starting from the above picture).

4. TSUNAMI FIELD SURVEYS

The postevent campaigns, performed to collect measurements and observations (three, at the beginning of 2003), focused more on the northern and northeastern coasts of Stromboli, approximately from Punta Labronzo, the north-western corner, to La Petrazza on the eastern coast. In Figure 3, the reader may find the area surveyed and the corresponding measured runup heights.

4.1. Spiaggia Longa

The tsunami impact here was not too evident, since the coast is high and rocky. Nevertheless, it was possible to identify some marks of tsunami attack at an altitude of 10.9 m asl, the highest runup height of the whole survey, and to quantify a range of 6.7–10.9 m for this portion of the coast. An interesting site is the narrow valley of Vallonazzo (marked with the letter V in the panel A of Figure 3), where

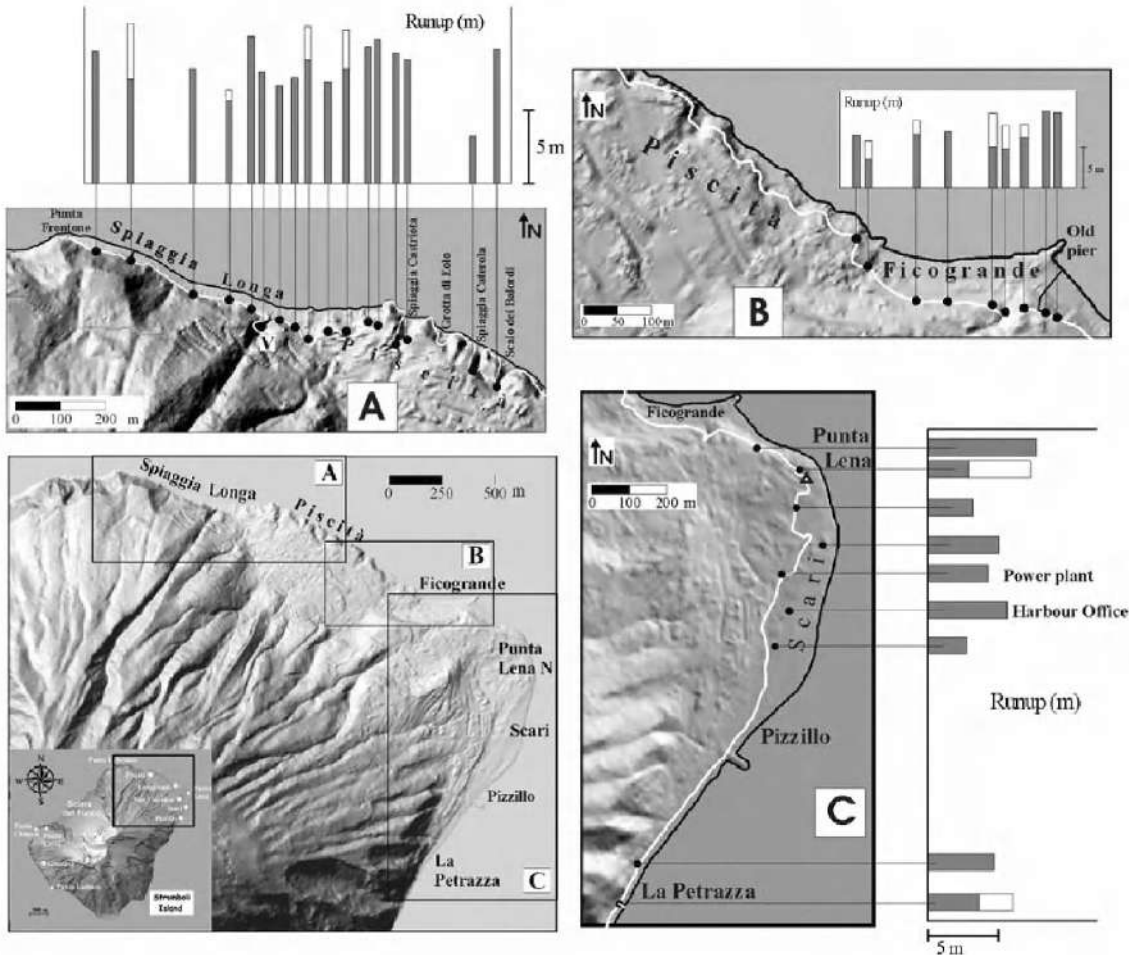


Figure 3. Sketch of the surveyed area (bottom left corner) with boxes delimiting zones A, B, and C, blown up in the crown panels also reporting histograms with observed runups. Note that in localities where more than one measure was taken, the minimum (gray) and maximum (white) values are graphed. The white line represents the maximum inland estimated penetration. Letter V in Figure 3a denotes the Vallonazzo site, where water channeling was observed.

the flattened vegetation evidenced the channeling of the sea water along the valley itself, reaching 7.6 m runup and horizontal inundation of 45 m.

4.2. Piscità

The village of Piscità is located just at the end of Spiaggia Longa and is characterized by a series of inlets separated by rocky promontories, as can be deduced from the figure (Figure 3a). Buildings up to 10–11 m were affected by the waves, with typical tsunami impact features: brick walls and balustrades knocked down, door and windows broken, sand deposits in the interior of the houses and along the streets,

small boats moved inland. The maximum runup here lies in the range 6.9–10.7 m, with a strong variability due to the local effects of shoreline and inlets.

4.3. Ficogrande

Tsunami effects here were particularly violent; some small buildings and some border walls were completely flattened. A considerable amount of sand, pebbles, and mid-sized boulders were deposited along the streets and inside the houses. In the northwestern part of Ficogrande, the measured runups lie between 3.5 and 6.5 m (Figure 3b). Moving eastward along the beach, the maximum runups tend to increase,

reaching 8.3–9.3 m with a corresponding flooding distance of approximately 65 m.

4.4. Punta Lena

Due to the construction of several houses close to the sea, the tsunami in this area was really destructive, transporting sand and pebbles on rooftops, at least 7 m asl. The maximum runup heights ranged between 2.9 and 7.7 m (see Figure 3c), with inland penetrations of 40–60 m.

4.5. Scari

The beach here is wide, and composed mainly of pebbles and sand, with a low-angle slope favoring the penetration of the tsunami. The biggest part of buildings, as well as the electric power plant, lies landward from the street in relation to the sea; distance from the water is actually greater than that in Ficogrande and Punta Lena, and this explains the lower damage suffered by this area. The power plant area, 4.3 m asl, was affected by the flooding, 134 m inland.

4.6. Tsunami Effects in the Aeolian Archipelago and in the Far Field

Within 20 min, the waves reached all the islands of the archipelago, from Panarea to Vulcano. Apart from Panarea, which was reached by 1-m waves, the effects of the tsunami elsewhere were generally negligible, although in some specific localities, some minor consequences were reported. A detailed description of field surveys conducted in the Aeolian archipelago can be found in Maramai *et al.* [2005a] and for the coasts of Campania in Nappi *et al.* [2003].

5. NUMERICAL SIMULATIONS

Simulations of the sliding motions along the SdF and of the generated tsunamis have been performed by means of numerical codes developed by the tsunami research team of the University of Bologna. For the landslides, codes UBO-BLOCK1 and UBO-BLOCK2 have been applied: these are the 1-D and 2-D versions of the same model, where the mass is considered to be split into blocks mutually interacting and conserving the volume, and the motion is computed by applying a Lagrangian approach. The main difference is that in the first case, the mass is discretized as a “chain” of blocks and, in the second, as a “matrix” of blocks [see Tinti *et al.*, 1997].

The propagation of the tsunami is computed by solving the Navier–Stokes equations of hydrodynamics in the shallow water approximation, adopting a finite element scheme:

the code UBO-TSUF, developed at the University of Bologna, discretizes the computational domain in triangular elements with size depending on the local depth of the sea. The link between the landslide and the tsunami simulation codes is the tsunami excitation term of the hydrodynamic equations (handled by the second code) that is computed from the landslide motion (output of the first code) through a suitable interface module: UBO-TSUIMP. This takes into account the filtering effect of the water depth and, through interpolation, passes data from the Lagrangian grid of the landslide simulation codes to the triangles grid of the code UBO-TSUF. More details on the tsunami model can be found, for example, in Tinti *et al.* [1994].

5.1. Simulation of the Landslides

To attain a better reconstruction of the landslide events, several landslide hypotheses have been investigated and run through our codes. We report the results only of those four cases that are the most relevant in our opinion:

1. Two cases for the submarine slide, case 1A and 1B, with a volume around 16 million m³, differ only for the initial mass distribution. Both have been simulated by means of code UBO-BLOCK2. Case 1A is characterized by longitudinal symmetry and by triangular cross-section; case 1B by an irregular mass distribution, thicker near the shore

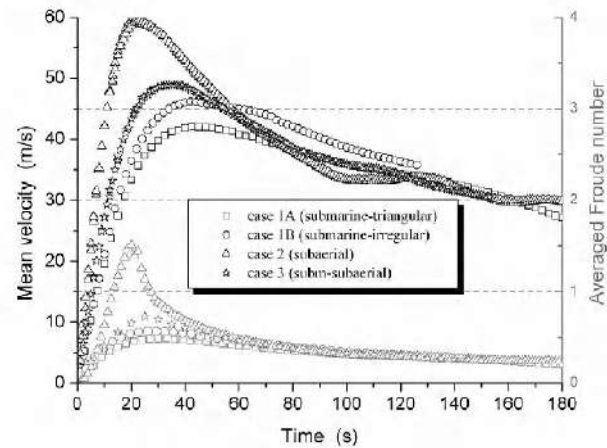


Figure 4. Average velocity (in black) of the four landslide cases versus time: case 2 (subaerial slide), starting in steeper slopes, reaches the highest velocity after 20 s. The same graph reports also the Froude number values (gray symbols), influencing the tsunamiogenic efficiency. In case 2, the Froude number exceeds the critical value 1, whereas for the other cases, it attains at most values of 0.6–0.7.

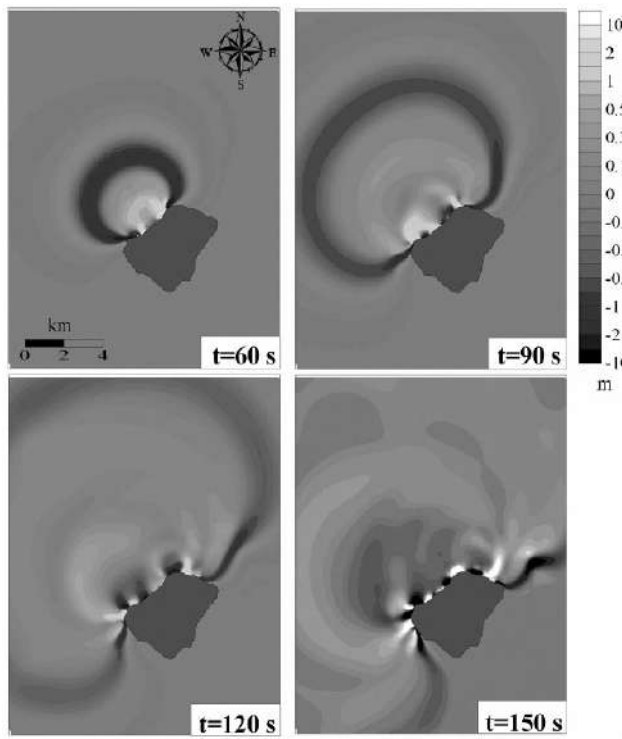


Figure 5. Tsunami field propagation for case 1B, at four different computation times. Black or dark gray areas denote negative signal; white and brighter zones denote positive wave.

(about 35 m) and thinning seaward. The initial position agrees with the findings of the postevent bathymetric surveys [Chiocci *et al.*, 2003].

2. Case 2 refers to the second event. It is a subaerial slide positioned in the northern part of SdF, with volume around 5 million m³. The 1-D model has been adopted, due to the narrowness of the body, which is better handled by the “chain of blocks” approach.

3. Case 3, simulated via UBO-BLOCK1, has a volume comparable to cases 1A and 1B and considers a slide partly subaerial and partly submarine. This hypothesis is presented for completeness.

The common feature of all cases (see Figure 4) is the strong initial acceleration, leading to peak speeds of 40–60 m/s after a few tens of seconds, which is followed by a slow deceleration phase, reflecting the fact that masses move along lower angle slopes. The difference between cases 1A and 1B reflects the different initial mass distribution: in case 1B, the center of mass (CoM) is located at a higher place than in case 1A, due to the slide mass concentration near the shore, and this corresponds to a higher potential energy available for the motion. The highest velocities are reached by the subaerial slide (case 2), for two main reasons—lack of water resistance and initial steeper slopes—whereas the submarine–subaerial slide (case 3) produces intermediate effects.

Figure 4 reports also the slide Froude number (in gray). This parameter measures the efficiency of the energy transfer

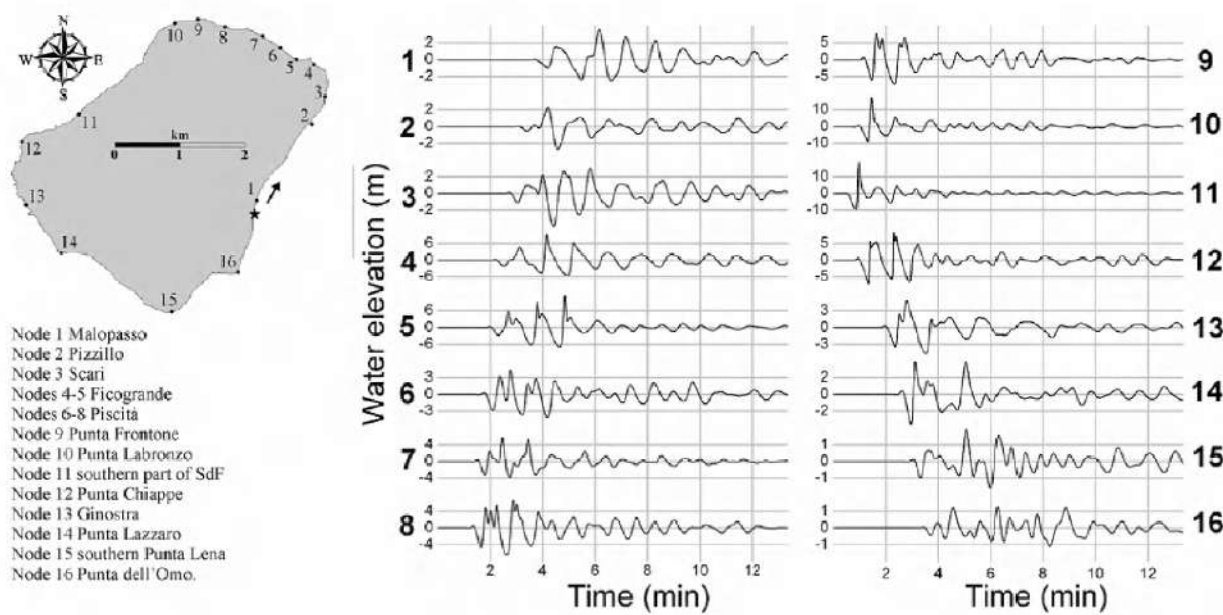


Figure 6. Synthetic marigrams computed in coastal nodes for case 1B, whose position and toponyms are indicated on the left.

from slide to the water wavefield, that is, the efficiency of the tsunami generation process; it is the ratio of the horizontal velocity of the moving body to the velocity of the wave that, in the shallow water approximation, is simply \sqrt{gh} . When this ratio approaches the critical value 1, the source and the wave are in resonance, and the generation power is maximum. All curves show an initial growth and a subsequent decrease, with a peak value corresponding more or less to the peak of maximum velocity. Only the subaerial case crosses the critical value, meaning that in this phase it is characterized by a considerable tsunamigenic efficiency.

5.2. Tsunami Simulations

The tsunami computational domain is represented in Figure 5. The figure portrays four snapshots for case 1B computed at different time instants of the tsunami propaga-

tion around Stromboli. Notice that the waves radiate from the area in front of SdF and propagate with radial fronts away from the source: they travel more slowly along the coast and faster in the open sea, due to the strong tsunami speed dependence on the sea depth. As a result, one observer sitting on the coast can see the tsunami front advancing almost normal to the shoreline at a certain distance offshore and attack the coast obliquely. This was the case reported by several eyewitnesses. When the coast bends suddenly, such as in Punta Lena, the northwestern head of Stromboli, the tsunami fronts also bend and may attack the coast normally. According to our simulations, within the first 2 min, the tsunami reaches more than one half of the Stromboli coast, and in less than 4 min, the entire island is affected.

The inspection of the computed tide gauges (Figure 6) shows almost everywhere a first negative leading signal, followed by a series of crests and troughs. The sites closer to

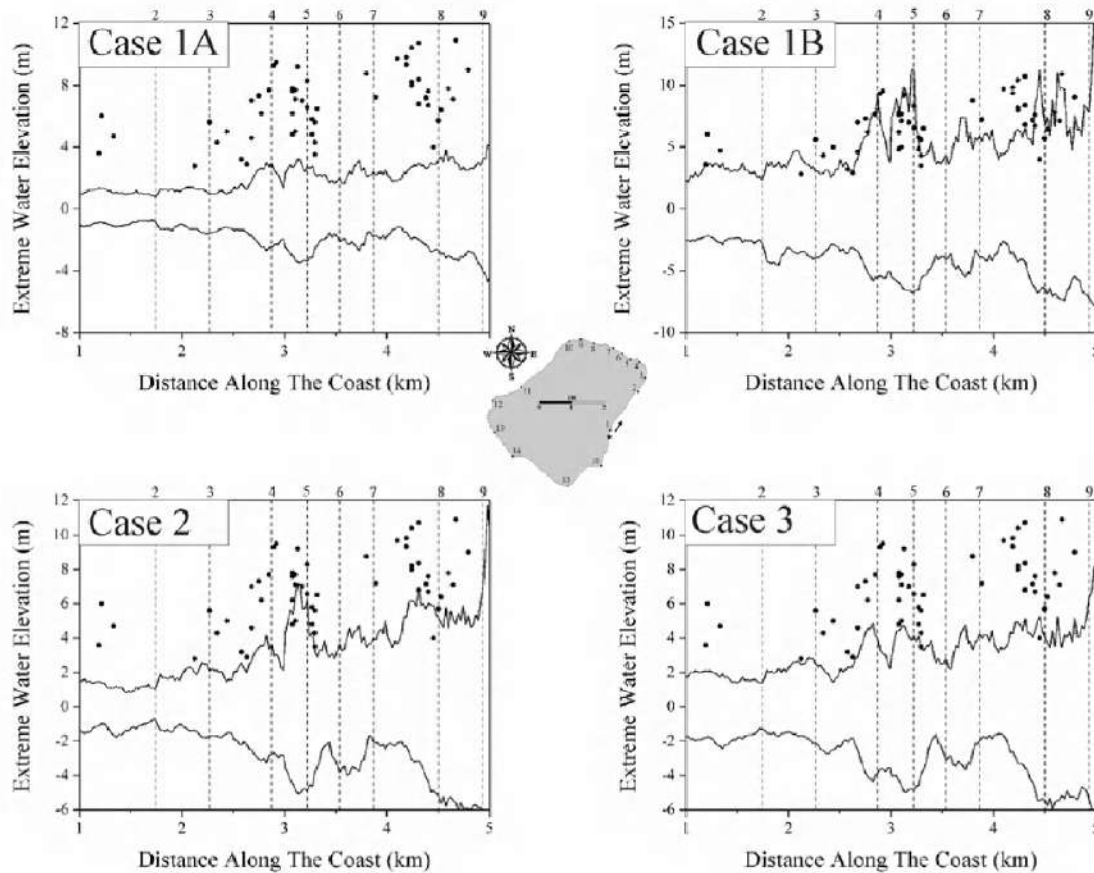


Figure 7. Comparison of the computed maximum and minimum elevations along the coast with the observed runups (black points), for the four cases considered. The abscissa is the linear distance from the origin point marked with a star in the map, on the eastern coast.

the source zone (points 10 and 11 in Figure 6) evidence the highest amplitudes and heights of the waves. In general, the most significant waves are two or three almost everywhere, but the first one is not always the highest. The wave period is approximately 60–80 s. These features are common to all the cases with the exception of the first polarity of the waves, which are negative for cases 1A, 1B, and 3, and is positive for case 2 concerning the subaerial landslide. For further details on the other cases results, see *Tinti et al.* [2006b, 2005a].

In Figure 7, the maximum and minimum water elevation along the coast are plotted for all simulations, over a segment going from point 2 (Pizzillo) to point 9 (Punta Froncone), that is, the area where the field surveys were carried out. The simulated heights are compared to the observed runup (black points). The best agreement is given by case 1B, especially between points 4 and 5, corresponding to the northeastern corner of the island. On the other hand, one may notice that somewhat big discrepancies, with regard to this case, come from the area between points 7 and 8, near Piscità, where a lot of inlets and promontories characterize the coast, strongly influencing the tsunami propagation with local effects. Also, case 2, which in general tends to underestimate the observed runup, shows a good fit around point 5. Cases 1A and 3, presented for completeness in this graph, provide low elevations compared to the observations.

The discrepancy in tsunami generation between cases 1A and 1B, having the same initial position and a similar initial dynamics, can be ascribed to the different initial shapes of the sliding body: the sliding body impulse is strongly filtered by the water depth, meaning that the higher contribution to the tsunami generation comes while the mass is shallower water. Case 1B presents an accumulation of material near the shore, while case 1A is characterized by a uniform mass distribution, and this is reflected in the size of the relative generated waves. The subaerial slide case shows that a mass that is considerably smaller than the submarine ones can generate a tsunami that is even larger than the one produced in cases 1A and 3; this is due to the steeper slope of its initial position and to the initial lack of water resistance, both contributing to a larger initial acceleration.

6. CONCLUSIONS

We have analyzed all the available data for the two major landslides and the corresponding tsunamis that occurred in Stromboli on 30 December 2002: instrumental data, eyewitness accounts, postevent field surveys, and numerical simulations. By putting together all the pieces, we were able to provide a consistent reconstruction of the events. Failure on the SdF started with a series of precursors (fissures) accompanying the ongoing eruption. One of the precursor was

a thin surface landslide taking place at 1311 LT. At 1315 LT, a major landslide of about 15–20 million m³ detached underwater causing the first tsunami that, in a few minutes, attacked disastrously all the coast of Stromboli with fronts traveling around the islands in both directions, south and north. In 5 min, the tsunami attacked Panarea. Case 1B is the most adequate simulation of this first event. The first landslide destabilized the slope above the sea level, which collapsed 7 min later and caused the second tsunami, better described by case 2. The tsunami arrived on the queue of the first and was not perceived by many as a second tsunami event. It is probable that the most severe damage was provoked by the first tsunami, but the second was not much weaker, although the mass involved in the generation was probably about one third of the first landslide.

REFERENCES

- Baldi, P., F. Belloli, M. Fabris, M. Marsella, R. Monticelli, and V. Signorotto (2003), La fotogrammetria digitale differenziale del versante della Sciara del Fuoco (isola di Stromboli) dopo l'evento del 30 Dicembre 2002, presented at 7a Conferenza Nazionale ASITA "L'informazione territoriale e la dimensione del tempo," (in Italian), Verona, Italy, 28–31 October 2003.
- Bonaccorso A., S. Calvari, G. Garfi, L. Lodato, and D. Patanè (2003), Dynamics of the December 2002 flank failure and tsunami at Stromboli volcano inferred by volcanological and geophysical observations, *Geophys. Res. Lett.*, 30(18), 1941, doi:10.1029/2003GL017702.
- Chiocci, F. L., A. Bosman, C. Romagnoli, P. Tommasi, and G. de Alteriis (2003), The December 2002 Sciara del Fuoco (Stromboli Island) submarine landslide: a first characterisation, presented at EGS–AGU–EUG Joint Assembly, Nice, France, April, Geophysical Research Abstracts, vol. 5, CD-ROM Version.
- Enet, F., and S. T. Grilli (2007), Experimental study of tsunami generation by three-dimensional rigid underwater landslides, *J. Waterw. Port Coastal Ocean Eng.*, 133(6), 442–454.
- La Rocca, M., D. Galluzzo, G. Saccorotti, S. Tinti, G. B. Cimini, and E. Del Pezzo (2004), Seismic signals associated to landslides and tsunami at Aeolian islands, Italy, *Bull. Seismol. Soc. Am.*, 94, 1850–1867.
- Maramai, A., L. Graziani, G. Alessio, P. Burrato, L. Colini, L. Cucci, R. Nappi, A. Nardi, and G. Vilardo (2005a), Near- and far-field survey report of the 30 December 2002 Stromboli (Southern Italy) tsunami, *Mar. Geol.*, 215, 93–106.
- Maramai, A., L. Graziani, and S. Tinti (2005b), Tsunami in the Aeolian islands (southern Italy): A review, *Mar. Geol.*, 215, 11–21.
- Nappi, R., G. Alessio, R. Nave, V. Sepe, V. Siniscalchi, and G. Vilardo (2003), Rilievo degli effetti del maremoto di Stromboli del 30.12.2002 (Costa Salernitana). INGV-Osservatorio Vesuviano, Open File Report N.2 (in Italian). Available online at: <http://www.ov.ingv.it/italiano/pubblicazioni/openfile/ofr0203.htm>.

- Pino, N. A., M. Ripepe, and G. B. Cimini (2004), The Stromboli volcano landslides of December 2002: A seismological description, *Geophys. Res. Lett.*, **31**, L02605, doi:10.1029/2003GL018385.
- Tinti, S., and C. Vannini (1995), Tsunami trapping near circular islands, *Pure Appl. Geophys.*, **144**, 595–619.
- Tinti, S., I. Gavagni., and A. Piatanesi (1994), A finite-element numerical approach for modelling tsunamis, *Ann. Geophys.*, **37**, 1009–1026.
- Tinti, S., E. Bortolucci, and C. Vanmimi (1997), A block-based theoretical model suited to gravitational sliding, *Nat. Hazards*, **16**, 1–28.
- Tinti, S., E. Bortolucci, and C. Romagnoli (2000), Computer simulations of tsunamis due to flank collapse at Stromboli, Italy, *J. Volcanol. Geotherm. Res.*, **96**, 103–128.
- Tinti, S., G. Pagnoni, F. Zaniboni, and E. Bortolucci (2003), Tsunami generation in Stromboli island and impact on the south-east Tyrrhenian coasts, *Nat. Hazards Earth Syst. Sci.*, **3**, 1–11.
- Tinti, S., A. Maramai, and L. Graziani (2004), The new catalogue of Italian tsunamis, *Nat. Hazards*, **33**, 439–465.
- Tinti, S., A. Armigliato, A. Manucci, G. Pagnoni, and F. Zaniboni (2005a), Landslides and tsunamis of 30th December 2002 at Stromboli, Italy: Numerical simulations, *Boll. Geofis. Teor. Applic.*, **46**(2–3), 153–168.
- Tinti, S., A. Manucci, G. Pagnoni, A. Armigliato, and F. Zaniboni (2005b), The 30th December 2002 landslide-induced tsunami in Stromboli: Sequence of the events reconstructed from the eye-witness accounts, *Nat. Hazards Earth Syst. Sci.*, **5**, 763–775.
- Tinti, S., A. Maramai, A. Armigliato, L. Graziani, A. Manucci, G. Pagnoni, and F. Zaniboni (2006a), Observations of physical effects from tsunamis of December 30, 2002 at Stromboli volcano, Italy, *Bull. Volcanol.*, **68**, 450–461.
- Tinti, S., G. Pagnoni, and F. Zaniboni (2006b), The landslides and tsunamis of 30th December 2002 in Stromboli analysed through numerical simulations, *Bull. Volcanol.*, **68**, 462–479.
- Ward, S. N (2001), Landslide tsunami, *J. Geophys. Res.*, **106**(B6), 11,201–11,216.

A. Armigliato, A. Manucci, G. Pagnoni, S. Tinti, R. Tonini, and F. Zaniboni, Department of Physics, Sector of Geophysics, University of Bologna, Viale Carlo Berti Pichat, 8 40127 Bologna, Italy.
(stefano.tinti@unibo.it; filippo.zaniboni@unibo.it)

L. Graziani and A. Maramai, Istituto Nazionale di Geofisica e Vulcanologia, Via di Vigna Murata 605, 00143 Rome, Italy.

Deep-Sea Deposits of the Stromboli 30 December 2002 Landslide

Michael P. Marani and Fabiano Gamberi

Istituto di Scienze Marine–CNR, Sede di Geologia Marina di Bologna, Bologna, Italy

Mauro Rosi

Dipartimento di Scienze della Terra, University of Pisa, Pisa, Italy

Antonella Bertagnini and Alessio Di Roberto

Istituto Nazionale di Geofisica e Vulcanologia, Sezione di Pisa, Pisa, Italy

Stromboli is a 3000-m-high island-arc volcano rising to 900 m above sea level. It is the most active volcano of the Aeolian archipelago in the Tyrrhenian Sea (Italy). In the last 13 ka, four large-volume (1-km³) flank collapses have shaped the northwestern flank [Sciara del Fuoco (SdF)] of the volcano with the potential to cause hazardous tsunamis. In addition, smaller volume, more frequent partial collapses of the SdF have been shown to be tsunami-generating events. One such partial collapse occurred on 30 December 2002. The resulting landslide generated a 10-m-high tsunami that impacted the island. Multibeam bathymetry, side-scan sonar, and seabed visual observations reveal that 25–30 × 10⁶ m³ of sediments were deposited on the offshore from the SdF landslide. Samples have led to the recognition of a proximal coarse-grained landslide deposit on the volcano slope and a distal, cogenetic, sandy turbidite 24 km from the Stromboli shoreline. The proximal landslide deposit consists of two contiguous facies: (1) a chaotic, coarse-grained deposit and (2) a sand facies that develops laterally with and over the coarse-grained deposits. Distally, a capping 2- to 3-cm-thick sand layer, not present in a prelandslide September 2002 core, represents the finer-grained turbidite equivalent to the proximal deposits. Characteristics of the SdF landslide deposits suggest that they derive from cohesionless, sandy matrix density flows. A range of density flow transitions, based principally on particle concentration and grain-size partitioning of cohesionless parent flows, can be identified in the proximal and distal deposits of this relatively small-scale landslide event on Stromboli.

1. INTRODUCTION

The Stromboli Volcano: An Integrated Study of the 2002–2003 Eruption
Geophysical Monograph Series 182
Copyright 2008 by the American Geophysical Union.
10.1029/182GM14

Landslides play a major role in the evolution of island volcanoes. Many large-scale landslide deposits covering many hundreds of kilometers squared of seafloor have been documented by detailed offshore studies, in some cases traveling

several hundreds of kilometers from the source [Moore *et al.*, 1989, 1994; Ollier *et al.*, 1998; Masson *et al.*, 2002; Wynn and Masson, 2003; Masson *et al.*, 2006].

In addition, much attention has been paid to island volcano landslides because of their tsunamigenic potential [e.g., Moore *et al.*, 1989; Masson *et al.*, 2006]. The hazard posed by subaerial volcaniclastic landslides entering the ocean or submarine landslides that are the result of flank collapse vary not only with the size of the landslide, but also with the specific process of transport of the collapsed material. Even relatively small landslides have the capacity to generate high runups due to their proximity to the coastline [Masson *et al.*, 2006]. This was the case for the partial collapse of the northwest flank of Stromboli Island that took place on 30 December 2002. This relatively small ($\approx 20\text{--}30 \times 10^6 \text{ m}^3$) landslide generated a tsunami of up to 10 m high on Stromboli and up to 2 m high on the neighboring islands of the Aeolian archipelago.

Submarine mass movements span a wide spectrum of gravity density flow processes because of the large variation in their physical properties of the slide material together with the consequential diversity of flow rheologies [Mulder and Cochonat, 1996; Masson *et al.*, 2006; Trofimovs *et al.*, 2006]. Moreover, transport processes of the material deriving from a single landslide may also evolve to form multiple density flows with distinctive properties [Kessler and Bédard, 2000; Sohn *et al.*, 2002].

This paper first identifies and characterizes the submarine deposits of the Stromboli 30 December 2002 landslide event. Based on the deposit properties, it then endeavors to decipher the deep-sea dynamics of sedimentary gravity flows offshore of the Stromboli volcano. The results provide a better understanding of the submarine transport and deposition mechanisms related to the Stromboli landslide that will improve our comprehension of the processes of submarine landslide deposition on other volcanic islands. The study is also applicable to both recent deposits and those preserved in the geological record. In addition, the flow dynamics and modes of deposition of the landslide material define baseline constraints for research directed at the modeling and evaluation of tsunamigenic hazards associated with island slope failure.

2. STROMBOLI ISLAND

Stromboli, the northernmost volcanic island of the Aeolian archipelago is located in the southern Tyrrhenian Sea (Figure 1). It is a large conical volcano rising to 900 m above sea level (asl) from a base that ranges between 2300 m below sea level (bsl) to the north and 1300 m bsl southward. Volcanism has been continuous since between the third and

seventh centuries A.D. Activity is principally mild intermittent and explosive, and punctuated by rare lava emissions and more violent explosions [Rosi *et al.*, 2001]. The active vents are located at 750 m altitude in the upper part of the Sciara del Fuoco (SdF), a horseshoe-shaped depression that occupies the northwestern flank of the volcano (Figures 1 and 2).

The SdF is probably the result of at least four flank collapses that have occurred during the last 13 ka, with each collapse involving volumes of material ranging from 0.73 ± 0.22 to $2.23 \pm 0.87 \text{ km}^3$ [Tibaldi, 2001]. The most recent event, which took place at ~ 5 ka [Bertagnini and Landi, 1996], resulted in the present-day form of the SdF depression, interpreted as a flank failure that generated an estimated collapse volume in the order of 0.7 km^3 . Numerical modeling indicates that the failure of these volumes would generate catastrophic tsunami waves, able to severely impact the Tyrrhenian coasts of Sicily and Calabria [Tinti *et al.*, 2003]. Nevertheless, observations and reports of recent small-scale tsunami events (five since 1906), all related to an increase in volcanic activity suggest that minor collapses, affecting only a part of the SdF, occur with a frequency certainly greater than the much larger failures [Maramai *et al.*, 2005].

3. THE SUBAERIAL SDF AND THE 30 DECEMBER 2002 PARTIAL COLLAPSE EVENT

The SdF is currently an unstable temporary storage area for volcaniclastic sediments derived from primary eruptive activity and by the subsequent, mostly mechanical, modification of the eruptive products. Clast populations within the SdF are primarily (40%–60%) medium-coarse sand to granule-sized scoria clasts [Kokelaar and Romagnoli, 1995]. The deposits filling the SdF prior to the December 2002 eruption consisted mainly of coherent slope-parallel ($30^\circ\text{--}40^\circ$ gradient) lava ribbons and spatter deposits (agglutinates) over which sheets of clastic material, comprising scoria, breccias, and loose sand, persistently moved downslope [Kokelaar and Romagnoli, 1995]. Small slope failures are common because of the alternation of coherent and loose layers.

The most recent partial collapse of the SdF took place at $\sim 13:20$ LT in 30 December 2002 [Bonaccorso *et al.*, 2003; Pino *et al.*, 2005]. The collapse followed a phase of lava effusion that began on 28 December 2002 along a fissure at the base of a crater at the altitude of the active vents (~ 750 m asl) [Bonaccorso *et al.*, 2003]. Seismic recordings [Pino *et al.*, 2004] and the postfailure bathymetric survey [Tinti *et al.*, 2006] identify the event as consisting of a submarine landslide followed by a subaerial failure from about 650 m elevation on the eastern side of the SdF. The submarine

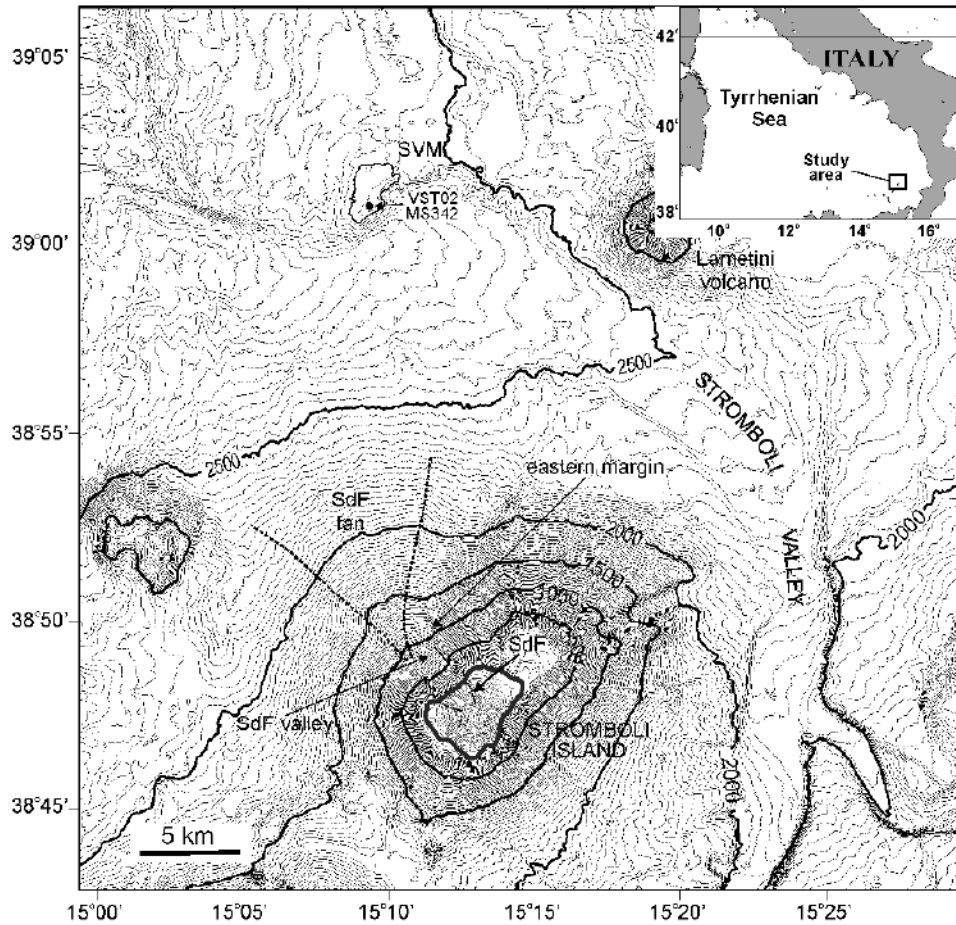


Figure 1. Topography of Stromboli Island (25 m contour interval) and prelandslide regional bathymetry of its offshore setting (25 m contour interval). Inset shows location of Stromboli Island within the southern Tyrrhenian Sea, bounded by box. The SdF on the northwestern flank of Stromboli Island is a horseshoe depression flanked by headwall scarps generated by repeated sector collapses. The 30 December 2002 partial collapse took place on the eastern portion of the SdF. The SdF scarps continue offshore delimiting the SdF valley to the east and the margin of the SdF fan (dashed lines) to the west. In its deeper reaches, the volcano flank progrades into the Stromboli Valley floor masking the left margin of the valley. The right SVM, in contrast, stands about 200 m above the valley floor. The plateau area where distal landslide-derived turbidite deposits were sampled (black circle) is outlined.

landslide affected the seafloor down to ~450 m depth. The slides produced a tsunami lasting several minutes [Tinti *et al.*, 2005]. Eyewitness accounts [Tinti *et al.*, 2005] and subsequent numerical simulations [Tinti *et al.*, 2006] suggest that the landslides generated two tsunamis. In about 90 s after the failures, the tsunami reached the northeastern coast of the island resulting in a maximum runup of 10 m and a maximum inland flooding distance of 100 m. The result was severe damage to Stromboli village. The tsunami also affected other nearby islands of the Aeolian archipelago and

the coasts of Calabria and Milazzo harbor, located on the northern coast of Sicily, 100 km south of Stromboli [Marani *et al.*, 2005].

Volume estimates for the submarine landslide, that affected the seafloor down to ~450 m depth, are in the order of $10.9 \times 10^6 \text{ m}^3$ [Baldi *et al.*, this volume], while the volume of the subaerial slide is estimated at $13.5 \times 10^6 \text{ m}^3$ [Baldi *et al.*, this volume]. The combined submarine and subaerial slide involved a considerable part, $\sim 2 \times 10^6 \text{ m}^3$, of newly formed lava flows [Baldi *et al.*, 2005; Calvari *et al.*, 2005].

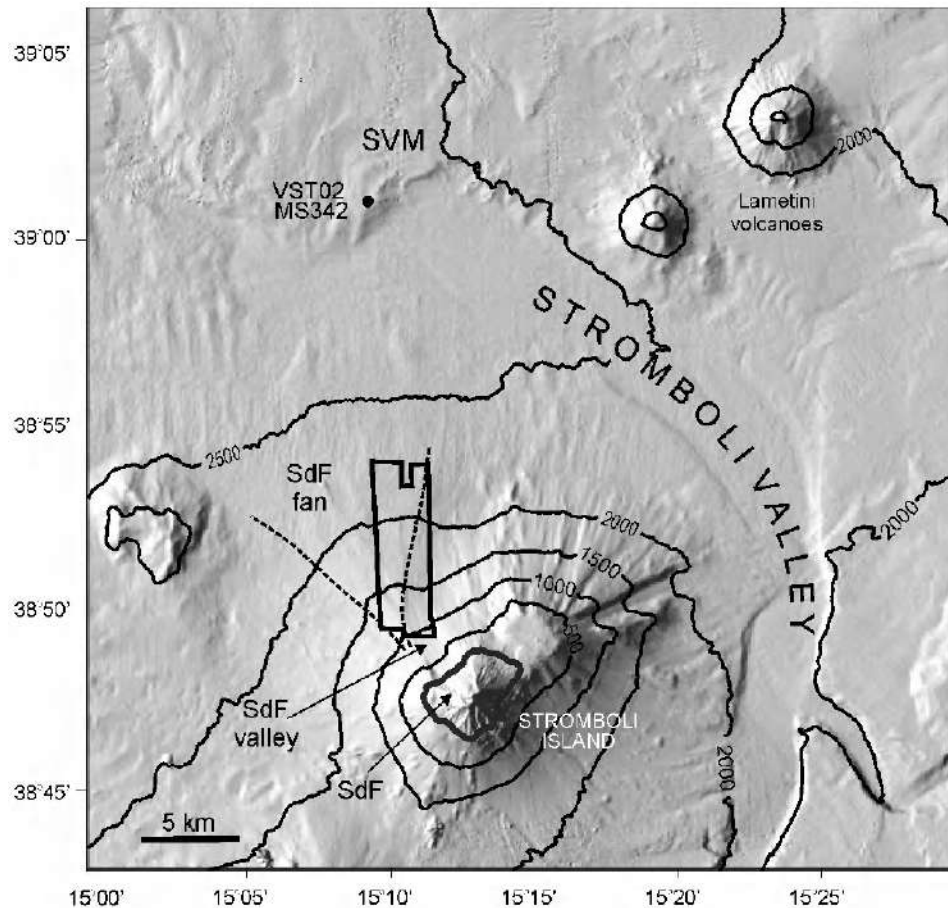


Figure 2. Prelandslide shaded relief bathymetry (Sun at 280°) of the Stromboli region. Illumination highlights the scarps delimiting the SdF and their continuation offshore. Also shown is the course of the Stromboli valley and one of its main tributaries. The Stromboli valley traces the eastern and northern perimeter of Stromboli volcano. SVM is the site of recovery of distal landslide deposits. Outline of black lines indicate the position of the 100-kHz SSS mosaic. Other features are the same as in Figure 1.

4. DATA AND METHODS

There have been a number of bathymetric and sidescan sonar (SSS) surveys in the Stromboli area mainly acquired in March 1999 and January 2003. A comprehensive prelandslide multibeam bathymetric coverage of the region is available (Figures 1 and 2). Additionally, a second swath bathymetric survey on the SdF flank took place a few days after the landslide event. The prelandslide survey was carried out utilizing an EM12dual multibeam system; postlandslide bathymetry was acquired with a deep-water (SeaBat 8160, max 3000 m) and a shallow-water (SeaBat 8125, max 120 m) system. The deep-water instruments have comparable,

range dependent, depth resolutions of 8.6 cm with footprints varying with water depth, while the shallow-water system was high resolution with a near-field depth resolution of <2.5 cm.

Further seafloor characterization, involving high-resolution deep-towed SSS and echosounder surveys, offshore of the SdF flank was undertaken in August 2004. The latest survey utilized a MAK-II sidescan system that was towed about 100 m above the seafloor. The total swath width was 2 km at 30 kHz during the regional survey of the submerged slope of Stromboli, followed by a 700-m-wide swath, 100 kHz higher resolution inspection of the most significant seafloor areas (Figure 2b). Small-scale seabed features of the

SdF flank were further investigated by three video-sled runs (across-slope at 1350 m, 1600 m, and 1800 m depths). These data were used to identify seafloor sites for sampling using box cores and video-guided grabs (Figure 3).

In order to detect the most distal landslide deposits, box cores were recovered in August 2004 (sample MS342) on an isolated, flat-topped, bathymetric high located on the right side of the Stromboli valley, about 200 m above the canyon floor (Figures 1 and 2). The same 2458-m-deep site, located opposite the SdF and along the path of the landslide, had previously been sampled with a gravity corer 3 months before the 30 December slide (sample VST02; Figures 1 and 2).

5. OUTLINE MORPHOLOGY

5.1. The Submarine SdF Valley

The submarine deep-water extension of the two NW trending scarps that delimit the subaerial SdF depression is discernible up to 900 m water depth (Figures 1 and 2). The submerged scarps delimit the shallower portion of a broad (~2 km wide), flat-bottomed valley, hereafter referred to as the SdF valley. Beyond 900 m depth, the deep-water eastern margin of the SdF valley consists of an incision connected to the eastern submarine scarp of the SdF that arches to a northward direction down to 1700 m, diminishing in relief with depth. To the west, the SdF valley is bounded by the subdued relief of the margin of a large fan (SdF fan), with apex at ~900 m water depth (Figure 2). The fan widens downslope, extending to ~2300 m depth.

The 100-kHz sidescan lines show the seafloor features of this region. The two easternmost lines (133 and 132) are characterized by curving streak bands that trace the SdF valley, following a northwest trend in shallower portions, turning to a northward trend downslope (Figure 3). A train of sediment waves develops between 1600 and 1800 m depths. The streak bands terminate at a NNW-trending alignment of large, high backscatter, positive relief features that develop between 1600 and 1850 m water depths (Figure 3). A number of smaller positive relief features also develop upslope from the alignment. The NNW alignment is interpreted as the deeper limit of the landslide-impacted seafloor region characterized by the seafloor elements shown in lines 133 and 132. This interpretation is also based on the comparison of the backscatter character of lines 134 and 135 that cover part of the SdF fan region. These lines show faint radial streaks over a mainly featureless seafloor, taken to represent the standard regime of sediment flows that characterizes the fan region.

On average, the slope gradient of the SdF valley is on the order of 10°. In particular, however, the gradient progressively decreases downslope from values of 19° between 200

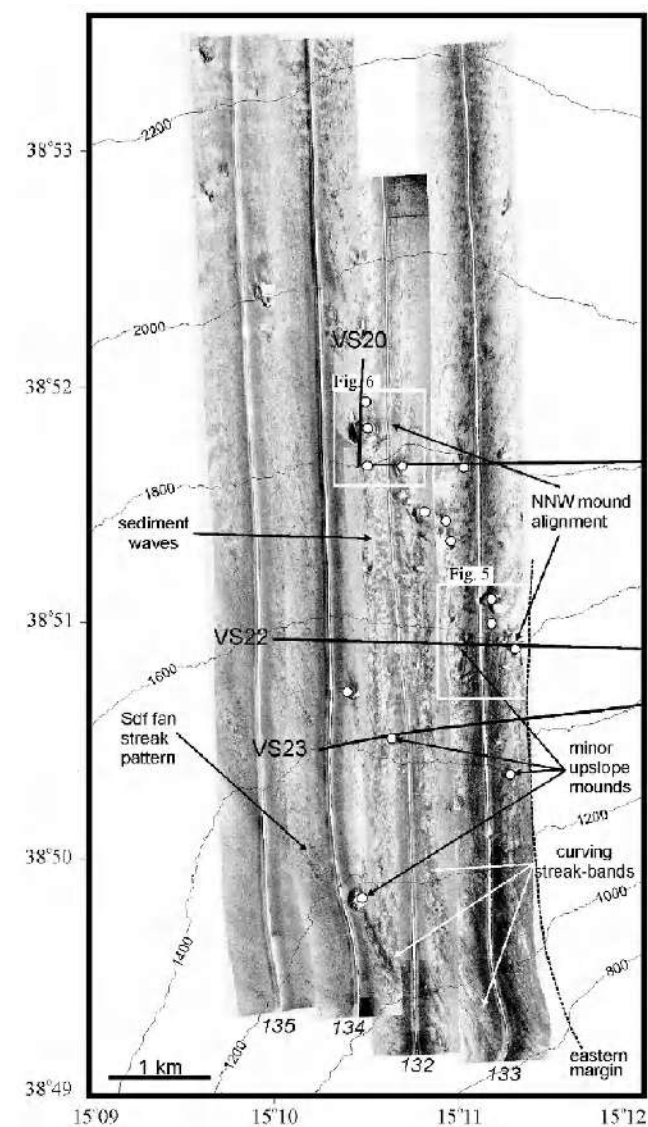


Figure 3. A 100-kHz SSS mosaic overlain by bathymetry at 200 m contour interval. High backscatter = dark tones. SSS track lines, sampling sites (white dots) and video-sled runs (black lines) undertaken on the volcano flank offshore of the SdF are shown. The majority of samples were collected by video-guided grab, providing additional video coverage and control of sample sites. High backscatter features with shadows (white) are the elevated mounds. The largest ones, aligned NNW from 1600 to 1900 m, form the principal limit of the landslide-impacted seafloor area. Upslope, smaller mounds and large bed forms are also present. The seafloor presents streak bands that are oriented NW upslope, the same trend of the submarine scarps of the SdF and curve northward following the eastern margin of the SdF valley (dashed line). In contrast, the SdF fan surface, presents weaker striations with a radially trending pattern. White boxes correspond to relative enlargements of Figures 5 and 6. For location, see Figure 2.

and 800 m, 12° between 800 and 1600 m, and 8° between 1600 m and the floor of the Stromboli Valley.

5.2. The Stromboli Valley Margin

To the north and east, the base of Stromboli volcano is bounded by the Stromboli Valley [Gamberi and Marani, 2007] that bends around the volcano changing from a S–N trend to an E–W course (Figures 1 and 2). The NNW-facing SdF flank of Stromboli extends seaward for 18 km and progrades over the left flank of the E–W-oriented Stromboli Valley at ~2600 m depth (Figures 1 and 2). Opposite the SdF, the relatively planar-floored canyon is 7 km wide and delimited by a sharp, 175-m-high right margin, termed the Stromboli Valley margin (SVM). Part of the SVM is rimmed by a flat, 2500-m-deep, 0.4 km² terrace region (Figures 1 and 2), isolated by the Lametini volcano cone to the east and several gullies that incise the margin to the west.

6. BATHYMETRIC DIFFERENCE ANALYSIS OF THE SDF FLANK

Comparison of the two multibeam data sets, acquired on the SdF flank before and after the December landslide reveals the main areas of seafloor change (Figure 4).

Difference analysis was performed by creating identical grids with 50-m cell sizes of the two bathymetric data sets and subtracting one from the other to produce a new grid displaying the positive and negative anomalies. Comparison with a more time-consuming triangular grid, with grid intervals increasing in proportion to increasing depth, did not yield a higher resolution. Gridding was performed in two software environments, GMT [Wessel and Smith, 1995] and Surfer® with no significant differences. Taking into account the possible errors in absolute values due to the different acquisition parameters of the bathymetric data sets, residuals with values ± 5 m were judged to be at the depth resolution limit and thus excluded from the volume assessment. Estimates of the volume change offshore of the SdF due to the landslide and associated processes indicate a total added volume to the SdF submarine slope in the order of $25\text{--}30 \times 10^6$ m³, a figure comparable to that calculated by other authors [Baldi *et al.*, this volume].

This is a minimum estimate that does not take into account the volume of finer sediment transported distally, beyond the SdF flank, by dilute gravity flows. Based on the discovery of a volcaniclastic layer associated with the landslide 24 km from the coastline of Stromboli Island (see below) and the probable dispersal path of the fines, the volume of this fine sediment is estimated to be 7×10^6 m³. The total volume of the landslide is thus estimated at $32\text{--}37 \times 10^6$ m³.

7. THE LANDSLIDE DEPOSITS

7.1. Proximal Facies

In the SdF flank region, positive-relief, high backscatter targets on the SSS lines (Figures 5 and 6) correspond to isolated high relief mounds consisting of fresh, cobble-sized scoria, clinker, and lava flow clasts (Figure 5) with a coarse sand matrix. The mounds are isolated from one another and have lateral dimensions between 100 and 250 m. The more extensive mounds follow a NNW trend that marks the deeper limit of landslide impact on the SdF flank seafloor (Figure 3). The greater part of the clasts sampled from the mounds are analogous to the eruptive products emitted by Stromboli shortly before the collapse event, porphyritic lavas with phenocrysts of plagioclase, clinopyroxene, and subordinate olivine. Crystals show no or very low alteration while the scoria and clinker fragments often contain abundant glassy

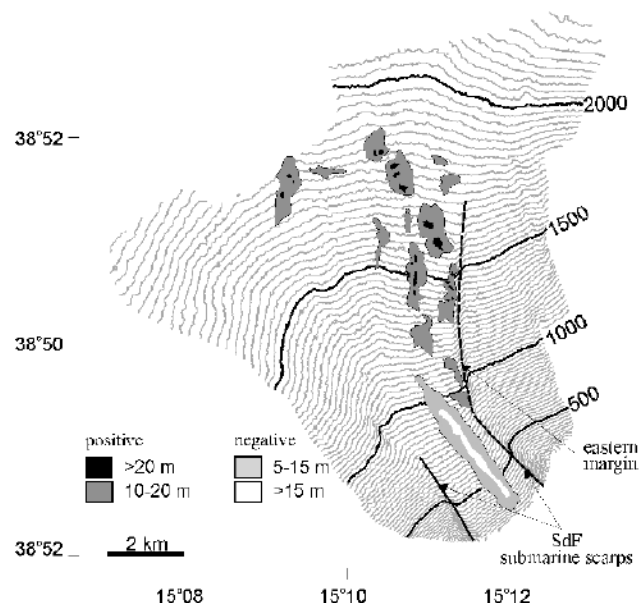


Figure 4. Foremost seafloor variations in the landslide-impacted seafloor of the SdF volcano flank shown by topographic difference map overlaid on 25 m contour postslide bathymetry. Residual values are indicated in the legend. A more extensive, background, positive anomaly (5–10 m added thickness) surrounds the regions of major positive residuals mapped in the figure. The sum of these characteristics, a proximal area of seafloor scouring upslope from the corresponding landslide material deposited at greater depths, corresponds to the principal seafloor modifications of the SdF submarine slope due to the 30 December 2002 landslide. The submarine SdF scarps are shown by black lines, northern extension of the SdF valley eastern margin in dashed line.

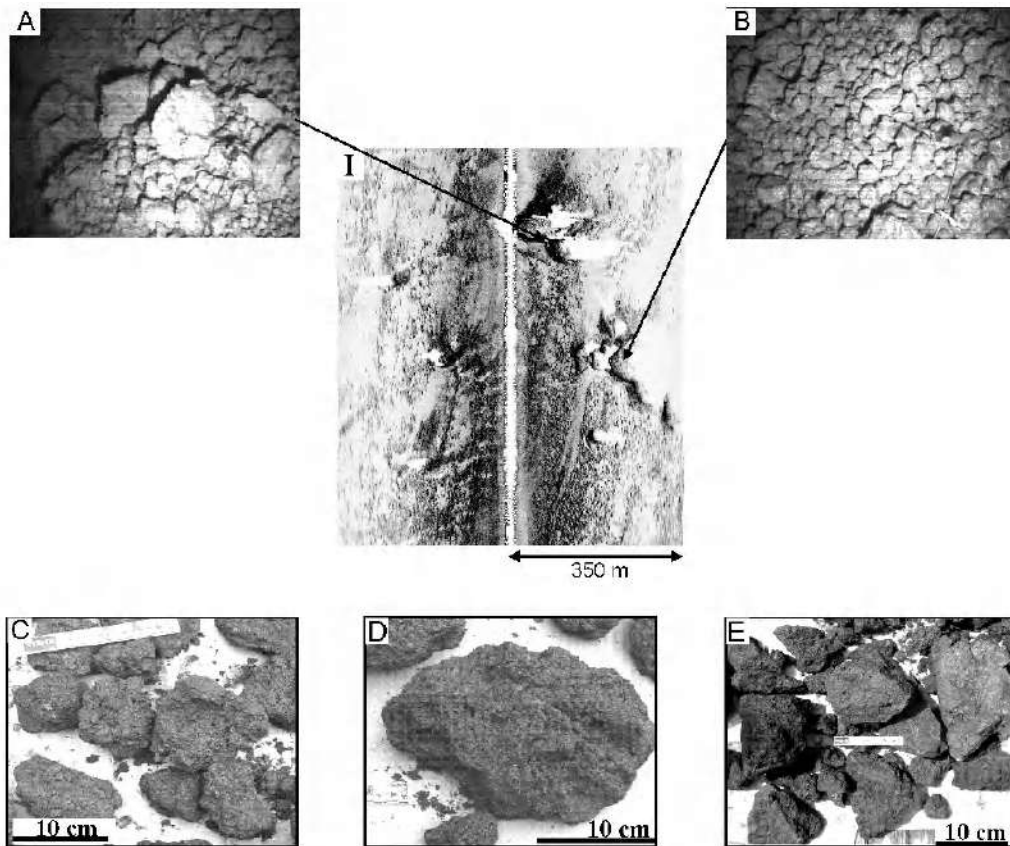


Figure 5. Seabed photographs of the mounded deposits of the landslide-impacted seafloor on the SdF flank with the associated side scan sonar imagery. Photo images are views of roughly $1.5 \text{ m} \times 2 \text{ m}$; high backscatter = dark tones. (I) SSS portion showing shallowest mounds (1600 m depth) located in the vicinity of the eastern scarp margin of the SdF valley (see location in Figure 3). (a) Margin of a mound displaying a variety of clast sizes and distribution of large boulders on mound top. Evidence of void-filling but not draping sand, may represent matrix remnants. (b) Zone of decimeter-sized, well-sorted clasts devoid of sand positioned in the main body of a 30-m thick deposit. Representative samples of the mound deposits are shown in: (c) black/reddish, vesicular, lava flow clinkers. (d) Black, highly vesiculated, crystallized scoria fragments. (e) Black, dense, crystallized lava flow fragments. These clast types, along with less abundant red-colored, altered lava fragments are characteristic of all the coarse mound deposits that were sampled.

matrix sometimes with iridescent surfaces and indicating both fast quenching and the freshness of the sample.

An extensive deposit of medium to coarse black sand, generally arranged in ripple bed forms (Figure 6) surrounds the mounds. The sand facies is composed of three units (Figure 6c): a lower, 30-cm-thick bed of cross-bedded coarse sands, marked by sand grain-size variations and pinch-outs, overlain by an intermediate unit of pebbly coarse sand. The topmost sand unit is arranged in ripple bed forms as shown at the seafloor surface. The ripples are regionally dispersed within the landslide-impacted seafloor area. In the lower

unit, some deformation of the upper beds is displayed in contrast to relatively undeformed lowermost beds (Figure 8c). Although deformation due to the coring process cannot be ruled out, it could alternatively be indicative of the effects due to the subsequent loading or traction of the upper, pebbly sand layer. In terms of the sedimentary components, the matrix sand and the contiguous sand deposit are alike and analogous to the clasts contained in the mounds. The landslide deposits contrast with the surrounding seafloor in being completely devoid of an otherwise ubiquitous hemipelagic sediment drape.

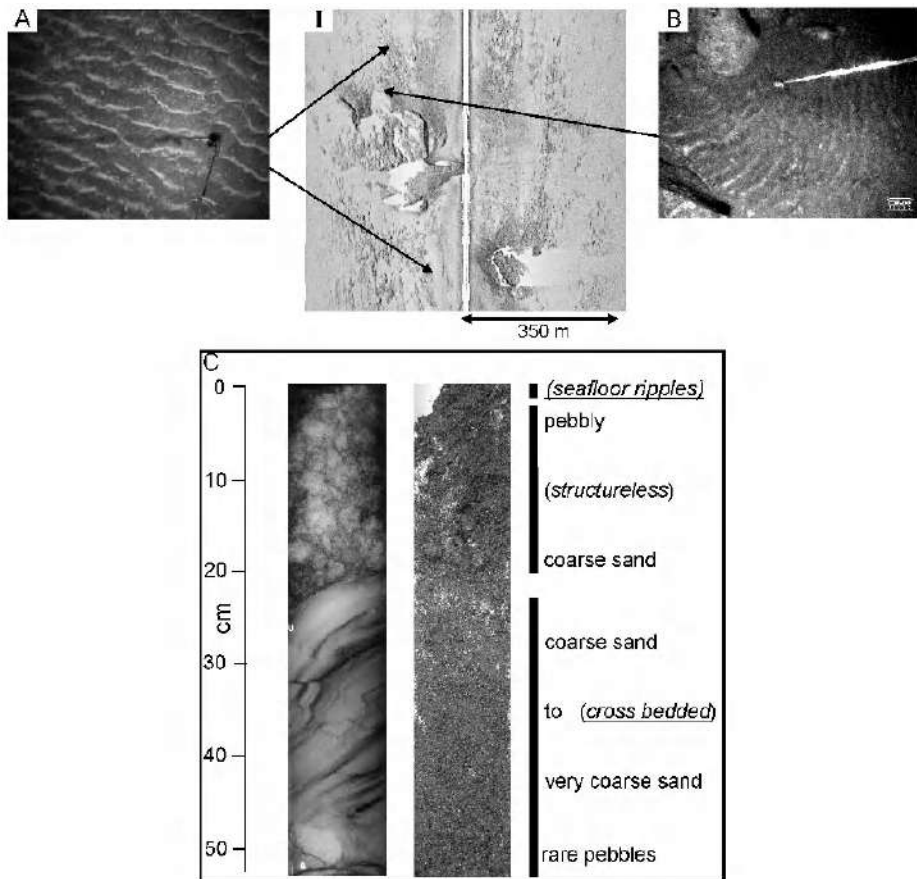


Figure 6. Seabed photographs and a core of the sand deposits of the landslide-impacted seafloor on the SdF flank associated with SSS imagery. Photo images are views of roughly 1.5×2 m, high backscatter = dark tones. (I) SSS portion of the deeper mound deposits (1900 m depth); black circle is the site of the core in figure. (a) Seafloor ripples developed in coarse black volcaniclastic sand downslope of the mound, underlined by finer-grained sediments in ripple troughs. Similar seafloor bed forms are common at the perimeter of the other larger coarse mounds. (b) Seafloor ripples developing laterally from sand-smothered margin of coarse deposit; the ripple pattern is indicative of flow interaction with mound topography. (c) Core and corresponding radiograph representative of the sand facies. The X-ray image provides evidence of the three-unit structure of the sand facies: a lower unit of cross-bedded coarse sand, an intermediate unit of structureless pebbly sand recovered in the core. The top of the coarse sand is arranged in ripple bed forms as observed at the seafloor surface. The cross-bedding of the lower unit displays some deformation of the upper beds but relatively undeformed lowermost beds. Although deformation due to the coring process cannot be ruled out, the observed structures could also be indicative of loading or traction exerted by the upper, pebbly sand layer.

7.2. Distal Facies

On the SVM, a virtually identical sequence of millimeter- to centimeter-thick, black layers of fine to medium sand alternating with up to 15-cm-thick, light brown, silty-mud hemipelagic beds was recovered in both the September 2002 gravity core and the August 2004 box core at a water depth of 2458 m (Figure 7). However, a topmost layer of medium/

fine volcaniclastic sand that caps the 2004 core is missing in the 2002 core (Figure 7c). The cores were collected from the same site, based on DGPS geographical coordinates, and thus, an error of about ± 15 m must be taken into account.

In view of the different sampling methods, particular attention was given to the inspection of the gravity core top, which ruled out any significant remobilization of the sediment–water interface, acknowledging the fact that the two cores

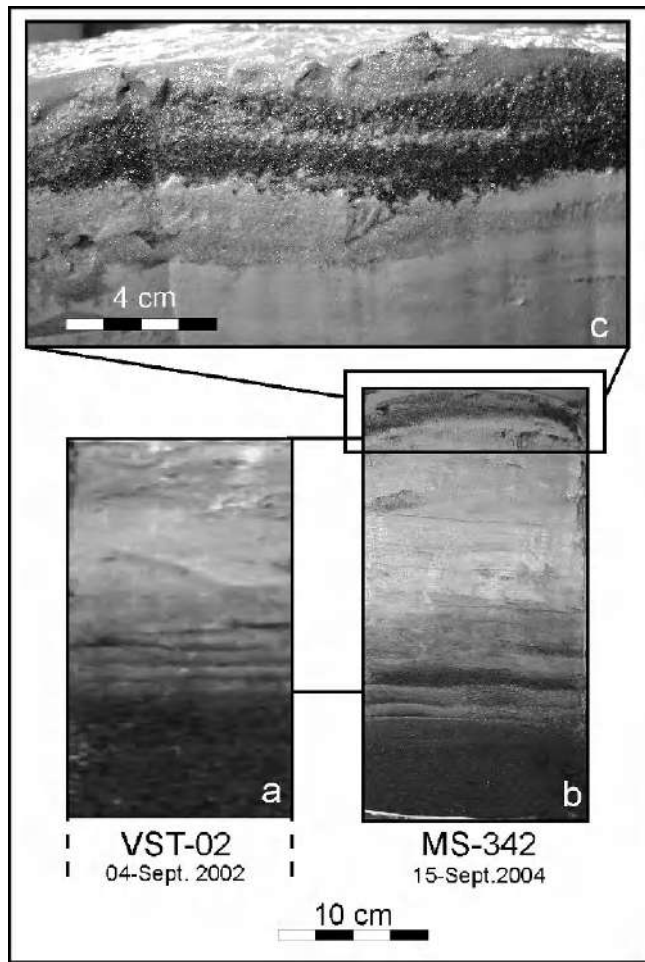


Figure 7. Stratigraphy of cores collected in the same site on SVM. Core sampled (a) 3 months before the 30 December 2002 Stromboli landslide and (b) about 2 years after the landslide. (c) Detail of the 2- to 4-cm-thick topmost layer of fine-medium uncompacted sand and silt interpreted as the distal turbidity current deposit co-genetic to the 30 December 2002 Stromboli landslide. See text for discussion.

are equivalent and in every respect comparable. A further factor favoring the stratigraphic comparability of the two cores is the complete lack of a hemipelagic drape above the sand layer in the box core, indicative of very recent deposition compatible with a post-2002 sedimentary event.

The topmost volcanic layer overlies a 10-cm-thick, bioturbated, silty-mud bed with centimetric silty lenses. The topmost layer is internally stratified and composed of a 2- to 3-cm-thick basal sand bed overlain by a 1- to 5-mm-thick, normally graded silty mud (Figure 7c). The contact between

the two beds is gradual suggesting that they originated from the same depositional event.

In order to assess the nature, grain size, and composition of the top volcaniclastic layer present only in the 2004 core, 80 g of the sand were sieved at one-phi intervals, and thin sections were prepared for component analysis. The basal layer is fine to medium-fine sand and consists almost entirely of volcaniclastic fragments represented, in decreasing order of abundance, by lava and clinker, plagioclase crystals, pyroclastic fragments, pyroxene, and olivine crystals. Pyroclastic fragments consist of mainly fresh, poorly vesicular, honey-colored glass containing abundant microlites of plagioclase and, subordinately, of highly vesicular, fresh, almost crystal-free clear-glass clasts. Pyroclastic fragments have prominent angular shape with very delicate, sharp edges indicating the lack of any mechanical interaction due to reworking (Figure 8).

The upper, normally graded, silty mud consists of volcaniclastic fragments similar to the underlying sand bed, however, with a significantly higher content of plagioclase and pyroclastic fragments compared to the other constituents. Texture and composition of the minerals present in both levels closely resemble those of the crystal-rich scoriae and lavas erupted by the present activity of Stromboli [Landi et al., 2004; Métrich et al., 2001]. Glass composition was also analyzed on unaltered fragments of both honey-colored and clear glass. Plots of the glass composition in the K_2O - SiO_2 classification diagram (Figure 8e) indicate the presence of two, well-defined, clusters. The honey colored glass has shoshonitic composition with (K_2O 3.7–5.8 wt %, SiO_2 52.7–55 wt %), the subordinate clear-glass fragments have shoshonitic–shoshonitic basalt composition with (K_2O 2.3–2.7 wt %, SiO_2 51.4–52.4 wt %). These clusters perfectly match the composition of the glassy groundmasses of, respectively, the crystal-rich and crystal-poor products emitted by the present activity of Stromboli volcano [Métrich et al., 2001, Landi et al., 2004 and unpublished data 2006].

The simultaneous presence of these two juvenile fractions typifies the present activity of Stromboli volcano at least since about the 3rd and the 7th century A.D. and is not recognized in products predating this period [Rosi et al., 2000]. Moreover, the Neostromboli eruptive cycle, preceding the recent Stromboli cycle is unique due to its potassic composition (HK series), its identification thus resulting straightforward.

As a whole, the layer has mineralogical and glass compositions fully consistent with the products of the present activity of Stromboli, matching the character of the material of the 2002 landslide, equivalent to the components of the SdF flank proximal facies deposits.

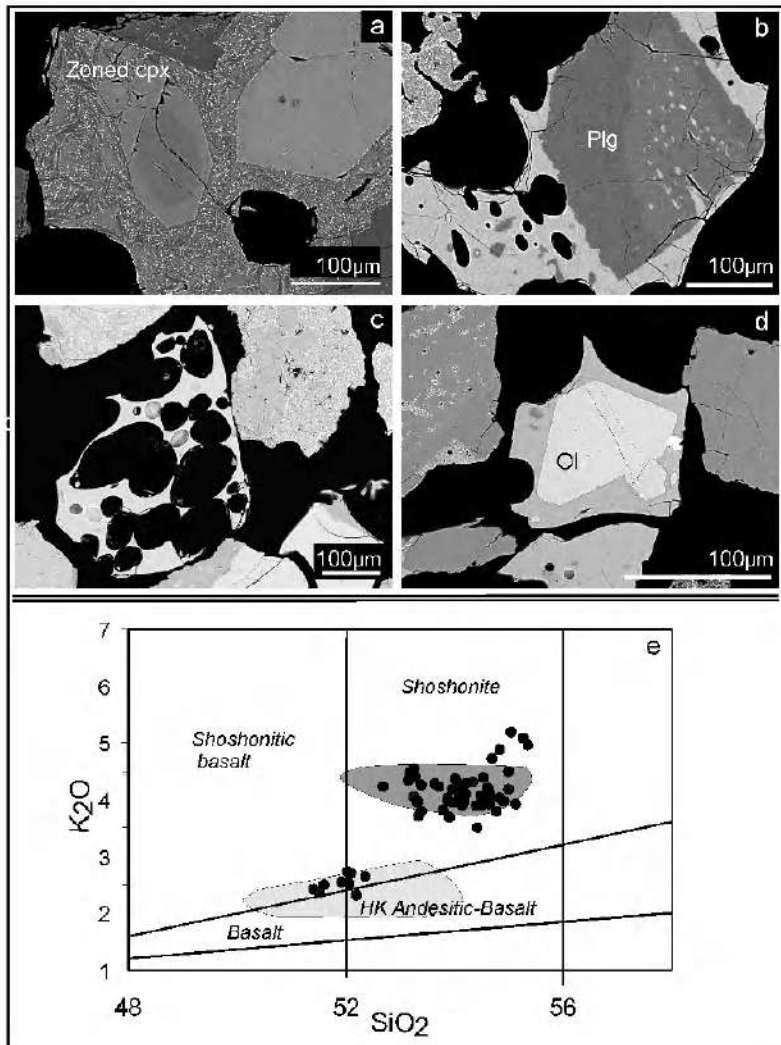


Figure 8. Scanning electron microscope images of volcanic clasts from the top sand bed: (a) clinopyroxenes crystals in microlite-rich groundmass holocrystalline lava fragment, (b) zoned plagioclase set in a poorly vesicular microlite bearing glass, (c) highly vesicular microlite-free glass. (d) Olivine crystal set in poorly vesicular glassy groundmass. (e) Classification of the glassy matrix of poorly vesicular and highly vesicular pyroclastic fragments (black dots) in the SiO₂-K₂O diagram [after Peccerillo and Taylor, 1976]; dark gray field = glassy matrix of the crystal-rich products of the present activity; light gray field = glassy matrix of the crystal-poor products of the present activity. Analyses and images were obtained with a Philips XL 30 scanning electron microscope equipped with EDAX X-4I at the Earth Science Department of Pisa University.

8. DISCUSSION

The data acquired on the SdF flank provide a comprehensive assessment of the deep-sea proximal deposit facies of the 30 December 2002 landslide. Moreover, the nature of these deposits, together with the characteristics of the distal dispersion of the finer fraction recovered from the SVM,

provides the opportunity to evaluate the subaqueous gravity flow processes that brought about such a style of deposition.

The series of observations concerning the SdF proximal deep-sea deposits of the Stromboli landslide material point to a transport process involving the development and evolution of a cohesionless, sand-matrix density flow [Mulder and Alexander, 2001; Kessler and Bédard, 2000; Sohn, 2000].

The impulsive entry of landslide material into the submarine environment, which can cause subaqueous gravity flows, informs which deposits, with similar characteristics to the deep-water Stromboli landslide deposits, are laid down [Mcleod *et al.*, 1999; Schneider *et al.*, 2004].

In the case of the 2002 Stromboli landslide, partitioning of the density flow into clast-rich mounds and sand-rich sectors was probably induced by evolving flow rheology resulting in the concentration of larger clasts into discrete flow regions. The high frictional energy loss due to focusing caused the larger clasts to become less mobile than the more dilute trailing flow regions. When the applied shear dropped below yield strength at the flow fronts, the coarser clasts interlocked and froze, resulting in rapid deposition of the coarse-clast mounds [Kessler and Bedard, 2000; Sohn 2000]. In this regard, both the mounds and the sand deposits of the proximal SdF flank facies resulted from density flow mobilization and segregation. Seafloor morphology controlled deposition and mound location on the SdF flank. Overall, the steadily declining gradient of the SdF slope must, at some level, attain the threshold point below which the yield strengths of the flows overcome the applied shear. This implies an interplay of gradient change and density flow types, determining variations of strength thresholds and ultimately leading to a diversity of depths for flow arrest and deposition.

The coarse to very coarse cross-bedded sands have characteristics similar to concentrated density flows [Mulder and Alexander, 2001] that are partly turbulent and have the capacity of producing a variety of tractional features and bed forms. Correspondingly, the intermediate deposit of the pebbly sand facies, lacking recognizable sedimentary structures, is texturally more akin to a gravelly, sand matrix density flow, or hyperconcentrated density flow [Mulder and Alexander, 2001].

In cases of increased velocity or lasting events, both flow types are liable to ingest seawater and to transform to low-density turbidity flows. Laboratory and field studies have also demonstrated that subaqueous, cohesionless density flows are capable of producing turbidity currents [Mohrig and Marr, 2003; Istad *et al.*, 2004; Elverhøi *et al.*, 2005], whereby the flow head transforms into a turbulent suspension of sediment, bringing about the transport of fine-grained material more distally and supporting the frontal deposition of the coarser clasts. Indeed, the ubiquitous ripple bed forms that cover much of the sandy seafloor of the proximal SdF flank region reflect deposition and reworking by turbulent low-density flows cogenetic to the parent coarser-grained flows.

The presence of the volcaniclastic layer in the SVM proves that these low-density flows retain the capacity to transport and disperse, through turbidity currents, a significant volume of material a long way from the landslide source area.

9. CONCLUSIONS

The integrated data set of seafloor images and sampling offshore of Stromboli demonstrate that a range of density flows can be readily identified in landslide deposits derived from island volcanoes. In the case of Stromboli, landslide sediments were distributed on the submerged volcano flank by largely unconfined, cohesionless granular density flows.

Partitioning of the cohesionless, sand-matrix density flow into sand-rich and clast-rich regions resulted in the formation of two principal deposit styles: coarse grained (meter- to centimeter-sized clasts), 15- to 30-m-thick mounds with a coarse-grained sand matrix and a medium- to coarse-grained sand deposit containing a lower cross-bedded sand unit, an intermediate structureless pebbly sand bed, and an upper cap of seafloor ripples.

The mounds result from rapid deposition due to the migration, segregation, and concentration of larger clasts to discrete regions of the density flow. Loss of fines and a drop in applied shear triggered grain interlocking and the arrest of the coarser-grained flow regions.

Two separate but interrelated flow types are the cause of the sand facies and correspond to the more dilute, trailing regions of the parent flow. The topmost layer of ripple bed forms is the result of turbidity currents derived from the further dilution of the sand facies.

Flow development of the dilute density flows are shown to have had a role in removing a significant volume of finer landslide-derived material into more distal regions, as indicated by the thin sand-rich turbidite bed found in the SVM, more than 24 km north of the SdF shoreline. In this respect, the concept of identifying and coring turbidite depositional environments offshore from active volcanoes is shown to be a powerful tool in acquiring information on the occurrence of failure events while providing baseline data for the future.

The present study demonstrates that some general inferences can be made about density flow properties, based on the resulting deposits. Grain-size partitioning and particle concentration seem to represent the dominant internal controls on flow rheology. General slope morphology, gradient, and preexisting topography are the basic external factors that constrain flow paths and maximum runout.

Recognition of several gravity flow types, resulting from a comprehensive cohesionless density-flow process, may have broader applications in providing key inputs to models of tsunami generation and runup scenarios in the context of island volcanoes. Furthermore, the prospective identification of a similar depositional assemblage to the 30 December 2002 event in older sequences offshore of the SdF may improve the likelihood of estimating landslide scale and recurrence cycles, augmenting correlation with island

sequences and additionally improving the appraisal of potential tsunami hazards.

Acknowledgments. This work was made possible by a Department of Civil Protection/GNV grant to M.M. Most of the data presented were acquired within the IOC/UNESCO Training Through Research Programme during cruises TTR12 and TTR14 aboard the *R/V Professor Logachev*; our sincere thanks go to the crew and shipboard scientific party.

REFERENCES

- Baldi, P., M. Fabris, M. Marsella, and R. Monticelli (2005), Monitoring the morphological evolution of the Sciara del Fuoco during the 2002–2003 Stromboli eruption using multi-temporal photogrammetry, *ISPRS J. Photogramm. Remote Sens.*, **59**(4), 199–211.
- Baldi, P., A. Bosman, F. L. Chiocci, M. Marsella, C. Romagnoli, and A. Sonnessa (2008), Integrated subaerial–submarine morphological evolution of the Sciara del Fuoco after the 2002 landslide, this volume.
- Bertagnini, A., and P. Landi (1996), The Secche di Lazzaro pyroclastics of Stromboli volcano: A phreatomagmatic eruption related to the Sciara del Fuoco sector collapse, *Bull. Volcanol.*, **58**(2–3), 239–245.
- Bonaccorso, A., S. Calvari, G. Garfi, L. Lodato, and D. Patané (2003), Dynamics of the December 2002 flank failure and tsunami at Stromboli volcano inferred by volcanological and geophysical observations, *Geophys. Res. Lett.*, **30**(18), 1941, doi:10.1029/2003GL017702.
- Calvari, S., L. Spampinato, L. Lodato, A. J. L. Harris, M. R. Patrick, J. Dehn, M. R. Burton, and D. Andronico (2005), Chronology and complex volcanic processes during the 2002–2003 flank eruption at Stromboli volcano (Italy) reconstructed from direct observations and surveys with a handheld thermal camera, *J. Geophys. Res.*, **110**, doi:10.1029/2004JB003129.
- Elverhøi, A., D. Issler, F. V. De Blasio, T. Ilistad, C. B. Harbitz, and P. Gauer (2005), Emerging insights into the dynamics of submarine debris flows, *Nat. Hazards Earth Syst. Sci.*, **5**, 633–648.
- Gamberi, F., and M. Marani (2007), Downstream evolution of the Stromboli slope valley (southeastern Tyrrhenian Sea), *Mar. Geol.*, **243**, 180–199.
- Ilistad, T., D. Issler, and J. G. Marr (2004), Subaqueous debris flow behaviour and its dependence on the sand/clay ratio: A laboratory study using particle tracking, *Mar. Geol.*, **213**, 415–438.
- Kessler, L. G., and J. H. Bédard (2000), Epiclastic volcanic debrites—Evidence of flow transformations between avalanche and debris flow processes, Middle Ordovician, Baie Verte peninsula, Newfoundland, Canada, *Precambrian Res.*, **101**, 135–161.
- Kokelaar, P. and C. Romagnoli (1995), Sector collapse, sedimentation and clast population evolution at an active island-arc volcano: Stromboli, Italy, *Bull. Volcanol.*, **57**, 240–262.
- Landi, P., N. Metrich, A. Bertagnini, M. Rosi (2004), Dynamics of magma mixing and degassing recorded in plagioclase at Stromboli (Aeolian Islands, Italy), *Contrib. Mineral. Petrol.*, **147**, 213–227.
- Maramai, A., L. Graziani, and S. Tinti (2005), Tsunamis in the Aeolian Islands (southern Italy): A review, *Mar. Geol.*, **215**, 11–21.
- Masson, D. G., A. B. Watts, M. J. R. Gee, R. Urgeles, N. C. Mitchell, T. P. Le Bas, and M. Canals (2002), Slope failures on the flanks of the western Canary Islands, *Earth Sci. Rev.*, **57**, 1–35.
- Masson, D. G., C. B. Harbitz, R. B. Wynn, G. Pedersen, and F. Lovholt (2006), Submarine landslides: Processes, triggers and hazard prediction, *Philos. Trans. R. Soc. Ser. A*, **364**, 2009–2039.
- McLeod, P., S. Carey, and R. S. J. Sparks (1999), Behaviour of particle-laden flows into the ocean: Experimental simulation and geological implications, *Sedimentology*, **46**, 523–536.
- Metrich, N., A. Bertagnini, P. Landi, and M. Rosi (2001), Crystallization driver by decompression and water loss at Stromboli volcano (Aeolian Islands, Italy), *J. Petrol.*, **42**, 1471–1490.
- Mohrig, D., and J. G. Marr (2003), Constraining the efficiency of turbidity current generation from submarine debris flows and slides using laboratory experiments, *Mar. Pet. Geol.*, **20**, 883–899.
- Moore, J. G., D. A. Clague, R. T. Holcomb, P. W. Lipman, W. R. Normark, and M. E. Torresan (1989), Prodigious submarine landslides on the Hawaiian Ridge, *J. Geophys. Res.*, **94**, 17,465–17,484.
- Moore, J. G., W. R. Normark, and R. T. Holcomb (1994), Giant Hawaiian landslides, *Annu. Rev. Earth Planet. Sci.*, **22**, 119–144.
- Mulder, T., and J. Alexander (2001), The physical character of subaqueous sedimentary density flows and their deposits, *Sedimentology*, **48**, 269–299.
- Mulder, T., and P. Cochonat (1996), Classification of offshore mass movements, *J. Sediment. Res.*, **66**, 43–57.
- Ollier, G., P. Cochonat, J. F. Lènat, and P. Labazuy (1998), Deep-sea volcanioclastic sedimentary systems: An example from La Fournaise volcano, Réunion Island, Indian Ocean, *Sedimentology*, **45**, 293–330.
- Pino, N. A., M. Ripepe, and G. B. Cimini (2004), The Stromboli Volcano landslides of December 2002: A seismological description, *Geophys. Res. Lett.*, **31**, L02605, doi:10.1029/2003GL018385.
- Rosi, M., A. Bertagnini, P. Landi (2001), Onset on the persistent activity of Stromboli volcano (Italy), *Bull. Volcanol.*, **62**, 294–300.
- Schneider, J. L., F. J. Pérez Torrado, D. G. Torrente, P. Wassmer, M. C. C. Santana, and J. C. Carracedo (2004), Sedimentary signatures of the entrance of coarse-grained volcanioclastic flows into the sea: The example of the breccia units of Las Palmas Detritic Formation (Mio-Pliocene, Gran Canaria, Eastern Atlantic, Spain), *J. Volcanol. Geotherm. Res.*, **138**, 295–323.
- Sohn, Y. K. (2000), Coarse-grained debris-flow deposits in the Miocene fan deltas, S. E. Korea: A scaling analysis, *Sediment. Geol.*, **130**, 45–64.
- Sohn, Y. K., M. Y. Choe, and H. R. Jo (2002), Transition from debris flow to hyperconcentrated flow in a submarine channel (the Cretaceous Cerro Toro Formation, southern Chile), *Terra Nova*, **14**, 405–415.

- Tibaldi, A. (2001), Multiple sector collapses at Stromboli volcano, Italy: How they work, *Bull. Volcanol.*, **63**, 112–125.
- Tinti, S., G. Pagnoni, and F. Zaniboni (2003), Tsunami generation in Stromboli Island and impact on the south-east Tyrrhenian coasts, *Nat. Hazards Earth Syst. Sci.*, **3**(5), 299–309.
- Tinti, S., A. Manucci, G. Pagnoni, A. Artigliato, and F. Zaniboni (2005), The 30 December 2002 landslide-induced tsunamis in Stromboli: Sequence of events reconstructed from the eyewitness accounts, *Nat. Hazards Earth Syst. Sci.*, **5**, 763–775.
- Tinti, S., G. Pagnoni, and F. Zaniboni (2006), The landslides and tsunamis of the 30th of December 2002 in Stromboli: Analysed through numerical simulations, *Bull. Volcanol.*, **68**, 462–479.
- Trofimovs, J., L. Amy, G. Boudon, C. Deplus, E. Doyle, N. Fournier, M. B. Hart, J. C. Komorowski, A. Le Friant, E. J. Lock, C. Pudsey, G. Ryan, R. S. J. Sparks, and P. J. Talling (2006), Submarine pyroclastic deposits formed at the Soufrière Hills volcano, Montserrat (1995–2003): What happens when pyroclastic flows enter the ocean?, *Geology*, **34**(7) 549–552, doi:10.1130/G22424.1.
- Wessel P., and W. H. F. Smith (1995), New version of the Generic Mapping Tool released, *Eos Trans. AGU*, **329**.
- Wynn, R. B., and D. G. Masson (2003), Canary Islands landslides and tsunami generation, in *Proceedings of the 1st International Symposium on Submarine Mass Movements and Their Consequences*, edited by J. Mienert and J. Locat, pp. 325–332, Springer, Dordrecht.
-
- A. Bertagnini and A. Di Roberto, Istituto Nazionale di Geofisica e Vulcanologia, Sezione di Pisa, Via della Faggiola 32, 56126 Pisa, Italy.
- F. Gamberi and M. P. Marani, Istituto di Scienze Marine–CNR, Sede di Geologia Marina di Bologna, Via Gobetti 101, 40129 Bologna, Italy. (michael.marani@bo.ismar.cnr.it)
- M. Rosi, Dipartimento di Scienze della Terra, University of Pisa, Via S. Maria 53, 56126 Pisa, Italy.

Integrated Subaerial–Submarine Morphological Evolution of the Sciara del Fuoco After the 2002 Landslide

Paolo Baldi,¹ Alessandro Bosman,² Francesco Latino Chiocci,³ Maria Marsella,⁴ Claudia Romagnoli,⁵ and Alberico Sonnessa⁴

In December 2002, an effusive eruption at Stromboli triggered a complex instability phenomenon, which affected both the subaerial and submarine portion of the Sciara del Fuoco slope, causing destructive landslide(s) and tsunami waves. Among the monitoring activities coordinated by the Italian Civil Defence Department, systematic photogrammetric and bathymetric surveys were carried out. Digital photogrammetry technique and multibeam soundings were used to obtain high-resolution digital elevation model of land and sea-floor surface of the NW flank of Stromboli (Sciara del Fuoco depression). Merging the subaerial and submarine data, and comparing multitemporal digital models, we first estimated the mass volumes involved in the failures of the subaerial and shallow submarine slope to be about $24 \times 10^6 \text{ m}^3$, and then, we monitored the continuous and relevant morphological changes induced by erosional–depositional processes during the various syneruptive and posteruptive stages. Filling processes of the scar by lava flow and debris and the morphological evolution of the slope in the 2 years after the event were described.

1. INTRODUCTION

¹ University of Bologna, Dip. Fisica, Viale Berti Pichat 8, Bologna, Italy.

² CNR Istituto di Geologia Ambientale e Geo-Ingegneria, Roma, Italy.

³ University “La Sapienza”, Dip. Scienze della Terra, Roma, Italy.

⁴ University “La Sapienza”, Dip. Idraulica, Trasporti e Strade, Roma, Italy.

⁵ University of Bologna, Dip. Scienze della Terra e Geologico-Ambientali, Bologna, Italy.

The monitoring of morphological changes in volcanic areas provides a fundamental contribution to the understanding of the dynamics of the volcanic system during the eruptions and in posteruptive stages. As pointed out by *Thouret* (1999), “rates of geomorphic processes acting at all scales on volcanoes need to be measured in order to reinforce the process-oriented aspect of volcanic geomorphology”. To document and quantitatively describe the morphological evolution induced by volcanic constructional and destructive processes, such as emplacement of lava flows, calderic collapses, gravitational instabilities, it is necessary to produce and compare multitemporal digital elevation models (DEM). On dangerous or inaccessible areas, a number of techniques based on remote-sensing sensors that can acquire 3D high-resolution data, such as airborne laser scanning and aerial photogrammetry, could be adopted for DEM extraction [Baldi *et al.*,

2002; *Haugerud et al.*, 2004]. For submarine areas, evolving acoustic techniques as interferometric or multibeam bathymetric surveys allow nowadays to investigate the seafloor with increasing detail and full coverage.

In this work, we present the result of the integration of photogrammetric and bathymetric surveys carried out before, during and after the 2002–2003 eruptive crisis at Stromboli, which was accompanied by a tsunamigenic submarine/subaerial landslide event at its beginning.

On 30 December 2002, after a period characterized by anomalous explosions and 2 days of relevant lava flows emitted from vents located below the NE crater [*Bonaccorso et al.*, 2003; *Calvari et al.*, 2005], a large-scale slope failure occurred triggering tsunami waves that propagated around Stromboli and on nearby islands, being felt as far as the Campanian, Calabrian, and Northern Sicily coast [*Maramai et al.*, 2005]. The reconstruction of the landslides, presented in full detail in *Tommasi et al.* (2005 and this volume) and in *Chiocci et al.* (2008a), was possible, thanks to the integration of data and knowledge from different research fields such as marine geology, applied geophysics, geotechnics, and volcanology.

The comparison of photogrammetric and bathymetric data collected before the 2002–2003 eruption and instability phenomena and those acquired a few days after the beginning of the eruption concurred to define the geometry and to estimate the mass volumes involved in the 30 December slope failure of the subaerial and submerged part of Sciara del Fuoco [*Baldi et al.*, 2005; *Chiocci et al.*, 2008a].

After the landslide, lava flowed along the slope mainly inside the scar and reached the sea building up a lava delta. Lava flows stopped entering the sea on mid-February 2003, while the eruption ended at mid-July of the same year. Nevertheless, in the months following the landslide, lava flows from a variable number of vents, together with moderate-sized landslides and rockfalls, continued to descend along Sciara del Fuoco. At the end of the eruption, the Sciara del Fuoco slope appeared strongly modified with respect to that observed before the eruption; the summit volcanic activity returned typically Strombolian-type, with variations in the intensity and frequency of explosions within normally observed limits.

Syneruptive photogrammetric and bathymetric surveys allowed the monitoring of continuous and relevant morphological changes induced both by the lava flow emplacement and by erosional–depositional processes during the eruptive crisis. Posteruptive stage data discussed in this paper are relevant to the first 2.5 years after the eruption, i.e., until the end of 2005. Surveys performed in the following months/years allowed to monitor the progression of erosional processes (such as minor landslides from the steep and unstable

flanks of the slide) and the morphological readjustment of the subaerial [*Baldi et al.*, 2008] and submarine [*Chiocci et al.*, 2008b] slopes, including the gradual scar infilling. Figure 1 shows the temporal distribution of the photogrammetric and bathymetric surveys carried out from 2001 to 2005. In 2007, a new eruption occurred constructing a large lava delta at the foot of Sciara del Fuoco and influenced the natural re-adjustment of the slope. New surveys were performed; however, our reconstruction do not encompasses the 2007 syneruptive and posteruptive periods.

2. FIELD SURVEYS AND DATA PROCESSING

2.1. Photogrammetry

In the frame of a research project of the Italian “National Group for Volcanology” (GNV), devoted to the development and application of remote sensing methods for the monitoring of active Italian volcanoes [*Baldi et al.*, 2006], at the end of May 2001, an aerial photogrammetric survey of Stromboli Island was carried out. The flight height, between the 900- and 1500-m above sea level (asl), concurred to obtain stereo images at a mean scale of about 1:5000 georeferenced by means of a GPS ground control network.

After the 30 December landslide and during the whole eruption period, Civil Protection Department coordinated the monitoring activities including also frequent aerial photogrammetric surveys. During the eruption, as a consequence of bad weather conditions or poor visibility on the flank, only 13 surveys were carried out [*Baldi et al.*, 2005]. The acquired images covered the NW side of the Island, furnishing stereo pairs over the Sciara del Fuoco and its surrounding area. Full stereoscopic coverage, including also the volcano top area up to 900 m asl, was obtained only starting from 21 February 2003. After the end of the eruption, additional photogrammetric surveys were performed in order to monitor the progression of erosion processes, such as minor landslides, small slumps and falls from the steep and unstable flanks of the slide, which continuously covered the lava flows along the subaerial slope with debris and filled in the submarine depression [*Baldi et al.*, 2008].

All the images, initially acquired on film, were digitized for being processed on a digital photogrammetry workstation obtaining a geometric resolution of 25 µm. This allowed dealing with ground pixel dimensions ranging from 15 to 40 cm in function of the relative image scale. In Table 1, the characteristics of all the available surveys are listed, evidencing those adopted for the analysis described in this paper.

Digital photogrammetry processing is based on image matching algorithms [*Kraus*, 1997; *Heipke* 1995] whose

Table 1. Date and Main Parameters of the Aerial Photogrammetric Surveys Until 2005

N°	Date	Film	Coverage	Photo Scale	Ground Resolution, m	Quality
1	29 May 2001	Color	ISLAND	1:5,000	0.13	High
2	05 Jan. 2003	B/W	SCIARA (0-650 m)	1:17,000	0.41	Poor
3	16 Jan. 2003	Color	SCIARA (0-400 m)	1:5,000	0.13	Fair
4	20 Jan. 2003	B/W	SCIARA (0-600 m)	1:8,000	0.20	Fair
5	27 Jan. 2003	B/W	SCIARA (0-600 m)	1:5,000	0.13	Good
6	06 Feb. 2003	B/W	SCIARA (0-600 m)	1:5,000	0.13	Fair
7	07 Feb. 2003	B/W	SCIARA (0-600 m)	1:8,000	0.20	Fair
8	21 Feb. 2003	B/W	SCIARA (0-600 m)	1:7,000	0.17	Fair
9	15 Mar. 2003	B/W	SCIARA (0-800 m)	1:7,000	0.17	Good
10	14 Apr. 2003	B/W	SCIARA (0-800 m)	1:13,000	0.32	Good
11	16 Apr. 2003	B/W	SCIARA (0-800 m)	1:8,000	0.20	Good
12	26 May 2003	Color	ISLAND	1:5,000	0.13	Good
13	16 Jun. 2003	B/W	SCIARA (0-800 m)	1:7,000	0.17	Fair
14	26 Jul. 2003	Color	SCIARA (0-800 m)	1:7,000	0.17	Good
15	04 Sep. 2003	B/W	SCIARA (0-800 m)	1:7,000	0.17	Good
16	04 Aug. 2004	Color	ISLAND	1:8,000	0.20	Good
17	02 Oct. 2005	Color	SCIARA	1:8,000	0.20	Fair

Acquisition time ranges between 1.00 and 4.00 pm to minimize shadow effects on the Sciara Slope.

capability to work at subpixel level allows to extract three-dimensional point measurements characterized by centimeter-level internal accuracy, in case of image scale large than 1:5000. Thus, the final precision of digital products (DEMs and orthophotos) depends on the robustness of the correlation algorithm and on the image geometric and radiometric resolution. In our case on smooth terrains and in good illumination conditions, we can expect to reach an accuracy ranging from 0.1 to 0.5 m, as also demonstrated by previous experiences performed on other volcanic areas [Baldi *et al.*, 2000, 2002]. The data presented in this paper were obtained using the Helava approach implemented into the DPW710 photogrammetric station [Muller *et al.*, 1992], which adopts a digital image matching procedure based on well-defined shape comparison techniques and grey level correspondence [Kraus, 1997].

A 5-m grid DEM and relative orthophoto were generated from images collected during each surveys. The data were filtered and validated using a supervised editing procedure conducted directly on the stereomodels, especially in the areas affected by shadowing or poor illumination, presenting very irregular morphological features and covered by vegetation. These procedures improve the quality of the DEM permitting to eliminate outliers and to measure new points to reconstruct the continuity of the ground surface.

The photogrammetric models used for DEMs generation at different epochs were all georeferenced in the same reference frame in order to perform a quantitative multitemporal analysis, which describes the surface modifications. Due to the impossibility of measuring a ground control network during the emergency period, this was accomplished by identi-

fying a posteriori well-defined natural control points visible on all the multitemporal models, whose coordinates have to be known in an external and stable (fixed in time) reference system. In our case, these points were identified outside the Sciara area and were measured on the models from the 2001 survey, which represents the reference dataset for the whole analysis. The 2001 survey was oriented with a rigorous approach by a GPS ground point network linked to GPS reference stations outside the island. The GCP control network was then remeasured in May 2003 to check its stability, and additional control points were established. The coordinates were then computed in the UTM-WGS84 system [Baldi *et al.*, 2006].

2.2. Bathymetry

In the framework of the Italian National Group for Volcanology (GNV) research activities, a pre-slide survey was carried out down to a depth of 1000 m, 10 months before the landslide event (February 2002). The first post-slide survey was carried out as soon as meteorological conditions allowed it (10 days after the landslide, on 9 January 2003) onboard a Coast Guard small vessel (CP 875) after the installation of a multibeam transducer on a movable, on purpose-made frame.

Serial multibeam surveys (Figure 1) have been carried out later on, onboard Italian oceanographic ships (*R/V Urania*, *Universitatis*, and *Thetis*) or by using smaller boats for shallow water surveys. These surveys allowed to monitor the morpho-sedimentary evolution of the landslide scar and to estimate the volumes of the infilling mass [Chiocci *et al.*,

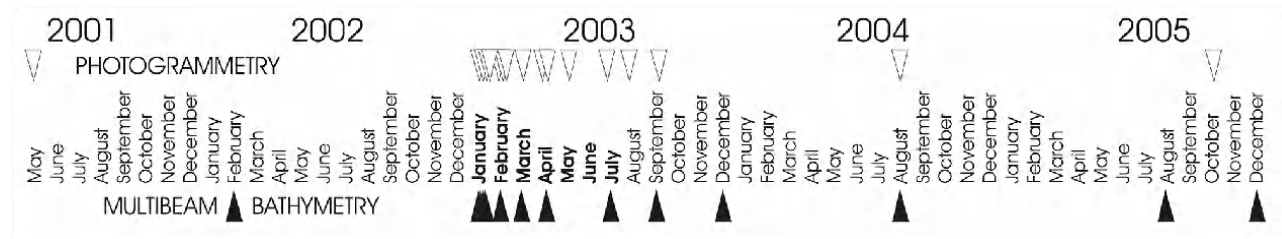


Figure 1. Multibeam marine and photogrammetric subaerial surveys performed on Sciara del Fuoco before, during and after the 2002–2003 eruption (months of the eruptions period are in bold).

2008a and 2008b]. Most of the post-slide surveys were directly funded by the Italian Civil Protection Department, the other ones were realized during transfer passages in the framework of other research projects, the last surveys were part of a specific project for Stromboli monitoring. In Table 2, all multibeam surveys, including those used for this study, are reported with the relevant technical details.

Differential GPS positioning was commonly adopted for georeferencing the surveys; two of them were positioned through real-time kinematic (RTK-GPS) and referred to a ground control point included in the photogrammetric GCP network.

DGPS positioning was used mainly during the deeper bathymetric surveys. In this case, the correspondence between the subaerial and submarine surfaces was assessed a posteriori, mainly verifying the congruency among morphological features. All data were then transformed in the UTM-WGS84 system.

The bathymetric surveys were carried out with Seabat multibeam systems at different resolutions, namely, 8125

(455 kHz) and 8101 (240 kHz) in shallow water and 8111 (100 kHz) and 8160 (50 kHz) in deep water.

Usually DEMs are generated by means of proprietary software (in this case of Reson PDS 2000, <http://www.reson.nl>), which adopt standard procedures based on statistically corrected grid data (thus averaging spikes and good soundings), increasing the cell size (thus lowering morphological resolution). Acquisition steps generally include: sound velocity profiling within the investigation area, patch test on specific targets through different surveys, redundant overlapping between swaths, acquisition along contours, with ship velocity varying with water depth. In this case, the processing was performed with “nonstandard” procedures. The raw data have been stored in XTF files and post-processed by using dedicated software (i.e., Caris Hips and Sips, <http://www.caris.com>) that recalculated all the ancillary data (navigation, patch test, instrumental offsets, tide gauge, and sound velocity profiler interpolation by nearest distance and/or in time etc.). Processing protocol then included: (a) removal of spikes and signal drift from navigation; (b) application

Table 2. List and Details of the Multibeam Surveys Carried out Offshore Sciara del Fuoco Until 2005

Survey	Date	Minimum Depth	Maximum Depth	Vessel	Positioning	Swath Angle	Frequency, kHz
Vulcan.it	24/02/02	-12	-1000	Thetis	DGPS	150°	100
Original*	30/12/02	-20	-320	-	-	-	-
CCE1	9/01/03	-20	-320	CP875	DGPS	150°	240
CCE2	15/01/03	-100	-1800	CP875	DGPS	150°	50
CCE3	20/01/03	-0.5	-120	CP875	DGPS	120°	455
ISMAR	18/01/03	-25	-1000	Thetis	DGPS	150°	240
Iddu	2/02/03	-38	-320	Urania	DGPS	150°	240
Iddutù	22/03/03	-10	-1000	Thetis	DGPS	150°	100
Iddutri	6/04/03	-10	-1000	Thetis	DGPS	150°	100
Iddufor	24/07/03	-0.5	-320	Alsea	RTK	120°–150°	240–455
Eleonora	26/09/03	-38	-2600	Urania	DGPS	150°	50
Iddufaiv	14/12/03	-0.5	-120	Alsea	RTK	120°	455
Iddusics	10/08/04	-20	-2600	Universitatis	DGPS	150°	50
Iddubos	11/08/05	-10	-600	Universitatis	DGPS	150°–120°	50–455
1908	01/12/05	-30	-500	Universitatis	DGPS	150°–120°	50–455

Asterisk refers to the original scar surface, virtually reconstructed by means of considerations exposed in the text.

of sound velocity profile in time stamp and nearest distance mode; (c) first manual despike across and along track on single swath (d) patch test on calibration line and check on overlapping soundings data line; (e) tide gauge correction; (f) further manual despike on all sounding line; (g) statistical filters based on depth standard deviation; (h) generation of digital elevation model by using weighted average, obtained by devalue of grazing angle average interpolation algorithms [Vásquez, 2007].

The precision of marine digital models is highly variable, depending first by positional modes and second by sensor frequency (in relation with depth). For GPS-RTK positioning in shallow water (from 0.5 to 50 m), we obtained a horizontal precision of ± 0.1 m and depth precision of ± 0.2 m (with tide gauge in situ); the maximum grid size is 0.5 m (with depth standard deviation of 0.2 m). In deeper water (from 50 to 300 m), DGPS positioning furnished a horizontal precision of ± 1 m, but depending to the footprint size, the grid size is 1 m (with depth standard deviation of 0.4 m).

3. DATA ANALYSIS AND DISCUSSION

3.1. Comparison Between Pre-Slide and Post-Slide Digital Terrain Models

Plate 1 shows the Sciara del Fuoco setting before (a, c) and after (b, d) the 30 December landslide. The map of residuals, obtained by subtracting the pre-slide and post-slide digital models, is also depicted. On the subaerial portion, the scar appears disarticulated into two different slabs (landslides β and γ in Tommasi *et al.* 2005 and this volume). At the coastline, the scar width appears reduced on its subaerial portion towards the NE side, due to the presence (at the time of the survey) of a sector of the slope that was later progressively removed. The shallower bathymetric surveys show a huge sub-circular slide scar, about 600 m wide and over 45 m deep, which can be related to the slide responsible for the tsunami event.

Volumetric estimates relevant to the landslide have been computed and are summarized in Table 3. By differencing the two subaerial DEMs (May 2001–January 5, 2003), the depression volume in the scar was estimated to be approximately 9×10^6 m³ [Baldi *et al.*, 2005; Marsella *et al.*, this volume] for the subaerial part. The total mass displaced on the 30 December resulted in 13.5×10^6 m³, accounting for a volume of 1.2×10^6 m³ attributed to the lava flow (flow b in Baldi *et al.*, 2005) emplaced on the surface of the future landslide in the first 2 days of the eruption, and for a volume of 3.3×10^6 m³ of the lava flow (flow c in Baldi *et al.*, 2005) that filled the scar between 30 December and 5 January (date

of the first photogrammetric survey). These estimates were obtained using a semiquantitative approach, based on extrapolated geometry of the lava flow field based the analysis of images acquired from helicopter and on average effusion rate obtained for the lava flow which was not involved in the landslide (flow a in Baldi *et al.*, 2005).

A bathymetric survey was performed a few days after the landslide (9 January 2002); detailed analyses were performed both on shallow-water (from -20 to -350 m) and deep-water (from -350 to over -1000 m) areas [Chiocci *et al.*, 2008a]. By comparison with the bathymetric survey carried out 10 months before the event (February 2002), the scar geometry and volumes of the failed mass were reconstructed.

From the comparison of pre-slide and post-slide DEMs, the material mobilized by the submarine slide down to -350 m is about 9.3×10^6 m³ (Table 3).

At the time of the first survey, the scar was empty except for a small depositional bulge due to the lava delta flow inside it. An “original” base surface was thus reconstructed by restoring the regularly concave surface in a section parallel to the coast and the original trend of isobaths in plan view. By subtracting this extrapolated surface from the bathymetry of the first survey, it has been hypothesized that 10 days after the event, i.e., on 9 January 2003, about 15% of the scar was filled by the submarine part of the first lava delta. This should prolong down to 150–180 m below sea level (bsl) as a wedge-shaped body, having a maximum thickness about 34 m offshore of the main entry point of lava flow to the sea; its volume was estimated as about 1.56×10^6 m³ [Chiocci *et al.*, 2008a; Table 3].

On the whole, the rock volume involved in the 30 December landslide (subaerial slope and shallow submarine) resulted in 24.4×10^6 m³, taking into account the volume of lava flows accumulated from the beginning of the eruption (December 28) to the date of the first surveys [Tommasi *et al.*, 2005].

It has to be noticed that while the data collected both on land and at sea have a very high precision [see Chiocci *et al.*, 2008a, Baldi *et al.*, 2005 for details], their uncertainties propagated to volume estimates providing a final error that has been estimated to not exceed 10%, the main source of error being the difficult discrimination between the areas influenced by lava accumulation and those more affected by debris erosion/accumulation processes.

3.2. Sciara del Fuoco Evolution

The availability of 16 photogrammetric and 14 bathymetric surveys before, during, and after the eruption period (Tables 1 and 2), made it possible to adequately monitor the erosional–depositional processes affecting the slope and the lava flow field evolution on the Sciara.

Table 3. Volumetric Estimations of the Landslide (in 10^6 m^3) in the Subaerial and Shallow-Water Parts (Down to -350 m) Derived From First Surveys (January, 5 on Land and January, 9 Offshore)

	Subaerial	Submarine
Scar volume at the time of first surveys	9	9.3
Volumes of lava flows emplaced from the eruption beginning to the time of the first surveys	4.5	1.56
Total volume displaced by the landslide	13.5	10.86

After the landslide, lava flowed within the slide scar from a new vent located at about 500–600 m above sea level, reached the sea, and accumulated along the coastline. In the first period, frequent changes in direction of the lava that flows from this vent [Calvari *et al.*, 2005] caused significant increase in the width and thickness of the lava flow field accumulated within the submarine scar [Chiocci *et al.*, 2008a].

At mid-February 2003 the lava flow stopped entering the sea and remained confined in a mid-slope field starting to build up lava terrace at about 600 m asl. During this stage, lava blocks often detached from the flow front in the upper subaerial slope and, rolling downslope, produced rock falls and grain flows. Finally, the eruption ended on 22 July of the same year. However, the morphological readjustment of the subaerial slope is a continuous process, after the end of the 2002–2003 eruption, the widening and upslope migration of the subaerial scar produced a large debris deposit at the foot of the slope and in the shallow water.

Plate 2 shows residual maps derived by the comparison of selected digital models. The slope evolution can be described according to the following stages:

- (a) During the first month after the landslide (Plate 2, a) accumulation areas (positive residuals) are present both on land and at sea, with maximum thickness of more than 20 m. On the submarine scar, lava mainly accumulated in the NE side. Erosion areas (negative residuals) are visible along the walls of the subaerial scar, caused by rock falls and small-scale slides which removed material up to some 10–20 m of thickness.
- (b) During the period end of January to mid-March (Plate 2, b), on the SW side of Sciara del Fuoco, the main landslide scarp continued to be eroded towards the crater area, forming deep gullies. The morphological readjustment of the subaerial slope continued, and the boundary of the scar enlarged, so that rockfalls and small landslides receded and concentrated mostly on the upper part of the scar. A lava flow developed at the very NE boundary of the subaerial slope, without reaching the coastline. On the marine part in this period, there is still a small amount of lava entering the sea until mid-February, but most of the positive re-

sidual is produced by slope readjustment. The debris tongues rest both on the submarine and on the lower subaerial slope within the scar, as witnessed by the marked continuity of residuals above and below sea level. The positive residuals show a shift in depocenters from SW to NE reflecting the migration of lava flows observed at the foot of the slope until mid-February [Chiocci *et al.*, 2008b].

- (c) From mid-March to mid-April (Plate 2, c), the most relevant differences are visible in the subaerial portion where the lava accumulated mainly in the upper sector of the slope, due to the marked reduction of the effusion rate. However, a small amount of debris formed by lava blocks and by the erosion of the landslide scarps reached the submarine sector.
- (d) From mid-April to end of July (Plate 2, d), lava flows were still active and confined in the upper subaerial slope of Sciara del Fuoco, accounting for the large area corresponding to positive residuals which reach more than 15 m. However, the breaching of the flows produced debris accumulating in the underlying slope, both above and below the sea level. Here the debris bypassed the shallow water area, where deposits were already emplaced. While lava flow was active on the northernmost part of the scar, on the southernmost one, the slope readjustment continued with the progression of erosion on the upper subaerial slope and of accumulation at lower elevation down to the very shallow water.
- (e) After the end of the eruption (July 2003) and in the following year (Plate 2, e), the slope continued to modify. As a matter of fact, the main slope readjustment is no more located at the tip of the 2002 landslide scar, but is concentrated on the lower subaerial slope. Here the loose volcanic debris, accumulated within the scar, is eroded by wave action during major storms and deposited downwards. This process transfers a huge amount of material from the subaerial slope to the submarine one.
- (f) In the following year (2004–2005, Plate 2, f), reduced erosion is visible on the subaerial slope, while a limited positive residual (i.e., accumulated volume) is present in the submarine sector.

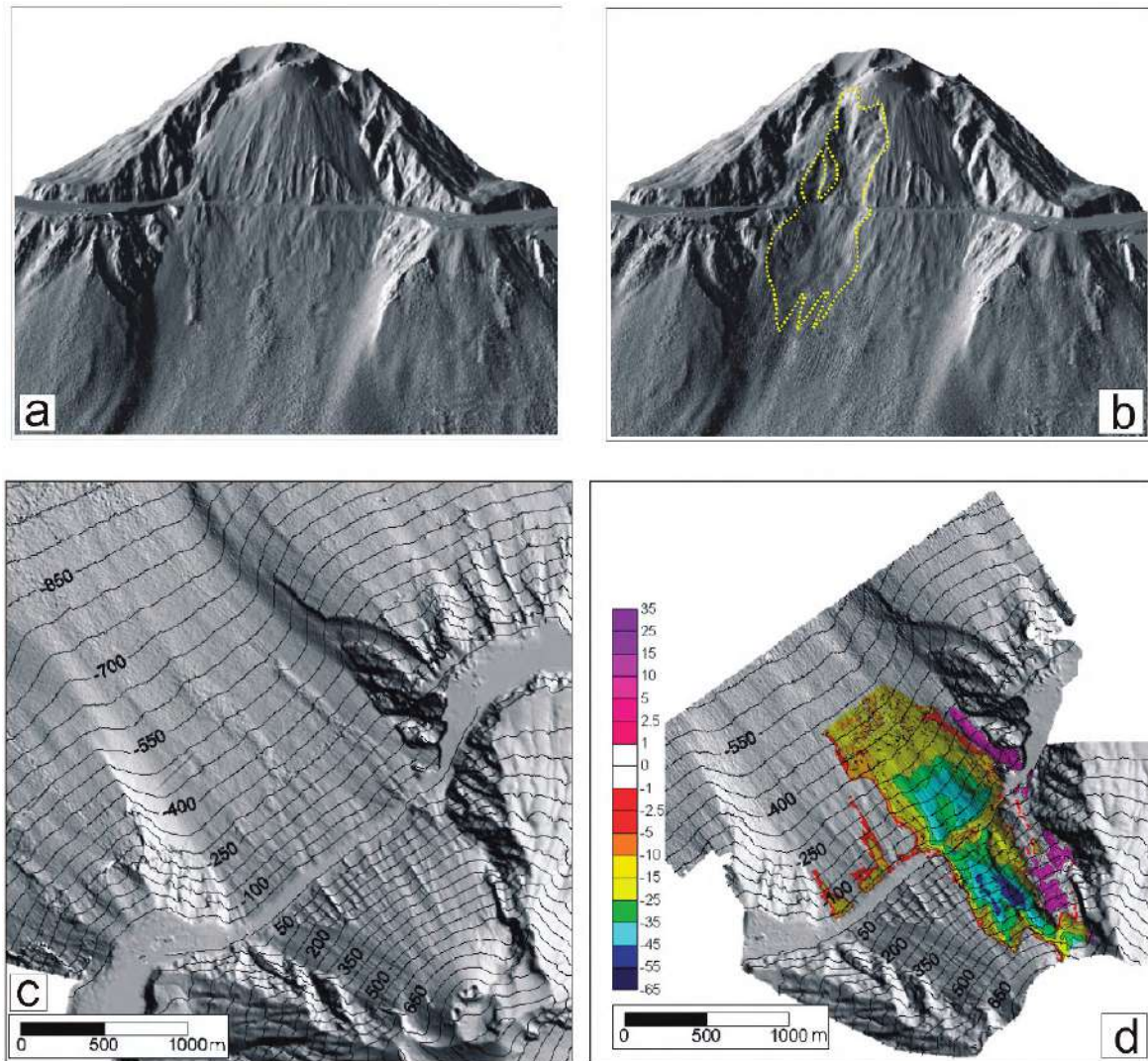


Plate 1. 3D and plan view of Sciara del Fuoco before (a, c) and after the landslide (b, d, with indication of the landslide scar limits and residual map between pre-event and post-event topography, respectively). Pre-slide digital models: 24 February 2002 (marine), 29 May 2001 (terrestrial); post-slide digital models: 9 January 2003 (marine), 5 January 2003 (terrestrial).

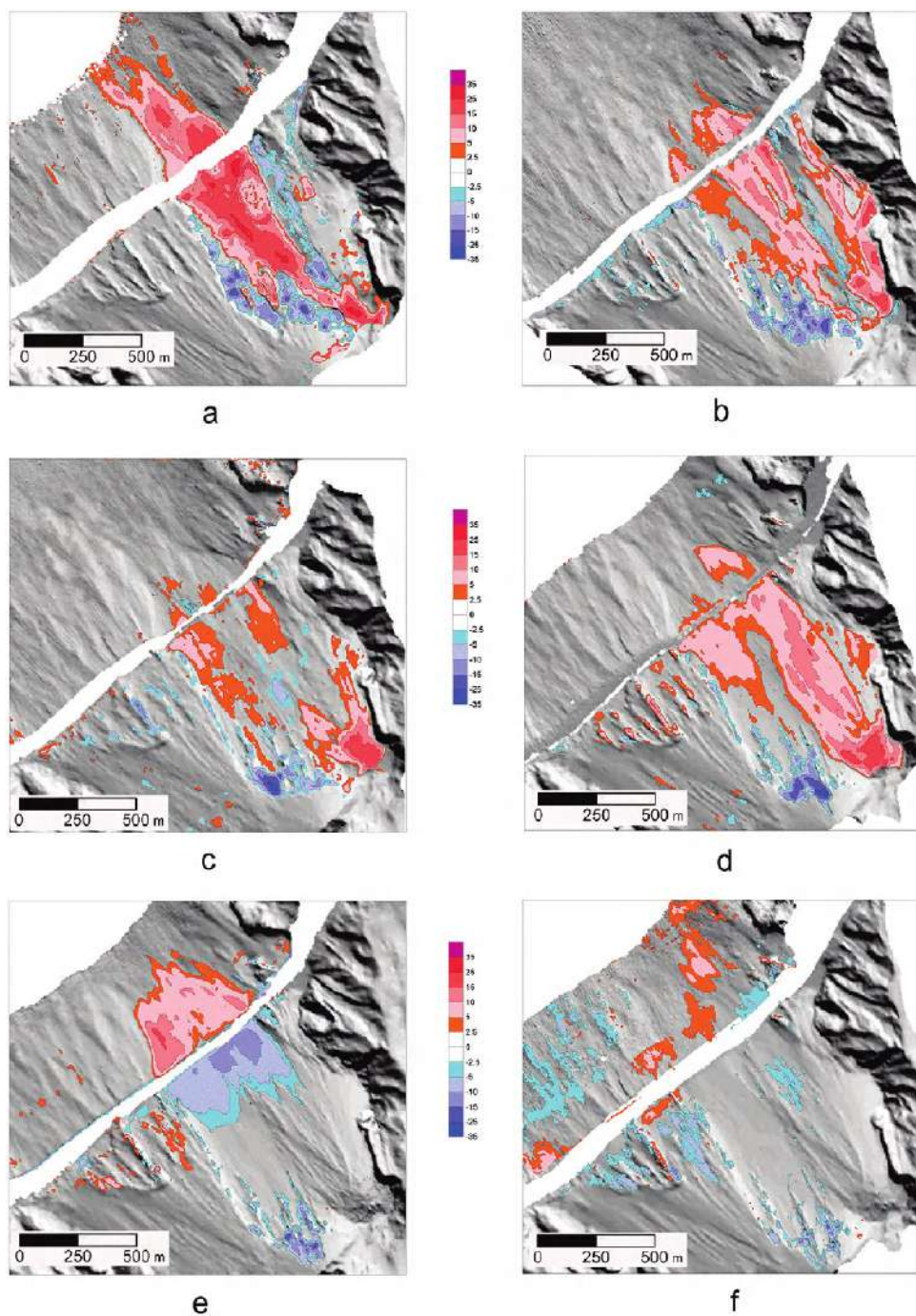


Plate 2. Residual maps (values in meters) derived from the comparison of subsequent surveys: (a) 27 January 2003 to 5 January 2003 for land, 2 February 2003 to 9 January 2003 for sea; (b) 15 March 2003 to 27 January 2003 for land, 22 March 2003 to 2 February 2003 for sea; (c) 16 April 2003 to 15 March 2003 for land, 6 April 2003 to 22 March 2003 for sea; (d) 26 July 2003 to 16 April 2003 for land, 24 July 2003 to 6 April 2003 for sea; (e) 4 August 2004 to 26 July 2003 for land, 10 August 2004 to 24 July 2003 for sea; (f) 2 February 2005 to 4 August 2004 for land, 1 December 2005 to 10 August 2004 for sea.

Its source appears to be confined in the very shallow water just above the deposit, where a small scar is only partially imaged by multibeam survey.

3.3. Differential and Cumulate Volumes

In Table 4 and in Figure 2, partial and cumulative volume differences between subsequent surveys, selected among those carried out on both the subaerial and submarine slope of Sciara del Fuoco, are reported. It can be noted that differential volumes tends to decrease with time from the eruption occurrence, becoming negative in the subaerial slope, as observed in the period 2003–2004. Cumulative volumes quickly increase in the first months after the landslide then, at the end of the eruption (July 2003), tends to stabilize around the value of $13 \times 10^6 \text{ m}^3$.

The whole evolution of the Sciara del Fuoco slope after the landslide is shown in Plate 3a. The lava flows, besides creating the lava terrace at 600 m asl close to the eastern side of Sciara del Fuoco, which partially filled the subaerial and submarine scar. A contribution to the scar infilling and to the morphological readjustment of the slope is also due to retrogressive erosion of the main landslide scarp towards the crater area. In Plate 3b, the morphological changes of the Sciara del Fuoco slope with respect to that observed before the landslide-eruption events are visible. The cumulative residuals show still a prevalent volume deficit, both in the subaerial and submarine slope, while the main accumulation by lava flows is responsible for positive residuals along the NE side of Sciara del Fuoco.

3.4. Erosional and Depositional Processes Within the Scar

The landslide that occurred on 30 December 2002 on the Sciara del Fuoco slope involved about $24.4 \times 10^6 \text{ m}^3$ if we limit the estimate to –350 m for the submarine extension. The availability of a multitemporal dataset of digital models describing both the subaerial and submarine slope morphol-

ogy allowed detecting and quantifying the superimposition of different processes that occurred during the post-slide evolution.

The total volume accumulated on the slope (lava flows emitted during the 2002–2003 eruptive crisis and debris due to erosional processes), estimated on the base of digital models comparison, is about $14 \times 10^6 \text{ m}^3$ [Baldi et al., 2005 and Chiocci et al., 2008a]. Lava flow emplacement greatly contributed to the scar's gradual infilling and to create a lava terrace of about $3 \times 10^6 \text{ m}^3$ at 600 m asl. On the submarine slope, the rate of infilling of the scar, due to lava flows entering the sea until mid-February 2003, has been estimated to be 50,000 m^3/day on average [Chiocci et al., 2008b].

During the eruption erosional–depositional processes affected both the subaerial and submarine portions of the slope. Erosion mainly involved progressive dismantling of the SW subaerial lateral scarp of the scar, removing up to $4.2 \times 10^6 \text{ m}^3$ through continuous minor slides and slumps. At least $1 \times 10^6 \text{ m}^3$ of remobilized debris partially filled the submarine scar in the period March to July 2003, corresponding to an infilling rate to some $2000 \text{ m}^3/\text{day}$. The decrease in the observed accumulation rate within the scar was due partly to temporary storage of debris along the coastal belt and partly to their sliding toward the deeper portion of the submarine slope.

In the post-eruption year (2003–2004), erosional processes on the subaerial flank remobilized some $1.3 \times 10^6 \text{ m}^3$ of debris especially at lower elevation; part of the removed debris (some $0.8 \times 10^6 \text{ m}^3$) accumulated in the first 200 m bsl within the submarine scar.

During the following year (2004–2005), erosional–depositional processes on the slope appear strongly reduced, testifying that the morphological readjustment was almost reached. Photogrammetric and bathymetric surveys carried out in the following years (2006 and 2007) did not show significant ongoing mass wasting. Major changes occurred at the beginning of 2007 when a new eruption started and a new lava delta was built.

Table 4. Partial and Cumulative Volume Differences Among Subsequent Surveys

Flight	Partial Vol. (10^6 m^3)	Cumulative Vol. (10^6 m^3)	Bathymetric Survey	Partial Vol. (10^6 m^3)	Cumulative Vol. (10^6 m^3)	Total Cumulative
May 01	–	–	24/02/02	–	–	–
05/01/03	–	–	09/01/03	–	–	–
27/01/03	2.20	5.50	02/02/03	1.12	2.68	8.18
15/03/03	2.25	7.75	22/03/03	0.63	3.31	11.06
16/04/03	0.75	8.50	06/04/03	-0.01	3.30	11.80
26/07/03	1.40	9.90	24/07/03	0.40	3.70	13.60
04/08/04	-1.30	8.60	10/08/04	0.77	4.47	13.07
02/10/05	0.0	8.60	01/12/05	0.22	4.69	13.29

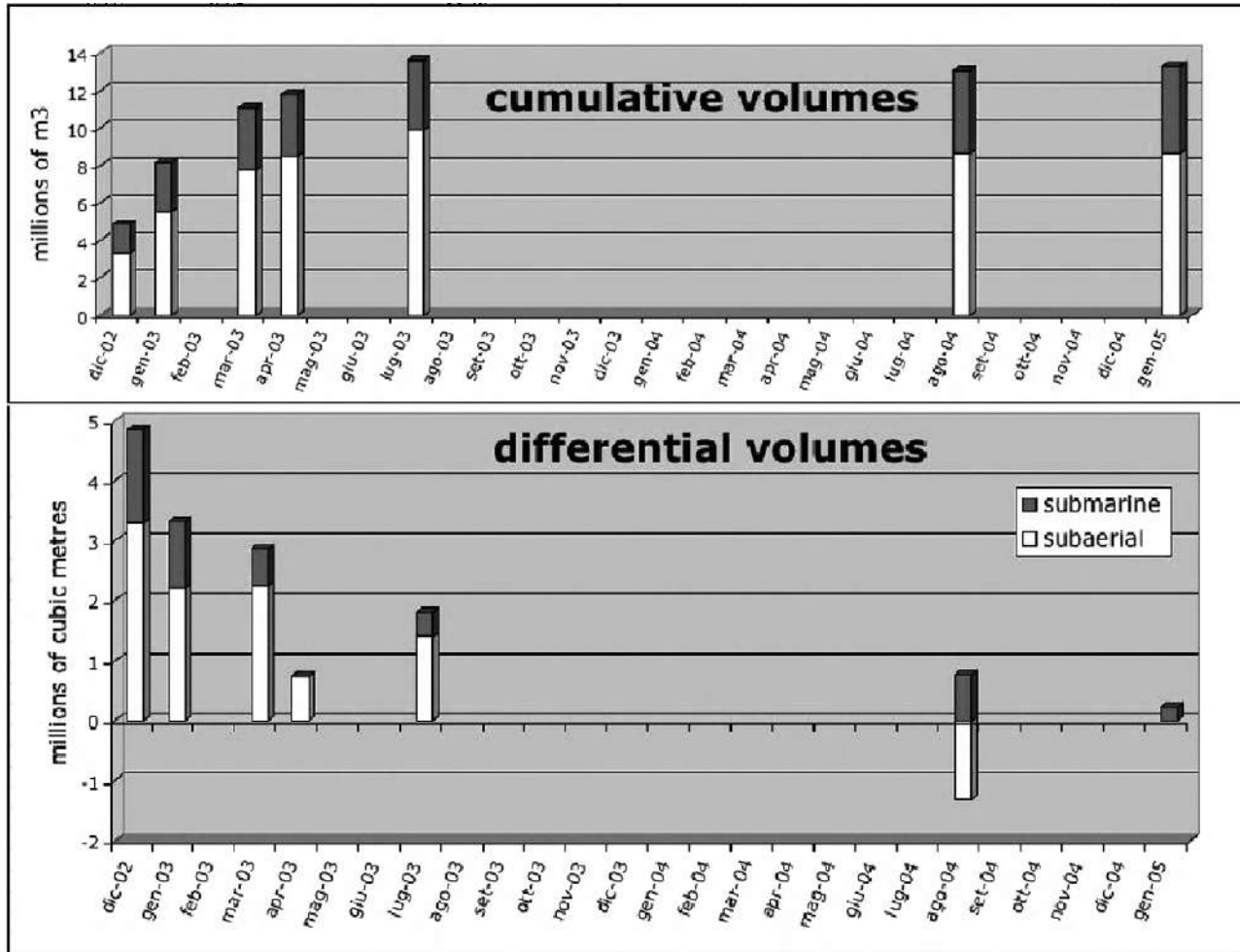


Figure 2. Cumulative and differential volumes estimated from digital models residuals on the subaerial and submarine slope of SdF.

4. CONCLUSIONS

Due to the need of the Civil Protection to first define causes and consequences of the tsunamogenic submarine landslide occurred at Stromboli on December 2002 and later on to monitor the evolution of the Sciara del Fuoco slope, a number of multibeam and aerophotogrammetric surveys were performed on the area. These furnished a unique opportunity to reconstruct the morphological features created by the instability phenomena and to follow the morphological recovering of the slide scar.

The total volume of the displaced mass by the 30 December 2002 landslide(s) is of about $24 \times 10^6 \text{ m}^3$. A further $7.7 \times 10^6 \text{ m}^3$ have been eroded on the seafloor deeper than 350 m by the transit of the failed mass. The landslide scar (extending

from about +650 m to -350 m with respect to sea level) was filled in both by lava flows (and related debris) and by the debris produced by the widening and smoothing of the harsh morphology left by the subaerial slide. When the lava ended entering the sea (mid-February 2003), the accumulation rate within the submarine scar sharply decreased to 1/20. On the subaerial scar, lava continued to accumulate until late July 2003 when eruption stopped and only a transfer of masses occurs between scar walls and the deeper portions of the scar. Noticeably, the debris produced on the subaerial slope accumulated on the coastal belt until it was eroded by wave action and distributed on the submarine slope.

In the 2 years after the event, i.e., in the time span dealt in by this article, the scar left by the December 2002 landslide was partially filled, even if its morphological evidence was

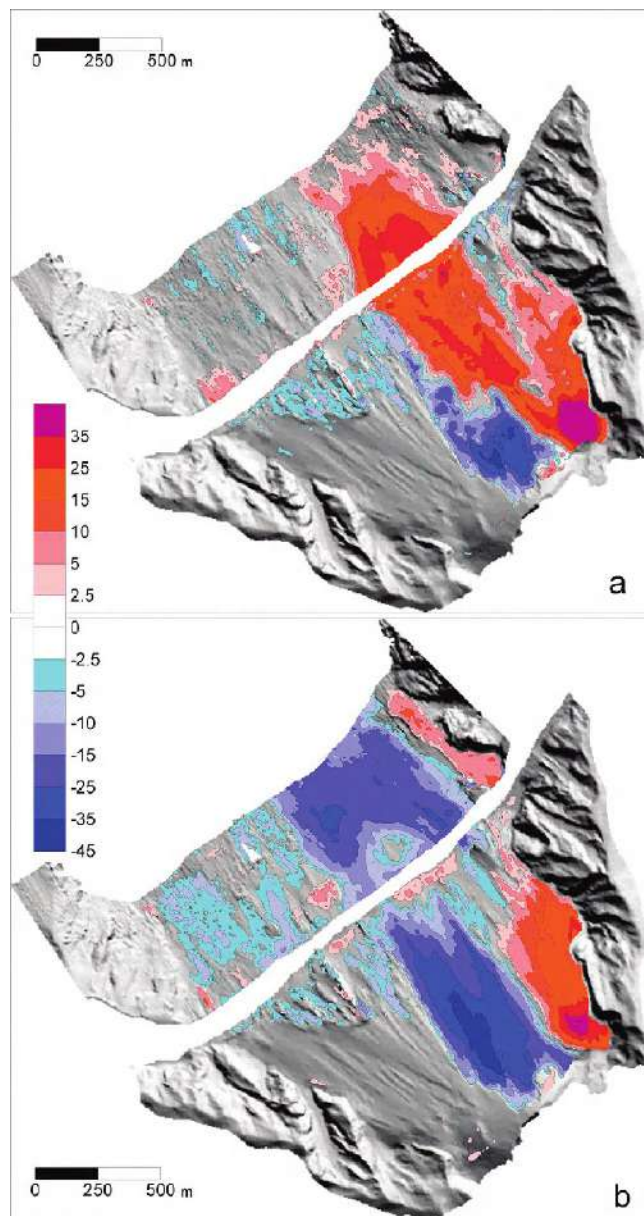


Plate 3. Total (cumulative) residual maps (values in meters), derived from the comparison of: (a) post-slide digital model (5 January 2003 on land, 9 January 2003 at sea) and the end of 2005 (surveys of 2 August 2005 on land, 1 December 2005 at sea); (b) pre-slide digital model (surveys of May 2001 for land, February 2002 at sea) and the end of 2005.

not still definitely erased. Nevertheless, since eruptive dynamics are active at Stromboli and morphological processes are very fast on this side of the volcano, monitoring activities on the subaerial and submarine slope are still going on.

Acknowledgments. This work was partially funded by National Department of Civil Protection (Italy). The authors are grateful to Ing. Massimo Fabris for the photogrammetric data analysis.

REFERENCES

- Baldi, P., S. Bonvalot, P. Briole, and M. Marsella (2000), Digital photogrammetry and kinematic GPS for monitoring volcanic areas, *Geophys. Journ. Int.*, 142(3), 801–811.
- Baldi P., S. Bonvalot, P. Briole, M. Coltellini, K. Gwinner, M. Marsella, G. Puglisi, and D. Remy (2002), Validation and comparison of different techniques for the derivation of digital elevation models and volcanic monitoring (Vulcano Island, Italy), *Int. J. Remote Sens.*, 22, 4783–4800.
- Baldi, P., M. Fabris, M. Marsella, and R. Monticelli (2005), Monitoring the morphological evolution of the Sciara del Fuoco during the 2002–2003 Stromboli eruption using multi-temporal photogrammetry, *J. Photogramm. Remote Sens.*, 59(4), 199–211.
- Baldi P., M. Fabris, M. Marsella, R. Monticelli, and V. Achilli (2006), Application of digital elevation model to volcanology, *Ann. Geophys.*, 49(4/5), 1059–1066.
- Baldi, P., M. Coltellini, M. Fabris, M. Marsella, and P. Tommasi (2008), High precision photogrammetry for monitoring the evolution of the NW flank of Stromboli volcano during and after the 2002–2003 eruption, *Bull. Volcanol.*, 70(6), 703–715, doi:10.10007/s00445-007-0162-1.
- Bonaccorso, A., S. Calvari, G. Garfi, L. Lodato, and D. Patanè (2003), Dynamics of the December 2002 flank failure and tsunami at Stromboli volcano inferred by volcanological and geophysical observations, *Geophys. Res. Lett.*, 30(18), 1941, doi:10.1029/2003GL017702.
- Calvari, S., L. Spampinato, L. Lodato, A. J. L. Harris, M. R. Patrick, J. Dehn, M. R. Burton, and D. Andronico (2005), Chronology and complex volcanic processes during the 2002–2003 flank eruption at Stromboli volcano (Italy) reconstructed from direct observations and surveys with an handheld thermal camera, *J. Geophys. Res.*, 110, B02201, doi:10.1029/2004JB003129.
- Chiocci, F. L., C. Romagnoli, P. Tommasi, and A. Bosman (2008a), The Stromboli 2002 tsunamigenic submarine slide: Characteristics and possible failure mechanisms, *J. Geophys. Res.*, doi:10.1029/2007JB005172, in press.
- Chiocci, F. L., C. Romagnoli, and A. Bosman (2008b), Morphologic resilience and depositional processes due to the rapid evolution of the submerged Sciara del Fuoco (Stromboli Island) after the December 2002 submarine slide and tsunami, *Geomorphology*, 100(3/4), 356–365 doi:10.1016/j.geomorph.2008.01.008.
- Haugerud, R., D. Harding, L. Mark, J. Zeigler, V. Queija, and S. Johnson (2004), Lidar measurement of topographic change during the 2004 eruption of Mount St. Helens, WA, *Eos Trans. AGU*, 85(47), Fall Meet. Suppl., Abstract V53D-01A.
- Heipke, C. (1995), State-of-the-art of digital photogrammetric Workstations for Topographic Applications, *Photogramm. Eng. Remote Sens.*, 61, 49–56.
- Kraus, K. (1997), *Photogrammetry*, vol. 2, Dummler Ed., Germany.
- Maramai, A., L. Graziani, G. Alessio, P. Burrato, L. Colini, L. Cucci, R. Nappi, A. Nardi, and G. Vilardo (2005), Near- and far-field survey report of the 30 December 2002 Stromboli (Southern Italy), *Mar. Geol.*, 215(1–2), 93–106.
- Marsella, M., M. Coltellini, S. Branca, C. Proietti, and R. Monticelli (2008), Lava flow eruption of Stromboli: A contribution to understanding lava discharge mechanism using periodic digital photogrammetry surveys, this volume.
- Müller, S., U. V. Helava, and K. Devenecia (1992), Softcopy photogrammetric work-station, *Photogramm. Eng. Remote Sens.*, 58, 77–83.
- Thouret, J. C. (1999), Volcanic geomorphology—an overview. *Earth Sci. Rev.*, 47, 95–131.
- Tommasi, P., P. Baldi, F.L. Chiocci, M. Coltellini, M. Marsella, M. Pompilio, and C. Romagnoli (2005), The landslide sequence induced by the 2002 eruption at Stromboli volcano, in *Landslide—risk analysis and sustainable disaster management*, edited by K. Sassa et al., pp. 251–258, Springer Verlag (Berlin), (ISBN: 3-540-28664-0).
- Tommasi, P., P. Baldi, F. L. Chiocci, M. Coltellini, M. Marsella, and C. Romagnoli (2008), Slope failures induced by the December 2002 eruption at Stromboli volcano, this volume.
- Vásquez, M. E. (2007) Tuning the CARIS implementation of CUBE for Patagonian Waters. Master Thesis of Science in Engineering, University of New Brunswick, 107 pp., http://www.caris.com/downloads/brochures/MScE_Miguel_Vasquez.pdf.

P. Baldi, University of Bologna, Dip. Fisica, Viale Berti Pichat 8, Bologna, Italy. (p.baldi@unibo.it)

A. Bosman, CNR Istituto di Geologia Ambientale e GeIngegneria, Roma, Italy. (alessandro.bosman@uniroma1.it)

F. L. Chiocci, University “La Sapienza”, Dip. Scienze della Terra, Roma, Italy. (francesco.chiocci@uniroma1.it)

M. Marsella, A. Sonnessa, University “La Sapienza”, Dip. Idraulica, Trasporti e Strade, Roma, Italy. (maria.marsella@uniroma1.it; alberico.sonnessa@uniroma1.it)

C. Romagnoli, University of Bologna, Dip. Scienze della Terra e Geologico-Ambientali, Bologna, Italy. (claudia.romagnoli@unibo.it)

Movements of the Sciara del Fuoco

A. Bonforte,¹ M. Aloisi,¹ G. Antonello,² N. Casagli,³ J. Fortuny-Guash,² L. Guerri,³ G. Nunnari,⁴
G. Puglisi,¹ A. Spata,⁴ and D. Tarchi²

The Sciara del Fuoco (SdF) landslides that occurred at the end of December 2002 prompted researchers to install geodetic networks to monitor deformations related to potential new slope failures. With this aim, an integrated multiparametric monitoring system was designed and deployed. In particular, this complex monitoring system is composed of four single systems: an electronic distance measurement network, installed immediately after the landslide events, a real-time GPS network, a ground-based interferometric linear synthetic aperture radar (GB-InSAR), and an automated topographic monitoring system (named Theodolite Robotic Observatory of Stromboli, or THEODOROS); the three last systems provided a continuous monitoring of selected points or sectors of the SdF. Data acquired from different systems have been jointly analyzed to reach a better understanding of the SdF dynamics. Displacement data obtained from the topographic systems are compared with those obtained from GB-InSAR, and the results of the comparison are analyzed and discussed. Furthermore, in this chapter, an example of a warning system that can detect slope instability precursors on the SdF based on a statistical analysis of the data collected by the THEODOROS system is reported.

1. INTRODUCTION

The Sciara del Fuoco (SdF) landslides that occurred at the end of December 2002 evidenced that a ground deformation monitoring system was required for the SdF to monitor

its stability. The aim was to detect the deformations related to potential new slope failures. The main difficulties in installing any instrumentation on the SdF are related to the very harsh environmental and topographic conditions, which prevented a similar initiative planned in the past. These conditions also require that the monitoring systems should be based on simplicity and robustness.

With this aim, together with the National Civil Protection Department, we planned to install a multiparametric monitoring system, based on the integration of different measurement techniques. The setup of this new monitoring system lasted several months and was developed in four steps. In fact, (1) electronic distance measurement (EDM) networks were immediately installed to start the ground deformation monitoring of the southern side of summit craters and SdF, (2) while an innovative real-time GPS network was being developed and then installed. (3) At the same time, an innovative ground-based interferometric linear synthetic aperture

¹Istituto Nazionale di Geofisica e Vulcanologia, Sezione di Catania, Catania, Italy.

²Joint Research Centre, European Commission, Ispra, Varese, Italy.

³Department of Earth Sciences, University of Firenze, Firenze, Italy.

⁴Dipartimento di Ingegneria Elettrica, Elettronica e dei Sistemi, Università degli Studi di Catania, Catania, Italy.

radar (GB-InSAR) was also set up and installed to monitor the northern side of the summit craters and of the upper part of the SdF. (4) The EDM monitoring continued throughout the eruption, until it was robotized, with the installation of a terrestrial geodetic monitoring system (named Theodolite Robotic Observatory of Stromboli, or THEODOROS) based on an automatic total station for routinely measuring the ground motion of the SdF. Comparisons among the data set of different monitoring systems were performed during the eruption and through the following years, confirming the congruence among different system. In addition, an early warning system, based on a statistical approach and soft-computing technique, was developed and tested on the THEODOROS data set.

2. MONITORING NETWORKS

2.1. First EDM Networks

On 16 January 2003, the geodetic monitoring started with EDM measurements on a continuously developing network (Plate 1); the very first EDM measurements were carried out from an iron pillar placed on “Il Pizzo Sopra la Fossa,” named STR (Plate 1). After installing the first network to monitor the crater terrace and a reference network outside the SdF, a further subnetwork consisting of six control points (labeled PST1 to PST6 in Plates 1 and 2) was placed within the scar of the 30 December landslide [Puglisi *et al.*, 2005]. These benchmarks were measured from the STR pillar, and two of them (PST4 and PST6) were equipped with two reflectors, to be measured also from another pillar located on the lower flank of the volcano, at Punta Labronzo (PLB in Plate 1).

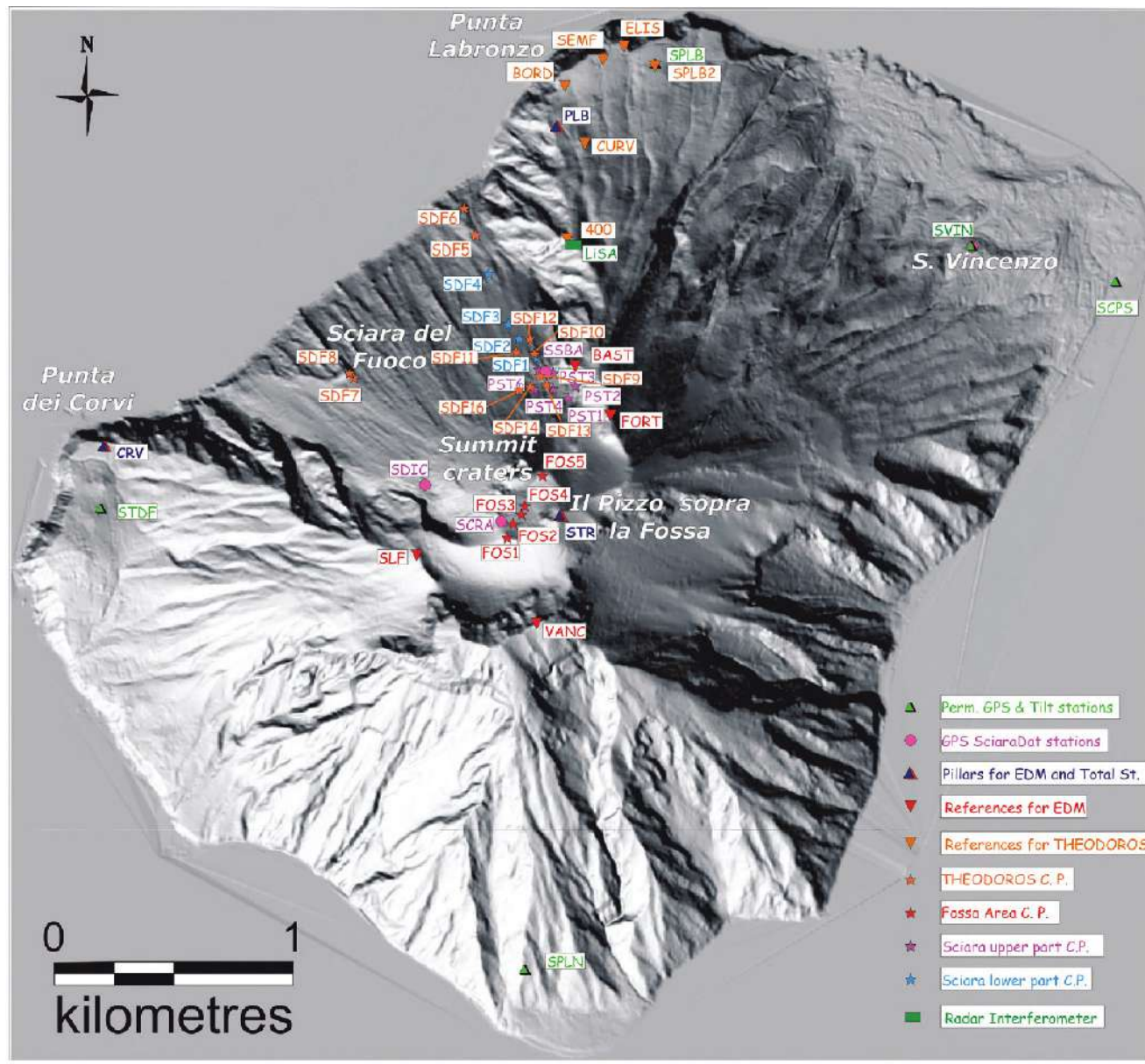
The PLB pillar was set up with the aim of monitoring the lower part of the SdF area, not visible from the STR pillar. Indeed, before the end of January 2003, the network was enlarged, including all the northern sector of the SdF, along the path of the 30 December 2002 landslide (SDF 1 to SDF6 in Plate 1). Finally, two other benchmarks were installed in the central part of the SdF (SDF7 and SDF8 in Plate 1), and a third pillar at Punta dei Corvi was set up (CRV in Plate 1), with the objective of monitoring the western sector of the SdF and eventually broadening the network. At the beginning of February 2003, the network was consisting of 22 monitoring points within the SdF and two pillars used for the EDM instruments.

The EDM data acquired from the PLB pillar were especially significant in describing the movement of the medium and lower part of the SdF involved in the landslide of 30 December 2002. Due to the peculiar geometry of the network, it should be highlighted that the most informative EDM measurements were those performed, almost daily, on the

highest benchmarks (i.e., SFD1, PST4, and PST6) because their positions with respect to the PLB pillar allowed the directions of the line of sight (LOS) of such measurements were almost coincident with that of the seaward movements. Occasionally, to obtain complete three-dimensional (3-D) information from the benchmarks installed in the SdF, measurements of azimuth and zenith angles have been carried out from the PLB pillar by using theodolite, but the difficulties of using this precise instrument in harsh operational conditions prevent to obtain 3-D information as accurate as necessary to measure the slow sliding of the flank. Despite these difficulties, the integration of angle and distance measurements allowed the detection of very large deformations on the highest part of the SdF, which are related to the opening of the vents that occurred on 16 February (see discussion in section 4.4). As concerning the monitoring of the stability of the SdF, the EDM data relevant to the SFD1, PST4, and PST6 benchmarks pointed out that the seaward movement of the sector of the SdF involved in the landslide of 30 December 2002 gradually decreased throughout February 2003. Unfortunately, the lava flows emplaced during the second half of February together with the pyroclastic products ejected during the 5 April paroxysm destroyed many of the benchmarks installed in the SdF, leaving only those located in its lowest part (SDF5, SDF6, SDF7, and SDF8), i.e., on a position nonoptimal in discriminating the sliding movements through EDM measurements. These situations spurred to assume new surveying techniques, allowing accurate and continuous 3-D positioning of the benchmarks; these solutions brought forth the design and the installation of the THEODOROS system, described in the section 2.4.

2.2. GPS “Real-Time” Network

The next step was the installation within the SdF of a permanent GPS network (circles in Plate 1), specifically designed for the real-time monitoring of movements in the core of the potential failure zone and close to the summit craters [Puglisi *et al.*, 2005]. The new GPS network, named SciaraDat, consisted of three stations, specifically designed and built for this network. They were installed around the summit craters during the first days of February; on 20 February, the lava flows covered the station installed northward to the crater (SSBA), while the paroxysm of 5 April definitively destroyed the remaining two stations of this network. The technical description of the SciaraDat network and the data set are described and discussed in the section 4.4 because they gave important information for both the dynamic of summit craters and the formation of the vents of the eruption. However, for the aim of this chapter, it is noteworthy to observe that the GPS data confirm a general stability of



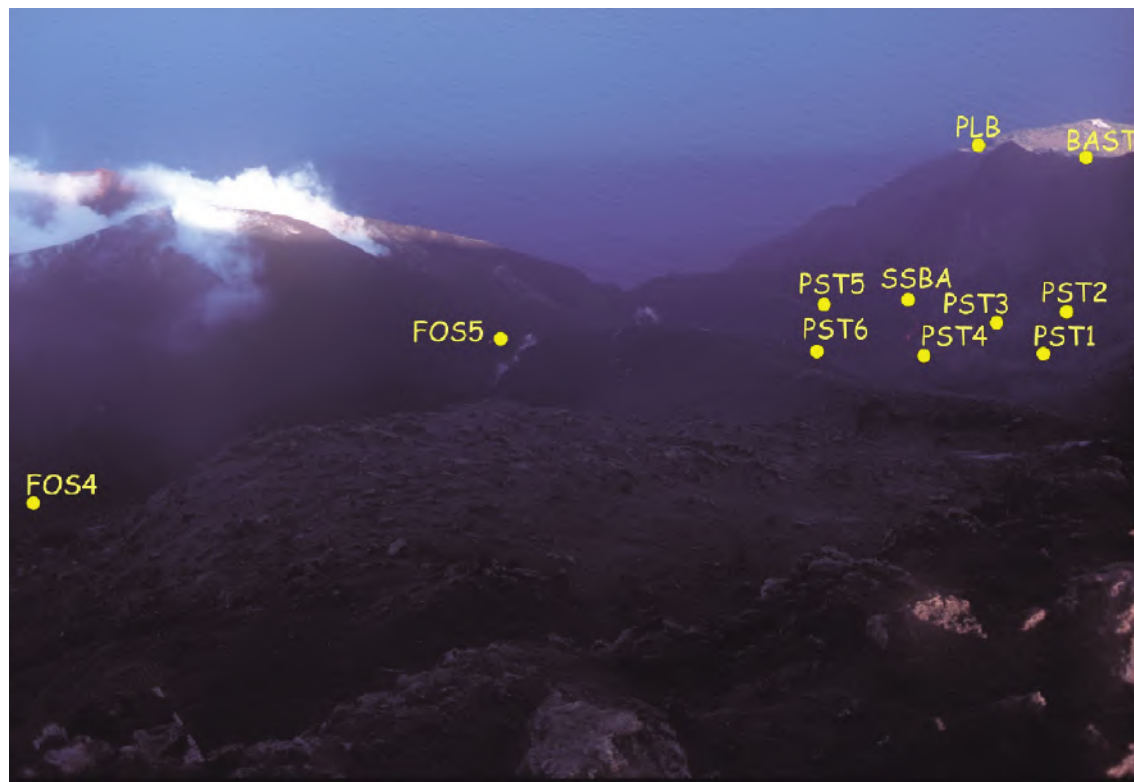


Plate 2. View from STR pillar on the upper SdF and craters area with location of the benchmarks for EDM measurements.

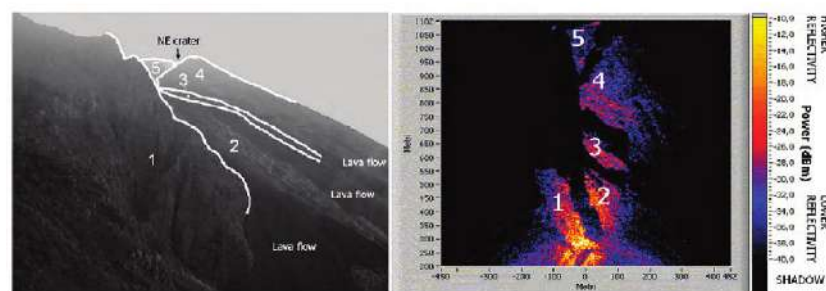


Plate 3. (left) Photo of the target area observed from the GB-InSAR showing the five sectors where it is possible to obtain radar images. (right) Synthesized SAR power image showing the same five sectors. 1, Stable flank of the SdF (Bastimento); 2, upper SdF (NE sector); 3, upper SdF (central sector); 4, flank of the NE crater; 5, rim of the NE crater.

the higher southern part of the SdF from February to April 2003.

2.3. InSAR Monitoring of the SdF

An innovative apparatus capable of a remote sensing monitoring of ground deformations on the SdF was set up on behalf of the National Department of Civil Protection [Antonello *et al.*, 2003, 2004a, 2004b, 2007; Casagli *et al.*, 2003, 2004]. The system consists of a GB-InSAR, also known as LiSA (linear SAR [Rudolf and Tarchi, 1999; Rudolf *et al.*, 1999; Tarchi *et al.*, 1997, 2000, 2003; Antonello *et al.*, 2004b]). The specific version of the instrument installed at Stromboli is composed of a continuous-wave step-frequency radar, a 3.0-m-long linear rail, and two antennas that move along it at steps of 5 mm forming a synthetic aperture. The microwave transmitter produces, step by step, continuous waves at 1601 discrete frequency values, sweeping the bandwidth from 17.0 to 17.1 GHz. The receiver acquires the in-phase and the quadrature components of the microwave signal backscattered by the target. Range and cross-range synthesis of complex images is obtained by coherently summing signal contributions relative to different antenna positions and different microwave frequencies. The system produces a synthesized radar image of the observed area every 12 min, night and day and in any visibility conditions (e.g., with fog or ash clouds), with a pixel resolution of about 2 m in range and 2 m on average in cross-range. The processing of the radar images is based on the radar interferometry technique [Zebker and Goldstein, 1986]. Interferograms are derived by using pairs of sequential images taken at different times from the same position in a zero baseline condition. The interferometric analysis of consecutive images gives a complete picture of the displacement field of the observed portion of the SdF and of the crater with an accuracy of about 1 mm [Antonello *et al.*, 2003].

The displacement is calculated from the phase difference between the backscattered signals received at different times, through the cross-correlation between two images. The resulting interferogram represents the displacement occurring along the LOS in the time interval, and it does not contain the topographic component, since the position of the antennas remains the same in all the acquisitions.

The observed area is shown in Plate 3 (left) and contains five sectors (numbered from 1 to 5), separated by morphological depressions, not visible by the GB-InSAR system. In Plate 3 (right), a radar power image of the target scene, projected on a horizontal plane, is shown. The color scale expresses the power of the backscattered signal. The above-mentioned five sectors, separated by shadow zones, are evident on the image and correspond to the five zones sketched

on the photo. The upper part of the SdF is represented in sectors 2 and 3.

A specific procedure for processing radar data acquired by the GB-InSAR instrument has been developed and implemented. This method, based on the selection over the whole SAR scene of pixels characterized by high-quality signal in terms of amplitude and coherence values, allows us to use a long time series of images, available from the beginning of 2003, for analyzing the temporal evolution of movements. The developed procedure enables estimating the atmospheric component of the interferometric phase by selecting, for each measurement point, a reference pixel located at the same distance from the system (isorange) but in a stable area (for the SdF, it generally corresponds to the Bastimento, area 1 in Plate 3). In this way, it is possible to remove the atmospheric artifacts and achieve better accuracy in the displacement measurements. During the first year of monitoring, the method was applied over a subset of the whole archive of SAR images. The observed portion of the SdF exhibits a complex displacement pattern, deriving from the superimposition and interference of the following geomorphic processes: (1) lava flows that move at high speeds, which are usually channeled into morphological depressions and are sometimes diverted over the slope; (2) gravitational sliding of the volcanoclastic materials on the SdF along a deep-seated slip surface related to the landslide of December 2002 [Tommasi *et al.*, 2003]; (3) gravitational slow viscous flow of cooling lava masses accumulated on the SdF.

These different processes can be observed separately on interferograms referring to different periods (Plate 4). On the short-period interferograms (i.e., 12 min), it is possible to detect rapid shallow movements associated with lava flows. The gravitational sliding is particularly evident on medium-period interferograms (i.e., 1 h), whereas the flow of cooling lava can clearly be observed only on long period interferograms (i.e., 24 h).

To assess the long-term evolution of the whole deformation field over the SdF, a new technique has been developed based on the creation of cumulative displacement maps (Plate 5). The retrieval of the cumulative displacement is based on the flattening of the phase of all the incremental coherence images and a subsequent averaging of large sets of images (usually 100). The flattening of the phase is done automatically using the Bastimento area (n.1 in Plate 3) as the reference. In this way, the distortion introduced with the changes of the radar refractivity index is significantly reduced. This technique has made it possible to increase the duration of the cumulated maps from a few days up to a few months. Plate 6 shows the plot of cumulated LOS displacement versus time of four points localized on the SdF, spanning a period from 25 February 2003 to 22 December 2003.

It is possible to identify a sharp decrease in the displacement rate starting from the end of the effusive phase of Stromboli in summer 2003.

2.4. The Continuous Topographic Monitoring of the SdF

After the explosion of 5 April 2003, only four EDM benchmarks (SDF5, SDF6, SDF7, and SDF8 in Plate 1) out of more than 20 remained in the SdF. Due to their position, the main component of the movement related to the SdF sliding is almost orthogonal to the LOS from the PLB pillar, thus, these benchmarks had nonideal positions for detecting this motion by using EDM only. The need to overcome these problems and monitor the movements of the SdF as frequently as possible is the basis of the decision to install of a new monitoring system. It was based on terrestrial geodetic techniques, allowing to perform continuous 3-D measurements and exploit the benchmarks that remained untouched by the volcanic activity. This new system, named THEODOROS, uses a remotely controlled total station located nearby the PLB pillar (Plate 7).

The design and installation of this new monitoring system take about four months, during which a network of reflectors was installed around the PLB pillar, outside the SdF, to build the reference system for the measurements of the THEODOROS system. Furthermore, another benchmark (CURV) was installed near the PLB pillar; together with the CRV, these two benchmarks had the two aims of checking the stability of the reference system and monitoring the deformations eventually occurring at the opposite side of the SdF. Thorough the 4 months, several tests were carried out to define the optimal measurement strategy. The total station, indeed, is remotely controlled by specific software installed on a PC in S. Vincenzo, which manages the measurement cycles, receives the data, and updates a local database, which is then downloaded from another PC in Catania, where software calculates the motion of each point, displaying them on plots. All these phases need to be optimized to avoid the backlog of data both on the database implementation and in the transfer of the data from the sensor to Catania. Finally, on August 2003, after the end of the effusion of the lava, new benchmarks were installed on the new lava field at about 500 m of altitude (reference for THEODOROS in Plate 1) and included in the new automated geodetic monitoring system.

The THEODOROS system was declared operational at the end of August 2003, allowing us to monitor the posteruptive behavior of the SdF. Due to a calibration error of the total station, the database of THEODOROS before June 2004 is different from that acquired after October 2004. However, for the aims of this chapter, the results of the analysis performed on the data set from August up to the end of Decem-

ber 2003 (Plate 8) are informative on its quality and on the pattern of the deformations observed in the SdF.

Considering the measurements carried out on the reference system and the two near (CURV) and far (CRV) benchmarks, we can confirm that the total station is stable. Moreover, the monitoring of the SdF enabled distinguishing different ground deformation patterns. First of all, the movements are detected only on the sector of the SdF, where 30 December 2002 landslides occurred, while on its central part (SDF7 and SDF8 benchmarks), the flank of the volcano is stable. Within the areas showing movements, different rates of deformations are observed between the lower and the upper parts of the slope. On the lower part (SDF5 and SDF6), the rates are relatively small (in the order of mm/day) and seem to increase on the lowest benchmarks. On the upper part of the SdF, on the benchmarks located on the recent lava flows field, we measured both horizontal and vertical movement rates up to 1 cm/day. However, we can distinguish different areas showing homogeneous rates. The fastest area is located along the northern boundary of SdF (SDF9, SDF10, and SDF12). SDF14 and SDF11 benchmarks seem located over another area where the rate of movement is in the order of 0.5 cm/day. A further block, where SDF16 is located, practically stopped its movement. However, the velocity of movement at all benchmarks decreased with time after the end of the eruption. These general behaviors of the movements in the SdF are confirmed in the following years.

3. COMPARISON AMONG EDM, THEODOROS, AND GB-InSAR DATA

One of the key points in setting up the integrated monitoring system of the SdF was the comparison among the data set provided by the different measuring techniques to check the congruence among them.

The first comparison was made during the installation of THEODOROS system, with the aim of checking the capability of the continuous measurements to follow those obtained in the previous months using EDM techniques. The agreement between these two data sets relevant to the distance measurements from the PLB pillar to the four benchmarks SDF5, SDF6, SDF7, and SDF8 is shown in Plate 9. The plot shows that the two time series agree except in a few days were specific tests for assessing the measurement strategies are carried out, during the first days of April 2003.

A second comparison was made between GB-InSAR and THEODOROS data sets. To do that, two preliminary operations are needed. From InSAR images, it is necessary to extract data at the same points where the THEODOROS benchmarks are located. To this end, an automatic procedure, based on the radar interferometry technique, has been

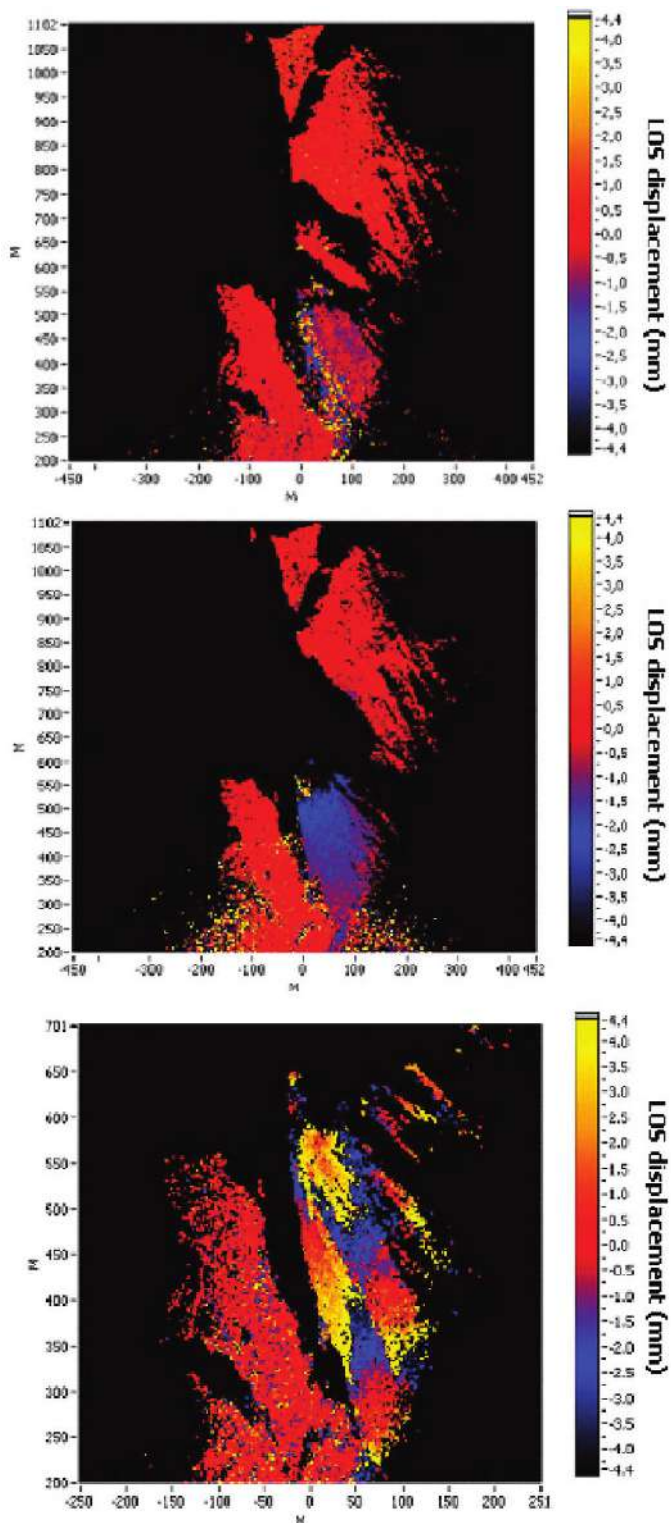


Plate 4. Examples of interferograms at different time intervals. From the top: 12-min interferogram showing lava flows over the slope; 1-h interferogram showing the gravitational sliding of volcanoclastic materials; detail of a 24-h interferogram of the SdF showing the gravitational slow viscous flow of cooling lava.

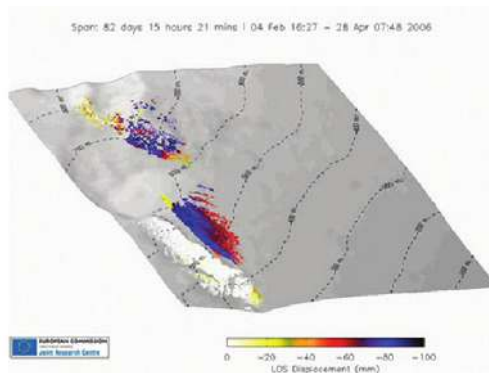


Plate 5. Example of cumulative displacement map from 4 February 2006 to 28 April 2006 (~8000 images processed).

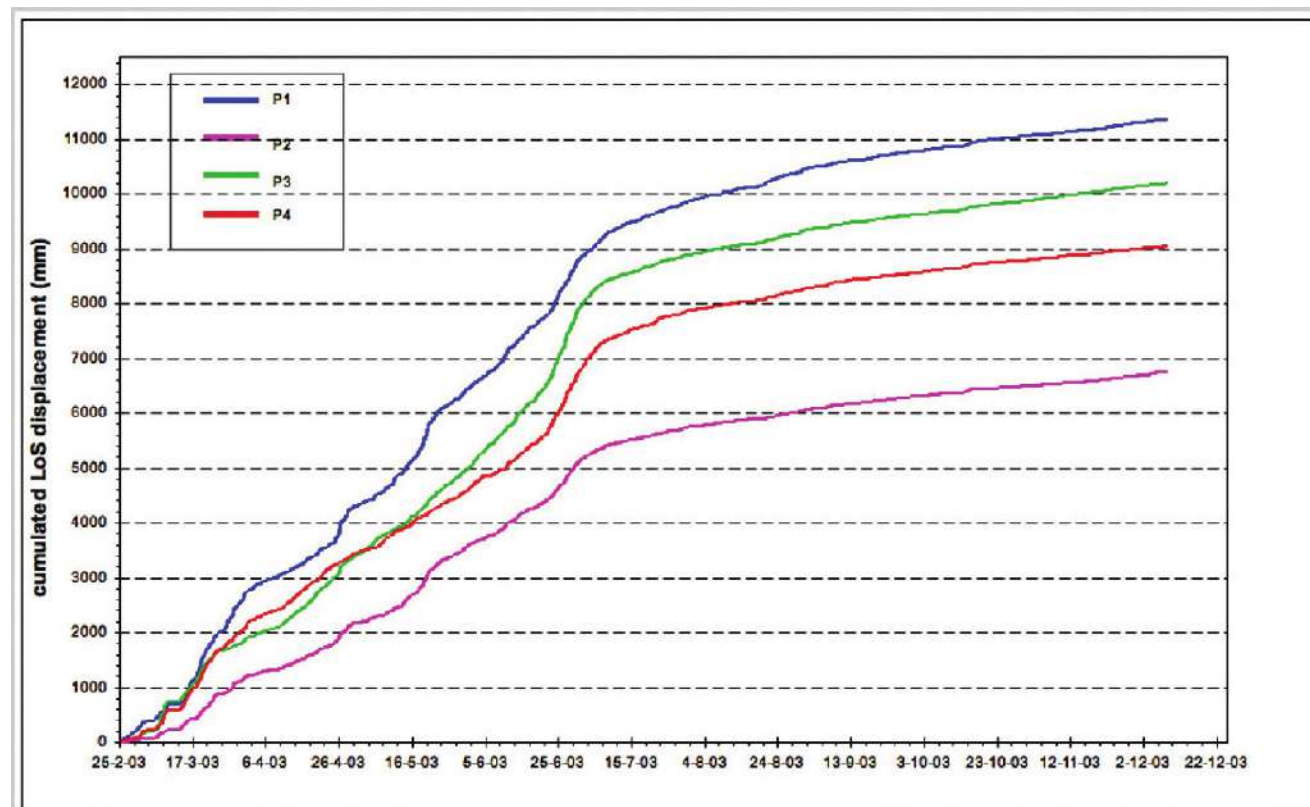


Plate 6. Plot of LOS cumulated displacement versus time assessed by the GB-InSAR on four pixels on the upper part of the SdF.

implemented for the extraction from SAR images of the motion history in selected points located in different sectors of the SdF. Furthermore, THEODOROS observations are not directly comparable with measurements extracted from InSAR images, but they must be projected along the LOS of the GB-InSAR.

Due to several technical and data processing improvements required during both the setting up and the first years of operation of these two systems, the comparison was carried out on data from February 2006 to April 2006. In the portion of the SdF observed by the GB-InSAR, two THEODOROS benchmarks (SdF11 and SdF13) are located. The position of both these benchmarks is considered representative of the average ground deformation observed on the SdF. In Plate 10, the extraction of InSAR measurements (red) corresponding to the THEODOROS benchmark SdF11 is plotted together with the projection of the same benchmark (blue) along the LOS of the GB-InSAR. As we can see in Plate 10, both observations are in good agreement in the periods from 4 February 2006 to 25 February 2006 and from 25 March 2006 to 22 April 2006. On the contrary, the displacements in the period from 25 February 2006 to 25 March 2006 are slightly different. We believe that this discrepancy may be attributed to local effects, which cannot be detected by the GB-InSAR technique, since it is based on algorithms that average both in space (a single pixel covers on average an area of 4 m²) and time (every acquisition spans a temporal interval of 12 min) the original data.

4. WARNING SYSTEM

For attempting to exploit the data provided by the THEODOROS system for assessing a warning system, a robust statistical method combined with a fuzzy processing has been developed. The statistical method is based on an opportunely modified version of the absolutely local index of change of the environment (ALICE) [Tramutoli, 1998] for the THEODOROS system. This index is then processed through suitable fuzzy rules to evaluate the alarm intensity (AI index), which gives a measure of the hazard connected with movements of the SdF area [Nunnari *et al.*, 2008].

The ALICE for THEODOROS system is defined as follows. Let $T_{SdFx}^i(t)$ be a generic feature of the benchmark SDFx (e.g., the slope distance between TS and the SdFx benchmark) at time t of day i . Let $\Delta T_{SdFx}^i(t)$ be the absolute value of the difference between two subsequent measurements at day i :

$$\Delta T_{SdFx}^i(t) = |T_{SdFx}^i(t - t_c) - T_{SdFx}^i(t)| \quad (1)$$

where t_c is the sample time. Let S be the set of the variables $\Delta T_{SdFx}^j(t)$ with $j < i$.

$$S = \left\{ \Delta T_{SdFx}^j(t) \mid j < i \right\} \quad (2)$$

The ALICE used to detect anomalous value of the variable $\Delta T_{SdFx}^i(t)$ is defined as

$$A_{\Delta T_{SdFx}^i(t)} = \frac{\Delta T_{SdFx}^i(t) - \mu_S}{\sigma_S} \quad (3)$$

where the quantities μ_S and σ_S are the mean value and standard deviation, respectively, of set S . In Figure 1, we show as example the behavior of ALICE computed for the slope-distance of SdF7 target plotted together with its statistical properties (mean and variance).

Although the index above defined is then suitable to identify anomalous variations of the movement of one benchmark, this is not enough to assess an effective warning system of the SdF, because the detected anomalies may have several origins, either techniques (e.g., malfunctioning of the sensor, temporal damages of the reference system, instability of the reflector) or volcanic (e.g., local instability of small part of the SdF, general instability of the SdF). Thus, it is necessary to set up a procedure able to evaluate if the detected anomalies are accompanied from other "symptoms" allowing discriminating their origin. A further complication is that this evaluation is mainly heuristic, because there is not a well-assessed dynamic or physical model allowing justifying the observed movements of the SdF.

Fuzzy logic is a suitable approach to map an input space to an output space when traditional methods are not applicable. Moreover, it provides a simple way to approximate nonlinear functions of arbitrary complexity. Fuzzy logic resembles the natural language to express concepts and is able to describe vague concepts (fuzzy set) in a framework of imprecise data; thus, it represents a good framework for the realization of a warning system for THEODOROS.

To perform the fuzzy processing of the ALICE, the following strategy was adopted. The benchmarks placed on the SdF have been grouped into three clusters depending on their averaged displacements. Three AI subindices are evaluated first for each individual cluster of benchmarks based on the actual measurements of the ALICE for each benchmark. As a second step, the AI subindices are integrated to acquire a value for AI, which takes into account the overall set of benchmarks [Nunnari *et al.*, 2008].

The composition of the rules for the fuzzy warning system follows a simple linguistic approach. For example, in the case of a cluster consisting of two reflectors, if the first value is "low" and the second one is "mean," then the AI will be "mean-low". Similarly, if one reflector is moving

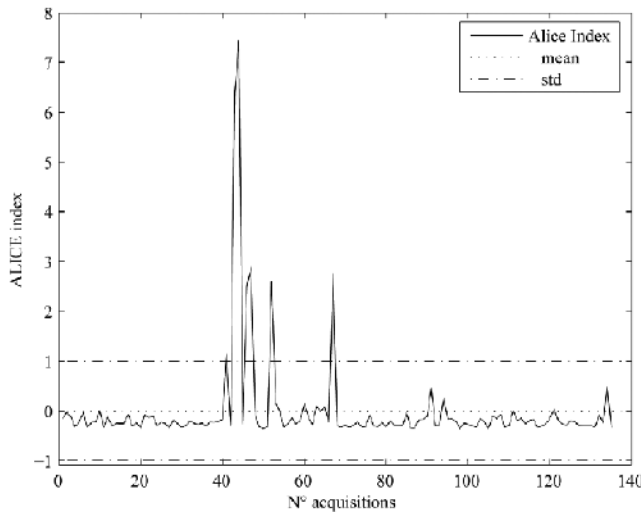


Figure 1. ALICE of SdF5 target-slope distance.

fast and the second is moving slowly, then the AI will result in a “mean,” and so on.

In Plate 11, we show the ALICEs of SDF7 and SDF10 benchmarks together with their sub-AI values. Near the 40th acquisition, some “mean” values of AI can be observed. A posteriori analysis has shown that they are all false alarms caused by malfunctioning of the acquisition system. After the acquisition system maintenance, the AI returned to normal level. Both the sub-AI and AI values are reported also as color bars to be more evident.

Similarly, the fuzzy evaluation performed on cluster consisting of benchmarks SDF9, SDF13, and SDF14 (Plate 12) has shown “mean” values of sub-AI in the same period. Finally, Plate 13 shows the total AI evaluation.

5. DISCUSSION AND CONCLUSIVE REMARKS

The 2002–2003 eruption marked the occasion for starting to monitor the SdF ground deformations, by using an extensive and multiparametric network of sensors. From general point of view, the different deformation monitoring systems revealed some interesting features related to both gravitational and volcanic dynamics never identified before the 2002–2003 eruption. The very prohibitive conditions to operate in the SdF, indeed, discouraged the setup of monitoring systems within the SdF during the normal activity of the volcano in the past years, while huge logistic efforts undertaken during the 2002–2003 eruption for improving the monitoring system of the volcano at whole allowed to overcome such difficulties.

After the first immediate measurements carried out by EDM techniques during the early stage of eruption, the monitoring network was continuously improved and extended to increase the amount of information both in time and in space. Thus, the preliminary one-dimensional data (EDM) were upgraded to a real 3-D monitoring (THEODOROS), improving the accuracy and precision of measurements. Furthermore, this experience allowed testing, for the very first time, the simultaneous application of both real-time geodetic monitoring techniques (GPS and terrestrial) and GB-InSAR on an active volcano. The first comparison among the different techniques confirm their suitability for monitoring purposes and congruence among them, evidencing some small discrepancies only when instantaneous point information (e.g., the measurements on single reflectors of the THEODOROS system) are compared with information averaged both in time and in space (e.g., the GB-InSAR time series).

The GB-InSAR was able to detect significant ground deformations related to the lava flows dynamics on the high SdF: either due to the expansion of compound lava flow fields during the eruption or due to the thermal compaction at the end of the eruption. Furthermore, GB-InSAR evidenced downslope movements of the new lava flow field due to its emplacement on a very steep slope, as an effect of gravitational sliding along a deep-seated slip surface.

The EDM, and later on, the THEODOROS system, measured a significant downslope motion affecting also the lower part of the SdF, even outside the new lava field, but confined to the northern half of the SdF.

In all cases, the velocity of the downslope motion decreased in time after the end of the eruption. These evidences suggest that the highest velocities of the gravitational movement were strictly related to the eruptive activity (both dike intrusions and lava loading) and that probably these movements were due to the reactivation of deep-seated slip surfaces associated with the landslides of December 2002 [Tommasi *et al.*, 2003].

One of the main conclusions of ground deformation monitoring within the SdF during the years following the 2002–2003 eruption is that different rates of movement characterize the ground deformation pattern on different sectors of the SdF. The central part of the SdF, indeed, remains fairly stable with respect to the northern part, which showed a continuous slow motion also several years after the end of the eruption. Furthermore, the highest velocities (in the order of 1 cm/day) are measured on the upper part of the SdF, from both GBInSAR and THEODOROS systems, while the smallest velocities (in the order of 0.5 cm/day) refer to lowest benchmarks.

Finally, the continuous data acquired by the THEODOROS system inside the SdF enabled us to test a statistical



Plate 7. View from PLB pillar on lower SdF area with location of the benchmarks for EDM measurements; AGA 6000 Geodimeter is placed on the PLB pillar, while TCA2003 robotized total station is visible.

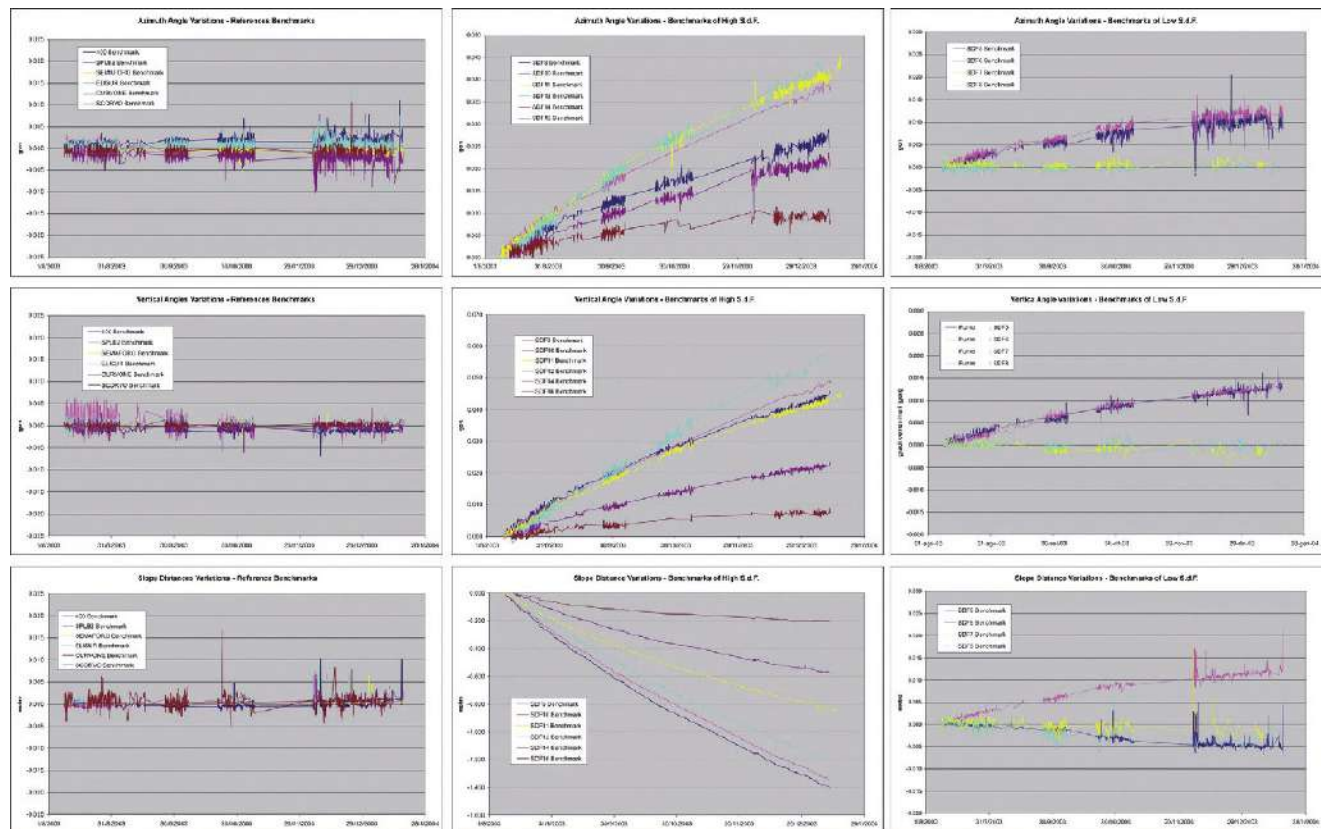


Plate 8. Different components of ground motion measured by the total station until December 2003 on all benchmarks.

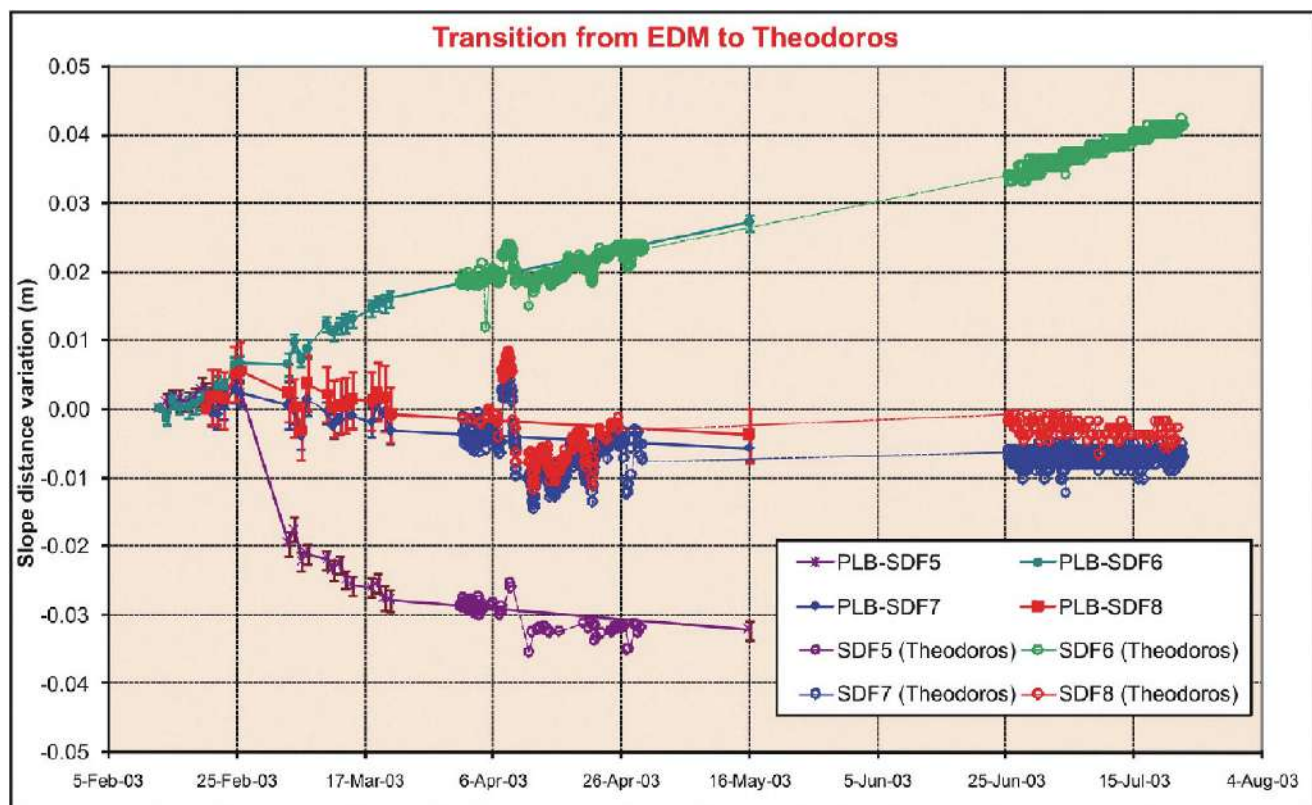


Plate 9. Plot showing the slope distances variation measured by EDM and THEODOROS. It is possible to see a very good overlap between the two techniques.

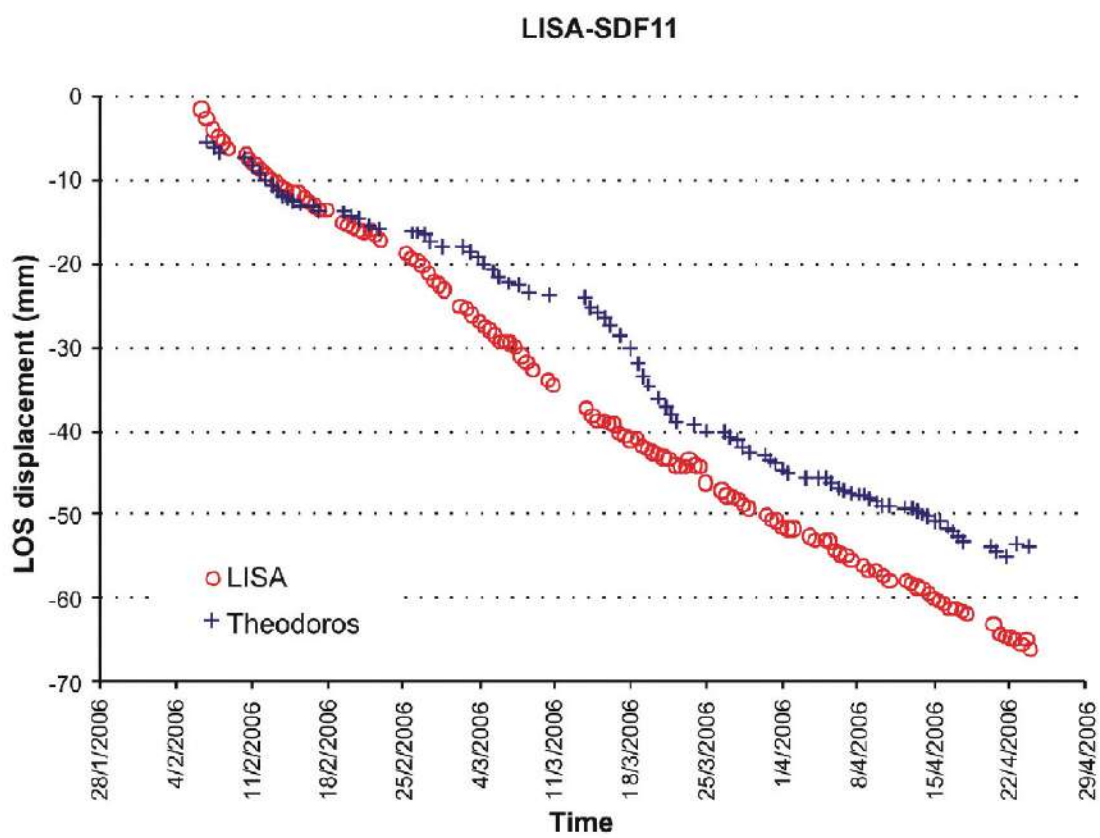


Plate 10. Comparison between the GB-InSAR and THEODOROS: SdF11 benchmark.

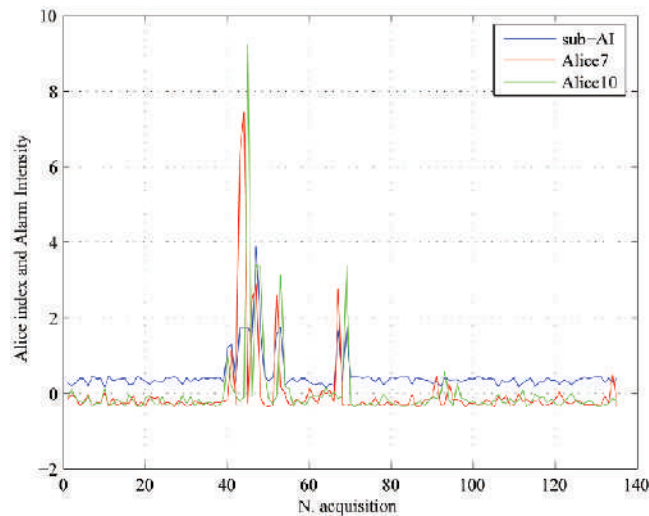


Plate 11. ALICEs of SDF7 (red), SDF10 (green), and their sub-AI (blue).

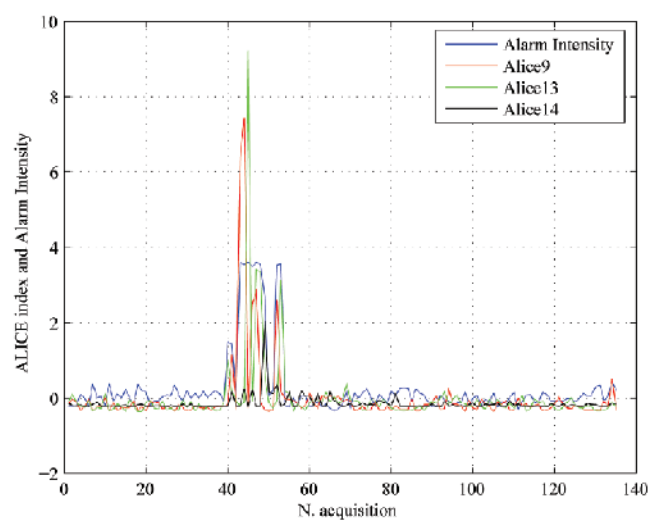


Plate 12. ALICEs of SDF9 (red), SDF13 (green), SDF14 (gray), and their sub-AI values (blue).

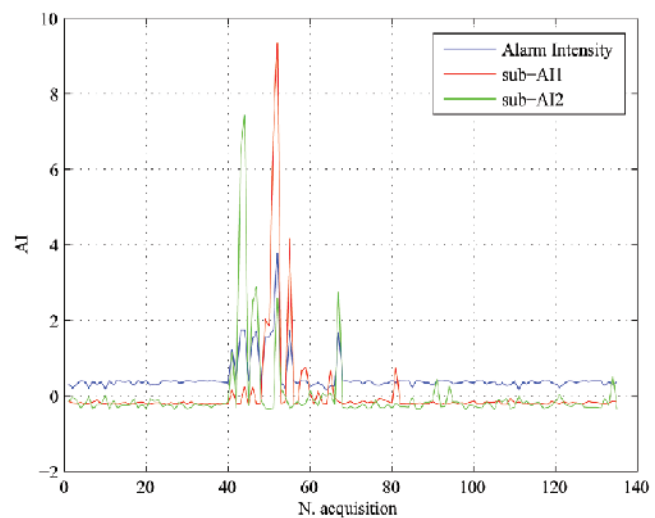


Plate 13. Total AI evaluation.

approach combined with a fuzzy processing aimed at calculating an alarm index for early warning applications. The preliminary results of this approach confirmed that it is able to identify anomalies in the data set, evidencing also if these anomalies are relevant to a single reflector or to a group of reflectors. These results spur to continue along this path to assess a future early warning system for the SdF.

Acknowledgments. This study was funded by the Italian Department of Civil Protection (DPC) through the Istituto Nazionale di Geofisica e Vulcanologia and DPC Stromboli Emergency Project V2-Monitoring and Research Activity at Stromboli and Panarea. The GB-InSAR system on the Stromboli volcano was set up by the Earth Science Department of the University of Florence, the Institute for the Protection and Security of Citizens of the Joint Research Centre and its spin-off company LisaLab, on behalf of DPC. B. De Bernardinis and his group at the Department of Civil Protection are acknowledged for the support to the project and for the permission given to the publication.

REFERENCES

- Antonello, G., N. Casagli, P. Farina, L. Guerri, D. Leva, G. Nico, and D. Tarchi (2003), SAR interferometry monitoring of landslides on the Stromboli volcano, in *Proceedings of FRINGE 2003 Workshop*, ESA/ESRIN, Frascati, Italy.
- Antonello, G., D. Tarchi, N. Casagli, P. Farina, L. Guerri, and D. Leva (2004a), SAR interferometry from satellite and ground-based system for monitoring deformation on the Stromboli volcano, in *Proceedings IGARSS 2004, International Geoscience and Remote Sensing Symposium*, pp. 633–636, IEEE Int., Piscataway, N. J.
- Antonello, G., N. Casagli, P. Farina, D. Leva, G. Nico, A. J. Sieber, and D. Tarchi (2004b), Ground-based SAR interferometry for monitoring mass movements, *Landslides*, 1, 21–28.
- Antonello, G., N. Casagli, F. Catani, P. Farina, J. Fortuny-Guash, L. Guerri, D. Leva, and D. Tarchi (2007), Real-time monitoring of slope instability during the 2007 Stromboli eruption through SAR interferometry, paper presented at Proceeding of 1st NACL, Veil, Colo.
- Casagli, N., P. Farina, L. Guerri, D. Tarchi, J. Fortuny, D. Leva, and G. Nico (2003), Preliminary results of SAR monitoring of the Sciara del Fuoco on the Stromboli volcano, *Occurrence and Mechanisms of Flow-like Landslides in Natural Slopes and Earthfills, Sorrento, Italy*, Patron Editore, Bologna.
- Casagli, N., P. Farina, D. Leva, and D. Tarchi (2004), Landslide monitoring on the Stromboli volcano through SAR interferometry, in *Proceedings of 9th International Symposium on Landslides*, Routledge, Abingdon, U. K.
- Nunnari, G., G. Puglisi, and A. Spata (2008), A warning system for Stromboli volcano based on statistical analysis, *Pure Appl. Geophys.*, in press.
- Puglisi, G., A. Bonaccorso, M. Mattia, M. Aloisi, A. Bonforte, O. Campisi, M. Cantarero, G. Falzone, B. Puglisi, and M. Rossi (2005), New integrated geodetic monitoring system at Stromboli volcano (Italy), *Eng. Geol.*, 79(1–2), 13–31.
- Rudolf, H., and D. Tarchi (1999), *LISA: The Linear SAR Instrument. DG JRC, Technical Note I.99.126*, European Commission, July.
- Rudolf, H., D. Leva, D. Tarchi, and A. J. Sieber (1999), A mobile and versatile SAR system, in *Proceedings of IGARSS 1999*, pp. 592–594, IEEE Int., Piscataway, N. J.
- Tarchi, D., H. Ohlmer, and A. J. Sieber (1997), Monitoring of structural changes by radar interferometry, *Res. Nondestruct. Eval.*, 9, 213–225.
- Tarchi, D., H. Rudolf, M. Pieraccini, and C. Atzeni (2000), Remote monitoring of buildings using a ground-based SAR, *Int. J. Remote Sens.*, 21(18), 3545–3551.
- Tarchi, D., N. Casagli, R. Fanti, D. Leva, G. Luzi, A. Pasuto, M. Pieraccini, and S. Silvano (2003), Landslide monitoring by using ground-based SAR interferometry: An example of application to the Tessina landslide in Italy, *Eng. Geol.*, 68, 15–30.
- Tommasi, P., F. L. Chiocci, M. Coltelli, M. Marsella, and M. Pomilio (2003), Analysis of the first data on the instability phenomena associated to the 2002–03 Stromboli volcano lava flow eruption, *Proceedings of the International Symposium of Flows*, Sorrento, Italy, May 15–16, 10 pp.
- Tramutoli (1998), Robust AVHRR Techniques (RAT) for environmental monitoring: Theory and applications, in *Earth Surface Remote Sensing II*, edited by G. Cecchi and E. Zilioli, *Proc. SPIE Int. Soc. Opt. Eng.*, 3496, 101–113, doi:10.1117/12.332714.
- Zebker, H. A., and R. M. Goldstein (1986), Topographic mapping from interferometric synthetic aperture radar observations, *J. Geophys. Res.*, 91, 4993–4999.

M. Aloisi, A. Bonforte, and G. Puglisi, Istituto Nazionale di Geofisica e Vulcanologia, Sezione di Catania, Piazza Roma, 2, I-95123 Catania, Italy.

G. Antonello, J. Fortuny-Guash, and D. Tarchi, Joint Research Centre, European Commission, Via Enrico Fermi 1, I-21020 Ispra, Varese, Italy.

N. Casagli and L. Guerri, Department of Earth Sciences, University of Firenze, Via la Pira 4, I-50121 Firenze, Italy.

G. Nunnari and A. Spata, Dipartimento di Ingegneria Elettrica, Elettronica e dei Sistemi, Università degli Studi di Catania, Viale Andrea Doria, I-95125 Catania, Italy.

Evolution of the Lava Flow Field by Daily Thermal and Visible Airborne Surveys

Letizia Spampinato,^{1,2} Sonia Calvari,¹ Andrew J. L. Harris,³ and Jonathan Dehn⁴

On 28 December 2002, an effusive flank eruption started at Stromboli volcano (Aeolian Islands, Italy). This lasted until 22 July 2003 and produced two lava flow fields that were emplaced onto the steep slopes of Sciara del Fuoco. The first flow field was fed by a vent that opened at 500 m elevation and was active between 30 December 2002 and 15 February 2003. The second was supplied by a vent at 670 m and was emplaced mainly between 15 February and 22 July 2003. Here we review the lava flow field emplacement based on daily thermal and visual surveys. The variable slopes on which the lava flowed yielded an uncommon flow field morphology. This resulted in a lava shield in the proximal area where flow stacking and inflation caused piling up of lava due to the relatively flat ground. The proximal area was characterized by a complex network of tumuli and associated tube-fed flows. The medial-distal lava flow field was emplaced on an extremely steep zone. This area showed persistent flow front crumbling, producing a debris field on which emplaced lava flows formed lava channels with excavated debris levées. This eruption provided an exceptional opportunity to examine the evolution of lava flow fields emplaced on steep slopes and proved the usefulness of thermal imagers for safe and efficient monitoring of the active lava flows. In addition, thermal monitoring allowed calculation of quantitative parameters, such as effusion rate, allowing constraint of the time varying nature of supply to this eruption.

1. INTRODUCTION

Although the Stromboli volcano is well-known for its persistent explosive activity, effusive flank eruptions are also

common and have a recurrence time of 5–15 years during the last few centuries [Barberi *et al.*, 1993]. Effusive activity does not pose a serious threat to the local community, and lava emplacement occurs exclusively on the barren Sciara del Fuoco (SdF) depression that cuts the NW flank of the volcano. The two previous effusive flank eruptions occurred in 1975 and 1985–1986, descriptions of which are provided by Capaldi *et al.* [1978] and De Fino *et al.* [1988], respectively.

The 2002–2003 eruption was the first of Stromboli's effusive eruptions for which a large amount of observational and geophysical data were available from continuous monitoring and routine observations. They allowed detailed reconstruction of the chronology of vent opening [Calvari *et al.*, 2005], the processes of lava flow field growth [Lodato *et al.*, 2007], quantification of effusion rate and accumulated lava volume [Calvari *et al.*, 2005; Harris *et al.*, 2005], the volume lost to the sea [Baldi *et al.*, 2008], sliding episodes that occurred at

¹Istituto Nazionale di Geofisica e Vulcanologia, sezione di Catania, Catania, Italy.

²Department of Geography, University of Cambridge, Cambridge, UK.

³HIGP/SOEST, University of Hawai'i, Honolulu, Hawaii, USA.

⁴Geophysical Institute, Alaska Volcano Observatory, University of Alaska Fairbanks, Fairbanks, Alaska, USA.

the lava flow field [Falsaperla *et al.*, 2008], and the relationship between effusive flank activity and summit explosive activity [Ripepe *et al.*, 2005].

Volcanological observation has recently been improved by the advent of portable thermal imaging cameras, which allow thermal mapping and tracking of active volcanic features [e.g., Calvari and Pinkerton, 2004; Andronico *et al.*, 2005; Burton *et al.*, 2005; Calvari *et al.*, 2005, 2006; Harris *et al.*, 2005; Patrick *et al.*, 2007; Spampinato *et al.*, 2008]. The use of the thermal camera to record the dynamics of the 5 April 2003 paroxysm at Stromboli is reviewed by Harris *et al.* [this volume] and detailed by Calvari *et al.* [2006]. However, thermal camera was also used during Stromboli's 2002–2003 effusive eruption to monitor the emplacement of the lava flow field and infer processes of flow field growth, as described by Calvari *et al.* [2005], Harris *et al.* [2005], and Lodato *et al.* [2007]. In addition, Ripepe *et al.* [2005] used satellite-based (Moderate Resolution Imaging Spectroradiometer-derived) volume flux data to show how the decline in effusion rate recorded during the eruption related to the reestablishment of "normal" Strombolian activity at the system. We here provide a review of the complex processes that occurred during this effusive eruption, the unusual emplacement mechanisms observed for these lava flows erupted onto steep slopes, and the time-varying character of the effusion rates.

2. METHODOLOGY

During the 2002–2003 effusive eruption, daily monitoring performed using a hand-held IR thermal camera (forward looking infrared, FLIR Systems), satellite (advanced very high resolution radiometer (AVHRR) and Moderate Resolution Imaging Spectroradiometer (MODIS)) images, and digital cameras proved essential for the tracking of lava flow field development and for the retrieval of daily variations in apparent temperature and effusion rate. Analysis of thermal images allowed daily mapping of active lava flows and the identification of lava flow field features, such as lava channels, lava tubes, ephemeral vents, skylights, and tumuli. Precise feature location and dimension estimates were obtained using laser ranger finders as well as triangulation using FLIR and digital camera images, with thermal and visible images being geolocated using GPS and ground control points. The quantitative analysis of thermal images proved useful to estimate temperatures of specific targets, thermal fluxes, and thus daily effusion rates. For this purpose, daily helicopter flights were performed at an altitude of ~1 km, each day repeating the same flight path to gather comparable thermal data of the entire lava flow field, as well as of the summit craters. Simultaneously, measurements of points, fixed us-

ing hand-held GPS, were carried out for pathlength estimation necessary for applying atmospheric corrections and pixel size calculations. These methodologies are detailed by Calvari *et al.* [2005], Harris *et al.* [2005], and Lodato *et al.* [2007].

3. CHRONOLOGY OF THE ERUPTION

After several months of strong explosive activity at the summit craters [Calvari *et al.*, 2005; Burton *et al.*, this volume], on 28 December, the first lava flow was erupted from a 300-m-long, NE-SW-trending fissure that opened at the northeastern flank of crater 1 (CR1 or north east crater, NEC) (Figure 1). This extended from the ~750 m elevation down to ~600 m [Calvari *et al.*, 2005; Lodato *et al.*, 2007], draining the shallow system immediately below the summit craters [Calvari *et al.*, 2005]. Debris from the breached flank of the crater mixed with a fast-moving lava flow and formed a hot avalanche that flowed down the SdF, reaching the sea at Spiaggia dei Gabbiani (Figure 1) and producing a ~4-m-thick reddish deposit of subrounded lava clasts and fine-grained ashy matrix [Calvari *et al.*, 2005; Pioli *et al.*, this

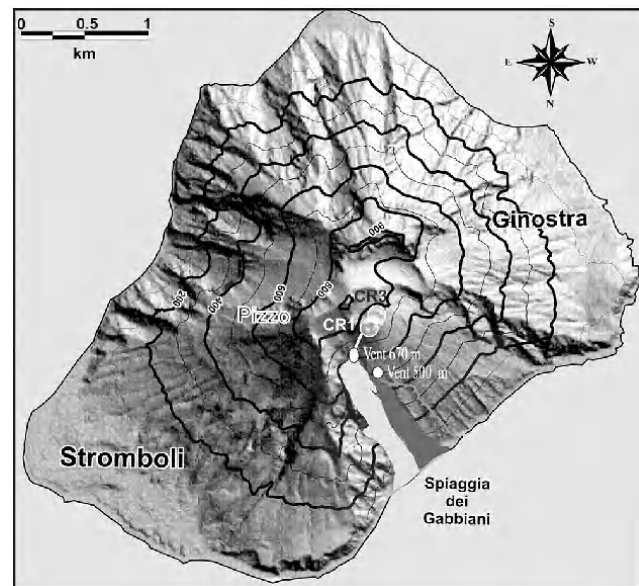


Figure 1. Shaded relief map of Stromboli Island showing SdF, the flank affected by the effusive activity, and by the 30 December landslides, the two main summit craters (CR1 and CR3), the NE-trending eruptive fissure in white, the two main effusive vents (500- and 670-m vent), the two distinct lava flow fields (in dark gray, the one fed by the 500-m vent, and light gray that fed by the 670-m vent), the Spiaggia dei Gabbiani beach, and the landslide scar (gray line) (modified after Calvari *et al.* [2005]).

volume]. This deposit was covered almost immediately by two 'a'a lava flows fed by the lowest segment of the eruptive fissure. These lava flows entered the sea after only 10–20 minutes after the eruption began, to give a time averaged velocity of 4–9 km h⁻¹ [Lodato et al., 2007]. The flows showed evidence of sliding, so that this velocity may well have been enhanced by the flows sliding down the steep slopes of the SdF [Lodato et al., 2007]. The western flow reached the sea at Spiaggia dei Gabbiani building a ~70-m-wide and 2-m-thick lava delta [Calvari et al., 2005; Lodato et al., 2007]. After 2 h of hiatus, the distal end of the eruptive fissure fed a new flow that was emplaced toward the middle section of the SdF.

By the morning of 29 December, at 1130 LT (all times are local), lava flows of the previous day were already inactive. Effusive activity resumed late in the same day. On the morning of 30 December, a thermal survey revealed the inactive 28 and 29 December flows, the cooling 30 December flows, and the opening of an effusive vent in the eastern upper portion of SdF at the 670-m elevation (Figure 1). It also revealed the development of a high-temperature fracture system along the SdF [Calvari et al., 2005]. Within a few hours, widening and extension of these fractures triggered the failure of two large portions of SdF (5×10^5 and 6×10^6 m³, respectively), which led to the generation of tsunami waves

as they entered the sea [Bonaccorso et al., 2003]. This loss in mass, along with the development and deepening of the fractures, allowed passive magma intrusion [Bonaccorso et al., 2003; Calvari et al., 2005] and eruption of lava through two new effusive vents at 500- and 550-m elevation, respectively (Figure 1). While the 550-m vent was active only for a few days, the 500- and 670-m vents were active for longer periods and built two spatially and temporally separated lava flow fields (Figure 1). Whereas the 500-m elevation vent fed lava flows until its abrupt closure on 15 February 2003, the 670-m vent was sporadic active during the first month and a half of eruption and stabilized in coincidence with the shutting of the lower 500-m vent.

Calvari et al. [2005] attributed the migration of effusive vents to higher elevations, with activity shifting from the 500-m to the 670-m vent on 15 February, to changes in magma level within the upper conduit (Figure 2). According to these authors, this process was enhanced by the proximity of the central upper conduit to the topographic surface due to the loss in rock volume after the 30 December landslides.

The 500- and 550-m vents erupted lava flows that filled the central-western sector of the SdF and entered the sea-forming lava deltas (lava field in dark gray in Figure 1). The 670-m vent also produced lava flows that reached the sea (lava field in light gray in Figure 1). However, after the

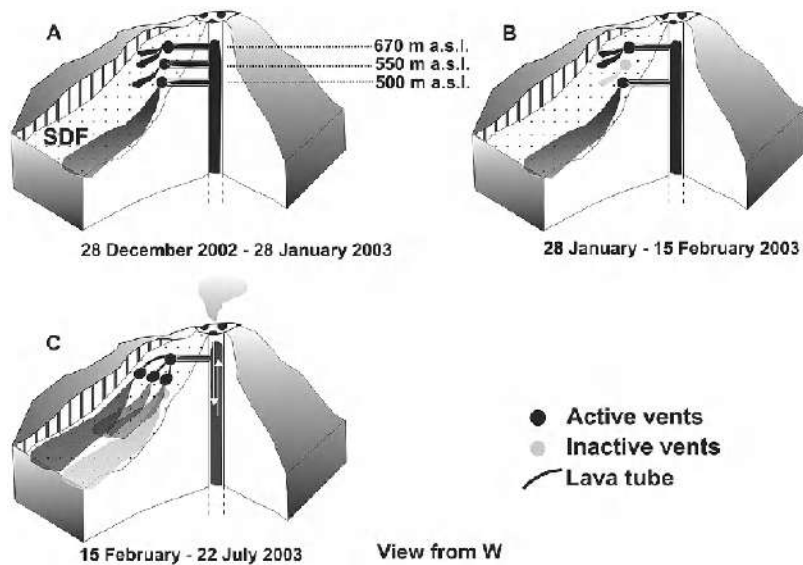


Figure 2. Qualitative models of Stromboli's 2002–2003 effusive eruption showing SdF, the site of lava emplacement, and the migration of effusive vent elevations between 28 December 2002 and 22 July 2003 (modified after Calvari et al. [2005]). (a) Three main effusive vents are simultaneously active at 670-, 550-, and 500-m elevation, respectively. (b) Only two main vents (670- and 500-m elevation, respectively) are feeding lava flows. (c) Only the 670-m elevation main effusive vent is active and supplying lava to the three secondary vents below through lava tubes.

occurrence of a major explosive event on 5 April, lava flows remained mainly confined to the proximal area until the end of the effusive eruption between 21 and 22 July 2003. A decline in lava output during the final months of the eruption was concomitant with the restart of the Strombolian activity at the summit craters [Ripepe *et al.*, 2005]. This suggested the gradual return of the volcanic system to the steady preeruptive state [Calvari *et al.*, 2005; Ripepe *et al.*, 2005; Salerno *et al.*, 2006].

4. LAVA FLOW FIELD EMPLACEMENT MECHANISMS

The first lava flows of 28 and 29 December were erupted from the lowest segment of the eruptive fissure with high effusion rates, the eruption rate on 28 December being $\sim 280 \text{ m}^3 \text{ s}^{-1}$. Such high effusion rates are to be expected in a situation where rapid drainage of a volcanic conduit occurs [e.g., Tazieff, 1977; Bertagnini *et al.*, 1990]. In the proximal area, these flows had an 'a'a surface morphology with narrow lava channels. Distally, they formed thick aprons of lava mixed with debris [Calvari *et al.*, 2005]. Features of the flows in section, as exposed at the Spiaggia dei Gabbiani beach (i.e., high amounts of entrainment, lack of basal clinker, patterns

of shear, and incorporation of underlying material), are consistent with the flows sliding down the steep underlying slope, which was composed by unconsolidated material capable of easy entrainment [Lodato *et al.*, 2007]. After this first stage of effusion, in which lava was supplied directly from a fissure opening from the base of the summit craters, the 7-month-long flank eruption was fed by the opening of topographically lower effusive vents. Here we detail the emplacement, development, closure, and features of the individual lava flow fields produced by the main effusive vents that opened at the 500- and 670-m elevations, respectively.

4.1. Lava Flow Field Fed by the 500-m Vent: 30 December 2002 to 15 February 2003

Between 30 December 2002 and 15 February 2003, persistent activity from the 500-m vent built an 'a'a compound lava flow field that was emplaced in the middle of SdF within the largest of the two 30 December landslide scars [Bonaccorso *et al.*, 2003; Calvari *et al.*, 2005] (Figures 1 and 3). This sector of the SdF was affected by collapses from failures at the boundaries of the landslide scars, as well as grain flow from failure at the active lava flow fronts [Lodato *et al.*, 2007]. Accumulation of this mixed debris modified

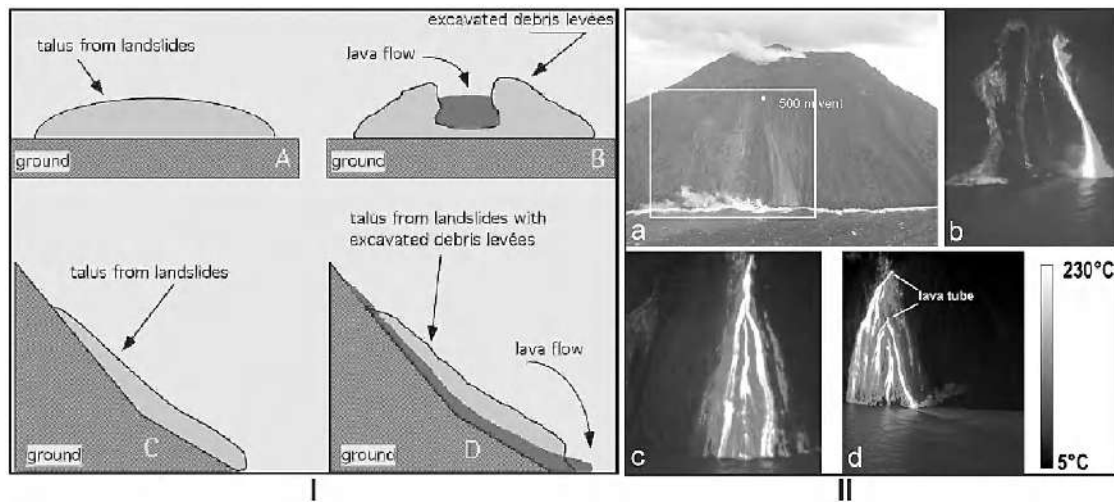


Figure 3. I. Sketch showing the formation of the excavated debris levées along the SdF. (a, b) Cross sections through the talus produced by the 30 December landslide events. (c, d) Longitudinal sections, respectively (modified after Calvari *et al.* [2005]). II. (a) Photo of SdF with the emplacement of lava flows from the 500-m vent. The white dot indicates the position of the 500-m effusive vent feeding the lava flows shown in Figures 3b–3d. The white rectangle shows the area of SdF imaged in Figures 3b–3d. The three thermal images show three different styles of lava flow emplacement associated with effusion rate variations: (b) emplacement of a single lava unit entering the sea with high effusion rates; (c) lava flow branching feeding multiple entries with moderate effusion rates; and (d) development of lava tubes and opening of ephemeral vents with low effusion rates (modified after Calvari *et al.* [2005]).

locally the topography, influencing lava flow paths and the morphology of lava flow channels. In fact, the combination of high slope gradient ($\sim 35^\circ$ – 45°) and the loose debris accumulation promoted the lava flow to mechanically erode the undelying debris, thus developing lava flow channels with excavated levées [Figure 3, I; Calvari et al., 2005].

Lava flowed as single units (Figure 3, IIb), branched flows (Figure 3, IIc), and within lava tubes, which fed flow from ephemeral vents and/or skylights (Figure 3, IIId) [Calvari et al., 2005].

The development of lava tubes on these steep slopes was favored by the continuous supply of debris from the landslide scar, which buried segments of active lava flows. The debris carpet would cover the active lava flows, which emerged from beneath the carpet at topographic breaks in slope. This initially gave the impression of effusive vent migration and downslope propagation of the feeder dike [Calvari et al., 2005].

The steady overlapping of lava flows formed a triangular lava flow field that eventually filled the largest of the 30 December landslide scars [Calvari et al., 2005]. This implied that in 19 days of activity, the 500-m elevation vent erupted a minimum lava volume $\sim 6 \times 10^6 \text{ m}^3$ (i.e., the volume of the filled scar), to give a time-averaged discharge rate of $\sim 3.7 \text{ m}^3 \text{ s}^{-1}$ [Calvari et al., 2005; Lodato et al., 2007]. Assuming a vesicularity of $\sim 22 \pm 12\%$ [Harris et al., 2000], this yielded a dense rock equivalent discharge rate of $2.9 \pm 0.4 \text{ m}^3 \text{ s}^{-1}$ [Calvari et al., 2005].

4.2. Lava Flow Field Fed by the 670-m Vent: 15 February to 22 July 2003

On 15 February, the 500-m elevation vent ceased its activity and effusion shifted to the bench at the base of CR1, where effusion had occurred sporadically between the end of December 2002 and February 2003 [Calvari et al., 2005; Lodato et al., 2007]. Over time, on this relatively gentle topography, lava flows fed by the 670-m vent built a complex, compound lava flow field (Figure 1), within which a number of secondary opened to feed tube-fed lava flows that piled up around the vent. The combination of lava flow stacking and inflation resulted in construction of a $\sim 50\text{-m}$ thick lava shield around the vent [Calvari et al., 2005; Lodato et al., 2007] (Figure 4). The development of lava tubes that were efficient in transferring lava from the main vent (670-m elevation) to lower elevations also resulted in lava flow field extension. This style of lava emplacement characterized the whole effusive period. Activity from this vent persisted through the 5 April explosive event, which changed the flow field morphology and SdF topography due to the accumulation of the 5 April deposits [Calvari et al., 2005; Lodato et al., 2007].

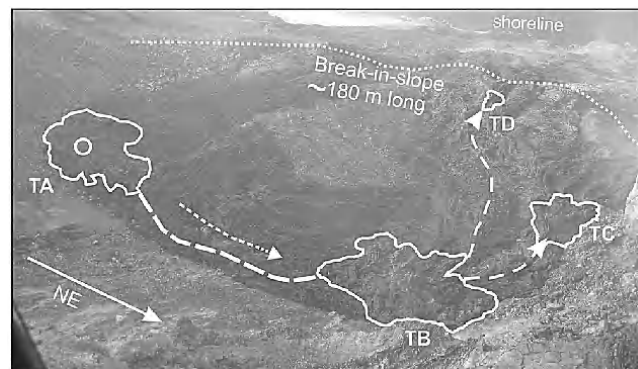


Figure 4. Photo of the upper portion of the lava flow field (top area of the light gray lava flow field in Figure 1) taken on 18 March 2003 during a helicopter survey. The four first-order tumuli (TA, TB, TC, and TD) are shown. The white dashed arrows indicate lava tube paths and lava flow direction; the break in slope at the $\sim 560\text{-m}$ elevation is also shown (modified after Lodato et al. [2007, Figure 6a] with kind permission of Springer Science+Business Media).

Thus, we split the development of the 670-m lava flow field into two periods spanning 15 February until 5 April and 5 April until the eruption end on 22 July.

4.2.1. Lava flow field development before the 5 April paroxysm. Effusive activity fed by the 670-m vent before 15 February produced numerous lava flows that spread westward but remained confined in the flat proximal area, forming a compound flow field. Flow that extended northward moved onto the steep slopes of the SdF excavating narrow lava channels and feeding crumbling flow fronts [Lodato et al., 2007]. As a result of flow front crumbling, much of the volume of these flows tumbled into the sea. Beginning on 15 February, lava rarely flowed down SdF and remained largely confined to the bench between 670 and 560 m (Figure 4). Here the continuous piling up of sheet flow lava units erupted by the 670-m vent led to the development of a domelike feature within the vent region. This structure was the result of endogenous growth due to lava injection and sheet flow inflation, as well as the exogenous piling up of flow units at the surface [Lodato et al., 2007]. Following the classification of Walker [1991], Rossi and Gudmundsson [1996] and Duncan et al. [2004], we term this feature a tumulus. This tumulus (tumulus A, TA) was the first in a series of four tumuli (tumulus B, TB; tumulus C, TC; and tumulus D, TD, in Figure 4 and Table 1) that formed across the proximal area. Except for TA, which was the main tumulus (primary focal tumulus following Duncan et al. [2004]) and developed over the main effusive vent, the others formed at exits of lava tubes that opened at topographic breaks in slope (Figure 4).

Table 1. Dates and Elevations of Tumuli Between 15 February and 22 July 2003

Order	Tumulus	Elevation, m asl ^a	Classification	Starting Day	Last Day	Duration, days
1	TA	670	Primary focal	15 Feb	22 Jul	156
1	TB	630	Secondary focal	18 Feb	22 Jul	154
1	TC	600	Primary satellite	22 Feb	11 Apr	48
1	TD	580	Primary satellite	17 Mar	9 Apr	23
2	T1	560	Secondary satellite	7 Apr	16 Jun	70
2	T2	560	Secondary satellite	7 Apr	9 Apr	2
2	T3	560	Secondary satellite	7 Apr	11 Apr	4
3	T1.1	560–630	Ephemeral	25 Jun	9 Jul	14
3	T1.2	560–630	Ephemeral	29 Jun	5 Jul	6
3	T1.3	560–630	Ephemeral	2 Jul	4 Jul	2

^aasl, m above sea level.

TA fed lava flows from its base and, eventually, from its summit until 16 February, when the development of a lava tube from its foot along the NE-trending fissure transferred lava output to a location 20–30 m below the tumulus (Figure 4). This tube became the main arterial path through which lava could reach the surface [Lodato *et al.*, 2007]. Successively, a number of short-lived lava flows piled up at the exit of this tube, generating a second focal tumulus structure (TB). By 17 March, the continuous repetition of this process had produced the development of additional tubes and tumuli (TC and TD), resulting in a complex network of tumuli connected by lava tubes (Figure 4).

4.2.2. Lava flow field development after the 5 April paroxysm. The 5 April paroxysm covered the proximal lava shield with a ~10-m-thick carpet of pyroclastics [Calvari *et al.*, 2005, 2006; Lodato *et al.*, 2007] (Figures 5a and 5b). This

caused a significant morphological change in the flow field surface, filling the depressions between single lava flows, and in the topography of SdF, extending the proximal bench ~10 m downslope (Figure 5a). However, the paroxysm did not affect lava effusion or the tube-tumulus network. In fact, after less than 2 h, lava emerged along the new break in slope, flowing through three main vents [Calvari *et al.*, 2005; Lodato *et al.*, 2007] (Figures 5a and 5b). Each of these vents was directly linked to the three buried tumuli (TB, TC, and TD) through tubes excavated within the low density and poorly consolidated debris (Figure 5b).

By 7 April, three second-order tumuli (tumulus 1, T1; tumulus 2, T2; tumulus 3, T3; Figure 5b) had developed at the location of the three vents (Figure 5b, Table 1). These linked effusion back to the three parental tumuli (TB, TD, and TC), as shown in Figure 5b. By 11 April, both T2 and T3 had deactivated, marking the death of both TD and TC

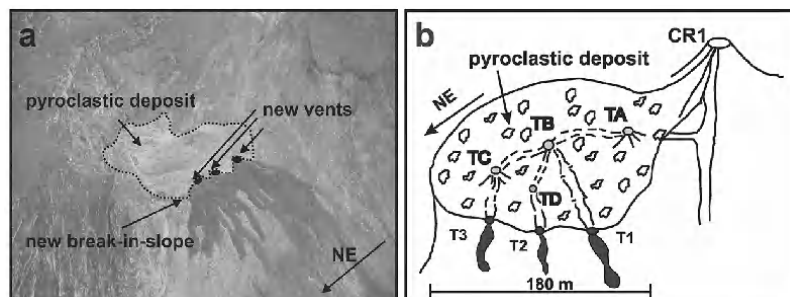


Figure 5. (a) Photo revealing the condition of the lava shield (the upper portion of the lava flow field in light gray in Figure 1) covered by the 10-m-thick pyroclastic deposit (area surrounded by the black dotted line) produced by the 5 April paroxysm and the new break in slope shifted ~10-m downslope. (b) Sketch of the lava shield with its tumuli and lava tubes buried by the 5 April deposits and the new effusive vents that opened along the new break in slope ~2 h after the paroxysm (modified after Lodato *et al.* [2007, Figure 8a] with kind permission of Springer Science+Business Media). The scale in Figure 5b indicates the maximum width of the lava flow field fed by the 670-m vent, measured in April 2003.

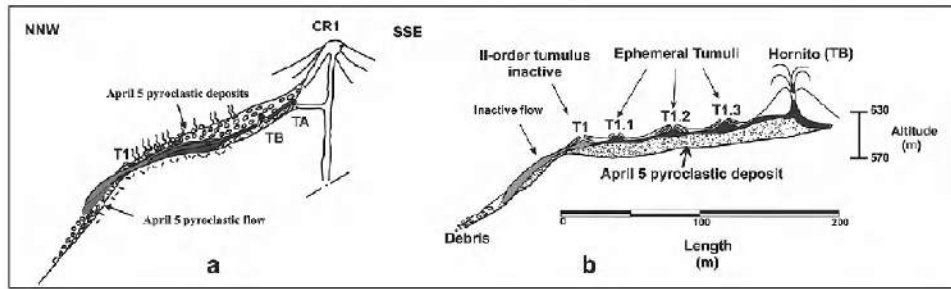


Figure 6. (a) Longitudinal section of the lava shield showing the 5 April deposit, two of the first order of tumuli TA and TB, the second-order tumulus T1, and the lava tube connecting TB to T1 (modified after Lodato *et al.* [1997, Figure 8c] with kind permission of Springer Science+Business Media). (b) Longitudinal section of the lava shield displaying the 5 April deposit, the first hornito that grew up atop TB, the lava tube TB–T1, and the third-order tumuli (ephemeral tumuli, T1.1, T1.2, and T1.3) that developed over TB–T1 tube (modified after Lodato *et al.* [2007, Figure 8d] with kind permission of Springer Science+Business Media).

and the beginning of the waning phase of the effusive activity [Lodato *et al.*, 2007]. From this point onward, lava output focused at T1, thus along the TA–TB–T1 alignment (Figure 6a).

The concentration of lava output at T1 allowed lava flows to extend down to the 300-m elevation and triggered the renewal of activity in the proximal area. Here TB emerged gradually from the 5 April pyroclastic deposit, displaying degassing and spattering activity that, by 18 April, had produced a hornito (Figure 6b). TB fed short, channelized lava flows that were emplaced onto its flanks, thus promoting further exogenous growth of TB. By 2 May, a second hornito had developed.

Effusion at T1 remained steady until the first half of June, when activity migrated back up the lava tube linking T1 with TB, over which three additional tumuli formed (T1.1, T1.2, and T1.3; Figure 6b). We named these third-order tumuli

“ephemeral tumuli” (Figure 6b, Table 1). Each formed progressively up-tube and were built by the superposition of short lava flows fed by skylights (Figure 6b). This mechanism of lava flow field regression persisted until late July, after which effusion occurred only at TB. On 22 July, the effusive eruption ended.

5. MAIN PARAMETERS CONTROLLING LAVA FLOW EMPLACEMENT

5.1. Effusion Rate

We present here data from Harris *et al.* [2005], Calvari *et al.* [2005], and Lodato *et al.* [2007], which combine effusion rates obtained from 64 FLIR thermal images and 25 AVHRR images (seven-point running in Figure 7). As shown by Calvari *et al.* [2005] and Harris *et al.* [2005], thermally derived

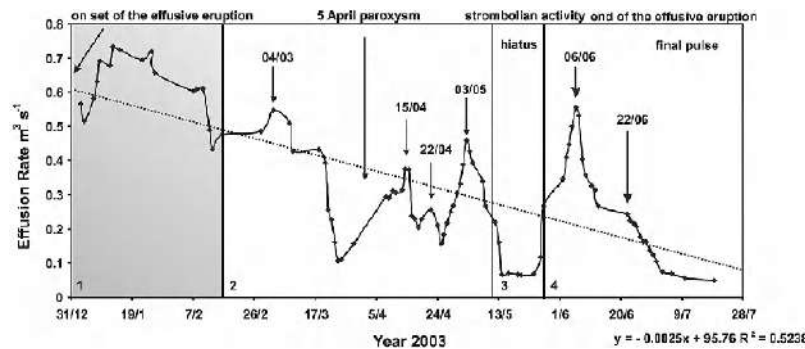


Figure 7. Seven-point running mean for effusion rate calculated using the FLIR and AVHRR data. The gray portion of the graph refers to the first effusive period (28 December 2002 to 15 February 2003) and the white to the second (15 February to 22 July 2003). The arrows mark the main events that occurred during the effusive activity, whereas the black dashed line shows the steady declining trend (modified after Lodato *et al.* [2007, Figure 9a] with kind permission of Springer Science+Business Media).

effusion rates from both data sets are consistent with field-based effusion rate measurements, with near-simultaneous results obtained from the FLIR and AVHRR data sets being consistent with one another.

Following the initial peak at the onset of the effusive activity on 28 December, effusion rate was characterized by a gradually declining trend (black dashed line in Figure 7) from $0.6\text{--}0.7 \text{ m}^3 \text{ s}^{-1}$ in January to $0.1 \text{ m}^3 \text{ s}^{-1}$ by July [Calvari *et al.*, 2005; Lodato *et al.*, 2007]. However, this behavior was not linear and displayed some significant fluctuations that allowed us to split the effusive eruption into four main periods (1, 2, 3, and 4 in Figure 7).

The first period (1) corresponded to the emplacement of the 500-m-fed lava field. This showed relatively high effusion rates ($0.6\text{--}0.5 \text{ m}^3 \text{ s}^{-1}$) that in the middle of January began to decline. By 13 February, 2 days before the shut down of the 500-m vent, effusion decayed between 0.5 and $0.4 \text{ m}^3 \text{ s}^{-1}$. The second period (2) displayed a phase of moderate effusion rate ($0.5 \text{ m}^3 \text{ s}^{-1}$), with a peak around 4 March. By 24 March, effusion decreased again reaching $\sim 0.1 \text{ m}^3 \text{ s}^{-1}$. The remaining days of this period were characterized by pulses, with two main peaks around 15 April and 3 May, separated by a smaller peak around 22 April (Figure 7). During the third period (3), effusion rates were stable and low ($\sim 0.1 \text{ m}^3 \text{ s}^{-1}$). The fourth period (4) began around 26–27 May with an

abrupt increase in effusion rate that peaked at $\sim 0.6 \text{ m}^3 \text{ s}^{-1}$ around 6 June. After that, effusion rates gradually declined to $\sim 0.1 \text{ m}^3 \text{ s}^{-1}$ by 3 July, remaining low until the end of the eruption on 22 July (Figure 7).

5.2. SdF Topography

It is well-known that topography can control lava flow paths and lava flow field morphology [e.g., Walker, 1973, 1991; Kilburn and Lopes, 1991; Calvari and Pinkerton, 1998]. To check the control of slope on flow field morphology, Lodato *et al.* [2007] divided the SdF into four sectors, a low-gradient proximal zone, an intermediate-gradient medial zone, a high-gradient medial-distal zone, and a low-gradient distal-toe zone, and examined the morphologies of each.

5.2.1. Low-gradient proximal zone. This zone represents the bench at the base of CR1 and proximal area of the lava field (Figure 8a). Here the gentle slopes, varying between 0° and 15° , allowed both endogenous (inflation and tumuli) and exogenous (lava piling up) processes. Tumuli, tumuli-fed ephemeral vents, 'a'a lava flows, tubes, skylights, and tube-fed flows built a complex flow field. Piling up of these features resulted in the formation of a proximal lava shield. Additionally, although the activity was dominated by

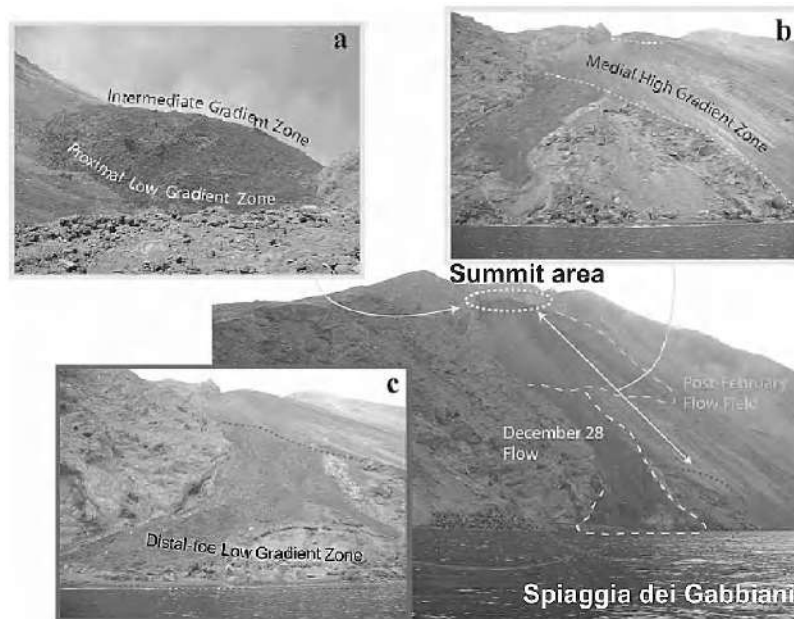


Figure 8. Photo showing the eastern edge of SdF with the four gradient zones. (a–c) Zooms of the gradient areas marked in the main photo: (a) low-gradient proximal and intermediate-gradient medial zones (view of the lava shield); (b) high-gradient medial-distal zone; (c) one of the two low-gradient distal-toe zones (modified after Lodato *et al.* [2007, Figure 4] with kind permission of Springer Science+Business Media).

emplacement of 'a'a lava flows, this was the only zone where pahoehoe flows were emplaced.

5.2.2. Intermediate-gradient medial zone. This zone includes the lava flow field emplaced between the 600- and 580-m elevations, where slopes were 15°–30° (Figure 8a). It represents a transitional region between the low-gradient proximal zone and the steeper distal zone. Here lava formed 'a'a lava flows, channels, tubes, tube-fed ephemeral vents, with channels being characterized by excavated levées [Calvari *et al.*, 2005].

5.2.3. High-gradient medial-distal zone. This zone was located below the 580-m elevation and was characterized by slopes greater than 30° (Figure 8b). Here 'a'a lava flows showed channels with excavated levées, lava tubes where segments of active lava flows were buried by debris, tube-fed ephemeral vents, skylights, and skylight-fed flows. Furthermore, due to the high gradient of the slope, this zone was the site of continuous lava flow front collapses.

5.2.4. Low-gradient distal-toe zone. This last zone comprises two low gradient areas. The first is located on the eastern edge of SdF and extends from the 300-m elevation to sea level (Spiaggia dei Gabbiani) (Figure 8c). The second is located 500 m west from the eastern edge of the SdF and extends from the 30-m elevation to the sea. Both zones were characterized by slopes varying between 5° and 15° promoting 'a'a flow, classical lava channels, dispersed flows, sea-entry flows, and lava deltas (Figure 8c).

6. DISCUSSION

The 2002–2003 effusive flank eruption of Stromboli provided a unique opportunity to study lava flow field morphology and emplacement on steep slopes. From a proximal shield, lava flowed through lava channels and tubes to feed the medial-distal portion of the flow field. Here the flows were emplaced on extremely steep slopes that promoted sliding, front crumbling, and autobrecciation. This caused an effective removal of lava volume from the slope to the sea and significantly reduced the measurable final volume of the flow field. In June 2004, for instance, the remaining volume of lava on the SdF was $\sim 2 \times 10^6 \text{ m}^3$. Based on the discrepancy between the time-integrated eruption rate measurements and the final flow field volume, 70% of the erupted volume is missing [Calvari *et al.*, 2005]. Lava front crumbling together with landslides, from the 30 December landslide scar, was responsible for the formation of a distal talus and burial of active flows to enhance tube formation.

In the medial-distal zones, accumulation of the fine-grained portion of this debris allowed for the formation of narrow lava channels characterized by excavated levées when active flow overrode such debris.

The morphology of the lava flows was not only governed by the slope gradient but also by effusion rate. During peaks in effusion rate, single 'a'a lava flows entered the sea, causing explosions at the flow fronts and accumulation of aprons of debris at the foot of the SdF (Figure 3, IIa,b). Decreases in effusion rate resulted in flow branching (Figure 3, IIc) to feed flow fields that widened the lava field in the middle of the SdF. Further decreases in effusion rate caused lava tube growth and tube-and-skylight-fed lava surface flows (Figure 3, IID). Commonly, in the proximal area, decreases in effusion rate corresponded to the growth of many small, short-lived vents. This suggested that high numbers of vents did not necessarily imply high effusion rates, but instead, the incapability of the supply system to feed single, well-fed, and long-lasting lava flows [Lodato *et al.*, 2007; Spampinato *et al.*, 2008]. The reverse was true when, after 11 April, effusion became focused at tumulus T1 and flow lengths increased. However, this was not triggered by an increase in the total effusion rate but by an increase in the local effusion rate to the T1-fed flows due to the concentration of the entire flux at one tumulus instead of three.

Overall, effusion rate revealed a gradual decreasing trend during the eruption (Figure 7). This declining rate has been shown to correlate with an increase in the free-surface level in the central conduit and the number of Strombolian events recorded at the crater terrace [Ripepe *et al.*, 2005]. Ripepe *et al.* [2005] concluded that reduced tapping of the central column by the flank effusive activity allowed magma levels in the conduit, and normal explosive activity, to steadily recover. However, this trend of declining effusion was interrupted by three significant peaks, each linked to distinct eruptive events, these being the sudden onset of effusive activity on 28 December, the 5 April paroxysm, and an increase in Strombolian activity at the summit craters during late May. The latter two revivals in effusion rate were thus associated with increases in the explosive activity at the summit craters and was followed by a period of steady effusion rate decline (Figure 7). This suggested that the eruption may have been punctuated by the arrival of three major batches of magma, the first causing the onset of the effusive eruption on 28 December and the second and third causing increases in effusion around the time of increase in explosive activity [Lodato *et al.*, 2007]. On a finer time scale, Harris *et al.* [2005] noted increases in effusion lasting a day or so following increases in vent temperature at the CR1. These were assumed to result from short-term oscillations in the

magma level in the central conduit, which increased the driving pressure for the magma erupting from the lateral vent, plausible increases in the magma-static head being consistent with the subsequent increase in effusion rate.

Because it was largely removed by collapse, the 2002–2003 effusive flank eruption produced a final lava flow field that was hard to distinguish from the preexisting morphology of the SdF. Mostly, this was because it did not exist—apart from the proximal shield it had all crumbled into Tyrrhenian. However, a total dense rock equivalent volume of $\sim 6 \times 10^6 \text{ m}^3$ was calculated by Calvari *et al.* [2005]. This, given an emplacement time of 156 days, yields mean output rate of $\sim 0.5 \text{ m}^3 \text{ s}^{-1}$. This is comparable to the mean output rate of the 1985–1986 effusive eruption ($0.3 \pm 0.2 \text{ m}^3 \text{ s}^{-1}$ [Rossi and Sbrana, 1988; Nappi and Renzulli, 1989; Harris *et al.*, 2000]), as well as the time-average supply rate calculated for normal Strombolian activity ($0.1\text{--}0.6 \text{ m}^3 \text{ s}^{-1}$ [Allard *et al.*, 1994; Harris and Stevenson, 1997]). This led Harris *et al.* [2005] to conclude that “the similarity between the erupted fluxes during these (2002–2003 and 1985–1986) effusive phases and the time-averaged supply during normal, persistent (non-effusive, Strombolian) activity, leads us to suggest that the 2002–2003 eruption comprises bleeding of the conduit at a flux typical for Stromboli.” The difference between the noneffusive and effusive phases is that the ascending (supplied) volume is not erupted in the former case but instead degasses and descends in the convecting conduit.

7. CONCLUSIONS

During the 2002–2003 effusive eruption of Stromboli, daily thermal surveys using a hand-held FLIR thermal camera allowed monitoring of the lava field emplacement and the retrieval of effusion rates.

This 7-month-long eruption was characterized by low effusion rates ($<1 \text{ m}^3 \text{ s}^{-1}$), which produced $\sim 6 \times 10^6 \text{ m}^3$ of lava and uncommon lava flow field morphologies. These uncommon morphologies were strongly controlled by the steep slopes on which lava emplaced. The result was a number of characteristic lava field features. Several papers deal with basaltic lava morphology flowing on relatively gentle surfaces, and our contribution provides a framework for tracking, understanding, and interpreting the evolution of lava flow fields emplaced on steep slopes. In addition, the thermal camera-data- and satellite-data-based effusion rates improved our understanding of the time-varying nature of effusion at Stromboli and its relation to the magma supply to the shallow system.

Acknowledgments. Two anonymous referees are acknowledged for their constructive reviews that significantly improved the

manuscript. L. S. thanks the project “Sviluppo di Sistemi di Monitoraggio” (Dipartimento di Protezione Civile di Regione Sicilia, INGV Catania Section, Italy) for funding her doctoral research.

REFERENCES

- Allard, P., J. Carbonelle, N. Métrich, H. Loyer, and P. Zettwoog (1994), Sulphur output and magma degassing budget of Stromboli volcano, *Nature*, **368**, 326–330.
- Andronico, D. *et al.* (2005), A multi-disciplinary study of the 2002–03 Etna eruption: Insights into a complex plumbing system, *Bull. Volcanol.*, **67**, 314–330.
- Baldi, P., M. Coltelli, M. Fabris, M. Marsella, and P. Tommasi (2008), High precision photogrammetry for monitoring the evolution of the NW flank of Stromboli volcano during and after the 2002–2003 eruption, *Bull. Volcanol.*, **70**, 703–715.
- Barberi, F., M. Rosi, and A. Sodi (1993), Volcanic hazard assessment at Stromboli based on review of historical data, *Acta Vulcanol.*, **3**, 173–187.
- Bertagnini, A., S. Calvari, M. Coltelli, P. Landi, M. Pompilio, and V. Scrivano (1990), The 1989 eruptive sequence, in *Mt. Etna: The 1989 Eruption, CNR GNV Spec. Issue*, edited by F. Barberi, A. Bertagnini, and P. Landi, pp. 10–22, Giardini, Pisa.
- Bonaccorso, A., S. Calvari, G. Garfi, L. Lodato, and D. Patanè (2003), Dynamics of the December 2002 flank failure and tsunami at Stromboli volcano inferred by volcanological and geophysical observations, *Geophys. Res. Lett.*, **30**(18), 1941, doi:10.1029/2003GL017702.
- Burton, M. R., *et al.* (2005), Etna 2004–2005: An archetype for geodynamically-controlled effusive eruptions, *Geophys. Res. Lett.*, **32**, L09303, doi:10.1029/2005GL022527.
- Burton, M., S. Calvari, L. Spampinato, L. Lodato, N. A. Pino, E. Marchetti, and F. Murè (2008), Volcanic and seismic activity at Stromboli preceding the 2002–2003 eruption, this volume.
- Calvari, S., and H. Pinkerton (1998), Formation of lava tubes and extensive flow field during the 1991–1993 eruption of Mount Etna, *J. Geophys. Res.*, **103**, 27,291–27,303.
- Calvari, S., and H. Pinkerton (2004), Birth, growth and morphologic evolution of the “Laghetto” cinder cone during the 2001 Etna eruption, *J. Volcanol. Geotherm. Res.*, **132**, 225–239.
- Calvari, S., L. Spampinato, L. Lodato, A. J. L. Harris, M. R. Patrick, J. Dehn, M. R. Burton, and D. Andronico (2005), Chronology and complex volcanic processes during the 2002–2003 flank eruption at Stromboli volcano (Italy) reconstructed from direct observations and surveys with a hand-held thermal camera, *J. Geophys. Res.*, **110**, B02201, doi:10.1029/2004JB003129.
- Calvari, S., L. Spampinato, and L. Lodato (2006), The 5 April 2003 vulcanian paroxysmal explosion at Stromboli volcano (Italy) from field observations and thermal data, *J. Volcanol. Geotherm. Res.*, **149**(1–2), 160–175.
- Capaldi, G., *et al.* (1978), Stromboli and its 1975 eruption, *Bull. Volcanol.*, **41**(3), 259–285.
- De Fino, M., L. La Volpe, S. Falsaperla, G. Fazzetta, G. Neri, L. Francalanci, M. Rosi, and A. Sbrana (1988), The Stromboli

- eruption of December 6, 1985–April 25, 1986: Volcanological, petrological and seismological data, *Rend. Soc. Ital. Mineral. Petrol.*, **43**, 1021–1038.
- Duncan, A. M., J. E. Guest, E. R. Stofan, S. W. Anderson, H. Pinkerton, and S. Calvari (2004), Development of tumuli in the medial portion of the 1983 'a'a flow-field, Mount Etna, Sicily, *J. Volcanol. Geotherm. Res.*, doi:10.1016/S0377-0273(03)00344-5.
- Falsaperla, S., V. Maiolino, S. Spampinato, O. Jaquet, and M. Neri (2008), Sliding episodes during the 2002–2003 Stromboli lava effusion: Insights from seismic, volcanic, and statistical data analysis, *Geochem. Geophys. Geosyst.*, **9**, Q04022, doi:10.1029/2007GC001859.
- Harris, A. J. L., and D. S. Stevenson (1997), Thermal observations of degassing open conduit and fumaroles at Stromboli and Vulcano using remotely sensed data, *J. Volcanol. Geotherm. Res.*, **76**, 175–198.
- Harris, A. J. L., J. B. Murray, S. E. Aries, M. A. Davies, L. P. Flynn, M. J. Wooster, R. Wright, and D. A. Rothery (2000), Effusion rate trends at Etna and Krafla and their implications for eruptive mechanisms, *J. Volcanol. Geotherm. Res.*, **102**, 237–270.
- Harris, A., J. Dehn, M. Patrick, S. Calvari, M. Ripepe, and L. Lodato (2005), Lava effusion rates from hand-held thermal infrared imagery: An example from the June 2003 effusive activity at Stromboli, *Bull. Volcanol.*, **68**(2), 107–117.
- Harris, A. J. L., M. Ripepe, S. Calvari, L. Lodato, and L. Spampinato (2008), The 5 April 2003 explosion of Stromboli: Timing of eruption dynamics using thermal data, this volume.
- Kilburn, C. R. J., and R. M. C. Lopes (1991), General patterns of flow field growth: Aa and blocky lavas, *J. Geophys. Res.*, **96**(B12), 19,721–19,732.
- Lodato, L., L. Spampinato, A. Harris, S. Calvari, J. Dehn, and M. Patrick (2007), The morphology and evolution of the Stromboli 2002–03 lava flow field: An example of basaltic flow field emplaced on a steep slope, *Bull. Volcanol.*, **69**, 661–679, doi:10.1007/s00445-006-0101-6.
- Nappi, G., and A. Renzulli (1989), Stromboli, *Bull. Volc. Eruptions*, **26**, 1–3.
- Patrick, M. R., A. J. L. Harris, M. Ripepe, J. Dehn, D. A. Rothery, and S. Calvari (2007), Strombolian explosive styles and source conditions: Insights from thermal (FLIR) video, *Bull. Volcanol.*, **69**, 769–784.
- Pioli, L., M. Rosi, S. Calvari, L. Spampinato, A. Renzulli, and A. Di Roberto (2008), The eruptive activity of 28 and 29 December 2002, this volume.
- Ripepe, M., E. Marchetti, G. Ulivieri, A. Harris, J. Dehn, M. Burton, T. Caltabiano, and G. Salerno (2005), Effusive to explosive transition during the 2003 eruption of Stromboli volcano, *Geology*, **33**, 341–344.
- Rossi, M., and A. Sbrana (1988), Stromboli, *Bull. Volc. Eruptions*, **25**, 7–8.
- Rossi, M. J., and A. Gudmundsson (1996), The morphology and formation of flow-lobe tumuli on Icelandic shield volcanoes, *J. Volcanol. Geotherm. Res.*, **72**, 291–308.
- Salerno, G., L. Spampinato, M. Burton, S. Calvari, L. Lodato, T. Caltabiano, D. Andronico, D. Condarelli, V. Longo, and F. Muré (2006), Hiatus in the typical Strombolian activity during the 2002–03 Stromboli effusive eruption: SO₂ flux degassing and thermal release relationship as a marker of anomalous activity, paper presented at GPL Walker Symposium 2006, Reykholt, Reykjavik, Iceland.
- Spampinato, L., S. Calvari, C. Oppenheimer, and L. Lodato (2008), Shallow magma transport for the 2002–3 Mt. Etna eruption inferred from thermal infrared surveys, *J. Volcanol. Geotherm. Res.*, in press.
- Tazieff, H. (1977), An exceptional eruption: Mt. Nyragongo, Jan. 10th, 1977, *Bull. Volcanol.*, **40**, 189–200.
- Walker, G. P. L. (1973), Lengths of lava flows, *Philos. Trans. R. Soc. London, Ser. A*, **274**, 107–118.
- Walker, G. P. L. (1991), Structure, and origin by injection of lava under surface crust of tumuli, "lava rises", "lava-rise pits", and "lava-inflation clefts" in Hawaii, *Bull. Volcanol.*, **53**, 546–558.

S. Calvari and L. Spampinato, Istituto Nazionale di Geofisica e Vulcanologia, sezione di Catania, Piazza Roma 2, I-95123 Catania, Italy.

J. Dehn, Alaska Volcano Observatory, Geophysical Institute, University of Alaska Fairbanks, Fairbanks, AK 99775, USA.

A. J. L. Harris, HIGP/SOEST, University of Hawai'i, 2525 Correa Road, Honolulu, HI 96822, USA.

Textural and Compositional Characteristics of Lavas Emitted During the December 2002 to July 2003 Stromboli Eruption (Italy): Inferences on Magma Dynamics

P. Landi,¹ L. Francalanci,² R. A. Corsaro,³ C. M. Petrone,^{2,4} A. Fornaciai,¹ M. R. Carroll,⁵ I. Nardini,² and L. Miraglia³

Periodic lava sampling was carried out at the active vents during the entire duration of the 28 December 2002 to 22 July 2003 effusive eruption. Major and trace element bulk rock analyses were performed at different laboratories, thereby acquiring four independent sets of analysis. Nd and Sr isotope ratios were obtained on whole rocks and groundmasses, together with micro-Sr isotope analyses on plagioclase and clinopyroxene by microdrilling technique. Crystal size distribution, mineral, and glassy matrix chemistry were analyzed on selected samples. The products show a fairly homogeneous composition, close to that of the crystal-rich scoria that erupted in the previous years. Slight variations of trace elements and isotope ratios between products that erupted before and after the 5 April paroxysm are likely accounted for by limited mixing between the fresh, volatile-rich magma that erupted during the paroxysm and the volatile-poor magma feeding the lava flow. Micro-Sr isotope data show large isotopic disequilibria pointing to the persistence of highly Sr-radioactive xenocrysts or crystal cores in the shallow magmatic system, probably recycled from the previous activity. Data rule out important changes in the dynamics of the plumbing system shortly before the eruption. A discrete input of deep magma into the lower part of the shallow system some months before the eruption may be at the origin of the increase of the magmatostatic pressure in the conduits, leading to the effusive eruption. An alternative hypothesis considers a nearly steady-state feeding system undergoing gradual, long-term pressure increase in its upper part, eventually leading to periodic lava effusions.

1. INTRODUCTION

Effusive episodes represent one of the manifestations that periodically interrupt the persistent Strombolian activity of

the volcano. Small volumes of lava flows are generally produced by overflows from the summit craters, whereas lateral vents opened a few hundred meters below the craters, which usually feed more voluminous lava flows. Only in 1955 was

¹ Istituto Nazionale di Geofisica e Vulcanologia, Sezione di Pisa, Pisa, Italy.

The Stromboli Volcano: An Integrated Study of the 2002–2003 Eruption
Geophysical Monograph Series 182
Copyright 2008 by the American Geophysical Union.
10.1029/182GM18

² Dipartimento di Scienze della Terra, Università degli Studi di Firenze, Florence, Italy.

³ Istituto Nazionale di Geofisica e Vulcanologia, Sezione di Catania, Catania, Italy.

⁴ Now at Department of Earth Sciences, Cambridge University, Cambridge, UK.

⁵ Dipartimento di Scienze della Terra, Università degli Studi di Camerino, Camerino, Italy.

it reported that an effusive vent had opened at shoreline level in the central part of the Sciara del Fuoco (SdF) [Abruzzese and Cavallaro, 1956]. Twenty-six effusive episodes were reported between 1888 and 2002. The duration of lava effusion ranges from a few days to 11 months, with an average time of about 90 d [Barberi *et al.*, 1993]. The volume of the two most recent lava flows (erupted in 1975 and 1985–1986) was estimated to be about 10^4 and $6 \times 10^6 \text{ m}^3$, respectively [Capaldi *et al.*, 1978; De Fino *et al.*, 1988].

The magma emitted during the effusive episodes is the same crystal-rich, volatile-poor magma with basaltic–shoshonitic composition, which commonly sustains the persistent Strombolian activity. This high-porphyritic magma significantly differs from the crystal-poor, volatile-rich magma produced during most paroxysmal explosive eruptions, in terms of crystal and volatile contents, mineral chemistry, Sr isotope ratios, and composition of the groundmass [Capaldi *et al.*, 1978; De Fino *et al.*, 1988; Francalanci *et al.*, 1999, 2004b, 2005; Metrich *et al.*, 2001; Landi *et al.*, 2004]. Nevertheless, the two magmas show minor differences in the bulk chemical composition (shoshonitic basalts and HK basalts, respectively). This suggests a magmatic system with a shallow degassed body, mainly resulting from the crystallization of deep volatile-rich magmas through decompression and water loss at low pressure [Metrich *et al.*, 2001].

While sampling of the erupted products, followed by petrological characterization during the eruption, has become a common monitoring tool for most effusive volcanoes, a systematic sampling of the products during the entire period of an effusive episode was carried out at Stromboli for the first time during the 2002–2003 eruption. The textural and compositional studies of the collected samples and the comparison with the large set of data available in the literature offer the opportunity to better evaluate the magma conditions related to an effusive episode at Stromboli and their relationships with the magmatic processes operating during normal Strombolian activity. Furthermore, the occurrence of a paroxysmal explosion during the effusive event on 5 April 2003 was an excellent opportunity to investigate how the transit of a batch of crystal-poor, volatile-rich magma through the shallow system can change the equilibrium of the shallow crystal-rich magma [Landi *et al.*, 2006].

2. THE 2002–2003 ERUPTIVE ACTIVITY

The lava flow eruption evolved through four main phases.

Phase I (28–30 December 2002): During the first 2 d, the activity was dominated by relatively high lava discharge rate from vents opened at the foot of the NE cone [≈ 650 and 600 m above sea level (asl)] and by contemporaneous gravity movements in the SdF (Figure 1), which culminated

in the cumulative collapse of $15\text{--}20 \times 10^6 \text{ m}^3$ of material on 30 December [Tommasi *et al.*, 2003, 2005]. The eruptive phenomena included a short-lived mild explosive episode from the lateral vent opened in the upper part of the SdF on the afternoon of 28 December; a lava overflow from the NE crater that, late in the afternoon of 28 December, descended at a high speed over the northeast slope of the SdF (Filo del Fuoco) down to the sea, producing a pahoehoe lava flow; a rootless lava flow, which descended along the easternmost border of the SdF late in the night of 28 December. According to Marsella *et al.* [this volume], a cumulative volume of $2 \times 10^6 \text{ m}^3$ with an average effusion rate of about $10 \text{ m}^3/\text{s}$ was erupted during this phase.

Phase II (31 December 2002 to 16 February 2003): Soon after the landslide, effusive activity concentrated in vents located from 500- to 550-m elevation within the scar left by the landslide. In addition, temporary halting of the lava emission from vents at 550 m asl was soon followed by lava outpouring from vents at 600 m asl at the foot of the NE cone in January. This phenomenon was sometimes accompanied by the apparent variations of the output rate. During the first days of February, active vents slowly moved at higher elevation (600 m asl), while lava effusion from the vent at 550 m asl ceased on 15 February. In this time span, effusion rate

Figure 1. Map of the SdF on the NE flank of Stromboli. Dark gray, lava field produced during the 2002–2003 effusive events; SWC, southwest crater; NEC, northeast crater. Modified from Landi *et al.* [2006].

progressively decreased from $6.4 \text{ m}^3/\text{s}$, measured during the early days of January, to $0.25 \text{ m}^3/\text{s}$ at the beginning of February [Marsella *et al.*, this volume].

Phase III (17 February to mid-April 2003): After a pause of 2 d on 17 February, lava effusion resumed from a vent located at about 580 m asl, at the foot of the Bastimento. This vent remained active until mid-April, giving rise to a compound lava field mainly restricted to the flat zone (Pianoro) between 550 and 600 m asl at the foot of the Bastimento (Figure 1). The effusion rate decreased from $0.7 \text{ m}^3/\text{s}$, in February, to $0.4 \text{ m}^3/\text{s}$, in April. In 5 April 2003, a major explosive eruption occurred from the summit craters. Effusive activity stopped for a couple of hours and then resumed from three vents at the edge of the Pianoro at about 600 m asl.

Phase IV (mid-April to late July 2003): Since 16 April 2003, weak degassing followed by spattering became progressively more evident from a site located in the middle part of the Pianoro. Significant spattering activity occurred there between 21 May and 3 June, resulting in the rapid growth of two hornitos up to 10 m high. In July, the effusion rate further decreased to less than $0.1 \text{ m}^3/\text{s}$, and lava output ended on 22 July.

2.1. Activity at the Summit Craters During the Effusive Period

The onset of the effusive phase from lateral vents in 28 December 2002 led to a drop of magma level in the central conduit and to the cessation of the Strombolian activity from the central crater. In March, moderate and discontinuous ejections of very fine grained, pink-colored ash resumed in the summit craters. This was followed by intensification of the explosions in the second half of April and by the gradual appearance of the glowing material starting from 3 May. The waning phase of the lava output (phase IV) was accompanied by a rapid rise of lava in the central conduit and the full resumption of normal Strombolian activity in all craters [Ripepe *et al.*, 2005].

3. SAMPLING

A total of 35 samples were collected during the whole eruptive episode [Landi *et al.*, 2006]. The products that erupted during the first phase of the effusive event were collected in the following days in the summit area, just near the effusive fissure, along the SdF, and on the coast. From January

Figure 2. Photomicrograph of the 2002–2003 lavas: (a) typical porphyritic texture of the lavas in which plagioclase is the dominant phase; (b) aggregate of clinopyroxene and olivine; (c) plagioclase with concentric zoning; (d) large clinopyroxene with resorbed cores and thin layer (more clear zones) with diopsidic composition.

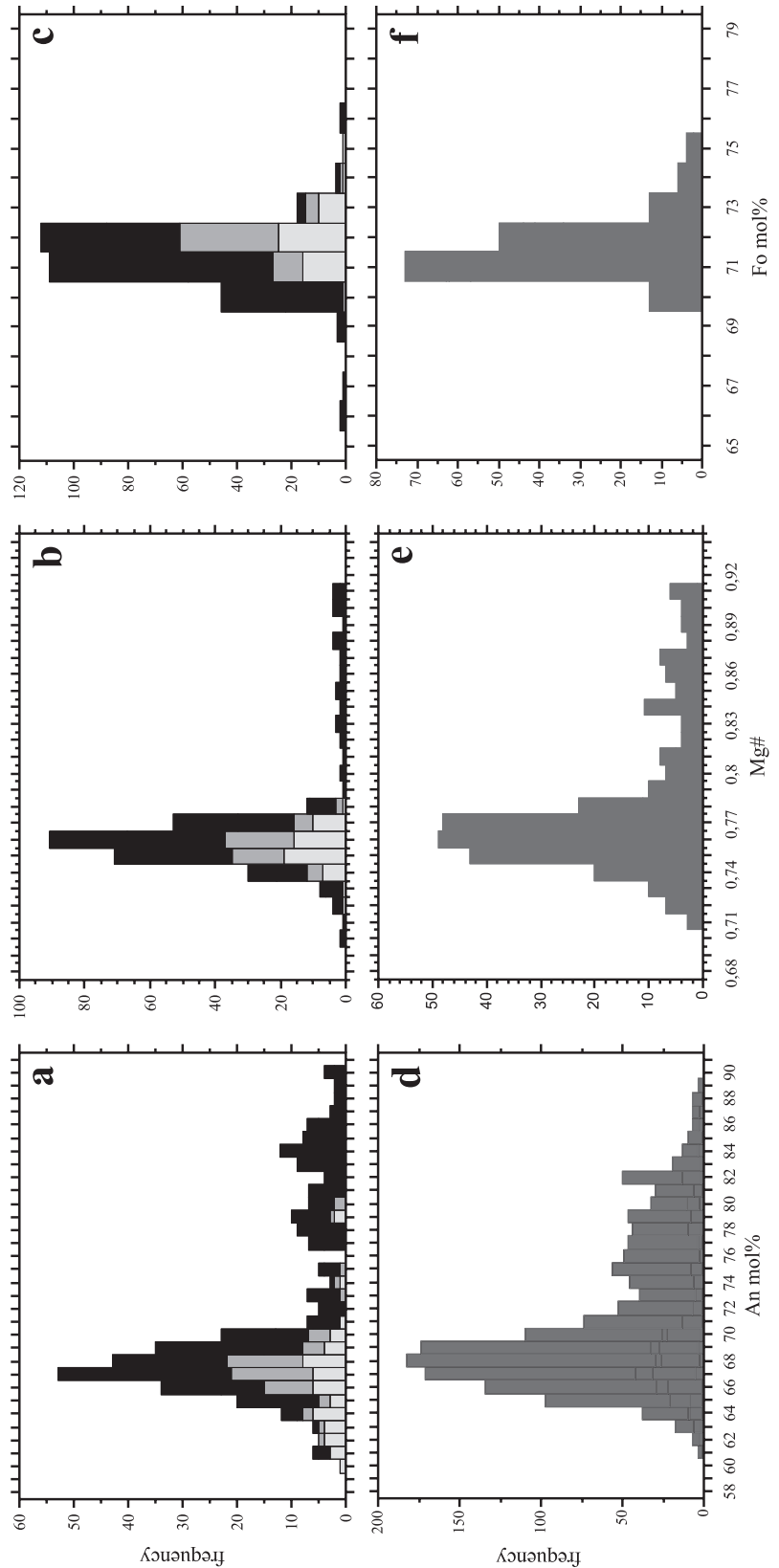


Figure 3. Cumulative (a) plagioclase, (b) clinopyroxene, and (c) olivine compositions of the 2002–2003 lavas. Black, interior part of the crystals; dark gray, crystal rims $<20\text{ }\mu\text{m}$ in the lavas that erupted before 5 April 2003; light gray, crystal rims $<20\text{ }\mu\text{m}$ in the lavas that erupted after 5 April 2003 (data from Landi *et al.* [2006]). (d–f) For comparison, the mineral compositions of the scoriae and lavas that erupted between 1985 and 2000 are reported (data from Métrich *et al.* [2004], Francalanci *et al.* [2001], and Landi *et al.* [2004, 2006]).

2003 onward, lava was sampled from the active channel in the lava field at 550–600 m asl, every 10–15 d on average. Most of these samples were quenched in water. The lavas that erupted during the phase II within the scar left by the landslide were not sampled because the lava channel was inaccessible. Unfortunately, the difficult access to the lava field and the very dangerous position of the active vents, just close to the summit craters, prevented a daily sampling. However, based on the characteristics of the crystal-rich products usually erupted at Stromboli and on the temporal variations observed during the lava effusion, we consider a suite of 35 samples representative of the magmatic processes involved in the 2002–2003 effusive eruption.

Scoriae emitted from the summit craters in November 2002 some days before the onset and after the end (on 6 September and 28 September 2003) of the 2002–2003 eruption were analyzed for a comparison.

4. PETROGRAPHY AND CHEMISTRY OF THE PRODUCTS

4.1. Mineral Chemistry and Composition of the Glassy Groundmass

Lavas and spatter collected during the eruption are crystal-rich products with 38–54 vol % (45 vol % on average) of euhedral phenocrysts represented by 23–31 vol % of plagioclase (0.1–2.5 mm in size), 5–19 vol % of clinopyroxene (0.5–5 mm), and 2–8 vol % of olivine (0.1–4 mm), set in a glassy to hypocrystalline matrix (Figure 2). Glomeroporphyritic aggregates up to 6–7 mm in diameter, mainly made up of clinopyroxene and olivine, are frequent (Figure 2b).

Plagioclase crystals are dominated by concentric zoning consisting of alternating layers (<10 to ~150 μm wide) of labradoritic (An_{60} – An_{70}) and bytownitic (An_{70} – An_{90}) plagioclase (Figures 2c and 3a). The plagioclase rims are labradoritic. In the lavas that erupted from December 2002 to March 2003, plagioclase crystals mainly have An_{70} – An_{65} composition, whereas in the lava emitted after April 2003, they eventually attain more sodic composition, up to An_{60} (Figure 3a). Clinopyroxene composition clusters around $\text{Mg} \# 0.74$ – 0.77 (= molar $[\text{Mg}/(\text{Mg} + \text{Fe}_t)]$) (Figure 3b). Mg-rich compositions ($\text{Mg} \# 0.8$ – 0.91) are present as corroded cores and/or thin layers with rounded boundaries (Figure 2d). Olivine composition is in the range Fo_{70} – Fo_{74} , the outer rims being on average more forsteritic (Fo_{71} – Fo_{73}) than the inner part of the crystals (Fo_{70} – Fo_{72} ; Fig. 3c). Crystals with more forsteritic rims, up to Fo_{76} , are rarely found in the samples that erupted at the end of the eruption. More evolved clinopyroxene with $\text{Mg} \# 0.70$ – 0.72 and olivine Fo_{66} – Fo_{69} are sporadically found in the cores of the crystals and/or

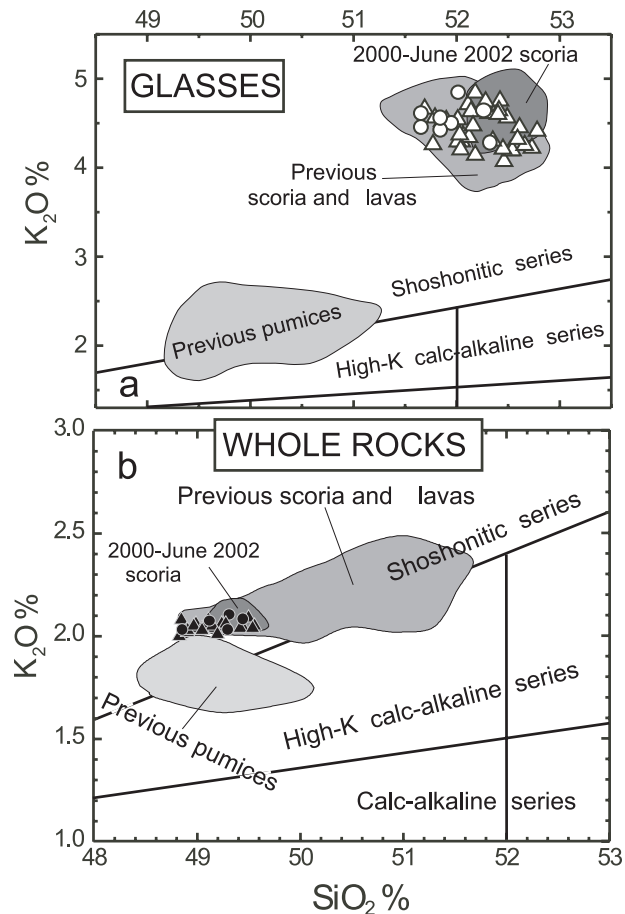


Figure 4. Classification diagrams for the whole rock and glassy groundmass of the products emitted in the 2002–2003 effusive events. Circle, scoria; triangle, lavas. Data are reported on water-free bases. The compositional fields of whole rock and groundmass of the products that erupted between 1900 and 2002 (both crystal-rich scoriae and crystal-poor pumice) are reported for comparison (data from Métrich et al. [2001], Francalanci et al. [2004b, 2005], and Landi et al. [2004, 2006]).

narrow layers in the inner part of them. Mineral composition of the 2002–2003 lavas are the same as those observed in the scoriae that erupted during normal Strombolian activity (Figures 3d–3f).

The microlite-free glassy groundmasses have a shoshonitic composition with SiO_2 (~52 wt %), fairly high K_2O content (4.2–4.8 wt %), and $\text{CaO}/\text{Al}_2\text{O}_3$ (0.46–0.48). In the $\text{K}_2\text{O}-\text{SiO}_2$ classification diagram, they plot in the same narrow field as the scoria bombs that erupted during the last decade (Figure 4). Small but systematic compositional variations can, however, be recognized between the products that

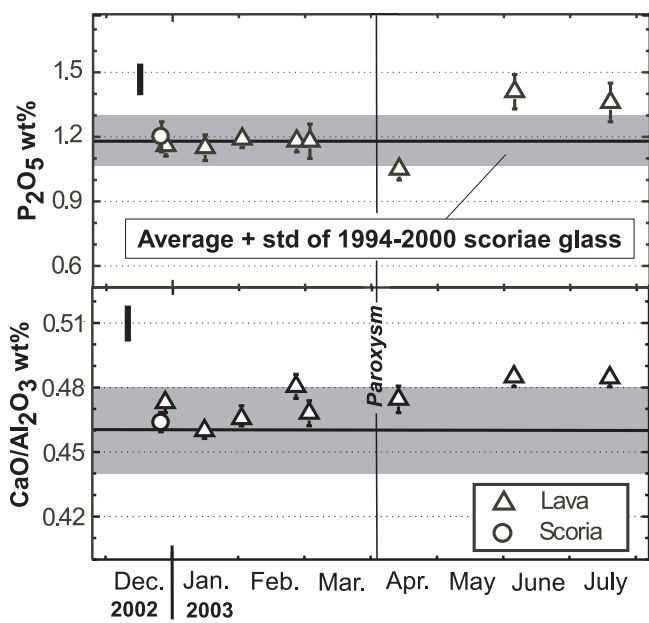


Figure 5. Variation diagram with time of $\text{CaO}/\text{Al}_2\text{O}_3$ and K_2O of the average composition of the groundmasses (four to eight quoted analyses for each sample). Bars indicate the standard deviation. Gray field, average composition of the glassy groundmasses of the scoria bombs that erupted from 1994 to June 2002 (data from *Fran-calanci et al. [2004b]*). Modified from *Landi et al. [2004]*.

erupted during the whole effusive eruption: $\text{CaO}/\text{Al}_2\text{O}_3$ ratio shows a general tendency to increase with time from 0.46 to 0.48; K_2O content slightly decreases after March 2003; the groundmasses of June and July 2003 display the highest P_2O_5 and lowest Na_2O contents (Figure 5).

4.2. Textural Features

The lavas produced during the effusive eruption of Stromboli in 2002–2003 are in general relatively homogeneous in texture. However, some textural differences were found between samples from the beginning of the eruption (end of December) and samples taken in February 2003. The samples taken in late December were collected at 250 m asl and represent the rootless flow involving the products that erupted in the afternoon of 28 December. Figure 6a shows a thin section of one of them and shows significant effects of resorption and development of sieve textures in plagioclase—interpreted to represent heating of preexisting crystals due to new (hotter) magma input (Carroll, unpublished data). In contrast, samples from February 2003 (Figure 6b) show euhedral crystals and no evidence of disequilibrium, suggesting that the magma system had achieved or approached a state of equilibrium.

The crystal size distribution (CSD) for plagioclase of 12 selected samples, which erupted during the effusive pe-

Figure 6. Photomicrograph showing (a) resorbed and sieve-textured plagioclase from samples of the rootless flow involving the products that erupted in the afternoon of 28 December (field of view, ~2 mm) and (b) euhedral plagioclase from sample taken in February 2003. Lack of resorption or disequilibrium features suggests the magma system has approached a state of equilibrium (field of view, ~2 mm).

riod, was measured using computer-based image analysis (Fornaciai et al., 2008; Dissolution–crystallization kinetics recorded in the 2002–2003 lavas of Stromboli (Italy), submitted to *Bulletin of Volcanology*, 2008, hereinafter referred to as Fornaciai et al., submitted manuscript, 2008). Mineral grain identification was performed by inspecting images of standard petrographic thin sections acquired with high-resolution film scanner [Tarquini and Armienti, 2001]. Image processing grain identification has been performed developing procedure with the VISILOG 6.1 package. The equivalent diameter of the crystals was measured [Tarquini and Armienti, 2001]. Stereological corrections based on the Schwartz–Saltykov algorithm [De Hoff and Rhines, 1972] are applied to the data to convert the two-dimensional measurements to a three-dimensional estimate of the population density. A total of 5000–6000 crystals were counted in each sample.

In the diagrams with size of crystals (D) versus $m[N(D)]$ ($N(D)$ = number density), the distribution of all the analyzed samples, in the entire representative size range of the plagioclase crystals (from 0.063 to ~ 1 mm), shows linear trends (Figure 7a) with slope (m) between –6.3 and –7.9 (average value = -7.1 ± 0.45) and intercept between 5.1 and 5.7 (average value = 5.4 ± 0.17). Most of the slope values (m) fall within the analytical error calculated as 1 standard deviation (Figure 7b). As a whole, CSD values of the lavas that erupted during the whole effusive period can be considered quasi-constant, with minor oscillations that fall within the value range covered by the crystal-rich scoriae that usually erupted during normal Strombolian activity (Figure 7b). The upturn in the CSD plot for small crystals ($D < 0.28$ mm) does not seem to be associated with the growth of microlite after the lava extrusion because (1) most of samples were collected at the active vents and immediately quenched in water and (2) microlites are on average <100 μm . Most likely, it represents the final phase of degassing, prior to the magma eruption (Fornaciai et al., submitted manuscript, 2008).

Linear trends of the CSD, with minor variation in m and $\ln N(D)$ is a feature of the crystal-rich products, both lavas and scoria, that erupted from Stromboli in the present-day activity [Armienti et al., 2007]. A plot in a semilogarithmic diagram of $\ln(n)$ versus the size of the class provides linear trends in a steady-state case, in which the slope is proportional to $-1/G\tau$ (where G is the crystal growth rate and τ is the time), and the intercept on the y axis yields the nucleation rate [Marsh, 1988; Cashman and Marsh, 1988]. This means that Stromboli works as a steady-state system controlled by continuous intrusions of deep, volatile-rich magma into the shallow, crystal-rich body and their mixing associated with mineral dissolution and crystallization.

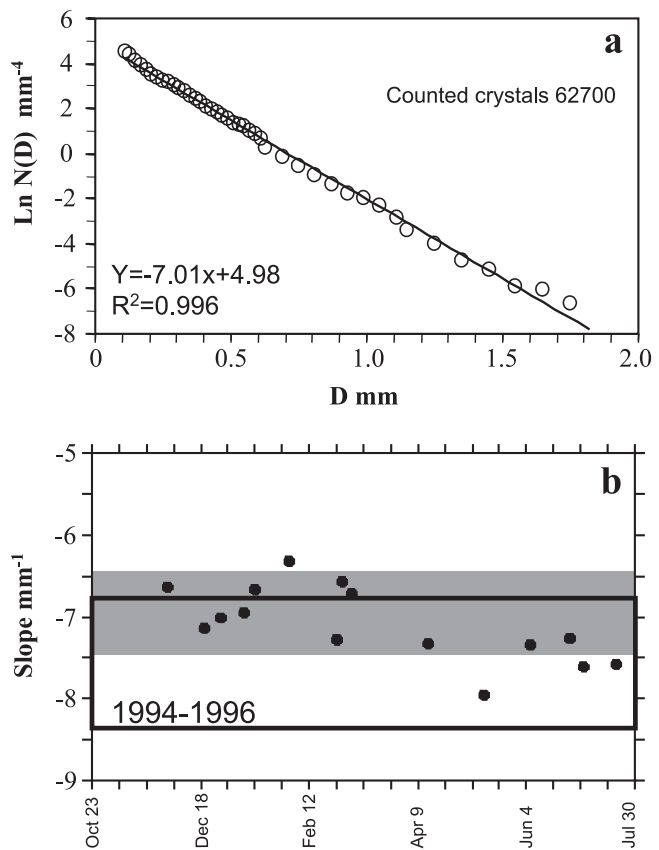


Figure 7. (a) Cumulative plagioclase size distribution of the 2002–2003 lavas. (b) Temporal variations of the slopes of the plagioclase CSDs in the 2002–2003 lavas. Gray, ± 1 standard deviation confidence intervals. Black rectangle contains the values of the plagioclase CSDs slope in Stromboli scoriae from April 1994 to September 1996 [Armienti et al., 2007].

4.3. Bulk Rock Chemical Composition

The whole-rock analyses of all samples were performed at different laboratories [Service d’Analyse des Roches et des Minéraux of Centre de Recherches Pétrographiques et Géochimiques—Centre National de la Recherche Scientifique (CNRS) of Nancy, France; Department of Earth Sciences of the University of Florence, Italy; Laboratoire Pierre Sue, Commissariat à l’Energie Atomique—CNRS, Gif-sur-Yvette, France; SGS Minerals Services of Toronto, Canada] and with different methods (inductively coupled plasma–mass spectrometry, instrumental neutron activation analysis, XRF; for more details, see Landi et al. [2006]).

Lava and pyroclastic rocks that erupted during the 2002–2003 event are all shoshonitic basalts with major and trace elements content very similar to those of the crystal-rich

Table 1. Major and Trace Element Contents of Selected Rocks Sampled During the 2002–2003 Effusive Event^a

Sample	STR281202a	STR281202c	STR291202	STR090103
Date	28 Dec 2002	28 Dec 2002	29 Dec 2002	9 Jan 2003
SiO ₂	50.09 (49.13–49.83)	49.97 (49.63–49.88)	50.28 (48.50–49.84)	50.37 (48.56–49.86)
TiO ₂	0.93 (0.89–0.99)	0.93 (0.90–0.98)	0.93 (0.88–0.99)	0.94 (0.87–0.96)
Al ₂ O ₃	17.27 (17.18–17.86)	17.19 (17.16–18.09)	17.42 (17.27–18.35)	17.39 (17.22–18.36)
Fe ₂ O ₃ T	8.88 (8.67–9.49)	8.84 (8.71–8.84)	8.92 (8.57–9.32)	8.92 (8.75–9.17)
MnO	0.16 (0.15–0.17)	0.16 (0.15–0.16)	0.15 (0.14–0.17)	0.16 (0.15–0.17)
MgO	6.19 (5.80–6.56)	6.11 (5.62–6.46)	6.09 (6.00–6.70)	6.10 (6.04–6.91)
CaO	11.23 (11.01–11.17)	11.12 (10.56–11.49)	11.19 (10.76–11.25)	11.23 (10.77–11.28)
Na ₂ O	2.50 (2.31–2.52)	2.48 (2.48–2.60)	2.51 (2.49–2.55)	2.51 (2.48–2.52)
K ₂ O	2.10 (2.07–2.42)	2.15 (2.14–2.22)	2.15 (2.07–2.26)	2.14 (2.01–2.24)
P ₂ O ₅	0.55 (0.37–0.56)	0.55 (0.40–0.55)	0.56 (0.38–0.56)	0.56 (0.36–0.55)
LOI	0.63 (0.23–0.63)	0.70 (0.21–0.69)	0.68 (0.23–0.68)	0.69 (0.21–0.69)
SUM	100.53	100.19	100.89	101.01
V	268 (261–268)	262 (248–262)	249 (249–268)	250 (250–262)
Cr	48 (48–55)	47 (47–63)	39 (39–54)	33 (33–59)
Co	30.6 (30.6–34)	34.7 (29–34.7)	31.9 (30–34)	30.6 (30.6–35)
Ni	39 (39–40)	35 (35–40)	36 (36–42)	36 (36–44)
Sc	32 (29.4–32)	30 (28.8–30)	30 (29.6–30)	30 (29.5–30)
Cu	123 (98–123)	98 (80–98)	117 (100–117)	114 (96–114)
Zn	77 (70–77)	75 (73–75)	69 (69–71)	67 (67–72)
Cs	4.5 (4.4–4.6)	4.8 (4.7–4.8)	4.6 (4.2–4.6)	4.5 (4.4–4.5)
Rb	65 (61–73)	71 (61–71)	69 (61–70)	67 (61–71)
Sr	773 (716–789)	744 (700–785)	745 (728–799)	734 (703–818)
Y	26.3 (26.3–27)	27.4 (25–27.4)	27.9 (26–27–9)	26.8 (26–27)
Zr	136 (136–170)	144 (144–177)	144 (144–170)	139 (139–164)
Nb	20.5 (19.2–21)	21.7 (17.8–22)	21.6 (18.3–22)	20.7 (18.1–23)
Ba	972 (935–986)	930 (930–974)	922 (922–988)	916 (916–1005)
La	42.9 (42.9–48)	46.5 (45–49)	45.5 (42–46)	45.4 (45–46.3)
Ce	92.7 (84–97)	103.4 (91–103.4)	99.5 (92–99.5)	98.1 (90–100)
Pr	11.1 (11.1–11.5)	12.1 (10.7–12.1)	11.9 (11–11.9)	11.6 (10.8–11.6)
Nd	42.5 (37–44)	46.0 (41–46)	45.4 (43–45.4)	44.9 (41–44.9)
Sm	8.40 (8.2–8.7)	9.11 (8.3–9.11)	8.76 (8.4–8.76)	8.79 (8.2–8.79)
Eu	2.19 (2.19–2.23)	2.43 (2.2–2.43)	2.32 (2.2–2.32)	2.30 (2.1–2.37)
Gd	6.84 (6.84–7.1)	7.46 (6.7–7.46)	7.20 (2.1–7.20)	7.22 (6.8–7.22)
Tb	1.03 (0.87–1.03)	1.14 (0.88–1.14)	1.07 (0.89–1.07)	1.08 (0.93–1.08)
Dy	5.02 (5.1–5.02)	5.63 (5.0–5.63)	5.33 (5.33–5.1)	5.29 (4.9–5.29)
Ho	0.95 (0.93–0.95)	1.06 (0.92–1.06)	1.01 (0.92–1.01)	0.99 (0.89–0.99)
Er	2.53 (2.5–2.53)	2.81 (2.5–2.81)	2.70 (2.5–2.70)	2.69 (2.4–2.69)
Tm	0.344 (0.344–0.36)	0.385 (0.35–0.385)	0.368 (0.36–0.368)	0.363 (0.36–0.363)
Yb	2.42 (2.4–2.4)	2.58 (2.3–2.58)	2.58 (2.3–2.58)	2.56 (2.3–2.56)
Lu	0.343 (0.343–0.37)	0.390 (0.35–0.390)	0.364 (0.36–0.364)	0.355 (0.35–0.355)
Ta	1.3 (1.28–1.3)	1.6 (1.22–1.6)	1.4 (1.27–1.4)	1.4 (1.18–1.4)
Hf	3.6 (3.6–4.0)	4.0 (3.7–4)	3.8 (3.7–4.0)	3.7 (3.6–4.2)
Pb	18 (18–26)	25 (20–25)	18 (16–22)	18 (14–18)
Th	15.3 (14.9–16.19)	16.5 (14.8–16.5)	15.8 (15.0–15.8)	15.7 (15.0–15.7)
U	3.65 (3.65–4.2)	4.08 (3.9–4.08)	3.87 (3.87–3.9)	3.75 (3.75–4.2)

Table 1. (continued)

Sample	STR150103		STR260203		STR130503		STR200703	
Date	15 Jan 2003		26 Feb 03		13 May 2003		20 Jul 2003	
SiO ₂	50.36	(48.93–49.85)	49.94	(48.57–49.84)	50.19	(49.11–49.85)	49.46	(48.87–49.68)
TiO ₂	0.93	(0.87–0.97)	0.92	(0.89–0.98)	0.93	(0.87–0.97)	0.93	(0.85–0.97)
Al ₂ O ₃	17.38	(17.21–18.14)	17.23	(17.20–18.11)	17.34	(17.22–17.85)	17.14	(17.22–18.06)
Fe ₂ O ₃ T	8.92	(8.56–9.25)	8.88	(8.68–9.40)	8.89	(8.63–9.20)	8.82	(8.71–9.29)
MnO	0.16	(0.15–0.16)	0.16	(0.16–0.16)	0.16	(0.16–0.16)	0.16	(0.16–0.17)
MgO	6.08	(5.89–6.46)	6.10	(5.89–6.70)	6.12	(5.95–6.65)	6.01	(6.04–6.46)
CaO	11.25	(10.86–11.43)	11.04	(10.79–11.53)	11.14	(10.91–11.53)	11.13	(11.04–11.30)
Na ₂ O	2.55	(2.44–2.52)	2.50	(2.50–2.66)	2.49	(2.47–2.48)	2.50	(2.44–2.51)
K ₂ O	2.14	(2.05–2.21)	2.19	(2.02–2.18)	2.12	(2.03–2.25)	2.19	(2.00–2.31)
P ₂ O ₅	0.56	(0.36–0.55)	0.56	(0.36–0.56)	0.56	(0.35–0.56)	0.56	(0.36–0.56)
LOI	0.68	(0.34–0.68)	0.68	(0.26–0.68)	0.73	(0.31–0.73)	0.66	(0.20–0.66)
SUM	101.02		100.20		100.67		99.56	
V	256	(256–268)	255	(248–259)	250	(250–259)	253	(253–262)
Cr	40	(40–61)	38	(38–57)	34	(34–54)	38	(38–54)
Co	31.5	(31.5–34)	34.2	(29–35)	32.4	(32–33)	26.6	(26.6–35)
Ni	36	(36–42)	35	(40–35)	35	(35–41)	35	(44–35)
Sc	31	(+)	29	(29–29.8)	29	(28.7–29)	30	(+)
Cu	116	(96–116)	114	(93–114)	113	(93–113)	114	(100–114)
Zn	70	(69–72)	63	(63–71)	67	(67–75)	65	(65–80)
Cs	4.7	(4.4–4.7)	4.5	(4.2–4.5)	4.5	(4.0–4.5)	3.9	(3.9–4.2)
Rb	70	(61–70)	71	(61–71)	69	(60–69)	59	(59–68)
Sr	749	(728–801)	740	(670–792)	739	(672–779)	745	(703–795)
Y	27.7	(26–27.7)	27.9	(24–27.9)	27.3	(24–27.3)	23.2	(23.2–27)
Zr	144	(144–159)	143	(143–174)	141	(141–157)	142	(142–159)
Nb	21.6	(18.1–22)	21.9	(17–21.9)	20.6	(17.2–21)	18.4	(18.0–22)
Ba	933	(933–962)	920	(887–989)	914	(883–958)	913	(913–928)
La	46.2	(46–47)	46.2	(43–46.3)	45.7	(43–50)	40.9	(40.9–50)
Ce	100.0	(92–100)	101.9	(86–101.9)	99.5	(86–99.5)	90.1	(90–94)
Pr	11.9	(11–11.9)	12.1	(10.2–12.1)	11.8	(10.2–11.8)	10.7	(10.6–10.7)
Nd	45.7	(42–49)	45.7	(40–45.7)	44.9	(42–44.9)	40.0	(40.0–47)
Sm	8.83	(8.3–8.83)	8.98	(7.9–8.98)	8.72	(8.9–8.72)	7.80	(7.80–8.2)
Eu	2.34	(2.2–2.34)	2.43	(2.1–2.43)	2.37	(2.0–2.37)	2.18	(2.1–2.18)
Gd	7.28	(6.8–7.28)	7.62	(6.6–7.62)	7.19	(6.3–7.19)	6.63	(6.6–6.63)
Tb	1.07	(0.94–1.07)	1.12	(0.89–1.12)	1.07	(0.86–1.07)	0.96	(0.93–0.96)
Dy	5.36	(5.1–5.36)	5.61	(4.8–5.61)	5.41	(4.7–5.41)	4.91	(4.9–4.91)
Ho	1.00	(0.91–1.00)	1.05	(0.87–1.05)	0.98	(0.84–0.98)	0.90	(0.89–0.90)
Er	2.68	(2.4–2.68)	2.86	(2.4–2.86)	2.66	(2.3–2.66)	2.43	(2.4–2.43)
Tm	0.367	(0.35–0.367)	0.372	(0.34–0.372)	0.354	(0.32–0.354)	0.322	(0.34–0.322)
Yb	2.57	(2.3–2.57)	2.60	(2.2–2.60)	2.53	(2.2–2.53)	2.26	(2.26–2.3)
Lu	0.367	(0.36–0.367)	0.383	(0.34–0.83)	0.383	(0.33–0.383)	0.341	(0.341–0.35)
Ta	1.4	(1.23–1.4)	1.7	(0.17–1.7)	1.3	(1.13–1.3)	1.3	(0.17–1.3)
Hf	3.8	(3.8–3.8)	4.0	(3.6–4.1)	3.8	(3.5–3.9)	3.4	(3.4–3.6)
Pb	18	(16–21)	19	(16–28)	19	(15–22)	17	(16–19)
Th	15.8	(15.4–15.8)	16.0	(14.4–16)	15.7	(13.2–15.7)	13.8	(13.7–13.8)
U	3.82	(3.82–3.9)	4.01	(3.8–4.2)	3.89	(3.4–3.89)	3.38	(3.38–3.6)

^a Data set obtained by ICP-MS at the SGS Minerals Services of Toronto, Ontario, Canada. The range of values obtained from different methods and laboratories are reported in brackets (see text for explanation). Data are from Landi et al. [2006].

(+) Only one value available.

products usually erupted from the present-day activity of Stromboli (K_2O 2–2.2 wt %; SiO_2 49.5–50.5 wt %; Figure 4 and Table 1).

Minor variations with time of major and trace element contents can be recognized during the entire effusive event [Landi *et al.*, 2006]. On the whole, volcanics that erupted during the first stages of the eruption (December 2002 to March 2003) show variations in trace element compositions that only rarely exceed 2 standard deviation analytical error. All data sets record random oscillations with comparable amplitudes, often uncorrelated. Compositional variations of most incompatible trace elements, larger than the analytical error are observed among the scoria bombs and lavas that erupted just before and at the very beginning of the effusive event (Figure 8 and Table 1). Moreover, after the paroxysmal episode of 5 April 2003, the variations in trace element composition become smaller (almost <5%), and all data sets point to a slight but systematic lowering of some incompatible elements (e.g., Ta, Th, U, Nb, Ba, Cs).

4.4. Sr and Nd Isotope Ratios

Sr and Nd isotope ratios on whole rocks and groundmasses have been analyzed at the Department of Earth Sciences, University of Florence, using standard chemical separation techniques and a thermal ionization mass spectrometer Finnigan Triton TI®, equipped with nine movable collectors [Avanzinelli *et al.*, 2005]. The same mass spectrometer was used for measuring the micro-Sr samples, which were prepared by previous microdrilling technique and chemical separation procedure at the University of Durham, England [Charlier *et al.*, 2006].

All the analyzed whole-rock samples show a small variation of Sr isotope ratios ($0.706146 \pm 7 - 0.706163 \pm 4$) and even a smaller variation of Nd isotope ratios ($0.512558 \pm 4 - 0.512567 \pm 4$; Table 2) [Landi *et al.*, 2006]. Sr isotope ratios of the groundmasses are generally lower than those of the respective whole rocks. This characteristic is more accentuated in the lava emitted after the 5 April paroxysm, but it is not present in the products that erupted in 28 December 2002. With respect to the previous scoria bombs of the 1994–2002 period, the Sr isotope ratios are generally lower (Figure 9). They increase from the scoria bombs of November 2002 toward the onset lava flow, then decrease again in the lavas that erupted later and especially after the paroxysm [Francalanci *et al.*, 2004a; Nardini *et al.*, *In situ* chemical and isotopic analyses in the Stromboli products of the 2002–2003 eruptive crisis: Micro-scale variations recording macro-scale processes, submitted to *Contributions to Mineralogy and Petrology*, 2008, hereinafter referred to as Nardini *et al.*, submitted manuscript, 2008]. Instead, a slight increase

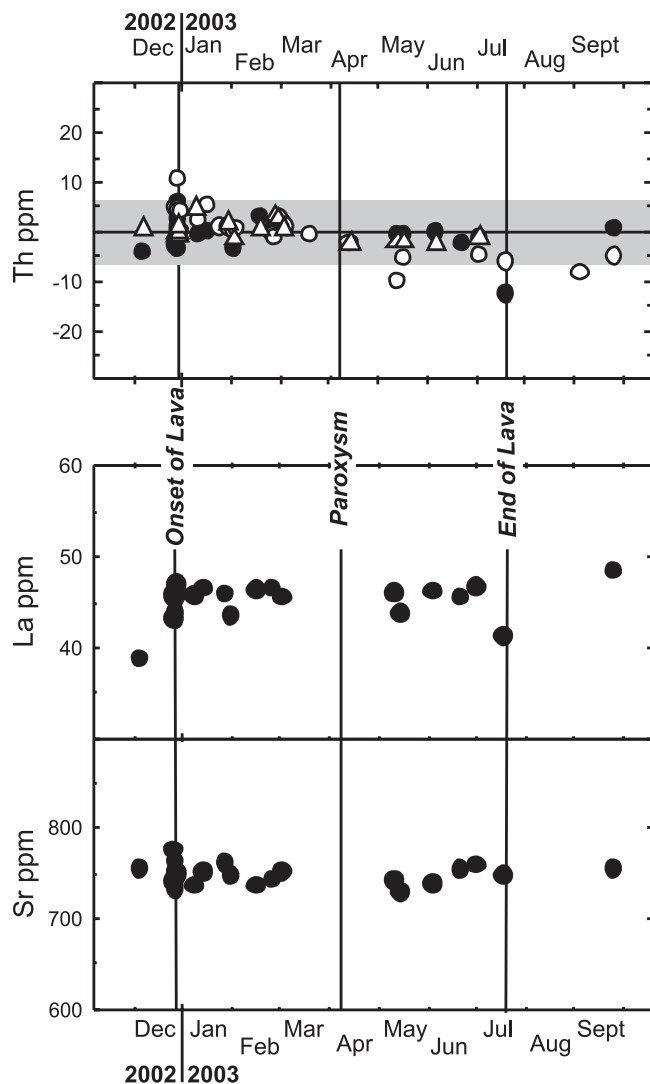


Figure 8. Time variations of the lavas emitted in the 2002–2003 effusive event. (a) Time variation of Th content reported as percentage deviations from the arithmetic means of each laboratory. A mean analytical error (1 standard deviation), expressed as percentage, is also reported as gray band. Filled circle, inductively coupled plasma–mass spectrometry (ICP–MS) analyses, SGS Minerals Services of Toronto, Canada; open circle, ICP–MS analyses, Service d’Analyse des Roches et des Minéraux of Centre de Recherches Pétrographiques et Géochimiques–CNRS of Nancy, France; open triangle, instrumental neutron activation analyses, Laboratoire Pierre sue, Commissariat à l’Energie Atomique–CNRS, Gif-sur-Yvette, France. (b) Variations of representative trace elements obtained by ICP–MS analyses from the SGS Minerals Services of Toronto, Canada. Errors can be estimated by the figures reported in Table 1. Modified from Landi *et al.* [2006].

Table 2. Sr and Nd Isotope Ratios of Representative Whole-Rock and Groundmass Samples From the 2002–2003 Effusive Event^a

Sample	Date	$^{87}\text{Sr}/^{86}\text{Sr}$	2σ	$^{143}\text{Nd}/^{144}\text{Nd}$	2σ
<i>STR 11/02p*</i>	7 Nov 2002	0.706146	0.000005	0.512565	0.000005
STR12/02a	28 Dec 2002	0.706160	0.000005	0.512558	0.000006
STR12/02b	28 Dec 2002	0.706163	0.000004	—	—
<i>STR 12/02b*</i>	28 Dec 2002	0.706158	0.000004	—	—
STR281202c	28 Dec 2002	0.706154	0.000006	0.512558	0.000004
<i>STR281202c*</i>	28 Dec 2002	0.706149	0.000006	—	—
STR150103	15 Jan 2003	0.706163	0.000005	—	—
STR010203	1 Feb 2003	0.706152	0.000006	0.512562	0.000004
STR170203	17 Feb 2003	0.706160	0.000007	—	—
<i>STR 170203*</i>	17 Feb 2003	0.706149	0.000008	—	—
STR040303	4 Mar 2003	0.706154	0.000006	—	—
<i>STR180303*</i>	18 Mar 2003	0.706151	0.000007	—	—
STR140403	14 Apr 2003	0.706156	0.000008	0.512564	0.000006
<i>STR140403*</i>	14 Apr 2003	0.706151	0.000007	—	—
STR130503	13 May 2003	0.706156	0.000006	0.512564	0.000005
STR060603	6 Jun 2003	0.706149	0.000007	0.512561	0.000006
STR030703	3 Jul 2003	0.706150	0.000008	0.512564	0.000005
STR200703	20 Jul 2003	0.706146	0.000007	0.512567	0.000004
<i>STR200703*</i>	20 Jul 2003	0.706134	0.000007	0.512559	0.000004
STR280903	28 Sep 2003	0.706154	0.000008	0.512559	0.000004

^a Italics with asterisks, groundmasses (data are from Nardini et al. [2008]; other data are from Landi et al. [2006]).

seems to occur in the scoria bomb erupted by the Strombolian activity of September 2003. An opposite behavior of $^{143}\text{Nd}/^{144}\text{Nd}$ with respect to the $^{87}\text{Sr}/^{86}\text{Sr}$ values also seems to be generally perceptible.

Micro-Sr isotope data on core–rim traverses of plagioclase and clinopyroxene have been performed on five lava samples chosen to represent the entire effusive period (Nardini et al., submitted manuscript, 2008). These data have been obtained by micromilling technique focusing the attention on the most zoned crystals. They show large Sr isotope disequilibria between the different crystal zones and the groundmasses (Figure 10). The internal parts of crystals, and especially the inner cores, often resorbed, have higher Sr isotope ratios than rims and groundmasses. These higher $^{87}\text{Sr}/^{86}\text{Sr}$ values are usually lower than 0.70640, a part from a value of 0.706647 ± 12 found in a plagioclase core of the onset lava flow. In the lavas that erupted after the 5 April paroxysm, isotope disequilibrium is also sometimes found between outer rims and groundmass (Figure 10) (Nardini et al., submitted manuscript, 2008).

5. DISCUSSION

All samples collected from the beginning to the end of the eruption do not show significant variations in textures, bulk chemical, and isotopic compositions with respect to those

of the crystal-rich magmas that erupted as lavas and scoria bombs during the past decades [Capaldi et al., 1978; De Fino et al., 1988; Bonaccorso et al., 1996; Francalanci et al., 1999, 2004b; Metrich et al., 2001; Landi et al., 2004]. CSD studies give results close to those for the crystal-rich products usually erupted from Stromboli (Figure 7). Chemical zoning of each mineral phase and the composition of the rims in equilibrium with the groundmass, both in 2002–2003 lavas and in the previous products, cover the same compositional intervals (Figure 3), and the composition of glassy groundmasses does not present substantial differences (Figure 4) [Francalanci et al., 2004b; Landi et al., 2004].

Nevertheless, small but significant compositional characteristics are worth noticing and contribute to understanding the behavior and evolution of the crystal-rich magmas and the relationships between compositional variations and eruptive dynamics during the 2002–2003 effusive event at Stromboli. Such characteristics include the compositional variability of the initial products, the compositional changes after the 5 April paroxysmal explosion, and slight variations in samples that erupted toward the end of the eruption [Landi et al., 2006].

The products emitted during the first phase of the eruption show the largest compositional variations of trace elements, both compatible and incompatible, with respect to the composition of the lavas that erupted during the whole effusive

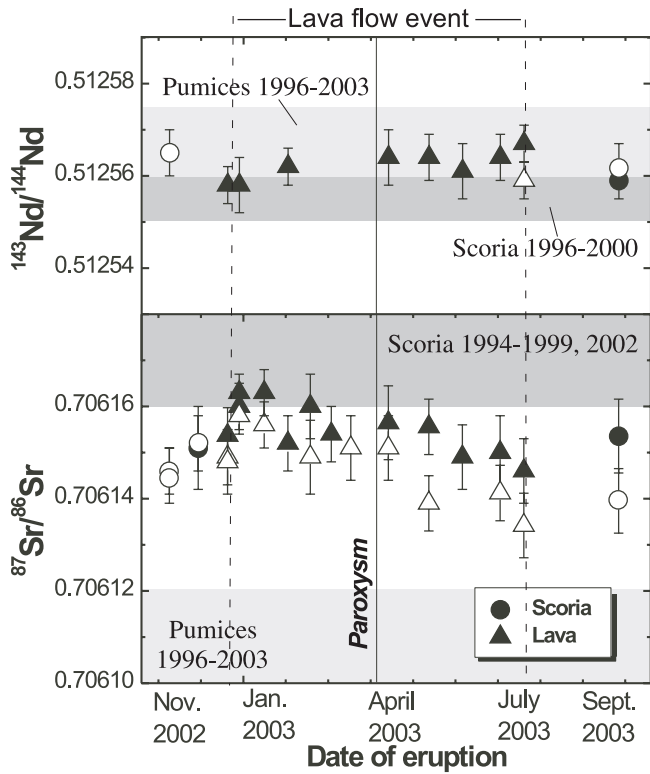


Figure 9. Variation of Sr and Nd isotope ratios in the products erupted by the present-day activity of Stromboli from November 2002 to September 2003. Full symbols, whole rocks; opens symbols, groundmasses. The gray fields are the compositional variations of the products previously that erupted as specified (data from Francalanci *et al.* [1999, 2004b, 2005]). Modified from Landi *et al.* [2006] and Nardini *et al.* (submitted manuscript, 2008).

period. The early phase of the eruption was characterized by high effusion rate (about $10 \text{ m}^3/\text{s}$ on average) and a cumulative volume of erupted products of about $2 \times 10^6 \text{ m}^3$ [Marsella *et al.*, this volume]. This has been associated with the rapid emptying of the topmost part of the conduit. We expect that this upper portion of the conduit is characterized by significant variations in physical conditions, induced by the complex dynamics of the Strombolian activity, which could produce textural and chemical zoning in the residing magma. As the gas bubbles rise and gases escape from the top of the conduit, liquid magma moves into the voids left by the arising gases [Chouet *et al.*, 2003, and references therein]. Downward magma movement in the conduit may induce some kind of crystal sorting, with accumulation of mafic phases at a lower buoyancy level.

The 5 April 2003 paroxysm determined a slight but systematic change in most of the chemical and textural param-

eters analyzed in the emitted lavas. Indeed, the lava samples collected after the paroxysm show a systematically lower content of some incompatible elements (e.g., Ta, Th, U, Nb, Ba, Cs) with respect to the lavas that erupted during the pre-paroxysm period (Figure 8 and Table 1) and a slight but significant decrease of Sr isotope ratios, better observed toward the end of the eruption (Figure 9 and Table 2). The paroxysmal eruption ejected a considerable amount of crystal-poor magma, characterized by lower incompatible trace element contents and $^{87}\text{Sr}/^{86}\text{Sr}$ values than the crystal-rich magmas. These compositional differences are due to the complex interplay of different processes, such as source heterogeneity, magma mixing and crystallization, and finally, crystal recycling and resorption. In particular, the lower Sr isotope ratios of the refilling crystal-poor magmas are likely due to a decrease of $^{87}\text{Sr}/^{86}\text{Sr}$ with time during the partial melting of the mantle source [Bertagnini *et al.*, this volume; Francalanci *et al.*, 1999, 2004a, 2004b, 2005, this volume; Landi *et al.*, 2004; Metrich *et al.*, 2005]. This leads to hypothesize that the chemical variations in lavas that erupted after the paroxysm are probably due to mixing between the crystal-rich magma occupying the shallow magmatic system and the refilling crystal-poor magma. Based on the differences in trace element contents, about $20 \pm 5 \text{ wt } \%$ of crystal-poor magma is calculated to be mixed with the crystal-rich magma. The lower mixed amount of 11 wt %, calculated on the basis of Sr isotope ratios, may be due to the recycling of cumulus phases with higher Sr isotope ratios (probably around 0.7063) into the crystal-rich magma reservoir during the refilling event (Figure 10) [Francalanci *et al.*, 2005]. The lower $^{87}\text{Sr}/^{86}\text{Sr}$ values of the glassy groundmasses of these rocks seem to confirm this hypothesis (Figure 9) [Francalanci *et al.*, 2004a].

An immediate textural response to the new input event is not observed. In fact, a slight m decrease of the CSD curves is only observed in the products that erupted in July (Fornaciai *et al.*, submitted manuscript, 2008).

The mixing process between crystal-poor and crystal-rich magmas after the paroxysm of 5 April 2003 is not recorded by the chemistry of the mineral phases or major element variations in the glassy groundmasses. This suggests that efficient mixing plus crystallization processes rapidly lead to the reequilibration of the minerals with the residual liquid during the ascent of magma to the surface [Landi *et al.*, 2004].

Products that erupted in the waning phase of the eruption have glassy matrices that tend to be slightly more evolved than those of the previous lavas. This is testified by the increase of $\text{CaO}/\text{Al}_2\text{O}_3$ value from 0.46 to 0.48 toward the end of the eruption, together with a slight P_2O_5 increase and Na_2O content decrease (Figure 5). Because of the absence

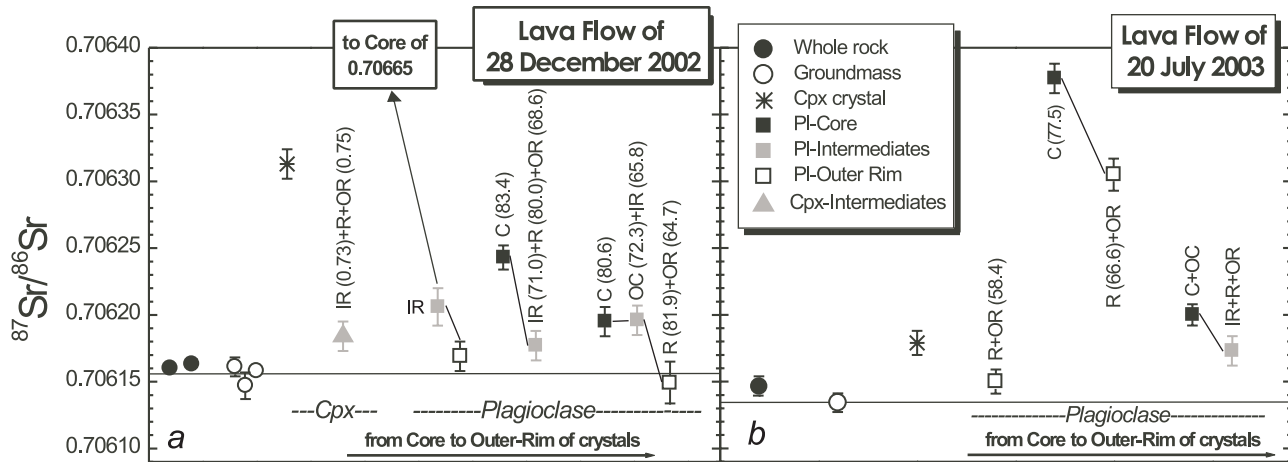


Figure 10. Micro-Sr isotope ratios analyzed in 28 December 2002 (onset lava flow) and 20 July 2003 lava flows. Sr isotope ratios have been analyzed on core to rim zones of plagioclase and clinopyroxene by microdrilling technique. $^{87}\text{Sr}/^{86}\text{Sr}$ values of whole rocks, groundmasses, and single clinopyroxene crystals have also been reported. Legend of the core–rim traverse of minerals: full black symbols, crystal cores; full gray symbols, intermediate zones of crystals; open black symbols, prevalent outer rims. C, core; OC, outer core; IR, inner rim; R, rim; OR, outer rim. Number in brackets indicates clinopyroxene and plagioclase composition in terms of $\text{Mg}/(\text{Mg} + \text{Fe}_t)$ and An mol %, respectively. Modified from Nardini et al. (submitted manuscript, 2008).

of apatite or other P_2O_5 -bearing mineral phases, P_2O_5 can be considered an incompatible element during present-day magma crystallization at Stromboli. Such slight variations may be related to the decline of the effusion rate recorded in the final phase of the eruption [Marsella et al., this volume; Ripepe et al., 2005]. It can induce both a reduction of the magma temperature in the topmost part of the conduit, thus a more extensive crystallization of the system and a more efficient degassing. Accordingly, a decrease in An content of the plagioclase rims is found in the lavas that erupted from April 2003 onward (Figure 3a).

Despite the almost homogeneous chemical, textural, and mineralogical characteristics of the products that erupted at the beginning and before the 2002–2003 eruption (since 1900 A.D.), some Sr isotopic differences are found in the products that erupted in the months before December 2002. In particular, the groundmasses of scoria that erupted in November 2002 have significantly lower Sr isotope ratios than the previous (from 1900 to June 2002) erupted magmas. The cause of this $^{87}\text{Sr}/^{86}\text{Sr}$ decrease in the crystal-rich magma has been attributed to mixing with the crystal-poor and less Sr-radiogenic magma. Thus, it has been interpreted as evidence of a higher supply rate of the shallow plumbing system by the deeper magma, which prevented an efficient mixing.

Our data have also pointed out that highly Sr-radiogenic xenocrysts or crystal cores still persist in the shallow mag-

matic system. They probably represent recycled crystals from a cumulus reservoir feeding the previous activity (at least since 10 ka ago) and erupting magmas with higher Sr isotope ratios than the present-day magmas [Francalanci et al., 2005; Nardini et al., submitted manuscript, 2008]. Some of these recycled crystals were probably formed around 10 ka ago, as demonstrated by the highest Sr isotope ratio found in a crystal core, which is similar to the $^{87}\text{Sr}/^{86}\text{Sr}$ values of magmas that erupted at Stromboli during the Neostromboli period (potassic magmas) [Francalanci et al., 1988, 2005]. The presence of minerals, entirely in isotopic disequilibrium with the groundmass in the magmas that erupted after the 5 April paroxysm, still suggests that these xenocrysts were brought into the shallow magma system by the refilling crystal-poor magmas [Francalanci et al., 2005; Nardini et al., submitted manuscript, 2008].

6. THE TRIGGER OF THE EFFUSIVE ACTIVITY

Macroscale and microscale variations in textural, mineralogical, chemical, and isotopic characteristics of the products erupted by active volcanoes can be directly linked with changes in the preeruptive magma conditions leading to vary the eruptive vigor of a volcano [Garcia and Wolfe, 1988; Thornber, 2003; Corsaro and Pompilio, 2004].

The constancy in major and trace element composition of the products erupted by the recent activity of the volcano,

both the shallow crystal-rich and the deeper crystal-poor magmas [Bertagnini *et al.*, this volume], makes it rather difficult to highlight possible destabilization of the shallow magmatic system due to events of refilling from depth. Indeed, a potential increase in the feeding rate from depth cannot easily change the whole chemistry of the shallow crystal-rich body and depending on the proportion between the refreshing volatile-rich magma and the residing crystal-rich one, the chemical variations can be close to the analytical error. In fact, at least in the past three important effusive events (1975, 1985–1986, 2002–2003), a variation in the eruptive style, from mild explosive to effusive, does not correspond to evident changes in the main composition of the erupted products [Capaldi *et al.*, 1978; De Fino *et al.*, 1988, Landi *et al.*, 2006]. In particular, the study of the periodic sampling carried out during the 2002–2003 effusive event reveals an absence of relevant differences in the textural, compositional, and isotopic characteristics of the lavas emitted in the early phase of the eruption with respect to those of the previous products. In addition, the nearly constant values of the CSD data observed in 2002–2003 lavas and in previous crystal-rich products suggest that the shallow reservoir of Stromboli operates as a steady-state system evolving close to the equilibrium, with only minor variation in time.

Only Sr isotope ratios reveal significant variations associated with large effusive episodes. A decrease in $^{87}\text{Sr}/^{86}\text{Sr}$ values and an increase in volume of the refreshing crystal-poor magmas were found to occur during the year preceding the 1985–1986 effusive eruption [Francalanci *et al.*, 1999, 2005]. Changes in the isotopic characteristics of the products that erupted in November 2002, moreover, suggest a higher supply rate for the shallow plumbing system by the deeper magma, possibly occurring some months before the lava effusion [Francalanci *et al.*, 2004a, 2004b; Nardini *et al.*, submitted manuscript, 2008].

Even if the 2002–2003 effusive eruption was not preceded by short-term variations of geophysical parameters and in the geochemistry of fluids [Bonaccorso *et al.*, 2003; Carapezza, 2004; Aiuppa and Federico, 2004], an increase in dissolved CO₂, H₂, and He in the thermal water from shallow wells located near the NE coast and an increase in sulfur degassing were measured some months before. These variations have been interpreted as due to the rise of deep magmatic gas [Carapezza, 2004; Aiuppa and Federico, 2004]. In addition, from May 2002 onward, an increase of the magma level in the conduit was recorded, resulting in more frequent explosions and in an overflow from the rim of a summit crater in November [Calvari *et al.*, 2005].

As a matter of fact, the onset of the effusive event is characterized by a state of high magmastic pressure in the conduit

and an immediate stress release during the first days through the emission of a large amount of magma, with a very high effusion rate (11.6 m³/s during the first 3 d [Marsella *et al.*, this volume]) when compared with that estimated during the normal Strombolian activity (0.1–0.3 and 0.06–0.6 m³/s [Giberti *et al.*, 1992; Allard *et al.*, 1994; Harris and Stevenson, 1997]).

Landi *et al.* [2006] proposed two alternative hypotheses to explain the high level of magma in the conduit, which leads to the effusive crisis of the volcano. A first interpretation is that a high volume of fresh crystal-poor magma arrived in the deeper part of the shallow system some months before the onset of the eruption, as suggested by the isotopic data. Possibly, this coincided with the anomalies observed in May–June in sulfur degassing and in geochemistry of the thermal waters. The subsequent mixing with the crystal-rich magma, crystallization, and degassing of this/these new batch/es of crystal-poor magma led the overlying magma column, constituted by the preexisting crystal-rich magma, to rise to a higher level in the conduit, inducing the beginning of the effusive event. The absence of variations in the geophysical and geochemical behavior, together with the absence of relevant differences in the textural, compositional, and isotopic characteristics of the lavas emitted in the early effusive phase with respect to those of the previous products, leads to ruling out an input event of fresh magma into the shallow part of the plumbing system shortly before the eruption. A second hypothesis considers a long-term, gradual pressure increase in the conduit, which started years before the eruption and culminating in 28 December 2002 with the failure of the conduit wall and the opening of vents 100–150 m below the summit craters. The 6.5-month duration of the effusion and the exponential decay of effusion rate with time might be the result of conduit wall relaxation and magma squeezing. In this case, Stromboli would operate as a nearly steady-state system with minor oscillations in the supply rate from depth, giving an average supply rate higher than the effusion rate.

REFERENCES

- Abbruzzese, D., and C. Cavallaro (1956), L'eruzione sottomarina di Stromboli del 28 Febbraio 1955, *Stromboli*, 4, 25–29.
- Aiuppa, A., and C. Federico (2004), Anomalous magmatic degassing prior to the 5th April 2003 paroxysm on Stromboli, *Geophys. Res. Lett.* 31, LI4607, doi:10.1029/2004GL020458.
- Allard, P., J. Carbonnelle, N. Métrich, H. Loyer, and P. Zettwoog (1994), Sulphur output and magma degassing budget of Stromboli volcano, *Nature*, 368, 326–330.
- Armenti, P., L. Francalanci, and P. Landi (2007), Textural effects of steady state behaviour of the Stromboli feeding system, *J. Volcanol. Geotherm. Res.*, 160, 86–98.

- Avanzinelli, R., E. Boari, S. Conticelli, L. Francalanci, L. Guarneri, G. Perini, C. M. Petrone, S. Tommasini, and M. Ulivi (2005), High precision Sr, Nd, and Pb isotopic analyses using new generation Thermal Ionisation Mass Spectrometer ThermoFinnigan Triton-Ti®, *Period. Mineral.*, 74–73, 147–166.
- Barberi, F., M. Rosi, and A. Sodi (1993), Volcanic hazard assessment at Stromboli based on review of historical data, *Acta Vulcanol.*, 3, 173–187.
- Bonaccorso, A., C. Cardaci, M. Coltell, P. Del Carlo, S. Falsaperla, S. Panucci, M. Pompilio, and L. Villari (1996), Annual report of the world volcanic eruptions in 1993, Stromboli, *Bull. Volc. Eruptions*, 33, 7–13.
- Bonaccorso, A., S. Calvari, G. Garfi, L. Lodato, and D. Patanè (2003), Dynamics of the December 2002 flank failure and tsunami at Stromboli volcano inferred by volcanological and geophysical observations, *Geophys. Res. Lett.*, 30(18), 1941, doi:10.1029/2003GL017702.
- Calvari, S., L. Spampinato, L. Lodato, A. J. L. Harris, M. R. Patrick, J. Dehn, M. R. Burton, and D. Andronico (2005), Chronology and complex volcanic processes during the 2002–2003 flank eruption at Stromboli volcano (Italy) reconstructed from direct observations and surveys with a handheld thermal camera, *J. Geophys. Res.*, 110, B02201, doi:10.1029/2004JB003129.
- Capaldi, G., et al. (1978), Stromboli and its 1975 eruption, *Bull. Volcanol.*, 41, 259–285.
- Carapezza, M. L., S. Inguaggiato, L. Brusca, and M. Longo (2004), Geochemical precursors of the activity of an open-conduit volcano: The Stromboli 2002–2003 eruptive event, *Geophys. Res. Lett.* 31, L07620, doi:10.1029/2004GL019614.
- Cashman, K. V., and B. M. Marsh (1988), Crystal size distribution (CSD) in rocks and the kinetics and dynamics of crystallization. II: Makaopuhi lava lake, *Contrib. Mineral. Petrol.*, 99, 292–305.
- Charlier, B. L. A., C. Ginibre, D. Morgan, G. M. Nowell, D. G. Pearson, J. P. Davidson, and C. J. Ottley (2006), Methods for the microsampling and high-precision analysis of strontium and rubidium isotopes at single crystal scale for petrological and geochronological applications, *Chem. Geol.*, 232, 114–133.
- Chouet, B., P. Dawson, T. Ohminato, M. Martini, G. Saccorotti, F. Giudicepietro, G. De Luca, G. Milana, and R. Scarpa (2003), Source mechanisms of explosions at Stromboli volcano, Italy, determined from moment-tensor inversions of very-long-period data, *J. Geophys. Res.*, 108(B1), 2019, doi:10.1029/2002BJ001919.
- Corsaro, R. A., and M. Pompilio (2004), Magma dynamics in the shallow plumbing system of Mt. Etna as recorded by compositional variations in volcanics of recent summit activity (1955–1999), *J. Volcanol. Geotherm. Res.*, 137, 55–71.
- De Fino, M., L. La Volpe, S. Falsaperla, G. Fazzetta, G. Neri, L. Francalanci, M. Rosi, and A. Sbrana (1988), The Stromboli eruption of December 6, 1985–April 25, 1986: Volcanological, petrological and seismological data, *Rend. Soc. Ital. Mineral. Petrol.*, 43, 1021–1038.
- De Hoff, R. T., and F. N. Rhines (1972), *Microscopie Quantitative*, 404 pp, Masson, Paris.
- Francalanci, L., M. Barbieri, P. Manetti, A. Peccerillo, and L. Tolomeo (1988), Sr-isotopic systematics in volcanic rocks from the island of Stromboli (Aeolian arc), *Chem. Geol.* 73, 164–180.
- Francalanci, L., S. Tommasini, S. Conticelli, and G. R. Davies (1999), Sr isotope evidence for short magma residence time for the 20th century activity at Stromboli volcano, Italy, *Earth Planet. Sci. Lett.*, 167, 61–69.
- Francalanci, L., C. M. Petrone, S. Conticelli, R. Vannucci, and E. Germiniani (2004a), The 2002–2003 eruptive crisis at Stromboli volcano, Italy: Mineralogical and geochemical characteristics of the erupted rocks and their inferences on the pre-eruptive processes, *Geophys. Res. Abstr.*, 6, 06412, 2004, SRef-ID:1607-7962/gru/EGU04-A-06412.
- Francalanci, L., S. Tommasini, and S. Conticelli (2004b), The volcanic activity of Stromboli in the 1906–1998 period: Mineralogical, geochemical and isotope data relevant to the understanding of Strombolian activity, *J. Volcanol. Geotherm. Res.* 131, 179–211.
- Francalanci, L., G. R. Davies, W. Lustenhouwer, S. Tommasini, P. R. D. Mason, and S. Conticelli (2005), Intra-grain Sr isotope evidence for crystal re-cycling and multiple magma reservoirs in the recent activity of Stromboli volcano, southern Italy, *J. Petrol.* 46, 1997–2021, doi:10.1093/petrology/egi045.
- Garcia, M. O., and E. W. Wolfe (1988), Petrology of the erupted lava, The Puu Oo eruption of Kilauea volcano, Hawaii: Episodes 1 through 20, January 3, 1983, through June 8, 1984, *U.S. Geol. Surv. Prof. Pap.*, 1463, 127–143.
- Giberti, G., C. Jaupart, and G. Sartoris (1992), Steady-state operation of Stromboli volcano, Italy: Constraints on the feeding system, *Bull. Volcanol.*, 54, 535–541.
- Harris, A. J. L., and D. S. Stevenson (1997), Magma budgets and steady-state activity of Vulcano and Stromboli, *Geophys. Res. Lett.* 24, 1043–1046.
- Landi, P., N. Métrich, A. Bertagnini, and M. Rosi, (2004), Dynamics of magma mixing and degassing recorded in plagioclase at Stromboli (Aeolian Arcipelago, Italy), *Contrib. Mineral. Petrol.*, 147, 213–227.
- Landi, P., L. Francalanci, M. Pompilio, M. Rosi, R. A. Corsaro, C. M. Petrone, I. Cardini, and L. Miraglia (2006), The December 2002–July 2003 effusive event at Stromboli volcano, Italy: Insights into the shallow plumbing system by petrochemical studies, *J. Volcanol. Geotherm. Res.*, 155, 263–284.
- Marsella M., M. Coltell, S. Branca, C. Proietti, and R. Monticelli (2008), 2002–2003 lava flow eruption of Stromboli: A contribution to understanding lava discharge mechanism using periodic digital photogrammetry surveys, this volume.
- Marsh, D. B. (1988), Crystal size distribution (CSD) in rocks and the kinetics and dynamics of crystallisation. I. Theory, *Contrib. Mineral. Petrol.*, 99, 277–291.
- Métrich, N., A. Bertagnini, P. Landi, and M. Rosi (2001), Crystallization driven by decompression and water loss at Stromboli volcano (Aeolian Islands, Italy), *J. Petrol.*, 42, 1471–1490.
- Métrich, N., A. Bertagnini, P. Landi, M. Rosi, and O. Belhadj (2005), Triggering mechanism at the origin of paroxysms at Stromboli (Aeolian Archipelago, Italy): The 5 April 2003 eruption, *Geophys. Res. Lett.*, 32, L10305, doi:10.1029/2004GL022257.

- Ripepe, M., E. Marchetti, G. Ulivieri, A. Harris, J. Dehn, M. Burton, T. Caltabiano, and G. Salerno (2005), Effusive to explosive transition during the 2003 eruption of Stromboli volcano, *Geology*, 33(5), 341–344.
- Tarquini, S., and P. Armienti (2001), Film color scanner as a new and cheap tool for image analysis in petrology. Determination of crystal size distributions of rocks by means of a color scanner, *Image Anal. Stereol.*, 20, 567–572.
- Thornber, C. R. (2003), Magma-reservoir processes revealed by geochemistry of the Puu Oo-Kupaianaha eruption, in *Puu Oo-Kupaianaha Eruption of Kilauea Volcano, Hawaii: The First 20 Years*, U.S. Geol. Surv. Prof. Pap., 1676, 121–136.
- Tommasi, P., F. Chiocci, M. Marsella, M. Coltellii, and M. Pompilio (2003), Preliminary analysis of the December 2002 instability phenomena at Stromboli volcano, *Symp. Flows, Sorrento, 15–16 May*.
- Tommasi, P., P. Baldi, F. L. Chiocci, M. Coltellii, M. Marsella, M. Pompilio, and C. Romagnoli (2005), The landslide sequence induced by the 2002 eruption at Stromboli volcano, in *Landslide-Risk Analysis and Sustainable Disaster Management*, pp. 251–258, Springer, Berlin.
-
- M. R. Carroll, Dipartimento di Scienze della Terra, Università degli Studi di Camerino, Via Gentile III da Varano, I-62032 Camerino, Italy.
- R. A. Corsaro and L. Miraglia, Istituto Nazionale di Geofisica e Vulcanologia, Sezione di Catania, Piazza Roma 2, I-95125 Catania, Italy.
- A. Fornaciai and P. Landi, Istituto Nazionale di Geofisica e Vulcanologia, Sezione di Pisa, Via della Faggiola 32, I-56126 Pisa, Italy. (landi@pi.ingv.it)
- L. Francalanci, I. Nardini, and C. M. Petrone, Dipartimento di Scienze della Terra, Università degli Studi di Firenze, Via La Pira 4, I-50121 Florence, Italy.
- C. M. Petrone, Department of Earth Sciences, Cambridge University, Downing Street, Cambridge CB2 3EQ, UK.

2002–2003 Lava Flow Eruption of Stromboli: A Contribution to Understanding Lava Discharge Mechanisms Using Periodic Digital Photogrammetry Surveys

Maria Marsella

Dipartimento di Idraulica, Trasporti e Strade, La Sapienza Università di Roma, Rome, Italy

Mauro Coltelli, Cristina Proietti, and Stefano Branca

Istituto Nazionale di Geofisica e Vulcanologia, Sezione di Catania, Catania, Italy

Roberto Monticelli

Dipartimento di Idraulica, Trasporti e Strade, La Sapienza Università di Roma, Rome, Italy

Photogrammetric surveys were performed between 5 January and 26 July 2003 for monitoring the NW flank of the Sciara del Fuoco (SdF) during the eruption of Stromboli that started on 28 December 2002. The collected data were used both for controlling morphological changes after the major landslide that occurred on 30 December 2002 and lava flow field evolution until the end of the eruption (22 July 2003). The latter objective was achieved by a quantitative analysis which allowed to estimate the total lava volume ($12.51 \times 10^6 \text{ m}^3$) emplaced on the SdF slope corresponding to an eruption rate of about $0.69 \text{ m}^3/\text{s}$. Thanks to the availability of multitemporal data set, which made this event the first well-documented and regularly surveyed Stromboli eruption, the cumulative volume and effusion rate trends were derived. A model for interpreting the behavior of the 2002–2003 Stromboli effusive eruption is also proposed: being the vents located very close to the volcano summit, a typical summit (terminal) basaltic lava flow eruption was expected; on the contrary, the observed effusion rate trend showed an initial peak followed by an exponential decline typical of flank (lateral) eruptions of basaltic volcanoes. We recognized in this trend a transition from a terminal (open conduit system) to a lateral (pressurized dike system) lava discharge followed by a longer period in which the elastic strain energy from the subvolcanic reservoir controlled the effusion rate; this effect counterbalanced the lava cooling at dike tip that tends to close the eruptive fissure causing the eruption end.

1. INTRODUCTION

The Stromboli Volcano: An Integrated Study of the 2002–2003 Eruption
Geophysical Monograph Series 182
Copyright 2008 by the American Geophysical Union.
10.1029/182GM19

From 28 December 2002 to 22 July 2003, the Sciara del Fuoco (SdF) slope (Stromboli Island) was interested by both instability phenomena and lava flow emplacement [Calvari

et al., 2005]. The effusive activity, started from a vent close to the foot of the Bastimento (about 600 m above sea level) on the 28 December 2002, was characterized by the subsequent opening and closing of more vents at different elevation (Figure 1). On 30 December, two large landslides destroyed a large portion of the submarine and subaerial SdF, causing a reorganization of the eruptive fissure setting and moving the main effusive vent. A paroxysmal explosive event at the summit craters, on 5 April, formed an eruptive column about 1000 m high above the volcano [Calvari *et al.*, 2005], while not influencing the effusive activity. The lava emplacement on the SdF resulted in a fan-shaped lava flow field open toward the sea and in the building of a lava megatumulus at the head of the flow field fed by several ephemeral vents. By the end of June, the lava flow activity was concentrated only on the megatumulus. Activity in the medial sections of the flow field ceased by 8 July; thereafter, all lava flows were confined to the top of the megatumulus. Finally the eruption ended on 22 July.

Photogrammetric techniques were adopted to monitor the evolution of both the instability phenomena and the lava flow emplacement. A photogrammetric survey conducted on July 2001 represented the preeruption surface; whereas repeated surveys (28 December 2002 to 26 July 2003) throughout the eruption allowed to collect a multitemporal cartographic data set formed by high-resolution digital elevation models (DEMs) and orthophotos. The analysis of this data set contributed to follow the evolution of the subaerial portion of

the SdF slope, due to the progression of the instability phenomena and to lava flow emplacement. DEM multitemporal analysis, which is the repeated comparison of two subsequent DEMs, allowed to evaluate, throughout the eruption, the volumes emplaced between two subsequent survey dates and the corresponding effusion rates. The effusion rate trend extrapolated from such values represented a useful data set for discussing about lava discharge mechanism.

2. REMOTE-SENSING TECHNIQUES FOR LAVA FLOW MONITORING

Different techniques can be used to estimate lava flow volumes or to define the geometry of the flow fields, such as area and thickness. Knowledge of these quantitative parameters is useful for evaluating the effusion rate variation during an eruption; if repeated, syn-eruption surveys are carried out [Baldi *et al.*, 2005]. Surveying techniques offering three-dimensional (3-D) mapping capability for directly estimating volumes of emitted lava use ground-based topographic instruments and airborne or satellite remote-sensing sensors. These methods are characterized by different ground resolutions, data density, and area coverage, as well as various operational constraints. Direct ground surveying by means of total stations or GPS receivers can be used to measure cross-sections and the perimeter of the lava field after the end of the eruption, then allowing for volume estimation using a planimetric approach. As an alternative, the same instruments can provide the measurements of

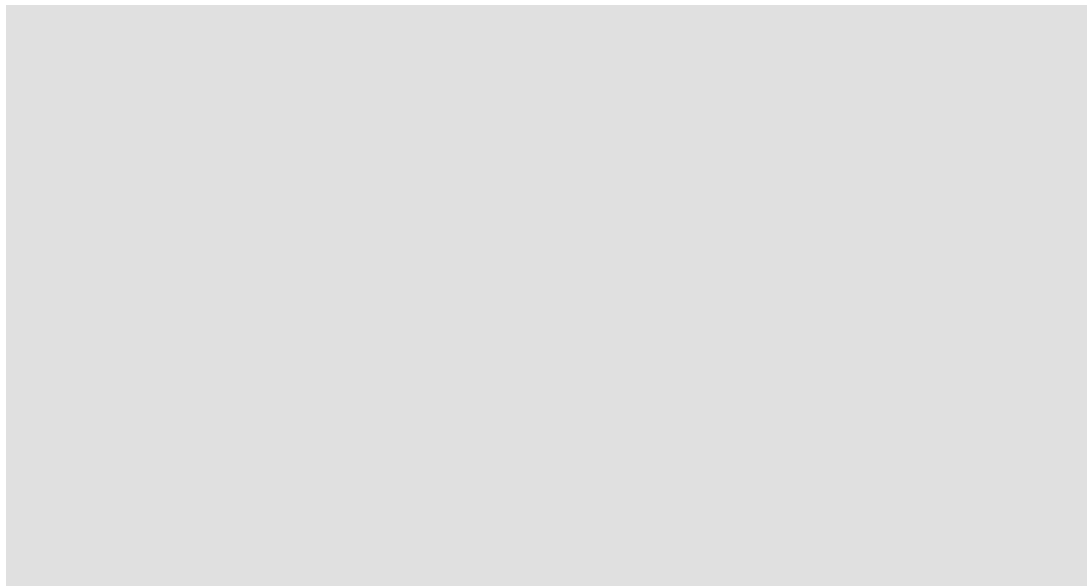


Figure 1. (a) Overview map of the Sciara del Fuoco (SdF) slope. (b) Detailed shaded relief map of the SdF slope; contour lines with 50 m interdistance and approximate location of the main eruptive vents (black triangles).

3-D points distributed over the whole lava field which allows the volume to be calculated if the preeruption surface is also available [Calvari *et al.*, 1994; Stevens *et al.*, 1997; Coltell *et al.*, 2007]. The quality of such volume estimates depends on the accuracy and density of the collected data, which are often constrained by the extent and accessibility of the area to be surveyed. Airborne or satellite surveying techniques, such as synthetic aperture radar interferometry (InSAR), airborne laser scanning (ALS), and aerial digital photogrammetry (ADP), are more suitable for acquiring dense 3-D data over large areas, thus resulting more appropriate to observe the evolution of the lava flow fields. Surveying frequency depends on the satellite-fixed acquisition time interval and on the availability of aerial platforms (helicopter or aircraft) close to the eruption site. From the comparison of subsequent surveys, the evolution of the flow field can be reconstructed, by means of a multitemporal analysis of DEMs, as carried out in this work. Data from remote-sensing techniques can also be adopted as constraints of indirect methods for measuring instantaneous effusion rate estimation such as those based on thermal images analysis [Harris *et al.*, 2000, 2005].

In the absence of dense 3-D data, the evolution of the lava flow can be followed by combining georeferenced and rectified digital images with observed thickness. Such images can be acquired by means of visible and thermal camera during close-range surveys (helicopter) as well as from satellite platforms.

ADP is one of the most flexible tools for acquiring, through semiautomatic procedures, a large amount of 3-D points for the generation of high spatial resolution DEMs and the relative rectified images. Aircraft surveys are preferred for 3-D data generation for their stable flying conditions and larger ground coverage. Conversely, images acquired during helicopter surveys are preferably adopted for extraction of 2-D features, after having applied a simplified procedure for their ortorectification (if a DEM is already available) and georeferencing. High accuracy 3-D models, with submeter elevation accuracy, can be obtained by images acquired at photo scales ranging between 1:5000 and 1:20,000. Direct georeferencing or, at least, sparse control network by means of GPS technology has now reduced the need for ground survey operations [Kraus, 1998].

The digital photogrammetry processing for 3-D point measurements is based on the application of image matching procedures. Autocorrelation algorithms, capable of working at subpixel level, are able to identify corresponding points/areas (well-defined shapes or gray level distribution) in stereomodels [Kraus, 1994; Heipke, 1995]. The final precision of digital products depends on the robustness of the matching, the geometric resolution of the images, the presence of shadows, and the roughness of the surface. Digital

photogrammetry has been used in many volcanic areas [e.g., Achilli *et al.*, 1998; Baldi *et al.*, 2000, 2002, 2006] demonstrating its capability to describe morphological features of inaccessible areas.

3. 2002–2003 STROMBOLI ERUPTION MONITORING

During the 2002–2003 Stromboli eruption, the Department of Civil Protection carried out systematic photogrammetric surveying activity with the aim of monitoring the morphological changes of the slope induced by both the evolution of the landslides that occurred 2 d after the onset of the eruption (30 December 2002) and the continuous lava flows piling on the slope from the 28 December 2002 to 22 July 2003 [Tommasi *et al.*, 2005; Baldi *et al.*, 2005]. Parallel bathymetric surveys provided data for estimating the accumulation rate on the submarine portion of the slope due to lava flowing into the sea until mid-February and additionally to the progressive erosion of landslide escarpments [Chiocci *et al.*, 2004, 2005].

Using the data collected during the photogrammetric surveys (Table 1) carried out through the eruption, DEMs with a 5×5 m grid spacing and an elevation accuracy ranging from 0.5 to 2 m, were extracted, together with the corresponding orthophotos. In some cases, lack of visibility, mainly around the summit crater area, prevented complete stereoscopic coverage. Data collected in 2001 provided the preeruption reference DEM and orthophoto [Baldi *et al.*, 2005]. Comparison with the data from the 5 January 2003, the first available survey which recorded the situation of the slope 8 d after the eruption beginning, revealed modifications of the SdF slope after the 30 December 2002 slope movements [Baldi *et al.*, this volume]. The survey performed on 26 July

Table 1. Photogrammetric Surveys Carried out During 2002–2003 Eruption and Used for Lava Flow Volume Estimation

Date	Film	Data Coverage
29 May 2001	Color	Island
5 Jan 2003	B/w	SdF up to 650 m
16 Jan 2003	Color	SdF up to 400 m
20 Jan 2003	B/w	SdF up to 600 m
27 Jan 2003	B/w	SdF up to 600 m
6 Feb 2003	B/w	SdF up to 600 m
21 Feb 2003	B/w	SdF up to 600 m
15 Mar 2003	B/w	SdF
16 Apr 2003	B/w	SdF
26 May 2003	Color	Island
16 Jun 2003	B/w	SdF
26 Jul 2003	Color	SdF

2003 is the last one considered within the scope of this work, the effusive activity having stopped on 22 July 2003.

The results presented in this work are obtained from a multitemporal analysis conducted on the data collected during the eruption. For the first few days of the eruption (28 December 2002 to 5 January 2003), the analysis was done using a semiquantitative approach, while for the rest of the eruption period (5 January 2003 to 22 July 2003), a quantitative approach was adopted.

4. METHOD ADOPTED FOR DEFINING THE LAVA FLOW FIELD AND VOLUME COMPUTATION

The estimation of the volumes of lava gradually added on the slope during the eruption was carried out by performing a comparative analysis between chronologically contiguous data (DEMs and orthophotos) obtained from the photogrammetric surveys listed in Table 1. On each pair of orthophotos, the lava flow field extension was defined with the aid of close range images taken during helicopter surveys. The field limits were then verified by checking their congruency with the altimetric residual maps (i.e., the height differences between two DEMs) which highlight, in this case, the areas where lava accumulated. In some cases, a detailed morphological and morphometric analysis of the pre- and post-eruption surfaces was conducted in the area surrounding the lava fields to solve interpretative ambiguities. Therefore, the analysis conducted in this work included the following steps: (1) delimitation of lava flow field extents through interpretation of images acquired from helicopter and during field observations; (2) multitemporal quantitative analysis, by subtraction of subsequent DEMs, in areas subjected to accumulation/erosion phenomena for discriminating material mobilized by the landslide scar evolution from that linked to the lava flow emplacement; (3) evaluation of lava volumes accumulated on the submerged portion of the slope in the first period of the eruption, as described in the following.

In the absence of independent measurements for assessing the DEMs' accuracy, we performed a statistical analysis on the height residuals with respect to a more accurate DEM. This analysis, conducted in areas not involved in the 2002–2003 instability and eruption phenomena (stable areas outside the SdF slope), provided an overall standard deviation of about 3 m, which was reduced, after a procedure for outlier detection and removal, to below 1 m on areas with good illumination and visibility conditions, smooth morphology, and absence of vegetation [Baldi *et al.*, 2005].

Volume values were calculated by summing the height variations obtained by differencing two subsequent DEMs multiplied by the cell area. The sum is limited to cells inside the lava flow field limits traced on the corresponding ortho-

photos. Thus, the associated uncertainties, deriving both from DEM (vertical and horizontal) and from orthophoto accuracy (only horizontal component), should be evaluated using the variance propagation law [Coltell *et al.*, 2007]. If we associate to DEMs and orthophotos adopted in this analysis a standard deviation of about 1–2 m, we obtain relative errors for the volume estimates that do not exceed 2% of their values as reported in Table 3. The same magnitude relative errors should be associated to the volumetric effusion rates recorded here. When pre- and posteruption DEMs are not available, the volumes are estimated by using a planimetric approach, that is, by multiplying the lava flow field area per an average flow thickness [Stevens *et al.*, 1997]. In such cases, the associated relative errors reach values close to 10–20% of the corresponding volumes [Coltell *et al.*, 2007]. A relative error of 20% was thus considered to evaluate the standard deviations of volumes emplaced between 28 and 30 December 2002 and between December 2002 and 5 January 2003 (Table 3).

5. ERUPTION NARRATIVE AND EVOLUTION OF THE LAVA FLOW FIELDS

During 2002, the eruptive activity at the summit craters of Stromboli volcano was characterized by a persistent Strombolian activity: one to four low-intensity explosions per hour were observed up to August. In this period only two paroxysmal explosions occurred, on 23 January and 24 July. Starting from September, both intensity and number of the Strombolian explosions gradually increased up to the 8 November when a continuous explosive activity, similar to fire fountaining, took place. After this unusually strong activity, an intense explosive activity continued, in the second half of November, producing also a very small lava overflow from the summit craters rim, and then gradually vanished at the beginning of December. A further sudden increase of the explosive activity started again on 24 December reaching the climax on 27 when an intense fire fountain activity heralded the new lava flow eruption that began in the afternoon of 28 December. The following description of the eruption, with the exception of the first few days (28 December 2002 to 5 January 2003), is organized accordingly to the periods between subsequent surveys; all the altitude values below reported were measured on the DEMs; main vent locations are approximately indicated in Figure 1.

5.1. 28 December 2002

At about 1830 LT, a NNE-directed eruptive fissure opened at the northern foot of the summit craters (named Terrazza Craterica) on the upper part of the SdF, between 650 and 600

m elevation, marking the onset of the eruption. Istituto Nazionale di Geofisica e Vulcanologia (INGV) surveillance camera recording and eyewitnesses' accounts indicate that the eruption started with a short-lived explosive episode from a lateral vent close to the foot of the Bastimento (probably at the lower end of the fissure) forming a hot avalanche that deposited on the northern shore of the SdF (Spiaggia dei Gabbiani). It was followed, about half an hour later, by a vigorous lava overflow from the upper part of the fissure. Lava discharge lasted about 1 h producing a thin pahoehoe-to-aa flow spilled over the northeast slope of the SdF (Filo del Fuoco) down to the sea, overlapping on the hot avalanche deposit (green flow area in Plate 1a). A branch from the break in slope at 570 m elevation, (blue flow area Plate 1a) diverged southward flowing in the central part of SdF reaching the shore divided in two fronts. Soon after, at about 2050 LT, a lava flow originated from another vent that opened on the northern slope of the summit craters at about 600 m and a few tens of meters west of the initial eruptive fissure. Also, this lava flowed down to the shore forming a lava fan in the central part of SdF that overlapped the previous lava flows.

5.2. 29 December 2002

The effusive activity resumed in the afternoon of 29 December from two more vents opened at about 600 and 550 m elevation located, respectively, at the foot of the Bastimento and on the northern flank of summit craters, at few tens of meters below the 600 m vent active the day before. Lava flows erupted by the upper vent partially covered the flow, active the previous day on the same area, without reaching the sea. Lava flows erupted from the lower vent forked immediately downslope, probably diverging in correspondence of the slope-breaks formed at the vent opening, and reached the sea building on the shoreline a thick fan of lava and blocks (yellow flow area in Plate 1a). On the whole, the discontinuous activity of the first 2 d generated, on the steep slope of the SdF, a branched lava field that reached the shoreline covering an area of about 0.2×10^6 m².

5.3. 30 December 2002

On 30 December, two large landslides occurred at 1315 and 1322 LT, respectively [Pino *et al.*, 2004], destroying a large portion of the submarine and subaerial SdF that included some small active lava tongues from one vent located at about 600 m elevation and others around 450 m elevation. The flank collapse caused a reorganization of the eruptive fissure setting. The subsequent main effusive vent opened within the detachment rim at 555 m elevation, in the place of the lower vent active on 29 December, forming a well-fed

lava flow that went straight to the sea (approximately following the same path of the yellow flow in Plate 1a). About 100 m below, a second vent generated a small lava flow that joined into the main flow.

5.4. 31 December 2002 to 14 February 2003

In the days after the SdF collapse, the lava emission from the vent at 555 m elevation was stable forming a narrow channel that delivered most of the molten lava directly into the sea. In 5 January 2003, the lava emission at this vent decreased, and the main vent moved down to 480 m elevation spreading the lava flows to form a fan-shaped lava flow field open toward the sea (Plate 2a). During January, a continuous and sustained lava emission at these vents increased the lava flow field extension (Plate 3a), and the new lava gradually refilled the landslide scar. In this period, the 555 m vent shifted to one at 535 m elevation, and the setting of the 480 m emission point became more complex with the opening of four vents located at 450, 470, and 480 m elevation. This evolving eruptive fissure confirmed that an ongoing dike intrusion was happening beneath the SdF. On 27 January, a wide fan-shaped lava flow field was mapped. It spread along the shoreline (Plate 3c) extending below sea level, as evidenced in Baldi *et al.* [this volume]. Between 28 January and 3 February temporary interruptions of the lava emission from lower vents were soon followed by lava outpouring from vents at around 600 m elevation. Limited lava effusion already occurred in this area immediately before the SdF collapse, in 30 December 2002 and also on 9 and 23 January. On 6 February, only the 470 m vent was active, and most of the lava passed through a tunnel down to an ephemeral vent located at 290 m elevation, generating a fan of lava flows that reached the sea (Plate 4a). This setting of the eruptive vents remained stable until 14 February producing a considerable thickening of the lava flow field.

5.5. 15 February to 15 March 2003

The most important modification of the effusive activity occurred on 15 February when the 470 m vent and the 290 m ephemeral vent shut down, and after a 1.5-d-long pause, a new vent opened on 17 February at 580–590 m elevation below the Bastimento in the same area as the 28 and 29 December vents. Very soon, a gradual increase of the lava output caused the formation of several ephemeral vents located between 550 and 590 m elevation on the break in slope between a quite flat area below the Bastimento and the SdF steep slope. By 21 February, the lava flow field spreading from the upper vents was characterized by two distinct lava flow branches whose fronts reached a minimum altitude

of about 250 and 100 m (Plate 4b). Between 21 February and 15 March, the eruptive activity was characterized by the sudden opening and closing of the ephemeral vents that fed toothpaste (close the vents) and aa (on the slope) lava tongues flowing mainly toward the northern wall of the SdF. The cooling-limited lava flow units started the construction of a lava megatumulus, named “lava shield” by *Calvari et al.* [2005] and *Lodato et al.* [2006], “Pianoro” by *Landi et al.* [2006], and “Lava Terrace” by *Baldi et al.* [2008], at the head of the flow field where the slope was gentler. Two or three vent systems were persistently active building small tumuli during February and March (Plate 4b). The lava flows generated from these short-lived ephemeral vents were superimposed in the middle-upper part of the SdF as a consequence of a gradual decrease in the lava output. Below the break in slope (at 550 m elevation), lava flow fronts traveled for tens to a few hundreds of meters and then broke, resulting in the detachment of blocks and slab from the lava flows. These rolled downslope, triggering the movement of unconsolidated coarse clasts as well as finer grained material (grain flows) along the slope down to the shoreline. By the middle of March, the lava flow field was formed by a main branch whose front went down to 20 m elevation, close to the shoreline (Plate 4c).

5.6. 15 March 2003 to 16 April 2003

A paroxysmal explosive event occurred at the summit craters at 0912 LT of 5 April forming an eruptive column about 1000 m high above the volcano and a block and spatter fallout on the upper slopes of the island [*Calvari et al.*, 2005]. A small pyroclastic flow was emitted during the explosive phase covering the area below the Bastimento where the active effusive vents were located. This explosive event did not produce any variation of the effusive activity, at that time characterized by the emission of small short-lived lava flows in the upper part of the SdF. In fact, a few hours after the event, lava emerged from three points below the pyroclastic deposit resuming the vent geometry observed before. In a few days, new tumuli were rebuilt on the pyroclastic deposit surface, and below the break in slope, the new lava flows continued to thicken mainly in the middle portion of the slope. The lava flow field produced between 15 March and 14 April covered an area of $0.11 \times 10^6 \text{ m}^2$ (Table 2) and formed two branches that reached a minimum altitude of about 260 m (Plate 5a).

5.7. 16 April 2003 to 26 May 2003 and to 16 June 2003

Moderate degassing activity was observed at the effusive vents on 16 April. At the same time, a renewal of the lava

output occurred producing lava flows that arrived near the shoreline. In the following days, the onset of lava spattering at these vents resulted in the rapid growth of two hornitos on the top of the tumuli at 650 m elevation. The lava was delivered by a braided tube system from the hornitos to ephemeral vents, mainly located on the slope break at 550 m, feeding short-lived flows moving on the central part of the SdF. In the first half of May, a regression of the active flow fronts was observed, due to a sudden decrease of the lava output. The lava flow field generated between 14 April and 26 May covered an area of $0.13 \times 10^6 \text{ m}^2$ (Table 2), and its main branch reached a minimum elevation of 15 m. Piling up of lava tongues, building the megatumulus [*Baldi et al.*, 2008], was recognized on the flat area below the Bastimento (Plate 5b).

Another spattering episode from the two hornitos occurred between 21 May and the beginning of June and marked the uprising of more gas-rich magma. Consequently, the effusive activity from ephemeral vents near the hornitos became more vigorous, increasing significantly the thickness of the megatumulus. In June, some ephemeral vents, located at the slope break (580–550 m elevation), fed a channel that drove most of the lava in the central portion of the SdF. Short-lived lava flows and hot block avalanches moved from their fronts and spread on the slope forming a main branch that reached the minimum altitude of 100 m above the shoreline (Plate 5c). The lava flow field formed between 26 May and 16 June covered an area of $0.12 \times 10^6 \text{ m}^2$.

5.8. 16 June 2003 to 26 July 2003

The upflow migration of the ephemeral vents began to be observed from 25 June, accompanied by a gradual withdrawal of the flow front positions to increasingly higher elevations. By the end of June, lava flow activity was concentrated on the megatumulus and just down the slope break between 550 and 610 m elevation, only grain flows moved on the distal section of the flow field (near the coast). Activity in the medial sections of the flow field (below the slope break) ceased by 8 July; thereafter, all lava flows were confined to the proximal zone, the top of the megatumulus. Consequently, a final thickening of the upper part of the flow field was observed [*Baldi et al.*, 2008]. Finally, by the half of July, only a few ephemeral vents were active at 620 m elevation generating very short lava flows (Plate 5d) as a consequence of the final decreasing in the lava output that vanished on 22 July. The lava flow field formed in this last eruptive period covered an area of $0.07 \times 10^6 \text{ m}^2$ (Table 2) and reached a minimum altitude of about 200 m, but only in the days immediately after the survey performed on 16 June.

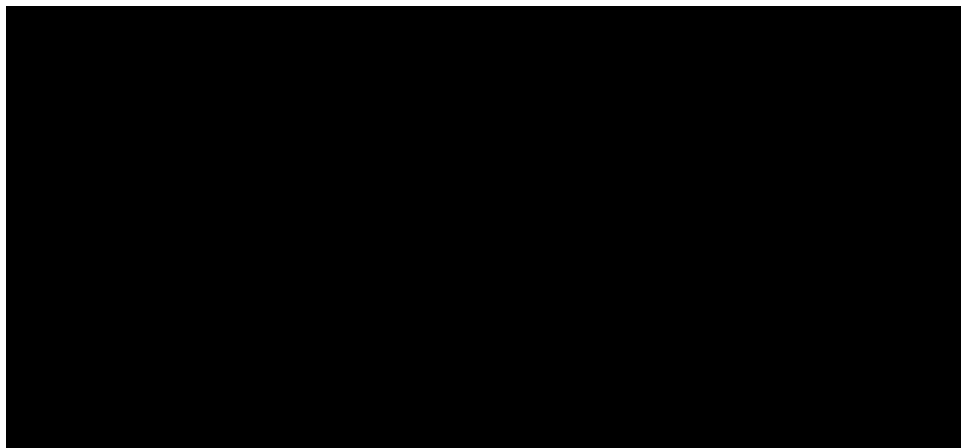


Plate 1. Reconstruction of lava fields between 28 December 2002 and 5 January 2003; (a) lava fields active in the whole period; in particular, the green flow area corresponds to the thin pahoehoe-to-aa flow overlapping the hot avalanche deposit of the 28 December 2002; the blue flow area corresponds to the flow flowed in the central part of SdF reaching the shore divided in two fronts. The yellow flow area corresponds to the 29 December flow which reached the sea building a fan on the shoreline. (b) DEM residuals 2001 to 27 January 2003 analyzed for estimating the thickness of lava flow (a) emplaced outside the 30 December landslide scar. (a) The limits of the scar is represented by the red dotted line to evidence the area where it was possible to estimate the lava thickness.

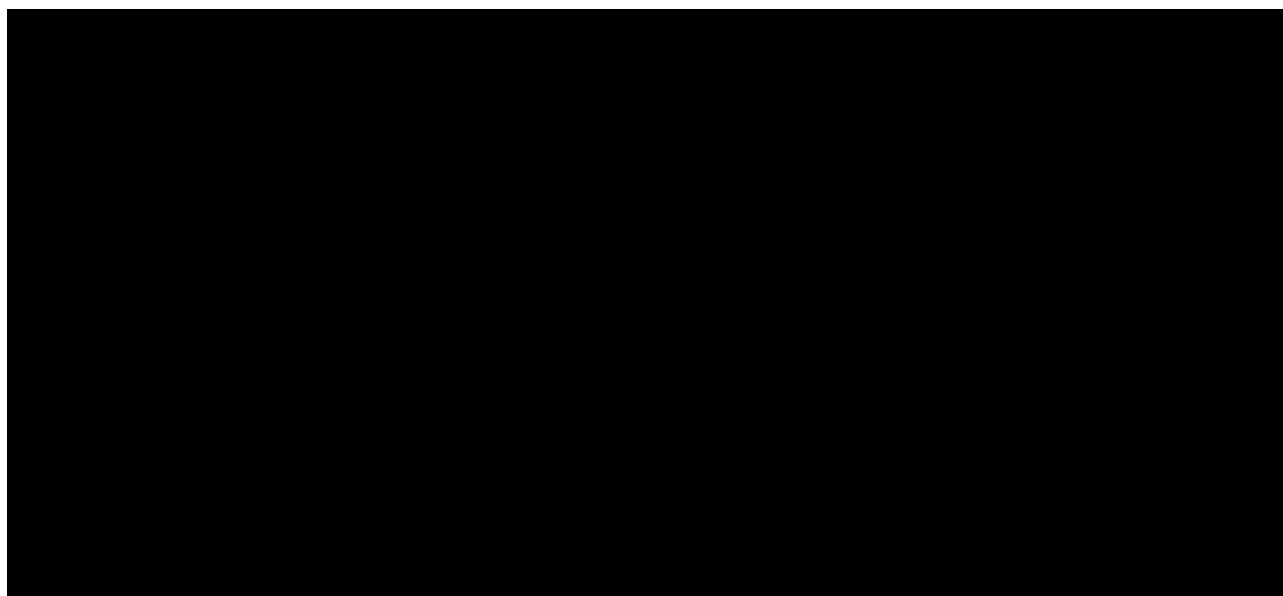


Plate 2. Reconstruction of lava fields between 30 December 2002 and 5 January 2003; (a) Lava flow field limits on 5 January 2003 orthophoto; black lines indicate the cross sections reported in Plate 2b. (b) Cross-sections used for supporting the volume estimation: black line, 29 May 2001; blue line, 5 January 2003; green line, 27 January 2003; red line, 26 May 2003.

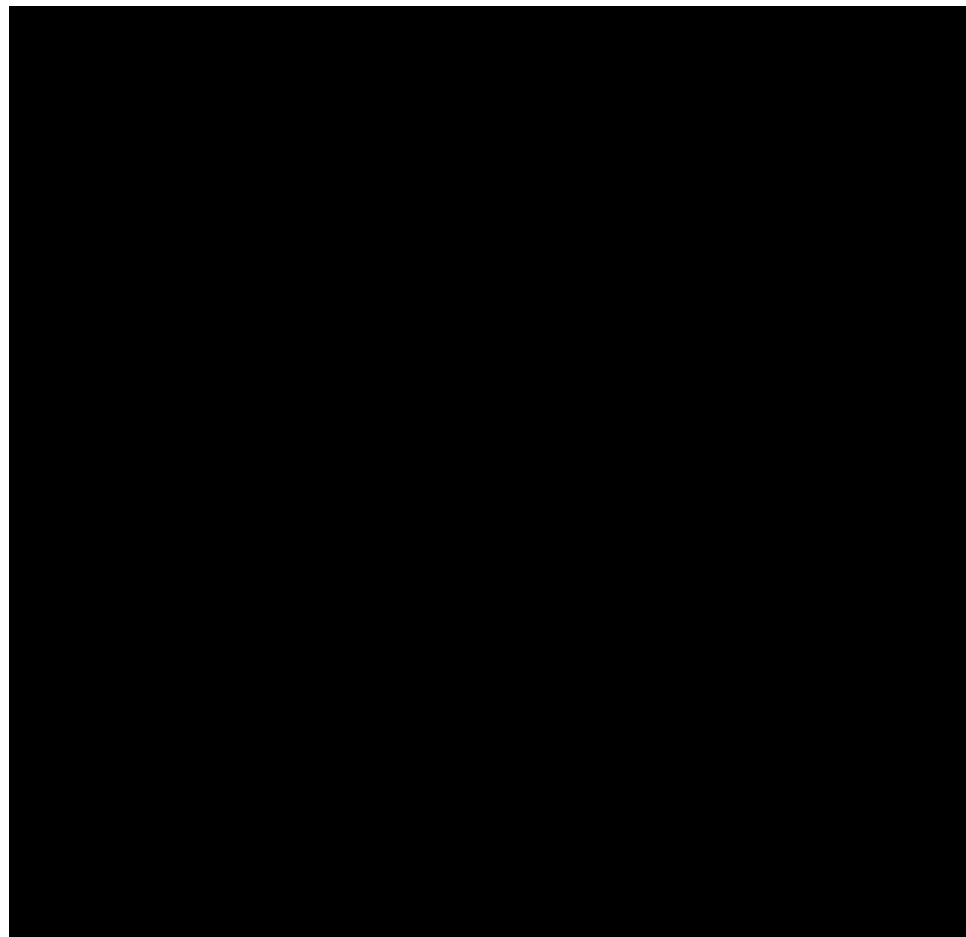


Plate 3. Reconstruction of lava fields between 5 and 27 January 2003; (a) Lava flow field limits on the 16 January 2003 orthophoto. (b) DEM residuals between 5 January 2003 and 16 January 2003. (c) Lava flow field limits on the 27 January 2003 orthophoto. (d) DEM residuals between 20 January 2003 and 27 January 2003.

Table 2. Geometrical Parameters for the Lava Flow Field Corresponding to the Dates of the Photogrammetric Surveys and Used for Lava Flow Volume Estimation^a

Observation Date	30 Dec 2002	5 Jan 2003	16 Jan 2003	20 Jan 2003	27 Jan 2003	6 Feb 2003	21 Feb 2003	15 Mar 2003	14 Apr 2003	26 May 2003	16 Jun 2003	26 Jul 2003
Time span, d	2	6	11	4	7	10	15	22	30	42	21	40
Flow field surface (10^6 m^2)	0.21	0.05	0.10	0.10	0.14	0.07	0.19	0.12	0.11	0.13	0.12	0.07
Observed volume (10^6 m^3)	2.00 ^b	2.50 ^b	1.05	0.27	0.63	0.21	0.95	0.78	0.77	0.61	0.51	0.29
Average thickness (m)	9.68	50.51	10.54	2.83	4.65	2.96	5.02	6.32	7.09	4.82	4.18	4.28
Estimated volume (10^6 m^3)	2.29	3.36	1.37	0.45	0.78	0.34	0.95	0.78	0.77	0.61	0.51	0.29

^a Lava volumes emplaced on the whole slope obtained adding the estimated contribution for the submerged portion, are also reported.

^b Volumes estimated by the planimetric approach.

6. RESULTS FROM THE PHOTOGRAHMETRIC SURVEYS

The availability of orthophotos and DEMs let us follow a quantitative approach for effusion rate estimations. Table 2 summarizes the area, thickness, and volume of the lava flow field evaluated at the same dates as the photogrammetric surveys carried out during 2002–2003 eruption; Table 3 contains the partial and cumulative volumes of lava as well as the time intervals. Most of the figures in Table 3 are computed from direct comparisons of photogrammetric DEMs or estimated by surface analysis. In order to estimate the amount of lava deposited along the submerged portion of the slope data from bathymetric surveys can be considered. Unfortunately, they were not performed at the same dates as the photogrammetric surveys; thus, it was necessary to extrapolate them by considering an average accumulation rate of $50,000 \text{ m}^3/\text{day}$ [Baldi *et al.*, this volume]. The obtained volume was reduced by the contribution attributed to the accumulation of landslide debris, which was estimated from the period when the lava was no longer reaching the sea [Baldi *et al.*, 2005]. Figure 2 shows the temporal evolution of cumulative lava volumes, from which we derived the average volumetric effusion rates. During the first period (28 December 2002 to 5 January 2003), there were a few direct observations on a limited part of the eruption theater, and inferences based on the reconstructed lava flow field and the eruption trend observed soon after had to be made.

From 5 January 2003, the volume estimates were always obtained by DEM differencing. For a few surveys, especially in the first months of the eruption, such as on 16 and 20 January, the collected data were insufficient for extracting reliable DEMs on the whole lava field. In order to avoid

a marked underestimation of the accumulated lava volumes due to missing 3-D data, we first attempted a manual refinement (integration) of the DEM data by measuring point coordinates directly on the stereo models. Then, in the cases of a lack of stereoscopic coverage, we estimated volumes from the analysis of images and orthophotos and by using geometrical constraints extrapolated from adjacent areas.

6.1. 28 December to 30 December 2002

The estimated volume includes contributions from partially overlapping lava flows (see eruption narrative) that we divided into two main branches (Plate 1a). The first takes into account lava that flowed on 28 December along the NE wall of SdF (green flow area in Plate 1a), while the second is the lava erupted from the 600 m vents from the evening of 28 December until the afternoon of 29 December (blue flow area in Plate 1a). The first lava branch was only partially removed by the landslides that occurred at 1315 LT on 30 December, while the second lava branch was completely removed by them.

Flow field areas were traced on the preeruption surface (2001 orthophoto) on the basis of the analysis of close range images taken during the helicopter overflights. Thicknesses, measured where the flows were not removed by the landslides (red dotted line in Plate 1a), were attributed to both the two lava flow branches. The volumes obtained were $0.8 \times 10^6 \text{ m}^3$ and $1.2 \times 10^6 \text{ m}^3$, respectively. Lava entering into the sea accounts for an additional volume of $0.3 \times 10^6 \text{ m}^3$. The total volume is considered an underestimate due to the following considerations: (1) lava flow fields are not correctly delimited on the upper portion of the slope due to poor visibility and plume coverage on the images taken on 28, 29, and 30 December; (2) the average thickness does not take into account the accumulation along the coastline and the

Table 3. Volume Accumulated on the Slope During the Time Spans Between Photogrammetric Surveys, Cumulated Volumes Throughout the Whole Eruption and Volumetric Effusion Rates^a

Observation Date	Day of Eruption	Time Span, d	Observed Lava Volume on Sub-aerial Slope in the Time Span, 10^6 m^3	Standard Deviation of Volume in the Time Span, 10^6 m^3 ^b	Cumulated Lava Volume on Subaerial Slope, 10^6 m^3
30 Dec 2002	2	2	2.00 ^c	0.40	2.00 ^c
5 Jan 2003	8	6	2.50 ^c	0.50	4.50 ^c
16 Jan 2003	19	11	1.05	0.02	5.55
20 Jan 2003	23	4	0.27	<0.01	5.82
27 Jan 2003	30	7	0.63	0.01	6.45
6 Feb 2003	40	10	0.21	<0.01	6.66
21 Feb 2003	55	15	0.95	0.02	7.62
15 Mar 2003	77	22	0.78	0.02	8.39
14 Apr 2003	107	30	0.77	0.02	9.16
26 May 2003	149	42	0.61	0.01	9.78
16 Jun 2003	170	21	0.51	0.01	10.29
26 Jul 2003	210	40	0.29	<0.01	10.58
Total		210	10.58		

Observation Date	Average Effusion Rate for the Sub-aerial Slope in the Time Span, m^3/s	Extrapolated Lava Volume on Submerged Slope in the Time Span, 10^6 m^3	Observed/Extrapolated Lava Volume on Subaerial and Submerged Slope in the Time Span, 10^6 m^3	Cumulated Lava Volume on Subaerial and Submerged Slope, 10^6 m^3	Average Effusion Rate for the Subaerial and Submerged Slope in the Time Span, m^3/s
30 Dec 2002	11.57	0.29	2.29	2.29	13.23
5 Jan 2003	4.82	0.86	3.36	5.65	6.48
16 Jan 2003	1.74	0.32	1.37	7.02	2.27
20 Jan 2003	0.78	0.18	0.45	7.47	1.31
27 Jan 2003	1.22	0.15	0.78	8.25	1.51
6 Feb 2003	0.49	0.13	0.34	8.59	0.78
21 Feb 2003	0.73	0.00	0.95	9.54	0.73
15 Mar 2003	0.41	0.00	0.78	10.32	0.41
14 Apr 2003	0.39	0.00	0.77	11.09	0.39
26 May 2003	0.17	0.00	0.61	11.70	0.17
16 Jun 2003	0.28	0.00	0.51	12.21	0.28
26 Jul 2003	0.08	0.00	0.29	12.51	0.08
Total	0.58	1.93	12.51		0.69

^a Volumes are computed using both aerial photogrammetry data for the subaerial slope and data extrapolated from accumulation rates reported for the submerged slope.

^b Standard deviation of the volume from DEM comparisons were evaluated as 2% of the volume, that estimated by the planimetric approach as 20% of their value.

^c Volumes estimated by the planimetric approach.

contribution of overlapped flows; (3) due to a lack of direct observation and survey data, it is very hard to account for the volume of lava entering into the sea in the first days.

6.2. 30 December 2002 to 5 January 2003

After the landslides, lava continued to flow within the scar contributing to its filling together with the debris from the

landslide escarpments, which partly remained along the sub-aerial slope and partly reached its submerged portion. Due to bad weather conditions, photogrammetric surveys were not carried out until 5 January. The corresponding lava volume (about $2.5 \times 10^6 \text{ m}^3$) emplaced on the slope was preliminary derived by extrapolating values from the average effusion rate observed in the subsequent period. This estimate is also in accordance with the one obtained by considering geometric

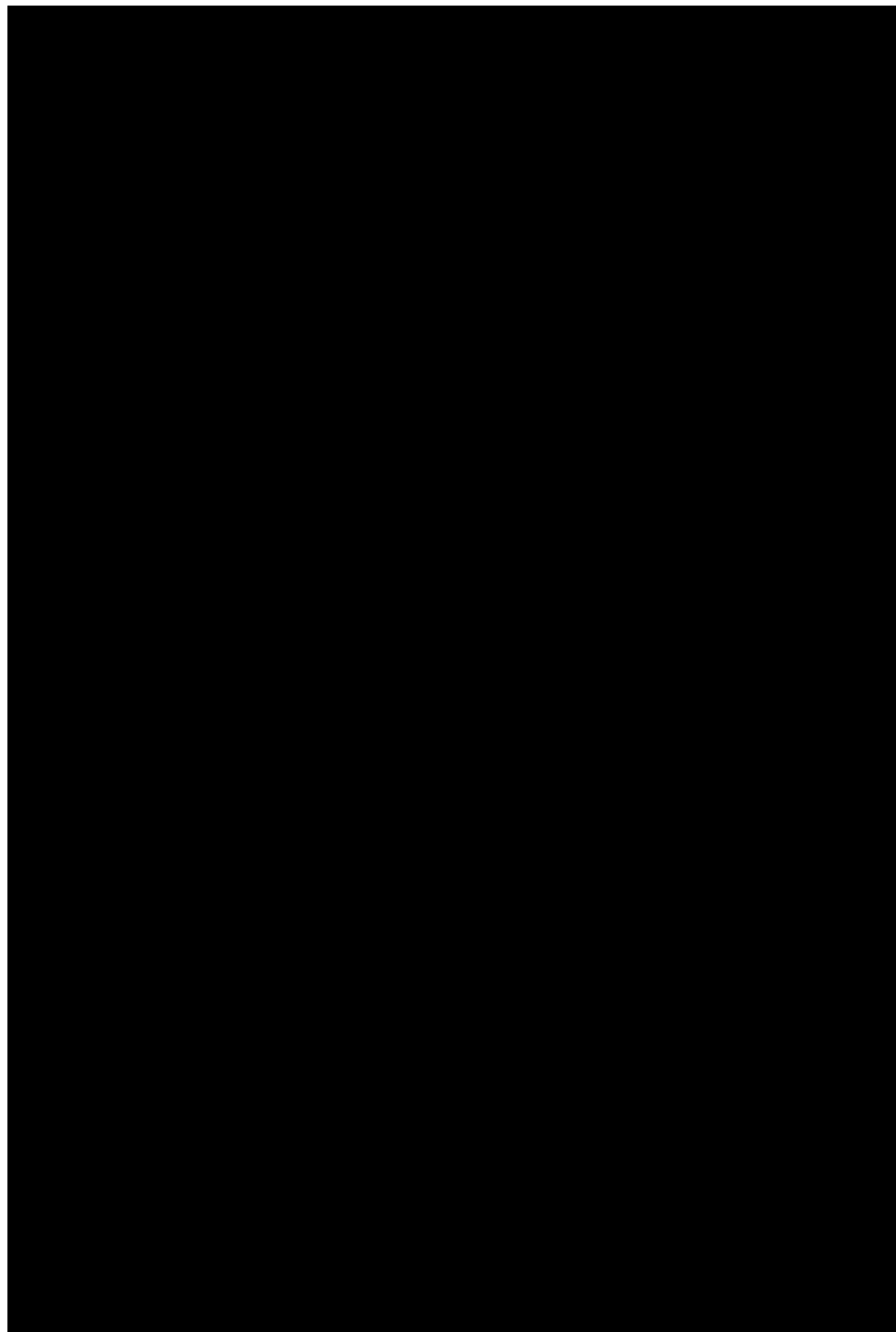


Plate 4. Reconstruction of lava fields between 27 January and 15 March 2003; (a) Lava flow field limits on 6 February 2003 orthophoto and DEM residuals 27 January 2003 to 6 February 2003. (b) Lava flow field limits on 21 February 2003 orthophoto and DEM residuals 6 February 2003 to 21 February 2003. (c) Lava flow field limits on 15 March 2003 orthophoto and DEM residuals 21 March 2003 to 15 March 2003.

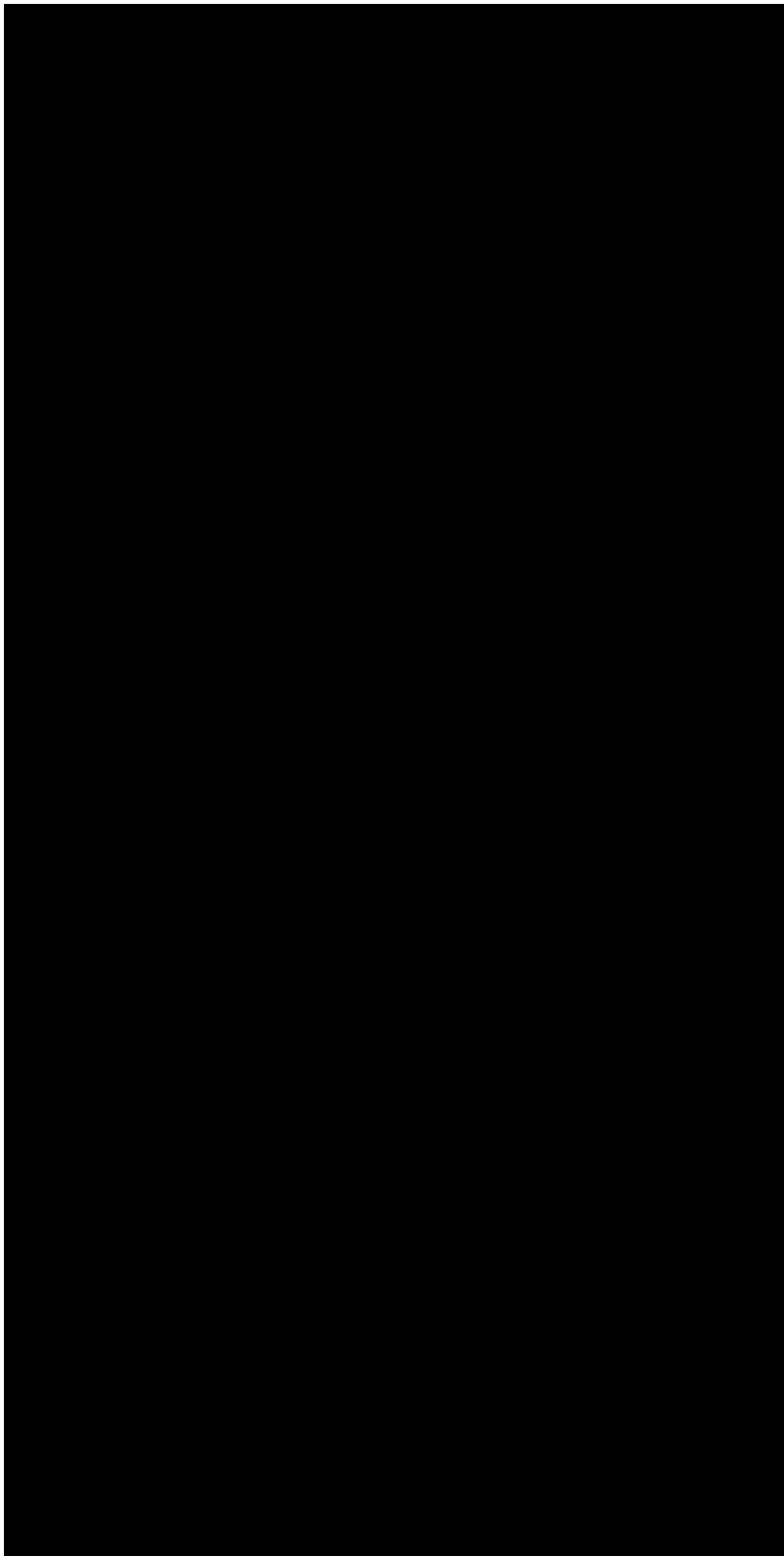


Plate 5. Reconstruction of lava fields between 15 March and 26 July 2003; (a) Lava flow field limits on 14 April 2003 orthophoto and DEM residuals 15 March 2003 to 14 April 2003; (b) Lava flow field limits on 26 May 2003 orthophoto and DEM residuals 14 April 2003 to 26 May 2003; (c) Lava flow field limits on 16 June 2003 orthophoto DEM residuals 26 May 2003 to 16 June 2003. (d) Lava flow field limits on the 26 July 2003 orthophoto DEM residuals 16 June 2003 to 26 July 2003.

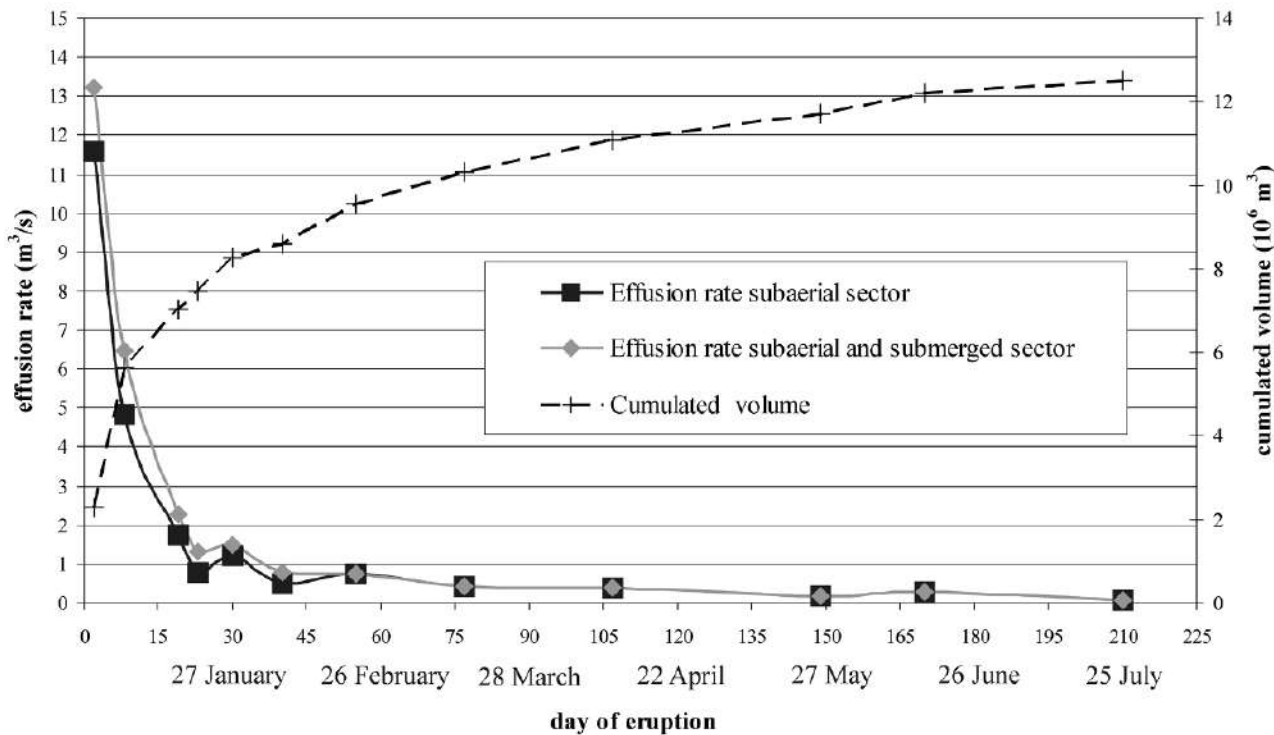


Figure 2. Temporal evolution of accumulated magmatic material volume and volumetric effusion rates.

constraints based on the cross-section analysis within the landslide scar (Plate 2b). By dividing the preliminary estimated volume by the active area traced on the 5 January orthophoto (Plate 2a), we obtain an averaged thickness of 70 m, which is fully compatible with that observed along the scar cross-sections. The volume was increased by about $0.8 \times 10^6 \text{ m}^3$ to take into account the contribution of the lava emplaced on the submarine slope, obtained by extrapolating backward the accumulation rates observed in the following days.

6.3. 5–16, 16–20, and 20–27 January 2003

As already mentioned, despite the availability of photogrammetric data starting from 5 January, the results of DEM analysis between 5 and 20 January underestimate the accumulated lava volumes because the stereoscopic coverage was not sufficient for extracting a DEM over the whole of the lava flow field; thus, some portions of the lava volume needed to be extrapolated. The first DEM comparison (5–16 January) gave the volume of accumulated lava ($0.9 \times 10^6 \text{ m}^3$) for almost the entire lava field. Additional volumes of 0.15×10^6 and $0.32 \times 10^6 \text{ m}^3$ were added to the observed value to take into account the lava emplaced on the upper

slope portion, on small lateral subaerial areas and on the submerged slope, respectively (Plate 3b). A total volume of $1.37 \times 10^6 \text{ m}^3$ was obtained.

For the second interval (16–20 January), an additional $0.07 \times 10^6 \text{ m}^3$ was added to the $0.2 \times 10^6 \text{ m}^3$ derived from DEM differencing by taking into account the upper and lower portions of the lava flow field (Plate 3b). Including also the lava deposited below the sea level gives a total of about $0.45 \times 10^6 \text{ m}^3$.

For the third time interval (20–27 January), we estimate a volume of $0.78 \times 10^6 \text{ m}^3$, that is, the sum of the DEM difference volume ($0.5 \times 10^6 \text{ m}^3$; Plate 3d) and that extrapolated using the planimetric approach on the subaerial slope ($0.13 \times 10^6 \text{ m}^3$) and that estimated for the submerged portion ($0.15 \times 10^6 \text{ m}^3$).

6.4. 27 January to End of Eruption (22 July 2003)

From 27 January to the end of the eruption, the volume estimates (Table 3) are based uniquely on DEM differencing. The contribution to the volume estimates coming from the lava entering into the sea was considered only until mid-February, that is, when the active lava flows retrograded

and covered only the subaerial portion of the slope. Seven surveys were repeated during this period with time spans ranging between 15 and 40 d. The volumes emplaced during each interval were 0.34×10^6 ; 0.95×10^6 ; 0.78×10^6 ; 0.77×10^6 ; 0.61×10^6 ; 0.51×10^6 , and $0.29 \times 10^6 \text{ m}^3$ for the periods 27 January to 6 February; 6–21 February; 21 February to 15 March; 15 March to 14 April; 14 April to 26 May; 26 May to 16 June, and 16 June to 26 July 2003, respectively (Table 3).

6.5. Total Volume of Erupted Lava (28 December 2002 to 22 July 2003)

The total lava volume emitted through the whole eruption (210 d) was evaluated, both for the subaerial and submerged slopes of the SdF, as the sum of the contributions described above for each time interval. The total volume emplaced on the subaerial slope of the SdF was $10.58 \times 10^6 \text{ m}^3$, whereas that on the submarine slope was $1.93 \times 10^6 \text{ m}^3$, giving a total outpoured volume of $12.51 \times 10^6 \text{ m}^3$, and an eruption rate (i.e., the total volume divided by the total eruption duration) of $0.69 \text{ m}^3/\text{s}$ (Table 3).

7. LAVA DISCHARGE BEHAVIOR DURING THE ERUPTION

Some insights into the lava discharge mechanism can be derived from the interpretation of Figure 2 which shows the effusion rate and the cumulative volume trends during the whole 2002–2003 lava flow eruption.

The observed effusion rate trend started on 28 December from an initial peak (it probably rose to this peak very rapidly in a few tens of minutes, see the eruption narrative) and then declined more slowly, resulting in an exponential decrease of eruption rate and diminishing growth of cumulative volume. This trend is typical of flank eruptions of basaltic volcanoes and can be explained by tapping of an enclosed pressurized system [Wadge, 1981]. However, we might have expected that, for Stromboli, lava flow eruptions would be characterized by steady outpouring and eruption rates and, hence, a linear increase in cumulative volume. Considering that the dike intrusion occurred very close to the summit vents level (less than 300 m of difference in height), the trend should be similar to that of a typical summit eruption of basaltic volcanoes (like Etna), which is related to overflow of the time-averaged magma supply. Harris *et al.* [2000] had attributed this style (their Type II) to the previous large effusive eruption of Stromboli that occurred in 1985–1986.

A conceptual model, for explaining the apparently contradictory behavior of 2002–2003 Stromboli lava flow eruption, was formulated starting from the results described above that makes this case the first well-documented and

regularly mapped lava flow eruption of this volcano. The onset (28 December 2002) of the lava flow eruption was characterized by a high effusion rate ($>13 \text{ m}^3/\text{s}$, Table 3), reconstructed by the subaerial lava volume emitted in the first 2 d of the eruption, as described before. The high value is in agreement with both the wide extent of the lava flows obtained from oblique helicopter photographs taken by the staff of INGV and with the eyewitnesses of the relevance of the initial eruptive phase. It is significant to observe that the initial hot avalanche and the subsequent sheet lava flow emitted from the upper part of the fissure system represent an unusual very strong overflow from the new dike emerging at the surface.

In the following days (29–30 December 2002), the activity was significantly lower until the large landslide-forming SdF-slope movement. This movement sharply decompressed the dike, enabling the opening of the eruptive vents at the lower tip of the intrusion and, consequently, giving rise to another period of strong effusion rate (30 December 2002 to 16 January 2003). The average value calculated for the first week of the eruption was $4.82 \text{ m}^3/\text{s}$ from the subaerial lava field that became $6.48 \text{ m}^3/\text{s}$ when including the lava flowed into the sea. In the next period (starting from 18 January), the effusion rate dropped down to about $2 \text{ m}^3/\text{s}$ and then below $1 \text{ m}^3/\text{s}$ in February when the emission from the lower vents stopped frequently, and lava was outpoured by vents opened at about 600 m elevation. On 17 February, effusion stopped at the lower vents, and new vents opened at 580 to 590 m elevation, starting to build up a new lava flow field on the upper slope. From this time, the evolution resembled that of a low-rate, long-lasting basaltic effusive eruption, with the emplacement of cooling-limited short-lived lava flow which, concentrating mainly around the vents, finally formed a megatumulus. The advancement of lava flow field was driven by both the stability of the main tube-channel, delivering lava out from the vent area (on the top of the megatumulus) to the steep slope sometimes allowing the lava field to approach the shoreline, mainly as autoclastic lava flows or block avalanches.

It is notable that the arrival of new magma in the upper plumbing system during the paroxysmal episode of 5 April did not change the declining trend of the effusion rate observed until the end of the eruption. Only a mild inflection point on the trend is visible in June after a short period (end of May to beginning of June) of spattering from the hornitos at the top of the megatumulus, coinciding with the resumption of the Strombolian activity at the summit craters. The eruption continued its slow decline until its end 1 month later, on 22 July.

The observed effusion rate trend (Figure 2) shows a very rapid increase followed, first, by a slower and, then, a much

slower decline. This is in accordance with the discharge variation model discussed by *Wadge* [1981] for lava flow eruptions from pressurized sources. Following the terminology of *Wadge* [1981], the effusion rate trend suggests the presence of an initial short period of waxing flow, not observed by our data, during the eruptive phase that preceded the landslide- and tsunami-forming SdF-slope movement. The initial peak observed in the first few hours of the eruption is not to be considered as the true effusion rate peak; conversely, we suggest that it had occurred in the hours/days immediately after the instability phenomenon that suddenly decompressed the dike-tip and opened the vigorous effusive vent at 500 m elevation. The occurrence of such effusion rate maximum after the SdF landslide is indirectly confirmed by the long period of waning flow observed afterward.

Even if this eruption showed a more complex evolution than that of standard basaltic flank eruptions, we can infer that the main process responsible for the observations reported here is the decompression of a very shallow magma reservoir, rather than the behavior of an open system. The effusion rate and cumulative volume trends never present the behavior described by *Harris et al.* [2000] for open system eruptions, that is a “persistent and steady leakage of a portion or all of the magma supply giving steady, but small effusion rates and a stable rate of volumetric emplacement”.

We have to consider that the main features of the 2002–2003 lava extrusion started from the breaking of the summit conduit, which was experiencing an unusual strong explosive activity. The 28 December activity then was an open conduit-style lava overflow that preceded the pressurized system-style waxing flow. The initial lava flow from the upper fissure was characterized by both high rate and short duration, due to the spill out of the lava stored in the higher portion of the plumbing system. Soon after, the opening of the 600 m vent represented the arrival at the surface of the tip of a dike connected with the deeper portion of the plumbing system and apart from the summit conduit.

Then, the eruption experienced an intermittent lava outpouring until the slope failures triggered a strong decompression at the tip of the dike feeding the main effusive eruption. This process produced at first the opening of a lower vent characterized by a very high effusion rate that soon reached the peak and then gave place to the waning flow. The exponential decline observed was stronger in the first 2 weeks after 30 December and very gentle afterward as highlighted by the two different slope gradients (Figure 2). In conclusion, we can divide the effusion rate in three phases ideally sketched out in Figure 3: the first one (28–30 December 2002) was characterized by transition from a terminal (open conduit system) to a lateral (pressurized dike system) spillage, in which the discharge from a broken conduit preceded

and probably accelerated the dike intrusion from depth; in the second one (30 December 2002–18 January 2003, which represent the intercept of the two curve slopes), the sudden slope decompression opened the lateral magma intrusion, decreasing the lithostatic load on the shallow dike and, thus, accelerating its elastic strain relaxation. This resulted in a lava discharge more efficient than that expected from pressurized sources. Finally, in the third longer phase (18 January to 22 July 2003), elastic strain energy from the subvolcanic reservoir controlled the effusion rate, counterbalancing the lava cooling along the wall and at the apical portion of the dike that tends to close the eruptive fissure [*Bruce and Huppert*, 1989].

The effusion rate trend of the 2002–2003 Stromboli eruption has been previously analyzed by other authors, such as *Calvari et al.* [2005], *Ripepe et al.* [2005], and *Lodato et al.* [2006], who obtained instantaneous effusion rates from the analysis of thermal images acquired both from satellite imagery [advanced very high resolution radiometer (AVHRR) and Moderate Resolution Imaging Spectroradiometer (MODIS)] and handheld thermal camera (FLIR). In *Calvari et al.* [2005], a 3-d running average interpolated the observed data to represent a trend for the whole eruption, for FLIR data, and from the eruption onset to the half of May, for AVHRR. Neglecting the discrepancy between their estimates and the large effusion rates obtained in this work for the first days of the eruption (28 December 2002 to 5 January 2003), the order of magnitude of the two data set is quite in agreement for the whole eruption; however, the general trends do not resemble the different phases we discussed in this work. In *Lodato et al.* [2006], a seven-point running mean on the FLIR data of *Calvari et al.* [2005] was used to obtain an effusion rate trend which shows a general decline through the whole eruption from an initial value of 0.6–0.7 m³/s. Furthermore, they distinguished three declining periods through the eruption, the first starting at the eruption onset and the following after two significant events, namely, the 5 April paroxysm and the early June spattering at hornitos. *Ripepe et al.* [2005] presented an effusion rate trend, through the whole eruption, evaluated from satellite remote-sensing thermal images (MODIS). A peak was measured during the first week of the eruption, then the measured fluxes decreased steadily until 21 June when they dropped below 0.2 m³/s. In particular, the peak phase showed significantly lower values for both the maximum (1.5 versus 13.2 m³/s) and the average (<1.0 versus >5.0 m³/s) values, whereas the declining phase is visually quite similar to that here presented. The results described above suggest that even if the flux rate trend from thermal imagery furnishes precious lava discharge data for monitoring a lava flow eruption, some problems raise if we attempt to extrapolate from them a general trend useful for

Figure 3. Schematic representation of the three-phase eruption evolution value between brackets are effusion rates from Table 3 (VH, very high; H, high; M, medium; L, low; VL, very low).

understanding the phenomenon evolution. First, the rate values do not furnish a volume estimate consistent with that obtained from geometric data from topographic measurements (i.e., DEMs differences). This inconsistency is more relevant for the higher rates. Second, the high scatter of thermal measurements can result in complex interpretations not always confirmed by independent observations including those performed with different thermal sensors. The effusion rate increase on 5 April is not confirmed by either DEM differencing (this work) or MODIS-derived data [Ripepe *et al.*, 2005], whereas that observed at beginning of June is evident in all data sets.

8. CONCLUDING REMARKS

The availability of repeated photogrammetric surveys during the eruption, starting 8 d after the first lava flow outbreak on 28 December 2002, allowed us to monitor the lava flow field evolution until the end of the eruption on 22 July 2003 and to produce a quantitative evaluation of the eruptive activity. The adopted method, based on the joint analysis of numerical photographic–cartographical (Orthophotos) and elevation (DEM) products, obviated the problems of collecting quantitative data (e.g., flow area and thickness) on the field. The adoption of the topographic method [Stevens *et al.*,

1997; Coltelli *et al.*, 2007] that is DEM differencing, to evaluate the lava flow volume, allowed also reducing the associated uncertainties with respect to the planimetric approach, generally adopted. The quantitative reconstruction of the lava flow field temporal evolution and the computation of the total lava volume erupted was performed. The 2002–2003 lava flow Stromboli eruption, lasting 210 d, emplaced on the subaerial slope of the SdF total lava volume of $12.51 \times 10^6 \text{ m}^3$, corresponding to an eruption rate of $0.69 \text{ m}^3/\text{s}$.

We used these data to test a model for explaining the unexpected behavior of the 2002–2003 lava flow eruption that was the first well-documented and regularly surveyed effusive eruption of Stromboli. Since the eruption vents were located less than 300 m in elevation from the volcano's summit vents, we expected a typical summit (terminal) basaltic lava flow eruption characterized by steady outpouring and eruption rates and, hence, a linear increase in cumulative volume. However, the observed effusion rate trend started on 28 December from an initial peak and then declined more slowly, resulting in an exponential decrease of the eruption rate in two steps (30 December 2002 to 18 January 2003 and 18 January to 22 July 2003) and a consequent diminishing growth of cumulative volume. This trend is typical of flank (lateral) eruptions of basaltic volcanoes and can be explained by tapping of an enclosed pressurized system

[Wadge, 1981]. We interpret the observed three phases of the eruption (Figure 3) as a transition from a terminal (open conduit system) to a lateral (pressurized dike system) lava discharge. In the first one, lava outpoured from an initial broken conduit, preceding and probably accelerating the dike intrusion from depth. In the second one, the sudden slope decompression opened the lateral magma intrusion, decreasing the lithostatic load on the shallow dike, and thus accelerating its elastic strain relaxation. Finally, in the third longer phase, elastic strain energy from the subvolcanic reservoir controlled the effusion rate, counterbalancing the lava cooling along the wall and at the apical portion of the dike that tends to close the eruptive fissure, ending the eruption.

Acknowledgments. The data used in this work were collected thanks to the support of the Dipartimento della Protezione Civile (DPC) during the 2002–2003 eruption; the results described were elaborated within the Project V1_2 of the 2002–2004 DPC–Istituto Nazionale di Geofisica e Vulcanologia (INGV) Research Program.

REFERENCES

- Achilli, V., P. Baldi, L. Baratin, C. Bonini, E. Ercolani, S. Gandolfi, M. Anzidei, and F. Riguzzi (1998), Digital photogrammetric survey on the island of Vulcano, *Acta Vulcanol.*, 10, 1–5.
- Baldi, P., S. Bonvalot, P. Briole, and M. Marsella (2000), Digital photogrammetry and kinematic GPS for monitoring volcanic areas, *Geophys. J. Int.*, 142(3), 801–811.
- Baldi P., S. Bonvalot, P. Briole, M. Coltelli, K. Gwinner, M. Marsella, G. Puglisi, and D. Remy (2002), Validation and comparison of different techniques for the derivation of digital elevation models and volcanic monitoring (Vulcano Island, Italy), *Int. J. Remote Sens.*, 22, 4783–4800.
- Baldi, P., M. Fabris, M. Marsella, and R. Monticelli (2005), Monitoring the morphological evolution of the Sciara del Fuoco during the 2002–2003 Stromboli eruption using multi-temporal photogrammetry, *ISPRS J. Photogramm. Remote Sens.*, 59(4), 199–211.
- Baldi P., M. Fabris, M. Marsella, R. Monticelli, and V. Achilli (2006), Application of digital elevation model to volcanology, *Ann. Geophys.*, 49(4/5), 1059–1066.
- Baldi P., M. Coltelli, M. Fabris, M. Marsella, and P. Tommasi (2008), High precision photogrammetry for monitoring the evolution of the NW flank of Stromboli volcano during and after the 2002–2003 eruption, *Bull. Volcanol.*, 70(6), 703–715, doi:10.1007/s00445-007-0162-1.
- Baldi P., A. Bosman, F. L. Chiocci, M. Marsella, C. Romagnoli, and A. Sonnessa, Integrated subaerial–submarine evolution of the Sciara del Fuoco after the 2002 landslide, *this volume*.
- Bruce P. M. and H. E. Huppert (1989), Thermal control of basaltic fissure eruptions, *Nature*, 342, 665–667.
- Calvari, S., M. Coltelli, M. Neri, M. Pompilio, and V. Scrivano (1994), The 1991–1993 Etna eruption: chronology and lava flow-field evolution, *Acta Vulcanol.*, 4, 1–14.
- Calvari, S., L. Spampinato, L. Lodato, A. J. L. Harris, M. R. Patrick, J. Dehn, M. R. Burton, and D. Andronico (2005), Chronology and complex volcanic processes during the 2002–2003 flank eruption at Stromboli volcano (Italy) reconstructed from direct observations and surveys with an handheld thermal camera, *J. Geophys. Res.*, 110, B02201, doi:10.1029/2004JB003129.
- Chiocci, F. L., C. Romagnoli, P. Tommasi, and A. Bosman (2004), The December 2002 submarine landslide at Stromboli volcano: Morphologic and tsunamogenic potential definition, *presented at 32nd International Geological Congress*, Florence, Italy, 20–28 August.
- Chiocci, F. L., C. Romagnoli, P. Tommasi, and A. Bosman (2005), The submarine slide causing the December 2002 tsunami at Stromboli (Tyrrhenian Sea, Italy), *presented at the 2nd Int. Symposium on Submarine Mass Movements and Their Consequences*, Oslo, Norway, 5–7 September.
- Coltell M., C. Proietti, S. Branca, M. Marsella, D. Andronico, and L. Lodato (2007), Analysis of the 2001 lava flow eruption of Mt. Etna from three-dimensional mapping, *J. Geophys. Res.*, 112, f02029, doi:10.1029/2006jf000598.
- Harris A. J. L., J. B. Murray, S. E. Aries, M. A. Davies, L. P. Flynn, M. J. Wooster, R. Wright, and D. A. Rothery (2000), Effusion rate trends at Etna and Krafla and their implications for eruptive mechanisms. *J. Volcanol. Geotherm. Res.*, 102, 237–270.
- Harris A. J., J. Dehn, M. Patrick, S. Calvari, M. Ripepe, and L. Lodato, (2005), Lava effusion rates from hand-held thermal infrared imagery: An example from the June 2003 effusive activity at Stromboli, *Bull. Volcanol.*, 68, 107–117, doi:10.1007/s00445-005-0425-7.
- Heipke, C. (1995), State-of-the-art of digital photogrammetric workstations for topographic applications, *ISPRS J. Photogramm. Remote Sens.*, 61, 49–56.
- Honda, K., and M. Nagai (2002), Real time volcano activity mapping using ground-based digital imagery, *ISPRS J. Photogramm. Remote Sens.*, 57, 159–168.
- Karras, G., and E. Petsa (1993), DEM Matching and detection of deformation in close range photogrammetry without control, *ISPRS J. Photogramm. Remote Sens.*, 59(9), 1419–1424.
- Kraus K. (1998), *Photogrammetry*, vol. 1, Dummler Ed., Germany.
- Landi, P., L. Francalanci, M. Pompilio, M. Rosi, R. A. Corsaro, C. M. Petrone, I. Nardini, and L. Miraglia (2006), The December 2002–July 2003 effusive event at Stromboli volcano, Italy: Insights into the shallow plumbing system by petrochemical studies, *J. Volcanol. Geotherm. Res.*, 155, 263–284.
- Lodato, L., L. Spampinato, A. J. Harris, S. Calvari, J. Dehn, and M. Patrick (2006), The morphology and evolution of the Stromboli 2002–2003 lava flow field: An example of a basaltic flow field emplaced on a steep slope, *Bull. Volcanol.*, 69, 661–679, doi:10.1007/s00445-006-0101.
- Pino N., A. M. Ripepe, and G. B. Cimini (2004), The Stromboli volcano landslides of December 2002: Aseismological description, *Geophys. Res. Lett.*, 31, L02605, doi:10.1029/2003GL018385.
- Stevens, N. F., J. B. Murray, and G. Wadge (1997), The volume and shape of the 1991–1993 lava flow field at Mount Etna, Sicily, *Bull. Volcanol.*, 58, 449–454.

Tommasi P., P. Baldi, F. L. Chiocci, M. Coltelli, M. Marsella, M. Pomilio, and C. Romagnoli (2005), The landslide sequence induced by the 2002 eruption at Stromboli volcano, in *Landslide—Risk analysis and sustainable disaster management*, edited by K. Sassa et al., pp. 251–258, Springer Verlag, Berlin, (ISBN: 3-540-28664-0).

Wadge, G. (1981), The variation of magma discharge during basaltic eruptions, *J. Volcanol. Geotherm. Res.*, 11, 139–168.

S. Branca, M. Coltelli, and C. Proietti, Istituto Nazionale di Geofisica e Vulcanologia, Sezione di Catania, Piazza Roma, 2, 95125 Catania, Italy. (branca@ct.ingv.it; coltelli@ct.ingv.it; proietti@ct.ingv.it)

M. Marsella and R. Monticelli, Dipartimento di Idraulica, Trasporti e Strade, La Sapienza Università di Roma, Roma Via Eudossiana 18, 00184 Rome, Italy. (maria.marsella@uniroma1.it)

Ground Deformations Related to the Effusive Eruptions of Stromboli: The 2002–2003 Case

M. Aloisi, A. Bonforte, M. Mattia, and G. Puglisi

Istituto Nazionale di Geofisica e Vulcanologia, Sezione di Catania, Catania, Italy

Stromboli volcano erupted suddenly on 28 December 2002 after a long period of typically persistent and moderate explosive activity. Lava flows outpoured from the northern wall of the NE crater and descended into the Sciara del Fuoco (SdF). On 30 December 2002, two landslides occurred on the northern part of the SdF, producing a tsunami that caused significant damage. This event led to the upgrading of the ground deformation monitoring system. The new requisite was the real-time detection of the deformation related both to the magma movements within the eruptive feeding system and to potential slope failures of the SdF. To this end, a remotely controlled monitoring system, based both on high-frequency (1-Hz) instantaneous GPS and terrestrial geodetic techniques (manual electronic distance measurements (EDM), transformed in automated terrestrial geodetic measurements) was planned and set up in a few months. During the recorded eruptive phases, the new monitoring system aided the Department of Civil Protection in making decisions related to hazards from landslides and volcanic activity and, more generally, on the evolution of volcanic phenomena throughout the eruption. The measurements carried out on the benchmarks located on the high flank allowed us to make some hypotheses on the dynamics of the craters. In particular, the behavior of the EDM baselines, showing alternating periods of increase and periods of stop in length variation, could be linked to movements of the magmatic column within the craters. Moreover, the monitoring system gave us the opportunity to observe the effects of an effusive vent opening on 16 February. The new geodetic network provided, for the first time, useful information on ground deformations due to shallow and very shallow volcanic sources at Stromboli.

1. INTRODUCTION

The volcanic phenomena occurring on Stromboli in December 2002 prompted the scientific community and the national Department of Civil Protection to implement new systems aimed at detecting and monitoring any movements within the

Sciara del Fuoco (SdF). These systems were primarily to provide information on the instability of the SdF and, furthermore, to monitor the dynamic of the area around the summit craters, for evaluating potential evolutions of the eruption, as is usually done on other active volcanoes. Due to these requirements, a monitoring system based on terrestrial geodetic techniques and a remotely controlled GPS station, with high-frequency (1-Hz) instantaneous positioning capabilities, were planned and set up around the summit craters in about 2 months.

The following chapter presents and discusses the data that this new geodetic monitoring system provided in the first

months of the eruption, i.e., before its complete destruction caused by the 5 April paroxysm. In particular, the chapter is principally devoted to the dynamic of the area around the summit craters, more or less directly linked to the magma movements within the shallow plumbing system of Stromboli.

2. MONITORING SYSTEM DESCRIPTION

Since 1993, Stromboli ground deformations have been monitored by GPS and clinometric techniques. Before the 2002–2003 eruption, the monitoring system on the island focused on measuring the effects of the plumbing system dynamic at medium-shallow depths (1–2 km below sea level) without the real-time detection requirement. To this end, four permanent GPS and three tiltmeter stations were set up between 1993 and 1997 at a lower altitude (50–150 m) around the island's perimeter (green points in Plate 1).

After the 30 December 2002 landslide, it became evident that the most urgent requirement of the monitoring system was to detect real-time deformations related to potential slope failures of the SdF. A new monitoring system, based on the integration of different measurement techniques (EDM, clinometric, and GPS), was planned and set up during the first two months of 2003 [Puglisi *et al.*, 2005]. Twenty-two EDM control points were installed within the Sciara, and three pillars were set up for the measurement instruments (Plate 1). Moreover, a permanent GPS network, specifically designed for the real-time monitoring of movement at the core of the potential failure zone and close to the summit craters, was built within the SdF (Plate 1). Finally, a robotized total station was installed to automate the terrestrial geodetic measurement along the northern sector of the SdF [Puglisi *et al.*, 2005].

The EDM was the first technique adopted to evaluate hazard evolution in the SdF during the initial days of the volcanic crisis. It was composed of four subnetworks. The first one (named “Fossa” in the following) was installed on the summit area of the volcano named Fossa area, the part of crater terrace included between the PSF and the craters. This subnetwork (Plate 1) consisted of five reflectors (named FOS1–FOS5) that were installed along a profile crossing several fractures and fumaroles on the ground. These control points were surveyed from the iron pillar set up at PSF (STR in Plate 1). The second subnetwork (named “Reference” in the following), composed of four reflectors (BAST, SLF, FORT, and VANC), was installed on the upper part of the volcano outside and around the SdF area, on sites located outside or along the rim of the Upper Vancori sector collapse [Tibaldi, 2001], thus considered stable with respect to the recent movements of the SdF (i.e., younger than 13 ka). This second one allowed us to check the actual stability of

these areas and verify the repeatability of the distance measurements carried out from the STR pillar, in order to detect systematic errors due, for example, to atmospheric effects. A third monitoring subnetwork (named “Bastimento” in the following) was installed below the Bastimento. This subnetwork consisted of six control points (from PST1 to PST6), placed in the area of the niche of the 30 December landslide (Plate 1). In particular, the first two (PST1 and PST2) were installed above the NE-trending eruptive fissure, which originated the first lava flows on 28–30 December, while the other four were distributed downslope from the fissure, on the lava flows produced in December. These benchmarks were measured from the STR pillar and two of them (PST4 and PST6) were equipped with two reflectors, in order to be measured also from another pillar, located on the lower flank of the volcano, at Punta Labronzo (PLB). This pillar was set up with the aim of enabling monitoring on the lower part of the SdF area, not visible from the STR pillar (the network of the benchmarks installed in the medium lower part of the SdF, measured from the PLB pillar, and the relevant data are discussed in Section 3.1). Throughout the EDM monitoring activities, angular measurements were sometimes carried out from the pillars by using a theodolite, in order to evaluate the three-dimensional (3-D) movements of the benchmarks.

After the events of 30 December, the Istituto Nazionale di Geofisica e Vulcanologia section of Catania, in conjunction with the national Department of Civil Protection, decided to set up a new GPS network (named “SciaraDat”), aimed at the real-time monitoring of displacements in the highest part of the SdF, under the realistic hypothesis that any future flank collapse would be preceded by initial deformations in these areas [Mattia *et al.*, 2004; Puglisi *et al.*, 2005]. SciaraDat consisted of four stations (SCRA, SDIC, SSBA, and SVIN; Plate 1). The stations were placed on the upper SdF slope and around the summit craters by using helicopters in order to work safely [Puglisi *et al.*, 2005]. The traditional approach based on the postprocessing of 24 h/d of GPS measurements, sampled every 30 s, was not able to give fast enough responses for early warning to the population of large regions of southern Italy, potentially affected by a large scale tsunami [Tinti *et al.*, 1999]. To provide data at suitable frequency, we adopted the CRNet software [Leica and Geodetics Inc., 2002], which applies the LAMBDA (Least squares AMBiguity DecorrelAtion technique [Teunissen, 1993]) method for the fast resolution of the phase ambiguities. The software is able to resolve the problem using the so-called epoch-by-epoch [Bock *et al.*, 2000] algorithm. Each time a single epoch of GPS data is collected, this algorithm produces a 3-D position of the remote stations, with respect to a “master” whose coordinates are assumed fixed (SVIN in our case). The levels of accuracy in positioning are in the

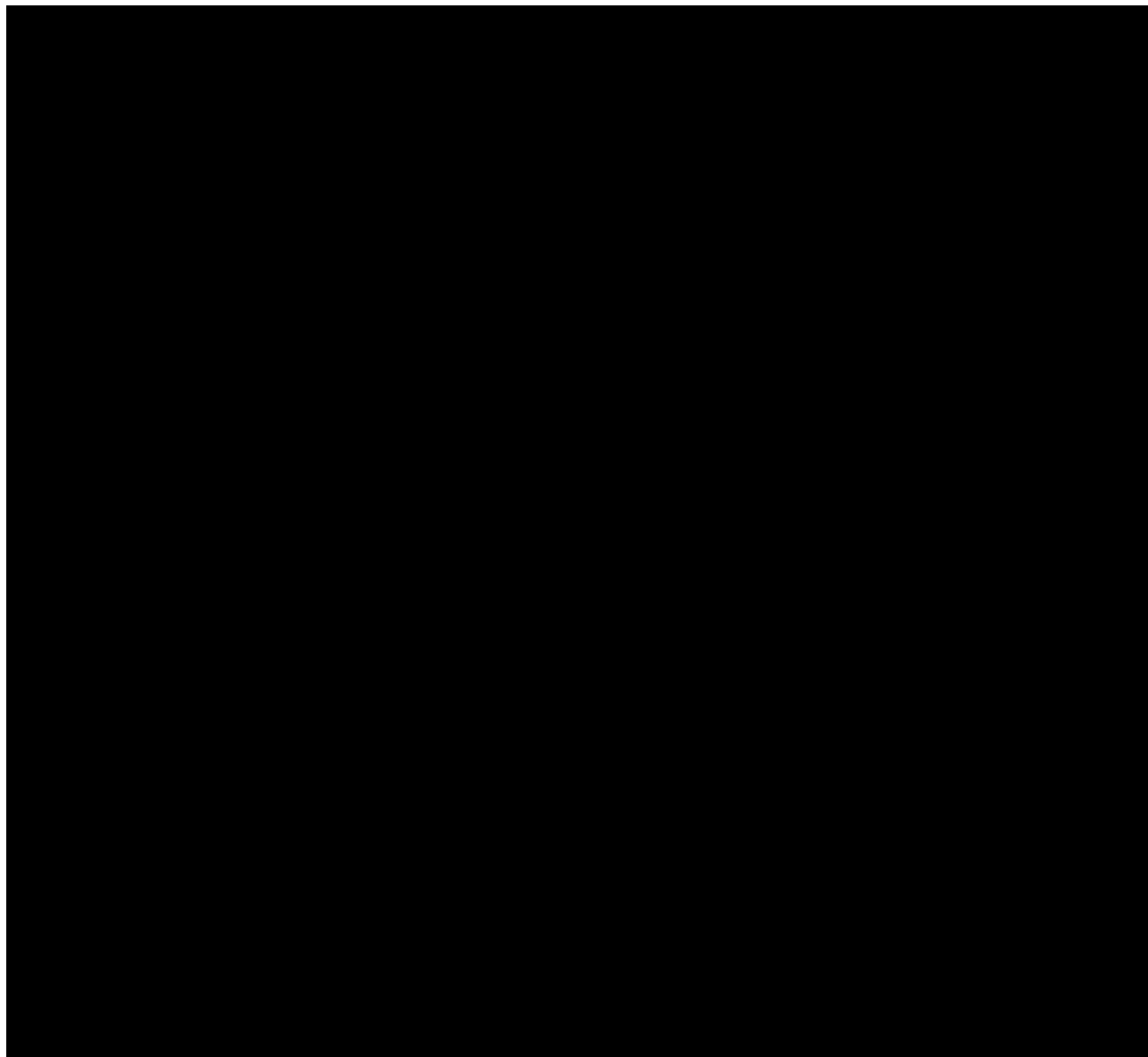


Plate 1. Ground deformation monitoring system after the 2002–2003 eruption onset. The map also shows the main volcanic features formed during the first two days of the 2002 eruption: the fracture opened on the northern flank of the NE crater (white line), the outpoured lava flows (black area), and the slid area (gray area). Inset, geographical setting of Stromboli volcano.

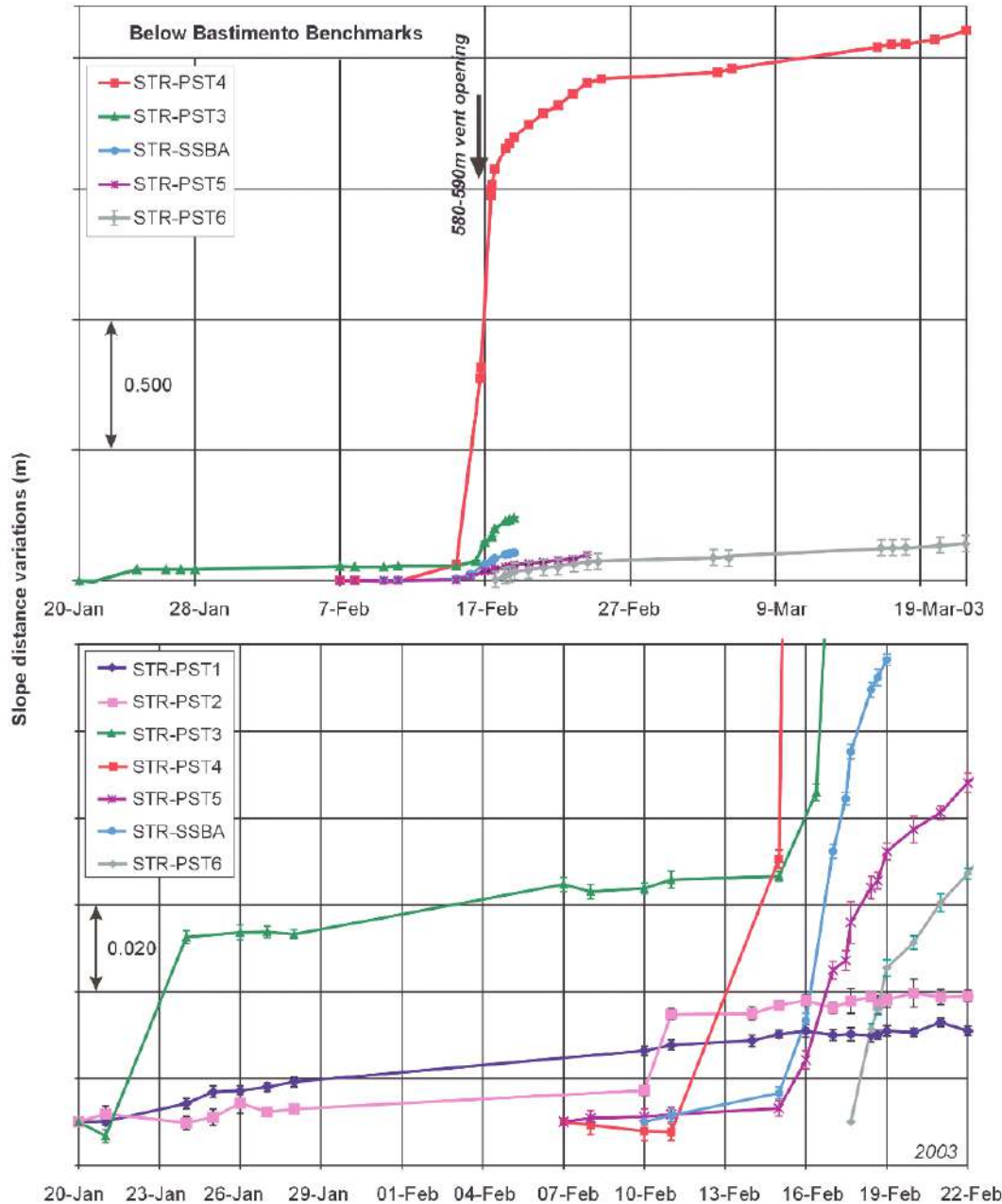


Plate 2. EDM data collected from STR pillar, related to the subnetwork, installed below the Bastimento. The data are shown in the top and bottom at different scale.

order of 1–2 cm in planimetry and 2–6 cm in altimetry, as demonstrated with internal tests performed on a selected baseline on Mount Etna during August 2002 [Mattia and Rossi, 2004]. We adopted 1 Hz as the sample frequency for SciaraDat. Usually, three kinds of result were produced for each remote station: the 1-Hz position, the median of 10-min of data positions and the median of 1 day of data positions.

One of the aims of this network was to trigger an alarm when significant deformation phenomena are observed on the GPS data. To achieve this, some useful statistics were introduced. CRNet multiepoch statistics are based on two robust estimators, the median and the interquartile range (IQR), which are less sensitive to data outliers than the traditional mean and standard deviation. When a data sample is drawn from a normal distribution, its mean very nearly equals its median and its standard deviation equals about three quarters of the IQR. For intervals longer than a single epoch, the position coordinates are determined as the median value of all single-epoch positions within the interval, excluding position coordinate outliers that are defined on an appropriate multiple of the IQR. Although the 1-Hz data are very precise, multipath effects and local transient radio signals can degrade the level of precision. For this reason, the alarm was set up using the median of a 10-min data set, with the threshold alarm at 0.1 m on planimetry and 0.2 m in altimetry.

3. DATA DISCUSSION

Data collected from this complex monitoring system allowed us to effectively monitor the deformations related both to the downslide movements of the SdF and to the evolution of the volcanic activity. In Section 3.1, we briefly discuss some significant aspects of the dynamics of the shallow plumbing system of the volcano, throughout the period of the lava effusion, while in Section 3.2, the geodetic data relevant to the stability of the SdF are discussed together with those provided by GBInSAR [Bonforte et al., 2008]. For simplicity, we can group the discussion by areas since there were specific events to be investigated in each of these.

3.1. Area Below Bastimento

The geodetic monitoring system enabled us to observe the effects of the migration of effusive activity from about 500 m of elevation to a new vent at 580–590 m of elevation, below Bastimento, occurring between 15 and 17 February [Marsella et al., 2008]. This phenomenon produced a deformation field, whose evolution was monitored both by GPS and EDM systems. From 15 February, several distances measured both from the STR and PLB pillars showed

significant variations with respect to the previous days, on benchmarks located below the Bastimento area (Plate 2). PST2 anticipated the deformation, showing a lengthening on 11 February. The climax of this phenomenon was on 16 February, just after the opening of the vent at 580–590 m of elevation that fed the lava flows until the end of the eruption, in July. After the vent opening, the SSBA GPS station, just installed, measured a significant NW displacement (Figure 1). The integration between the 3-D movement detected by the GPS station and the displacements relevant to dense distribution of the reflectors installed below the Bastimento, measured from PLB pillar (Figure 2), enabled us to characterize the spatial and temporal evolution of this phenomenon. Only benchmark PST4 recorded a very high ground deformation (about 80 cm between 15 and 16 February), while the other benchmarks close to PST4 (within a radius in the order of one hundred of meters) recorded smaller movements by two orders of magnitude (Figure 2). The abrupt spatial decay of the deformation and the stability of the reference points on the summit area, as well as the absence of movements at the GPS permanent network at the foot of the volcano, confirmed that this phenomenon was local and did not affect either the entire volcano or the whole unstable flank. This sustained the hypothesis of a very shallow migration of magma toward the new active vent that opened on 16 February, at 580–590 m elevation. All these data were provided in real time to the scientists involved in

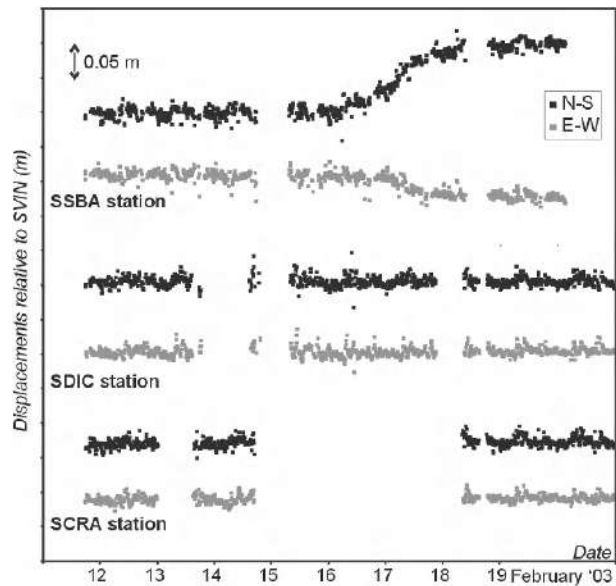


Figure 1. Ten-minute average values of 1-Hz displacement time series of the three GPS stations station from the start of operation on 11 February until the destruction of SSBA station caused by the lava on 20 February.

Figure 2. Three-dimensional vector deduced by EDM and theodolite measurements at PST4, from 13 to 19 February. To show the abrupt decay of the deformation, we reported a table with the modules and the vertical variations of many points located near PST4.

monitoring activities. This capability, the appropriate dense network configurations and the integration between information provided by different techniques, enabled giving accurate and timely information to the Department of Civil Protection, avoiding raising a false alarm of the potential major failure of the SdF flank. A few days after the beginning of the deformation episode, a new vent opened and the lava flow emitted by this vent destroyed the SSBA station on 20 February 2003. The activity of the vent at 580–590 m destroyed many reflectors installed below the Bastimento and on the SdF slope. However, there was no flank failure. A simple elastic source model for this episode was not feasible because of its very limited spatial extent and lack of data in the far field where the elastic conditions are satisfied.

On the basis of the results of the above analysis, we think that a similar ground deformation pattern evolution, even if with smaller magnitude, also occurred during the opening of the 670-m vents (Figure 2), in the January–February pe-

riod [Calvari *et al.*, 2005]. From 20 January to 7 February, only three benchmarks were measured in the Bastimento area (Plate 2), two of these (PST1 and PST2) located uphill from the eruptive fissure formed during the first days of the eruption, thus in a relatively stable area (Figure 2). The third benchmark (PST3) recorded an abrupt and permanent deformation between 21 and 24 January (Plate 2), of about 4 cm, which was confirmed by the subsequent measurements until 28 January. We think that this deformation was related to the opening of the 670-m vent on 23 January [Calvari *et al.*, 2005]. The next measurement, on 7 February, recorded another deformation of about 1.5 cm, which probably was due to the repeated opening of the 670-m vent on 28, 29, 30, and 31 January and on 1, 2, and 3 February [Calvari *et al.*, 2005]. However, only the measurements on the PST3 benchmark were suitable for this period in this area, preventing any further analysis on the spatial evolution of the deformation pattern as above performed for the 15–17 February event.

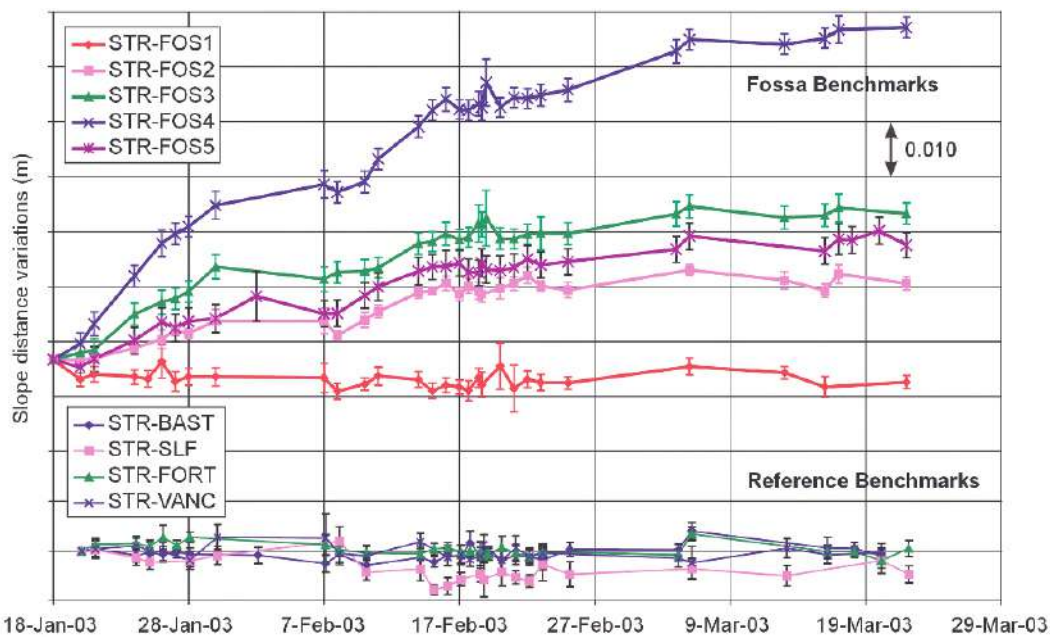


Plate 3. EDM data collected from STR pillar, related to the Reference and Fossa subnetworks.

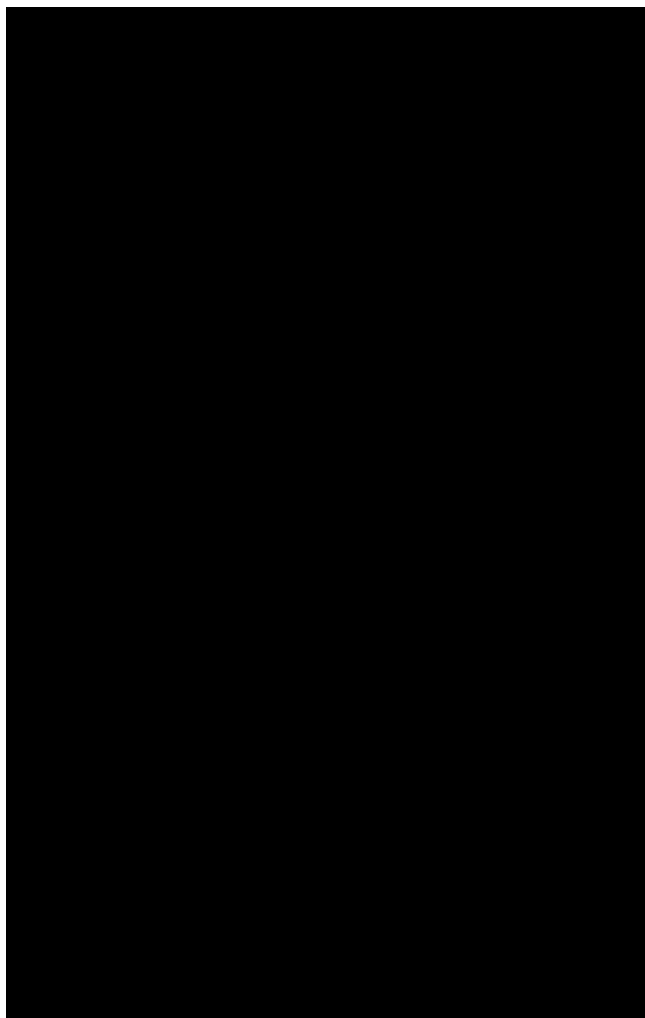


Plate 4. Scheme of the interpretation of the phenomena originating the variations in the EDM measurements collected by the Fossa subnetwork. (a) During the first phase (corresponding to the period of no-lengthening of distances), the landslide in the SdF is stable and the passive fingering is not fed, thus the level in the conduit of the craters remains stable. (b) During the second phase (corresponding to the lengthening of distances), the movement of the landslide induces the feeding of the passive fingering, producing a lowering of the magma level within the conduits.

3.2. Fossa and Summit Area

Two questions arose during the first days of the eruption, both concerning the stability of critical parts of the volcano: the summit craters and the SdF. It is obvious, indeed, that if either the summit craters or the SdF should collapse, the risk would dramatically increase not only for the Stromboli island but also for the Aeolian Archipelago and south Italy as a whole.

The EDM measurement carried out on the two subnetworks Fossa and Bastimento, together with the data provided by the SciaraDat network, allowed us to investigate the dynamics of these areas and provide information about the evolution of the volcanic risk during the first week of the eruption.

Since the first measurements collected from the STR pillar, the reference subnetwork installed around the summit area of the Stromboli confirmed that the Pizzo area, as well as the upper part of the rim of the SdF (from Bastimento to SLF station), was stable. In fact, the EDM measurement did not record any significant deformation of the reference subnetwork (Plate 3). This was the first significant result of the monitoring geodetic activities, which excluded the possibility of a sector collapse involving the Pizzo area that might produce a large phreatomagmatic explosion and a giant tsunami. The hypothesis of the sector collapse was based on previous studies of the evolution of SdF [Tibaldi, 2001], which showed that this phenomenon occurred a few times, through the evolution of the volcano, alternating with growth phases (the Vancori Collapse, ~13 ka according to Tibaldi [2001]). According to Tibaldi [2001], “the younger sliding planes tended to become more superficial and to decrease the areal extent” involving the low-middle sector of the SdF. Our observations concur with this scheme of the evolution of the SdF and suggest that its current dynamic was not evolving toward catastrophic events, which might involve a sector collapse.

The increase in the distances between the STR pillar and the benchmarks of La Fossa area (Plate 3) allowed making some hypotheses on the dynamic of the craters. The deformation pattern was characterized by a period of a quasi-linear distance increase at the beginning, followed by a pause, and then a second phase of deformation starting after 7 February. This peculiar behavior could be linked either to the sliding toward the sea of the summit craters and SdF, altogether, or to the movements of the magmatic column within the craters. In order to discriminate between these two possible origins of the observed movements, we may consider the measurement performed at the two GPS stations, SDIC and SCRA (Figure 1). The absence of significant movements at these stations, during their working period, suggests exclud-

ing the sliding phenomena of the summit craters, at least with velocities and pattern comparable to those measured by the EDM Fossa subnetwork ranging from 1 to 5 cm/month. Thus, the movement measured by the EDM network should be related to a local phenomenon, probably due to the movement of the magmatic column within the conduits.

It is noteworthy that the principal increases of the distance between the crater flanks and the STR pillar occurred during two main periods: from the beginning (18 January) until 30 January and from 7 to 16 February, approximately. These periods correspond to the rising of the vents from 500 m up to about 580–590 m or 670 m of elevation [Calvari et al., 2005; Marsella et al., 2008]. Thus, it is reasonable to assume that the increase in the distance was related to vent migration, which in turn was related to the variation of magmatic column within the shallow plumbing system. In this view, the vents “represented the passive fingering of magma from the central conduit and NE fissure” [Calvari et al., 2005].

Above, we showed how the ground deformations pattern related to the second of these periods was characterized by a high areal gradient measured by both EDM and GPS networks, suggesting that its origin was very local and shallow. Unfortunately, during the first of these periods, the geodetic monitoring system installed below Bastimento area was incomplete because only the PST1, PST2, and PST3 EDM benchmarks were installed. However, it is noteworthy that the PST3 distance jumped on 24 January, with respect to the measurement carried out on 21 January (Plate 2).

The data discussed until now highlight that the movements measured during the first months of the eruption at the benchmarks located both at “La Fossa” and “below Bastimento” areas are temporally associated to the development of the “temporary” vents on the SdF, observed from about 500 m up to about 600 m [Calvari et al., 2005; Marsella et al., 2008]. Considering that both these vents and the benchmarks are located within the α slide [Tommasi et al., 2008], it seems reasonable to assume that the movement of the α slide is at the origin of both the EDM movements and the vent formation. The mechanism we assume is that irregular movements of portions of the α slide induced the infiltration of magma within the body of the slide, from the central conduit (Plate 4b); these infiltrations were forming the new “temporary” vents, which remained active for a few hours or days, i.e., until the magma could flow through the body of the slide, before its cooling. Consequently, this passive fingering produced a lowering of the magma column top. So, we were able to deduce that the increase in the distances should be related to the lowering of the top of the magma column within the conduits (Plate 4b) for feeding the vent in the SdF (580–590 m, or 670 m in our case) and to

the consequent lowering of the SE rim of the craters area (Plate 4b).

Conversely, the periods of stopping in length variation could be linked to a stasis of the magmatic column within the craters, during the magma emission from the 500-m elevation vent (Plate 4a).

Although this hypothesis needs more investigation to understand the role of the fractures existing between STR and the craters in the Fossa area and to explain the absence of significant movements at the SCRA station, it is noteworthy that similar phenomena, even with larger morphological evidences, occurred during the first days of the 2007 eruption. The Fossa area, indeed, completely collapsed within the craters, while the seaward flank of the craters remained relatively stable and the collapse evolved along a ring-shaped fracture system very similar to that observed during 2002–2003 eruption.

4. CONCLUSIONS

The geodetic monitoring of the Stromboli volcano enabled us to collect important data on the dynamic of the eruption. In particular, we were able to investigate the opening of eruptive vents on 16 February and elaborate a model of magmatic column movements within the shallow plumbing system of the craters during the first month of the eruption.

We explained the EDM baselines lengthening on the Fossa area as the result of the movements of the magmatic column within the craters, when new vents in the SdF were forming. Thus, the pauses we measured in the increase in the distances between the STR pillar and the benchmarks of La Fossa area were related to a stasis of the magmatic column within the craters.

Moreover, the local effects of an effusive vent opening on 16 February were observed. During this phenomenon, the very high ground deformation recorded only locally and the abrupt spatial decay of the deformation around the benchmark where the maximum of deformation was measured, as well as the stability of the points on the summit area and at the foot of the volcano, meant excluding the possibility of an imminent flank failure and contributed to the decision to avoid declaring a state of emergency. A deep deformation source, which could trigger a new landslide, indeed, should produce a wider ground deformation field than the one actually measured. Furthermore, the opening of the vents from about 500 m up to about 600 m of elevation during the January–February period possibly produced a similar ground deformation pattern, even with smaller magnitude, which was not investigated due to the suitability of only one benchmark in this area during this period.

All this information certainly represents a valuable data set for future research to understand how the plumbing system of this volcano works, especially during eruptive events. The twofold aspect (eruption and landslide) of the Stromboli volcanic crisis emphasized the role of geodetic monitoring activities on active volcanoes. The strategy adopted at Stromboli was to implement many different types of real-time or near real-time survey techniques, taking cost-effective and logistic constraints into account.

Our experience underlines that the current development of surveying techniques allow performing a detailed real-time monitoring of ground deformations, in a very wide spectrum of operational conditions. The achievable accuracies in 3-D positioning are suitable for scientific and early warning purposes. These positive results then suggest that Stromboli monitoring system will be a useful tool to identify movements for forecasting large future landslides that could occur on the SdF.

REFERENCES

- Bock, Y., R. Nokolaidis, P. de Jong, and M. Bevis (2000), Instantaneous geodetic positioning at medium distances with the Global Positioning System, *J. Geophys. Res.*, **105**(B12), 28,223–28,253.
- Bonforte, A., M. Aloisi, G. Antonello, N. Casagli, J. Fortuny-Guash, L. Guerri, G. Nunnari, G. Puglisi, A. Spata, and A. Tarchi (2008), Movements of the Sciara del Fuoco, this volume.
- Calvari, S., L. Spampinato, L. Lodato, A. J. L. Harris, M. R. Patrick, J. Dehn, M. R. Burton, and D. Andronico (2005), Chronology and complex volcanic processes during the 2002–2003 flank eruption at Stromboli volcano (Italy) reconstructed from direct observations and surveys with a handheld thermal camera, *J. Geophys. Res.*, **110**, B02201, doi:10.1029/2004JB003129.
- Leica and Geodetics Inc. (2002), *Software CRNet User Manual*, Leica and Geodetics Inc., San Diego, Calif.
- Marsella, M., M. Coltelli, S. Branca, C. Proietti, and R. Monticelli (2008), 2002–2003 Lava flow eruption of Stromboli: Contribution to understanding lava discharge mechanism using period digital photogrammetry surveys, this volume.
- Mattia, M., and M. Rossi (2004), Sperimentazione di un sistema di monitoraggio vulcanico per mezzo di tecniche GPS in tempo reale, *INGV-CT Internal Report*, INGV-CT, Catania.
- Mattia, M., M. Rossi, F. Guglielmino, M. Aloisi, and Y. Bock (2004), The shallow plumbing system of Stromboli Island as imaged from 1 Hz instantaneous GPS positions, *Geophys. Res. Lett.*, **31**, L24610, doi:10.1029/2004GL021281.
- Puglisi, G., A. Bonaccorso, M. Mattia, M. Aloisi, A. Bonforte, O. Campisi, M. Cantarero, G. Falzone, G. Puglisi, and M. Rossi (2005), New integrated geodetic monitoring system at Stromboli volcano (Italy), *Eng. Geol.*, **79**(1–2), 13–31, doi:10.1016/j.enggeo.2004.10.013 (Correction, *Eng. Geol.*, **82**(2) 136, doi:10.1016/j.enggeo.2005.10.002, 2005.)

- Teunissen, P. J. G. (1993), Least-squares estimation of the integer GPS ambiguities, *LGR Series 6*, Delft Geodetic Computing Centre, Delft, Netherlands.
- Tibaldi, A. (2001), Multiple sector collapses at Stromboli volcano, Italy: How they work, *Bull. Volcanol.*, *63*, 112–125, doi:10.1007/s004450100129.
- Tinti, S., E. Bortolucci, and C. Romagnoli (1999), Computer simulations of tsunamis due to flank collapse at Stromboli, Italy, *J. Volcanol. Geotherm. Res.*, *96*, 103–128.
- Tommasi, P., A. Bosman, P. Baldi, F. L. Chiocci, M. Coltellini, M. Marsella, and C. Romagnoli (2008), Morphological evolution of the Sciara del Fuoco, this volume.

M. Aloisi, A. Bonforte, M. Mattia, and G. Puglisi, Istituto Nazionale di Geofisica e Vulcanologia, Sezione di Catania, Piazza Roma 2, Catania 95123, Italy. (aloisi@ct.ingv.it)

Gas Flux Rate and Migration of the Magma Column

Emanuele Marchetti, Maurizio Ripepe, and Giacomo Olivieri

Dipartimento di Scienze della Terra, Università di Firenze, Firenze, Italy

Michael R. Burton, Tommaso Caltabiano, and Giuseppe Salerno

Istituto Nazionale di Geofisica e Vulcanologia, Sezione di Catania, Catania, Italy

The 2002–2003 effusive eruption of Stromboli volcano represents an excellent opportunity to investigate the transition from effusive to explosive activity at an open-conduit basaltic system, when activity migrated from effusive vents, at the base of the craters, to summit explosions. The transition is investigated here through the analysis of very long period seismicity, delay times between infrasonic and thermal onsets of explosions, and SO₂ flux recorded during a 1-year period. The synergy of the multiple geophysical observations points to a magma-driven migration of the magma column. Here the increased magma supply at the eruption onset lead to opening of effusive fissures, which draining the magma in the shallow conduit caused the decrease of the magma level. The decrease of the magma supply at the end of the effusion lead to sealing of effusive fissures, upraise of the magma level within the conduit, and reestablishment of explosive activity from the summit vents.

1. INTRODUCTION

Basaltic explosive activity is directly related to the presence of dissolved gas within the magma, unless gas is lost before eruptions [Parfitt, 2004]. Two distinct models have been proposed to explain the different explosive styles observed on basaltic volcanoes. The rise speed-dependent model [Wilson, 1980] implies a two-phase flow of melt and exsolved gas within the conduit and predicts varying explosive styles for varying rise rates of magma and gas. The collapsing foam model [e.g., Jaupart and Vergniolle, 1989] infers a separate flow of gas within the magma and explains the different explosive styles in terms of different gas fluxes and conduit geometry. Despite the model, the primary role

of gas flux is commonly accepted, but its dynamism within the magma column has to be further investigated, by means of geophysical observations, to better constrain the two-phase flow dynamics driving volcanic activity.

Thanks to its persistent activity and easy access to the summit craters, Stromboli has greatly contributed to the understanding of the magma–gas interactions driving volcanic explosions and to promote new research directions in volcanology. In particular, the broadband seismology [e.g., Neuberg *et al.*, 1994; Dreier *et al.*, 1994; Chouet *et al.*, 1999], infrasound acoustics [Braun and Ripepe, 1993; Vergniolle and Brandeis, 1994; Buckingham and Garcés, 1996], and ground-based IR thermometry [Ripepe *et al.*, 2002] have been applied and/or developed here in the last decade. However, the 2002–2003 eruptive crisis has produced such an abundant set of data to still offer excellent opportunities to further discuss some of the main aspects of the magma–gas dynamics in basaltic systems. Here the dense monitoring network installed during the first months of the eruption, in

The Stromboli Volcano: An Integrated Study of the 2002–2003 Eruption
Geophysical Monograph Series 182

Copyright 2008 by the American Geophysical Union.

10.1029/182GM21

response to increased level of alert produced by the flank instability and tsunami, provided a detailed geophysical and geochemical description [e.g., *Bonaccorso et al.*, 2003; *Brusca et al.*, 2004; *Burton et al.*, 2004; *Ripepe et al.*, 2004; *Capasso et al.*, 2005; *Puglisi et al.*, 2005] of this effusive activity interrupting the persistent explosivity of the volcano.

Thermal analysis based on the combination of data provided by ground- and satellite-based IR thermal imageries and the integration of multiple geophysical parameters allowed to track the end of the effusive eruption at the end of July 2003 [*Ripepe et al.*, 2005]. They defined the transition between the end of June and the end of July 2003, when the lava effusion dropped rapidly to less than $0.1 \text{ m}^3/\text{s}$ and a weak explosive activity from the summit vents was newly observed [*Ripepe et al.*, 2005]. In this study, we focus on the geophysical and geochemical changes produced during the 2003 eruption with the aim of underlining its transition from the effusive to explosive activity.

2. DATA ACQUISITION

The volcanic activity at Stromboli is currently monitored by a dense geophysical network developed during the last eruptive crises of 2002–2003 and 2007. This network is based on broadband seismology [*Ripepe et al.*, 2004; *Auger et al.*, 2006], infrasound acoustics [*Ripepe et al.*, 2007], IR thermometry [*Ripepe et al.*, 2004; *Calvari et al.*, 2005], ground deformation [*Puglisi et al.*, 2005], and geochemistry [*Brusca et al.*, 2004; *Burton et al.*, 2004; *Capasso et al.*, 2005; *Cigolini et al.*, 2005]. All geophysical data are radio-transmitted to the recording center (COA) of the Italian Civil Protection in the village of Stromboli, where data are collected and processed in real time.

In this study, we focus on seismic, infrasonic, and thermal data collected by two permanent stations deployed on the summit of Stromboli volcano (Figure 1). These stations consist of five-channel 16-bit acquisition systems, operating at 18.5 ms sampling rate, equipped with Guralp CMG-40T broadband seismometers with eigenperiod of 30 s and sensitivity of $800 \text{ V/m}^{-1} \text{ s}^{-1}$, preamplified Monacor condenser microphones with sensitivity of 46 mV/Pa in the frequency range 3–20 Hz as infrasonic sensors and Omega OS series IR thermometers with 15° field of view (FOV) targeting the summit vents.

During the 2002–2003 eruption, SO_2 flux was measured almost everyday by helicopter- and boat-based correlation spectrometer (COSPEC) and mini-differential optical absorption spectroscopy (DOAS) spectrometer [*Salerno et al.*, 2004]. Since the end of 2003, a network of scanning ultraviolet spectrometers has allowed automatic measurement of SO_2 flux from the volcano [*Burton et al.*, 2004].

3. VERY LONG PERIOD EVENTS AND GAS FLUX DURING THE ERUPTION

The typical explosive activity from the summit craters at Stromboli is associated with long-lasting ($\sim 10\text{--}20$ s) emergent seismic transients rich in a very long period (VLP) component (>3 s) [e.g., *Chouet et al.*, this volume]. Seismological investigations [e.g., *Chouet et al.*, 2003] and laboratory experiments [e.g., *Ripepe et al.*, 2001; *James et al.*, 2004; 2006] suggest that VLP seismic transients may be produced by the rapid expansion of a large gas volume, acting, as inferred from source location of VLP events [e.g., *Chouet et al.*, 2003], at shallow depth within the conduit. The gas expansion might result from shallow gas coalescence and expansion [e.g., *Ripepe et al.*, 2001] or from expansion of a gas slug formed at greater depth (~ 3000 m) and rising through the shallow conduit system [*Burton et al.*, 2007b]. Despite the model, the VLP events are the evidence of an active gas dynamics as the source process of Strombolian explosions.

The VLP seismic events show during the eruption an oscillatory pattern around a mean value of 13 events per hour (eph; Figure 2); their rate has been larger at the beginning

Figure 1. Map of Stromboli volcano showing the position of the seismic-acoustic-thermal stations (STR and ROC) whose data are presented in this work. Station ROC is deployed on the NE flank of the volcano, at an elevation of ~ 750 m above sea level (asl) and at a distance of ~ 450 m from the summit crater. Being line of sight to the summit craters, the station is equipped with a 15° field-of-view IR thermometer, targeting the summit craters. Station STR is deployed at an elevation of ~ 800 m asl and at a distance of ~ 400 m from the summit vent. Data are radio-transmitted to the recording center (COA) of the Department of Italian Civil Protection in the village of Stromboli. The two stations are part of the integrated geophysical monitoring network operated by the Department of Earth Sciences, University of Firenze. The gray area corresponds roughly to the lava flow.

of 2003, during the effusive phase, and then decreased with the reestablishment of the explosive activity from the summit vents (Figure 2a). The mean rate of VLP seismicity for the effusive (15.3 eph) and explosive (11.4 eph) phases are evaluated from the slope of the cumulative number of VLP

events which shows a clear change before and after 21 July 2003 (Figure 2c). The latter mean value is close to the rate of VLP (~ 11 eph) calculated from August 2003 to December 2007 and might be considered as the typical value of the VLP seismicity rate for Stromboli during the last 4 years.

Figure 2. (a) Daily number (gray diamonds) of VLP seismic events recorded at Stromboli in 2003. The number of VLP events has been evaluated from seismic data recorded at Station STR. The vertical dashed line corresponds to the end of the eruption (21 July 2003) defined by *Ripepe et al.* [2005] and is repeated in the following figures for better comparison. (b) COSPEC measurements of SO_2 fluxes at Stromboli volcano during 2003. Error bars reflect the standard deviation between the single transverse measurements carried on during each survey and the mean value (gray points). (c) Cumulative curves of VLP events and of SO_2 flux in 2003 (gray lines). Their slope, evaluated from linear fitting (dashed black lines), allows identification of mean VLP number and mean SO_2 fluxes during the effusive and explosive phases.

The number of VLP events decreased in July 2003, between the effusive and explosive phases, and is marking the clear change in slope of the cumulative distribution of the number of VLP events. This indicates that during the effusive phase, when no explosive activity was observed at the summit craters, the VLP source process did not cease, but was rather acting at a rate ~25% larger than its typical value. The persistency of VLP events suggests that the same preeruptive source process was still active within the system also during the effusive eruption.

The SO₂ flux at Stromboli volcano was measured almost everyday between 23 January and 11 November 2003, providing a 65% coverage for the eruptive time interval. The daily SO₂ flux value was determined by averaging up to nine transverse COSPEC measurements (mean = 4.2, standard deviation = 1.5) of the volcanic plume, collected during one or two daily surveys carried out using a helicopter or a boat, depending on weather and sea conditions.

The variations in the SO₂ rates appeared to cover a large range (mean = 510 t/d, standard deviation = 197 t/d) with values spanning between 168 t/d (standard deviation = 69 t/d) on 28 October and 1573 t/d (standard deviation = 484 t/d) on 22 February 2003 (Figure 2b). From the raw data set, four main phases are visible in the SO₂ flux distribution (Figure 2b). From January to March, the SO₂ flux was highly variable around an average of ~500 t/d and increased during March to April up to ~700 t/d. From April to July, SO₂ flux showed variable values with rather flat trend with an average of ~500 t/d and eventually dropped to an average of ~300 t/d after the eruption. As for the number of VLP events, the long-term SO₂ flux can also be represented in terms of cumulative distribution. This way of representing the measured flux better evidences a clear trend of large SO₂ emission during the effusive phase, followed by a sharp decrease with the reestablishment of explosive activity. From the slope of the cumulative flux (Figure 2c), we can derive that the mean SO₂ flux was of ~450 t/d between January and July 2003, during the effusive phase, and decreased to ~260 t/d after July 2003 at the end of the eruption.

The SO₂ flux and the number of VLP events appear to follow a similar trend for most of the observation period (February–November 2003), suggesting a direct link between these two parameters. They are, in fact, both characterized by a clear change of 30%–40% in the slope of their cumulative distribution after 21 July 2003, when the effusive eruption ended, and the summit explosive activity started again. These empirical observations during the 2002–2003 eruption indicate that the gas process controlling the rate of the VLP seismicity is directly related to the SO₂ supply rate (Figure 2c), where a higher gas flux rate leads to an increase of the rate of the VLP seismicity.

4. MAGMA SUPPLY RATE, LAVA EFFUSION, AND SO₂ FLUX

Magma supply rate can be determined in two ways, one assuming complete degassing of sulfur from magma and the second assuming that all the supplied magma is erupted by measuring the lava effusion rate. Estimates for the lava effusion rate during the 2002–2003 eruption are reported by Landi *et al.* [2006]. Lava effusion progressively decreased between 31 December 2002 and 15 February 2003 from 6.4 m³/s (measured in early January) to 0.25 m³/s at the beginning of February. After 15 and 16 February, the effusion rate slightly increased (0.7 m³/s), and the lava flowing along the eastern border of the Sciara del Fuoco (SdF) reached the shoreline on the early days of March. From this date, the progressive decline (0.4 m³/s) resulted in the formation of shorter lava tongues, and then the effusion rate slowly decreased to 0.1 m³/s in July, before stopping completely on 22 July [Landi *et al.*, 2006].

The SO₂ flux measurements after the 2003 eruption indicate that its rate during the normal stage of the explosive Strombolian activity varies between 100 and 200 t/d [Burton *et al.*, 2007a]. Assuming a complete degassing of the magma, this SO₂ flux is consistent with a magma supply rate of 0.1–0.2 m³/s [see Allard *et al.*, 1994; Burton *et al.*, 2007a]. During the eruption, the four main phases of SO₂ flux can be converted in the following magma supply rate: 0.5 m³/s in January–March, 0.7 m³/s in March–April, 0.5 m³/s in April–July, and 0.3 m³/s between July and December. These values are strongly comparable to the magma supply rate determined from the lava effusion rates and allow us to assume, as a first-order approximation, that all magma that degassed also erupted.

5. INFRASONIC–THERMAL DELAY TIMES AND POSITION OF THE MAGMA COLUMN

Explosive eruptions produce infrasonic transients in the atmosphere and are recorded as thermal transients when hot gas and ejecta, emitted by an explosion, exit the vent and enter the FOV of IR thermometers. In the assumption that thermal and infrasonic waves share the same source-to-receiver travel distance (first in the conduit and then in the atmosphere), the delay times between thermal (t_T) and infrasonic (t_I) onsets of explosions provide indications about the position of the magma-free surface within the conduit [Ripepe *et al.*, 2001, this volume]. Here the delay times ($dt = t_T - t_I$) are a function of the distance between the vent rim and the receiver (D), the sound velocity in air ($c_a \sim 340$ m/s), and in the conduit (c_c) and the mean velocity of the expanding gas and fragments (U) between the fragmenta-

tion level (h) and the surface [see *Ripepe et al.*, this volume, equation (1)].

The acoustic onset will be defined by the travel time of the sound first in the conduit (h/c_s), from the fragmentation level to the vent rim (h), and then in the atmosphere (D/c_a), between the vent rim and the receiver (D). The thermal onset will be defined by the travel time of the gas/fragments in the conduit (h/U) and is then immediately recorded when hot gas/vapor and ejecta appear out of the crater rim, being the thermal radiation traveling at the speed of light. Accordingly, the travel time of thermal radiation between the crater rim and the recording station can be neglected.

Therefore, once the onset of the acoustic wave is corrected for the vent-to-receiver distance, the delay time between the two onsets will entirely depend on the travel history within the conduit, where the sound is moving much faster ($440 < c_c < 710$ m/s) than the gas/fragments mixture ($10 < U < 150$ m/s) (see *Ripepe et al.* [this volume] for details).

Infrasonic and thermal data have been recorded at station ROC (Figure 1), positioned at a distance (D) of $\sim 450\text{--}680$ m

from the NE and SW crater, respectively. The proper vent-to-receiver distance (D) is obtained from the infrasonic location [*Ripepe et al.*, 2007] of each infrasonic transient. Delay times have been measured for $\sim 10,000$ explosive events between May 2003, when the first weak explosions occurred during the effusive eruption [*Ripepe et al.*, 2007], and December 2003 (Figure 3a). The delay times were long (>1 s) during the effusive phase and decreased rapidly (<0 s) in July 2003 with the end of the effusive phase (Figure 3b).

The delay times depend both on the position of the magma-free surface within the conduit (h) and on the velocity of the gas/fragments (U), and accordingly, they do not allow without additional constraints to solve the ambiguity between these two parameters. Therefore, the short delay times (<0 s) observed after July 2003 are consistent with both a larger gas expansion velocity and/or shallower position of the explosive source.

According to *Ripepe et al.* [this volume, equation (1)], it is evident how the depth of the fragmentation level (h) is so less sensitive to changes in the sound velocity within the

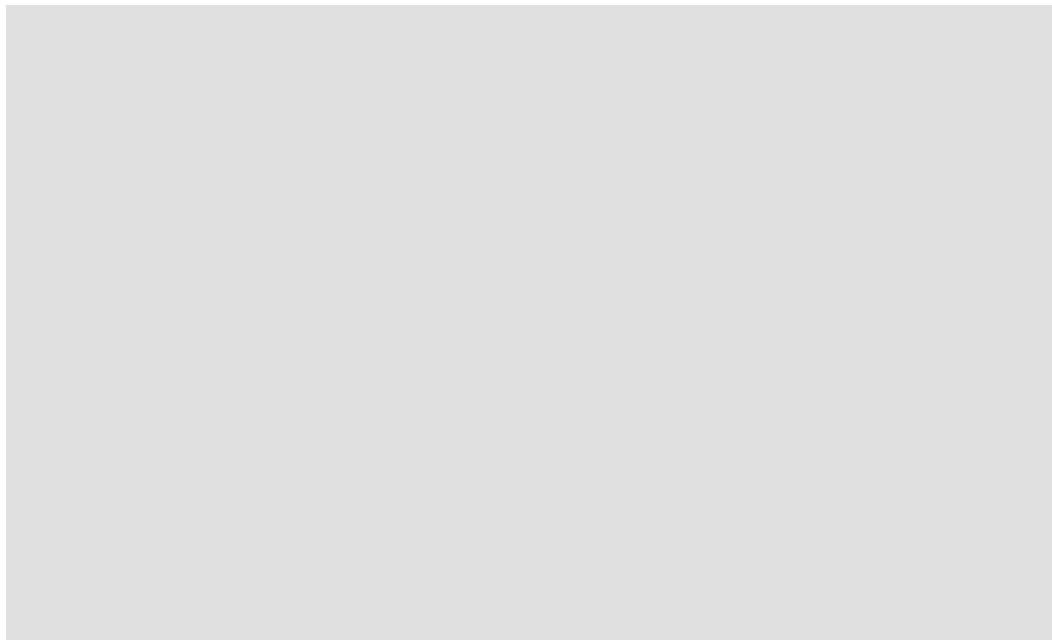


Figure 3. Mean daily values (gray points) of (a) Infrasonic amplitude and (b) delay times between the thermal and infrasonic onsets evaluated from 9042 explosions recorded between May 2003 and January 2004 with clear thermal and infrasonic onsets. (c) Depth of the explosive sources evaluated from thermal–infrasonic delay times by taking into account a gas expansion velocity of 40 m/s and a sound velocity in the conduit of 440 (gray line) and 710 m/s (dashed black line). The depth lines (Figure 3c) results from a five-data-point smoothing procedure. The depth of the explosive source is so less sensitive to the sound speed within the conduit.

conduit (c), which was assumed to range between 440 m/s (for steam at 373°K) and 710 m/s (for air at 1250°K), while it is strongly related to changes in the gas velocity (U).

Assuming a mean gas/fragments velocity of 40 m/s [Delle Donne *et al.*, 2006; Patrick *et al.*, 2007] and sound velocities within the conduit of 440 and 710 m/s, the measured delay times can be converted in magma-free surface depth (Figure 3c). During the end of the eruption, this value was changing from a few hundred meters (300 m) before June 2003 to a few tens of meters (approximately 2–30 m below the summit craters) at the end of the eruption in July 2003, when the explosive activity was visible again at the summit craters (Figure 3c). The longer delay times (1–2 s) observed in August 2003 are most probably related to the temporary reactivation of explosive activity within the SW crater [Ripepe *et al.*, 2007].

The migration of the magma column, as deduced from the decreasing delay times, is consistent with other geophysical evidences such as the progressive increase of the explosive activity at the craters, the increase of tremor, and reestablishment of puffing activity from the summit vents [Ripepe *et al.*, 2005]. Besides, it quite nicely agrees also with the volcanological observations. In fact, at the end of June 2003, the magma level was sufficiently high to be again visible within the NE conduit.

Without a robust constraint on the gas/fragments mean velocity in the conduit (U) for each of the explosive signals, the delay times cannot be converted in absolute position of the fragmentation level in the magma column but rather can allow monitoring relative variations in the depth of the magma-free surface. Therefore, the large values of the fragmentation depth (~300 m) estimated in May 2003 during the effusive phase, might be overestimated as a consequence of the assumed mean gas exit velocity of 40 m/s. This consideration seems quite reasonable, if considering that the ash-rich explosive activity recorded in May–June 2003 was associated to weak (20 Pa) infrasonic transients (Figure 3a), which indicates a low gas overpressure and then a quite low gas exit velocity.

6. MIGRATION OF THE VLP SEISMIC SOURCE

The observed VLP seismic transients are most probably the result of an extended source, where different sections of the conduit radiate simultaneously or at different times, different contributions of energy. However, considering the long wavelength ($>10^4$ m) of the VLP seismic signals, it is reasonable to make the point source assumption and to locate the VLP events using moment tensor inversion [Chouet *et al.*, 2003] or signal directivity [Marchetti and Ripepe, 2005]. These location methods provide an estimate of the

source centroid, which represents the center of distribution of the real source volume. Accordingly, any change in the position of the centroid of the VLP source will indicate a change in the position and/or geometry of the source volume, whereas an upraise of the VLP source centroid should indicate a migration of the source with fixed volume toward the surface or a progressive expansion of the source volume toward the surface.

Particle motion and source location of VLP events recorded on the summit of Stromboli in January 2003, just 5 d after the eruption onset, pointed to a slight change in the position of the centroid [Marchetti and Ripepe, 2005]. Given the large wavelength of the VLP signal, an efficient correction of the effect of the free surface on the polarization vector is not possible. Therefore, the use of the polarization to determine the absolute position of the VLP source centroid is not possible, and we use here the changes of the polariza-

Figure 4. Back azimuth and the takeoff angle for VLP seismic events recorded during 2003 at stations (a) STR and (b) ROC. The black circles represent the mean daily values of azimuth and takeoff, while gray error bars correspond to the variance of the daily distribution.

zation direction as an indication of a relative change in the source position.

The long-term analysis of the back azimuth and takeoff angle recorded at two stations (Figure 4) in 2003 show the same general trend. While the back azimuth is quite stable in 2003, the takeoff angle at both stations shows comparable variations of $\sim 4^\circ$ at STR and $\sim 6^\circ$ at ROC stations, toward the surface. This general trend is interrupted only once just after the major 5 April paroxysm, when the back azimuth moved $\sim 3^\circ$ toward west in the craters direction and takeoff increased $\sim 2^\circ$ at STR and $\sim 4^\circ$ at ROC, indicating a shallower position of the VLP source (Figure 4).

Besides this short episode, the takeoff angle shows, in general, a long-term migration toward the surface (Figure 4) indicating that just after the onset of the eruption, the centroid of the VLP source was acting deeper in the conduit and slowly moved toward the surface, recovering the initial position only in December 2003, 5 months after the effusive eruption ended. However, this upward migration trend of the centroid does not coincide with the reduction of the delay times between the acoustic and the thermal onsets (Figure 3b), and it seems then decoupled from the position of the magma column within the conduit.

7. CONCLUSION

The integration of seismic, infrasonic, thermal, and SO_2 flux data provides a detailed description of the geophysical aspects involved in the 2002–2003 eruption of Stromboli volcano. During the effusive phase, which lasted from December 2002 to June 2003, volcanic activity was characterized by an increase in the VLP seismic rate and SO_2 emissions as a consequence of the larger magma supply rate.

The increase of magma supply at the onset of the eruption leads to the opening of the effusive fractures. The large lava flow from lateral vents caused the drop of the magma column in the central conduits. The higher magma supply is exsolving large quantities of gas in the melt, as revealed by the increased SO_2 flux measurements (Figures 2b and 2c). This large gas concentration leads to a more active gas dynamics, which is most probably responsible for the increased VLP seismic rate (Figures 2a and 2c), which was acting deeper in the conduit (Figures 3 and 4) and did not produce visible explosive activity at the summit vents.

The reduction of the magma supply at the end of the effusive activity is marked by the decrease in the SO_2 emission (Figures 2b and 2c). As a consequence, the reduced magma supply is mainly responsible for the sealing of the effusive fracture along the SdF scarp and for the progressive migration of the magma within the central conduits [Ripepe *et al.*, 2005]. This process is evidenced by the reduction

of the delay times between thermal and infrasonic onsets (Figure 3b).

The delay times between the thermal and the infrasonic onsets generated by the explosions indicate that the position of the magma-free surface was deeper (<300 m) in the conduit during the effusive phase. This is consistent with a deeper position of the centroid indicating the possible position of the VLP source volume, as inferred from the polarization of VLP seismic waveforms. After July 2003, when the effusive activity ceased and the explosive activity at the summit vents was finally reestablished, the SO_2 flux rate decreased in good agreement with the reduction of the VLP seismic rate. In harmony with these observations, the delay times between the acoustic and the thermal explosive onset decreased, while the takeoff angle of the VLP seismic polarization vector moved toward the surface, suggesting an upward migration of the magma column within the conduit.

The trend of the takeoff angle variation of VLP seismic events (Figure 4) is, however, different from the rate at which the infrasonic and thermal onset delay times decreased (Figure 3b). The delay times point to a more rapid upraise of the magma column and coincide with the visual observation, while the shift of the VLP takeoff angle is slower and long-lasting, reaching the preeruptive values only in December 2003 when activity was fully reestablished at all the craters [Ripepe *et al.*, 2007]. This suggests a more complex effect of the position of the magma column on the centroid of VLP seismicity.

The transition from the effusive to explosive phase thus appears to have been controlled by the progressive reduction in the magma supply, as marked by the reduction of SO_2 emission and by the number of VLP events (Figure 2) and by the increase of the magma level within the conduit, as indicated by the short delay times between thermal and infrasonic onsets (Figure 3) and by the upward migration of the VLP seismic activity (Figure 4). These evidences point to a transition from explosive to effusive activity driven by magma supply.

Acknowledgments. The authors thank the Italian Civil Protection for funding and support during the 2002–2003 eruption of Stromboli volcano. Phillip Dawson and an anonymous reviewer are greatly acknowledged for their careful and critical reviews, which greatly improved the manuscript.

REFERENCES

- Allard, P., J. Carbonnelle, N. Metrich, H. Loyer, and P. Zettwoog (1994), Sulphur output and magma degassing budget of Stromboli volcano, *Nature*, 368, 326–330.

- Auger, E., L. D'Auria, M. Martini, B. Chouet, and P. Dawson (2006), Real-time monitoring and massive inversion of source parameters of very-long period seismic signals: An application to Stromboli volcano, Italy, *Geophys. Res. Lett.*, 33, L04301, doi:10.1029/2005GL024703.
- Bonaccorso, S., S. Calvari, G. Gafri, L. Lodato, and D. Patanè (2003), Dynamics of the December 2002 flank failure and tsunami at Stromboli volcano inferred by volcanological and geophysical observations, *Geophys. Res. Lett.*, 30(18), 1941.
- Braun, T., and M. Ripepe (1993), Interaction of seismic and air waves as recorded at Stromboli volcano, *Geophys. Res. Lett.*, 20, 65–68.
- Brusca, L., S. Inguaggiato, M. Longo, P. Madonia, and R. Maugeri (2004), The 2002–2003 eruption of Stromboli (Italy): Evaluation of the volcanic activity by means of continuous monitoring of soil temperature, CO₂ flux, and meteorological parameters, *Geochem. Geophys. Geosyst.*, 5, Q12001, doi:10.1029/2004GC000732.
- Buckingham, M. J., and M. A. Garcés (1996), Canonical model of volcano acoustics, *J. Geophys. Res.*, 101, 8129–8151.
- Burton, M., T. Caltabiano, G. Salerno, F. Mure, and D. Condarelli (2004), Automatic measurements of SO₂ flux on Stromboli using a network of scanning ultraviolet spectrometers, *Geophys. Res. Abstr.*, 6, 03970.
- Burton, M. R., H. M. Mader, and M. Polacci (2007a), The role of gas percolation in quiescent degassing of persistently active basaltic volcanoes, *Earth Planet. Sci. Lett.*, 264(1–2), 46–60.
- Burton, M. R., P. Allard, F. Murè, and A. La Spina (2007b), Magmatic gas composition reveals the source depth of slug-driven Strombolian explosive activity, *Science*, 317, 5835, 227–230, doi:10.1126/science.1141900.
- Calvari, S., L. Spampinato, L. Lodato, A. J. L. Harris, M. R. Patrick, J. Dehn, M. R. Burton, and D. Andronico (2005), Chronology and complex volcanic processes during the 2002–2003 flank eruption of Stromboli volcano (Italy) reconstructed from direct observations and surveys with a handheld thermal camera, *J. Geophys. Res.*, 110, B02201, doi:10.1029/2004JB003129.
- Capasso, G., M. L. Carapezza, C. Federico, S. Inguaggiato, and A. Rizzo (2005), Geochemical variations in fluids from Stromboli volcano (Italy): Early evidences of magma ascent during 2002–2003 eruption, *Bull. Volcanol.*, 68, 118–134.
- Chouet, B., P. Dawson, T. Ohminato, M. Martini, G. Saccorotti, F. Giudicepietro, G. De Luca, G. Milana, and R. Scarpa (2003), Source mechanisms of explosions at Stromboli Volcano, Italy, determined from moment-tensor inversions of very-long-period data, *J. Geophys. Res.*, 108(B1), 2019.
- Chouet, B., P. Dawson, and M. Martini (this volume), Upper conduit structure and explosion dynamics at Stromboli.
- Chouet, B. A., G. Saccorotti, P. Dawson, M. Martini, R. Scarpa, G. De Luca, G. Milana, and M. Cattaneo (1999), Broadband measurements of the sources of explosions at Stromboli Volcano, Italy, *Geophys. Res. Lett.*, 28, 1937–1940.
- Cigolini, C., G. Gervino, R. Bonetti, F. Conte, M. Laiolo, D. Coppoli, and A. Manzoni (2005), Tracking precursors and degassing by radon monitoring during major eruptions at Stromboli volcano (Aeolian Islands, Italy), *Geophys. Res. Lett.*, 32, L12308, doi:10.1029/2005GL022606.
- Delle Donne, D., G. Lacanna, E. Marchetti, M. Ripepe, and G. Ulivieri (2006), Monitoring explosive volcanic activity using thermal images, Stromboli Volcano, Italy, *Eos Trans. AGU*, 87(52), Fall Meet. Suppl., Abstract V43B-1795.
- Dreier, R., R. Widmer, R. Schick, and W. Zurn (1994), Stacking of broadband seismograms of shocks at Stromboli, *Acta Vulcanol.*, 5, 165–172.
- James, M. R., S. J. Lane, B. Chouet, and J. S. Gilbert (2004), Pressure changes associated with the ascent and bursting of gas slug in liquid-filled vertical and inclined conduits, *J. Volcanol. Geotherm. Res.*, 129, 61–82.
- James, M. R., S. J. Lane, and B. A. Chouet (2006), Gas slug ascent through changes in conduit diameter: Laboratory insights into a volcano-seismic source process in low-viscosity magmas, *J. Geophys. Res.*, 111, B05201, doi:10.1029/2005JB003718.
- Jaupart, C., and S. Vergniolle (1989), The generation and collapse of a foam layer at the roof of a basaltic magma chamber, *J. Fluid Mech.*, 203, 347–380.
- Landi, P., L. Francalanci, M. Pompilio, M. Rosi, R. A. Corsaro, C. M. Petrone, I. Cardini, and L. Miraglia (2006), The December 2002–July 2003 effusive event at Stromboli volcano, Italy: Insights into the shallow plumbing system by petrochemical studies, *J. Volcanol. Geotherm. Res.*, 155, 263–284.
- Marchetti, E., and M. Ripepe (2005), Stability of the seismic source during effusive and explosive activity at Stromboli Volcano, *Geophys. Res. Lett.*, 32, L03307, doi:10.1029/2004GL021406.
- Neuberg, J., R. Luckett, M. Ripepe, and T. Braun (1994), Highlights from a seismic broadband array on Stromboli volcano, *Geophys. Res. Lett.*, 21, 749–752.
- Parfitt, E. A. (2004), A discussion of the mechanism of explosive basaltic eruptions, *J. Volcanol. Geotherm. Res.*, 134, 77–107.
- Patrick, M. R., A. J. L. Harris, M. Ripepe, J. Dehn, D. A. Rothery, and S. Calvari (2007), Strombolian explosive styles and source conditions: Insights from thermal (FLIR) video, *Bull. Volcanol.*, 69, 769–784, doi:10.1007/s0044500601070.
- Puglisi, G., A. Bonaccorso, M. Mattia, M. Aloisi, A. Bonforte, O. Campisi, M. Cantarero, G. Falzone, B. Puglisi, and M. Rossi (2005), New integrated geodetic monitoring system at Stromboli volcano (Italy), *Eng. Geol.*, 79, 13–31.
- Ripepe, M., S. Ciliberto, and M. Della Schiava (2001), Time constraints for modeling source dynamics of volcanic explosions at Stromboli, *J. Geophys. Res.*, 106(B5), 8713–8727.
- Ripepe, M., A. J. L. Harris, and R. Carniel (2002), Thermal, seismic and infrasonic evidences for variable degassing rates at Stromboli volcano, *J. Volcanol. Geotherm. Res.*, 54, 335–351.
- Ripepe, M., E. Marchetti, P. Poggi, A. J. L. Harris, A. Fiaschi, and G. Ulivieri (2004), Seismic, acoustic and thermal network tracks in real time the 2003 eruption of Stromboli volcano, *Eos Trans. AGU*, 85, 329–332.
- Ripepe, M., E. Marchetti, G. Ulivieri, A. J. L. Harris, J. Dehn, M. Burton, T. Caltabiano, and G. Salerno (2005), Effusive to explosive transition during the 2003 eruption of Stromboli volcano, *Geology*, 33(5), 341–344, doi:10.1130/G21173.1.
- Ripepe, M., E. Marchetti, and G. Ulivieri (2007), Infrasonic monitoring at Stromboli Volcano during the 2003 effusive eruption:

- Insights on the explosive and degassing process of an open conduit system, *J. Geophys. Res.*, 112, B09207, doi:10.1029/2006JB004613.
- Ripepe, M., D. Delle Donne, A. J. L. Harris, E. Marchetti, and G. Olivieri (this volume), Dynamics of Strombolian activity.
- Salerno, G., M. Burton, T. Caltabiano, E. Longo, F. Mure, and D. Condarelli (2004), Insights into the 2002–2003 eruption of Stromboli from daily measurements of SO₂ emission rates, *Geophys. Res. Abstr.*, 6, 04175.
- Vergniolle, S., and G. Brandeis (1994), Origin of the sound generated by Strombolian explosions, *Geophys. Res. Lett.*, 21, 1959–1962.
- Wilson, L. (1980), Relationships between pressure, volatile content and ejecta velocity in three types of volcanic explosion, *J. Volcanol. Geotherm. Res.*, 8, 297–313.

M. R. Burton, T. Caltabiano, and G. Salerno, Istituto Nazionale di Geofisica e Vulcanologia, Sezione di Catania, Piazza Roma, 95123 Catania, Italy.

E. Marchetti, M. Ripepe, and G. Olivieri, Dipartimento di Scienze della Terra, Università di Firenze, Via G. La Pira 4, 50121 Firenze, Italy.

Variations of Soil Temperature, CO₂ Flux, and Meteorological Parameters

Paolo Madonia, Lorenzo Brusca, Salvatore Inguaggiato, Manfredi Longo, and Sabina Morici

Istituto Nazionale di Geofisica e Vulcanologia, Sezione di Palermo, Palermo, Italy

The detailed analysis carried out on the data, acquired in two continuous monitoring stations during the 2002–2003 Stromboli eruption, integrated by daily field observations of the scientific personnel working at the volcanological observatory, showed that CO₂ flux and soil temperature are strictly related to volcanic events. Furthermore, the recorded signals showed a strong correlation with wind speed and direction, revealing that during the eruption, in the summit area of Stromboli, air movements were related not only to atmospheric circulation, but were also significantly affected and, in certain cases, caused by volcanic activity. The possible volcanic origin of a peculiar type of air circulation identified in the summit area of Stromboli suggests that the separation between volcanic and atmospheric signals might not be obvious, requiring monitoring of atmospheric parameters over a wide area, rather than a single location.

1. INTRODUCTION

Continuous monitoring of CO₂ flux from soil plays a very important role in the geochemical monitoring network operating at Stromboli. As an example, the onset of the 28 December 2002 eruption was clearly heralded by strong anomalies of carbon dioxide fluxing from the soil [Federico *et al.*, this volume].

As described by Brusca *et al.* [2004], some side parameters, like wind speed and direction, air and soil temperature and humidity, atmospheric pressure are normally acquired in addition to CO₂ in order to look for possible environmental noise masking the volcanic signal.

However, in certain cases, some of the above mentioned parameters are not driven by exogenous phenomena, but their anomalies appear to be a direct consequence of transitions of the volcanic system between two different states of activity.

The Stromboli Volcano: An Integrated Study of the 2002–2003 Eruption
Geophysical Monograph Series 182
Copyright 2008 by the American Geophysical Union.
10.1029/182GM22

The work of Brusca *et al.* [2004] deeply investigated the mutual relationships between air circulation over Stromboli and soil temperature and CO₂ flux from soil during the 2002–2003 eruption. The authors highlighted how wind speed influenced the recorded parameters, but on the other side, the wind field was the result of the interactions between the normal atmospheric circulation and the air turbulence provoked by the volcanic activity. In other words, during an eruption, the boundary between the volcanic system and the external universe does not coincide with the shallowest portion of the lithosphere, but also the very low strata of the atmosphere are involved as a part of the volcanic processes.

De Gregorio *et al.* [2007] analyzed continuous data of soil temperatures, acquired in the summit fumarolic system, and total dissolved gas pressure (TDGP), measured in a well-located area very close to the shoreline. They demonstrated that their simultaneous anomalies, mainly due to endogenous phenomena like earthquakes and/or energetic explosions, clearly indicate how also the hydrogeologic system is part of a unique process that at Stromboli involves the feeding magmatic system, the shallowest soil horizons, the hydrosphere, and the low atmosphere.

In this contribution, we focus our attention on the description of the complex system above described, with special reference to the observation made during the effusive period of the 2002–2003 eruption, trying to fix a new perspective in the separation between environmental noise and volcanic anomalies.

In particular, more data and a deeper interpretative lecture have been added to the work by *Brusca et al.* [2004], which represents the main core of this contribution.

First, we present a new subdivision of the 2002–2003 eruption into different phases, analyzing their functional relationships with the degassing style evidenced by the signals recorded in the continuous monitoring stations. Then,

introducing new geochemical information from the spot measurements done during the eruption on the coastal aquifer, we better clarify the link between this last and the soil degassing, framing the fluid transfer process from the lithosphere to the atmosphere into a unique phenomenon.

2. STRUCTURE OF THE MONITORING NETWORK

Carbon dioxide flux, together with other meteorological parameters, have been continuously measured since 1999 at two automatic stations, named STR01 and STR02 (Figure 1), located in relative high flux zones, installed the former in

Figure 1. Location of multiparametric stations and monitored wells at Stromboli Island.

December 1999 and the latter in July 2000 [Carapezza *et al.*, 2002]. They were manufactured by West Systems and use the accumulation chamber method [Chiodini *et al.*, 1998].

Carbon dioxide flux, together with wind speed and direction, air temperature and relative humidity, soil temperature, water content, and atmospheric pressure, are acquired every hour and transmitted to the operative Istituto Nazionale di Geofisica e Vulcanologia geochemical center in Palermo directly via GSM modem (STR01) or by radio transmission to the Centro Operativo Avanzato (Advanced Operative Center) volcanological and civil protection presidium in Stromboli (STR02).

Carbon dioxide is measured by a Dräger Polytron IR spectrometer, in the interval 0–0% with a precision of $\pm 0.01\%$, soil temperature by a PT100 probe, with a precision of $\pm 0.1^\circ\text{C}$, air temperature and relative humidity by a combined sensor Mod. LSI DMA570 with a precision of $\pm 0.2^\circ\text{C}$ and $\pm 0.2\%$, respectively.

Wind speed and direction are measured by a Lastem combined sensor, with a precision of $\pm 0.001 \text{ m/s}$ in speed and $\pm 0.5^\circ$ in direction.

3. SYNTHESIS OF THE ERUPTION PHASES

The 2002–2003 eruption may be subdivided, under the light of the possible relationships between volcanological events and anomalies of the previously described parameters, into four different steps:

1. The preparatory phase, characterized by a long period of increased Strombolian activity, started in May 2002 and signed by clear geochemical anomalies recorded in the thermal waters and soil gas emanations, like concentrations and isotopic composition of helium and carbon [Capasso *et al.*, 2003; Carapezza *et al.*, 2004].
2. The effusive phase, began on 28 December, with emission of highly variable amounts of gas with no scoria. However, the presence of continuous very long period events, registered by the local seismic network, testified the ongoing Strombolian activity in the conduit, due to the lower level of the magmatic column with respect to normal conditions [Ereditato and Luongo, 1997; Ripepe *et al.*, 2003].
3. The large explosion of 5 April occurred from the NE crater which was due to the ascent of a new batch of gas-rich magma, freeing the conduit obstructed by collapsed rocky material.
4. The last phase, after the explosions, during which the lava outpouring gradually declined. The magma started to rise in the conduit towards the summit craters, whose activity increased until the restoration

of the typical Strombolian character on 21 July, when the effusive phase finally stopped.

4. DATA PRESENTATION AND DISCUSSION

Soil temperature and CO₂ flux measures from both the STR01 and STR02 stations are presented in Figure 2, where 24-h running averages for both the parameters are draft; data refer to the period January–September 2003 because before that date STR01 station was not operating in its actual location, and no meteorological data are available from STR02.

Carbon dioxide anomalies recorded at STR02 before the eruption onset have been already exhaustively described by Federico *et al.* [this volume]; what we observed at the beginning of the investigated period is something we define as the “tail” of the high CO₂ flux that characterized the preeffusive stage. The upraising of a batch of gas-rich magma considerably enhanced the release of volatiles, mainly water vapor and carbon dioxide, from the soil. Until the middle of February, the average CO₂ daily flux was about 13,000 and 75 g m⁻² d⁻¹ at STR02 and STR01, respectively.

Once the contribution of the new magma to the degassing was exhausted, CO₂ flux halved in a very few days since the middle of February, when different trends of the signals were recorded in the two measuring sites. We define this new phase of the eruption as “effusive” period, subdivided in two subperiods having the 5 April explosion as a divide and ending at the beginning of May, when the lava flow from the effusive fissures stopped definitely. At STR02, we observed an increasing trend modulated by high-frequency anomalies of wide amplitude (several thousands grams per square meter per day), lasting until the end of March, a few days before the 5 April explosions. Since the end of March, a new phase of degassing style took place, characterized by a decrease modulated by the same high amplitude anomalies observed during the initial increase. More in general, during all the effusive phase, the signal recorded at STR02 showed variability much higher than in the next phases.

On the contrary, at STR01, the signal was much more constant during the effusive period. The different behaviors recorded in the summit and the coastal stations are due to the very different characteristics of the sites. STR02 is located within a fumarolic field very close to the summit craters, in strict hydraulic contact with the volcanic conduit through which the most part of the degassing takes place. Variations of the degassing rate are immediately reflected in the amount of volatiles fluxing through the soil, revealed by the high frequency-amplitude anomalies recorded at STR02.

The fast-changing signal that characterizes the eruptive phase probably depends on the continuous changes in the geometry and effusion rates from the vents at that time. The

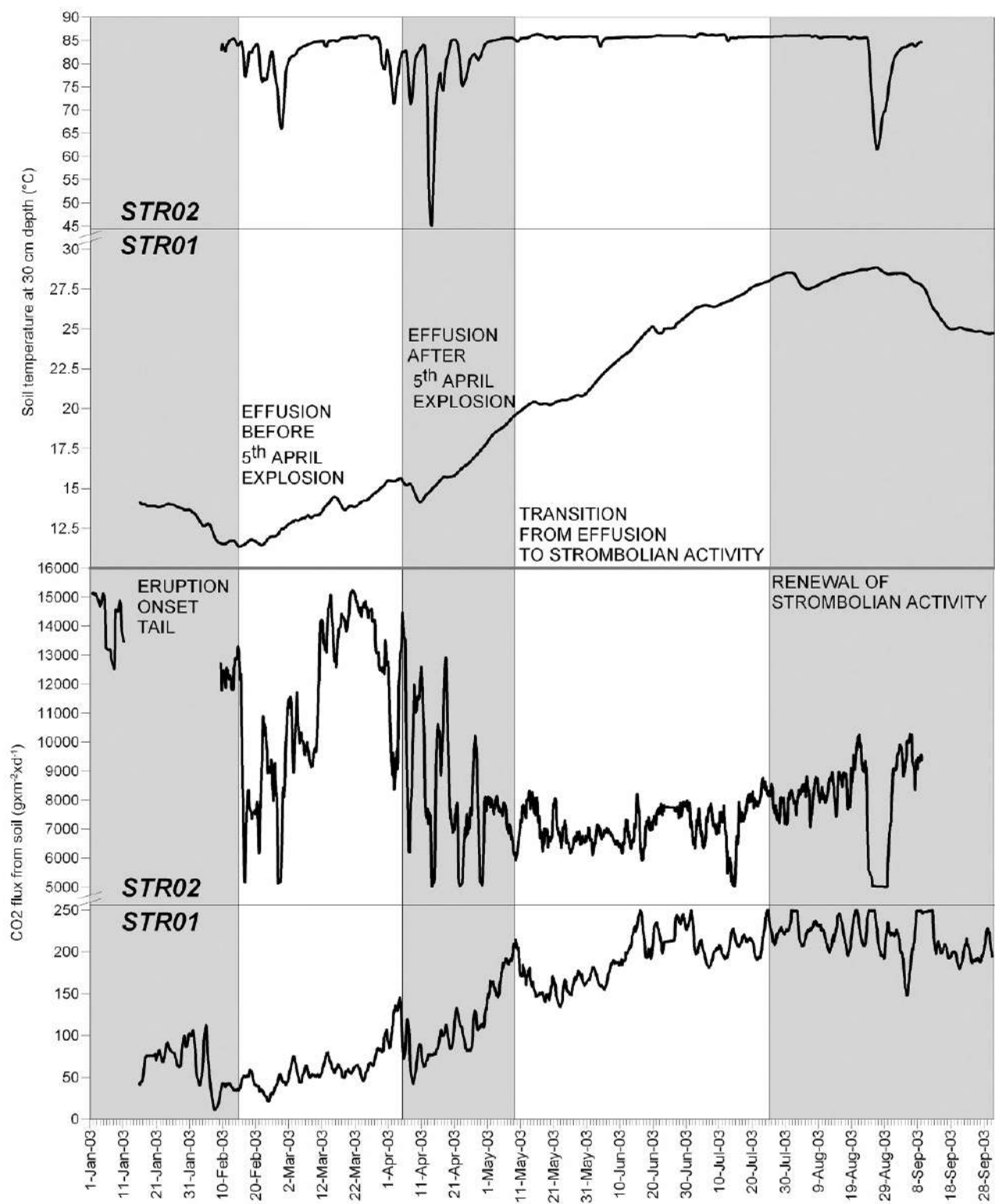


Figure 2. Running 24-h averages of (bottom) CO₂ flux data and (top) soil temperatures registered at STR01-02 stations.

opening and closure of the basal vents, the variations in the lava flow rate, the presence of rocky material inside the main conduit, and oscillations in the height of the magma may have influenced the partitioning between the vents themselves and the soil of the volatiles released by the volcanic system.

On the contrary, STR01 is located far away from the conduit, in a little coastal plain under which an aquifer is present a few meters below the topographic surface. Excess CO₂, generated by an increase in degassing, chemically interacts with the aquifer, and only a reduced amount is released from the aquifer to the overlying soil; the presence of this chemical tampon acts as a low-pass filter on the signal recorded at ground level, which is characterized by low absolute values, modulated by smooth anomalies. Under these condition, the variation style of the signal is similar to that one expected in a nonvolcanic area: lower values during the cold season, gently increasing toward higher values in the warm season, when soil respiration is enhanced due to the higher temperatures induced by the higher solar radiation. Only very strong variations in degassing due to endogenous causes are then visible as anomalies in the signal recorded at STR01.

The gentle increase from 50 to 200 g m⁻² d⁻¹ observed from February (the coldest month of the year, in this area) to July (the warmest month) is, in our opinion, only due to the seasonal cycle. The only significant anomalies are the two slope ruptures observed in coincidence with the 5 April explosion and with the end of the lava flow.

Since 24 March, the increasing trend was steeper than in the previous period, with a culmination on 5 April and a successive sudden decrease of the flux. The same behavior was observed in coincidence with the complete closure of the eruptive vents, which occurred on the first days of May. No other anomalies were observed at STR01 during the transition phase and the final renewal of Strombolian activity.

The different variation styles of the soil temperature signals reflect exactly what we have observed about CO₂ flux. At STR01, the driving mechanisms of soil temperature variations may be completely attributed to the effect of the solar irradiance: low temperatures during the cold season, higher temperatures during the warm months, no significant high-frequency anomalies.

On the contrary, at STR02, we observe a very clear volcanic signal. First of all, the absolute values of temperature (more than 80°C) is not compatible with the simple contribution of the solar irradiance, but must be explained involving a heat carrier of endogenous nature. In the specific case, the heat carrier is represented by the water vapor fluxing through the soil.

Moreover, the temperature signal highlights the presence of two very different eruption phases: a first period, from February to May, characterized by continuous variations in both the parameters and, a second one, from May to the end of the considered time window (i.e., September), having a quite flat signal, which is interrupted by a single episode right at the beginning of September. The dividing point between the two periods coincides with the beginning of the transition from the effusive phase of the eruption to the closure of the eruptive fractures and the reactivation of the summit craters.

When the effusive vents located on the Sciara del Fuoco (SdF) began to close, the magma column started to rise up through the conduit toward the summit craters. As the summit vents were large enough to ensure the release of large amounts of volatiles, the geometry of the vents did not vary, and the source of gas/vapor was very close to the detection point, no more variations were observed in soil temperature and at STR02 station. The only perturbation that occurred during this second phase was registered during the first days of September, after a minor episode of decreased volcanic activity (from Strombolian to degassing).

Finally, soil temperatures recorded at STR02 have been compared with CO₂ and TDGP measured in the wells of the geochemical monitoring network (Table 1), under the retrospective light of the relationships found by *De Gregorio et al.* [2007] and already discussed in the introductory chapter.

As clearly evidenced in the table, showing the variance of the measures, the variability of the gas content in the coastal aquifer was higher during the effusive phase than in the later transitional phase, reproducing the same variation style just described for STR02.

The coastal aquifer was reactive to the turbulent degassing regime that accompanied the lava flow, but all the gas excess was digested by itself. This is the reason why we

Table 1. Variance of CO₂ and TDGP Measured in the Wells of the Geochemical Monitoring Network [*Capasso et al.*, 2005] During the Effusive (February–April) and Transitional (May–July) Phases

Eruption Phase	Fulco		Zurro		Cusolito	
	CO ₂	TDGP	CO ₂	TDGP	CO ₂	TDGP
Effusion	5.394E-3	6.945E-2	3.265E-3	1.310E-1	7.000E-4	4.770E-2
Transition	4.853E-3	2.923E-2	6.590E-6	2.519E-2	2.000E-4	3.320E-2

Values are expressed in atmosphere.

did not observe any significant variation at STR01. These observations teach us a very important concept in designing a volcano monitoring network. What is important is the right comprehension of all the physical components of a specific volcanic system and their mutual relationships. In other words, the coastal aquifer, monitored by the well network, showed a geochemical behavior much more similar to a measuring point located in the summit area (STR02) rather than the same kind of station directly lying a few meters over it (STR01). The reason is that the degassing system directly interacts with the aquifer and the summit station, whereas STR01 records a signal filtered by the interposition of a media (the aquifer) able to strongly smooth any possible anomaly.

The last nodal point over which we like to focus attention is the meaning of the observed anomalies in meteorological parameters, and in the wind speed and directions in particular.

As already discussed by *Brusca et al.* [2004], a relative minima of both soil temperature and CO₂ flux at STR02 appear to be related to relative maxima of wind speed (Figure 3). Wind can affect the measurements for several reasons:

1. dilution of water vapor and CO₂ in the soil near the surface [*Fukuda*, 1955]; this effect might be particularly significant because the station is located on the top of a thin ridge, whose flanks are well exposed to winds;
2. transformation of the heat exchange processes from convective to a forced-convective system;
3. emptying of the accumulation chamber due to high lateral wind pressures;
4. faster evaporation of condensed steam from the ground surface.

Moreover, the higher thermal gradient inside the soil, due to the higher cooling, causes the increase in CO₂ flux [*Garcia et al.*, 2000]. The processes just described explain the effect of wind but do not explain why CO₂, temperature anomalies, and wind speed peaks occur in correspondence with volcanic events.

The possible mechanism individuated by *Brusca et al.* [2004] refers to a local air circulation induced by volcanic activity.

Figure 3. Running 24-h averages of soil temperature and CO₂ flux compared with wind speed data recorded at STR02.

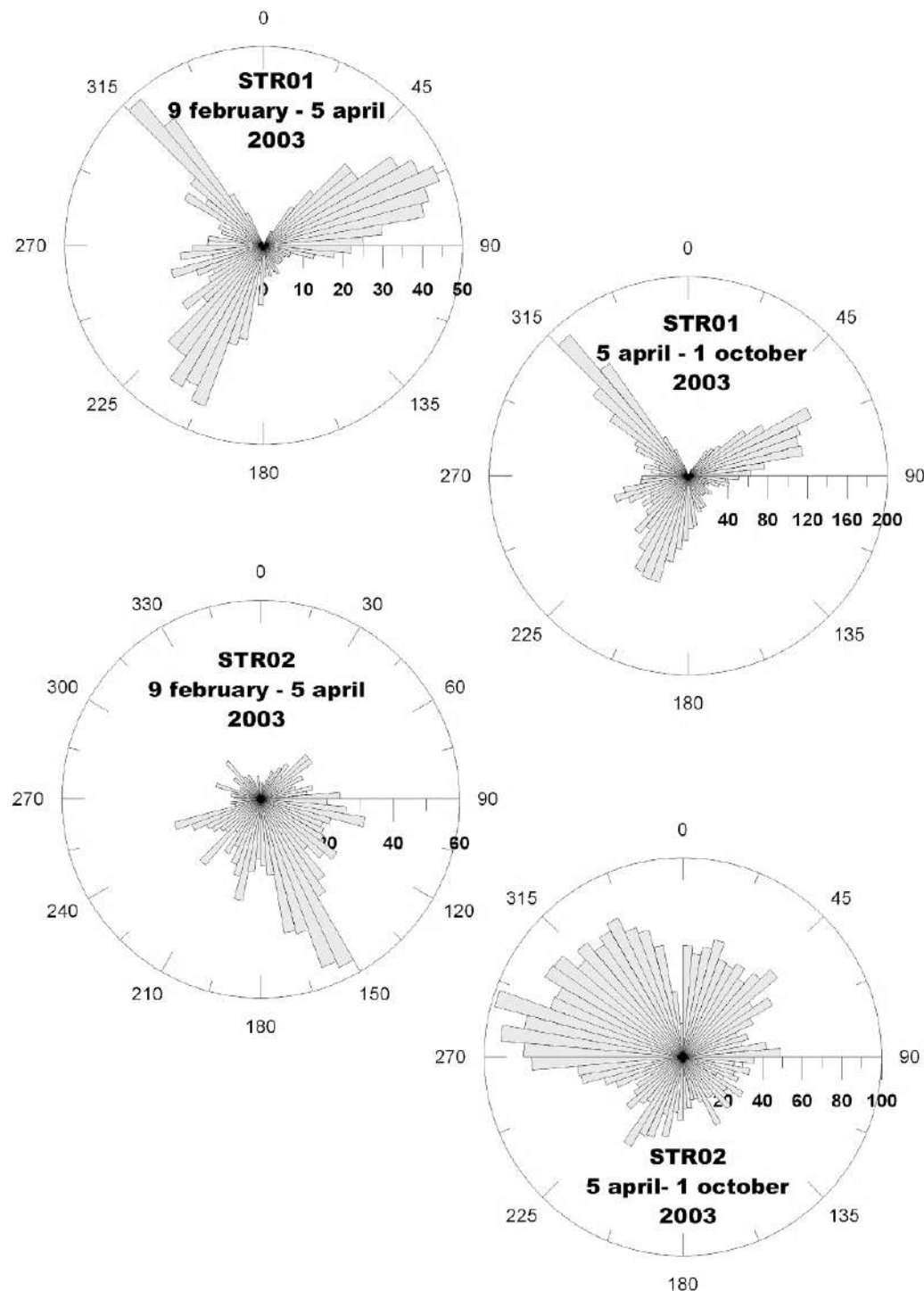


Figure 4. Frequencies of wind directions recorded at STR01 and STR02 before and after the 5 April explosion.

In particular, during the effusive phase of the eruption, the thermal energy released by the summit and basal vents, as well as by the lava field on the SdF, could have generated an upwelling hot air column, on its own, generating a low atmospheric pressure area centered somewhere in the middle between the summit vents and the lava field. Air claimed in from all directions generated a local centripetal wind cell that could have been revealed by STR02 data as a prevailing wind from SE.

After the late transition to Strombolian activity, and the de-activation of the lava field, the preeruptive conditions of air circulation over Stromboli were restored.

Figure 4 shows frequencies and speed of wind versus direction for both STR01 and STR02 stations, plotted in separated polar diagrams for the periods before and after the 5 April explosion. At STR01 station, far from the craters, no differences either in frequencies or wind speed exist between the two periods. In contrast, at STR02 station, we clearly observed that before the 5 April event, the dominant winds were from SE. An inversion of 180° occurred after the 5 April event, when both STR01 and STR02 started to show the same dominant winds. This observation agrees with the existence of a local wind cell caused by the lava field, that, however, no longer seems to be effective after the reactivation of the summit craters.

5. CONCLUDING REMARKS

Signals recorded in the summit continuous monitoring station STR02 during the 2002–2003 Stromboli eruption evidenced anomalies both in CO₂ and soil temperatures.

These anomalies appear strictly related to the different phases of the eruption and can be explained involving specific volcanic events.

In particular, variations in effusion rates, height of the magmatic column inside the conduit, partial and/or complete opening and closure of the effusive fissures, have been identified as mechanisms able to change the partition ratio of the volcanic volatiles between the conduit and the soil and, in the last instance, to control CO₂ and water vapor flux through it.

Furthermore, the relative minima and maxima of the two parameters showed a strong correlation with wind speed and direction. The analysis of the wind data, particularly the relationships between wind speed and direction, air and soil temperature, and local circulation of atmospheric air masses revealed that, during the eruption, in the summit area of Stromboli, air movements were related not only to atmospheric circulation, but were also significantly affected and, in certain cases, caused by volcanic activity.

Data acquired in the coastal STR01 station, located far away from the main degassing system, appear to be strongly filtered by the interposition of water in liquid phase (aquifer), showing a dominant control acted by exogenous causes and, in particular, by solar irradiance.

Finally, the volcanic origin of the peculiar type of air circulation identified in the summit area of Stromboli suggests that the separation between volcanic and atmospheric signals might not be obvious, requiring monitoring over a wide area, rather than a single location.

Acknowledgments. The researches whose results have been presented in this article have been carried out as a part of the monitoring activity of Italian active volcanoes promoted and financially supported by the “Presidenza Consiglio dei Ministri, Dipartimento Nazionale di Protezione Civile (Italian National Department for Civil Defense).”

REFERENCES

- Brusca, L., S. Inguaggiato, M. Longo, P. Madonia, and R. Maugeri (2004), The 2002–2003 eruption of Stromboli (Italy): Evaluation of the volcanic activity by means of continuous monitoring of soil temperature, CO₂ flux, and meteorological parameters, *Geochemistry, Geophysics, Geosystems*, 5(12), doi:10.1029/2004GC000732.
- Capasso, G., M. L. Carapezza, C. Federico, S. Inguaggiato, and A. Rizzo (2003), Long term geochemical monitoring of Stromboli volcano (Italy): Clues on 2002–2003 eruption from gas chemistry, helium and carbon isotopes, *Eos Trans. AGU*, 84(46), Fall Meet. Suppl., Abstract V52C-01.
- Capasso G., M. L. Carapezza, C. Federico, S. Inguaggiato, and A. Rizzo (2005), Geochemical monitoring of the 2002–2003 eruption at Stromboli volcano (Italy): Precursory changes in the carbon and helium isotopic composition of fumarole gases and thermal waters, *Bull. Volcanol.*, 68, 118–134.
- Carapezza, M. L., M. Guidi, and S. Inguaggiato (2002), Soil CO₂ degassing on Stromboli island: Influence of environmental parameters and insights on volcanic activity, EGS 27th General Assembly, Nice, *Geophys. Res. Abstract*, Vol. 4, Abs. Numb. 02-A-06737.
- Carapezza, M. L., S. Inguaggiato, L. Brusca, and M. Longo (2004), Geochemical precursors of the activity of an open-conduit: The Stromboli 2002–2003 eruptive events, *Geophys. Res. Lett.*, 31, L07620, doi:10.1029/2004GL019614.
- Chioldini, G., R. Cioni, M. Guidi, B. Raco, and L. Marini (1998), Soil CO₂ flux measurements in volcanic and geothermal areas, *Appl. Geochem.*, 13(5), 543–552.
- De Gregorio, S., P. Madonia, S. Gurrieri, G. Giudice, and S. Inguaggiato (2007), Contemporary total dissolved gas pressure and soil temperature anomalies recorded at Stromboli volcano (Italy), *Geophys. Res. Lett.*, 34, L08301, doi:10.1029/2007GL029578.
- Ereditato, D., and G. Luongo (1997), Explosion quakes at Stromboli (Italy), *J. Volcanol. Geotherm. Res.*, 79, 265–276.

- Federico C., L. Brusca, M. L. Carapezza, C. Cigolini, S. Inguaggiato, A. Rizzo, and D. Rouwet, Geochemical evidences of the incoming 2002–03 Stromboli eruption: Variations in CO₂ and Rn emissions and He isotopes before 28th December 2002, *this volume*.
- Fukuda, H. (1955), Air and vapor movement in soil due to wind gustiness, *Soil Sciences.*, 79, 249–256.
- Garcia, R., G. Natale, M. Monnin, and J. L. Seidel (2000), Shock wave radon surface signals associated with the upsurge of T-P politons in volcanic systems, *J. Volcanol. Geotherm. Res.*, 96, 15–24.
- Ripepe, M., E. Marchetti, A. Flaschi, and G. Ulivieri (2003), Seismo-acoustic monitoring of the Dec.2002 eruption of Stromboli volcano, *Eos Trans. AGU*, 84(46), Fall Meet. Suppl., Abstract V52C-03.

L. Brusca, S. Inguaggiato, M. Longo, P. Madonia, and S. Morici, Istituto Nazionale di Geofisica e Vulcanologia, Sezione di Palermo, Via Ugo La Malfa 153, I-90146 Palermo, Italy. (p.madonia@pa.ingv.it)

Seismological Insights on the Shallow Magma System

M. Martini, L. D'Auria, T. Caputo, F. Giudicepietro, R. Peluso, A. Caputo, W. De Cesare,
A. M. Esposito, M. Orazi, and G. Scarpato

Istituto Nazionale di Geofisica e Vulcanologia, Sezione di Napoli, Osservatorio Vesuviano, Naples, Italy

We present an overview of the volcanic seismicity recorded at Stromboli from January to September 2003. The data set starts a few weeks after the onset of the eruption and covers most of the effusive phase and the subsequent recovery of the explosive activity. The most important variations occurred between May and July coinciding with the waning of the lava flow and the reappearance of Strombolian activity at the summit craters. All the parameters indicate that the shallow magmatic system has not undergone permanent changes during this period. The only significant variation related to the shallow conduit is the increase in volcanic tremor amplitude and the change in the spectral content of long-period events during the transition between effusive and explosive activity. A slight increase in the very long period (VLP) events source elevation seems to mark the rise of the magma at the end of the effusive phase. The variations in the VLP events occurrence rate are more likely to be attributed to changes in the gas flow rate and the bubble coalescence mechanism, therefore, to a deeper portion of the magmatic system. The 5 April paroxysm is associated only with a small increase of the activity in the following days.

1. INTRODUCTION

Starting from 16 January 2003, a digital broadband seismic network was deployed in Stromboli by the Istituto Nazionale di Geofisica e Vulcanologia (INGV) (Plate 1). In September 2003, the network consisted of 10 seismic stations. Most of them were installed before the end of February. Each station consists of a Guralp CMG-40T sensor (60-s period), a digital 24-bit data logger GAIA, and a UHF radio modem. Power supply is provided by solar panels and batteries. The data are acquired from two local acquisition centers, one in

Stromboli for the stations situated on the northern part of the island and one in Lipari island (40 km south of Stromboli) for stations located in the southern part. Data were locally stored and sent in real time through Internet connections to INGV departments in Naples, Catania, and Rome.

A surprising feature of the observed seismicity was the persistence of very long period (VLP) events, long-period (LP) events, and volcanic tremor during the effusive phase. These events have been traditionally linked to the bursting of gas slugs (VLP and LP) [Chouet *et al.*, 2008] and smaller bubbles (tremor) at the magma-air interface [Ripepe *et al.*, 1996] typically related to Strombolian activity. The new observations shed a different light on the physical mechanisms at the base of the volcano seismicity of Stromboli during effusive eruptions since they persist even when the vents are obstructed by debris [Calvari *et al.*, 2005].

Here we analyze different seismological parameters and try to interpret them.

2. VOLCANIC TREMOR

The persistent volcanic tremor at Stromboli has been linked to the impulsive bursting of gas bubbles at the magma–air interface [Ripepe *et al.*, 1996]. After the onset of the effusive eruption and the obstruction of the summit craters with debris [Calvari *et al.*, 2005], the volcanic tremor was still recorded, even if with a reduced amplitude. Its overall amplitude remained low since the beginning of June (Plate 2) then started to increase. From 23 and 25 June, the amplitude increased dramatically and remained high until the beginning of September when it stabilized on average values.

The relative amplitude of volcanic tremor has been shown to be a good indicator of its source location [Aki and Ferrazzini, 2000]. In Plate 2, we show the amplitude ratio between two mid-elevation stations (STR1 and STR7) and a summit station (STR2). The overall trend indicates a decrease of both ratios. The considered frequency band (1–6 Hz) excludes a significant seismic wave propagation effects [Chouet *et al.*, 1997]. The most likely interpretation to the observed variation should be attributed to a decrease of the volcanic tremor source depth or alternatively to the appearance of a new source at shallower depth.

3. LP EVENTS AND EXPLOSION QUAKES

Strombolian explosions are usually accompanied by LP events, which often contain a seismoacoustic transient. For this reason, they are usually also called explosion quakes [Ripepe and Braun, 1994]. LPs were recorded in Stromboli also during the effusive phase with significant amplitudes (Plate 3), so they are not simply linked to the bursting at the summit craters but to processes involving the whole shallow conduit.

The spectral analysis of LP events is a very important tool for understanding variations in volcanic and geothermal systems [Kumagai and Chouet, 1999, 2001]. The spectra of these events are usually characterized by discrete peaks linked to the resonant modes of the conduit. Each resonant mode is characterized by a frequency and a quality factor Q , which is indicative of the amplitude decay rate of the oscillations because of damping effects. Both parameters are related to the physical properties of the resonant structure (i.e., the volcanic conduit) and less to the excitation mechanisms [Nakano *et al.*, 1998]. However, depending on the mechanism, some resonant modes can be triggered more strongly than others [Chouet, 1986].

The spectra of LP events at Stromboli during 2003 (Plate 4) show some spectral peaks common to many events. The peaks at 1.8, 2.3, and 2.7 Hz are observed in most of the events until July. New spectral peaks (at 3.4 and ~4 Hz) ap-

pear in May, but they become clearer at the end of June, and after August, they became dominant. This behavior is common to many stations, and the considered frequencies correspond to wavelengths (>1 km) long enough to exclude consistent seismic wave path effects [Chouet *et al.*, 1997].

If there is a change in the conduit structure, we would expect a progressive shift of the spectral peaks [Neuberg *et al.*, 2000]. Otherwise, if there is only a change in the source mechanism, we would expect that some spectral peaks decrease in amplitude or disappear, while others increase their amplitude and/or new peaks appear. The latter hypothesis seems to fit better with the data shown in Plate 4.

The persistence of common spectral peaks means that the resonating structure responsible for LP events generation did not change much during the considered period. A further confirmation of the previous statement comes from the analysis of the quality factors of the resonant modes [Nakano *et al.*, 1998]. Plate 5 shows that the quality factor Q exhibits no significant trends. The only evident feature is that higher-frequency spectral components, appearing in May–June, have also a higher Q , but this can depend solely on the overall properties of the conduits.

4. VLP EVENTS

The occurrence of VLP events at Stromboli is well known [Neuberg *et al.*, 1994; Chouet *et al.*, 1999; Wielandt and Forbringer, 1999]. They have been interpreted as the result of a sudden expansion and bursting of gas slugs coming from deeper part of the conduit [Chouet *et al.*, 2003]. The depth of slug coalescence zone inferred from geochemistry is ~3 km [Burton *et al.*, 2007].

A detailed analysis of their source functions has shown that they are related to volumetric variation of the shallow plumbing system consisting of a dike oriented NE–SW with a dip of ~60° toward the Sciara del Fuoco [Chouet *et al.*, 2003, 2008].

In Plate 6, we show their average hourly occurrence rate from January to September; until June their rate was between 15 and 25 events/hour. This value is a higher than the average rate at Stromboli (12–13 events/hour) but is within the overall statistics of the volcano (see histogram in Plate 6). At the end of June, they reached a peak of ~28 events/hour and then started diminishing, reaching 10 events/hour, at the end of August.

VLP events at Stromboli have usually a very simple radial particle motion, pointing toward the source centroid [Chouet *et al.*, 2003]. The polarization analysis of the VLP waveforms then is a good indicator of relative variations in the source position. In Plate 7, we show the azimuth and the inclination of the principal polarization vector at STR8

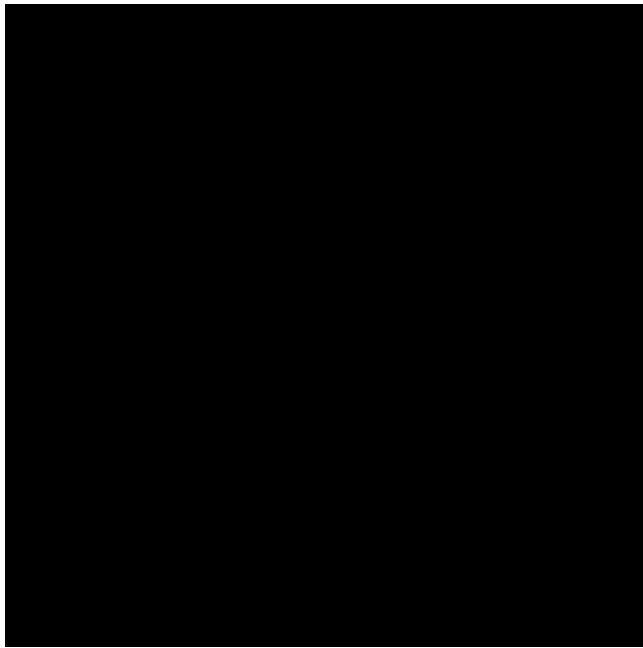


Plate 1. Map of the INGV broadband seismic network. Seismic stations are indicated by black dots. The inset in the lower part shows the position of the Stromboli Island in the Tyrrhenian Sea (southern Italy).

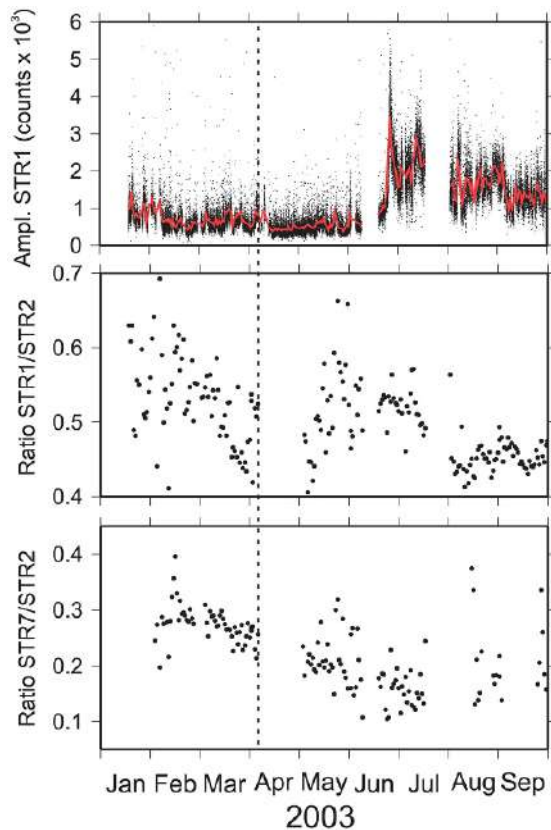


Plate 2. (top) Temporal variation of the volcanic tremor amplitude at STR1 EW component. Each single dot represents the average tremor amplitude in the time interval between two consecutive explosion quakes and in the frequency band 1–6 Hz. The red line is the daily average. (bottom) Daily average of the ratio between the volcanic tremor amplitude at STR1 EW component [570 m above sea level (asl)] and STR2 EW component (840 m asl) and between STR7 EW component (632 m asl) and STR2 EW component. The vertical dashed line marks the 5 April paroxysm.

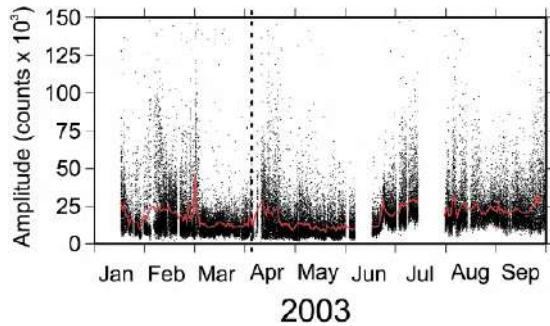


Plate 3. Amplitude of LP events at STR1 EW component. Each dot represents a single event. Note the high variability of values. Daily averages are indicated by the red line. The vertical dashed line marks the 5 April paroxysm.

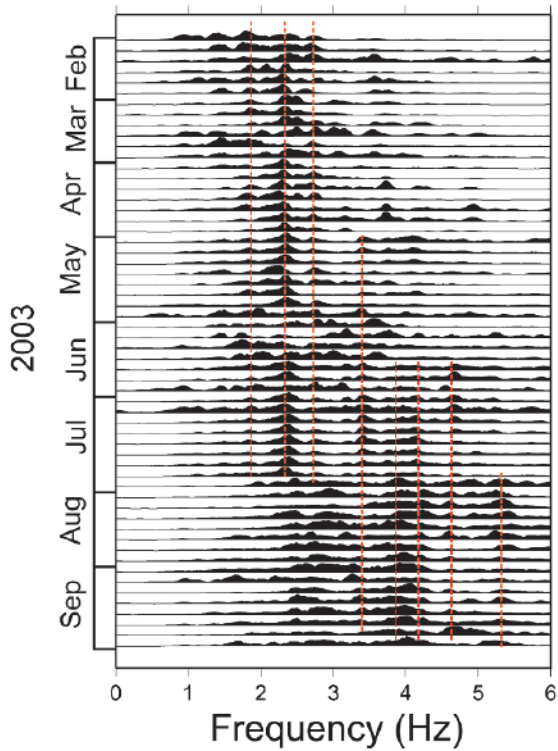


Plate 4. Normalized spectra of 58 LP events from February to September. Dashed red lines mark significant common spectral peaks.

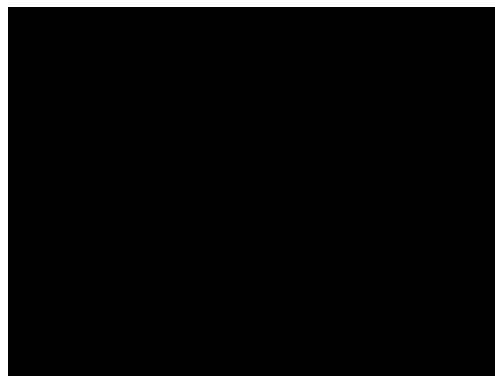


Plate 5. Complex spectral components of the same LP events as Plate 4. Each dot represents a spectral component, with its frequency (vertical axis) and quality factor (see color scale).

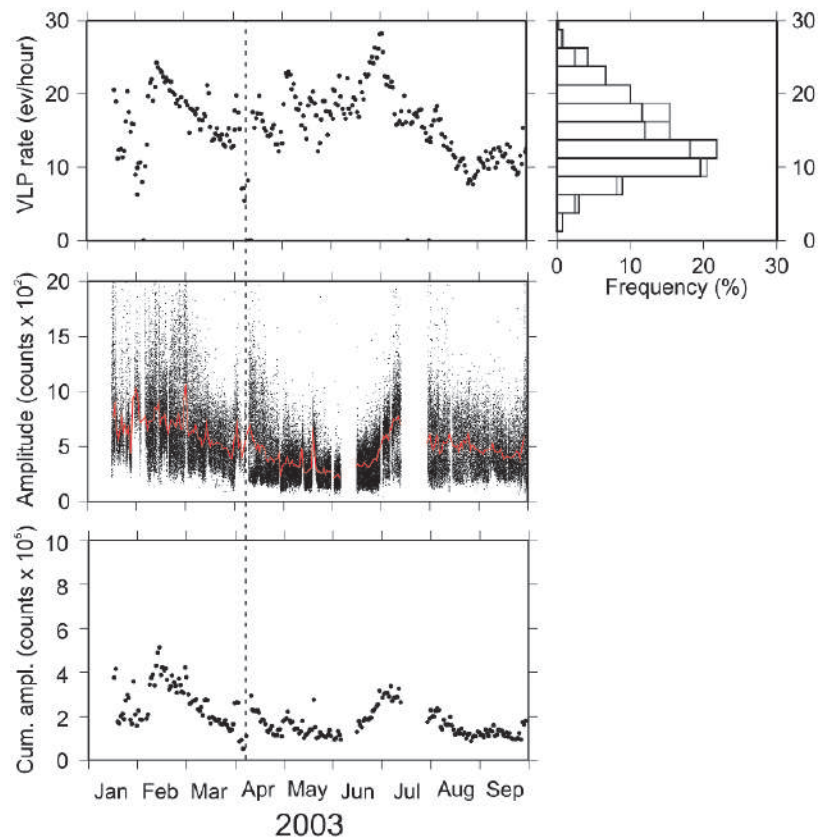


Plate 6. (top) Occurrence rate of VLP events. For comparison, the black histogram on the left is representative of the whole 2003–2008 period, while the gray histogram is representative of 2003 only. (middle) Amplitude of VLPs at station STR1 with its daily average (red line). (bottom) Cumulative daily VLP amplitude (average amplitude by VLP rate). The dashed line marks the 5 April paroxysm.

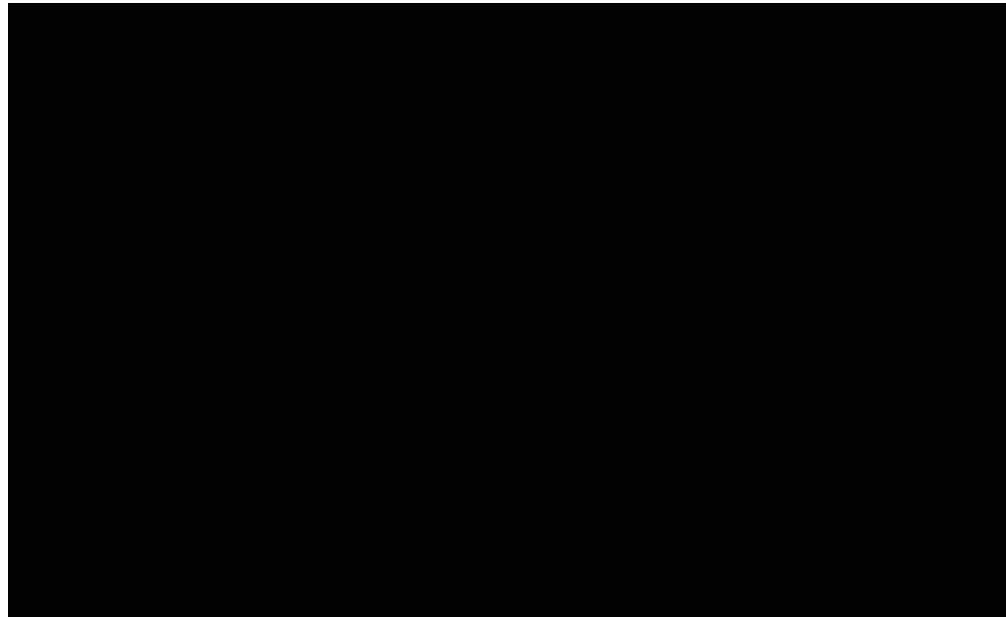


Plate 7. VLP polarization parameters for STR8 and STR9. Darker shades indicate higher concentration of values. Gray areas represent lack of data.

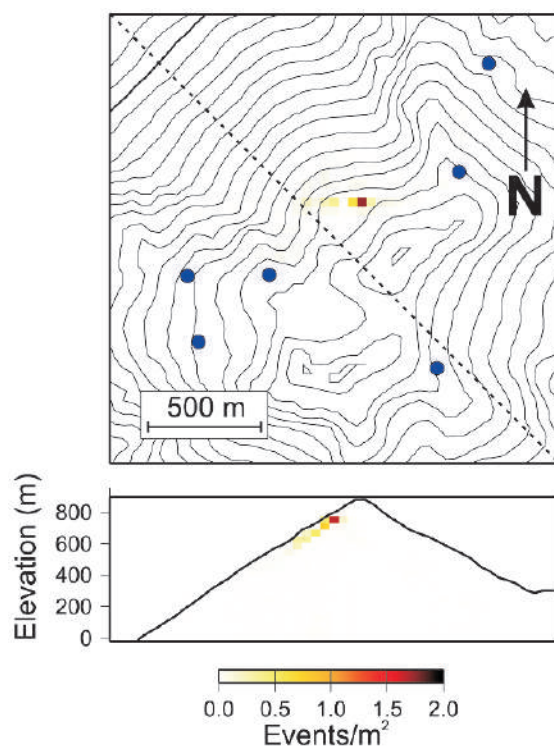


Plate 8. Locations of ~15,000 selected VLPs in the time interval February–September 2003. The upper map shows the event density projected on the horizontal plane, while the lower map shows its projection along a NW–SE cross section (dashed line). Blue dots are seismic stations (see Plate 1).

and STR9. In the period between January and March and in September, the polarization values are poorly indicative because they are affected by the low-frequency seismic noise of marine origin. At STR8, the polarization does not exhibit significant features, with a limited variation in July when the azimuth shifted of few degrees. Most of the other stations show similar patterns. The only exception is STR9, which is close to the VLP source (<500 m). Starting, at least, from June, the inclination suggests a progressive shallowing of the source. The total variation is less than 10°, suggesting a change of less than 100 m. This is confirmed by the location of ~15,000 VLPs, using the polarization, during the whole period (Plate 8). The map shows a clustering of hypocenters in a very small volume. It should be emphasized that the location shown in Plate 8 is not absolute because of the well-known problem of particle motion distortion, due to the topography [Chouet *et al.*, 2003]. A possible explanation for the VLP source shallowing can be the progressive refilling of the conduit when the lava flow ceased.

The amplitude of VLP events (Plate 6, middle) was quite high until March, then decreased until the end of June, when it increased again, together with the volcanic tremor (Plates 2 and 6).

In Plate 6 (bottom), we show the cumulative daily amplitude of VLPs (i.e., the average daily amplitude multiplied by the daily occurrence rate). The graph shows a background rate with two episodes of temporary increase, in January–March and June–August. The two episodes have a similar shape. The plateau value between April and May is the same as the one between August and September. The occurrence rates were ~20 and 10 events/hour, respectively.

Variations in the VLP amplitudes can be explained in two ways. The first is just a variation in the slug masses, while the second is a variation in the efficiency of the slug expansion mechanism. These two mechanism can act simultaneously since they are independent, the first being related to the slug formation processes occurring in the deeper part of the conduit [Burton *et al.*, 2007], while the second is related to the shallow conduit [Chouet *et al.*, 2003].

5. DISCUSSION

The most important changes in the seismicity occur at the transition from the effusive to explosive activity between June and August. This phase is marked by the clearing of the vents obstructed by debris, the rise of the magma column, and the reappearance of the genuine Strombolian activity [Calvari *et al.*, 2005; Ripepe *et al.*, 2005].

ummit craters during the effusive phase [Calvari *et al.*, 2005] seems to indicate that the debris obstructing the vent were quite permeable, allowing the transit of gases but not

the generation of significant infrasonic transients [Ripepe *et al.*, 2005]. Since the volcanic tremor and LP events were observed also during the effusive phase, the bursting of gas bubbles and slugs was also possible in an obstructed conduit probably because of the permeability of the debris plug. Instead of bursting at the magma/air interface, bubbles and slugs released gases at the magma/plug boundary with a dynamics able to generate seismic waves but not infrasonic transients.

The spectral properties of LP events during the effusive phase are quite homogeneous. Since we do not observe sudden or gradual changes in the spectra of LPs, we infer that the resonant part of the conduit has not undergone significant structural changes during this period.

During the effusive phase, the VLP event rate remained quite constant (~20 events/hour), while the amplitude decreased significantly. It is difficult to discern between a deep and shallow cause of this variation. Further seismological studies and correlations with observed gas flow rates are needed.

The vent clearing phase is marked by an increase in the amplitude of volcanic tremor and by a change in its source position. This seems to indicate that the volcano was switching back to the usual seismoacoustic mechanism, with the main source located at very shallow depth. This is supported by the variations in the LP spectra. In fact, we observe during this transition the coexistence of spectral peaks typical of the effusive phase and the waxing of others that become dominant during the following explosive phase.

The end of the effusive phase is also associated with the refilling of the shallow conduit system as evidenced by the slight rising of the VLP source centroid (Plate 7).

The 5 April paroxysm was a remarkable event from both a volcanological and a seismological point of view [Calvari *et al.*, 2006; D'Auria *et al.*, 2006]. However, the only evident variations in the seismicity were moderate increases in the LP and VLP amplitudes, lasting for a few weeks after the event (Plates 3 and 6).

Acknowledgment. We would like to acknowledge two anonymous reviewers for their valuable comments, which improved this paper.

REFERENCES

- Aki, K., and V. Ferrazzini (2000), Seismic monitoring and modeling of an active volcano for prediction, *J. Geophys. Res.*, 105(B7), 16,617–16,640.
- Burton, M., P. Allard, F. Muré, and A. L. Spina (2007), Magmatic gas composition reveals the source depth of slug-driven Strombolian explosive activity, *Science*, 317, 227–230, doi:10.1126/science.1141900.

- Calvari, S., L. Spampinato, L. Lodato, A. J. L. Harris, M. R. Patrick, J. Dehn, M. R. Burton, and D. Andronico (2005), Chronology and complex volcanic processes during the 2002–2003 flank eruption at Stromboli volcano (Italy) reconstructed from direct observations and surveys with a handheld thermal camera, *J. Geophys. Res.*, 110, B02201, doi:10.1029/2005JB003129.
- Calvari, S., L. Spampinato, and L. Lodato (2006), The 5 April 2003 Vulcanian paroxysmal explosion at Stromboli volcano (Italy) from field observations and thermal data, *J. Volcanol. Geotherm. Res.*, 149, 160–175.
- Chouet, B. (1986), Dynamics of a fluid-driven crack in three dimensions by the finite difference method, *J. Geophys. Res.*, 91(B14), 13,967–13,992.
- Chouet, B., G. Saccorotti, M. Martini, P. Dawson, G. De Luca, G. Milana, and R. Scarpa (1997), Source and path effects in the wave fields of tremor and explosions at Stromboli volcano, Italy, *J. Geophys. Res.*, 102(B7), 15,129–15,150.
- Chouet, B., G. Saccorotti, P. Dawson, M. Martini, R. Scarpa, G. D. Luca, G. Milana, and M. Cattaneo (1999), Broadband measurements of the sources of explosions at Stromboli volcano, Italy, *Geophys. Res. Lett.*, 26(13), 1937–1940.
- Chouet, B., P. Dawson, T. Ohminato, M. Martini, G. Saccorotti, F. Giudicepietro, G. D. Luca, G. Milana, and R. Scarpa (2003), Source mechanisms of explosions at Stromboli volcano, Italy, determined from moment-tensor inversions of very-long-period data, *J. Geophys. Res.*, 108(B1), 2019, doi:10.1029/2002JB001919.
- Chouet, B., P. Dawson, and M. Martini (2008), Upper conduit and explosion dynamics at Stromboli, this volume.
- D'Auria, L., F. Giudicepietro, M. Martini, and R. Peluso (2006), Seismological insight into the kinematics of the 5 April 2003 vulcanian explosion at Stromboli volcano (southern Italy), *Geophys. Res. Lett.*, 33, L08308, doi:10.1029/2006GL026018.
- Kumagai, H., and B. Chouet (1999), The complex frequencies of long-period seismic events as probes of fluid composition beneath volcanoes, *Geophys. J. Int.*, 138, F7–F12.
- Kumagai, H., and B. A. Chouet (2001), The dependence of acoustic properties of a crack on the resonance mode and geometry, *Geophys. Res. Lett.*, 28(17), 3325–3328.
- Nakano, M., H. Kumagai, M. Kumazawa, K. Yamaoka, and B. A. Chouet (1998), The excitation and characteristic frequency of the long-period volcanic event: An approach based on an inhomogeneous autoregressive model of a linear dynamic system, *J. Geophys. Res.*, 103(B5), 10,031–10,046.
- Neuberg, J., R. Luckett, M. Ripepe, and T. Braun (1994), Highlights from a seismic broadband array on Stromboli volcano, *Geophys. Res. Lett.*, 21(9), 749–752.
- Neuberg, J., R. Luckett, B. Baptie, and K. Olsen (2000), Models of tremor and low-frequency earthquake swarms on Montserrat, *J. Volcanol. Geotherm. Res.*, 101, 83–104, doi:10.1016/S0377-0273(00)001694.
- Ripepe, M., and T. Braun (1994), Air-wave phases in Strombolian explosion-quake seismograms: A possible indicator for the magma level?, *Acta Vulcanol.*, 5, 201–206.
- Ripepe, M., P. Poggi, T. Braun, and E. Gordeev (1996), Infrasonic waves and volcanic tremor at Stromboli, *Geophys. Res. Lett.*, 23(2), 181–184.
- Ripepe, M., E. Marchetti, G. Olivieri, A. Harris, J. Dehn, M. Burton, T. Caltabiano, and G. Salerno (2005), Effusive to explosive transition during the 2003 eruption of Stromboli volcano, *Geol. Soc. Am.*, 33(5), 341–344.
- Wielandt, E., and T. Forbringer (1999), Near-field seismic displacement and tilt associated with the explosive activity of Stromboli, *Ann. Geofis.*, 42(3), 407–416.

L. D'Auria, A. Caputo, T. Caputo, W. De Cesare, A. M. Esposito, F. Giudicepietro, M. Martini, R. Peluso, M. Orazi, and G. Scarpato, Istituto Nazionale di Geofisica e Vulcanologia, Sezione di Napoli, Osservatorio Vesuviano, Via Diocleziano 328, 80124 Naples, Italy. (martini@ov.ingv.it)

Fluid Circulation and Permeability Changes in the Summit Area of Stromboli Volcano

Anthony Finizola

*Laboratoire Géosciences Réunion, Université de La Réunion, Institut de Physique du Globe de Paris, CNRS, UMR 7154,
Saint Denis, La Réunion, France*

Francesco Sortino

Istituto Nazionale di Geofisica e Vulcanologia, Sezione di Palermo, Palermo, Italy

The main problem posed by the 2002–2003 eruptive crisis at Stromboli was in assessing the flank stability of the volcanic edifice. Indeed, this eruptive crisis has been characterized by important effusive and collapse events inside the Sciara del Fuoco sector collapse area: in particular, two flank sector collapses in the aerial and submarine part of the edifice and the opening of a fracture set close to gliding plane in the summit part of the Sciara del Fuoco sector collapse. Detailed fluid flow mapping and reiterative profiles carried out with self-potential, temperature, and soil gas measurements since 1994 in the Fossetta–Sciara del Fuoco–Fossa area, show the importance of old structural boundaries, such as the Large Fossa crater, in the opening of part of the 2002–2003 set of fractures. Within this structural framework, other morphological changes occurred during the eruptive crisis, such as the opening of new sets of fracture and collapse events. These were probably located along other crater boundaries formed since the largest paroxysmal event of September 1930, which dramatically modified the morphology inside the Large Fossa crater area. The multidisciplinary approach to fluid flow measurements during an eruptive crisis demonstrates the powerful potential of these techniques as a complement to deformation measurements in assessing the weakness planes of a volcanic edifice and the risk of sector collapses.

1. INTRODUCTION

Since 1994, we have conducted a water and gas flow survey at Stromboli volcano, involving self-potential (SP), temperature (T), and soil gas measurements. The aim of this multidisciplinary approach, involving geoelectrical and

geochemical techniques with a step of measurement varying from 1 to 20 m, was to study in detail the fluid flow in the summit crater area [Finizola *et al.*, 2003; Revil *et al.*, 2004], and to put it back in the general context of fluid flow at the island scale [Finizola *et al.*, 2002]. Moreover, in the summit area, a strategic profile has been reiterated since 1994 with the above-mentioned techniques to assess fluid flow variations in time. These different surveys characterized the fluid flow before the Stromboli 2002–2003 eruptive crisis.

Finizola *et al.* [2002] identified at the island scale one hydrothermal system intersected by two regional faults. In the summit (Fossa–Pizzo) area, close to the active craters, SP,

T, and CO₂ soil measurements revealed anomalies related to hot fluid migration along faults bordering the rims up today (NE and SW) of active craters, and other anomalies associated with older crater boundaries called Large Fossa crater and Pizzo crater [Finizola *et al.*, 2003; Revil *et al.*, 2004].

In January, March, and April 2003, we carried out a reiteration campaign in SP, T, and soil CO₂ measurements at Stromboli volcano to assess the disruptions in fluid flow that occurred in the summit area during the 2002–2003 eruptive crisis.

The crisis, which began on 28 December 2002, involved important changes in the eruptive activity associated with several drastic morphological changes [Bonaccorso *et al.*, 2003; Calvari *et al.*, 2005, 2006] shown in Plate 1:

1. Lava flow emission in the northern part of the Sciara del Fuoco area from an eruptive fissure that opened on 28 December 2002, and that was associated with a partial collapse of the external northern flank of the NE crater. This event was followed 2 days later, on 30 December 2002, by:

2. Two sector collapses ($\sim 20 \times 10^6$ m³) in the submarine and aerial parts of the same area of the Sciara del Fuoco [Baldi *et al.*, 2005], causing two tsunamis that damaged Piscità, Ficogrande, and Scari's houses located in the north-eastern coast of Stromboli island [Maramai *et al.*, 2005]. During the next 7 months, these two aerial sector collapses were totally refilled by the persistent effusive activity, which stopped on the 22 July 2003 [Calvari *et al.*, 2006].

3. Collapse on the inside of the summit craters, with the union of the central and NE craters, and partial collapses of the SW crater.

4. The development of a set of fractures cutting all of the Fossa area, some of them associated with vapor emission and with a maximum of horizontal and vertical displacements reaching in some points 15 and 20 cm, respectively.

Appearing at the beginning of the eruptive crisis, these different collapses and fractures posed the need to assess the flank stability of the volcanic edifice. In particular, the worst case hypothesized was the possible reactivation of the old sliding plane of the entire aerial and submarine Sciara del Fuoco sector collapse area (Plate 1). With a volume of about 1 km³ [Tibaldi, 2001], this represents 50 times the volume involved at the beginning of the eruptive crisis. Such a collapse scenario would generate a huge tsunami that could severely impact not only on the coast of Stromboli island, but also the whole Aeolian Archipelago and the Sicilian and Calabrian shores [Tinti *et al.*, 2003].

Consequently, an important volcano monitoring network was quickly developed by volcanologists and the Italian Civil Protection Institute. Plate 1 summarizes the different permanent monitoring stations used by different volcanological groups at the beginning of the crisis, including a Global Positioning System (GPS) network, an electronic distance

measurement (EDM) network, and synthetic aperture radar techniques. These reflect the importance of having volcanologists assigned to monitoring and assessing the Sciara del Fuoco flank stability. The aim of our work was to support this topic using additional parameters to monitor the evolution of the fracture set that appeared in the summit area of the volcano (Plates 1 and 2). Several techniques were used to monitor changes in soil permeability; in particular, techniques related with fluid migration such as self-potential, temperature, and soil gas techniques were applied.

Thanks to the detailed field works carried out in the summit area since 1994 [Finizola *et al.*, 2003; Revil *et al.*, 2004], a precise comparison of the fluid flow before and during the eruptive crisis has been possible. The three main topics that will be discussed in this work are: (1) the possible causes involved in the opening of the fracture system of the summit area; (2) the changes in fluid flow and heat transfer that occurred during the eruptive crisis; and (3) the strategic use of SP, T, and soil gas techniques as a complementary method to assess the flank stability of a volcanic edifice.

2. FLUID FLOW MEASUREMENT TECHNIQUES

In this section, we give a short description of the three different techniques (SP, T, and soil gas) used in this work, as related to fluid flow detection.

2.1. Self-Potential Measurement

SP consists of measuring the natural electric potential on the ground surface. In a volcanic context, this electrical potential represents the electrical field signature of some polarization mechanisms occurring at depth. These SP signals are created by electrokinetic coupling of fluid flow dragging the excess of charges located in the vicinity of the pore water/mineral interface. For silicates or aluminosilicate rocks, this electrical diffuse layer is generally positive and induces an excess of positive charges toward the flow direction [e.g., Ishido and Mizutani, 1981; Jouniaux *et al.*, 2000; Pride, 1994; Revil *et al.*, 1999a, 1999b; Lorne *et al.*, 1999a, 1999b; Revil and Leroy, 2001; Revil *et al.*, 2003a, 2003b; Ishido, 2004]. Therefore, SP is frequently used on active volcanoes to identify, through positive anomalies, uprise of hydrothermal fluids [e.g., Zablocki, 1976; Malengreau *et al.*, 1994; Lénat, 1998; Finizola *et al.*, 2002, 2003, 2004].

2.2. Temperature Measurements

At a short distance from active craters, where hot steam reaches or condenses near the surface, thermal supply is generally sufficient to support shallow hydrothermal systems.

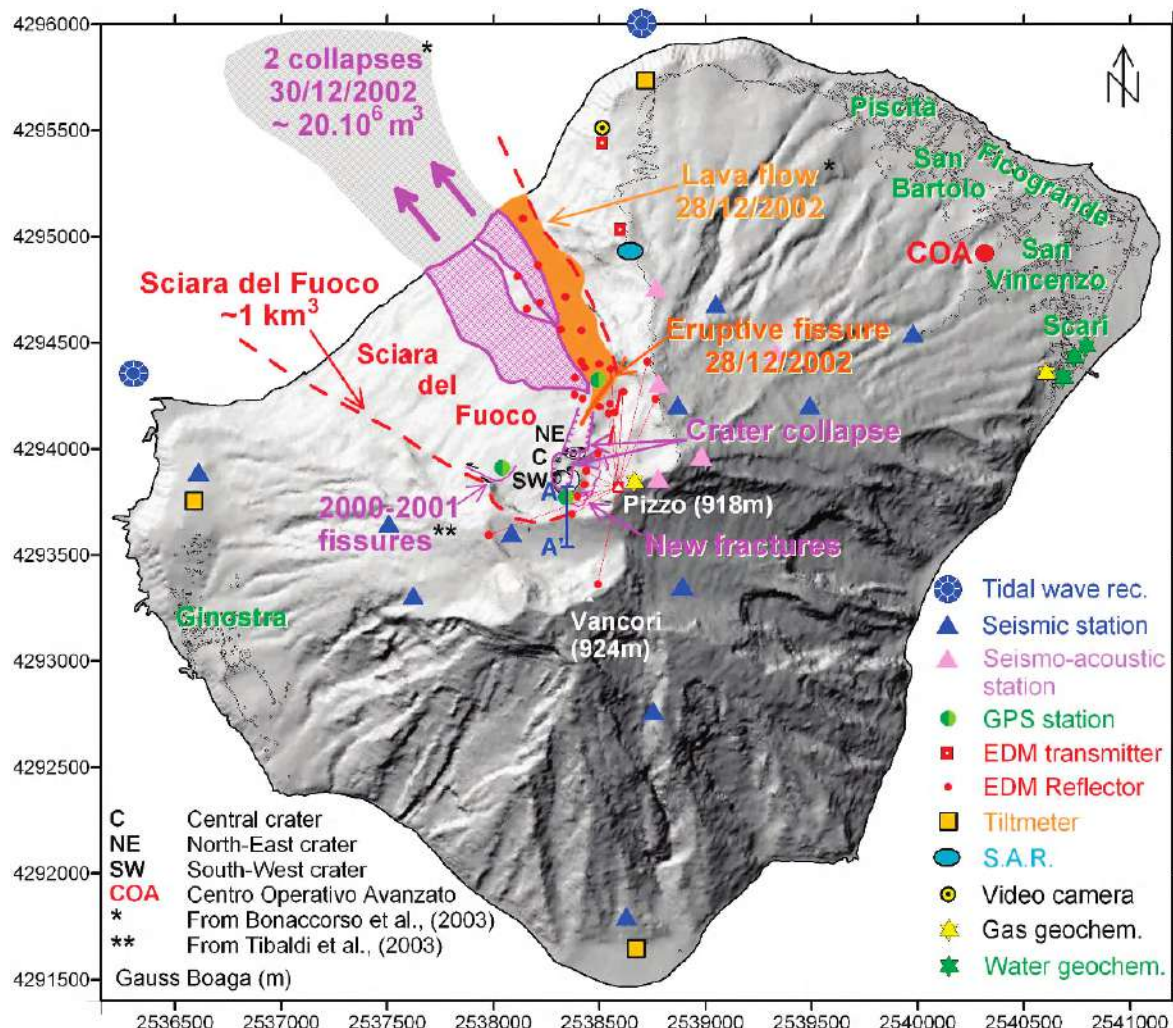


Plate 1. Shaded relief map of Stromboli island showing the effusive and collapse events that occurred at the beginning of the 2002–2003 eruptive crisis. This Plate displays the monitoring strategy used at the beginning of the eruptive crisis by the Italian volcanologists to assess flank stability in the Sciara del Fuoco sector collapse area, by way of the numerous scientific instruments located in the area. The A–A' profile corresponds to the reiterated self-potential, temperature, and soil gas measurements along a north–south direction crossing the Sciara del Fuoco sector collapse, Pizzo crater, Large Fossa crater, and SW crater boundaries.

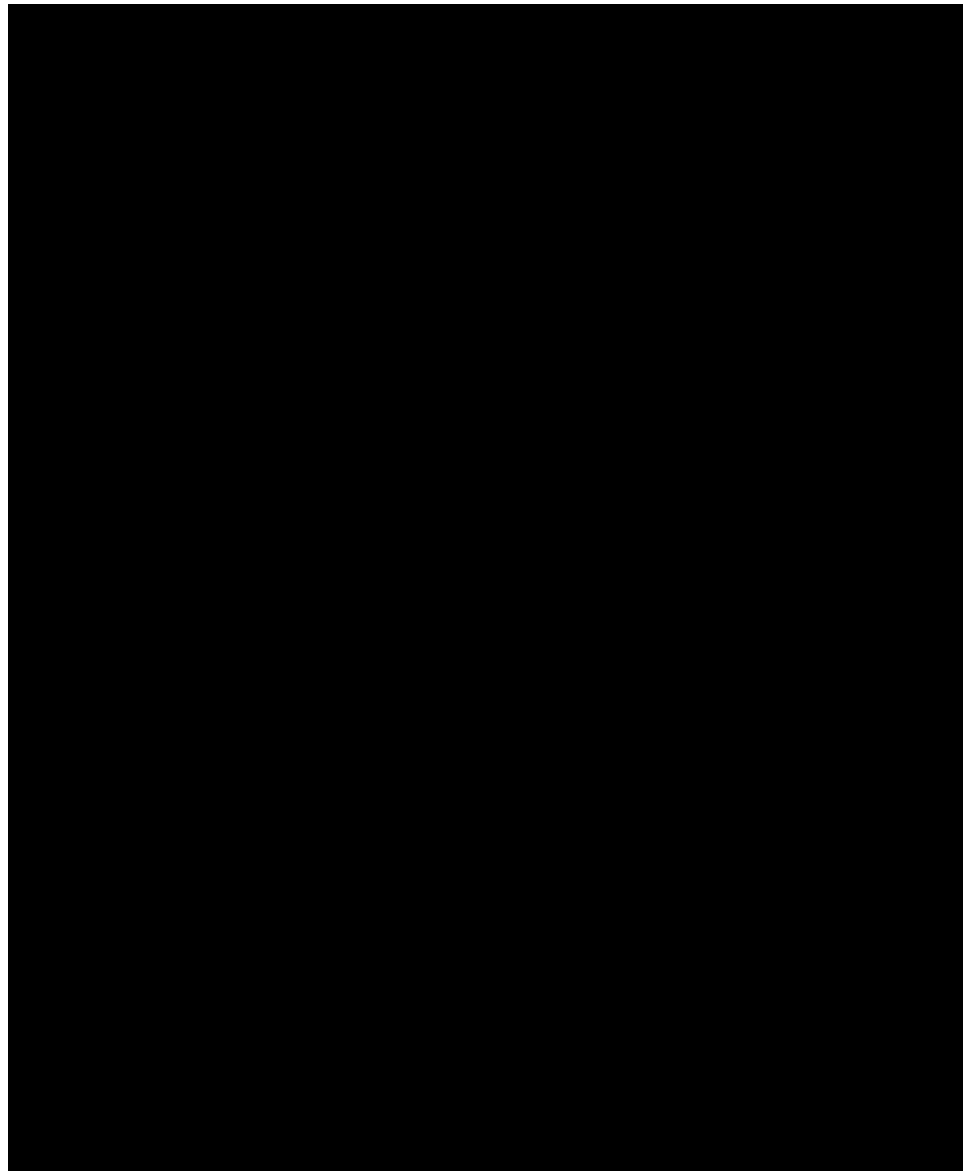


Plate 2. Photographs showing the fracture set opened in the summit part of Stromboli at the beginning of the 2002–2003 eruptive crisis. F1, F2, ..., P1, P2, ... represent the maxima of the thermal anomalies found in 1999 in the Fossa and Pizzo areas, respectively. Numbers 1–7 (in pink) in Plate 2c are outcrops also shown in Figures 3, 4, 7, 8, and 9. The A–A' profile corresponds to the reiterated self-potential, temperature, and soil gas measurements along a north–south direction crossing the Sciara del Fuoco sector collapse, Pizzo crater, Large Fossa crater, and SW crater boundaries. Numeration of the fractures is discussed in the text.

These fumarolic and subfumarolic areas have been evidenced in several surveys by temperature anomalies measured at several tens of centimeters' depth, and show a good correlation with SP maxima [Ballestracci, 1982; Nishida and Tomiya, 1987; Aubert and Baubron, 1988; Matsushima et al., 1990; Aubert, 1999; Finizola et al., 2003; Lewicki et al., 2003].

2.3. CO_2 Soil Gas Measurements

On active volcanoes, CO_2 anomalies are generally associated with highly permeable zones, which may also drain heat and other fluids. Indeed, surveys coupling soil gas and T measurements over active fissures show a good correlation between these parameters [e.g., Aubert and Baubron, 1988; Finizola et al., 2003; Lewicki et al., 2003].

3. DATA ACQUISITION

During the 2002–2003 eruptive crisis, detailed mapping of the fractures that appeared in the Fossa area was carried out in the middle of January 2003, and at the beginning of April 2003, to identify and check a possible extension of the fracture set (Plate 3). T and CO_2 soil gas measurements were also acquired inside all the fractures with a step of 5 m.

Moreover, before the eruptive crisis, SP, T, and CO_2 soil gas measurements were performed along a north–south profile (A–A' in Plates 1, 2c, and 3) in August 1994, August 1995, May 2000, May 2002, and October 2002, and reiterative profiles were carried out during the eruptive crisis in the middle of January 2003 and at the beginning of March 2003. All of the measurements were consistently taken at the same place by using benchmarks (wooden markers) installed every 5 m along the A–A' profile since 1994. SP data were acquired every 1 m, and T and CO_2 data every 2.5 m along the 315-m length of the A–A' profile.

3.1. SP Measurements

The SP equipment consisted of a high-impedance voltmeter, a pair of Cu/Cu SO_4 nonpolarizing electrodes, and an insulated electric cable. The reference potential (0 mV) was taken in the Fossetta area (A' in Plates 2c and 3), 200 m away from the huge fluid migration system of the Fossa area. The electrical contact with the ground was always good (always $<100 \text{ k}\Omega$) because moisture was consistently found a few centimeters below the surface.

3.2. T Measurements

Thermal probes and a digital thermometer were used for the ground temperature measurements. Readings were

taken to a tenth of degree. Each T measurement was taken by following four steps: (1) burrowing of a hole to a precise depth of 30 cm with a steel rod, 2 cm in diameter; (2) insertion of a thermal probe into the hole at the precise depth of 30 ± 1 cm by means of a graduated wooden stick; (3) filling and compaction of the hole; and (4) a temperature reading was taken after 10–15 min (in order to achieve thermal equilibrium).

3.3. CO_2 Soil Gas Measurements

CO_2 emanation data can be obtained by two different types of measurements: concentration and flux. Etiope et al. [1999] showed evidence that a general linear relationship exists between concentration and flux. For practical reasons (i.e., lighter weight, smaller size, lower power requirement, and cost), we chose to measure CO_2 concentrations. We discuss later the limitations of this approach, especially in areas with high permeability. In this technique, gas was pumped through a copper tube 2 mm in diameter, inserted in the soil to a depth of 0.5 m, and analyzed in the field by infrared spectrometry. The analytical uncertainty is 5% of the value.

4. RESULTS

4.1. Location of the new Fractures in the Fossa Area

At the beginning of the eruptive crisis a set of fractures appeared in the Fossa area, around the SW, central, and NE active craters (Plates 1, 2, and 3). Thus, EDM reflectors and GPS stations were installed between these fractures and the active craters (Plates 1 and 2b) to monitor their evolution in time [Puglisi et al., 2005].

Detailed mapping of these fracture systems (Plate 3), combined with data from the thermal map created in August 1999 at 30 cm depth [Finizola et al., 2003], allows us to distinguish two types of fractures:

1. A NW–SE-oriented set (A–B–C–D–E, B–Q, C–R fractures in Plate 3), perfectly superimposed on the maxima of the F1–F3 thermal anomalies identified in 1999, and defining the border of the Large Fossa crater [Finizola et al., 2003].

2. A set roughly NE–SW-oriented, not related to previously defined thermal anomalies (E–F, G–H–I, J–K–L, M–N, O–P, S–H, T–U, V–W fractures in Plate 3).

The entire opened-fracture set is located inside or along the structural boundary of the Large Fossa crater, along which fluids already migrated preferentially before the eruptive crisis (see F1, F3, and F6 T anomalies in Finizola et al. [2003]).

4.2. Fracture Mapping and T and CO₂ Measurements Along the Open Fractures in January–April 2003

4.2.1. Reiterative mapping of the fractures. The reiteration between the middle of January and the beginning of April 2003 of the detailed fracture mapping shows, in less than 3 months, a lateral extension of about 10 m at the end of numerous fractures (see blue segments in A, E, F, G, J, L, and S in Plate 3), and also the appearance of a new fracture (X-Y in Plate 3).

4.2.2. T measurements along the fractures. A comparison between T measured in August 1999 in the Fossa area (background of Plates 4a and 5) and T measured in January 2003 along the fractures (color dots in Plate 4a) shows a significant increase at several points in the Fossa area. These temperature changes, from August 1999 to January 2003, can be more easily compared in Plate 5 along the profile cutting the A-B-C-D-E-F-G-H-I-J-K-L-V-W fractures. In the southern part of the Fossa area, a T increase from 45°–55°C to more than 90°C can be noted, whereas in the northern part, the “cold zone” defined in 1999 [Finizola *et al.*, 2003], have been observed only seasonal variations of temperature.

Between the middle of January 2003 (Plates 4a and 5) and the beginning of April 2003 (Plates 4c and 5), the T went on increasing along several fractures in the southern part of the Fossa area (e.g., T-U and S-H in Plate 4c), whereas T remained cold in the northern cold zone.

The increase in T in the southern part of the Fossa area is in good agreement with continuous data recorded by a temperature monitoring system installed near the F1 anomaly from March to May 2003. This also revealed a general increase in temperature at 30 cm depth of more than 20°C between March and the beginning of April 2003.

4.2.3. CO₂ measurements along the fractures. The CO₂ soil concentrations measured along the fractures in the middle of January and at the beginning of April 2003 (Plates 4b, 4d, and 5) display always high concentrations throughout the Fossa area, except in the cold zone which remained permanently impermeable to gas ascent. It is important here to keep in mind that the measured parameter is CO₂ concentration and not CO₂ flux.

4.3. SP, T, and CO₂ Reiteration Along the A–A' Profile

Measurements of SP, T, and CO₂ soil concentration have repeatedly been recorded along the A–A' profile since August 1994. This profile (Plates 2 and 3) strategically crosses four structural boundaries that preferentially direct the shallow fluid migration close to the active crater area: (1) the SW

crater, (2) the Large Fossa crater, (3) the Pizzo crater, and (4) the Sciara del Fuoco sector collapse [Finizola *et al.*, 2003; Revil *et al.*, 2004]. To simplify the description and interpretation of the A–A' profile, it has been subdivided into nine sectors delineated by CO₂ soil gas concentrations (Plate 6): sectors 2, 4, 6, and 8 correspond to higher CO₂ concentration, and the intermediate sectors to lower CO₂ concentration.

4.3.1. SP measurements. SP measurements were reiterated from August 1995 to March 2003 along the A–A' profile. During this period, the SP data (Plate 6) display no significant variation in the southern part of the profile (sectors 5–9). In contrast in the northern part of the profile, a huge variation in the SP signal can be noted, especially in sectors 4 and 2 associated with the F1 and F2 T and CO₂ anomalies, respectively. In January 2003, the highest SP value (F1 anomaly) measured in the same place in 1995 and 2000 (boundary between sectors 4 and 5) shifted by 12 m to the north, making a striking superposition between SP, T, and CO₂ maxima and the A-B fracture (Plates 2 and 3) that appeared at the beginning of the 2002–2003 eruptive crisis.

In March 2003, SP values for the F1 and F2 anomalies were the highest levels ever recorded. In particular, in sector 2, the F2 anomalies changed through time from an SP minimum (1995–2000) to an SP maximum (2002–2003).

In sector 1, we observed a decrease in SP values between January and March 2003.

4.3.2. T measurements. F1 and F2 anomalies (sectors 4 and 2, respectively, in Plate 6) display no significant change in T maxima before and during the eruptive crisis, whereas in December 2002, the A-B opened fracture appeared exactly on the T maximum of the F1 anomaly. A slight increase in T, SP, and CO₂ was observed at the X-Y fracture between January–March 2003.

The T profiles also reveal a reduction in the width of the F1 and F2 anomalies between 1994–1995 and 2002–2003. Also, in sector 3, the T measured in 1994–1995 are about 20°–30°C higher than the T measured in 2002–2003. Although T in the first period were measured in August and in the second period in January, March, and May, the variations cannot be explained by seasonal variations alone. This aspect will be discussed later.

During the eruptive crisis (between January and March 2003), sector 1 displays a sharp T decrease of more than 20°C. For cold temperature areas (sectors 6, 7, 8, and 9) outside of the preferential F1 and F2 fluid rising systems, the differences observed are clearly due to seasonal variations.

4.3.3. Soil CO₂ measurements. For CO₂ soil concentration measurements, the main changes occurred in sector 7 (Plate 6).

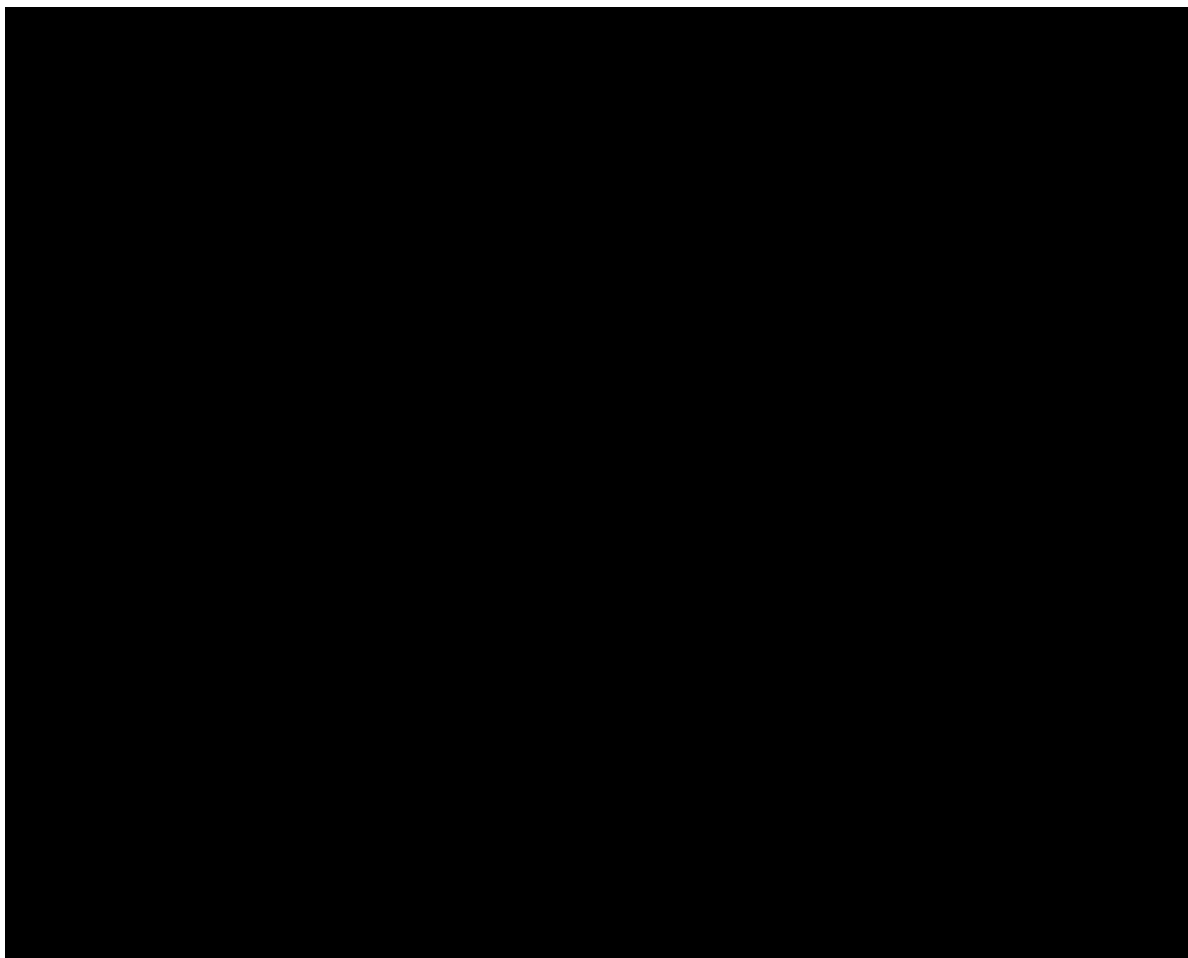


Plate 3. Map of the new set of fractures for January and April 2003 superimposed on the thermal map at 30 cm depth carried out in August 1999 with structural boundaries inferred by self-potential, temperature, and soil-gas measurements [modified from Finizola *et al.*, 2003]. F1, F2, ..., P1, P2, ... represent the maxima of the thermal anomalies detected in 1999 in the Fossa and Pizzo areas, respectively. Numbers 1–7 (in pink) are outcrops. The A–A' profile is as in Plate 2.

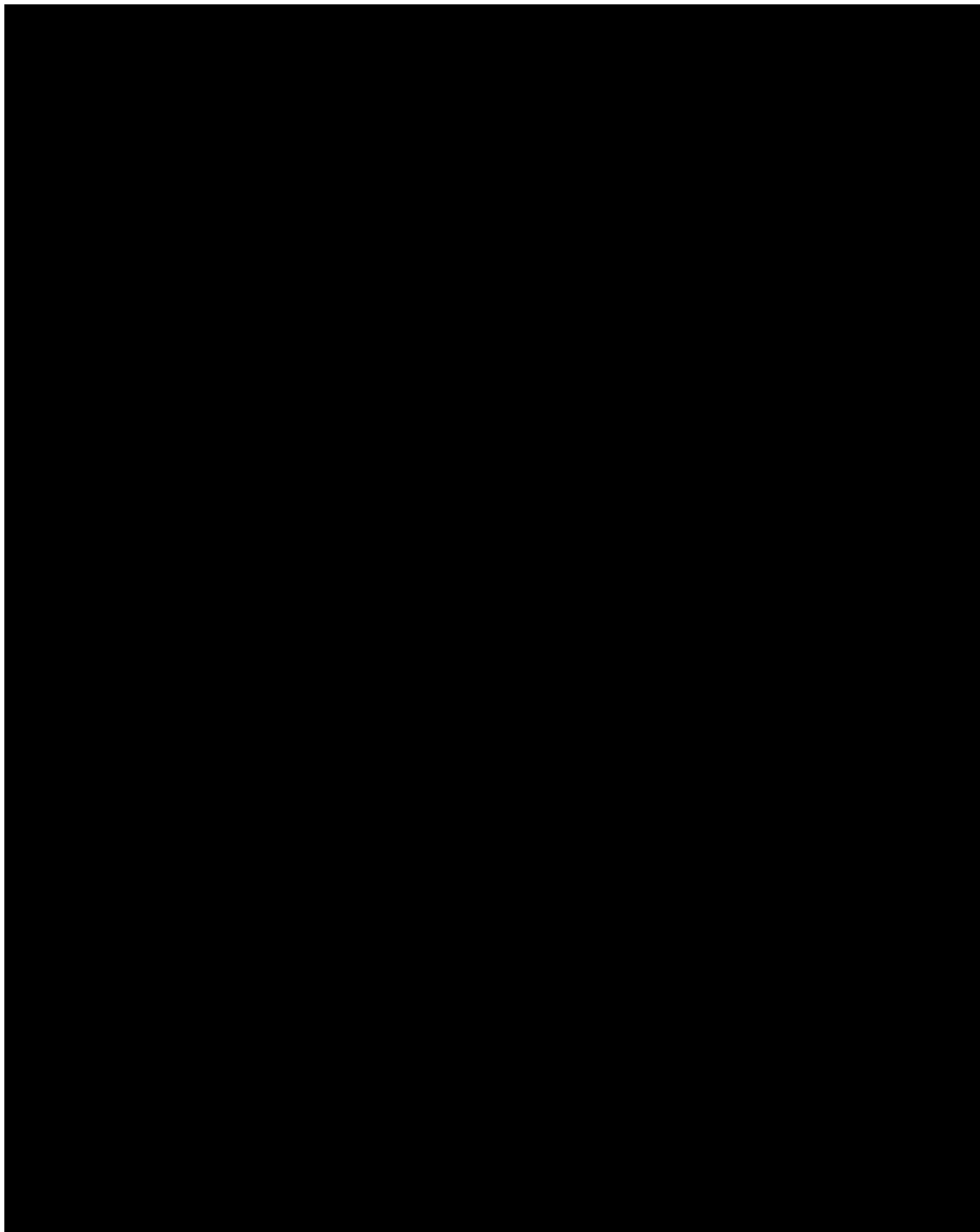


Plate 4. Thermal measurement sites at 30 cm depth and CO₂ concentration measurements (colored dots) carried out along the opened fracture system in January and April 2003 superimposed on the thermal map at 30 cm depth carried out in August 1999 [modified from *Finizola et al.*, 2003]. (a) Temperature measurements in January 2003. (b) CO₂ measurements in January 2003. (c) Temperature measurements in April 2003. (d) CO₂ measurements in April 2003. F1, F2, ..., P1, P2, ... represent the maxima of the thermal anomalies encountered in 1999 in the Fossa and Pizzo areas, respectively. Numbers 1–7 are outcrops (pink). The A–A' profile is as in Plate 2.

In October 2002, before the eruptive crisis, two distinct CO₂ peaks were identifiable, coinciding with the Sciara del Fuoco sector collapse boundary (sector 8) and the rim of Pizzo crater (sector 6). These two peaks were separated by very low CO₂ concentrations, showing a preferential gas migration along these two structural boundaries. In January 2003, a sharp increase in CO₂ concentrations occurred in the space between the two structural boundaries, removing the previous recognition of two distinct anomalies. The data acquired in March 2003 display a general decrease in CO₂ concentration along the entire profile, but no important variations have been detected at the top of the F1 and F2 anomalies. Stability in the maximum CO₂ peaks on F1 and F2 anomalies is mainly due to the saturation of the signal, because the parameter measured is CO₂ concentration (buffered, by definition, close to 100%) and not CO₂ flux. This shows the limitations of using CO₂ concentration versus CO₂ flux as the concentration signal can reach saturation level (i.e., 100%) in case of very high ground permeability. However, for lower ground permeability, such as in sectors 1, 3, and 5–9, the dynamics of the CO₂ concentration signal can be easily observed.

5. INTERPRETATION AND DISCUSSION

The data acquired before and during the 2002–2003 eruptive crisis allows discussion of three main questions:

1. What are the parameters involved in the opening of the fracture system across the Fossa area?
2. What changes occurred in fluid flow and heat transfer during the 2002–2003 eruptive crisis, and what are the consequences in terms of volcanic hazards?
3. How can SP, T, and soil gas techniques be strategically implemented to monitor the fracture system of a volcanic edifice?

5.1. Changes in Fluid Flow and Heat Transfer Along the Summit Fractures During the Eruptive Crisis

The reiteration of SP, T, and CO₂ soil gas measurements along the A–A' profile allow better understanding of the parameters involved in the morphological changes that occurred during the 2002–2003 eruptive crisis.

The most striking result obtained by contemporaneously using these three techniques is that the different methods do not always reveal the same variations through time. Considering that all of the methods are sensitive to fluid flow (liquid or gas), the main problem is therefore to understand why the different types of signal variations observed are not always comparable.

During the eruptive crisis, three geographic areas with high variations in SP, T, and/or CO₂ soil gas signal were observed (Plate 6):

1. Sector 7, corresponding to the southern Sciara del Fuoco sector collapse boundary;
2. Sectors 4 (F1) and 2 (F2) corresponding respectively to the fracture area and to the upper external flank of the SW crater;
3. Sector 1 corresponding to the inner flank of the SW crater.

(1) In January 2003, sector 7 was characterized by a drastic increase in CO₂ soil gas concentration in comparison to the October 2002 measurements, but without significant change in SP or T signals. Because we are dealing with CO₂ concentration and not flux, two hypotheses can be suggested to explain these observations: (a) an increase in CO₂ concentration in the magmatic source or (b) an increase in permeability in sector 7. The first hypothesis can be dismissed because an increase in CO₂ concentration from a magmatic source would affect also the neighboring sectors 7. Therefore, this increase in CO₂ concentrations between the Sciara del Fuoco sector collapse and Pizzo crater can be explained by an increase in permeability in this area. This suggests that the southern Sciara del Fuoco sector collapse area has probably been slightly affected by the two collapses that occurred in the northern part of the Sciara del Fuoco on 30 December 2002 (Plate 1).

The data acquired in March 2003 show a general decrease in CO₂ concentration along the entire profile, which can be interpreted as:

- A lower input of CO₂ coming from depth;
- Dilution of CO₂ rich gases by water vapor or atmospheric air.

According to the SP and T measurements taken before and during the eruptive crisis, no significant changes were observed in sector 7. This suggests that the increase in permeability was sufficient to allow higher gas flux transfer, but not enough to allow also higher liquid transfer in this area. This difference in gas and water transfer according to rock permeability will be discussed in more detail in the section dealing with monitoring techniques.

(2) Since January 2003, sectors 4 and 2 have been characterized by a sharp increase in SP values, reaching highest levels ever recorded in March 2003. This result agrees with the general lengthening of the fracture system in the Fossa area observed between January and April 2003 (Plate 3). These fracturing processes induced a permeability increase during the first months of the 2002–2003 eruptive crisis allowing a major water/steam flux to reach the surface and therefore

generate a higher amplitude streaming potential signal along the fracture system. The SP data show that not only the fractures of the F1 anomaly (Plate 6) showed a permeability increase during the eruptive crisis, but the same was also true for the F2 anomaly (Plate 6), which was not affected at the surface by visible fracture system. As described in Chapter 5.1, F1 and F2 anomalies are each supposed to be expression of a double fracture system related respectively to (1) the Large Fossa crater and the 1930s crater boundary and (2) the 1934–1950s crater and the SW crater boundary (Plate 6). According to the SP maximum peaks that can be observed at each of these four structural boundaries, it can be hypothesized that during the first months of the eruptive crisis the permeability increased along all of these limits (Plate 6) [Rittmann, 1931; Bullard, 1954].

However, this general increase in permeability and fluid flow rising along the fracture system during the first months of the eruptive crisis could appear inconsistent compared with T data; whereas SP data display an increase in the amplitude of SP anomalies, T anomalies do not display any significant variation in amplitude for the same F1 and F2 anomalies. This absence of increase in the amplitude of T anomalies can be easily explained by considering the presence of a hydrothermal system [Finizola *et al.*, 2003] between the magma body and the surface, buffering the T maximum at a T not exceeding the boiling point of water.

Looking in more detail at the SP and T signals (Plate 6), two striking characteristics appear. (1) The first concerns the F2 SP anomaly where the signal has been inverted from a minimum between August 1995–May 2000 to a maximum peak between May 2002–March 2003 period. (2) The second concerns the width of the F1 and F2 T anomalies, which showed a significant decrease between the August 1994–August 1995 period and the May 2002–March 2003 period.

In hypothesizing a common phenomenon to explain these two results, drastic changes in fluid flow and heat transfer should be considered during May 2000–May 2002, before the 2002–2003 eruptive crisis.

To explain the change observed in the F2 SP anomaly, an inversion in fluid flow direction could be suggested; during the period August 1995–May 2000, a preferential water infiltration system dragging down positive charges along this structural boundary could be responsible for the SP minimum, whereas since May 2002, the SP maximum could be induced by a preferential fluid rising system dragging positive charges toward the surface. Such a drastic change in fluid flow could be the consequence of a permeability increase along this structural boundary between May 2000 and May 2002, thereby allowing major heat transfer along this boundary.

The hypothesis of a permeability increase along the structural boundaries associated with F1 and F2 anomalies can

also explain, by changes in heat transfer, the decrease in width of the F1 and F2 T anomalies also observed after May 2000–May 2002. Considering that the heat transfer of hydrothermal systems is through both transport by advection and also release by steam condensation [Chiodini *et al.*, 2005], an increase of permeability will involve an easier heat transfer toward the surface. However, above a threshold of permeability, part of the advection can reach the surface and the atmosphere, and in this case, the energy coming from steam condensation will be released outside of the soil and will not heat the system. In this case, for a major rising fluid flow, the width of the associated T anomalies will be smaller and the temperature minimum between the two anomalies will be also lower because part of the steam condensation energy will be lost in the atmosphere. Hence, a hypothesis of permeability increase along the F1 and F2 anomalies between May 2000 and May 2002 can explain both SP and T changes observed after this period.

Moreover, the above hypothesis agrees with the opening of fractures observed 300 m lower, in the Sciara del Fuoco area, between November 2000 and April 2001 exhibiting a maximum total of 45 cm of pure dilatation [Tibaldi *et al.*, 2003].

It is interesting to note on the T and CO₂ maps from January and April 2003 (Plate 4) that T propagation along the fracture system was slower than CO₂ propagation. Indeed, by January 2003 the values of CO₂ (Plate 4b) were already high and very similar to those of April 2003 (Plate 4d), whereas for the T maps, a significant T increase was observed between January 2003 (Plate 4a) and April 2003 (Plate 4c). This time delay for T propagation in a fractured system in comparison to CO₂ ascent could be explained by considering that the heating processes of hydrothermal systems near the surface also involves an important contribution of heat conduction [Chiodini *et al.*, 2005], and this needs more time to propagate heat throughout the entire fracture system.

(3) From January to March 2003, we also observed a sharp decrease in SP and T measurements inside the SW crater (sector 1 in Plate 6). This result is probably related to a cooling phenomenon inside the SW crater, due to descent of the magma (the heat source) inside the conduits to sustain lower-elevation lava flows in the Sciara del Fuoco area.

The reiteration of SP, T, and soil gas measurements before and during the 2002–2003 eruptive crisis along the A–A' profile allowed us to identify that:

- The two important collapse events that occurred on 30 December 2002 in the northern part of the Sciara del Fuoco sector collapse area increased the permeability of the southern part of the Sciara del Fuoco area

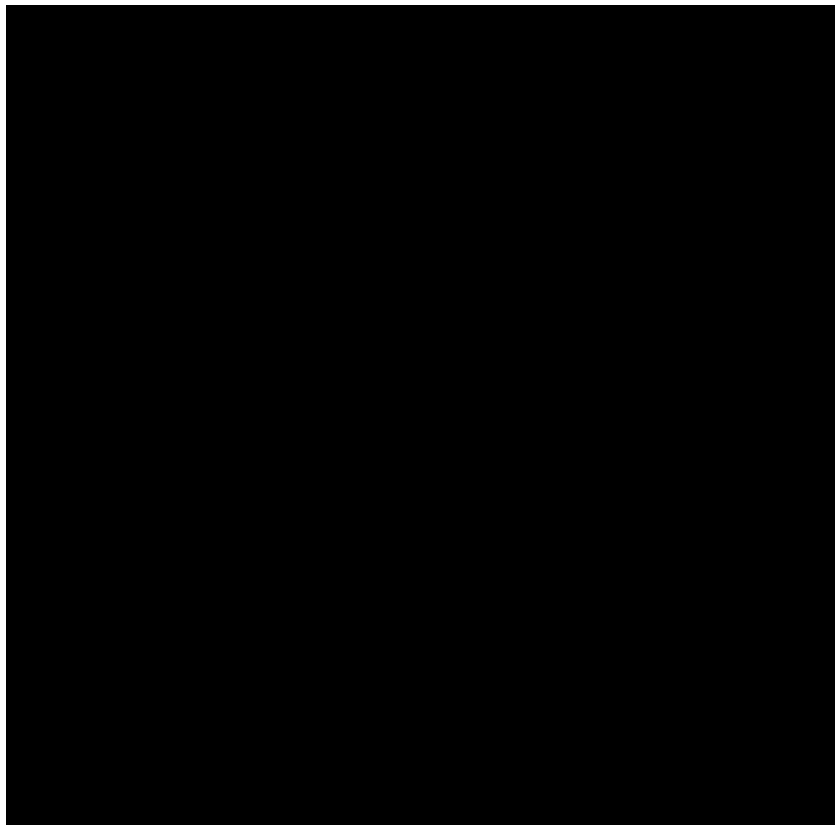


Plate 5. Reiteration in January and April 2003 of temperature (at 30 cm depth) and CO₂ soil concentration measurements along the new fractures crossing the entire Fossa area.

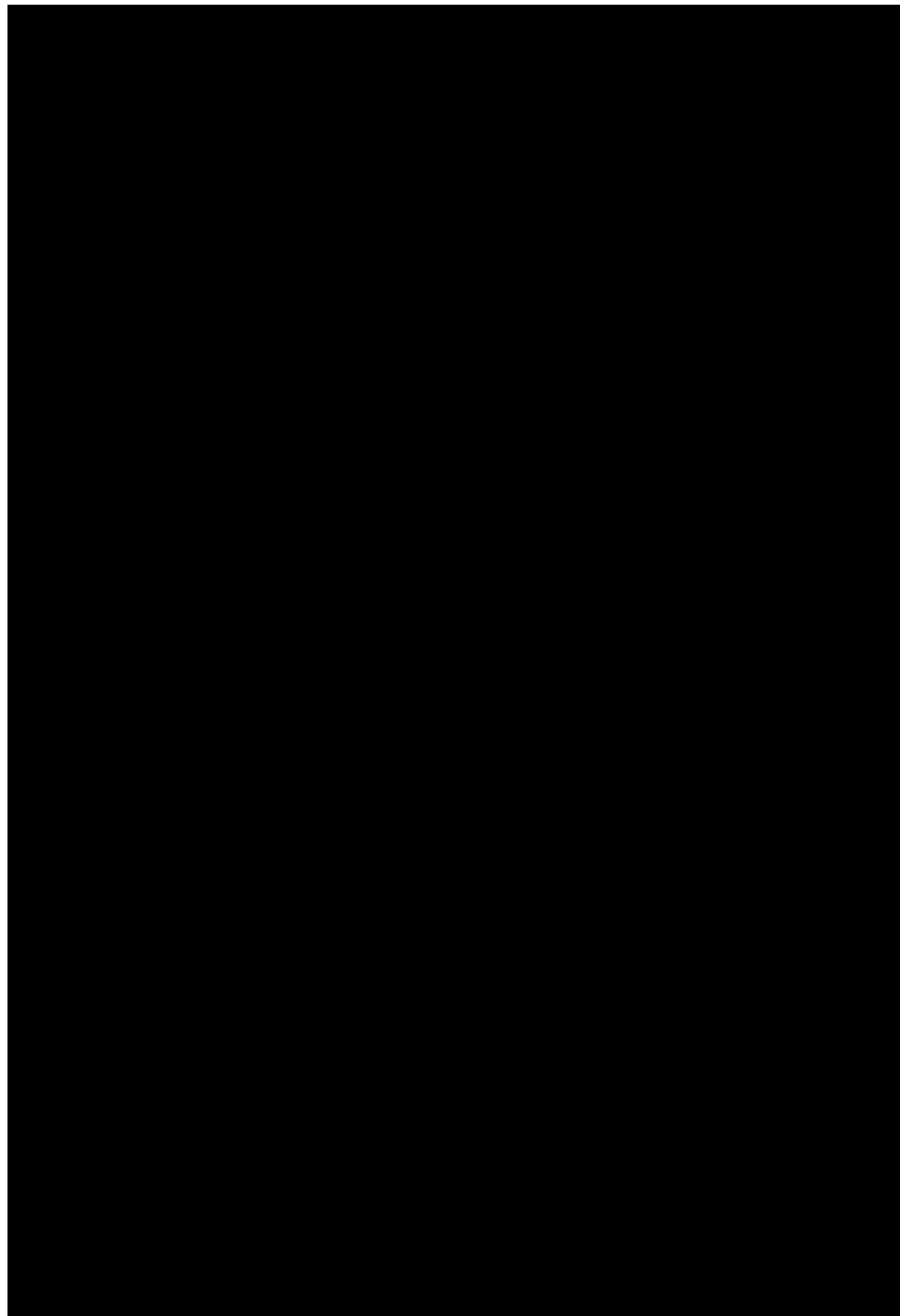


Plate 6. Reiteration of self-potential, temperature (at 30 cm depth), and CO₂ soil concentration measurements along the A–A' profile shown in Plates 1, 2, and 3, before and during the 2002–2003 eruptive crisis. Sectors 1 to 9 are discussed in the text.

- in January 2003, but this phenomenon subsequently stopped, according to the March 2003 data set.
- b) In the Fossa area, the F1 and F2 anomalies identified since 1994 have both been affected by a double fracture system related to crater boundaries, increasing their permeability from January to March 2003.

In terms of the collapse hazard, this means that the southern Sciara del Fuoco collapse has been slightly affected by this eruptive crisis. However, the higher permeability in January 2003 stopped increasing in the southern Sciara del Fuoco area, whereas the fracture phenomenon of the Fossa area remained active, increasing from January to March 2003. According to the evolution in permeability of the structural boundaries in the summit area during the first months of the eruptive crisis, it can be hypothesized that the most probable collapse event would be linked to the collapse of old crater boundaries inside the Fossa area rather than the destabilization of the entire Sciara del Fuoco area. However, the increase in permeability in the southern part of the Sciara del Fuoco sector collapse area at the beginning of the eruptive crisis, and the potential consequences of a such a collapse event in terms of tsunami generation affecting all of the Tyrrhenian sea coasts, suggest the need for a permanent monitoring system in this area.

Our SP and T results also show changes in fluid flow and heat transfer that reveal an increase in permeability along the main structural boundaries of the Fossa area during the period of May 2000–May 2002, before the 2002–2003 eruptive crisis. This agrees with the opening fractures observed in the upper southern part of the Sciara del Fuoco area by *Tibaldi et al.* [2003]. These events revealed, even before the 2002–2003 eruptive crisis, the importance of the instability processes in the upper southern part of the Sciara del Fuoco area.

5.2. Use of SP, T, and Soil Gas Methods as a Fracturing Monitoring Technique

The contemporaneous use of different methods such as SP, T, and soil gas measurements appears to be a powerful tool for assessing the evolution of permeability of a fracture system. The multidisciplinary approach applied here before and during the Stromboli 2002–2003 eruptive crisis revealed three interesting aspects from a monitoring point of view: (1) the identification before a collapse event of the weakness planes of a volcanic edifice, (2) the importance in the location of the different sensors for a monitoring system installation, and (3) the complementary aspect of the three techniques for interpreting fluid flow variations.

(1) The different works carried out in the Fossa area before the eruptive crisis [*Finizola et al.*, 2003; *Revil et al.*, 2004] identified precisely through SP, T, soil gas, and high-resolution resistivity tomography the main drains for fluid migration.

The comparison in Plate 7 between the high-resolution resistivity tomography carried out along the A–A' profile in May 2002 before the eruptive crisis [*Revil et al.*, 2004], and the fracture system opened during the 2002–2003 eruptive crisis, shows that the two areas that played a major role during the eruptive crisis both correspond to drastic transitions in resistivity (sector 4 with the opened fractures and sector 7 with the increase in permeability, see Plate 6). These, both of which are related with structural boundaries, subdivide areas with high differences in permeability representing weakness zones of a volcanic edifice.

(2) A detailed identification of these weakness zones through SP, T, soil gas, and resistivity tomography surveys is of utmost importance for the installation of a permanent monitoring system:

a) For SP monitoring, it is only at the maximum at these anomalies that the dynamics of the signal can be recorded (F1 and F2 anomalies in Plate 6). Note that 20 m south of the F1 anomaly, corresponding to the opened fracture area, the SP signal remained unchanged both since 1995 and during the eruptive crisis. This surprising result emphasizes the fact that the installation of an SP network on an active volcano to monitor permeability and steam flux variations needs a previous detailed SP survey in order to accurately install the monitoring electrodes over the anomalies. Consequently, these electrodes must be able to resist temperatures up to 100°C, which is not a characteristic previously considered in the construction of traditional SP monitoring electrodes [*Perrier et al.*, 1997; *Petiau*, 2000]. Hence, a new generation of SP electrodes for hydrothermal system monitoring applications needs to be developed. Moreover, our SP data set acquired during the 2002–2003 eruptive crisis also shows that at small distances (several tens of meters) from a major active fracture (e.g., sector 5 in Plate 6), the SP signal remained stable in time throughout the eruptive crisis. Note that the SP reference electrodes were positioned at A', located in the cold Fossetta area, 315 m away from the beginning of the profile (sector 1 in Plate 6). That means that for a permanent SP hydrothermal system monitoring application, only a small distance between the two electrodes can be sufficient to have relative stability of the reference electrode in order to measure the dynamics of the SP signal over

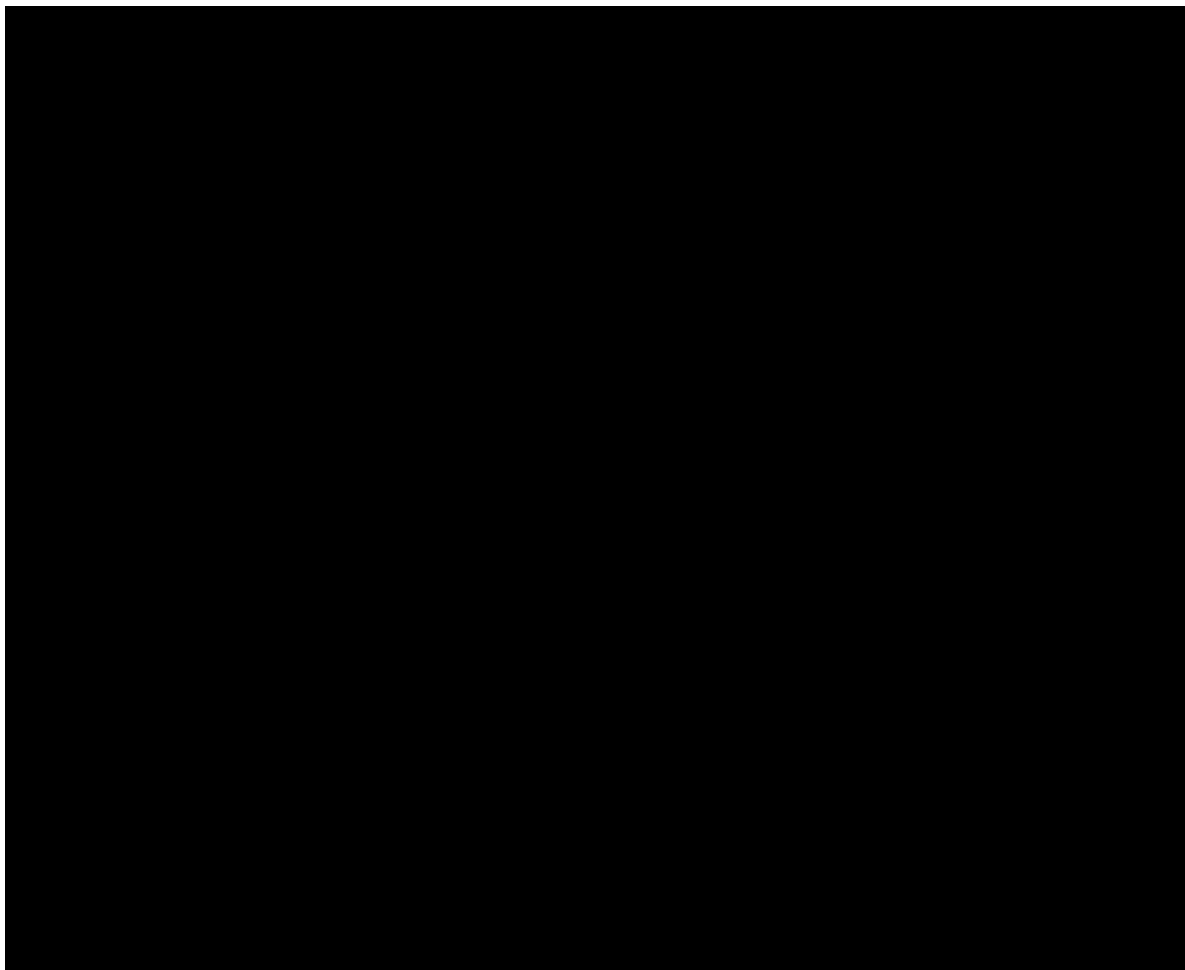


Plate 7. Correlation between old structural boundaries and the opened fractures in the Fossa area during the 2002–2003 eruptive crisis. Note that the Large Fossa crater and the 1934–1950s crater boundary have been defined from self-potential and temperature measurements [Finizola *et al.*, 2003], whereas the 1930s crater boundary comes from the correlation between the 2002–2003 opened fractures and the sketch map of Rittmann [1931].

- the SP anomalies, as generated by the hydrothermal up flow.
- b) For T measurements, in the presence of a hydrothermal system the sensors' installation at the top of the anomalies would not be of high interest. Indeed, as hydrothermal systems buffer the temperature at the boiling point of water, it is better to install a temperature flux monitoring system in warm areas (40° – 70°C), rather than at the top of the anomalies.
 - c) CO_2 soil gas concentration monitoring can be used to detect changes in areas of lower permeability. At the top of the anomalies, the CO_2 signal may be buffered by the concentration of the gas. This problem can be solved by monitoring the CO_2 flux instead of CO_2 concentration. However, the measurement of soil gases in areas such as F1 or F2 anomalies, characterized by high steam flux, would pose a lot of technical problem, in order to filtrate the water component, for instance. As a consequence, the CO_2 soil gas monitoring technique appears to be the best method to control permeability variations in areas of weaker degassing.

(3) Our multidisciplinary data set involving SP, T, and CO_2 data also demonstrates the complementary aspect of these three techniques in terms of their different indicators of permeability increase. Indeed, for the lowest permeability increase at depth, soil gas appears as the most sensitive technique to assess these variations. Then, for higher permeability increases, allowing a steam rising system at depth, SP can record an associated signal. Finally, if the permeability increase reaches the subsurface, T increases can also be detected.

Therefore, the systematic application of these three techniques on areas that can be affected by fracture systems (e.g., sector collapse areas) appears to be a powerful tool for detecting changes in permeability, due to the propagation of creeping phenomenon at depth, even before observing a displacement at the surface.

6. CONCLUSION

The combination of geoelectrical, temperature, and soil gas techniques both before and during the 2002–2003 Stromboli eruptive crisis showed that the heterogeneity of the Fossa area in terms of old structural boundaries plays a prominent part in the opening of fractures and in the collapse of several areas.

The use of these three techniques before the 2002–2003 eruptive crisis revealed the most permeable areas corresponding to the weakness planes of the volcanic edifice, which later evolved in opened fractures during the eruptive

crisis. These methods also showed the permeability changes during the eruptive crisis, and the related disruptions in fluid flow transport along several structural boundaries.

As shown in this survey, the identification of strategic areas in which to install a permanent monitoring system, where the dynamics of the signal is significant during an eruptive crisis, requires previous detailed mapping of the upper part of a volcano using these three techniques.

Therefore, fluid circulation surveys from geoelectrical, temperature, and soil gas measurements appears to be a powerful tool in recognizing (1) from a structural viewpoint, discontinuities inside a volcanic edifice involving differential fluid flow pathways, and (2) from a sector's collapse hazard assessment viewpoint, areas of lower coherency that represent a higher risk in favoring sliding planes.

Acknowledgments. We are grateful to the Italian Civil Protection Institute in providing us the great support of the Air Walser helicopter during the 2002–2003 eruptive crisis. The three field campaigns carried out in 2003 have been supported by Italian Civil Protection Institute funding. A. F. acknowledges the “Conseil Régional d’Auvergne” in France for a research grant during 2002–2003 period, and particularly thanks Jean Todt (sports director of Formula One Scuderia Ferrari), Giancarlo Minardi (director of the Minardi Formula One team), Flavio Briatore (ex-director of the Formula One Benetton team), and Marc Demougeot (director of Sparco-France) for their help in obtaining Formula One fireproof equipment. Without it, measurements near the active craters during the 2002–2003 eruptive crises could not have been carried out for security reasons. The authors wish to thank Nicolas Fournier and James Cowlyn for constructive comments and corrections on the English on earlier versions of this manuscript. This is IPGP contribution number 2382.

REFERENCES

- Aubert, M. (1999), Practical evaluation of steady heat discharge from dormant active volcanoes: Case study of Vulcano fissure (Mount Etna, Italy), *J. Volcanol. Geotherm. Res.*, 92, 413–429.
- Aubert, M., and J. C. Baubron (1988), Identification of a hidden thermal fissure in a volcanic terrain using a combination of hydrothermal convection indicators and soil-atmosphere analysis, *J. Volcanol. Geotherm. Res.*, 35, 217–225.
- Baldi, P., M. Fabris, M. Marsella, and R. Monticelli (2005), Monitoring the morphological evolution of the Sciara del Fuoco during the 2002–2003 Stromboli eruption using multi-temporal photogrammetry, *ISPRS J. Photogramm. Remote Sens.*, 59(4), 199–211, doi:10.1016/j.isprsjprs.2005.02.004.
- Ballestracci, R. (1982), Self-potential survey near the craters of Stromboli volcano (Italy). Inference for internal structure and eruption mechanism, *Bull. Volcanol.*, 45, 349–365.
- Bonaccorso, A., S. Calvari, G. Garfi, L. Lodato, and D. Patanè (2003), Dynamics of the December 2002 flank failure and tsunami at Stromboli volcano inferred by volcanological and

- geophysical observations, *Geophys. Res. Lett.*, 30(18), 1941, doi:10.1029/2003GL017702.
- Bullard, F. M. (1954), Activity of Stromboli in June and December 1952, *Bull. Volcanol.*, 15, 91–98.
- Calvari, S., L. Spampinato, L. Lodato, A. J. L. Harris, M. R. Patrick, J. Dehn, M. R. Burton, and D. Andronico (2005), Chronology and complex volcanic processes during the 2002–2003 flank eruption at Stromboli volcano (Italy) reconstructed from direct observations and surveys with a handheld thermal camera, *J. Geophys. Res.*, 110, B02201, doi:10.1029/2004JB003129.
- Calvari, S., L. Spampinato, and L. Lodato (2006), The 5 April 2003 vulcanian paroxysmal explosion at Stromboli volcano (Italy) from field observations and thermal data, *J. Volcanol. Geotherm. Res.*, 149, 160–175, doi:10.1016/j.jvolgeores.2005.06.006.
- Chioldini, G., D. Granieri, R. Avino, S. Caliro, A. Costa, and C. Werner (2005), Carbon dioxide diffuse degassing and estimation of heat release from volcanic and hydrothermal systems, *J. Geophys. Res.*, 110, B08204, doi:10.1029/2004JB003542.
- Etiope, G., P. Beneduce, M. Calcara, P. Favali, F. Frugoni, M. Schiattarella, and G. Smriglio (1999), Structural pattern and CO₂–CH₄ degassing of Ustica Island, Southern Tyrrhenian basin, *J. Volcanol. Geotherm. Res.*, 88, 291–304.
- Finizola, A., F. Sortino, J. F. Lénat, and M. Valenza (2002), Fluid circulation at Stromboli volcano (Aeolian Island, Italy) from self-potential and CO₂ surveys, *J. Volcanol. Geotherm. Res.*, 116(1–2), 1–18.
- Finizola, A., F. Sortino, J. F. Lénat, M. Aubert, M. Ripepe, and M. Valenza (2003), The summit hydrothermal system of Stromboli: New insights from self-potential, temperature, CO₂ and fumarolic fluids measurements, with structural and monitoring implications, *Bull. Volcanol.*, 65, 486–504, doi:10.1007/s00445-003-0276-2.
- Finizola, A., J. F. Lénat, O. Macedo, D. Ramos, J. C. Thouret, and F. Sortino (2004), Fluid circulation and structural discontinuities inside Misti volcano (Peru) inferred from self-potential measurements, *J. Volcanol. Geotherm. Res.*, 135, 343–360, doi:10.1016/j.jvolgeores.2004.03.009.
- Ishido, T. (2004), Electrokinetic mechanism for the “W”-shaped self-potential profile on volcanoes, *Geophys. Res. Lett.*, 31, L15616, doi:10.1029/2004GL020409.
- Ishido, T., and H. Mizutani (1981), Experimental and theoretical basis of electrokinetic phenomena in rock–water systems and its applications to geophysics, *J. Geophys. Res.*, 86, 1763–1775.
- Jouiniaux, L., M. L. Bernard, M. Zamora, and J. P. Pozzi (2000), Streaming potential in volcanic rocks from Mount Pelée, *J. Geophys. Res.*, 105(4), 8391–8401.
- Lénat, J. F., B. Robineau, S. Durand, and P. Bachéléry (1998), Etude de la zone sommitale du volcan Karthala (Grande Comore) par polarisation spontanée, *C. R. Acad. Sci.*, 327, 781–788.
- Lewicki, J. L., C. Connor, K. St. Amand, J. Stix, and W. Spinner (2003), Self-potential, soil CO₂ flux, and temperature on Masaya volcano, Nicaragua, *Geophys. Res. Lett.*, 30(15), 1817, 1–4, doi:10.1029/2003GL017731.
- Lorne, B., F. Perrier, and J. P. Avouac (1999a), Streaming potential measurements: 1. Properties of the electrical double layer from crushed rock samples, *J. Geophys. Res.*, 104, 17,857–17,877.
- Lorne, B., F. Perrier, and J. P. Avouac (1999b), Streaming potential measurements: 2. Relationship between electrical and hydraulic flow patterns from rock samples during deformation, *J. Geophys. Res.*, 104, 17,879–17,896.
- Malengreau, B., J. F. Lénat, and A. Bonneville (1994), Cartographie et surveillance temporelle des anomalies de Polarisation Spontanée (PS) sur le Piton de la Fournaise, *Bull. Soc. Géol. Fr.*, 165, 221–232.
- Maramai, A., L. Graziani, G. Alessio, P. Burrato, L. Colini, L. Cucci, R. Nappi, A. Nardi, and G. Vilardo (2005), Near- and far-field survey report of the 30 December 2002 Stromboli (Southern Italy) tsunami, *Mar. Geol.*, 215(1–2), 93–106, doi:10.1016/j.margeo.2004.11.009.
- Matsushima, N., M. Michiwaki, N. Okazaki, N. Ichikawa, A. Takagi, Y. Nishida, and H. Y. Mori (1990), Self-potential study in volcanic areas—Usu, Hokkaido Komaga-take and Me-akan, *J. Fac. Sci. Hokkaido Univ., Ser. VII*, 8, 465–477.
- Nishida, Y., and H. Tomiya (1987), Self-potential studies in volcanic areas—Usu volcano, *J. Fac. Sci. Hokkaido Univ., Ser. VII*, 8, 173–190.
- Perrier, F., et al. (1997), A one-year systematic study of electrodes for long period measurements of the electric field in geophysical environments, *J. Geomagn. Geoelectr.*, 49(11–12), 1677–1696.
- Petiau, G. (2000), Second generation of lead–lead chloride electrodes for geophysical applications, *Pure Appl. Geophys.*, 157(3), 357–382.
- Pride, S. R. (1994), Governing equations for the coupled electromagnetics and acoustics of porous media, *Phys. Rev. B*, 50, 15,678–15,696.
- Puglisi, G., A. Bonaccorso, M. Mattia, M. Aloisi, A. Bonforte, O. Campisi, M. Cantatero, G. Falzone, B. Puglisi, and M. Rossi (2005), New integrated geodetic monitoring system at Stromboli volcano (Italy), *Eng. Geol.*, 79(1–2), 13–31, doi:10.1016/j.enggeo.2004.10.013.
- Revil, A., and P. Leroy (2001), Hydroelectric coupling in a clayey material, *Geophys. Res. Lett.*, 28, 1643–1646.
- Revil, A., P. A. Pezard, and P. W. J. Glover (1999a), Streaming potential in porous media. 1. Theory of the zeta potential, *J. Geophys. Res.*, 104, 20,021–20,031.
- Revil, A., H. Schwaeger, L. M. Cathles, and P. D. Manhardt (1999b), Streaming potential in porous media: 2. Theory and application to geothermal systems, *J. Geophys. Res.*, 104, 20,033–20,048.
- Revil, A., V. Naudet, J. Nouzaret, and M. Pessel (2003a), Principles of electrography applied to self-potential electrokinetic sources and hydrogeological applications, *Water Resour. Res.*, 39(5), 1114, doi:10.1029/2001WR000916.
- Revil, A., G. Saracco, and P. Labazuy (2003b), The volcano-electric effect, *J. Geophys. Res.*, 108(B5), 2251, doi:10.1029/2002JB001835.
- Revil, A., A. Finizola, F. Sortino, and M. Ripepe (2004), Geophysical investigations at Stromboli volcano, Italy: Implications for ground water flow and paroxysmal activity, *Geophys. J. Int.*, 157, 426–440, doi:10.1111/j.1365-246X.2004.02181.x.
- Rittmann, A. (1931), Der Ausbruch des Stromboli am 11 September 1930, *Z. Vulkanol.*, 14, 47–77.

- Tibaldi, A. (2001), Multiple sector collapse at Stromboli volcano, Italy: How they work, *Bull. Volcanol.*, **63**, 112–125.
- Tibaldi, A., C. Corazzato, T. Apuani, and A. Cancelli (2003), Deformation at Stromboli volcano (Italy) revealed by rock mechanics and structural geology, *Tectonophysics*, **361**, 187–204, doi:10.1016/S0040-1951(02)00589-9.
- Tinti, S., G. Pagnoni, F. Zaniboni, and E. Bortolucci (2003), Tsunami generation in Stromboli island and impact on the Southeast Tyrrhenian coasts, *Nat. Hazards Earth Syst. Sci.*, **3**, 1–11.
- Zablocki, C. J. (1976), Mapping thermal anomalies on an active volcano by the self-potential method, Kilauea, Hawaii, *Proceedings, 2nd UN Symposium of the Development and Use of Geothermal Resources*, San Francisco, Calif., May 1975, 1299–1309.
-
- A. Finizola, Laboratoire Géosciences Réunion, Université de La Réunion, Institut de Physique du Globe de Paris, CNRS, UMR-7154-Geologie des Systèmes Volcaniques, 15 avenue René Cassin, BP 7154, 97715 Saint Denis cedex 9, La Réunion, France. (anthony.finizola@univ-reunion.fr)
- F. Sortino, Istituto Nazionale di Geofisica e Vulcanologia, Via Ugo la Malfa, 153, Sezione di Palermo, 90144 Palermo, Italy. (f.sortino@pa.ingv.it)

The 5 April 2003 Explosion of Stromboli: Timing of Eruption Dynamics Using Thermal Data

Andrew J. L. Harris

HIGP/SOEST, University of Hawai‘i, Honolulu, Hawaii, USA

Maurizio Ripepe

Dipartimento di Scienze della Terra, Università di Firenze, Firenze, Italy

Sonia Calvari, Luigi Lodato, and Letizia Spampinato

INGV-Catania, Catania, Italy

Stromboli’s 5 April 2003 explosion sent an ash plume to 4 km and blocks to 2 km, representing one of the most powerful events over the past 100 years. A thermal sensor 450 m east of the vent and a helicopter-flown thermal camera captured the event dynamics allowing detailed reconstruction. This review links previous studies providing a complete collation and clarification of the actual event chronology, while showing how relatively inexpensive thermal sensors can be used to provide great insight into processes that cannot be observed from locations outside the eruption cloud. The eruption progressed through four phases, comprised 29 discrete explosions, and lasted 373 s. The opening phase (phase 1) comprised ~30 s of precursory ash emission, with stronger emission beginning after 17 s. This was abruptly terminated by the main blast of phase 2 that comprised emission of a rapidly expanding ash cloud followed, after 0.4 s, by a powerful jet with velocities of up to 320 m/s. A second explosive phase (phase 3) began 38 s later and involved ascent of a phoenix cloud and explosive emission above a lateral vent lasting 75 s. This was followed by a 175-s-long phase of weaker, pulsed emission. The eruption was terminated by a series of three explosions (phase 4) sending ash to ~600 m at velocities of 27–45 m/s and lasting 87 s. Together, these results have shown that a low-energy opening phase was followed by the highest-energy phase. Each phase itself comprised groups of discrete explosions, with energy of the explosions diminishing during the two final phases.

1. INTRODUCTION

The Stromboli Volcano: An Integrated Study of the 2002–2003 Eruption
Geophysical Monograph Series 182
Copyright 2008 by the American Geophysical Union.
10.1029/182GM25

An effusive eruption began at Stromboli (Aeolian Islands, Italy) on 28 December 2002. This continued until July 2003 and was punctuated, on 5 April 2003, by a major explosive event or paroxysm [Calvari *et al.*, 2005; Rosi *et al.*, 2006].

The onset of effusive activity, plus the associated flank instabilities and tsunami hazard [Bonaccorso *et al.*, 2003; Pino *et al.*, 2004; Tinti *et al.*, 2003, 2006], accelerated the deployment of an extensive instrument array. This included a thermo-acoustic-seismic array, of which the infrasonic portion had been installed during autumn 2002 [Ripepe *et al.*, 2004a]. It initially comprised a five-element infrasound array and a four-station broadband seismometer network [Ripepe *et al.*, 2004a, 2004b]. Three 15° field of view (FOV) thermal (8–14 μm) sensors were added in May 2002 [Harris *et al.*, 2005]. These were initially located at the Pizzo Sopra La Fossa, a position ~250 m SE and ~150 m above Stromboli's active summit craters, with a second thermal station being added ~450 m east of the summit craters in February 2003 (Figure 1a). Further geophysical installations after the onset of the eruption included eight broadband seismometers installed by INGV-Osservatorio Vesuviano [D'Auria *et al.*, 2006], two web cameras, and three summit GPS stations deployed by INGV-Catania [Mattia *et al.*, 2004]. In addition, once the eruption was underway, a thermal IR camera was used to track both the lava flow field and the summit craters during daily monitoring flights [Calvari *et al.*, 2005, 2006; Harris *et al.*, 2005; Lodato *et al.*, 2007].

All permanently installed thermal and infrasonic sensors were operational at the time of the 5 April 2003 paroxysm, except the summit web cameras, and the helicopter carrying the daily monitoring crew was in the air acquiring thermal images of the summit craters and flow field (Figure 1a). This presence yielded an integrated data set that allowed a detailed event chronology to be put together, with timings accurate to tenths of a second. While the event chronology drawn from the thermal camera and digital photo data is described by Calvari *et al.* [2006], that drawn from the thermo-acoustic-seismic array is given by Ripepe and Harris [2008]. The latter data were used in combination with a posteruption examination of the deposits by Rosi *et al.* [2006] to more fully understand the dynamics and mass fluxes involved in the 5 April event. All three studies are complimentary and provide full documentation of the explosion dynamics of the 5 April paroxysm. In this work we draw these studies together to provide a full review of the 5 April event chronology.

2. THE 5 APRIL PAROXYSM

The 5 April paroxysm had several precursors. Radon anomalies developed about 2 weeks before the event [Cigolini *et al.*, 2005]. In addition, CO₂ anomalies developed in the week before the eruption, with peaks in H₂ and He being recorded a few days before 5 April [Carapezza *et al.*, 2004]. Anomalously high SO₂/HCl ratios were noted 2–3 days before 5 April [Aiuppa and Federico, 2004], and de-

formation was recorded by two GPS stations 30 s prior to the explosion [Mattia *et al.*, 2004]. These precursors have been interpreted as the geochemical signatures from a sulfur-rich magma batch ascending into the shallow system [Aiuppa and Federico, 2004; Carapezza *et al.*, 2004] to cause inflation just before the event followed by deflation as the pressure was released during the explosion [Mattia *et al.*, 2004]. The broadband seismometer network recorded an ultralong period (>20 s) signal beginning ~4 min before the eruption. This was also interpreted as the effect of radial ground tilt caused by pressurization of the conduit due to vesiculation in the rapidly ascending magma batch [D'Auria *et al.*, 2006; Ripepe and Harris, 2008]. The onset of a high-frequency (<0.1 s) signal, related to vesiculation of the rising batch, was recorded ~1 min before the explosion with a very-long-period (VLP) signal at 0713:35 UT marking the onset of fragmentation [D'Auria *et al.*, 2006; Ripepe and Harris, 2008]. This is consistent with the geochemical analysis of erupted samples, which indicates that the eruption involved melt that rose through, and interacted with, overlying (slightly more evolved) melt to finally mingle with the shallow crystal-rich magma just before eruption [Métrich *et al.*, 2005]. The same broadband data have also been used to infer slow slip movement along a preexisting fracture in the minutes prior to eruption [Cesca *et al.*, 2007]. This may indicate reopening of the uppermost ~250 m of the conduit, which had previously been blocked [Calvari *et al.*, 2006], to allow a few seconds of ash emission followed by the main blast as the pathway opened up [Cesca *et al.*, 2007].

The ensuing eruption began with a cannon-like detonation accompanied by a shock wave that broke windows at Ginostra, a village ~2 km from the vent [Calvari *et al.*, 2006; Rosi *et al.*, 2006; Figure 1a]. Given the delay time between the infrasonic and thermal signals generated by the initial explosion, the source was extremely shallow—just 80–150 m below the crater rim—and likely involved a total gas mass of 3×10^6 kg [Ripepe and Harris, 2008]. The event that followed sent an eruption column to a height of ~4 km and ejected 2–3 m³ bombs as far as Ginostra where they caused some damage [Rosi *et al.*, 2006]. All the explosive emissions lasted ~8 min and involved four distinct phases with the second, and most violent, phase lasting 39 s and erupting a total mass of $1.1\text{--}1.4 \times 10^8$ kg [Rosi *et al.*, 2006].

3. EFFECTS ON THE INSTRUMENT ARRAYS AND THERMAL IMAGE ACQUISITION

Our network of thermal, seismic, and infrasonic sensors was subjected to fallout of hot juvenile and lithic fragments within a few seconds of the event onset. The first damage, however, was inflicted by the pressure wave that spread from

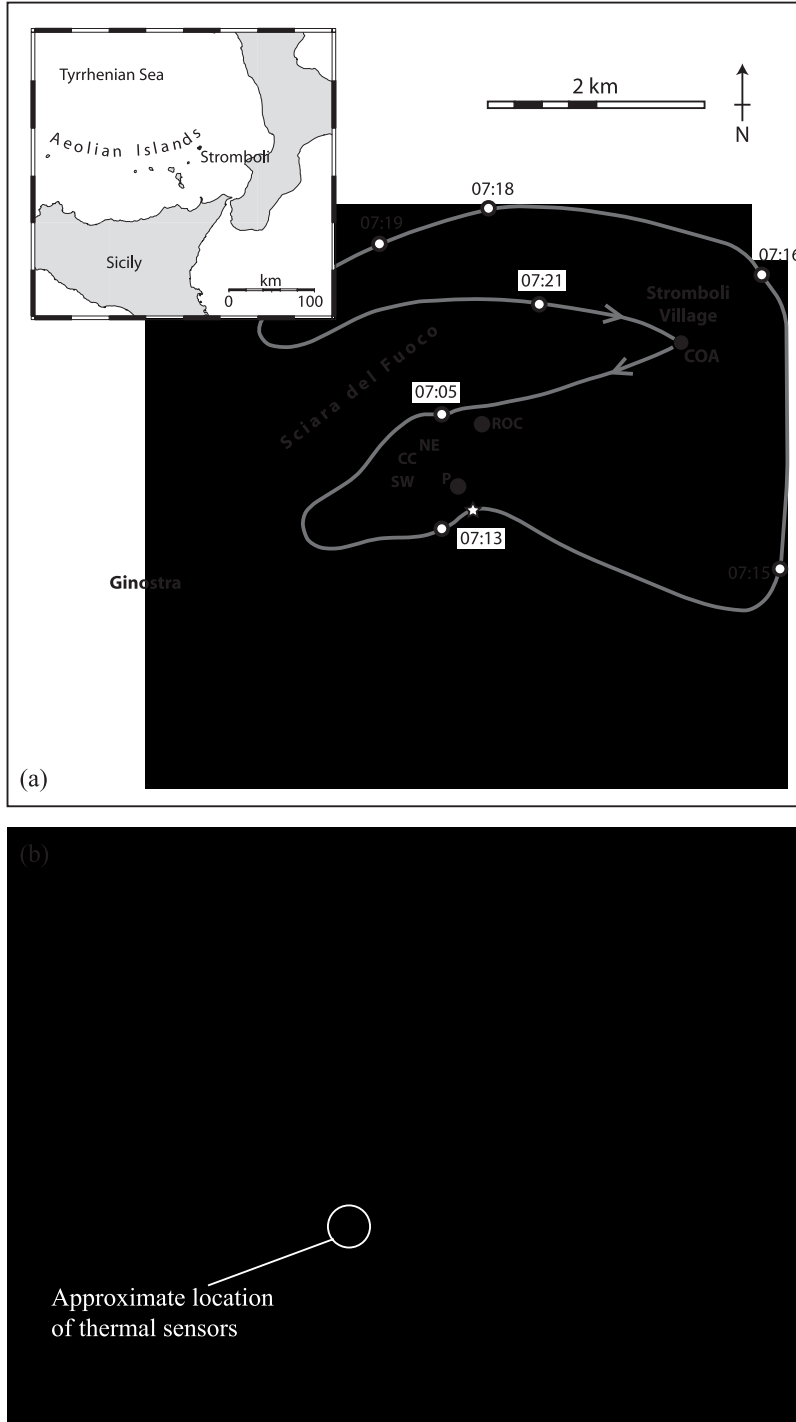


Figure 1. (a) Stromboli showing locations of the SW, central, and NE craters (SW, CC, and NE). The two thermal sensor sites to the southeast (P) and northeast (ROC) of the summit craters and the Civil Protection Operations Center (COA) are given, as is the 5 April helicopter flight path (gray line; from *Calvari et al. [2006]*), on which approximate times for the helicopter location at each point are marked. Note the sharp turn to the SE (marked with a star) just after 0713 UT forced by the paroxysm onset. (b) The 5 April 2003 paroxysmal eruption viewed from the east at 0714:15 showing the main column of phase 2 and location of ROC thermal station within the column. Black curtains of ballistic fallout are apparent at the plume margins, as is a small cloud rising above the phase 3 pyroclastic flow. The plume front has the form of a well-developed thermal. Insets are photographs of the thermal sensor bunker upon installation in May 2002 at the Pizzo (top) and immediately after the 5 April event (bottom) (from *Harris et al. [2005]*).

the vent at the explosion onset. The damage inflicted on the bunker housing the IR thermometers was consistent with the pressure wave entering the viewing slot and exiting through the roof that was partially peeled back by the exiting wave. The following fallout then covered and partially collapsed the outer box (Figure 1b). The instrument boxes within the outer box, however, remained secure, and the thermal sensors survived unscathed recording good, unsaturated signal throughout the event (Figure 2) from a location situated on the edge of the column (Figure 1b). The instruments in operation were Omega OS43 thermal IR thermometers [Harris *et al.*, 2005]. This instrument detects emitted radiation across the 8- to 14- μm range, converting the recorded voltage to temperatures in the -40° to 1200°C range integrated across a 15° FOV. These were installed in protective, gas-proof cases to view the target through thermally transmissive germanium–arsenide–selenium windows [Harris *et al.*, 2005]. The eastern (ROC, Figure 1) site is ~ 450 m to the east of the craters, which means the FOV will have a diameter of 120 m (D_{FOV}), and thus will relate to the thermal emission of the plume over the first 120 m of ascent. The Omega OS43 outputs a continuous signal as a voltage, where 1 mV is equivalent to 1°C , which we sample at a rate of 54 Hz. A good portion of our seismic network also survived, with three of the four CMG40T broadband seismometers surviving (see Marchetti and Ripepe [2005] for instrument details and capabilities). However, the signal was too intense, and all seismic signals were saturated and clipped. The infrasonic microphones used

in the five-element array had sensitivities of 0.54 V/Pa in the infrasonic (1–20 Hz) range [Ripepe *et al.*, 2004b]. However, the entire infrasonic array was destroyed due to bomb impact within a few seconds of the eruption beginning.

At the time of the explosion, thermal images and digital photographs were also being collected from a helicopter flying over the summit craters (see Figure 1a for flight path). A FLIR systems TM 695 thermal (7.5–13 μm) camera was being operated, which collects 320×240 -pixel images of calibrated temperature at one of three gain settings covering the temperature ranges of -40° to 120°C , 0° to 500°C , and 350° to 1500°C . In practice, temperatures exceeding these maximum limits can be retrieved. For example, the low gain mode is capable of recording up to 232°C . Images were collected at a frame rate of one image per second initially using the low-gain setting, allowing temperatures of up to 232°C to be recorded [Calvari *et al.*, 2006]. Data collection began at 0703 (all times are UT), with 286 images being acquired of the active lava flow field and Sciara del Fuoco (Figure 1a). The overflight began targeting the summit craters ~ 20 s before the paroxysm, so that 16 images of the persistent gas plume were obtained, from a location ~ 350 m to the south of the summit craters and roughly level with them, in the seconds prior to the event. Five images of the emerging plume and ejecta were then obtained as the helicopter banked rapidly and began evasive action, diving to the south and away from the blast. A further 440 images of the plume and hot deposits lying on the volcano flanks were then acquired from

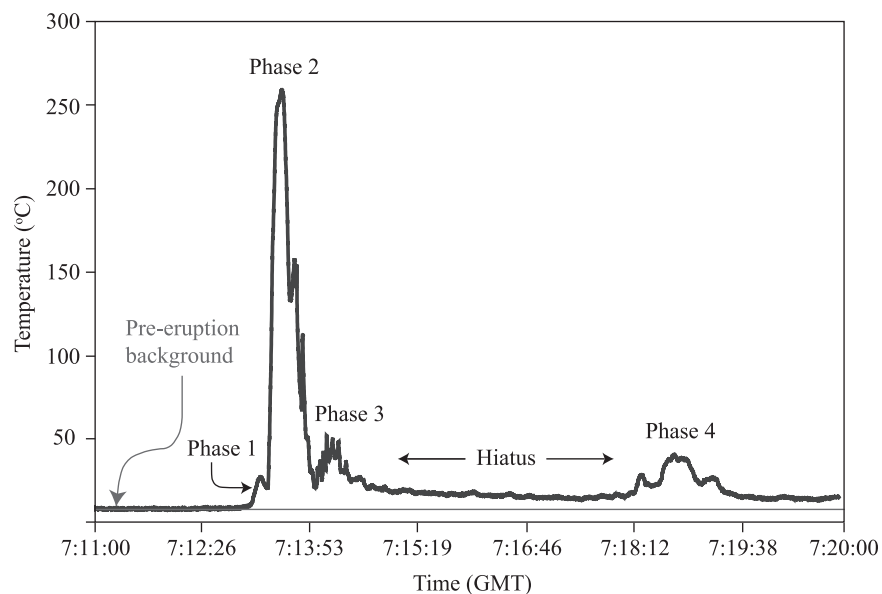


Figure 2. Overview of the thermal signal obtained for the 5 April paroxysm. The opening phase (phase 1) and three main explosive phases (2 to 3) defined using these thermal data by Rosi *et al.* [2006] are marked.

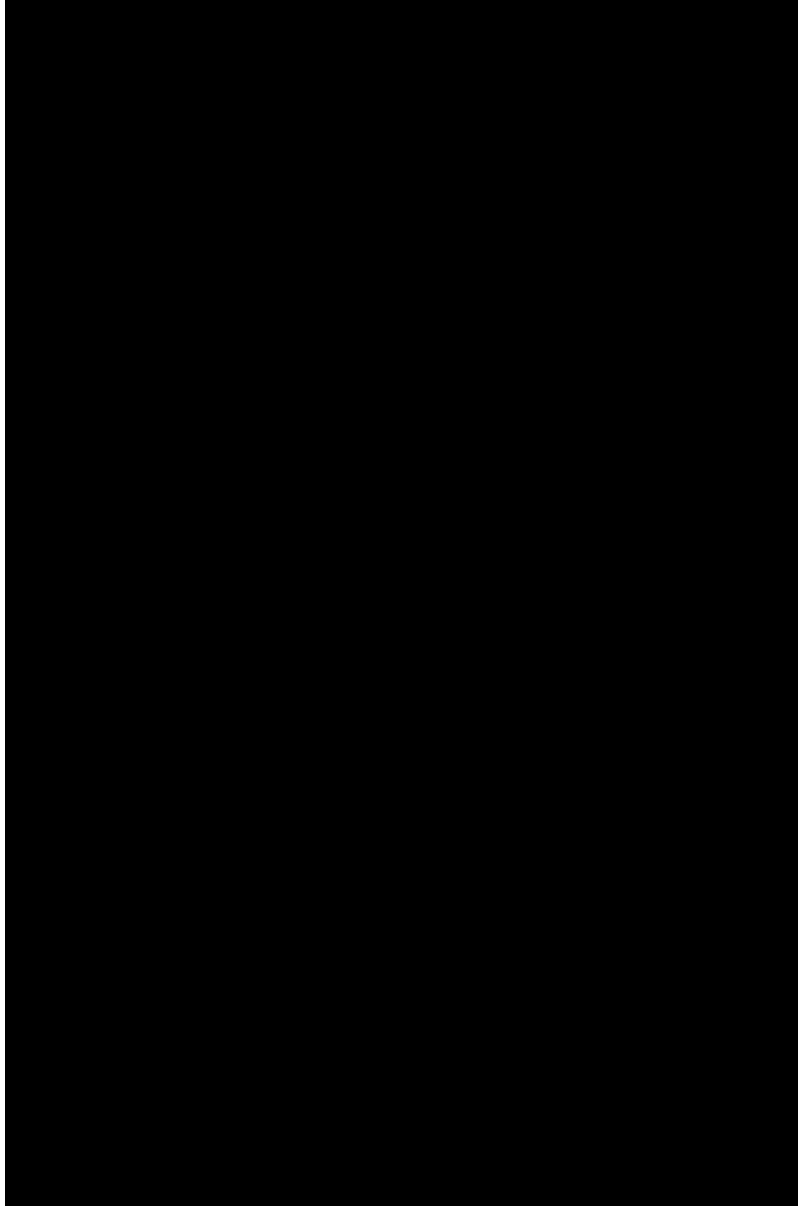
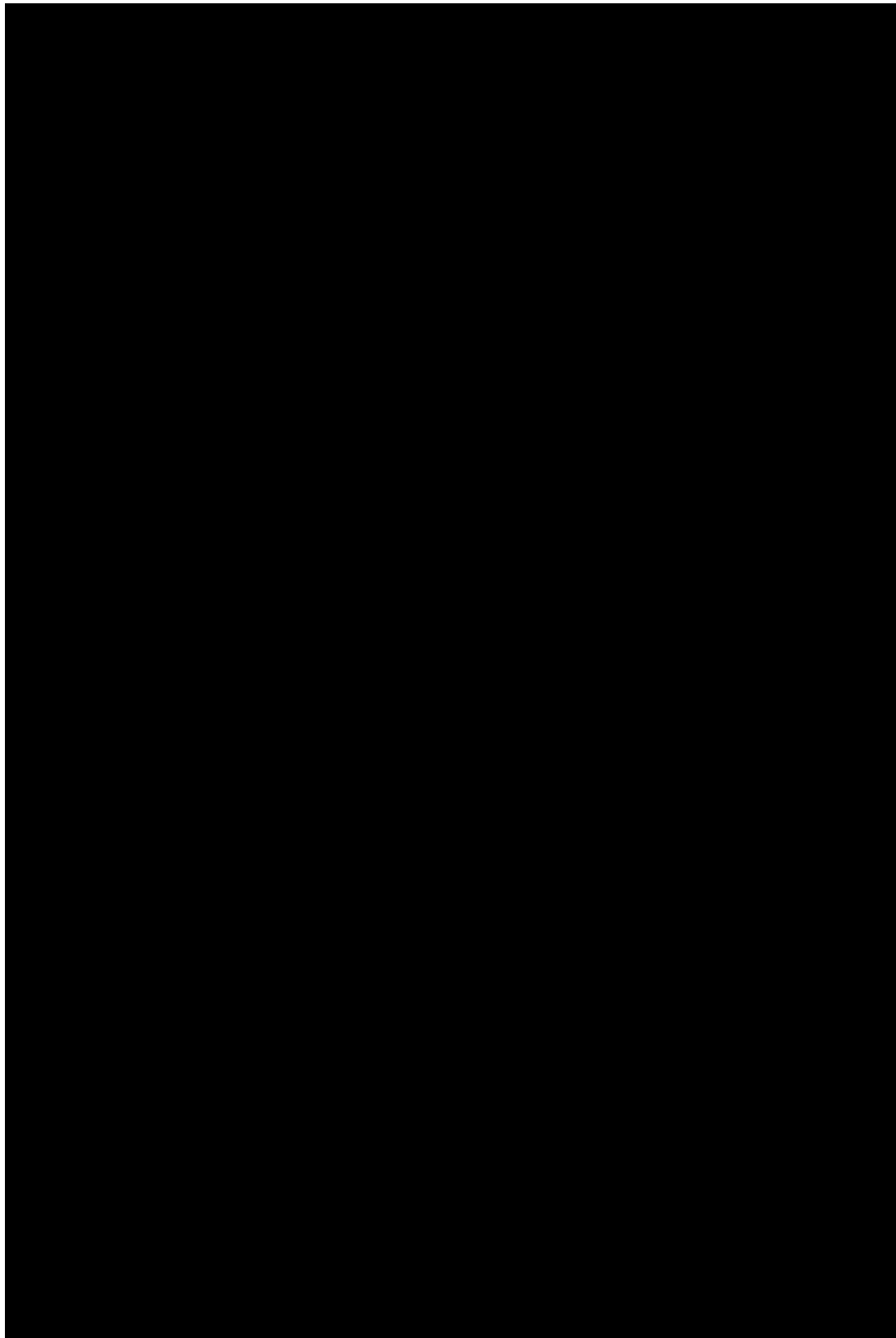


Plate 1. Digital photo sequence of the 5 April paroxysm. Timings are set by correcting the digital camera time using the difference between the thermal-IR thermometer-derived onset for phase 2 (0713:38 UT) and the camera time of the same event. This time is also used as time zero. (a) View from the west of Stromboli's summit craters ~2 min before phase 2, showing a normal condensed plume emitted from the NE, central, and SW craters as well as the proximal section of the active lava flow field (p). (b) View from the south showing slight reddening of the plume due to emission from the central and NE craters, followed by (c) slightly more intense emission from NE crater to form a darker, billowing cloud in the seconds before the main phase 2 blast. (d) The expanding cloud and finger jet components of the phase 2 emission imaged ~2 s after the blast onset. (e) View from the east showing the eruption plume ~20 s after the onset of phase 3, showing well-developed phoenix cloud from the scoria flow and thermal from the phase 2 emission. (f) View from the NE showing (1) thermal generated by the phase 3 phoenix cloud and (2) two pulses of light gray ash most likely (given their source location) from the lateral vent. (g) View from the NE showing (1) pulsing plume characteristic of the hiatus, (2) steam rising from hot, wet deposits emplaced on the active flow field, and (3) location of the ROC thermal sensor (black dot). (h) Phase 4 plume ~1 min and 15 s after initial emission showing the plumes from each of the three pulses (O, P, and Q, Table 1) that comprised this three-explosion phase, as well as the steam plume (s) generated by hot deposits over the lateral vent/shield.



~2 km to the south beginning around 0715, by which time the event had been underway for ~2 min, and the camera gain setting have been changed to the midgain mode. Acquisition ended at 0726, ~13 min after the event began. In addition, 101 photographs were taken (using a Canon A40 digital camera) from the helicopter, 29 photographs being acquired in the minutes before the event, and 72 during the event itself.

4. EVENT CHRONOLOGY

Thermal imagery of the summit craters on 1 April 2003 showed the NE crater to be obstructed and lacking high-temperature vents, with talus covering the crater floor [Calvari *et al.*, 2006]. Although the craters remained obstructed just before the 5 April explosion, an increase in maximum temperature was noted in the thermal imagery for fumaroles within the NE crater beginning ~3 min before the blast [Calvari *et al.*, 2006]. This ties in with the onset of the ultralong-period seismic signals that began ~4 min before the eruption [D'Auria *et al.*, 2006] and may represent the onset of opening/charging of the uppermost section of the conduit.

Examination of the digital photographs show a white, heavily condensed plume, typical of persistent gas emission from Stromboli's active vents immediately prior to the explosion (Plate 1a). The eruption began with a weak emission of red ash from the NE and central craters. This mixed with the gas plume and drifted SW due to the strong wind, causing a slight reddening of the plume (Plate 1b). After 17 s, the emission became more intense, and the NE crater became the source of a gray emission (Plate 1c) with a cauliflower shape [Calvari *et al.*, 2006]. The increase in intensity was also apparent from an increase in plume temperature above the crater (Plates 2a–2d). This opening phase lasted ~30 s [Rosi *et al.*, 2006], with the NE crater emission being detected as a low-amplitude thermal oscillation in the IR thermometer data beginning at 0713:24 and lasting 13 s (Figure 3a). This first phase has been interpreted by Cesca *et*

al. [2007] as being due to opening of the blocked upper section of the conduit to feed minor ash emission in the seconds before the main blast.

The paroxysm thus began with a low-energy opening phase and was followed by three main explosive events. These events were identified and defined by Rosi *et al.* [2006] using the thermal IR thermometer record and visual documentation (Figure 2). The opening phase (phase 1) was abruptly terminated at 07:13:38 by the first main explosive event (phase 2). The phase 2 thermal onset followed the most powerful VLP seismic signal by ~2.5 s, the VLP being recorded at 0713:35.5 [D'Auria *et al.*, 2006]. The opening events of phase 2 were also captured by the helicopter-borne thermal and digital camera [Calvari *et al.*, 2006; Rosi *et al.*, 2006]. This showed that phase 2 began with emission of a rapidly expanding, dark-colored cloud that, seconds later, was overtaken by multiple hot (finger) jets of juvenile material from both the NE and SW craters (Plate 1d). The thermal imagery show emission of a rapidly expanding hot cloud behind a leading edge composed of ballistics (Plates 2e–2f). Unfortunately, the maximum cloud temperature cannot be determined because it exceeded the upper range of our gain setting, that is, 232°C. As described by Calvari *et al.* [2006] and Rosi *et al.* [2006], this first main explosive phase fed a 4-km-high convective column with a well-developed thermal (Figure 1b). Fallout of a large number of blocks and bombs (Figure 1b) reached distances of up to 2 km from the vent [Rosi *et al.*, 2006]. The first thermal peak during phase 2 was reached after 0.37 s (B in Figure 3a), making this peak almost synchronous with the 07:13:37 seismically recorded arrival of the blast wave reported by D'Auria *et al.* [2006]. This is assumed to mark emission of the second plume of multiple jets captured in Plate 1d. This onset time can be used, following the methodology of Harris and Ripepe [2007], to give a thermal-data-derived ascent velocity of ~320 m/s for the second finger-jet forming (and blast-wave-associated) plume [Rosi *et al.*, 2006]. Calvari *et al.* [2006] obtained a velocity of 80 m/s from the thermal

Plate 2. (Opposite) Thermal camera time series for (a–f) phases 1–2, (g–l) the hiatus, and (m–r) phase 4. Timings are set by correcting the digital camera time using the difference between the thermal-IR thermometer-derived onset for phase 2 (0713:38 UT) and the camera time of the same event. This time is also used as time zero. (a–d) Increasing emission from NE and SW craters during the opening phase (phase 1), interrupted (e–f) by emission of the phase 2 plume. This initially comprised an expanding cloud of high-temperature ash (ec) behind a leading edge of ballistics (bl). (g–i) The pulsing plume of the hiatus, revealing the SW crater as its source (j–l). Also apparent is the hot fallout from phase 2 mantling the upper sections of the outer flank and extending down a gully (g–l). Approximate outer flank altitude range covered by images in g–i and j–l is given, as is the approximate scale for the image position of the SW crater plume. The location of the ROC IR thermometer (open circle), Pizzo Sopra La Fossa (p; 918 m above sea level) and NE crater (ne) are given. NE crater flank is mantled by a near-continuous cover of high-temperature (200°–400°C) fallout (j–l). (m–r) Record emission of the phase 4 plume, showing the starting plumes and thermals associated with the three explosion events (1–3). The plume from the second explosion forms three discrete thermals (2a, 2b, and 2c). Where given, vertical (white) scale line is 150 m. Images given in Plates 2a–f are obtained over a viewing distance of ~450 m and thus cover a ~150 × 200 m field of view at the plume location.

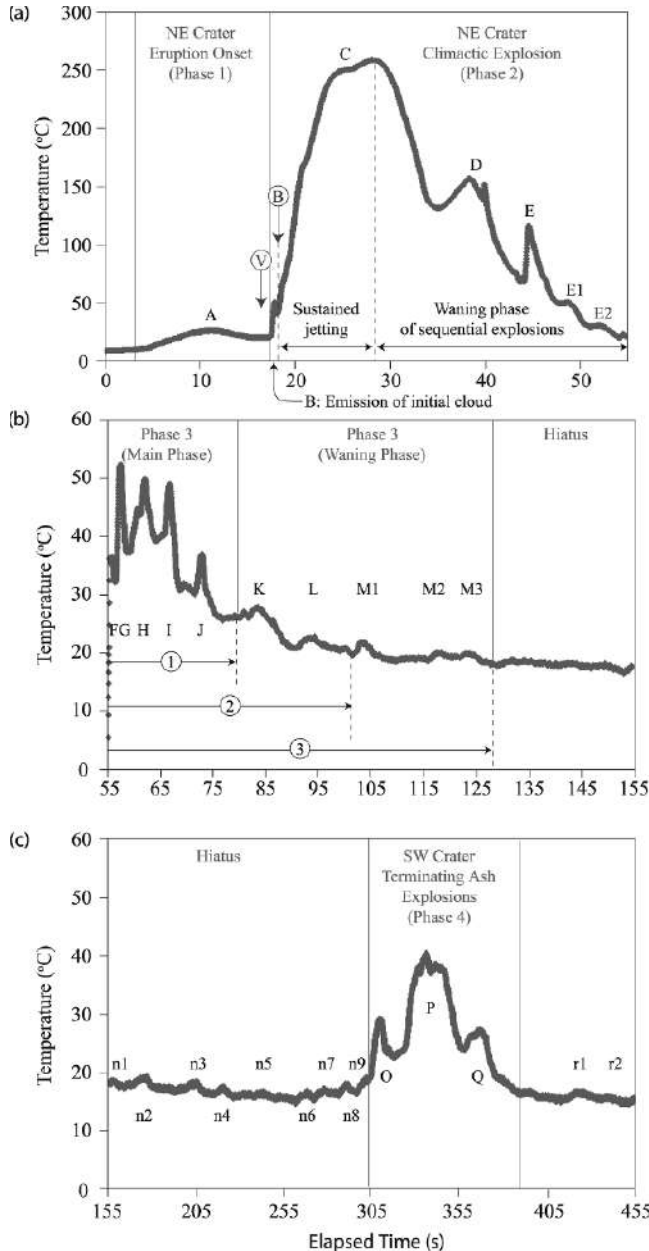


Figure 3. Detail of the thermal IR thermometer signal obtained during (a) phases 1–2, (b) phase 3, and (c) phase 4. Time is in seconds since 0713:18 UT. Each of the main pulses that comprise each phase and hiatus are lettered (see Table 1). The four main eruption phases defined by Rosi *et al.* [2006] using these data are also marked. Arrows labeled V and B mark the seismically recorded arrivals of the most powerful VLP and blast wave, respectively. In Figure 3b, numbered arrows indicate the minimum [Rosi *et al.*, 2006], median [Harris and Ripepe, 2007], and maximum likely duration of phase 3.

image data. This lower velocity relates to the cloud front of the expanding plume associated with the first emission, showing that velocities for the second jet-like plume were at least three times faster than those of the first expanding plume. Velocities at Stromboli during normal Strombolian have been measured at up to 101 m/s (mean = 34 m/s) for eruptions dominated by coarse ballistics, with a maximum of 58 m/s (mean = 19 m/s) measured during ash-rich eruptions [Patrick *et al.*, 2007]. Velocities during the opening seconds of phase 2 were thus higher than during normal Strombolian activity.

The thermal signal during phase 2 reached a peak after 10 s, by which time thermal image acquisition had temporarily ceased. This period likely represents a sustained period of jetting [Rosi *et al.*, 2006]. The signal then waned over 28 s to give a total phase 2 duration of 38 s (Figure 3a). Closer examination of the waning thermal signal reveals that it comprised four sequential subevents, each apparent from oscillations in the time series (D–E2, Figure 3a). These likely represent a series of shorter explosions [Rosi *et al.*, 2006], which decreased in thermal amplitude as phase 2 proceeded and had onsets of between 0.31 and 1.19 s. These onsets (δt) give (following Harris and Ripepe [2007], $V = D_{FOV}/\delta t$) ascent velocities of 100–320 m/s (mean = 230 m/s, standard deviation = 95 m/s).

Rosi *et al.* [2006] estimate an erupted mass of $1.1\text{--}1.4 \times 10^8$ kg during phase 2, which (for a 38-s duration) gives a time-averaged discharge rate of $2.8\text{--}3.6 \times 10^6$ kg/s. Assuming that most of the material was emitted in the first 10 s of jetting indicates that the discharge rate probably peaked at $1.0\text{--}1.2 \times 10^7$ kg/s [Rosi *et al.*, 2006]. This is much higher than masses typically erupted during normal Strombolian activity at Stromboli, where a maximum of ~ 6000 kg is erupted in any single event [Ripepe *et al.*, 1993; Patrick, 2005] which, for a mean eruption duration of ~ 8 s [Ripepe *et al.*, this volume], converts to a time-averaged discharge rate 750 kg/s during a single normal event.

The beginning of a second main explosive phase (phase 3) was marked by a reversal of the waning trend in the thermal IR thermometer data (Figure 2). Phase 3 was coincident with the formation of a scoria flow and the concurrent rise of a phoenix plume [Rosi *et al.*, 2006]. Phase 3 began at 0714:15 and, like phase 2, comprised a number of sequential thermal events (Figure 3b; Table 1) associated with the phoenix plume that rose from the scoria flow active between the instruments and the vent (Plate 1e). It is possible that the spikes recorded in the thermal data during this phase (Figure 3b) record a series of explosions from a lateral vent. This lateral vent would have been at the head of the dyke extending NE from the summit craters and which was feeding the ongoing lava flow [Rosi *et al.*, 2006]. This is consistent with the digital camera data showing plumes from two explosions

Table 1. Thermal-IR Thermometer-Derived Event Chronology

Phase	Event (Figure 3)	Start Time (UT)	Finish Time (UT)	Duration (hhmm:ss.0)	Notes
<i>Three-Phase Eruption Sequence (Modified from Rosi et al. [2006])</i>					
1		0713:24	0713:37	0013	Eruption onset (vent opening phase)
2		0713:38	0714:15	0037	Climactic explosion
3		0714:15	0715:30	0115	Pyroclastic flow and smaller explosions
Hiatus		0715:30	0718:24	0254	Persistent, low intensity, pulsed emission
4		0718:24	0719:51	0127	Terminating ash emission from SW crater
Post-4		0720:17	0721:19	0102	Final bursts
<i>Detail from Thermal IR Thermometer Log</i>					
Phase 1: Eruption onset (vent opening phase)					
1	A	0713:24	0713:37	0000:12:6	Opening phase of NE crater (NEC)
Phase 2: Climactic explosion					
2	B	0713:37	0713:37	0000:00.7	Initial explosion (NEC explosion 1) to feed expanding plume
2	C	0713:37	0713:54	0000:17.1	Main pulse (NEC explosion 2) to feed sustained jetting
2	D	0713:54	0714:03	0000:08.8	Third pulse (NEC explosion 3)
2	E	0714:03	0714:08	0000:04.2	Fourth pulse (NEC explosion 4)
2	E1	0714:08	0714:10	0000:02.7	Fifth pulse (NEC explosion 5)
2	E2	0714:11	0714:14	0000:02.9	Sixth pulse (NEC explosion 6)
Phase 3: Pyroclastic flow and smaller explosions (from lateral vent?)					
3	F	0714:15	0714:16	0000:01.3	Initial pulse (Lateral vent explosion 1)
3	G	0714:16	0714:19	0000:02.7	Main pulse 1 (Lateral vent explosion 2)
3	H	0714:19	0714:24	0000:05.3	Main pulse 2 (Lateral vent explosion 3)
3	I	0714:24	0714:27	0000:02.4	Main pulse 3 (Lateral vent explosion 4)
3		0714:27	0714:32	0000:04.9	Inter-pulse
3	J	0714:32	0714:37	0000:05.5	Waning pulse 1 (Lateral vent explosion 5)
3		0714:37	0714:42	0000:04.8	Inter-pulse
3	K	0714:42	0714:51	0000:08.8	Waning pulse 2 (Lateral vent explosion 6)
3	L	0714:51	0714:57	0000:05.8	Waning pulse 3 (Lateral vent explosion 7)
3	M1	0714:57	0715:16	0000:19.8	Waning pulse 4 (Lateral vent explosion 8)
3	M2	0715:16	0715:22	0000:05.9	Waning pulse 5 (Lateral vent explosion 9)
3	M3	0715:22	0715:30	0000:07.3	Waning pulse 6 (Lateral vent explosion 10)
Hiatus (H): Persistent, low-intensity, pulsed emission from SW crater (SWC)					
H	N1	0715:56	0716:02	0000:06.1	Hiatus pulse #1 (SWC burst)
H	N2	0716:09	0716:23	0000:14.4	Hiatus pulse #2 (SWC burst)
H	N3	0716:34	0716:55	0000:20.3	Hiatus pulse #3 (SWC burst)
H	N4	0716:57	0717:07	0000:10.7	Hiatus pulse #4 (SWC burst)
H	N5	0717:20	0717:31	0000:10.6	Hiatus pulse #5 (SWC burst)
H	N6	0717:42	0717:53	0000:10.6	Hiatus pulse #6 (SWC burst)
H	N7	0717:53	0718:06	0000:13.4	Hiatus pulse #7 (SWC burst)
H	N8	0718:06	0718:17	0000:10.3	Hiatus pulse #8 (SWC burst)
H	N9	0718:17	0718:24	0000:07.2	Hiatus pulse #9; interrupted by explosive onset of phase 4
Phase 4: Terminating ash emission from SW crater					
4	O	0718:24	0718:39	0000:15.1	First explosion
4	P	0718:39	0719:19	0000:39.7	Second explosion
4	Q	0719:19	0719:51	0000:32.1	Third explosion
Final bursts					
	R1	0720:17	0720:37	0000:19.7	Minor (low thermal amplitude) emission #1
	R2	0720:54	0721:19	0000:25.8	Minor (low thermal amplitude) emission #2

at this location to feed two plumes of light gray ash that rose in front of the darker plume from the summit craters (Plate 1f). These events occurred at 0714:51 and 0715:25, tying in with oscillations recorded by the IR sensor (L–M1 and M2–M3, Figure 3c; Table 1). The onset times for the five thermal oscillations that comprised the main phase of this series of lateral vent explosions (F–J, Figure 3c) give ascent velocities for these explosions of 40–85 m/s (calculated for a source that is 225 m from the sensor so that FOV height, D_{FOV} , is 60 m; consistent with emission from the lateral vent). The phase 3 thermal signal began to wane after the fourth event (Figure 3b) (i.e., at 0714:27), ending around 0715:30 (Table 1). Given the photographic evidence, the main phase is likely related to ascent of the phoenix plume, and the waning phase to small explosive emissions of discrete, light gray plumes (Plate 1f) from the lateral vent. With clearance/dispersal of the phoenix plume following the main phase, a clear line-of-sight into the summit craters was reestablished.

There followed a 174-s long hiatus. Throughout the hiatus, the thermal signal remained elevated (Figure 2). Examination of the thermal signal revealed that low intensity emissions continued to give nine low amplitude thermal oscillations (N1–N9, Figure 3c; Table 1). Thermal imagery for this phase shows high-temperature (up to 400°C) fallout mantling the upper flanks and extending down some gullies, with isolated hot spots at lower altitudes locating bombs from phase 2 (Plates 2g–2l). The thermal imagery and digital photos show a persistent, low intensity, pulsing emission from the SW crater (Plates 1g and 2g–2l), explaining the oscillating thermal signal during the hiatus in terms of continued, but lower intensity, pulsed emission. The digital photos also show a persistent steam cloud rising above hot deposits emplaced on the proximal section of the active flow field [Calvari *et al.*, 2006; Rosi *et al.*, 2006; Plate 1h]. Emission of the steam plume begins only after the two lateral vent explosive bursts (Plates 1e–1g). At the location of the thermal IR thermometer, however, the steam plume was below the line of sight (Plate 1g), so that the instrument had an unimpeded view of activity within the summit craters.

At 0718:24, the final major explosive phase began (phase 4, Figure 2). This comprised three discrete explosions at the SW crater, each apparent from oscillations in the thermal signal (Figure 3c), and lasted 1 min 27 s [Rosi *et al.*, 2006]. The digital photos show a billowing red-brown emission from the SW crater overtaking the lighter color emission of the hiatus (Plate 1h). This fed a plume front that, by 0719:23 (~1 min after phase 4 began), had reached a height of ~600 m above the SW crater (Plate 1h). Likewise, the thermal imagery revealed the persistent, low-intensity plume of the hiatus being replaced by a stronger (higher temperature) plume from the SW crater (cf. Plates 2l and 2m). The thermal am-

plitude of the hiatus oscillations also appeared to pick up just before phase 4 (events N6–N9; Figure 3c), with the final oscillation (N9) being interrupted by the first explosion of phase 4 (Figure 3c). This is also consistent with the thermal imagery, which shows emission of a more intense ash plume just before phase 4 (compare Plates 2j–2k and 2l).

The thermal images captured during phase 4 show that the three explosions fed emissions that began, following the terminology of Turner [1969], with emission of a starting plume rooted to the vent, which then developed into buoyantly rising thermals (Plates 2m–2r). The plume emitted by the second explosion developed into three thermals (Plates 2p–2r) and likely explains why the thermal signal associated with this event (P, Figure 3c) has a broad peak, which itself contains three oscillations. The three explosions of phase 4 had thermally IR-thermometer-derived velocities of 25, 30–40, and 45 m/s, respectively. This compares well with thermal-image-derived velocities. The thermal image data places the plume front from the first explosion at ~190 m above the vent after 7 s (Figure 3m), that of the second explosion at ~250 m after 7 s (Figure 3n), and that of the third at ~180 m after 4 s. These give velocities of 27, 36, and 45 m/s for the three pulses, respectively. The paroxysm was effectively over by 0719:51, with the main explosive emission having lasted 6 min and 13 s, and comprising three main phases (Figure 2) and 29 discrete explosions (Table 1).

5. TIMING ERRORS AND UNCERTAINTIES

Recovery of the analog signal from the German-transmitted time code (DCF; <http://www.hopf-time.com/en/dcf-info.htm>) allowed Ripepe and Harris [2008] to better synchronize the thermal events, with timings given by Rosi *et al.* [2006] and Harris and Ripepe [2007] being offset by 17 s. Although this does not affect the event chronology or durations, all absolute times given in these earlier studies will be 17 s too early. Correct absolute times are given by Ripepe and Harris [2008] and in this work (Table 1).

Assigning onset and termination points for specific events involve manual picking of onsets, many of which are not steplike, but instead turn around gradually over up to 1 s. This means that errors of 1 s may be applied to most times, so that timings given here may differ by ~1 s from those given by Rosi *et al.* [2006]. Assigning a termination time to phase 3 was particularly problematic, it being characterized by a waning thermal signal that is not abruptly terminated by a new explosive event, as at the end of phase 2 (Figure 2). Rosi *et al.* [2006] assigned a duration of 25 s—a consideration that includes the four main high-amplitude thermal events comprising this explosion cluster, plus the first event of the waning phase (events F–J, Figure 3b). However, this excludes

two moderate amplitude events (K–L, Figure 3b) which, if included, place the termination of this event at 0714:57, to give a duration of 42 s [Harris and Ripepe, 2007]. If the termination is set at the point at which the waning tail flattens out, and the final three low amplitude thermal events of the waning tail (M1–M3, Figure 3b) are included, the duration increases to 75 s. This also means that the hiatus period may be between 175 s (Table 1) and 225 s [Rosi *et al.*, 2006] in duration, depending on choice for phase 3 termination. Given that the low-amplitude events M1–M3 can be linked to emissions from the lateral vent activity, we ascribe these to the lateral vent eruption phase therefore preferring 75 s for the duration of phase 3 (lateral vent) activity. Finally, two extremely low thermal amplitude thermal oscillations occurred after phase 4 (R1–R2, Figure 3c). These began at 0720:17 and ended at 0721:19 (Table 1); beginning 26 s after phase 4 ended. Including these two events (as well as the opening phase: phase 1) as part of the emission associated with the paroxysm increases the duration to ~8 min [Rosi *et al.*, 2006].

6. CONCLUSIONS

Integration of thermal, seismic, and acoustic data collected during explosive eruptions is becoming an increasingly useful tool in tracking event dynamics (see Harris and Ripepe [2007] for review). Simultaneous collection of seismic and infrasonic data has been relatively widely reported in the literature, where studies at Stromboli include those of Braun and Ripepe [1993], Ripepe and Braun [1994], Chouet *et al.* [1997], and Ripepe *et al.* [2001]. Addition of a thermal IR sensor to the array allows further constraint of the shallow system dynamics, including explosion source depth and ascent velocity [Harris and Ripepe, 2007]. The first experiment integrating a calibrated thermal IR sensor was conducted on Stromboli in 1999 [Ripepe *et al.*, 2002]. Recently, the advent of lightweight, portable thermal cameras capable of collecting images of calibrated temperature at frame rates of up to 30 Hz has added to this capability, allowing improved analysis of the plume ascent dynamics following emission [Patrick *et al.*, 2007; Patrick, 2007]. The use of both permanently deployed thermal IR sensors and helicopter-flown thermal imagers during Stromboli's 5 April explosion greatly enhanced our ability to produce a detailed chronology of this explosive event [Calvari *et al.*, 2006; Rosi *et al.*, 2006; Ripepe and Harris, 2008; Table 1], with the addition of seismic and infrasonic data allowing a full consideration of the event dynamics [Ripepe and Harris, 2008]. For comparison, the dynamics of normal Strombolian events at Stromboli, obtained through an identical integration of thermal, seismic, and acoustic data, are reviewed by Ripepe *et al.* [this volume].

The highly detailed information provided by the thermal record reveals important new insights into the dynamics of an explosive paroxysm. Possibly the most profound is that even a short explosive event is not necessarily composed of a single, simple event, as already observed during previous major explosions at this volcano [Bertagnini *et al.*, 1999]. Instead, it is a complex emission comprising numerous individual pulses. As a result, the eruption comprises a pulsing emission, with explosions grouping together to define individual explosive phases. Even the most apparently simple explosive event is thus a complex phenomena comprising, itself, of a series of explosive events. These complex dynamics can be clearly tracked using suitably placed and protected thermal instruments, revealing processes invisible to the more distant observer. For such observers, after the initial emission, the dynamics at the core of the plume are hidden from view by the optically thick ash at the plume edge. Placement of sensors within the plume reveals these invisible dynamics, yielding new insights into the rapidly evolving and complex behavior of an explosive volcanic eruption.

Acknowledgments. We wish to thank G. Bertolaso and the Italian Civil Protection for their substantial support of our activities; M. Zaia (Zazà) for field assistance; the Air Walser helicopter pilots for allowing us to collect the daily thermal and visual images of the activity; colleagues of INGV from Catania, Palermo, Napoli, Roma, Pisa, and Milano who helped during the monitoring effort.

REFERENCES

- Aiuppa, A., and C. Federico (2004), Anomalous magmatic degassing prior to the 5th April 2003 paroxysm on Stromboli, *Geophys. Res. Lett.*, 31, L14607, doi:10.1029/2004GL020458.
- Bertagnini, A., M. Coltellini, P. Landi, M. Pompilio, and M. Rosi (1999), Violent explosions yield new insights into dynamics of Stromboli volcano, *Eos Trans. AGU*, 80(52), 633–636.
- Bonaccorso, A., S. Calvari, G. Garfi, L. Lodato, and D. Patané (2003), Dynamics of the December 2002 flank failuzre and tsunami at Stromboli volcano inferred by volcanological and geophysical observations, *Geophys. Res. Lett.*, 30(18), 1941, doi:10.1029/2003GL017702.
- Braun, T., and M. Ripepe (1993), Interaction of seismic and air waves as recorded at Stromboli Volcano, *Geophys. Res. Lett.*, 20(1), 65–68.
- Calvari, S., L. Spampinato, L. Lodato, A. J. L. Harris, M. R. Patrick, J. Dehn, M. R. Burton, and D. Andronico (2005), Chronology and complex volcanic processes during the 2002–2003 flank eruption at Stromboli volcano (Italy) reconstructed from direct observations and surveys with a handheld thermal camera, *J. Geophys. Res.*, 110, B02201, doi:10.1029/2004JB003129.
- Calvari, S., L. Spampinato, and L. Lodato (2006), The 5 April 2003 vulcanian paroxysmal explosion at Stromboli volcano (Italy)

- from field observations and thermal data, *J. Volcanol. Geotherm. Res.*, **149**, 160–175.
- Carapezza, M. L., S. Inguaggiato, L. Brusca, and M. Longo (2004), Geochemical precursors of the activity of an open-conduit volcano: The Stromboli 2002–2003 eruptive events, *Geophys. Res. Lett.*, **31**, L07620, doi:10.1029/2004GL019614.
- Cesca, S., T. Braun, E. Tessmer, and T. Dahm (2007), Modelling of the April 5, 2003, Stromboli (Italy) paroxysmal eruption from the inversion of broadband seismic data, *Earth Planet. Sci. Lett.*, **261**, 164–178.
- Chouet, B., G. Saccorotti, M. Martini, P. Dawson, G. De Luca, G. Milana, and R. Scarpa (1997), Source and path effects in the wave fields of tremor and explosions at Stromboli Volcano, Italy, *J. Geophys. Res.*, **102**, 15,129–15,150.
- Cigolini, C., G. Gervino, R. Bonetti, F. Conte, M. Laiolo, D. Coppoli, and A. Manzoni (2005), Tracking precursors and degassing by radon monitoring during major eruptions at Stromboli Volcano (Aeolian Islands, Italy), *Geophys. Res. Lett.*, **32**, L12308, doi:10.1029/2005GL022606.
- D'Auria, L., F. Giudicepietro, M. Martini, and R. Peluso (2006), Seismological insight into the kinematics of the 5 April 2003 vulcanian explosion at Stromboli volcano (southern Italy), *Geophys. Res. Lett.*, **33**, L08308, doi:10.1029/2006GL026018.
- Harris, A. J. L., and M. Ripepe (2007), Synergy of multiple geophysical approaches to unravel explosive eruption conduit and source dynamics—A case study from Stromboli, *Chem. Erde*, **67**, 1–35.
- Harris, A., D. Pirie, K. Horton, H. Garbeil, E. Pilger, H. Ramm, R. Hoblitt, C. Thornber, M. Ripepe, E. Marchetti, and P. Poggi (2005), DUCKS: Low cost thermal monitoring units for near-vent deployment, *J. Volcanol. Geotherm. Res.*, **143**, 335–360.
- Lodato, L., L. Spampinato, A. Harris, S. Calvari, J. Dehn, and M. Patrick (2007), The morphology and evolution of the Stromboli 2002–03 lava flow field: An example of basaltic flow field emplaced on a steep slope, *Bull. Volcanol.*, **69**, 661–679.
- Marchetti, E., and M. Ripepe (2005), Stability of the seismic source during effusive and explosive activity at Stromboli Volcano, *Geophys. Res. Lett.*, **32**, L03307, doi:10.1029/2004GL021406.
- Mattia, M., M. Rossi, F. Guglielmino, M. Aloisi, and Y. Bock (2004), The shallow plumbing system of Stromboli island as imaged from 1 Hz instantaneous GPS positions, *Geophys. Res. Lett.*, **31**, L24610, doi:10.1029/2004GL021281.
- Métrich, N., A. Bertagnini, P. Landi, M. Rosi, and O. Belhadj (2005), Triggering mechanism at the origin of paroxysms at Stromboli (Aeolian Archipelago, Italy): The 5 April 2003 eruption, *Geophys. Res. Lett.*, **32**, L10305, doi:10.1029/2004GL022257.
- Patrick, M. (2005) Strombolian eruption dynamics from thermal (FLIR) video imagery, Ph.D. dissertation, 281 pp., Department of Geology & Geophysics, Univ. of Hawaii.
- Patrick, M. (2007), Dynamics of Strombolian ash plumes from thermal video: Motion, morphology, and air entrainment, *J. Geophys. Res.*, **112**, B06202, doi:10.1029/2006JB004387.
- Patrick, M. R., A. J. L. Harris, M. Ripepe, J. Dehn, D. Rothery, and S. Calvari (2007), Strombolian explosive styles and source conditions: Insights from thermal (FLIR) video, *Bull. Volcanol.*, **69**, 769–784, doi:10.1007/s00445-006-0107-0.
- Pino, N. A., M. Ripepe, and G. B. Cimini (2004), The Stromboli volcano landslides of December 2002: A seismological description, *Geophys. Res. Lett.*, **31**, L02605, doi:10.1029/2003GL018385.
- Ripepe, M., and T. Braun (1994), Air-wave phases in Strombolian explosion-quake seismograms: A possible indicator for the magma level?, *Acta Vulcanol.*, **5**, 201–206.
- Ripepe, M., and A. J. L. Harris (2008), Dynamics of the 5 April 2003 explosive paroxysm observed at Stromboli by a near-vent thermal, seismic and infrasonic array, *Geophys. Res. Lett.*, **35**, L07306, doi:10.1029/2007GL032533.
- Ripepe, M., M. Rossi, and G. Saccorotti (1993), Image processing of explosive activity at Stromboli, *J. Volcanol. Geotherm. Res.*, **54**, 335–351.
- Ripepe, M., S. Ciliberto, and M. Della Schiava (2001), Time constraints for modeling source dynamics of volcanic explosions at Stromboli, *J. Geophys. Res.*, **106**(B5), 8713–8727.
- Ripepe, M., A. J. L. Harris, and R. Carniel (2002), Thermal, seismic and infrasonic insights into conduit process at Stromboli volcano, *J. Volcanol. Geotherm. Res.*, **118**, 285–207.
- Ripepe, M., E. Marchetti, P. Poggi, A. J. L. Harris, A. Fiaschi, and G. Ulivieri (2004a), Seismic, acoustic, and thermal network monitors the 2003 eruption of Stromboli volcano, *Eos Trans. AGU*, **85**(35), 329–332.
- Ripepe, M., P. Poggi, and E. Marchetti (2004b), Small aperture infrasonic array monitors activity of Stromboli Volcano, *Inframatics*, **7**, 1–14.
- Ripepe, M., D. Delle Donne, A. Harris, E. Marchetti, and G. Ulivieri (2008), Dynamics of strombolian activity, this volume.
- Rosi, M., A. Bertagnini, A. J. L. Harris, L. Pioli, M. Pistolesi, and M. Ripepe (2006), A case history of paroxysmal explosion at Stromboli: Timing and dynamics of the April 5, 2003 event, *Earth Planet. Sci. Lett.*, **243**, 594–606.
- Tinti, S., F. Pagnoni, F. Zaniboni, and E. Bortolucci (2003), Tsunami generation in Stromboli island and impact on the south-east Tyrrhenian coasts, *Nat. Hazards Earth Syst. Sci.*, **3**, 299–309.
- Tinti, S., A. Maramai, A. Armigliato, L. Graziani, A. Maucci, G. Pagnoni, and F. Zaniboni (2006), Observations of physical effects from tsunamis of December 30, 2002 at Stromboli volcano, southern Italy, *Bull. Volcanol.*, **68**, 450–461.
- Turner, J. S. (1969), Buoyant plumes and thermals, *Annu. Rev. Fluid Mech.*, **1**, 29–44.

S. Calvari, L. Lodato, and L. Spampinato, INGV-Catania, Piazza Roma 2, 95123 Catania, Italy.

A. J. L. Harris, HIGP/SOEST, University of Hawai'i, 1680 East West Road, Honolulu, HI 96822, USA. (harris@higp.hawaii.edu)

M. Ripepe, Dipartimento di Scienze della Terra, Università di Firenze, Via La Pira 4, 50121 Firenze, Italy.

The Paroxysmal Event and Its Deposits

Marco Pistolesi,¹ Mauro Rosi,¹ Laura Pioli,² Alberto Renzulli,³ Antonella Bertagnini,⁴ and Daniele Andronico⁵

The 5 April 2003 eruption of Stromboli volcano (Italy) was the most violent of the past 50 years. It was also the best documented due to the accurate geophysical monitoring of the ongoing effusive eruption. Detailed field studies carried out a few hours to a few months after the event provided further information that were coupled with visual documentation to reconstruct the explosive dynamics. The eruption consisted of an 8-min-long explosive event preceded by a short-lived precursory activity that evolved into the impulsive ejection of gas and pyroclasts. Meter-sized ballistic blocks were launched to altitudes of up to 1400 m above the craters falling on the volcano flanks and on the village of Ginostra, about 2 km far from the vent. The vertical jet of gas and pyroclasts above the craters fed a convective plume that reached a height of 4 km. The calculated erupted mass yielded values of $1.1\text{--}1.4 \times 10^8$ kg. Later explosions generated a scoria flow deposit, with an estimated mass of $1.0\text{--}1.3 \times 10^7$ kg. Final, waning ash explosions closed the event. The juvenile fraction consisted of an almost aphyric, highly vesicular pumice mingled with a shallow-derived, crystal-rich, moderately vesicular scoria. Resuming of the lava emission a few hours after the paroxysm indicate that the shallow magmatic system was not significantly modified during the explosions. Combination of volume data with duration of eruptive phases allowed us to estimate the eruptive intensity: during the climactic explosive event, the mass discharge rate was between 10^6 and 10^7 kg/s, whereas during the pyroclastic flow activity, it was $2.8\text{--}3.6 \times 10^5$ kg/s. Strong similarities with other historical paroxysms at Stromboli suggest similar explosion dynamics.

¹Dipartimento di Scienze della Terra, Università di Pisa, Pisa, Italy.

²University of Oregon, Eugene, OR, USA.

³Istituto di Scienze della Terra, Università di Urbino, Urbino, Italy.

⁴Istituto Nazionale di Geofisica e Vulcanologia, Sezione di Pisa, Pisa, Italy.

⁵Istituto Nazionale di Geofisica e Vulcanologia, Sezione di Catania, Catania, Italy.

The Stromboli Volcano: An Integrated Study of the 2002–2003 Eruption
Geophysical Monograph Series 182
Copyright 2008 by the American Geophysical Union.
10.1029/182GM26

1. INTRODUCTION

The current activity of Stromboli has likely persisted since the fourth to the seventh century A.D. [Rosi *et al.*, 2000]. Activity has been dominated by low-energy, Strombolian explosions that usually occur at intervals of 10–20 min from vents within an elliptical, SW–NE elongated crater area located at an elevation of 750 m. This normal activity is occasionally broken by discrete, violent explosions called “paroxysms.” Paroxysms are short-lived explosive events, forming a vertical column of gas and pumice rising up to several kilometers and launching blocks up to 2–3 km from the vent, eventually damaging the settled areas. These events

occur suddenly, often during persistent mild activity and appear not to be preceded by any significant instrumental precursors. Because of their violent and unpredictable nature, paroxysms represent a major threat to people either visiting the volcano summit or living in the settled areas. After pioneering works by *Perret* [1915] and *Rittman* [1931], studies on paroxysmal activity have been limited to compositional characteristics of the juvenile ejecta and general descriptions [*Barberi et al.*, 1993; *Rosi et al.*, 2000; *Bertagnini et al.*, 2003; *Francalanci et al.*, 2004]. However, quantification of the physical characteristics of the eruption, particularly the aerial distribution and variability of the deposits, is fundamental for the evaluation of the eruptive parameters and eruption modeling.

The paroxysmal eruption occurred on 5 April 2003, at 0713:24 UT, while an effusive eruption was in progress [*Harris et al.*, this volume]. The paroxysm was observed, photographed, and filmed by several researchers. From an examination of the visual documentation, geophysical data, and deposit analysis, it was possible to define four main phases [*Rosi et al.*, 2006] summarized as follows:

- Phase 1: eruption onset
- Phase 2: climactic explosive event
- Phase 3: pyroclastic flow and smaller explosions
- Phase 4: final ash explosions

Accurate field analyses of pyroclastic deposits were carried out shortly after the paroxysm, when the deposit was pristine. Laboratory analyses were performed to assess the physical characteristics of the ejecta and make inferences about the origin of the different eruptive products. Integration of all data sets provides a compelling quantitative reconstruction that sheds new light on the physical volcanology of the event.

2. METHODS

Sample collection and mapping across the distal and proximal areas started just a few hours after the eruption and was carried out during several fieldtrips, until April 2004. During fieldwork, thickness and mass/unit area of the fallout deposit were mapped on flat to gently inclined areas. In the summit area, a series of sites were chosen to cover a horseshoe-shaped zone equidistant from the vents. Grainsize, componentry analyses, and petrographic observation of both juvenile and lithic fragments were conducted on selected samples. In each site, all the material was picked up and weighed from a 1 × 1- to 5 × 5-m square that was set depending on mean granulometry or continuity of the blanket. In distal areas (Punta Lena, southern tip

of the island), sampling sites were located on flat roofs of houses.

Impact crater mapping was performed during multiple field surveys; in addition, analysis and comparison of images obtained during aerial photogrammetric surveys made 1 month before (15 March, scale 1:7000) and a few days after the eruption (16 April, scale 1:8000, and 26 May 2003, scale 1:5000) were kindly made available by M. Marsella [*Baldi et al.*, 2003]. Comparison with field observations indicates that aerial images showed only blocks exceeding 2 m in diameter.

Bulk density measurements were performed on juvenile fragments from the main fallout deposit (total of 120 clasts), following the method of *Polacci et al.* [2001]. As juvenile clast densities vary with size, only clasts from a restricted size fraction were used (diameters ranging from 4 to 10 cm), large enough such that they are indistinguishable in density from bigger clasts but small enough to be reasonably common in the deposit.

3. DEPOSIT FEATURES

All studied deposits consist of coarse pyroclasts (bombs and lapilli) with subordinate amounts of fine ash. Pumice lapilli were observed floating in the sea south of the island immediately after the eruption and were washed ashore on the southern coast of Stromboli in the hours following the event. Five categories of deposits can be identified: (a) “ballistic fallout,” (b) “fallout tephra,” (c) “pyroclastic flow,” (d) “late ash and lapilli fallout,” and (e) “secondary flows” (Figure 1).

3.1. Ballistic Fallout

A total of 37 impact craters were mapped, covering an area of about 0.3 km² on the northeastern flank of the volcano (Figure 1a).

The zone of maximum concentration of the lithic ejecta was located between 750 and 1350 m NE of the crater area. Most of the blocks were measured and sampled between 450 and 650 m above sea level (asl), from the Vallonazzo to the northern edge of the Sciara del Fuoco (SdF; Figure 1a). The blocks that fell in this area ranged from decimeter size to meter size and were often coated by light-colored highly vesicular pumice (Figure 2a). The largest block (3.5 × 1.5 × 1.5 m) was encountered on the upper northeastern flank at an elevation of 450 m asl and 1 km from the craters. It formed a 1.5- to 2-m-deep elliptical impact crater of 13.5 × 8.5 m (Figure 2b). Blocks that fell on hard rocks mostly fragmented upon impact, ejecting centimeter- to decimeter-sized shards up to tens of meters from the impact site (Figure 2c).

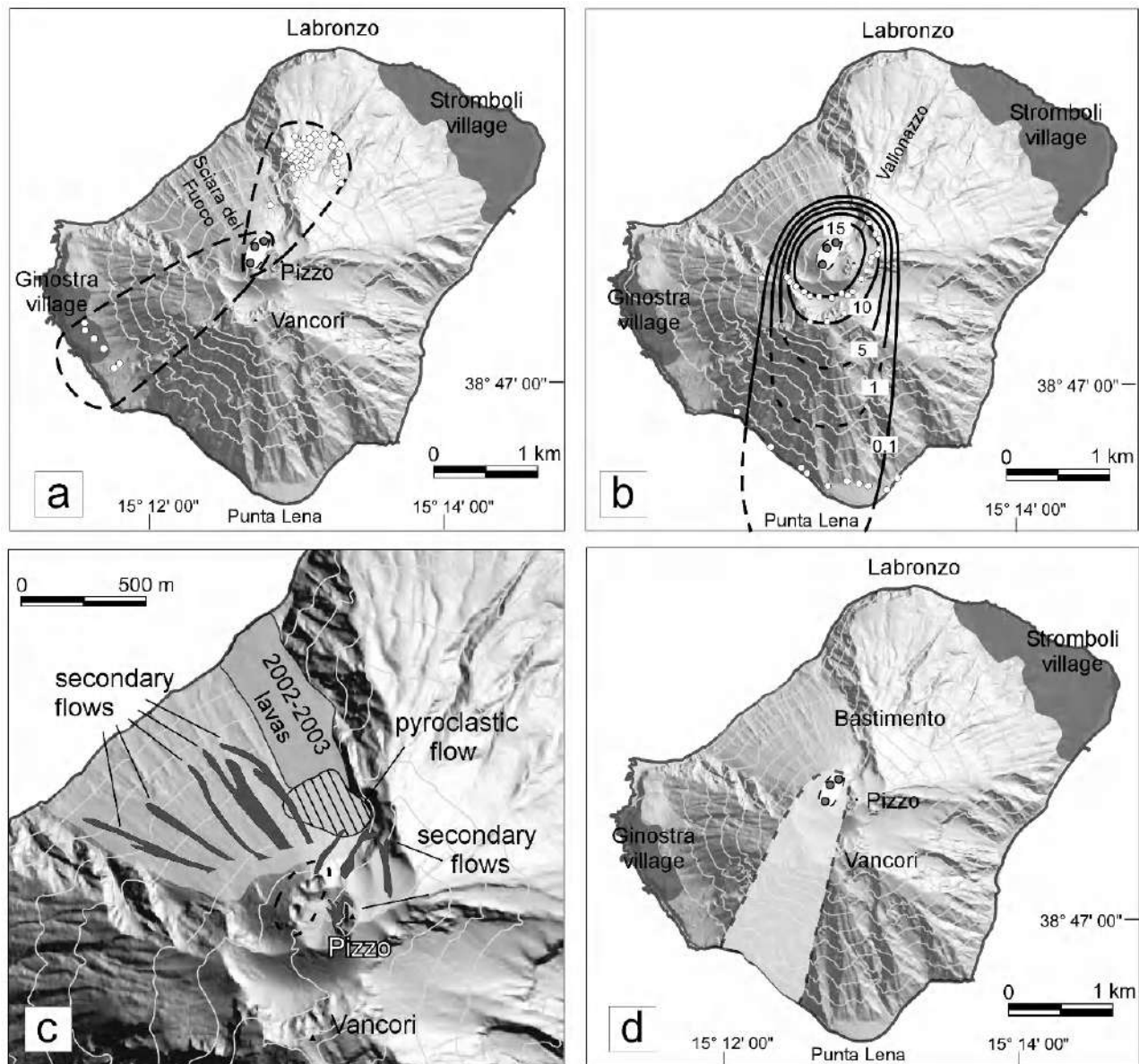


Figure 1. (a) Mapped impact craters from larger ballistic blocks emitted during phase 2. Dashed lines enclose the areas of higher concentration of blocks. Measurements of blocks and GPS locations of 16 impact craters were performed during field surveys made in April and May 2003. Impact craters produced by blocks with diameter ≥ 2 m were also mapped using data of aerial photogrammetric surveys of the island (15 March 2003, scale 1:7000; 16 April scale 1:8000, and 26 May 2003, scale 1:5000) [Baldi et al., 2003]. (b) Isomass map of fallout deposit (values are in kg/m²). (c) Aerial dispersion of secondary flow (dark gray), and pyroclastic flow (striped area) deposits. (d) Dispersion of final ash (phase 4). Modified from Rosi et al. [2006].

Blocks that fell over vegetation or soft soil along the volcano slopes slipped for tens of meters, leaving paths on the ground (Figure 2b) and in some cases setting fire to vegetation. Many blocks fell west and southeast of the vents, including the village of Ginostra (seriously damaging a house,

a road, and a water tank). Eyewitness accounts reported the fall of several ejecta along the western flank of the volcano and in the sea in front of Ginostra at the beginning of the main explosive phase. The distribution of the impact craters was strongly asymmetrical, being concentrated in two narrow

Figure 2. Ballistic blocks. (a) The coating of a block by highly vesicular LP magma. (b) One of the largest blocks ~1 km NE of the vents. (c) Decimeter-sized shard ejected after fragmentation of a block upon impact near Ginostra village and jabbed in a prickly pear (picture courtesy of K. Cashman). (d) Radial fractures due to the impact in a meter-sized block.

sectors with a 30°–35° aperture oriented to the NE and WSW, respectively (Figure 1a).

3.2. Fallout Tephra

The wind-blown fallout deposit consisted of variably expanded and mingled pumice clasts and lithic fragments. On the east part of the island, the most distal juvenile material was found at 650 m asl (Bastimento area) consisting of isolated spatter fragments (25–30 cm). Gray-colored “fresh” lithic blocks were also present together with subordinate hydrothermally altered ejecta. South of the summit vents, in the valley between the Pizzo Sopra la Fossa and the Vancori peaks (Figure 3a), the deposit formed a continuous bed extending up to 0.6 km from the vent, reaching maximum thickness of 15 cm. In this sector, juvenile material was made up by highly vesicular pumiceous lapilli

(10–15 cm). Lithic material was dominantly composed by altered clasts, although fresh lava fragments are still present. Southwest of the vents, the deposit had an average thickness of 2 cm, was very well sorted ($\sigma = 0.89\phi$), mainly comprising coarse-grained lapilli ($Md\phi = -3.61\phi$) and a significant amount of ash finer than 1 mm ($F1 = 4.34 \text{ wt } \%$). The juvenile component accounted for 63 wt % of the deposit (Figure 4), whereas the lithic component mainly consisted of hydrothermally altered clasts. Westward of the crater area, the deposit was represented by a carpet of scattered spatters. Lithic material was composed of spongy scoria clasts, fresh lava blocks, and variably altered lava and scoria blocks. A moderately sorted, incipiently welded spatter deposit was observed across the summit area of the volcano. In a site located 350 m NE of crater 1, this deposit was 1-m thick, and consisted of decimeter-sized spatter fragments mixed with subordinate amounts of centimeter- to decimeter-sized

Figure 3. (a) Fallout deposit blanketing the area between Pizzo and Vancori. (b) Welded deposit in proximal area. (c) Active lava flows covering deposits of pyroclastic flows, photographed on 18 April 2003. Hot avalanche lobes overlap the scoria flow deposit on northern side of the lava field. (d) Secondary flow lobe in the area between the active craters and Bastimento ridge.

accidental lithic clasts (Figure 3b). Individual juvenile clasts were flattened and elongated due to splashing upon landing and limited downhill flowage.

In medial–distal locations, the deposit was dispersed only southward and consisted of a discontinuous blanket of scoriaceous pumice and lithic fragments. Lithic material was made up of millimetric to centimetric fragments of dark gray clasts or more frequently by red or brown material.

The mass of the juvenile material increased linearly from west to east, with minimum values of 0.4 kg/m^2 to maximum values of 20 kg/m^2 south of Pizzo Sopra la Fossa, in coincidence with the dispersal axis of the fallout (Figure 5). Values further decreased (5 kg/m^2) toward the eastern sector. In proximal locations, lithic/juvenile ratios (Figure 4) ranged from 0.30 to 4.95, increasing from east to west.

The isomass map was drawn by interpolating measurements of mass loading per unit area made along three

transects across the deposit at increasing distance from the craters and at scattered sites in proximal area (Figure 1b). It indicates a dispersal axis oriented to the south of the vents.

Loading per unit area of fallout deposit versus isomass area plot indicates a single exponential decay law. Total erupted mass calculated according to *Pyle* [1989], yielded values of $1.1\text{--}1.4 \times 10^8 \text{ kg}$, with erupted magma accounting for $0.8\text{--}1.1 \times 10^8 \text{ kg}$ (estimated maximum error = 10%).

3.3. Pyroclastic Flow

A coarse-grained pyroclastic flow deposit was emplaced on top of the active lava flow field on the upper, eastern sector of the SdF. The deposit was dispersed over an area of 0.05 km^2 with an average thickness of 1 m (Figures 1c and 3c) corresponding to a volume of $0.9\text{--}1.1 \times 10^4 \text{ m}^3$ (corresponding to a mass of $1.0\text{--}1.3 \times 10^7 \text{ kg}$).

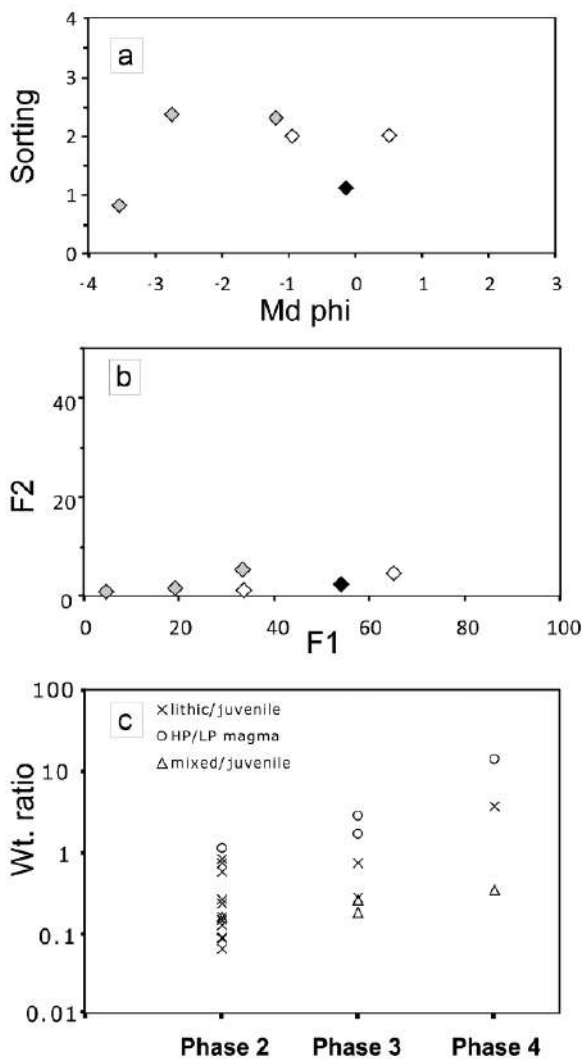


Figure 4. Grainsize features and componentry of the analyzed samples. (a) Sorting versus median grainsize ($Md\phi$), (b) F_1 versus F_2 . Gray diamonds, phase 2 samples; white diamonds, phase 3 samples; black diamonds, phase 4 sample. (c) Relative proportion between lithic and juvenile (black, golden, and mixed) material during the subsequent phases of the event.

Field inspection was made on 13 May 2003 when most of the deposit had already been completely covered by new lava. However, limited portions of the deposit had been pushed upward onto the surface of the lava field, possibly as a result of lava injection from below. Grain-size analysis of a 2-kg sample of the uplifted deposit indicates that the deposit matrix was poorly sorted ($\sigma = 2.16\phi$), medium-coarse ash ($Md\phi = 0.44\phi$). Pyroclastic flow material contains juvenile clasts (57 wt %) mainly composed of crystal-rich, vesicle-

poor, scoria and subordinate pumice clasts (Figures 4 and 6a) of variable size, far denser than the fallout material and showing plastic deformation, welding, compaction, and a characteristic color from brown to red, probably due to oxidation that occurred after high temperature emplacement (Figure 6a).

The aerial distribution of the scoria flow deposit closely matches the source area of the ground-hugging ash plume visible during phase 3 in the photographic records.

3.4. Late Ash and Lapilli Fallout

A red ash and lapilli bed up to 5-cm thick covered the pumice deposit in a narrow sector S-SW of crater 3 (Figure 1d). A representative sample taken about 300 m S-SW of crater 3 revealed that the deposit was fine grained ($F_1 = 53.86$ wt %, $Md\phi = -0.10\phi$) and well sorted ($\sigma = 1.10\phi$). The deposit is mainly represented by altered lava fragments (79 wt %) with subordinate amounts of fresh crystalline scoria fragments (Figure 4). The dispersion and lithology of the bed matches the dispersion direction and color of the short-lived plume emitted during phase 4.

3.5. Secondary Flows

Hot avalanche deposits resulted from sliding, and secondary mass flowage of fall deposits accumulated on steep slopes ($>10^\circ$ – 20°) around the crater area and in the SdF (Figures 1c and 3c). The flow formed up to 4-m wide, 3-m thick, and a few tens of meters long, steep-sided lobes that accumulated on the southern edge of the lava field. Field observations made in the days after the event showed that the deposit originated from the sliding of the spatter agglutinate deposit about 300 m upslope of the accumulation site. In this sector, the flow deposit consisted of juvenile clasts showing clear evidence of plastic deformation and agglutination (Figure 6b).

Other lobes on the northern flank of Pizzo flowed for distances of about 50 m, with lateral extent of 2–4 m and front thickness of 1 m (Figure 3d). The deposits had massive to inversely graded structure.

4. PHYSICAL FEATURES OF THE ERUPTED MATERIAL

4.1. Juvenile Component

The juvenile material is composed of black, crystal-rich scoria and tan, nearly aphyric, pumice corresponding to the well-known HP (highly porphyritic) and LP (low porphyritic) magma types described by *Corsaro et al.* [2004],

Figure 5. Loading/unit area of material for proximal and distal deposits (graphs). Lithic/juvenile ratios are shown in the pie charts on the maps (dark gray for lithic and light gray for juvenile material).

Francalanci et al. [this volume], and *Métrich et al.* [2001]. The great majority of the clasts displays intermediate features and mingling of the two magma types up to millimeter scale (Figure 6c). Very rare juvenile fragments consist of a single magma type; about 10 vol % of them also contains small

(millimeter-sized) lithic fragments dispersed in the glassy matrix. The proximal fallout deposit was mainly composed of spatter (10–30 cm in size; Figures 6d to 6f) and highly vesicular pumice fragments (≤ 10 cm). Vesicularity and mean vesicle size increases from the rim to the inner portion of the

Figure 6. (a) Oxidized scoria from pyroclastic flow deposit. (b) Ribbon scoria from secondary flow deposit. (c) Mingled clast of distal (Punta Lena) fallout deposit. (d) Exceptionally expanded clast with a central main cavity surrounded by a smooth microvesicular glassy rim. (e) Spatter clast with engulfed lithic fallen in proximal area. (f) Twisted bomb. Scale bars in Figures 6a, 6c, and 6d are 5 cm long.

clasts, as the result of postfragmentation expansion. Some exceptionally expanded clasts displayed a central main cavity surrounded by a microvesicular glassy rim less than 1 cm thick (Figure 6d). Pumiceous bombs are glassy with few crystals (≤ 5 vol %) with phenocrysts of plagioclase, clinopyroxene, and olivine. HP magma fragments have similar mineralogy but higher crystallinity (45–50 vol %).

The clasts have densities ranging from 580 to 1840 kg/m³ (mean value = 1080 ± 250 kg/m³), corresponding to vesicularities of 35 to 79 vol % (mean = 61 vol %), calculated using a dense rock equivalent (DRE) density of 2880 kg/m³ (Table 1). Clast vesicularities have unimodal distribution with a dense tail represented by about 10% of clasts (Figure 7).

The broad spectrum of vesicularity of the analyzed clasts likely corresponds to different proportion of the two magmas (HP and LP) mingled up to centimeter scale: denser clasts have higher proportions of HP magma, whereas lighter clasts are composed almost entirely of LP magma.

4.2. Lithic Component

The most common lithotypes that erupted as lithic blocks during phase 2 consist of a light gray to gray holocrystalline subvolcanic rock (type 1 igneous ejecta, Figures 2, 8, and 9) with a relatively homogeneous structure, varying from fine to medium-grained; clasts that fell over the north to east

Table 1. DRE Values Obtained With Powder Density Measurements^a

Sample	Lithotype	DRE, kg/m ³	SD
ST 325 A	5 April LP pumice	2860	0.02
ST 325 B	5 April LP pumice	2860	0.03
ST 317	5 April HP scoria	2840	0.02
ST 320	5 April HP scoria	2860	0.03
ST 212	HP scoria (recent activity)	2890	0.02
ST 140	LP pumice (historical activity)	2980	0.03
STR 060303	6 March 2003 lava	2870	0.01
STR 130503	13 May 2003 lava	2900	0.02

^a Four samples of 5 April were analyzed (two golden pumice and two black scoria) together with two lava samples of 2002–2003 effusive activity (one before and one after 5 April paroxysm). A pumice and a scoria sample of preceding activity (1996–2000) were also analyzed for comparison.

side of the volcano are often coated with the highly vesicular magma (Figure 2a). The phenocryst assemblage consists of plagioclase (~28% volume, up to 3 mm in size), clinopyroxene (~15% volume, up to 7 mm in size), and olivine (~5% volume, up to 3 mm in size). Finer-grained crystals of plagioclase, sanidine, clinopyroxene, olivine, opaque minerals (Ti-magnetite and ilmenite), apatite, and phlogopite interstitially crystallized between the “phenocrystic” phases [for the mineral chemistry, see *Francalanci et al.*, this volume]. Plagioclase phenocrysts and microphenocrysts often show igneous lamination (Figure 8a). Sanidine forms a finer-grained interstitial component as anhedral–poikilitic phase and as rim overgrowths, up to 50 µm thick, on plagioclase phenocrysts (Figure 8b). These fragments have the same texture; chemical and mineralogical composition of the HP magma erupted during the present-day activity and the 2002–2003 crisis [*Bertagnini et al.*, this volume; *Francalanci et al.*, this volume; *Landi et al.*, this volume]. Such characteristics suggest an origin from the complete crystallization of the crystal-rich degassed magma that resides in the shallow magmatic system. Miarolitic cavities (up to a few centimeters in size) occur and can be partially to completely filled by millimeter-sized phlogopite (up to 7 mm), hyperstene, sanidine (<150 µm), Fe–Ti oxides ± clinopyroxene, and silica phases.

Type 2 ejecta consist of composite lithic blocks (subvolcanic breccia), where light gray angular blocks (a few millimeters to 0.5 m in size) are set in sharp contact with a dark gray, vesicular, porphyritic lava component (Figures 8c–8e). Although finer-grained and porphyritic (Figure 8d), the dark gray lava in these ejecta shows a similar mineralogy to the coarser-grained type 1 rocks and exactly the same chemi-

cal bulk composition [*Francalanci et al.*, this volume]. The groundmass of the dark gray lava-like component of these composite ejecta is microcrystalline to cryptocrystalline made of interstitial sanidine, plagioclase, clinopyroxene, and opaque minerals. Contacts between the two components of the composite blocks usually show brittle features with broken crystals of the light gray igneous component and millimeter-sized vesicles on the dark gray lava-like component (Figure 8e). Type 2 ejecta appear to be therefore formed by the intrusion of the HP magma (then crystallized and yielding the dark gray lava-like) into the light gray, crystallized subvolcanic rocks (already in the subsolidus range).

A third type of igneous ejecta consists of strongly shattered fragments of the light gray (i.e., type 1) subvolcanic rocks (from a few millimeters to 30 cm) kneaded by black scoriae to form a rather unconsolidated, poorly welded concrete-like volcanic breccia (type 3, Figure 9a).

Some ejecta that erupted on 5 April 2003 are also characterized by a thin red film of exogenous alteration due to the exposure to acid gases and often showing radial fractures as the result of the impact (type 4, Figures 2d and 9b). In thin sections, they are very different from the most common type 1 igneous ejecta, being characterized by a microstructure which is very similar to that found in some shoshonitic dykes exposed near the summit craters [*Corazzato et al.*, 2008]. These blocks are therefore fragments of dykes which were already exposed to the atmosphere at the time of the paroxysmal event.

Fragments of vesicular lavas, belonging to the stratigraphy of the Stromboli cone of the last 10–13 ka were also erupted as blocks and lapilli. The lavas are commonly altered to Mg–Al–Na–hydrous sulfate and hydroxysulfate,

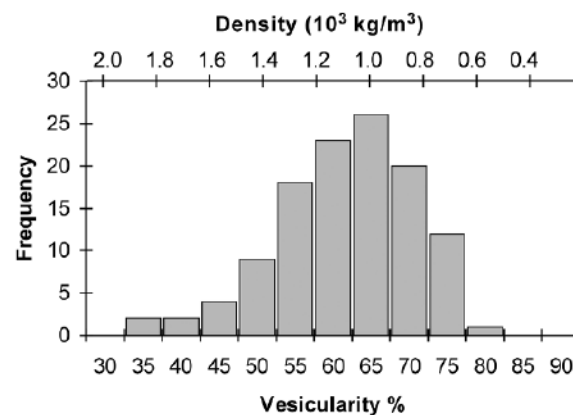


Figure 7. Frequency histogram for vesicularity distribution of 120 analyzed specimens from a sample collected in the Punta Lena coast. Density range is shown in upper horizontal axis.



Figure 8. Macroscopic and microscopic features of the type 1 (lava) and type 2 (breccia) lithic ejecta. Type 1 thin-section images: (a) igneous lamination of plagioclases, (b) sanidine rim on plagioclase phenocryst, scanning electron microscope backscattered images, (c) type 1 lava, (d) dark gray lava of the type 2 block, and (e) contact between the two igneous components in the type 2 breccia. Broken plagioclase crystals can be seen at the center of the photo, whereas vesicles (on the right) occur along the contact in the dark gray porphyritic component.

such as pickeringite and natroalunite (argillic facies), likely by hydrothermal and fumarolic alteration (Figure 9c).

5. ERUPTIVE DYNAMICS

The event started with initial ash emission from all three summit craters [Harris *et al.*, this volume]. The ash emission could be due to early gas leakage and/or sliding of the crater walls induced by the rapid ground deformation. The ash was not dispersed beyond the craters and was negligible with respect to the total erupted mass. After this initial phase, a vertical jet formed above the craters and meter-sized blocks and bombs were ejected. A convective column extending to a height of about 4 km formed above the craters in the following minutes eventually feeding a plume that dispersed

southward [Rosi *et al.*, 2006]. Field data indicate that most of the pyroclastic material was emitted during this phase, that lasted 38 s. Average mass discharge rate yielded values of $2.8\text{--}3.6 \times 10^6 \text{ kg/s}$, with a possible peak of $1.0\text{--}1.2 \times 10^7 \text{ kg/s}$, assuming that the jet was sustained only during the main, 10-s-long thermal pulse [Harris *et al.*, this volume]. Block ejection velocities were calculated following Martin [1991] by using field data and images of the eruptions. The zone of maximum concentration of blocks was located between 750 and 1350 m NE of the crater area. Most of the blocks landed within the first 30 s of the main climactic event. This is consistent with minimum launch velocities of 150 m/s, ejection angles ranging from 70° to 85° and maximum heights of about 1050 m above the craters [Rosi *et al.*, 2006].

ing the normal Strombolian explosions or lava flows but arrested in situ and completely degassed within the uppermost subvolcanic system. The asymmetrical distribution and different nature of lithic blocks (hydrothermally altered fragments, material altered from fumarolic activity and vesicular altered lavas to the SW of crater 3, and fresh, holocrystalline subvolcanic blocks to the NNE of crater 1) and visual observation of the eruption [Calvari *et al.*, 2006] indicate eruption from at least two vents systems.

High vesicularity of the juvenile clasts, associated with proximal welding and postfragmentation expansion (suggesting low viscosity at the time of landing and high eruption temperatures) are indicative of magmatic fragmentation. Furthermore, a progressive increase of HP/LP magma and lithic/juvenile ratios from phase 2 to phase 4 coupled with eruption intensity decrease, also suggests that the explosivity was mainly driven by fast ascent of water-rich LP magma.

6. COMPARISON WITH OTHER PAROXYSMAL EVENTS

Any paroxysmal event is characterized by the emission of aphyric, highly vesicular LP magma (“golden pumice” of Bertagnini *et al.* [1999]) that is dispersed over large areas [Rosi *et al.*, 2000] and is not erupted during normal Strombolian explosions. A list of the main eruptive events of the last century is given by Capaldi *et al.* [1975] and Barberi *et al.* [1993]. Dispersal of pumice along the volcano slopes to the sea is described for the 1883 [Mercalli, 1884], 1891 [Riccò and Mercalli, 1891], 1906 [Riccò, 1907], 1907 [Platania, 1908], 1912 [Perret, 1915], 1919 [Ponte, 1919], 1930 [Rittmann, 1931], 1936 [Abbruzzese, 1937], and 1944 [Cavallaro, 1955] explosive events. Emission of a large amount of lithic blocks is also reported for most of these eruptions. Characteristics of the most common lithic ejecta erupted during the 11 September 1930, 13 November, and 10 December 1915 (when some of them were also coated by highly vesicular glass) events [Ponte, 1919, 1921; Rittmann, 1931] are similar to the type 1 lavas.

Among the descriptions of historical paroxysms, the report of the 1930 event is particularly detailed and accurate [Rittmann, 1931]. The eruption sequence, the dispersal of the deposit, and the nature of the ejecta have striking similarities with the 5 April eruption: the 1930 event started suddenly interrupting “normal” Strombolian activity with mild explosions emitting ash, followed by two, closely spaced, extremely violent explosions clearly felt up to tens of kilometers away. Meter-sized lithic blocks were launched on the SW and NNE flanks, and a heavy rain of meter-sized spatter clasts, decimeter-sized bombs, lapilli, and ash fell on the volcano. It is noteworthy that the lithic block emission is

Figure 9. (a) Type 3 volcanic breccia clast. (b) Type 4 ejecta characterized by a thin red alteration rim due to exposure to acid gases before being erupted. (c) Block affected by strong fumarolic and hydrothermal alteration (picture courtesy of S. Del Moro).

Phase 3 formed a pyroclastic flow that spread onto the lava field and had a total duration of 75 s [Harris *et al.*, this volume]. Average mass discharge rate during this phase decreased to $1.3\text{--}1.7 \times 10^5 \text{ kg/s}$. Images, field and geophysical evidences [Rosi *et al.*, 2006; Harris *et al.*, this volume] strongly suggest that the flow was emitted from a lateral vent, likely located NE of the summit craters, at the head of the dyke that was feeding the ongoing lava flow.

The final waning phase of the eruption had a pulsatory dynamics emitting lithic fragments, a subordinate amount of crystal-rich scoria and scarce pumice clasts from crater 3 (Figure 1d). Hot avalanche deposits resulting from sliding and secondary mass flowage of fall deposits accumulated on steep slopes around the crater area and in the SdF.

Juvenile material is mainly composed of black, phenocryst-rich, scoria and tan, aphyric pumice, corresponding to HP and LP magma types described by Bertagnini *et al.* [1999, 2003], Francalanci *et al.* [2004], and Métrich *et al.* [2001], displaying intermediate features and mingling of the HP and LP magma types up to millimeter scale. This suggests that the eruption involved a batch of magma compositionally distinct from the degassed, crystal-rich magma that was feeding the ongoing lava flow. Lithic blocks mainly consisted of holocrystalline shallow subvolcanic rocks and variously altered blocks. The fresh subvolcanic ejecta represent the slowly cooled equivalents of the HP magmas feed-

fully comparable both in terms of launch directions (the affected zone in 1930 were Ginostra and Labronzo) and zonation of type of material; in both cases, fresh holocrystalline gray to light gray blocks of very shallow subvolcanic origin such as type 1 ejecta, were launched towards NE slope, while altered material from fumarolic and hydrothermal activity fell on the opposite side. Also, juvenile material showed the same characteristics: both expanded pumice with smooth surface and a hollow internal cavity associated with black scoriaceous material were emitted. Finally, both events produced pyroclastic flows. The end of the 1930 paroxysm was marked by ash explosions and lava emission from the summit craters. As a whole, these features suggest that whatever the conditions of the uppermost part of the feeding system, the overall eruptive dynamics display similar characteristics. These conditions were open vents in 1930 (as well as in 1916 and 1919 events) and debris-clogged vents and lava effusion during 5 April. This strongly suggests that this type of explosive activity at Stromboli is accounted well for by the same mechanism as proposed for the 5 April 2003 event.

7. CONCLUSIONS

Analysis and integration of visual and field data during and after the 5 April 2003 paroxysmal eruption of Stromboli provided an outstanding opportunity to observe and study deposit features in order to assess the dynamics of this eruption.

Collected data indicate that the dynamics of the 5 April 2003 Stromboli paroxysm was an impulsive, short-lived pulsatory event. The explosions initially involved the summit vent systems and then propagated to lateral lava boccas. Maximum intensity was reached within the first minute, peaking to values comparable to subplinian basaltic eruptions [Rose *et al.*, 2007; Stelling *et al.*, 2002], when the highest proportion of volatile-rich LP magma was emitted. The progressive increase of lithic/juvenile ratio and the decrease of the relative proportion of LP magma from phase 2 to phase 4 (Figure 4) suggest that the explosive dynamics was mainly controlled by the LP, volatile-rich magma. The nature of the erupted lithic ejecta and the occurrence of both LP and HP magma coating indicate incorporation of fragments from igneous wall rocks and subvolcanic breccias surrounding the shallow conduit in the ascending magmatic mixture (types 1–3 ejecta). Further lithic fragments (type 4, vesicular slightly altered lavas and strongly altered blocks affected by hydrothermal and fumarolic activity) represent the material located at the surface or the inner parts of the summit cones, disrupted during the paroxysm. Lava flow emission was only temporarily interrupted by the paroxysm: active lava flows outpoured from vents at ~600 m asl, less than 2 h after the eruption [Calvari *et al.*, 2006] suggest-

ing that the shallow magmatic system was not significantly modified by the event.

Finally, our data indicate that the paroxysm dynamics was likely related to magmatic fragmentation of volatile-rich LP magma subjected to fast ascent and decompression eventually rising through, and effectively mingling with, a superficial reservoir constituted by a degassed, more crystalline HP magma. The emitted products, impulsive nature of the event, and eruptive dynamics make the eruptive event of 5 April 2003 fully comparable with other historical paroxysms of Stromboli volcano that have occurred both in open and closed vent conditions, suggesting that the paroxysms are driven by sudden input of LP magma, regardless of conditions in the shallow reservoir.

Acknowledgments. This work was financially supported by the Istituto Nazionale di Geofisica e Vulcanologia and Dipartimento di Protezione Civile in the framework of the project “Monitoring and Research Activity at Stromboli and Panarea” (V2/10, V2/09, and V2/18, for M.R., A.B., and A.R., respectively). L.P. was partly funded by NSF EAR0510493. The Italian Civil Protection is acknowledged for logistic support and helicopter use during field activities. The volcanological guides of Stromboli Island and the Guardia di Finanza alpine guides are acknowledged for having provided fundamental support during field activities throughout and after the 2002–2003 eruptive crisis. K. Cashman, S. Del Moro, M. Menna, and A. Harris are acknowledged for fruitful discussions and having kindly shared data and some field pictures with the authors. K. Cashman is also acknowledged for a revision of an early version of the manuscript. M. Marsella provided aerial pictures and technical support for mapping of ballistic blocks.

REFERENCES

- Abbruzzese, D. (1937), Attività dello Stromboli dal 1930 al 1934, *Boll. Sismol. Soc. Ital.*, 33, 118–125.
- Baldi, P., F. Belloli, M. Fabris, M. Marsella, R. Monticelli, and V. Signoretto (2003), La fotogrammetria digitale differenziale per il monitoraggio del versante della Sciara del Fuoco (Isola di Stromboli) dopo l’evento del 30 dicembre 2002, 7° National ASITA Meeting, Verona, Italy.
- Barberi, F., M. Rosi, and A. Sodi (1993), Volcanic hazard assessment at Stromboli volcano based on review of historical data, *Acta Vulcanol.*, 3, 173–187.
- Bertagnini, A., M. Coltellini, P. Landi, M. Pompilio, and M. Rosi (1999), Violent explosions yield new insights into dynamics of Stromboli volcano, *Eos Trans. AGU*, 80, 633–636.
- Bertagnini, A., N. Métrich, P. Landi, and M. Rosi (2003), Stromboli volcano (Aeolian Archipelago, Italy): An open window on the deep-feeding system of a steady state basaltic volcano, *J. Geophys. Res.*, 108(B7), 2336, 1–15.
- Bertagnini, A., N. Metrich, L. Francalanci, M. Landi, S. Tommasini, and S. Conticelli (this volume), Volcanology and magma

- geochemistry of the present-day activity: Constraints on the feeding system.
- Calvari, S., L. Spampinato, and L. Lodato (2006), The 5 April vulcanian paroxysmal explosion at Stromboli volcano (Italy) from field observation and thermal data, *J. Volcanol. Geotherm. Res.*, **149**, 160–175.
- Capaldi, G., et al. (1975), Stromboli and its 1975 eruption, *Bull. Volcanol.*, **41**, 259–285.
- Cavallaro, C. (1955), Attività dello Stromboli dal 1940 al 1953, *Boll. Acc. Gioenia*, **3**, 525–532.
- Corazzato, C., L. Francalanci, M. Menna, C. Petrone, A. Renzulli, A. Tibaldi, and L. Vezzoli (2008), What factors control sheet intrusion in volcanoes? Structure and petrology of the Stromboli sheet complex, Italy, *J. Volcanol. Geotherm. Res.*, **173**(1–2), 26–54, doi:10.1016/j.jvolgeores.2008.01.006.
- Corsaro, R. A., L. Miraglia, and V. Zanon (2004), Petrologic monitoring of glasses in the pyroclastites erupted in February 2004 by the Stromboli volcano, Aeolian islands, southern Italy, *J. Volcanol. Geotherm. Res.*, **139**, 339–343.
- Francalanci, L., S. Tommasini, and S. Conticelli (2004), The volcanic activity of Stromboli in the 1906–1998 AD period: Mineralogical, geochemical and isotope data relevant to understanding of the plumbing system, *J. Volcanol. Geotherm. Res.*, **131**, 179–211.
- Francalanci, L., A. Bertagnini, N. Métrich, A. Renzulli, R. Vannucci, P. Landi, S. Del Moro, M. Menna, C. M. Petrone, and I. Nardini (this volume), Mineralogical, geochemical and isotopic characteristics of the ejecta from the 5 April 2003 paroxysm at Stromboli, Italy.
- Harris, A. J. L., M. Ripepe, S. Calvari, L. Lodato, and L. Spampinato (this volume), The 5 April 2003 explosion of Stromboli: Timing of eruption dynamics using thermal data.
- Houghton, B. F., and C. J. N. Wilson (1989), A vesicularity index for pyroclastic deposits, *Bull. Volcanol.*, **51**, 451–462.
- Landi, P., L. Francalanci, R. A. Corsaro, C. Petrone, A. Fornaciai, M. Carroll, I. Nardini, and L. Miraglia (this volume), Textural and compositional characteristics of the lavas erupted in the December 2002–July 2003 effusive events at Stromboli, Aeolian Island, Italy.
- Mastin, L. G. (1991), A simple calculator of ballistic trajectories for blocks ejected during volcanic eruptions, *U.S. Geol. Surv. Open File Rep.*, 1–45.
- Mercalli, G. (1884), Notizie sullo stato attuale dei vulcani italiani. *Atti Soc. Sci. Nat.*, **28**, 184–198.
- Métrich, N., A. Bertagnini, P. Landi, and M. Rosi, (2001), Crystallization driven by decompression and water loss at Stromboli volcano (Aeolian Islands), *J. Petrol.*, **42**, 1471–1490.
- Perret, F. A. (1916), The lava eruption of Stromboli, summer-autumn 1915, *Am. J. Sci.*, **192**, 443–463.
- Platania, G. (1908), I fenomeni eruttivi dello Stromboli nella primavera del 1907, *Ann. Uff. Cent. Metereol. Geodin.*, **30**, 3–29.
- Polacci, M., L. Pioli, and M. Rosi (2004), The Plinian phase of the Campanian Ignimbrite eruption (Phlegrean Fields, Italy): Evidence from density measurements and textural characterization of pumice, *Bull. Volcanol.*, **65**, 418–432.
- Ponte, G. (1919), La catastrofica esplosione dello Stromboli, *R. Accad. Naz. Lincei*, **28**, 89–94.
- Ponte, G. (1921), La formidabile esplosione dello Stromboli del 1916, *Mem. R. Com. Geol. It.*, **7**, 1–34.
- Pyle, D. M. (1989), The thickness, volume and grainsize of tephra fall deposits, *Bull. Volcanol.*, **51**, 1–15.
- Riccò, A. (1907), Sull'attività dello Stromboli dal 1891 in poi, *Boll. Sismol. Soc. Ital.*, **12**, 205.
- Riccò, A., and G. Mercalli (1892), Sopra il periodo eruttivo dello Stromboli cominciato il 24 Giugno 1891, *Ann. Uff. Cent. Meteorol. Geodin. Ital.*, **11**, 189–221.
- Rittmann, A. (1931), Der Ausbruch des Stromboli am 11 September 1930, *Zeits Vulkanol.*, **14**, 47–77.
- Rose, W. I., S. Self, P. J. Murrow, C. Bonadonna, A. J. Durant, and G. G. J. Ernst (2007), Nature and significance of small volume fall deposits at composite volcanoes: Insights from the October 14, 1974, Fuego eruption, Guatemala, *Bull. Volcanol.*, **70**, 1043–1067, doi:10.1007/s0044500701875.
- Rosi, M., A. Bertagnini, and P. Landi (2000), Onset of the persistent activity at Stromboli volcano (Italy), *Bull. Volcanol.*, **62**, 294–300.
- Rosi, M., A. Bertagnini, A. J. L. Harris, L. Pioli, M. Pistolesi, and M. Ripepe (2006), A case history of paroxysmal explosion at Stromboli: Timing and dynamics of the April 5, 2003 event, *Earth Planet. Sci. Lett.*, **243**, 3–4, 594–606.
- Stelling, P., J. Beget, C. Nye, J. Gardner, J. D. Devine, and R. M. M. George (2002), Geology and petrology of ejecta from the 1999 eruption of Shishaldin Volcano, Alaska, *Bull. Volcanol.*, **64**, 548–561.
-
- D. Andronico, Istituto Nazionale di Geofisica e Vulcanologia, Sezione di Catania, Catania, Piazza Roma 2, 95123 Catania, Italy.
- A. Bertagnini, Istituto Nazionale di Geofisica e Vulcanologia, Sezione di Pisa, Via della Faggiola 32, 56123 Pisa, Italy.
- L. Pioli, University of Oregon, Eugene, OR, USA.
- M. Pistolesi, and M. Rosi, Dipartimento di Scienze della Terra, Università di Pisa, Via S. Maria 53, 56126 Pisa, Italy. (pistolesi@dst.unipi.it)
- A. Renzulli, Istituto di Scienze della Terra, Università di Urbino, Campus Scientifico, 61029 Urbino, Italy.

Mineralogical, Geochemical, and Isotopic Characteristics of the Ejecta From the 5 April 2003 Paroxysm at Stromboli, Italy: Inferences on the Preeruptive Magma Dynamics

Lorella Francalanci,¹ Antonella Bertagnini,² Nicole Métrich,^{2,3} Alberto Renzulli,⁴
Riccardo Vannucci,⁵ Patrizia Landi,² Stefano Del Moro,⁴ Michele Menna,⁴
Chiara Maria Petrone,¹ and Isabella Nardini¹

The 5 April 2003 explosive eruption at Stromboli emplaced typical basaltic scoria, pumice, and lithic blocks. This paper reports a detailed set of mineralogical, geochemical, and isotopic data on the juvenile ejecta and fresh subvolcanic blocks, including micro-Sr isotope analyses and major and dissolved volatile element contents in olivine-hosted melt inclusions. The juvenile ejecta have compositions similar to those of their analogs from previous paroxysms; the 2003 pumice, however, does not contain stable high-MgO olivine, usually typical of large-scale paroxysms and has lower compatible element contents. Texture, composition, and Sr isotope disequilibrium of crystals in pumice indicate that most of them are inherited from the shallow crystal-rich magma and/or crystal mush. The most primitive magma is recorded as rare melt inclusion in olivine Fo_{85-86} . It has a typical S/Cl (1.1) and a total volatile content of 3.1 wt % from which the total fluid pressure was evaluated ≥ 240 MPa. Hence, moderate pressure conditions can be envisaged for the mechanism triggering the April 2003 paroxysm. The subvolcanic blocks are shoshonitic basalts with 45–50 vol % of phenocrysts (plagioclase + clinopyroxene + olivine). The late-stage crystallization of the crystal-rich magma lead to the formation of Na-sanidine with plagioclase An_{60-25} + olivine Fo_{68-49} + Ti-magnetite \pm apatite \pm phlogopite \pm ilmenite assemblage. Mineralogy, chemistry, and Sr–Nd isotopic signatures of the subvolcanic blocks indicate they represent the slowly cooled equivalents of batches of crystal-rich basaltic magma stored in the uppermost subvolcanic feeding system during the last few years. Cooling might be facilitated by short breaks in the summit crater activity.

¹Dipartimento di Scienze della Terra, Università degli Studi di Firenze, Firenze, Italy.

²Istituto Nazionale di Geofisica e Vulcanologia, Sezione di Pisa, Pisa, Italy.

³Laboratoire Pierre Sue, CEA-CNRS, CE-Saclay, Gif-sur-Yvette, France.

⁴Istituto di Scienze della Terra, Università degli Studi di Urbino, Campus Scientifico, Urbino, Italy.

⁵Dipartimento di Scienze della Terra, Università di Pavia, e CNR-IGG, Pavia, Italy.

1. INTRODUCTION

The paroxysm of 5 April 2003 has been the most violent event of the past 50 years. The eruption occurred while lava emission was in progress from lateral vents and consisted of an 8-min-long explosive sequence. The most energetic explosion launched meter-sized ballistic blocks that fell on the volcano flanks and on the village of Ginostra, about 2 km far from the vent. A vertical gas/pyroclastic jet rose above the craters, feeding a convective plume that reached a height of up to 4 km. A fallout deposit of coarse pyroclasts (bombs and blocks) with subordinate amount of fine ash blanketed the upper part of the cone, while a shower of light pumice fell on the southern slopes of the volcano, down to the sea.

The juvenile clasts mainly consisted of light-colored, crystal-poor pumice variably mingled with dark-colored, crystal-rich scoria, which was formed by the same magma feeding the lava flows. Lithic fragments were very abundant and consisted of cognate, angular holocrystalline igneous rocks and variably altered volcanic scoria and lava [Rosi *et al.*, 2006; Pistolesi *et al.*, this volume].

Pumice and scoria bombs (hereafter pumice and scoria) and the most common and fresh lithics, mostly represented by subvolcanic rocks, were sampled for mineralogical, geochemical, and isotopic studies.

Bulk samples, matrix glasses, and minerals were analyzed for major and trace elements in different laboratories using a variety of bulk and in situ methods. Major and volatile elements were also determined in olivine-hosted silicate melt inclusions (MI) from pumices. Sr and Nd isotope data were performed on bulk samples and glassy groundmasses, whereas micro-Sr isotope ratios were determined on plagioclase and clinopyroxene of pumice and scoria by the micro-drilling technique [I. Nardini, L. Francalanci, D. G. Chertkoff, M. Tiepolo, R. Avanzinelli, J. P. Davidson, and R. Vannucci, *In-situ* chemical and isotopic analyses in the Stromboli products of the 2002–2003 eruptive crisis: Micro-scale variations recording macro-scale processes, submitted to *Contributions to Mineralogy and Petrology*, 2008, hereinafter referred to as Nardini *et al.*, submitted manuscript, 2008]. Separation procedures were applied to obtain pumice and scoria fractions from the mingled ejecta for whole-rock analyses. About 90 clinopyroxene and 600 olivine crystals were carefully hand-picked from the 1- to 0.25-mm grain-size pumice fraction for petrographic and MI analyses [Métrich *et al.*, 2005].

2. JUVENILE EJECTA

2.1. Petrography and Major and Trace Element Composition of Minerals

The 5 April scoria samples have petrographic and mineralogical characteristics similar to those of the scoria erupted

by the normal Strombolian activity; they have highly porphyritic texture (~45–55 vol % of phenocrysts and microphenocrysts) and mainly hyaline to cryptocrystalline groundmass. Olivine (~5 vol %), up to 3 mm in size, clinopyroxene (~15 vol %), up to 0.5 cm in size, and plagioclase (~35 vol %), up to 2 mm in size represent the phenocrysts, whereas microphenocrysts are mostly represented by plagioclase and rare olivine. The prevailing composition of olivine from scoria is forsterite (Fo) 70–73%, with small normal or reverse zoning. Clinopyroxene shows oscillatory zoning, from Mg # [mole Mg/(Mg + Fe)] 0.89 to 0.75. Resorbed clinopyroxene cores are often present. Plagioclase from scoria displays a large spectrum in anorthite (An) contents (65–86%), with outer rims generally showing the lowest An values. The largest plagioclase crystals usually have resorbed cores with concentric compositional and textural zoning.

In situ trace element contents were analyzed by laser ablation (LA) inductively coupled plasma (ICP) mass spectrometry (MS) (see Tiepolo *et al.* [2003] for instrumentation and analytical procedures) on some plagioclase and clinopyroxene crystals (Figures 1a and 1b). Chondrite-normalized [Anders and Grevesse, 1989] patterns indicate positive anomalies for Ba, Sr, and Eu in plagioclase, with no correlation between An and trace element contents. Only Th and Ta contents seem to be higher in the rim with lower An component than the outer core (Figure 1a). Chondrite-normalized trace element values of clinopyroxene are in the range between 0.1 and 100. For zones with Mg # <0.82, heavy rare earth element (REE_N) are around 10, and middle and light REE_N and Ni_N are >10. Zones with Mg # >0.82 have lower Hf_N, Zr_N, Y_N, and REE_N. The light REE have convex upward patterns, similar in both Mg-rich and Mg-poor zones. The latter are characterized by small negative Eu anomalies (Eu/Eu* around 0.8), possibly suggesting lower oxygen fugacity of the host magma with respect to the crystallizing conditions of the Mg-rich zones (Figure 1b).

The 5 April pumice samples carry up to 15–20 vol % of crystals settled in a glassy groundmass. As previously verified in other paroxysmal events, most of them (the dominant proportions of minerals in grain sizes >1 mm) are “xenocrysts” of plagioclase, clinopyroxene, and olivine-entrained and inherited from the shallow crystal-rich magma body [Métrich *et al.*, 2001; Francalanci *et al.*, 2004b].

In grain sizes <1 mm, olivine shows a broad compositional and textural heterogeneity. The most abundant olivine crystals are represented by (1) euhedral crystals with homogeneous Fe-rich cores (Fo_{66–71}), surrounded by a heterogeneous mottled zone of variable width, and a thin Mg-richer outer rim (Fo_{82–86}; Figure 2a); (2) heterogeneous patchy-zoned euhedral crystals (Fo_{75–83}) surrounded by outer Mg-rich rims (Fo_{82–87}). The chemical variability, systematic reverse zoning, and resorption textures indicate that these olivine

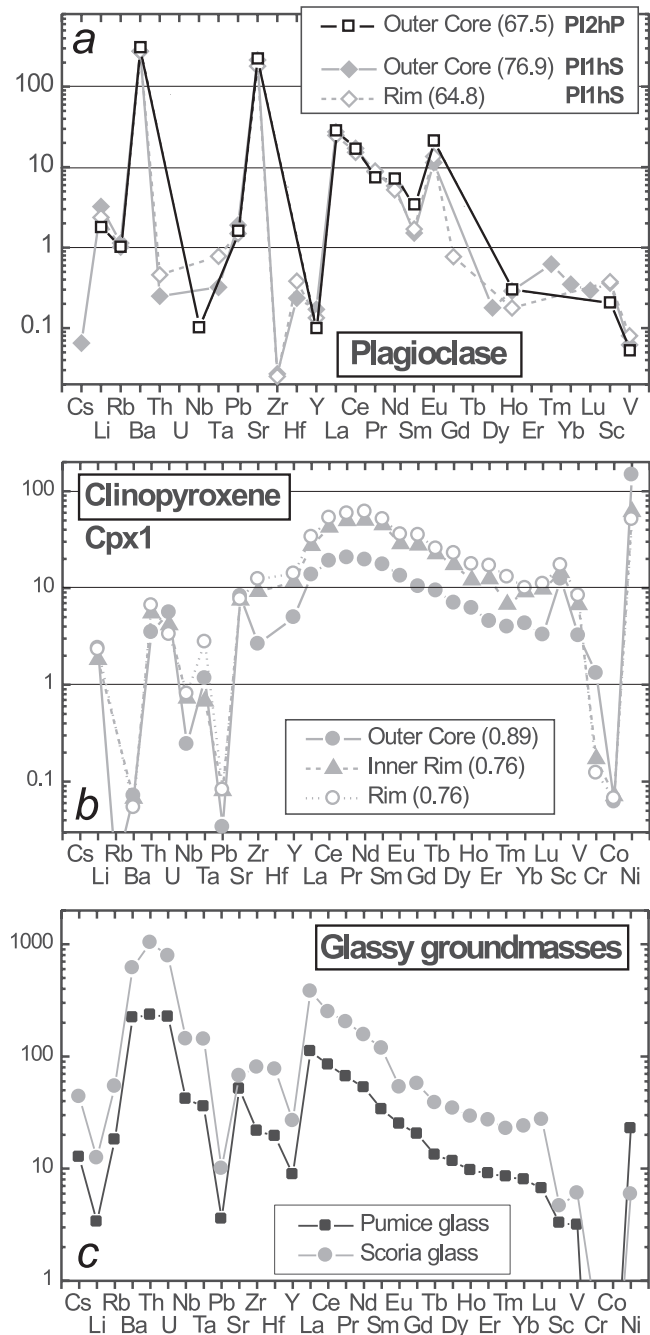


Figure 1. Chondrite-normalized [Anders and Grevesse, 1989] trace element patterns for (a) plagioclase, (b) clinopyroxene, and (c) matrix glasses of scoria (gray) and pumice (black). Trace elements were determined by LA ICP-MS at CNR-IGG, Pavia. An % for plagioclase and Mg # [mole Mg/(Mg + Fe)] for clinopyroxene of the analyzed zones are also given in the legends. PI1hS, PI2hP, and Cpx1 are referred to the name of crystals drilled for micro-Sr isotope ratios and reported in Figure 5. Element ordering: rare earth elements have been reported separately from the other elements, which are in order of increasing compatibility into a basaltic mineral assemblage.

crystals (1 and 2) represent different stages of reaction with a more primitive melt than their host liquid. Crystals with Fe-rich cores (Fo_{66-71}) are interpreted as drained-back from the shallow magmatic body and/or from the most evolved parts of the upper plumbing system, as already observed in the Stromboli pumice [Métrich *et al.*, 2001; Francalanci *et al.*, 2004b, 2005]. Variable growth of reaction zones indicates different times of reaction and, thus, residence of recycled crystals in pumice-like melts. The patchy-zoned olivine (Fo_{75-83}) is indicative of unstable conditions during resorption-crystallization processes, a feature previously observed [see Bertagnini *et al.*, 2003, for discussion]. Minor anhedral crystals (Fo_{79-82}) with lobate margins (Fo_{84-85}) are also present (Figure 2b). A very small fraction (~1%) of the handpicked olivine is constituted by euhedral microphenocrysts (nearly 0.5 mm in size) with a restricted compositional range (Fo_{85-87} ; Figure 2c). They are either slightly normally or reversely zoned [Métrich *et al.*, 2005].

Clinopyroxene crystals show similar characteristics. Only a few homogenous $\text{Wo}_{45-48}-\text{Fs}_{7-8}$ microphenocrysts are present, while most of the studied crystals are reversely zoned with resorbed cores and variable (50–500 μm) rims of composition $\text{Wo}_{44-48}-\text{Fs}_{7-10}$. Besides, the core chemistry is that expected for clinopyroxene in equilibrium with the shallow-sited magma ($\text{Wo}_{43-46}-\text{Fs}_{12-16}$), more Fe-rich and less calcic compositions are frequent ($\text{Wo}_{38-41}, \text{Fs}_{17-19}$) [Métrich *et al.*, 2005].

Most of the plagioclase crystals have compositional range (An_{64-86}), zoning, and texture similar to those shown by their analogs from scoria, indicating their origin from the shallow crystal-rich magma reservoir. Only rare plagioclase microphenocrysts have high An contents (from core to outer rim, 85%–89%), representing the minerals in equilibrium with the pumice magma, crystallized for water lost at the ultimate stage of their transfer to the surface. These high An contents were also found in pumice from the previous small-scale paroxysms that occurred between 1996 and 2000 [Francalanci *et al.*, 2004b].

A plagioclase outer core from pumice has a chondrite-normalized trace element pattern similar to that of plagioclase from scoria, including the amplitude of Ba-, Sr-, and Eu-positive anomalies (Figure 1a). The low An content (67%) of this plagioclase is also indicative of its origin from the crystal-rich magma.

2.2. Major and Trace Element Compositions of Whole Rocks and Matrix Glasses

The bulk pumices emitted on 5 April 2003 plot on the boundary line between shoshonitic and high-K basalts of the K_2O versus silica classification diagram, similarly to the previously erupted pumices (Table 1). They belong to the

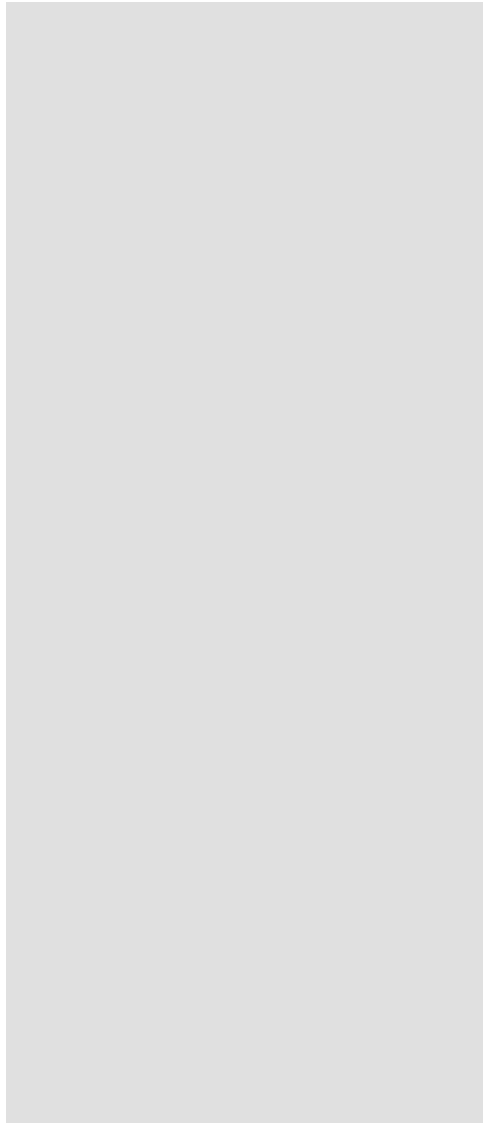


Figure 2. Backscattered electron microphotographs of olivine from pumice of the 5 April 2003 paroxysm. (a) Euhedral crystals with homogeneous Fe-rich cores and more forsteritic rims. (b) Anhedral olivine with a large amount of MI's, open gulls (embayments), and bubbles, testifying to the ultimate stage of crystallization. (c) Primitive euhedral olivine with isolated MI's.

typical domain of the historical to present-day pumices with respect to their major and trace element compositions, except for their slightly lower Cr contents (28–40 ppm with respect to 45–55 ppm of previous pumice; data ranges based on different analytical methods).

Because of the diffuse mingling between scoria and pumice, bulk-rock chemical analyses of the two lithotypes could not be completely representative of the two end members, despite our efforts in separating the two fractions. Bulk-rock

composition of 5 April scoria, however, seems to strictly resemble that of the previous crystal-rich magmas (Table 1). Furthermore, major and trace element contents of the scoria glassy groundmasses closely match those of the earlier crystal-rich products, with K_2O 4.0–4.7 wt % and Al_2O_3 15–16 wt % (Table 2; Figure 3).

The matrix glasses of 5 April 2003 pumice show higher MgO , CaO , and Al_2O_3 (17.4–18.2 wt %) and lower FeO , TiO_2 , K_2O (1.9–2.2 wt %), Na_2O , P_2O_5 , and incompatible trace element contents than the glassy groundmasses of the coeval scoria (Table 2, Figures 1c and 3). These compositional variations are those typically observed between scoria and pumice matrix glasses from the recent Strombolian activity. As already observed for whole rocks, glassy groundmass of 5 April 2003 pumice is similar in composition to the previous pumices, except for slightly lower Cr and Sc contents of the former [Francalanci *et al.*, 2004a].

Chondrite-normalized trace element patterns for both pumice and scoria show large overall REE-negative fractionation, positive Th and U, and negative high field strength elements spikes, as usually observed in Stromboli K-enriched series [Francalanci *et al.*, 1989; Tommasini *et al.*, 2007]. Noticeably, higher abundance levels, coupled with negative Sr and Eu anomaly, characterize scoria matrix glasses, in agreement with the crystallization of a plagioclase-bearing mineral assemblage in the crystal-rich magma (Figure 1c).

2.3. *Sr, Nd, and Micro-Sr Isotope Data in Pumice and Scoria*

Whole-rock and matrix glass of 5 April 2003 pumice show comparable $^{87}Sr/^{86}Sr$ values, i.e., ~0.70611. This value falls in the isotopic range of the previously erupted pumice since 1996 (Table 3, Figure 4). A higher $^{87}Sr/^{86}Sr$ value (~0.70615) is shown by the glassy groundmass of scoria. This value well compares with those for 2002–2003 lavas erupted before and a few days after (14 April 2003) the 5 April paroxysm (Table 3).

Nd isotope ratios of bulk rock and groundmass of 5 April 2003 pumice and scoria are around 0.51257, akin to the values measured in 1996 and 1999 pumices [Francalanci *et al.*, 2004b, unpublished data]. $^{143}Nd/^{144}Nd$ of scoria groundmass is about 0.512556 (Table 3), a value well in the range of 1996–2000 scoria [Landi *et al.*, this volume; Nardini *et al.*, submitted manuscript, 2008]. Accordingly, Nd isotope ratios between 5 April 2003 scoria and pumice are less variable than Sr isotope ratios, and this makes the Nd isotopes less relevant for understanding the magma dynamics at Stromboli.

Micro-Sr isotope data have been performed on core–rim traverses of plagioclase and clinopyroxene by microdrilling

Table 1. Major and Trace Element Analyses of Representative Whole Rock Samples of Pumice and Scoria

Sample	STR ^a 050403hP pumice	STR ^b 050403hP pumice	STR ^a 050403k pumice	STR ^b 050403k pumice	ST ^c 317 pumice	ST ^c 320 pumice	ST ^c 333 pumice	ST ^c 300 pumice	ST ^c 325a scoria	ST ^c 325b scoria
SiO ₂ , wt %	49.23	49.44	49.77	49.34	48.38	48.63	48.99	49.51	49.22	49.31
TiO ₂	1.01	0.91	0.98	0.91	0.90	0.91	0.91	0.92	0.91	0.92
Al ₂ O ₃	17.06	17.60	16.85	17.32	17.21	17.45	17.14	17.06	17.33	16.93
Fe ₂ O ₃	3.27	8.81	3.03	8.71	8.95	8.84	8.80	8.76	8.75	8.74
FeO	5.84	—	5.76	—	—	—	—	—	—	—
MnO	0.17	0.16	0.17	0.16	0.16	0.16	0.16	0.15	0.16	0.16
MgO	6.70	6.07	6.86	5.98	6.64	6.36	6.33	6.36	6.24	6.19
CaO	11.72	11.56	11.67	11.65	12.01	11.92	11.80	11.76	11.54	11.24
Na ₂ O	2.41	2.45	2.47	2.48	2.40	2.43	2.44	2.43	2.52	2.55
K ₂ O	1.84	1.89	1.77	1.77	1.84	1.87	1.89	1.85	2.08	2.15
P ₂ O ₅	0.37	0.55	0.37	0.53	0.59	0.61	0.56	0.54	0.61	0.57
LOI	0.39	0.44	0.30	0.74	0.78	-0.02	0.33	0.43	0.22	0.19
CaO/Al ₂ O ₃	0.69	0.66	0.69	0.67	0.70	0.68	0.69	0.69	0.67	0.66
K ₂ O/Na ₂ O	0.76	0.77	0.72	0.72	0.77	0.77	0.77	0.76	0.83	0.84
V, ppm	279	254	273	251	286	278	280	279	272	282
Cr	36	29	31	28	40	36	39	35	47	52
Co	37	31.0	34	34.6	35	34	34	34	33	34
Ni	—	34	—	34	44	41	41	41	40	41
Sc	—	29	—	29	—	—	—	—	—	—
Cu	118	132	112	126	—	—	—	—	—	—
Zn	72	62	71	64	—	—	—	—	—	—
Cs	—	3.5	—	3.7	3.4	3.5	3.7	3.6	4.2	4.5
Rb	51	56	52	59	57	58	60	59	67	71
Sr	787	722	778	716	715	730	729	740	731	753
Y	25	24.7	25	27.1	25	25	26	26	26	27
Zr	144	127	132	123	145	146	149	149	159	167
Nb	19	17.6	18	18.9	16	16	16	16	18	19
Mo				1.18	1.16	1.21	1.21	1.27	1.44	1.52
Ba	857	826	825	801	841	860	874	878	940	984
La	42	37.9	42	41.1	40	41	42	42	45	47
Ce	99	84.2	85	91.1	82	84	85	86	91	94
Pr	—	10.1	—	11.1	9.8	10.03	10.17	10.25	10.77	11.06
Nd	44	38.7	43	42.6	39	40	40	41	42	43
Sm	—	7.65	—	8.26	7.8	7.9	8.0	8.0	8.4	8.6
Eu	—	2.15	—	2.40	2.1	2.2	2.2	2.2	2.2	2.3
Gd	—	6.47	—	7.03	6.5	6.6	6.5	6.7	6.8	7.0
Tb	—	0.97	—	1.07	0.90	0.91	0.92	0.94	0.95	0.96
Dy	—	4.94	—	5.36	4.81	4.87	4.96	5.01	5.03	5.18
Ho	—	0.90	—	1.01	0.89	0.89	0.90	0.92	0.93	0.93
Er	—	2.47	—	2.71	2.33	2.37	2.43	2.43	2.45	2.51
Tm	—	0.329	—	0.361	0.34	0.35	0.35	0.35	0.35	0.37
Yb	—	2.27	—	2.49	2.18	2.21	2.24	2.27	2.32	2.39
Lu	—	0.338	—	0.375	0.34	0.34	0.35	0.35	0.36	0.36
Hf	—	3.3	—	3.5	3.3	3.4	3.4	3.4	3.6	3.8
Ta	—	1.3	—	1.4	1.02	1.05	1.05	1.09	1.19	1.23
Pb	19	15	20	17	14	16	18	17	17	17
Th	—	12.1	—	13.0	11.4	12.0	12.4	12.3	14.2	14.9
U	—	2.90	—	3.20	2.94	3.08	3.15	3.14	3.67	3.81

^a All elements were analyzed by XRF at the Department of Earth Science of Florence, Italy.^b Major elements were analyzed by XRF and trace elements by ICP–atomic emission spectrometry + ICP–MS at the SGS Minerals Services of Toronto, Ontario, Canada.^c All elements were analyzed at Service d'Analyse des Roches et des Minéraux, CRPG, Nancy, France.

Table 2. Representative Compositions of MIs in Olivine From 5 April 2003 Pumice and of Matrix Glass in Pumice and Scoria

Sample	ST304	ST300	ST300	ST300	ST300	ST304	ST304	ST304	ST306p	ST304s
Inclusion ^a	3a (3)	34a (4)	34b (2)	33a (1)	33d (1)	19a (4)	22-2 (1)	22-2 (1)	mg (5)	mg (5)
SiO ₂ , wt%	47.77	47.93	47.55	47.45	47.15	47.23	47.34	49.07	48.98	52.36
TiO ₂	0.91	0.87	0.87	0.91	0.96	0.88	0.91	1.14	0.98	1.59
Al ₂ O ₃	16.83	16.57	16.59	16.60	17.55	16.93	17.16	17.37	17.63	15.52
FeO total	7.73	8.49	8.21	8.49	7.75	8.12	7.96	8.12	8.13	10.05
MnO	0.13	0.12	0.17	0.13	0.06	0.13	0.22	0.30	0.19	0.20
MgO	6.42	6.75	6.69	6.04	5.85	6.47	6.18	6.20	5.97	3.22
CaO	12.81	11.78	11.55	11.73	12.08	12.06	11.51	11.52	11.57	7.11
Na ₂ O	2.03	2.41	2.31	2.17	2.41	2.15	2.61	2.45	2.53	3.40
K ₂ O	1.41	1.65	1.68	1.48	1.66	1.51	1.94	1.90	1.92	4.25
P ₂ O ₅	0.66	0.56	0.57	0.56	0.49	0.58	0.60	0.60	0.61	1.19
S	0.157	0.128	0.140	0.148	0.119	0.152	0.097	0.060	0.022	0.009
Cl	0.154	0.155	0.151	0.133	0.128	0.191	0.139	0.144	0.114	0.118
H ₂ O	2.5	2.0	2.1	N.D.	N.D.	N.D.	0.8	0.5	N.D.	
CO ₂ , ppm	1673	1428	1603	2123	1301	1094	368	N.D.	N.D.	
Total	99.71	99.58	98.73	96.05	96.35	96.52	97.46	99.38	98.65	99.02
Olivine, Fo mol %	86.4	85.8	86.1	83.8	85.0	85.7	84.6	84.6		
% PEC	0.04	0.06	0.07	0.10	0.03	0.04	0.03	0.00		
CaO/Al ₂ O ₃	0.76	0.71	0.69	0.70	0.69	0.71	0.67	0.66	0.66	0.46
S/Cl	1.02	0.82	0.92	1.12	0.93	0.80	0.69	0.41	0.20	0.08
K ₂ O/Na ₂ O	0.69	0.69	0.73	0.68	0.69	0.70	0.74	0.77	0.76	1.25
Pressure, MPa ^b (4)	299	244	270				61			

Major and volatile elements are corrected for olivine postentrainment crystallization (% PEC). Fo mol% = [100 × Mg/(Fe + Mg)].

^a In parentheses is the number of analyzed points per inclusion and matrix glass (mg). p, pumice; s, scoria; N.D., not determined.

^b Pressure calculated using VolatileCalc [Newman and Lowernstern, 2002]. Analytical techniques are from Métrich *et al.* [2005].

technique. The analyses were generally focused on crystals showing marked zoning. The different crystal zones were sampled by a Micromill instrument, and Sr isotope ratios

were analyzed using standard chemical separation techniques (at the University of Durham, UK) and a thermal ionization mass spectrometer (at the University of Florence, Italy; specific procedures according to Charlier *et al.* [2006]). Pronounced isotopic disequilibria were found in most of the crystals analyzed both in pumice and scoria (Figure 5). The cores and intermediate zones of minerals generally have higher Sr isotope ratios than outer rim and groundmasses, signifying they were crystallized from more Sr-radiogenic magmas than the host melt. Only the internal zone of one clinopyroxene grain, which included a large Mg-rich ($Mg \# > 0.82$) band, has given quite low Sr isotope ratios. On the other hand, $^{87}\text{Sr}/^{86}\text{Sr}$ values comparable with those of groundmasses were observed in two outer rims of coexisting plagioclase and clinopyroxene from scoria; this suggests that isotopic equilibrium was achieved during the final magma crystallization stages (Figure 5) [Nardini *et al.*, submitted manuscript, 2008].

Sr isotopic disequilibria were already reported for the shallow crystal-rich magmatic system of the present-day Stromboli, at least since 1984. It has been suggested that the deeper and crystal-poor magma periodically recharging the shallow crystal-rich reservoir passes through an old cumu-

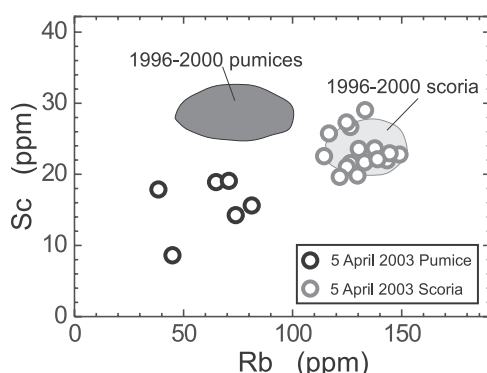


Figure 3. Rb versus Sc diagram for the matrix glass compositions of scoria and pumice from the 5 April 2003 paroxysm. Compositional fields of the matrix glasses of scoria–pumice pairs from the 1996–2000 paroxysms are also reported for comparison. All data are analyzed by LA ICP–MS at CNR-IGG, Pavia.

Table 3. Representative Sr and Nd Isotope Ratios of Ejecta From the 5 April 2003 Paroxysm

Sample	Ejecta	$^{87}\text{Sr}/^{86}\text{Sr}$	2 SD	$^{143}\text{Nd}/^{144}\text{Nd}$	2 SD
STR050403k ^a	Pumice	0.706098	0.000007	0.512567	0.000004
STR050403hP ^a	Pumice	0.706111	0.000007	0.512574	0.000004
STR050403h ^a	Pumice gdm	0.706116	0.000005	0.512572	0.000004
STR050403i ^a	Scoria gdm	0.706150	0.000007	0.512558	0.000004
STR050403r	Lithic	0.706159	0.000006	0.512563	0.000005
STR050403s	Lithic	0.706160	0.000006	0.512563	0.000004
STR050403t	Lithic	0.706171	0.000008	—	—
STR050403y	Lithic	0.706152	0.000006	—	—
<i>Micro-Sr analyses</i>					
STR050403f ^a	Scoria	0.706401	0.000011	Plagioclase 3 core	
STR050403f ^a	Scoria	0.706183	0.000009	Plagioclase 3 rim	
STR050403h ^a	Scoria	0.706146	0.000008	Olivine crystal	
STR050403hP ^a	Pumice	0.706234	0.000015	Plagioclase 2 middle	
STR050403hP ^a	Pumice	0.706290	0.000008	Plagioclase 2 rim	

^a Data from Nardini et al. [submitted manuscript, 2008]. Analyses were performed by thermal infrared multispectral scanning at the Department of Earth Sciences of Florence according to Avanzinelli et al. [2005] and for micro-Sr analyses, to Nardini et al. [submitted manuscript, 2008]. Replicate measurements of NBS 987 [0.710249; Thirlwall, 1991] and La Jolla [0.511856; Thirlwall, 1991] standards during the period of these analyses gave mean values of $^{87}\text{Sr}/^{86}\text{Sr} = 0.710250 \pm 0.000012$ (2 SD, $n = 78$) and $^{143}\text{Nd}/^{144}\text{Nd} = 0.511847 \pm 0.000007$ (2 SD, $n = 21$). gdm, groundmass.

lus and more Sr-radiogenic crystal-mush reservoir. Minerals from the old and more Sr-radiogenic reservoir are thus sampled by the uprising crystal-poor magma and transported

into the shallower reservoir where mixing and crystallization processes led to the development around crystals of outer rims in isotopic equilibrium with the residual liquids [Francalanci et al., 2005]. The in situ isotope data reported on 5 April 2003 juvenile ejecta suggest that crystal recycling still persist, and the plumbing system behaves as in the previous two decades at least.

2.4. Major and Volatile Element Data of Olivine-Hosted Melt Inclusions in Pumice

Major and volatile element compositions of MI, textures, and compositions of their host olivine were systematically studied in seven pumice samples both from distal and proximal fallout deposits [Métrich et al., 2005].

Brownish MI in Fe-rich olivine ($\leq\text{Fo}_{71}$) are compositionally equivalent ($\text{CaO}/\text{Al}_2\text{O}_3 < 0.5$, $\text{K}_2\text{O} > 3.5$ wt %) to the glassy groundmass of the crystal-rich magma residing at shallow level. Melt (inclusions, embayments) trapped in large quantity in patchy-zoned olivine (Fo_{75-83}) systematically show variable enrichment in their Fe and Ca content and depletion in alkalis, in agreement with successive dissolution-crystallization events, as reported by Bertagnini et al. [this volume]. Instead, the chemical magma variability is recorded in MI and embayments (gulfs) that are entrapped in Fo_{87-79} olivine, and it is accompanied by a change in size and morphology of inclusions and by textural evolution of

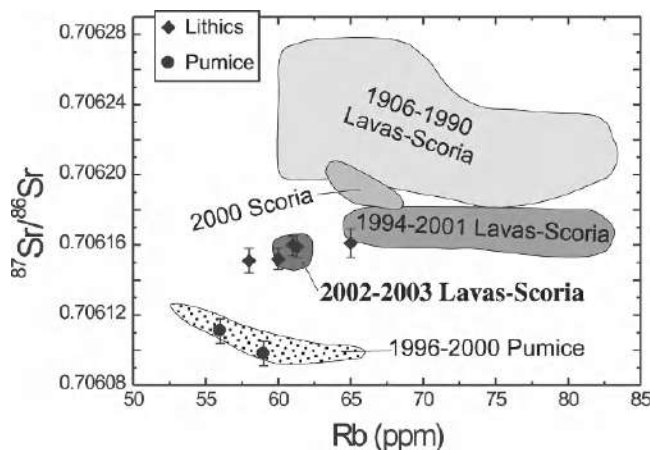


Figure 4. $^{87}\text{Sr}/^{86}\text{Sr}$ versus Rb for 5 April 2003 pumice and subvolcanic lithics, with compositional fields of previously erupted products since 1900 activity. The variation field of the nearly coeval 2002–2003 lavas and scoria is also separately reported. It is worth noting that the youngest products of the previous activity generally plot at lower Sr isotope ratios. Data for fields from Francalanci et al. [1999, 2004b, 2005], Landi et al. [2006, this volume], and Nardini et al. [submitted manuscript, 2008].

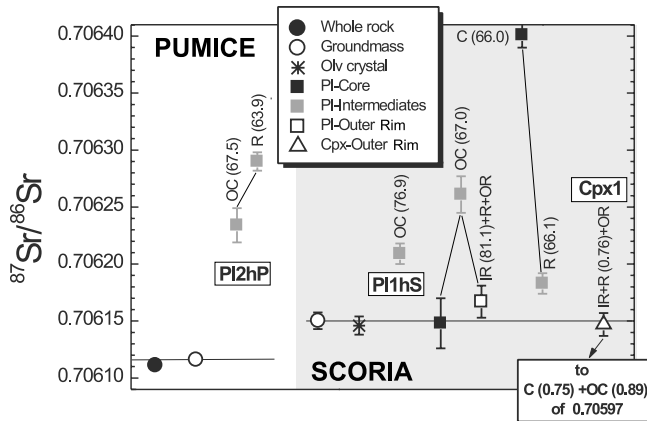


Figure 5. Micro-Sr isotope ratios for core–rim traverses in clinopyroxene and plagioclase of 5 April 2003 pumice and scoria. Isotope data on a separated olivine crystal, on whole rocks, and groundmasses are also reported. The white and gray areas of the diagram indicate the pumice and scoria portions, respectively. Micromillings of the different crystal zones and the Sr chemical separation have been performed at the University of Durham, whereas the Sr isotope ratios were measured at the University of Florence; Sr and Nd isotope analyses of bulk rocks and groundmasses have been entirely carried out at the University of Florence (see Avanzinelli *et al.* [2005] for instrumentation and methods). Legend of the core–rim traverse of minerals: full black symbols, crystal cores; full gray symbols, intermediate zones of crystals; open black symbols, prevalent outer rims; C, core; OC, outer core; IR, inner rim; R, rim; OR, outer rim. Pl2hP, Pl1hS, and Cpx1 refer to crystals also analyzed for trace elements by LA ICP–MS and reported in Figures 1a and 1b. (Modified after Nardini *et al.* [submitted manuscript, 2008].)

their host olivine. Euhedral microphenocrysts (Fo_{83-87}) host HK-basaltic MI that are more primitive than the bulk pumice ($CaO/Al_2O_3 \leq 0.70$; Figure 6). In contrast, anhedral crystals (Fo_{79-82}) with lobate margins (Fo_{84-85}) trapped a large amount of melt and bubbles (Figure 2b). Their MI and embayments (gulfs) chemically resemble the matrix, and these crystals probably represent the ultimate stage of crystallization, just prior to eruption. The overall evolution tracked by the olivine-hosted MI would be explained by the combined effect of crystal fractionation and mixing. Upon ascent, mixing would occur at least at local scale, between HK-basaltic magmas that slightly differed in their evolution degrees and possibly in their initial K_2O content (on average, K_2O/Na_2O ratio varies from 0.67 to 0.76) [Métrich *et al.*, 2005].

As a whole, the dissolved contents of H_2O (from 2.5 to 0.5 wt %; Figure 7a) and CO_2 (from 0.21 to 0.037 wt %; Figure 3b) widely vary. MI and embayments in anhedral olivine (Fo_{79-82}) track syn-eruptive degassing of water and

decrease in the S/Cl ratio ($2.0 > H_2O \geq 0.8$; $0.8 > S/Cl \geq 0.6$; Figure 7a). MI ($CaO/Al_2O_3 \sim 0.69-0.70$) in single olivine (Fo_{83-86}) show the broadest extents of variation in CO_2 (0.21–0.11 wt %; Figure 7b) and lowering in their S/Cl ratio (from 1.12 to 0.8). Since immiscible sulfide globule has not been observed, the combined decrease in S/Cl ratio and CO_2 content has been related to degassing and melt entrapment during decompression, in agreement with high and variable proportions of melt and bubble entrapped in this olivine. Kinetic effects, however, resulting in local enrichment in CO_2 dissolved in melt cannot be totally excluded. It is worth noting the water richness (up to 2.5 wt %) of the most primitive inclusions in Fo_{85-87} and their high S/Cl ratio (1.1), typical of HK-basaltic magma at Stromboli [Métrich *et al.*, 2001].

The total fluid pressures, assuming gas magma saturation, were assessed from the few available values of CO_2 and H_2O in primitive MI. The pressures ($P_{CO_2} + P_{H_2O}$) were computed between 240 and 300 MPa (Table 2), using VolatileCalc [Newman and Lowernstern, 2002], and for a basalt containing 48 wt % SiO_2 , as deduced from the coefficient [Dixon, 1997]. Using Papale's [1999] model, they shift to higher values up to 400 MPa. The effect of water on the CO_2 solubility in basaltic melts at high pressure limits the application of the available models. It is worth noting, however, that the 5 April 2003 samples plot in the pressure domain defined

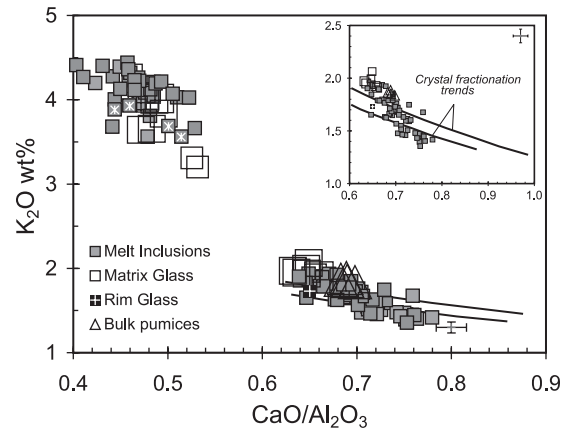


Figure 6. Variation of K_2O versus CaO/Al_2O_3 in olivine-hosted MI, matrix glasses and bulk rocks from the 5 April 2003 eruption [squares with an asterisk correspond to evolved MI in olivines (Fo_{66-71}) with reaction zones]. Trends of fractional crystallization are calculated with MELTS [Ghiorso and Sack, 1995] for parental melts containing 1.45 and 1.35 wt % K_2O , respectively, between 300 and 250 MPa and 1180°–1130°C. The inset shows the enlargement of the chemical variation of MI in olivine Fo_{79-87} . Modified from Métrich *et al.* [2005].

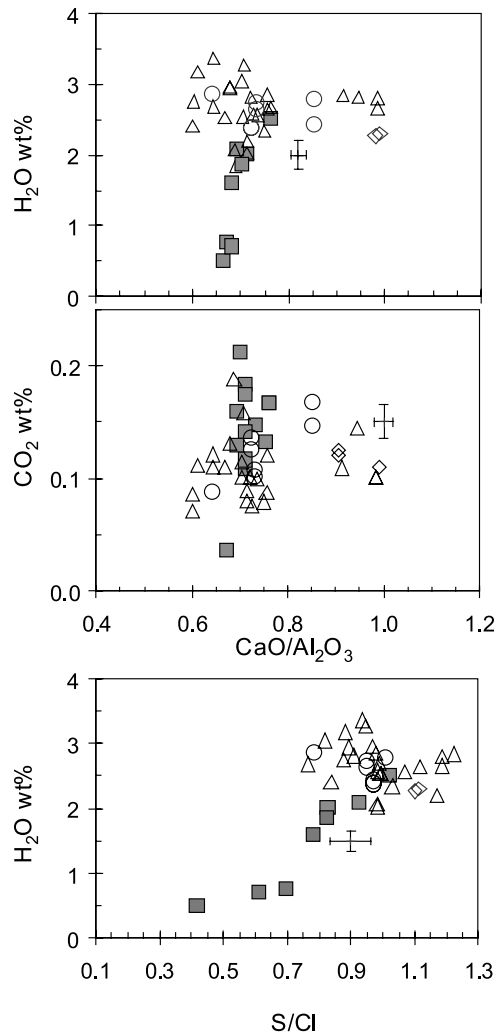


Figure 7. Volatile variability in MI hosted in olivine crystals from 5 April 2003 pumice (filled symbols) and from pumices emitted (triangle, samples ST81; diamond, ST79, 207; circle, ST82) during the most violent historical paroxysms (empty symbols) [Métrich et al., 2001; Bertagnini et al., 2003, unpublished data]. Modified from Métrich et al. [2005].

from the olivine-hosted MI of the large-scale historical paroxysms [Métrich et al., 2001; Bertagnini et al., 2003].

3. SUBVOLCANIC LITHIC EJECTA

3.1. Petrography and Mineral Chemistry of the Lithic Ejecta

Subvolcanic igneous blocks consist of gray holocrystalline rocks (type 1; Figure 8), locally brecciated and more

or less welded by a dark gray vesicle-rich lava-like or scoria lithotype (types 2 and 3 ejecta, respectively; Pistolesi et al., this volume; A. Renzulli, S. Del Moro, M. Menna, P. Landi, and M. Piermattei, Transient processes in the shallow basaltic system of Stromboli (Aeolian Islands, Italy) inferred from dolerites and magmatic breccias erupted as blocks during the paroxysm of 5 April 2003, submitted to *Bulletin of Volcanology*, 2008, hereinafter referred as Renzulli et al., submitted manuscript, 2008). They are phaneritic with phenocrysts of plagioclase (~28 vol %), clinopyroxene (~15 vol %), and olivine (~5 vol %). Interstitial crystallization of thinner-grained plagioclase, sanidine, clinopyroxene, olivine, opaque minerals (Ti-magnetite and ilmenite), apatite, and phlogopite also occurs (Figure 8). Sanidine is usually present in the finer-grained interstitial component as anhedral-poikilitic phase and as rims overgrowth, up to 50 µm

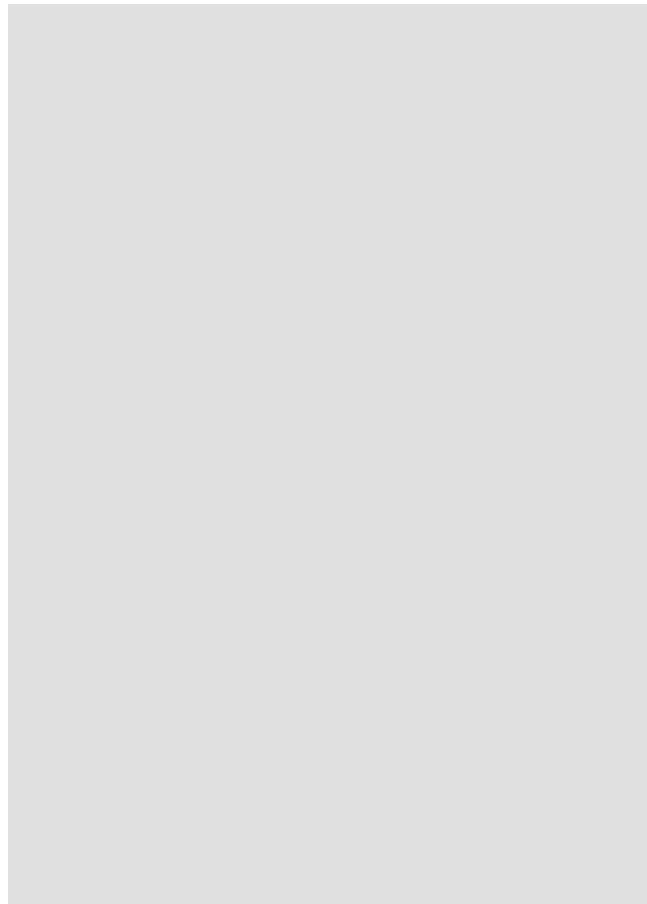


Figure 8. Macroscopic and microscopic (SEM) features of the 5 April 2003 subvolcanic igneous ejecta [type 1: Pistolesi et al., this volume].

thick, on plagioclase phenocrysts (Figure 8). At the micro-scale, igneous lamination is ubiquitous, involving plagioclase phenocrysts and microphenocrysts showing a clear preferred orientation. When the subvolcanic blocks are brecciated and welded (type 2), the closely associated dark gray vesicle-rich lava-like component [Pistolesi *et al.*, this volume] is porphyritic, with about 50 vol % of olivine, clinopyroxene, and plagioclase phenocrysts whose grain size resembles those of the gray igneous lithotype (Figure 8). Its groundmass is microcrystalline to cryptocrystalline, made of abundant sanidine, plagioclase, clinopyroxene, opaque minerals, and rare pigeonite and olivine. Sanidine is commonly interstitial, but it also occurs as rare, thin overgrowths on plagioclase. Contacts between the two components of the subvolcanic welded breccias usually show brittle features with broken crystals of the gray subvolcanic igneous block. Enrichment of vesicles in the dark gray rock often occurs close to the contact zone [Pistolesi *et al.*, this volume].

Texture and composition of inner plagioclase, olivine, and clinopyroxene phenocrysts from subvolcanic igneous blocks are closely similar to those of the same minerals from crystal-rich scoriae and lavas of the present-day Stromboli activity [Métrich *et al.*, 2001; Francalanci *et al.*, 2004b; Landi *et al.*, 2004, 2006; Bertagnini *et al.*, this volume] (Figures 9 and 10). Conversely, the composition is more evolved towards

the rims and in the interstitial grains of the groundmass, up to plagioclase An_{25} , olivine Fo_{50} , and augite $Wo_{5-9}-En_{61-62}-Fs_{30-33}$ (Figures 9 and 10). Alkali feldspar, occurring as plagioclase rims and anhedral-poikilitic phase, shows a Na-sanidine composition ($Or_{49-56}-Ab_{40-44}-An_{4-7}$) and high BaO contents (up to 4.2 wt %).

In addition, Mg-pigeonite microlites are found in the dark gray vesicle-rich component of the welded breccias. The presence of pigeonite could be explained by the expansion of the pigeonite stability field with the increasing differentiation degree and iron enrichment of the residual melt. Expansion of the pigeonite stability field appears to be a transient phenomenon [Renzulli *et al.*, submitted manuscript, 2008].

Opaque minerals are represented by both Ti-magnetite and ilmenite. Equilibrium temperatures of these oxide pairs range between 790° and 830°C using the geothermometers of Powell and Powell [1977] and Spencer and Lindsay [1981]. These temperatures are between the HM and NNO buffers, indicating a log fO_2 ranging from -13.8 to -12.9. Since the opaque mineral pairs represent the late-stage magmatic crystallization, the above temperature values are supposed to approach the solidus curve of the shoshonitic basalts which formed the shallow-level subvolcanic body. It is worth noting that ilmenite is not found throughout the shoshonitic basalts (scoria or lavas) of the present-day

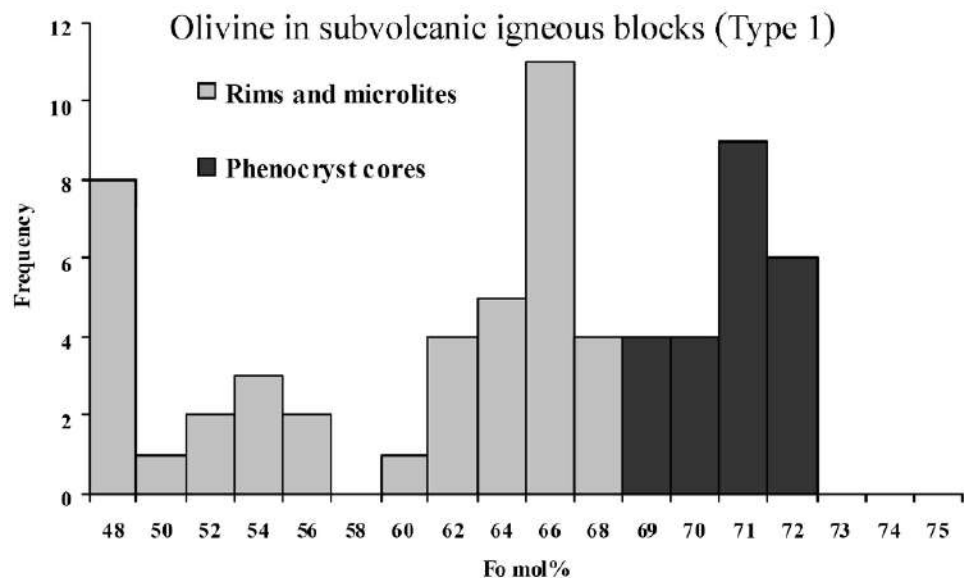


Figure 9. Olivine composition in the most common subvolcanic lithotype ejecta (type 1). It is worth noting that olivine phenocryst cores have the same composition of the phenocrysts and microphenocrysts of the highly porphyritic scoriae and lavas, whereas olivine rims and microlites of the subvolcanic lithotype are significantly enriched in iron. (Modified after Renzulli *et al.* [submitted manuscript, 2008].)

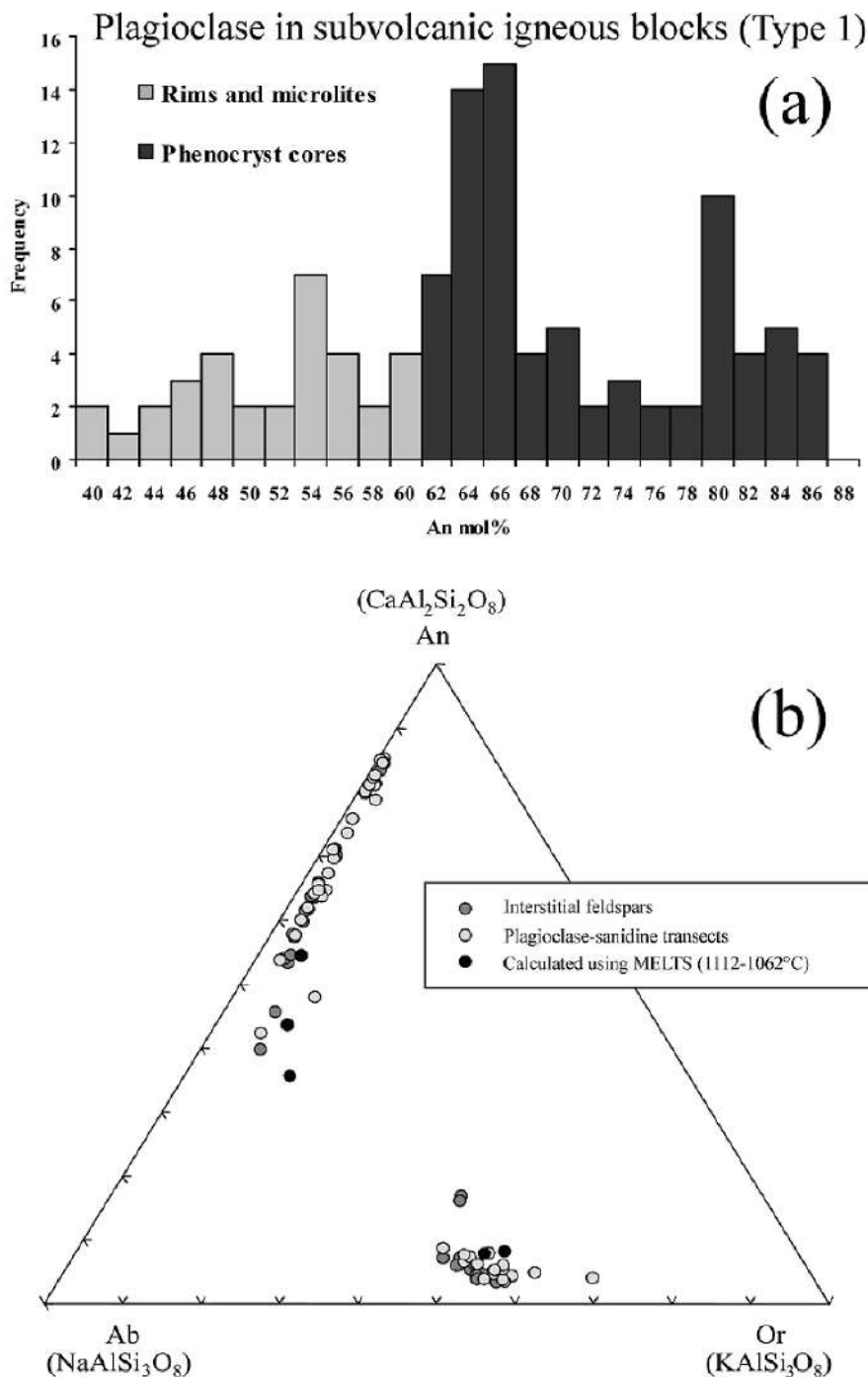


Figure 10. (a) Plagioclase composition in the most common subvolcanic lithotype ejecta [type 1: *Pistolesi et al.*, this volume]. It is worth noting that plagioclase phenocryst cores have the same composition of the phenocrysts and microphenocrysts of the highly porphyritic scoriae and lavas, whereas plagioclase rims and microlites of the subvolcanic lithotypes are significantly enriched in the Ab molecule. (b) Feldspar ternary diagrams for the subvolcanic type 1 ejecta. (Modified after Renzulli et al. [submitted manuscript, 2008].)

activity. This is because the porphyritic basalts are normally erupted at temperature of $\sim 1090^{\circ}\text{C}$ [Freda *et al.*, 2005], well above the ilmenite liquidus. Ilmenite may, therefore, crystallize when some residual liquids become enriched in TiO_2 and temperature is low enough to equilibrate oxide pairs [Renzulli *et al.*, submitted manuscript, 2008].

3.2. Whole-Rock Geochemistry and Glass Composition of the Lithic Ejecta

The subvolcanic igneous blocks are shoshonitic basalts, with major and trace element compositions similar to the crystal-rich scoria and lavas (Figure 4), suggesting these blocks could simply represent small batches of crystal-rich magma arrested in the uppermost plumbing system of the present-day activity [Renzulli *et al.*, 2004, submitted manuscript, 2008; Cortés *et al.*, 2006]. In the breccias, both the gray vesicle-free and the dark gray vesicle-rich rocks have comparable major and trace element contents (Table 4).

Sr isotope ratios of the subvolcanic blocks show small variation, ranging from 0.706151 to 0.706175. Both Sr and Nd isotope ratios of the studied lithics have values similar to those of the products from the most recent Strombolian activity (Table 3; Figure 4). Indeed, Sr isotope ratios generally decrease with time after 1985, starting from a value of about 0.70626 [Francalanci *et al.*, 1999]. Accordingly, the $^{87}\text{Sr}/^{86}\text{Sr}$ values of subvolcanic blocks akin to those of the scoria and lavas erupted during the last 10 years (Figure 4). This is also in agreement with the freshness of these lithics [Francalanci *et al.*, 2003].

Rare glassy mesostasis of trachyte composition were detected (by scanning electron microscopy with energy dispersive system analyses) in the subvolcanic blocks of 5 April 2003. In addition, according to mass balance calculations, the composition resulting from bulk rock of the subvolcanic ejecta minus their “phenocrystic” components (i.e., the coarser-grained crystals) closely matches that of the glassy groundmass of the erupted crystal-rich basalts of the present-day activity. This means that the silicate liquid normally frozen as glass in the crystal-rich lavas and scoria is the same from which the interstitial, finer-grained mineral assemblage of the subvolcanic blocks is crystallized. According to MELTS code (Melts-Linux-RH-ELF 3.0.5; Ghiorso and Sack, 1995; Asimow and Ghiorso, 1998), the melt otherwise quenched as glass in the extrusives may produce a liquid line of descent that passes through the residual glassy mesostasis of the subvolcanic blocks. MELTS calculations were investigated within the quartz–fayalite–magnetite buffer, at temperatures lower than the eruption temperatures of the crystal-rich basaltic magma and considering a pressure of 0.5 kbar. This pressure value is compatible with the stationary level of the

crystal-rich basaltic magma of Stromboli being considered within the volcanic cone by geophysical and petrological evidences. Along this liquid line of descent, the mineralogy (olivine, Fo_{56-60} ; clinopyroxene, En_{37-44} , Fs_{13-17} , Wo_{41-42} ; plagioclase, Ab_{43-51} , An_{36-50} , Or_{7-13} ; sanidine, Or_{51-55} , An_{4-8} , Ab_{37-45}) obtained by MELTS calculations is similar to that of the finer-grained minerals of the type 1 subvolcanic blocks. The crystallization of the finer-grained phases of type 1 blocks are therefore normally precluded in the present-day crystal-rich basalts because of the high degree of undercooling of the erupted magmas [Renzulli *et al.*, submitted manuscript, 2008].

4. CONCLUSIONS

Available chemical information on whole rocks, matrix glasses, and minerals shows that pumices and scoria erupted by the 5 April paroxysm generally have textural, mineralogical, major and trace elements, and isotopic characteristics similar to those of their analogs erupted by the earlier paroxysms. Nevertheless, some significant differences have been recognized: (1) the 5 April 2003 pumices do not carry Mg-rich olivines ($\text{Fo} \sim 90$) with Ca-rich primitive MI that testify to magma input in the deep-feeding system as recognized for the large-scale paroxysms [Bertagnini *et al.*, this volume]; (2) the olivine + clinopyroxene mineral assemblage, usually observed in equilibrium with the crystal-poor magma erupted as pumice, is rarely found; (3) the bulk-rock and glassy matrix chemistry of 5 April 2003 pumice is characterized by lower Cr and Sc contents than previously erupted pumices.

Both the mineralogy of the 5 April 2003 pumice and the chemistry of the olivine-hosted MI imply that the gas/particle jets were driven by the fragmentation of a volatile-rich, strongly mixed and mingled magma batch. Most of the crystals show resorption features to variable extents that prove their entrainment from the more evolved parts of the plumbing system. Furthermore, the Sr isotope disequilibrium between groundmass and minerals suggest the inner parts of the zoned crystals are xenocrysts derived from a cumulus crystal-mush zone. These xenocrysts crystallized from previous magmas (>1900 A.D.), when the volcanic products were more Sr-radiogenic than those erupted at present. Noticeably, Sr isotope disequilibrium is also found between outer rims and groundmass of crystals from the 2003 post-paroxysm lavas; this provides evidence that the uprise of crystal-poor magmas brought new xenocrysts in the shallow magmatic system [Landi *et al.*, this volume; Nardini *et al.*, submitted manuscript, 2008].

A few olivine crystals (Fo_{85-87}) record the involvement of a more primitive melt with a total dissolved volatile content of 3.1 wt % (H_2O , CO_2 , S, Cl), which allows estimating a total

Table 4. Major and Trace Element Data of Subvolcanic Lithic Blocks

	STR ^a 050403r	STR ^b 050403r	STR ^a 050403s	STR ^b 050403s	STR ^a 050403t	STR ^a 050403y	STR ^b 050403y	5437a1 ^c	5437a2/v ^c	5437f/v ^c	5437g1 ^c	5437g2/v ^c	54314/Sc ^c	54314/Ch ^c
SiO ₂	50.98	50.27	50.58	49.96	50.70	50.91	50.11	50.10	49.55	49.79	50.00	49.44	49.47	49.64
TiO ₂	0.82	0.94	0.88	0.93	0.83	0.78	0.94	0.95	0.91	0.92	0.94	0.90	0.94	0.94
Al ₂ O ₃	18.78	17.44	17.95	17.29	18.62	18.69	17.39	17.01	16.67	16.42	16.84	16.48	17.22	17.04
Fe ₂ O ₃	1.16	8.89	3.06	8.86	1.59	1.28	8.90	8.80	8.76	8.81	8.84	8.83	8.69	8.84
FeO	6.10	—	4.82	—	5.81	5.73	—	—	—	—	—	—	—	—
MnO	0.14	0.16	0.15	0.15	0.14	0.16	0.16	0.16	0.16	0.16	0.16	0.16	0.15	0.15
MgO	6.33	6.12	6.64	6.11	6.12	6.84	6.09	6.07	6.41	6.56	6.23	6.50	5.88	6.10
CaO	10.35	11.11	10.56	11.19	10.52	10.24	11.17	11.09	11.17	11.52	11.19	11.28	11.18	11.12
Na ₂ O	2.53	2.52	2.55	2.51	2.65	2.55	2.47	2.52	2.56	2.51	2.54	2.59	2.59	2.60
K ₂ O	2.20	2.15	2.20	2.15	2.45	2.27	2.11	2.28	2.25	2.27	2.29	2.28	2.17	2.21
P ₂ O ₅	0.50	0.55	0.43	0.56	0.49	0.52	0.55	0.55	0.53	0.51	0.54	0.52	0.55	0.55
LOI ^d	0.09	0.01	0.18	0.01	0.08	0.07	0.01	—	—	—	—	—	—	—
Tot	99.98	100.14	100.00	99.71	100.01	100.02	99.89	99.15	98.80	99.25	99.20	98.84	98.53	98.76
V	231	252	252	256	230	226	255	236	240	231	226	226	226	223
Cr	50	38	49	45	54	49	43	54	59	67	57	59	35	41
Co	29	32.1	31	33.5	29	29	31.8	29	29	28	27	28	27	28
Ni	—	35	—	36	—	—	36	52	41	43	38	40	37	38
Sc	—	29	—	29	—	—	30	—	—	—	—	—	—	—
Cu	89	102	93	109	109	103	114	132	57	53	125	49	96	68
Zn	56	65	62	65	56	55	65	87	91	83	80	82	84	81
Ga	—	—	—	—	—	—	—	16	16	15	16	15	16	16
Cs	—	4.0	—	5.0	—	—	3.8	6.3	4.0	4.6	4.7	3.2	4.6	3.2
Rb	61	68	61	72	69	60	69	74	69	69	71	66	70	69
Sr	778	735	787	750	812	776	749	836	840	794	775	796	843	833
Y	25	25.9	26	27.7	26	25	27.4	28	28	27	27	27	27	28
Zr	141	140	149	143	151	142	142	175	170	158	158	163	158	164
Nb	19	20.6	21	21.4	22	20	21.5	20	20	20	21	20	21	22
Ba	1055	930	1013	932	1149	1060	928	1100	1090	1040	1100	1050	1060	1070
La	46.5	44.0	51.8	47.4	51.6	46.9	45.6	52.5	50.6	51.2	51.9	52.8	50.2	49.5
Ce	95.3	95.8	100.2	104.1	97.0	103.2	100.6	103.9	98.5	100.0	102.8	103.4	101.0	98.0
Pr	—	11.3	—	12.4	—	—	12.1	10.6	10.1	10.3	10.5	10.6	10.3	10.1
Nd	44.9	42.8	48.5	46.9	43.3	48.8	44.7	43.2	41.8	43.2	43.0	43.8	41.8	41.5
Sm	—	8.4	—	9.1	—	—	8.7	8.7	8.4	8.7	8.7	8.8	8.6	8.3
Eu	—	2.3	—	2.5	—	—	2.3	2.3	2.2	2.3	2.2	2.3	2.3	2.2
Gd	—	7.0	—	7.7	—	—	7.3	7.5	7.2	7.5	7.3	7.6	7.3	7.4
Tb	—	1.1	—	1.1	—	—	1.1	1.1	1.0	1.1	1.0	1.1	1.1	1.0
Dy	—	5.2	—	5.7	—	—	5.4	5.3	5.1	5.3	5.3	5.2	5.2	5.1
Ho	—	1.0	—	1.1	—	—	1.0	1.0	0.9	0.9	0.9	0.9	0.9	0.9
Er	—	2.6	—	2.8	—	—	2.7	2.8	2.7	2.8	2.7	2.8	2.7	2.7
Tm	—	0.35	—	0.37	—	—	0.37	0.37	0.37	0.38	0.37	0.39	0.38	0.38
Yb	—	2.4	—	2.6	—	—	2.5	2.4	2.2	2.3	2.4	2.3	2.3	2.3
Lu	—	0.36	—	0.39	—	—	0.38	0.36	0.35	0.37	0.36	0.34	0.36	0.36
Ta	—	1.4	—	1.5	—	—	1.4	1.1	1.1	1.1	1.1	1.1	1.0	1.1
Hf	—	3.7	—	3.8	—	—	3.8	4.3	4.2	4.2	4.0	4.4	4.0	4.2
Pb	16	18	17	17	15	13	17	15	16	14	13	17	15	12
Th	—	15.1	—	16.1	—	—	15.4	16.1	15.2	15.7	15.6	16.1	15.6	15.4
U	—	3.72	—	3.97	—	—	3.76	4.14	3.99	4.08	4.04	4.25	4.09	4.06

^aAll the elements were analyzed by XRF at the Department of Earth Science of Florence, Italy.^bMajor elements were analyzed by XRF and trace elements by ICP–atomic emission spectrometry + ICP–MS at the SGS Minerals Services of Toronto, Canada.^cMajor elements were analyzed by ICP–optical emission spectroscopy and trace elements by ICP–MS at the Actlabs Laboratory, Ontario, Canada.

fluid pressure ≥ 240 MPa. The involvement of a more primitive melt relative to that poured out as pumice is testified by olivine hosted MI; however, its imprint on the composition of the erupted magma is weak. This is a recurrent characteristic of the Stromboli paroxysms and strongly indicates that the “deep” magma blobs—uprising from depths corresponding to 200–300 MPa P conditions—have small volumes. In turn, this implies that the driving force for triggering magma ascent is chiefly supplied by gas bubbles. The high volume ratio between gas and melt is testified by the heterogeneous trapping of gas and melt within crystals [Métrich *et al.*, 2005], with possible gas differential transfer from a bubble-rich layer where gas bubbles accumulated and coalesced in the range of pressure reported above [Allard, 2004].

The slightly lower contents of compatible trace elements of 5 April pumice, relative to that of older pumices, suggest that the 5 April crystal-poor magmas fractionated a higher amount of femic phases (mainly clinopyroxene).

En route to the surface, the gas-rich and crystal-poor magma blob interacts and mixes with overlying melts, filling the feeding system of the volcano [Bertagnini *et al.*, 2003]. It also continues to exsolve volatiles that promote bubble growth and expansion. Following this line of reasoning, the crystal-poor magma erupted by the 5 April paroxysm most likely represents the upper part of the deep plumbing system that is still able to generate pumice. In the final stage, immediately before magma fragmentation and explosion, this “balloon” of vesicular magma rapidly rises through and mingles with the denser, degassed magma residing in the uppermost part of the cone.

The subvolcanic blocks ejected during the 5 April 2003 paroxysm have the same uniform chemical and isotopic composition, which characterizes the crystal-rich products erupted during the present-day explosive and effusive activity of the volcano. Microstructures and chemistry of crystals larger than 100–150 μm closely match those of the phenocrysts and microphenocrysts of the crystal-rich scoriae and lavas. Crystal Size Distribution [Renzulli *et al.*, submitted manuscript, 2008] give a residence time for the finer-grained interstitial olivine of about 100 d, assuming a crystal growth value for olivine of 10^{-8} mm/s [Armienti *et al.*, 1994]. As a result, finer-grained mineral assemblage (finer than 100 μm) could be crystallized during brief periods in which small batches of crystal-rich magma arrest and crystallize in the uppermost part of the subvolcanic system. The cause of the complete solidification of the present-day crystal-rich basaltic magma might be ascribed to the drainage of magma from the surface to lower levels, which occurred at the beginning of the effusive event, and its crystallization during the short break of the summit explosive activity in the period 28 December 2002–early March 2003 [Renzulli *et al.*, submitted manuscript, 2008].

Acknowledgments. We would like to thank Maurizio Ulivi, Elena Boari, and Massimo Tiepolo for laboratory assistance. Riccardo Petrini is acknowledged for the critical revision of the manuscript. This research was financially supported by INGV and Italian Civil Defence (DPC).

REFERENCES

- Allard, P. (2004), Stromboli, an erupting system powered by steady and catastrophic gas transfer. INGV Workshop: L’eruzione di Stromboli (28 Dicembre 2002–20 Luglio 2003), 21–24 May 2004, Catania, Italy, Abstract, p. 7.
- Anders, E., and N. Grevesse (1989), Abundances of the elements: Meteoric and solar, *Geochim. Cosmochim. Acta*, 53, 197–214.
- Armienti, P., M. T. Pareschi, F. Innocenti, and M. Pompilio (1994), Effects of magma storage and ascent on the kinetics of crystal growth. The case of 1991–93 Mt. Etna eruption, *Contrib. Mineral. Petrol.*, 115, 402–414.
- Asimow, P. D., and M. S. Ghiorso (1998), Algorithmic modifications extending MELTS to calculate subsolidus phase relations, *Am. Mineral.*, 83, 1127–1132.
- Avanzinelli, R., E. Boari, S. Conticelli, L. Francalanci, L. Guarneri, G. Perini, C. M. Petrone, S. Tommasini, and M. Ulivi (2005), High precision Sr, Nd, and Pb isotopic analyses using new generation Thermal Ionisation Mass Spectrometer ThermoFinnigan Triton-Ti®, *Period. Mineral.*, 74–73, 147–166.
- Barberi, F., M. Rosi, and A. Sodi (1993), Volcanic hazard assessment at Stromboli based on review of historical data, *Acta Vulcanol.*, 3, 173–187.
- Bertagnini, A., N. Métrich, P. Landi, and M. Rosi (2003), Stromboli volcano (Aeolian Archipelago, Italy): An open window on the deep-feeding system of a steady state basaltic volcano, *J. Geophys. Res.*, 108(B7), 2336, doi:10.1029/2002JB002146.
- Charlier, B. L. A., C. Ginibre, D. Morgan, G. M. Nowell, D. G. Pearson, J. P. Davidson, and C. J. Ottley (2006), Methods for the microsampling and high-precision analysis of strontium and rubidium isotopes at single crystal scale for petrological and geochronological applications, *Chem. Geol.*, 232, 114–133.
- Cortés, J. A., M. Wilson, E. Condiffe, and L. Francalanci (2006), The occurrence of forsterite and highly oxidizing conditions in basaltic lavas from Stromboli volcano, Italy, *J. Petrol.*, 47, 1345–1373.
- Dixon, J. B. (1997), Degassing of alkalic basalts, *Am. Mineral.*, 82, 368–378.
- Francalanci, L., P. Manetti, and A. Peccerillo (1989), Volcanological and magmatological evolution of Stromboli volcano (Aeolian islands): The roles of fractional crystallisation, magma mixing, crustal contamination and source heterogeneity, *Bull. Volcanol.*, 51, 355–378.
- Francalanci, L., S. Tommasini, S. Conticelli, and G. R. Davies (1999), Sr isotope evidence for short magma residence time for the 20th century activity at Stromboli volcano, Italy, *Earth Planet. Sci. Lett.*, 167, 61–69.
- Francalanci, L., M. Rosi, S. Tommasini, S. Conticelli, E. Germiniani, C. Petrone, A. Bertagnini, P. Landi, and R. Vannucci (2003),

- Caratteristiche mineralogiche, geochemiche ed isotopiche dei prodotti emessi durante l'attuale crisi eruttiva di Stromboli: Implicazioni sui meccanismi pre-eruttivi del sistema vulcanico. GNV-INGV, General Assembly, Roma, Giugno, Abstracts, 30–31.
- Francalanci, L., I. Nardini, D. G. Chertkoff, S. Conticelli, and J. P. Davidson (2004a), The pre-eruptive processes involved in the 2002–2003 crisis at Stromboli volcano, Italy: Inferences from detailed mineralogical, geochemical and isotopic data on the erupted products. Italia 2004, 32° International Geological Congress, Firenze, Agosto, Abstracts, Part 2, 207–205, p. 967.
- Francalanci, L., S. Tommasini, and S. Conticelli (2004b), The volcanic activity of Stromboli in the 1906–1998 AD period: Mineralogical, geochemical and isotope data relevant to understanding of the plumbing system, *J. Volcanol. Geotherm. Res.*, **131**, 179–211.
- Francalanci, L., G. R. Davies, W. Lustenhouwer, S. Tommasini, P. R. D. Mason, and S. Conticelli, (2005), Old crystal re-cycle and multiple magma reservoirs in the plumbing system of the present day activity at Stromboli volcano, South Italy: Sr-isotope in situ microanalyses, *J. Petrol.*, **46**, 1997–2021, doi:10.1093/petrology/egi045.
- Frederick, C., D. R. Baker, and P. Scarlato (2005), Sulfur diffusion in basaltic melts, *Geochim. Cosmochim. Acta*, **69**, 5061–5069.
- Ghiorso, M. S., and R. O. Sack (1995), Chemical mass transfer in magmatic processes; IV, A revised and internally consistent thermodynamic model for the interpolation and extrapolation of liquid–solid equilibria in magmatic systems at elevated temperatures and pressures, *Contrib. Mineral. Petrol.*, **119**, 197–212.
- Landi, P., N. Métrich, A. Bertagnini, and M. Rosi (2004), Dynamics of magma mixing and degassing in plagioclase at Stromboli (Aeolian Archipelago, Italy), *Contrib. Mineral. Petrol.*, **147**, 213–227.
- Landi, P., L. Francalanci, M. Pompilio, M. Rosi, R. A. Corsaro, C. M. Petrone, I. Nardini, and L. Miraglia (2006), The December 2002–July 2003 effusive event at Stromboli volcano, Italy: Insights into the shallow plumbing system by petrochemical studies, *J. Volcanol. Geotherm. Res.*, **155**, 263–284.
- Landi, P., L. Francalanci, R. A. Corsaro, C. M. Petrone, A. Fornaciai, M. Carroll, I. Nardini, and L. Miraglia (2008), Textural and compositional characteristics of the lavas erupted in the December 2002–July 2003 effusive events at Stromboli, Aeolian Island, Italy, this volume.
- Latypov, R. M., M. I. Dubrovskii, and T. T. Alapeti (2001), Graphical analysis of the orthopyroxene–pigeonite–augite–plagioclase equilibrium at liquidus temperatures and low pressure, *Am. Mineral.*, **86**, 547–554.
- Métrich, N., A. Bertagnini, P. Landi, and M. Rosi (2001), Crystallisation driven by decompression and water loss at Stromboli volcano (Aeolian Islands), *J. Petrol.*, **42**, 1471–1490.
- Métrich, N., A. Bertagnini, P. Landi, M. Rosi, and O. Belhadj (2005), Triggering mechanism at the origin of paroxysms at Stromboli (Aeolian archipelago, Italy): The 5 April 2003 eruption, *Geophys. Res. Lett.*, **32**, L10305, doi:10.1029/2004GL022257.
- Newman, S., and J. B. Lowernstern (2002), VolatileCalc: A silicate melt–H₂O–CO₂ solution model written in Visual Basic Excel, *Comput. Geosci.*, **28**, 597–604.
- Papale, P. (1999), Modeling of the solubility of two-component H₂O–CO₂ fluid in silicate liquids, *Am. Mineral.*, **84**, 477–492.
- Pistolesi, M., M. Rosi, L. Pioli, A. Renzulli, A. Bertagnini, and D. Andronico (2008), The paroxysmal explosion and its deposits, this volume.
- Powell, M., and R. Powell (1977), Geothermometry and oxygen barometry using coexisting iron titanium oxides: A reappraisal, *Mineral. Mag.*, **41**, 257–263.
- Renzulli, A., P. Landi, A. Bertagnini, M. Rosi, M. Menna, and S. Del Moro (2004), Subvolcanic crystallization of the present-day shoshonitic basalts of Stromboli: Evidence from the ejecta erupted on April 5th 2003. Incontro Scientifico dell'INGV “L'eruzione di Stromboli (28 Dicembre 2002–20 Luglio 2003),” 20–21 Maggio 2004, Catania.
- Rosi, M., A. Bertagnini, A. J. L. Harris, L. Pioli, M. Pistolesi, and M. Ripepe (2006), A case history of paroxysmal explosion at Stromboli: Timing and dynamics of the April 5, 2003 event, *Earth Planet. Sci. Lett.*, **243**(3–4), 594–606.
- Spencer, K. J., and D. H. Lindsley (1981), A solution model for coexisting iron–titanium oxides. *Am. Mineral.*, **66**, 1189–1201.
- Thirlwall, M. F. (1991), Long-term reproducibility of multicollector Sr and Nd ratio analyses, *Chem. Geol.*, **94**, 85–104.
- Tiepolo, M., P. Bottazzi, M. Palenzona, and R. Vannucci (2003), A laser probe coupled with ICP—Double-focusing sector-field mass spectrometer for in situ analysis of geological samples and U–Pb dating of zircon, *Can. Mineral.*, **41**, 259–272.
- Tommasini, S., A. Heumann, R. Avanzinelli, and L. Francalanci (2007), The fate of high angle dipping slabs in the subduction factory: An integrated trace element and radiogenic isotope (U, Th, Sr, Nd, Pb) study of the Stromboli volcano, Aeolian arc, Italy, *J. Petrol.*, **48**(12), 2407–2430.
-
- A. Bertagnini and P. Landi, Istituto Nazionale di Geofisica e Vulcanologia, Sezione di Pisa, Via della Faggiola 32, 56126 Pisa, Italy.
- S. Del Moro, M. Menna, and A. Renzulli, Istituto di Scienze della Terra, Università degli Studi di Urbino, Campus Scientifico, 61029, Urbino, Italy.
- L. Francalanci, I. Nardini, and C. M. Petrone, Dipartimento di Scienze della Terra, Università degli Studi di Firenze, via La Pira 4, 50121, Firenze, Italy. (lorella.francalanci@unifi.it)
- N. Métrich, Laboratoire Pierre Sue, CEA-CNRS, CE-Saclay, 91191 Gif-sur-Yvette, France.
- R. Vannucci, Dipartimento di Scienze della Terra, Università di Pavia, e CNR-IGG, via Ferrata 1, 27100 Pavia, Italy.

The 5 April 2003 Paroxysm at Stromboli: A Review of Geochemical Observations

A. Rizzo, A. Aiuppa, G. Capasso, F. Grassa, S. Inguaggiato, and M. Longo

Istituto Nazionale di Geofisica e Vulcanologia—Sezione di Palermo, Palermo, Italy

M. L. Carapezza

Istituto Nazionale di Geofisica e Vulcanologia—Sezione di Roma I, Rome, Italy

This paper reviews the published geochemical variations observed during the 2002–2003 eruption at Stromboli volcano. At the end of 2002, a new eruption began at Stromboli with a lava flow that lasted until the end of July 2003. In 5 April 2003, an explosive paroxysm occurred with the ejection of bombs that reached the village of Ginostra, about 4 km from the craters. During the eruption, specific variations in chemical composition of groundwaters and summit fumaroles were recorded before the explosion, most of them for the first time. The water pH decreased significantly (0.5 units), and the dissolved CO₂ increased in two thermal wells (Cusolito and Zurro) located near Stromboli harbor from March until 5 April. Peaks in the dissolved He were also observed at all the sampling sites. All of these changes in the thermal aquifer suggested a pressurization of the system due to the degassing of a volatile-rich magma at depth. In the summit area, the SO₂/HCl and SO₂/HF ratios in the plume increased suddenly between 1 and 3 April due to the degassing of an S-rich magma that was approaching the shallow levels of the plumbing system, and this was involved in the explosion that occurred a few days later. This eruption was the first at Stromboli to be analyzed using geochemical models. The variations observed in the basal aquifer and in the summit area occurred on very different timescales: a few weeks and a few days, respectively.

1. INTRODUCTION

The Italian volcano Stromboli is internationally famous because to its persistent activity characterized by mild explosions every 15–20 min fed by three vents located in the crater area, at an elevation of 700 m above sea level (asl). The present-day activity is sustained by a degassed, crystal-rich shoshonitic magma residing in the shallow plumbing system

of the volcano [Landi *et al.*, 2006]. This magma is continuously crossed by gas bubbles coming from a crystal-poor, volatile-rich magma located in the deep portion of the feeding system, whose ascent and bursting is probably responsible for the Strombolian activity at the surface [Ripepe *et al.*, 2002; Chouet *et al.*, 2003; Metrich *et al.*, 2005]. Sometimes, this persistent activity is interrupted by lava effusion onto the Sciara del Fuoco (SdF) flank and/or by more violent and dangerous paroxysmal explosions. The latter result in the ejection of bombs that often reach a few kilometers from the crater area and comprise golden pumice and mingled blocks due to the coexistence of dark-colored, crystal-rich scoria, and crystal-poor pumice [Landi *et al.*, 2006].

The persistent volcanic activity at Stromboli provides a unique opportunity for scientists to develop and test new models as well as to apply the established ones. Work performed during the past 10 years has revealed the great potential of fluid geochemistry to both explain and predict the degassing mechanisms and eruptive activity of this volcano. Geochemical monitoring in Italian volcanic areas has demonstrated the usefulness of investigating plume chemistry [Aiuppa *et al.*, 2002, 2004; Allard *et al.*, 2004], He and C isotopes in both gases and waters [Caracausi *et al.*, 2003; Capasso *et al.*, 2005; Rizzo *et al.*, 2006; Federico *et al.*, this volume], and soil gas emissions [Badalamenti *et al.*, 2004; Carapezza *et al.*, 2004]. Similar investigations carried out in other active volcanoes such as Masaya (and others in this list) in Nicaragua [Duffell *et al.*, 2003], Galeras in Colombia [Sano *et al.*, 1997], Sakurajima in Japan [Hirabayashi *et al.*, 1986], and Oshima Island in Japan [Sano *et al.*, 1988] have demonstrated that geochemical studies can be used to predict the eruptive activity of a volcano. For example, a marked increase in the SO_2/HCl ratio in the plume was recorded before the 23 April 2001 explosion at Masaya, and this was attributed to scrubbing of water-soluble magmatic gases by a rejuvenated hydrothermal system [Duffell *et al.*, 2003]. Helium-isotope variations were recorded in high-temperature fumaroles during an increase in the activities of the Oshima Island and Galeras volcanoes and were considered indicative of the injection of mantle-derived volatiles [Sano *et al.*, 1988, 1997]. A marked increase in helium concentration in fumarolic samples at Galeras was also recorded during the same investigative period preceding its eruptive activity [Fischer *et al.*, 1997]. The H_2 concentration measured in gas from a hot spring at Sakurajima increased a few weeks before the resumption of intense explosive activity [Hirabayashi *et al.*, 1986]. These reports represent a very small proportion of the many examples of geochemical variations observed in volcanic systems worldwide that testify to the usefulness of geochemical investigations in the volcanic natural environment.

At Stromboli, a preliminary geochemical investigation carried out at the end of 1992 by Capasso and Carapezza [1994] identified two areas characterized by anomalous CO_2 soil emissions: (1) Pizzillo, located in the northeastern part of the island near the inhabited area, and (2) Pizzo Sopra La Fossa (PSF), along the crater rim. These anomalies were investigated by Carapezza and Federico [2000], whose systematic CO_2 soil flux survey aimed at identifying the main volcanotectonic structures controlling the gas ascent from depth. Automatic stations for continuously monitoring CO_2 soil flux and environmental parameters (STR01 and STR02) were installed in July 1999 at the two anomalous sites of Pizzillo and PSF [Carapezza and Inguaggiato, 2001]. The

volcanotectonic structure has been further investigated by Finizola *et al.* [2002, 2003], who identified a summit hydrothermal system beneath the La Fossa crater depression using self-potential, temperature, CO_2 , and fumarolic fluid measurements. The investigation of gases dissolved in water revealed a contribution of magmatic fluids in some thermal wells located near the inhabited area of Stromboli that showed an unexpected high $^3\text{He}/^4\text{He}$ ratio (≈ 4.1 Ra; Inguaggiato and Rizzo [2004]), suggesting the presence of a basal hydrothermal system that needed to be monitored. Indeed, previous investigations had established that the helium-isotope signature for Stromboli was typically 3.0–3.5 [Carapezza *et al.*, 2000].

The monitoring of gases for 6 years at site SC5 in the summit area (a fumarole located in the anomalous area of PSF) showed a clear magmatic contribution to the emitted fluids [Carapezza and Federico, 2000]. The total plume output of acid gases and SO_2 was quantified several times by airborne and ground-based filter-pack sampling combined with correlation spectrometry measurements [Allard *et al.*, 1994, 2000; Aiuppa *et al.*, 2005], which revealed the great importance of evaluating the budget of gases released to the atmosphere and of estimating the magma volume that participated in a recharge toward the surface.

In this paper, we present a review of the geochemical variations observed during the 2002–2003 eruptive period at Stromboli, focusing on the paroxysm that occurred on 5 April 2003.

2. ERUPTIVE ACTIVITY DURING 2002–2003

The 2002–2003 volcanic activity of Stromboli was characterized by a new flank eruption that started on 28 December 2002 and lasted until 22 July 2003. Since May 2002, a considerable increase in Strombolian activity coupled with small lava overflows from the summit craters was recorded by an INGV-CT web camera located at PSF [Bonaccorso *et al.*, 2003]. Apart from the spectacular but innocuous lava flow that started on 28 December from a fissure located in SdF between 550 and 650 m asl, this eruption will be remembered for two dangerous phenomena that caused concern to scientists and the Italian Civil Defence: (1) flank landslides of SdF and the associated tsunami that caused damage around the island on 30 December 2002 [Bonaccorso *et al.*, 2003; Pino *et al.*, 2004]; and (2) the explosive paroxysm that occurred at the craters on 5 April 2003, which lasted a few minutes and was characterized by a vertical gas emission into the atmosphere accompanied by the fallout of bombs and blocks that reached the village of Ginostra, and was the strongest event recorded at Stromboli since the 1930 paroxysm [Rittmann, 1931; Barberi *et al.*, 1993]. Similar to

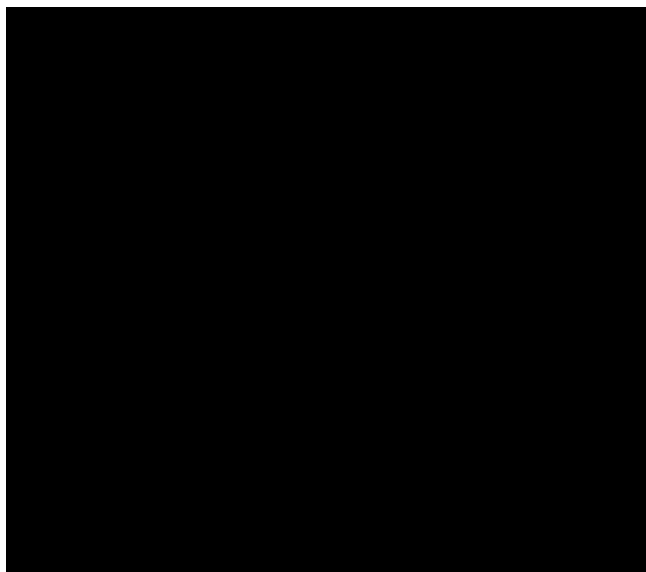


Plate 1. Sketch map showing the locations of monitored sites (modified from <http://www.celestiamotherlode.net>).

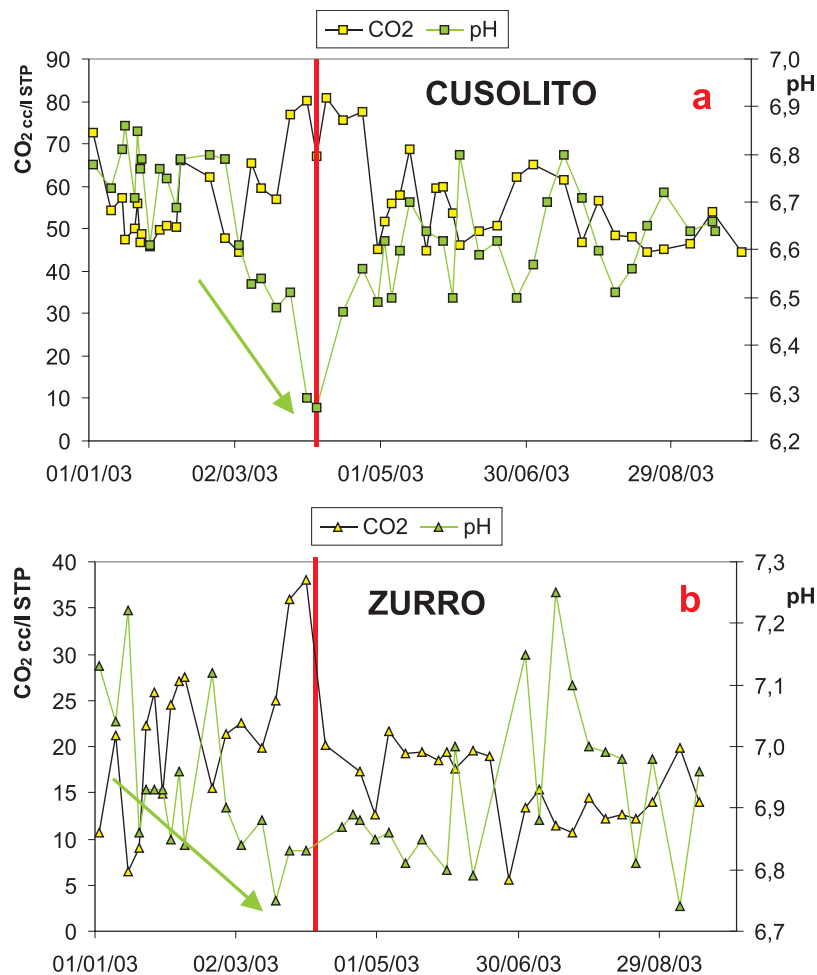


Plate 2. Temporal variations in pH and dissolved CO₂ in the waters of Cusolito (a) and Zurro (b) wells [Carapezza et al., 2004]. Colored arrows indicate the decreasing trend in pH preceding the explosion. Vertical red line indicates the 5 April paroxysm.

previous energetic events that occurred in the known history of the volcano, the explosion was accompanied by the presence of two HK-basaltic components that resulted from the sudden ascent of crystal-poor, gas-rich magma through the resident magma, which is degassed and crystal-rich [Metrich *et al.*, 2001; Landi *et al.*, 2004; Metrich *et al.*, 2005; Rosi *et al.*, 2006]. It is worth noting that the paroxysm occurred while the lava emission was still in progress from a vent located at 600 m asl and that the summit craters were clogged with debris [Rosi *et al.*, 2006].

After 5 April, normal Strombolian activity gradually resumed at the summit craters due to the progressive ascent of the magma level in the conduits. This resulted in effusive vents gradually moving up the slope until the flow field was active in SdF [Calvari *et al.*, 2006].

3. METHODS

Thermal waters have been collected since 1999 from three wells (named Cusolito, Fulco, and Zurro) with depths from a few to a few tens of meters (Plate 1) located in the northeastern part of Stromboli about 5 km from the craters. The sampling frequency was once per month during the normal Strombolian activity and increased up to twice per week during the 2002–2003 eruption. All of the collected waters have been analyzed in the INGV-PA laboratories for their chemical composition, as have the He and C isotopic compositions of the dissolved gases. The sampling and analytical techniques are described by Capasso and Inguaggiato [1998], Inguaggiato and Rizzo [2004], and Capasso *et al.* [2005a]. The chemical content of dissolved gases is expressed as cubic centimeters of gas per liter of water at standard temperature and pressure conditions ($\text{cm}^3 \text{ L}^{-1}$ STP). Helium isotopes are reported as Rc/Ra , which is the ratio corrected for air contamination on the basis of ${}^4\text{He}/{}^{20}\text{Ne}$ ratio measured in the same gas [Inguaggiato and Rizzo, 2004]. Carbon isotopic composition is reported as $\delta^{13}\text{C}$ in parts per thousand versus Peedee belemnite (PDB) [Capasso *et al.*, 2005b]. Temperature, pH, conductivity, and Eh have been directly measured in the field during water sampling.

The carbon dioxide flux and certain meteorological parameters (e.g., soil temperature and humidity) have been measured hourly by an automatic station (STR02; Plate 1) installed in 1999 at PSF. Further details about the technical specifications of the system are provided by Carapezza *et al.* [2002, 2004], Brusca *et al.* [2004], Federico *et al.* [this volume], and Madonia *et al.* [this volume].

The contents of SO_2 , HCl, and HF (expressed in micrograms per cubic centimeter) in the Stromboli plume were measured using diffusive (passive) samplers equipped with an NaOH-impregnated sorbent. These diffusive tubes were

exposed to the atmosphere (protected from rainwater) at PSF (Plate 1) at 1.0–2.5 m above ground for a duration determined by the ability to climb in the crater area. After exposure, filters were eluted in $\text{H}_2\text{O}-\text{H}_2\text{O}_2$ solution, then analyzed for Cl^- , F^- , and SO_4^{2-} by ion chromatography. This technique for volcanic plume monitoring is described by Aiuppa and Federico [2004] and Aiuppa *et al.* [2004].

4. GEOCHEMICAL CHANGES HERALDING THE 5 APRIL PAROXYSM

Most of the gases released from the magma in a volcanic system are degassed to the atmosphere via the plume that is continuously emitted from the craters. However, some of this gas is also released near the crater area via fractures connecting the volcanic conduit with the surface or diffusively from the soil and at the base of the volcanic cone, and near the coast where gas of deeper provenance interacts with the shallow aquifer to generate thermal waters. The shallow geothermal Strombolian aquifer has been intercepted by a few wells drilled in the northeastern part of the island near the harbor of Stromboli [Grassa *et al.*, this volume].

This study focused on the gases discharged from the soil in the crater area and from the plume emitted from the craters. We also investigated the thermal waters to better understand gas–water interaction processes and their possible relation with the volcanic activity.

4.1. Basal Thermal Aquifer

The collected thermal waters have a temperature ranging from 34.7°C (Zurro well) to 44°C (Cusolito well) and contain between 9000 and 40,000 mg L^{-1} dissolved salts due to the variable contribution of seawater to the aquifer. The wells have a depth ranging from a few to a few tens of meters, depending on the altitude at which they are drilled because the water table is constantly a few meters below sea level. Interactions between the rocks and deep hot waters have been confirmed by the anomalous enrichment in some elements with respect to a mixing between shallow meteoric waters and seawater [see Capasso *et al.*, 2005a; Grassa *et al.*, this volume]. The pH of collected waters varies with the investigated site, but is always less than the typical value of marine water ($\text{pH} = 8.3$). During the 2002–2003 eruption, the pH ranges were 6.27–6.86, 6.17–6.56, and 6.7–7.3 at the Cusolito, Fulco, and Zurro wells, respectively. These values are consistent with dissolution in the water of acid species such as carbon dioxide. Indeed, the CO_2 in dissolved gases varied with the sampled well, being 44–81, 76–210, and 6–91 $\text{cm}^3 \text{ L}^{-1}$ STP at Cusolito, Fulco, and Zurro, respectively. These values are well above the normal content of CO_2 dissolved in

air-saturated seawater ($\approx 0.25 \text{ cm}^3 \text{ L}^{-1}$ STP). These anomalous values of dissolved CO_2 , coupled with the $\delta^{13}\text{C}$ of CO_2 being from -9 to $-1.1\text{\textperthousand}$ versus PDB, suggest a magmatic origin of the fluids interacting with the shallow aquifer. The measured carbon-isotope values in the dissolved gases are indeed comparable with those in the crater fumaroles [Finizola and Sortino, 2003; Capasso *et al.*, 2005; Federico *et al.*, this volume]. The measured ranges of He content in dissolved gases were 1.99×10^{-4} – $8.56 \times 10^{-3} \text{ cm}^3 \text{ L}^{-1}$ STP at Cusolito, 2.05×10^{-4} – $1.58 \times 10^{-2} \text{ cm}^3 \text{ L}^{-1}$ STP at Fulco, and 1.86×10^{-4} – $6.47 \times 10^{-3} \text{ cm}^3 \text{ L}^{-1}$ STP at Zurro. The carbon dioxide content was sensibly higher than that in air-saturated water (ASW; $4.55 \times 10^{-5} \text{ cm}^3 \text{ L}^{-1}$ STP). Helium-isotope values were in the range of 3.49 – 4.56 Ra , confirming the magmatic signature of the dissolved gases in the thermal waters. Specifically, the recorded values were higher than those measured at the SC5 crater fumarole ($\approx 3 \text{ Ra}$; Carapezza and Federico [2000]; Inguaggiato and Rizzo [2004]; Federico *et al.* [this volume]) and comparable to those at the active fumarole field located near the northeastern crater (4.3 Ra ; Finizola and Sortino, [2003]). Finally, the O_2 content dissolved in collected waters never exceeded $2.8 \text{ cm}^3 \text{ L}^{-1}$ STP, whereas ${}^4\text{He}/{}^{20}\text{Ne}$ was in the range 1 – 10.66 (in ASW: $\text{O}_2 = 6.37 \text{ cm}^3 \text{ L}^{-1}$ STP, ${}^4\text{He}/{}^{20}\text{Ne} = 0.285$), suggesting a low atmospheric contribution. Therefore, an interaction process between deep magmatic gases and shallow waters is well recognized, confirming the usefulness of monitoring these basal thermal wells to provide evidence of anomalous degassing related to depressurization upon ascent of new magma batches, such as the ones that trigger explosive paroxysms.

These geochemical parameters have been regularly monitored since 1999 and have displayed anomalous variations during periods of intense Strombolian activity and before the onset of the 2002–2003 eruption [Carapezza *et al.*, 2004a; Capasso *et al.*, 2005; Federico *et al.*, this volume]. We now report the most indicative variations recorded across the 5 April paroxysm.

Starting from the end of February 2003, the pH progressively decreased, and the dissolved CO_2 simultaneously increased in Cusolito and Zurro waters (Plate 2). These variations were also accompanied in all the monitored wells by the amount of He dissolved in water peaking at one to two orders of magnitude higher than the average (Plate 3). Also, the Fulco water showed synchronous anomalies in pH, temperature, and dissolved CO_2 . An experimental continuous station, designed by the IGG-CNR, Pisa, was installed in this well in the beginning of February. The temperature, pH, conductivity, Eh, and dissolved CO_2 and CH_4 were measured every second (for technical details, see Carapezza *et al.* [2004b]). In the period preceding the 5 April paroxysm, temperature and dissolved CO_2 increased, and pH decreased.

These trends reversed soon after the explosion, in agreement with data from the intermittent sampling.

An anomalous ${}^4\text{He}/{}^{20}\text{Ne}$ peak of more than 10 was also observed at Cusolito about 2 weeks before the 5 April paroxysm (Plate 4), which had never been measured before in the basal thermal aquifer. This suggests a decrease in the shallow atmospheric component of the incoming CO_2 also dissolved in the water. The observed variations suggested a pressurization of the shallow geothermal system by the degassing of magmatic gases at depth. After the explosive event, He and CO_2 contents as well as ${}^4\text{He}/{}^{20}\text{Ne}$ ratios decreased toward the average values recorded before the paroxysm, whereas the water pH returned to 6.6 and 6.9 at the Cusolito and Zurro wells, respectively (Plates 2, 3, and 4).

Helium isotopes displayed almost synchronous variations at all the sampling sites, suggesting that they had a common deep magmatic source. At the end of January (Plate 5), the ${}^3\text{He}/{}^4\text{He}$ ratio reached the highest value ever measured at Stromboli of 4.56 Ra [Capasso *et al.*, 2005; Federico *et al.*, this volume], after which a progressive decrease in ${}^3\text{He}$ content characterized the Cusolito, Fulco, and Zurro waters until the end of March, with the trend thereafter reversing at Fulco and Zurro. In particular, on 23 March, the value at the Fulco well reached its lowest value of 3.58 Ra . The Cusolito site displayed a different trend, showing a minimum ${}^3\text{He}/{}^4\text{He}$ ratio of 3.83 Ra on 5 April. After the paroxysm, helium isotopes showed almost identical trends in all the thermal wells, with pulsing variations that accompanied the resumption of normal Strombolian activity.

The variations observed in ${}^3\text{He}/{}^4\text{He}$ ratios can be ascribed either to a variable contribution of a crustal ${}^4\text{He}$ -rich term mixed with the magmatic component or, more likely, to a variable extent of magma degassing at depth, in which the decrease in helium-isotope ratios could be due to the loss of ${}^3\text{He}$ during magma degassing and depressurization. In contrast, increases in ${}^3\text{He}/{}^4\text{He}$ ratios can be ascribed to a replenishment of a new deep magma batch that is rich in ${}^3\text{He}$.

Similar variations in helium-isotope ratios were also recorded at the Oshima Island and Galeras volcanoes during an increase in the volcanic activity, and were unequivocally interpreted as indicative of the injection of mantle-derived volatiles [Sano *et al.*, 1988, 1997]. In view of the observed variations, the ${}^3\text{He}/{}^4\text{He}$ ratio peak recorded at the end of January would suggest the degassing of a new deep magma batch that is rich in ${}^3\text{He}$, which probably rose toward the surface and fed the lava effusion. It cannot be ruled out that this new magma batch was involved in the paroxysm that occurred 2 months later. This is supported by the lack of further increases in helium-isotope ratios before then. The ${}^3\text{He}/{}^4\text{He}$ ratio decrease observed in March at the Fulco well could be due to a minor interaction of magmatic gases with the shallow aquifer.

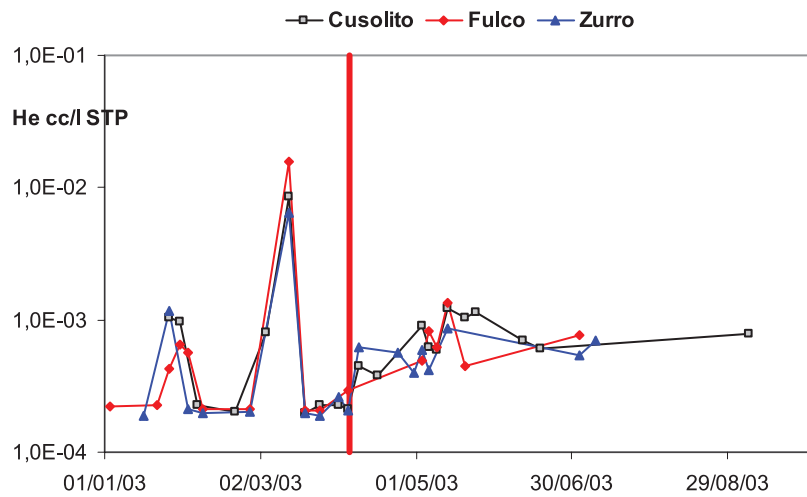


Plate 3. Temporal variations in dissolved He in the waters of all the sampled wells [Carapezza *et al.*, 2004]. Vertical red line indicates the 5 April paroxysm.

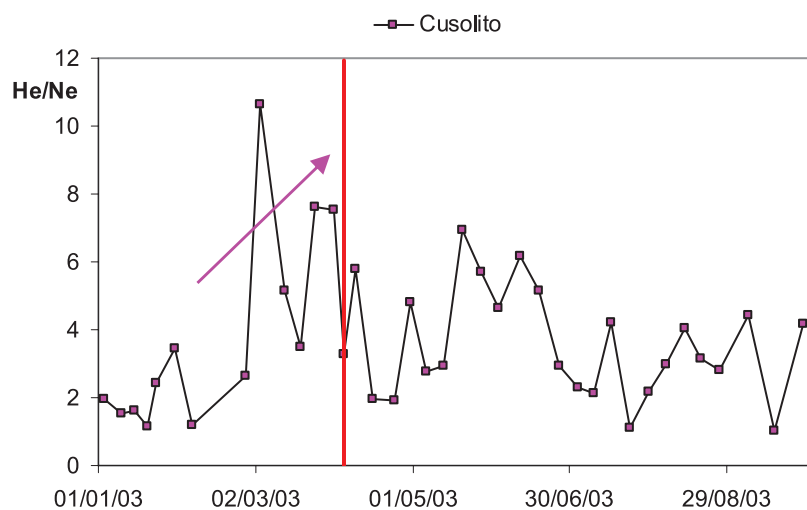


Plate 4. Temporal variations in the ${}^4\text{He}/{}^{20}\text{Ne}$ ratio in the waters of the Cusolito well. Colored arrow indicates the increasing trend preceding the explosion. Vertical red line indicates the 5 April paroxysm.

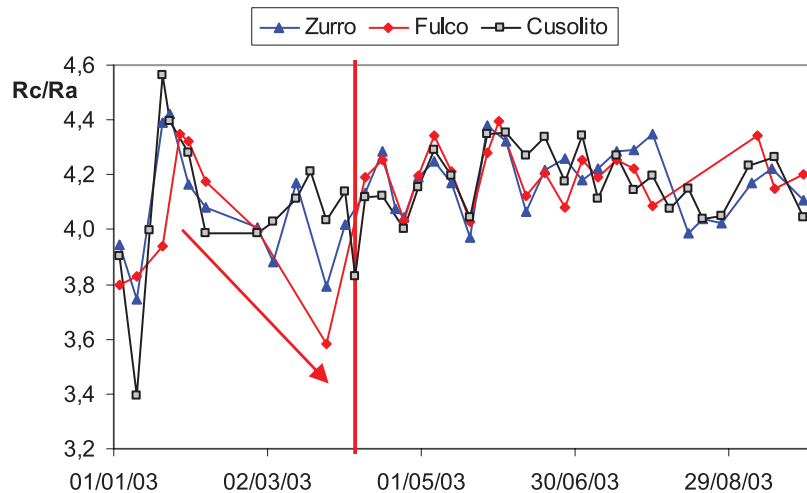


Plate 5. Temporal variations in Rc/Ra ratios in the waters of all the sampled sites [Capasso *et al.*, 2005]. Colored arrow indicates the decreasing trend preceding the explosion. Vertical red line indicates the 5 April paroxysm.

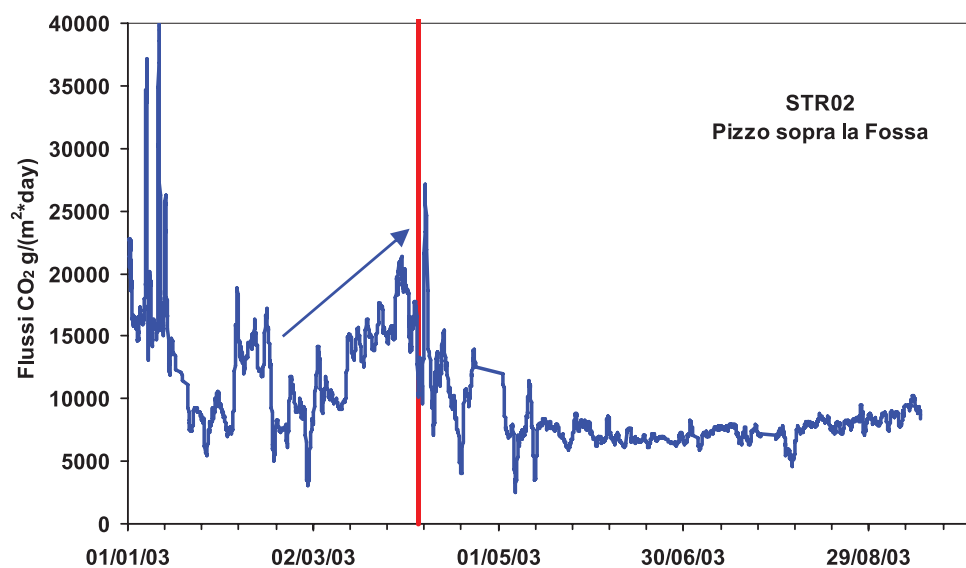


Plate 6. Temporal variations in CO_2 flux emitted from the soil at Pizzo Sopra La Fossa, reported as twenty 4-point moving averages (equating to averaging over about 1 day; Carapezza *et al.* [2004]). Colored arrow indicates the increasing trend preceding the explosion. Vertical red line indicates the 5 April paroxysm.

4.2. Summit Area

Continuous monitoring at an automatic station since July 1999 revealed that the daily average CO_2 soil flux at PSF was 5000–6000 $\text{g m}^{-2} \text{ day}^{-1}$ during periods of normal Strombolian activity. There was an anomalous increase in CO_2 released from soil for 1 week before the onset of the 2002–2003 eruption, which reached values in excess of 80,000 $\text{g m}^{-2} \text{ day}^{-1}$ [Carapezza et al., 2004; Federico et al., this volume], the highest ever measured since its installation. It is noteworthy that there was no lava effusion at Stromboli from 2000 to 2002. After the onset of the 2002–2003 eruption, the CO_2 flux decreased to an average value of 10,000 $\text{g m}^{-2} \text{ day}^{-1}$ without further variations as clear as those recorded before 28 December 2002. High values were recorded again in January 2003, but they were only nearly half those recorded before the eruption onset (Plate 6). A slight increasing trend was observed for about 1 month before 5 April (Plate 6), reaching about 20,000 $\text{g m}^{-2} \text{ day}^{-1}$. After the paroxysm, the CO_2 flux decreased slowly to 7000 $\text{g m}^{-2} \text{ day}^{-1}$ and remained nearly constant throughout the remaining eruptive period.

In the summit area of Stromboli, the clearest signals heralding the 5 April paroxysm were in the plume chemistry. Previous investigations of its chemical composition demonstrated that SO_2 was the third major component (after H_2O and CO_2) of the volatile phase degassed from magma [Allard et al., 1994]. Minor species degassed from magma at shallow depth are acid gases such as HCl and HF , with the latter coupled with SO_2 collected in the crater rim area (Plate 1) using diffusive tubes (see analytical techniques section) since April 1. During the investigated period, the SO_2 content in the atmosphere surrounding the craters ranged between 6500 $\mu\text{g m}^{-3}$ before the paroxysm and 42 $\mu\text{g m}^{-3}$ at the end of September, when the Strombolian activity had already resumed, and the eruption had ended about 2 months previously. These values exceed the atmospheric background at Stromboli (17 $\mu\text{g m}^{-3}$), suggesting a magmatic origin of SO_2 as the unique explanation of these measured high contents. In contrast, HCl and HF appeared to vary randomly during the observation period, with concentrations ranging from 77 to 1175 and from 20 to 207 $\mu\text{g m}^{-3}$, respectively. An analysis by Aiuppa and Federico [2004] indicated that the recorded data were unlikely to be influenced by wind, rainfall, or barometric pressure.

Plate 7 shows temporal variations in the SO_2/HCl and SO_2/HF molar ratios during the investigated period. Both ratios increased rapidly a few days before the 5 April explosion, with SO_2/HCl increasing from 4.5 to about 9 in less than 1 day. Values of SO_2/HCl before the paroxysm were the highest ever measured in the area since the development of this technique and significantly above the normal passive degas-

sing at Stromboli [Allard et al., 1994, 2000; Burton et al., 2001; Burton and Murè 2002], suggesting an involvement of degassing of an SO_2 -rich magma just before the explosion. This hypothesis is strongly supported by the observations of Bertagnini et al. [2003], who ascribed the major explosion and paroxysm to the rapid ascent of primitive gas-rich magma toward the shallow plumbing system [Francalanci et al., this volume]. Indeed, after 5 April, SO_2/HCl and (to a lesser extent) SO_2/HF decreased substantially until the end of the effusion. Further decreases were observed when the Strombolian activity gradually replaced the lava effusion, with the values eventually stabilizing at around the average values characteristic of normal passive degassing at Stromboli.

5. CONCLUDING REMARKS

The Stromboli 5 April explosive paroxysm was preceded by geochemical changes in both the basal thermal aquifer and the crater area. The main anomalies were recorded from 1 month to a few days before the explosion. From the beginning of March, the pH of the thermal waters of Cusolito and Zurro wells progressively decreased, with a corresponding increase in dissolved CO_2 . A significant peak in dissolved He was also observed in all wells by the middle of March, followed by a marked decrease in the $^3\text{He}/^4\text{He}$ ratio at the Fulco and Zurro sites. CO_2 released from soil measured at PSF (in the summit area) increased moderately from 1 month before the paroxysm. A few days before 5 April, the SO_2/HCl and SO_2/HF ratios in the plume suddenly increased, which had never been recorded previously. After the major explosion, all the monitored geochemical parameters returned to their average values contemporarily to the resumption of normal Strombolian activity and the end of the eruption.

These geochemical variations observed across the 5 April event identified—1 month in advance—the progressive pressurization of the basal thermal aquifer due to the degassing of a volatile-rich magma at depth. The plume chemistry 40–60 h before the paroxysm indicated an important degassing event of the S-rich magma approaching the shallow plumbing system, which was probably involved in the subsequent explosive event. The resumption of normal Strombolian activity was not accompanied by further input of magma.

The geochemistry at Stromboli was monitored from 1999 until late 2002, during which no lava effusion occurred. This permitted the collection of a set of data representative of a long intereruption period that has successfully been used as a reference background to recognize anomalies heralding important changes in the eruptive regime of the volcano. Despite the dense geophysical network operating at Stromboli, no geophysical precursors were observed for the 5 April paroxysm, with the only forerunning phenomena being the

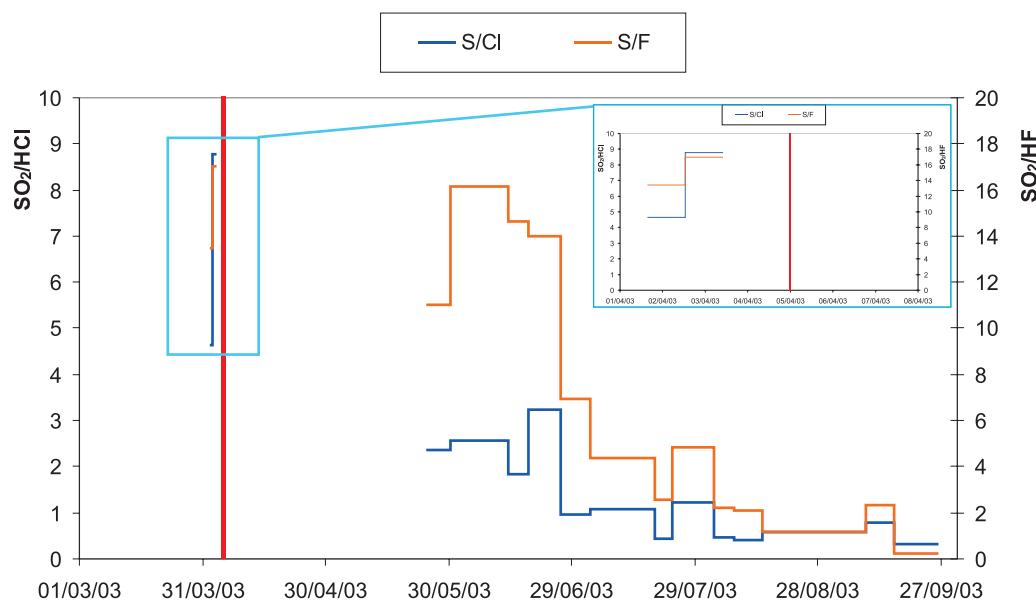


Plate 7. Temporal variations in SO_2/HCl and SO_2/HF molar ratios measured in the atmosphere surrounding the craters [Aiuppa and Federico, 2004]. Horizontal bars represent time-weighted SO_2/HCl and SO_2/HF molar ratios during each exposure period, computed from the cumulative amounts of acidic gases that accumulated on the samplers throughout that time. Vertical red line indicates the 5 April paroxysm. A magnification of the first week of April is also shown to clarify the variations recorded just before the explosion.

described geochemical variations. This confirms the crucial importance of fluid geochemistry in the monitoring of open-conduit volcanoes, and encourages further developments in this area.

Acknowledgments. We are grateful to all our collaborating colleagues at INGV-PA during the eruptive event. We especially thank Giusy Volpicelli, who actively participated in the fieldwork during the eruption and in the laboratory analyses. The presented results were obtained within the framework of the GNV “Stromboli volcanic hazard” project and by the volcano monitoring activities of INGV-PA.

REFERENCES

- Aiuppa, A., and C. Federico (2004), Anomalous magmatic degassing prior to the 5th April 2003 paroxysm on Stromboli, *Geophys. Res. Lett.*, 31(L14607), doi:10.1029/2004GL020458.
- Aiuppa, A., C. Federico, A. Paonita, G. Pecoraino, and M. Valenza (2002), S, Cl and F degassing as an indicator of volcanic dynamics: The 2001 eruption of Mount Etna, *Geophys. Res. Lett.*, 29–11, S4–S1/S4–S4.
- Aiuppa, A., C. Federico, G. Giudice, S. Gurrieri, A. Paonita, and M. Valenza (2004), Plume chemistry provides insights into mechanisms of sulfur and halogen degassing in basaltic volcanoes, *Earth Planet. Sci. Lett.*, 222, 469–483.
- Aiuppa A., S. Inguaggiato, A. J. S. Mcgonigle, M. O'dwyer, C. Oppenheimer, M. J. Padgett, D. Rouwet and M. Valenza (2005), H₂S fluxes from Mt. Etna, Stromboli, and Vulcano (Italy) and implications for the sulphur budget at volcanoes, *Geochim. Cosmochim. Acta*, 69(7), 1861–1871.
- Allard, P., J. Carbonelle, N. Metrich, et al. (1994), Sulphur output and magma degassing budget of Stromboli volcano, *Nature*, 368, 326–330.
- Allard, P., A. Aiuppa, H. Loyer, et al. (2000), Acid gas and metal emission rates during long-lived basalt degassing at Stromboli volcano, *Geophys. Res. Lett.*, 27, 1207–1210.
- Allard, P., M. Burton, and F. Muré (2004), Spectroscopic evidence for a lava fountain driven by previously accumulated magmatic gases, *Nature*, 433, 407–410.
- Badalamenti, B., N. Bruno, T. Caltabiano, F. Di Gangi, S. Giannamico, and G. Salerno (2004), Continuous soil CO₂ and discrete plume SO₂ measurements at Mt. Etna (Italy) during 1997–2000: A contribution to volcano monitoring, *Bull. Volcanol.*, 66, 80–89, doi:10.1007/s00445-003-0305-y.
- Barberi, F., M. Rosi, and A. Sodi (1993), Volcanic hazard assessment at Stromboli based on review of historical data, *Acta Vulcanol.*, 3, 173–187.
- Bertagnini, A., N. Métrich, P. Landi, and M. Rosi (2003), Stromboli volcano (Aeolian Archipelago, Italy): An open window on the deep-feeding system of a steady state basaltic volcano, *J. Geophys. Res.*, 108(B7), 2336, doi:10.1029/2002JB002146.
- Bonaccorso, A., S. Calvari, G. Garfi, L. Lodato, and D. Patanè (2003), Dynamics of the December 2002 flank failure and tsunami at Stromboli volcano inferred by volcanological and geophysical observations, *Geophys. Res. Lett.*, 30(18), 1941, doi:10.1029/2003GLO17702.
- Brusca, L., S. Inguaggiato, M. Longo, P. Madonia, and R. Maugeri (2004), The 2002–2003 eruption of Stromboli (Italy): Evaluation of the volcanic activity by means of continuous monitoring of soil temperature, CO₂ flux, and meteorological parameters, *Geochem. Geophys. Geosyst.*, 5(12), 1525–2027, doi:10.1029/2004GC000732.
- Burton, M., and F. Murè (2002), Helicopter-borne FTIR measurements of the summit crater plume of Stromboli, Open file report, INGV-CT, Catania, Italy.
- Burton, M., P. Allard, L. Brusca, and F. Murè (2001), High resolution spectroscopic analysis of volcanic gas composition during passive and explosive degassing at Stromboli volcano, Italy, paper presented at the Assembly, Eur. Geophys. Soc., Nice, France, 25 March.
- Calvari S., L. Spampinato, and L. Lodato (2006), The 5 April 2003 vulcanian paroxysmal explosion at Stromboli volcano (Italy) from field observations and thermal data, *J. Volcanol. Geotherm. Res.*, 149, 160–175.
- Capasso, G., and M. L. Carapezza (1994), A geochemical survey of Stromboli, *Acta Vulcanol.*, 6, 52–53.
- Capasso, G., and S. Inguaggiato (1998), A simple method for the determination of dissolved gases in natural waters. An application to thermal waters from Vulcano Island, *Appl. Geochem.*, 13, 631–642.
- Capasso, G., M. L. Carapezza, C. Federico, S. Inguaggiato, and A. Rizzo (2005a), Geochemical monitoring of the 2002–2003 eruption at Stromboli volcano (Italy): Precursory changes in the carbon and helium isotopic composition of fumarole gases and thermal waters, *Bull. Volcanol.*, 68, 118–134, doi:10.1007/s00445-005-0427-5.
- Capasso, G., R. Favara, F. Grassia, S. Inguaggiato, and M. Longo (2005b), On-line technique for preparing and measuring stable carbon isotope of total dissolved inorganic carbon in water sample ($\delta^{13}\text{C}_{\text{TDIC}}$), *Ann. Geophys.*, 48, 159–166.
- Caracausi, A., R. Favara, S. Giannamico, F. Italiano, P. M. Nuccio, A. Paonita, G. Pecoraino, and A. Rizzo (2003), Mount Etna: Geochemical signals of magma ascent and unusually extensive plumbing system, *Geophys. Res. Lett.*, 30(2), 1057, doi:10.1029/2002GL015463.
- Carapezza, M. L., and C. Federico (2000), The contribution of fluid geochemistry to the volcano monitoring of Stromboli, *J. Volcanol. Geotherm. Res.*, 95, 227–245.
- Carapezza, M. L., and S. Inguaggiato (2001), Interaction between thermal waters and CO₂-rich fluids at Stromboli volcano (Italy), Proc. WRI-10, Balkema, Rotterdam, vol. 2, 791–794.
- Carapezza, M. L., M. Guidi, and S. Inguaggiato (2002), Soil CO₂ degassing on Stromboli island: Influence of environmental parameters and insights on volcanic activity, paper presented at EGS 27th General Assembly, Eur. Geophys. Soc., Nice, France.
- Carapezza, M. L., S. Inguaggiato, L. Brusca, and M. Longo (2004a), Geochemical precursors of Stromboli 2002–2003 eruptive events, *Geophys. Res. Lett.*, 31(7), doi:10.1029/2004GL019614.

- Carapezza, M. L., R. Cioni, M. Guidi, L. Pruitt, and A. Scozzari (2004b), Experimentation of an automatic continuous monitoring station in a thermal well of Stromboli volcanic island (Italy). *Proc. WRI-11*, vol. 1, edited by R. B. Wanty, and R. R. Seal, pp. 95–99, Balkema, Rotterdam.
- Chouet, B., P. Dawson, T. Ohminato, M. Martini, G. Saccorotti, F. Giudicepietro, G. De Luca, G. Milana, and R. Scarpa (2003), Source mechanisms of explosions at Stromboli determined from moment tensor inversions of very-long-period data, *J. Geophys. Res.*, 108(B1), 2019, doi:10.1029/2002JB001919.
- Duffell, H. J., C. Oppenheimer, D. M. Pyle, B. Galle, A. McGonigle, and M. R. Burton (2003), Changes in gas composition prior to a minor explosive eruption at Masaya volcano, Nicaragua, *J. Volcanol. Geotherm. Res.*, 126, 327–339.
- Finizola A., F. Sortino, J.-F. Lénat, and M. Valenza (2002), Fluid circulation at Stromboli volcano (Aeolian Island, Italy), from self-potential and CO₂ surveys, *J. Volcanol. Geotherm. Res.*, 116(1–2), 1–18.
- Finizola, A., F. Sortino, J.-F. Lénat, M. Aubert, M. Ripepe, and M. Valenza (2003), The summit hydrothermal system of Stromboli: New insights from self-potential, temperature, CO₂ and fumarolic fluids measurements, with structural and monitoring implications, *Bull. Volcanol.*, 65, 486–504, doi:10.1007/s00445-003-0276-2.
- Fischer, T. P., G. B. Arehart, D. Counce, N. D. Sturchio, and S. N. Williams (1997), The chemical and isotopic composition of fumarolic gases and spring discharges from Galeras Volcano, Colombia, in *Galeras Volcano, Colombia: Interdisciplinary Study of a Decade Volcano*, edited by J. Stix., M. L. Calvache, and S. N. Williams. *J. Volcanol. Geotherm. Res.*, 77, 229–253.
- Hirabayashi, J., J. Ossaka, and T. Ozawa (1986), Geochemical study on volcanic gases at Sakurajima volcano, Japan, *J. Geophys. Res.*, 91(B12), 167–176.
- Inguaggiato, S., and A. Rizzo (2004), Dissolved helium isotope ratios in ground-waters: A new technique based on gas–water re-equilibration and its application to a volcanic area, *Appl. Geochim.*, 19, 665–673.
- Landi, P., N. Métrich, A. Bertagnini, and M. Rosi (2004), Dynamics of magma mixing and degassing recorded in plagioclase at Stromboli (Aeolian Archipelago, Italy), *Contrib. Mineral. Petrol.*, 147, 213–227, doi:10.1007/s00410-004-0555-5.
- Landi, P., L. Francalanci, M. Pompilio, M. Rosi, R. A. Corsaro, C. M. Petrone, I. Nardini, and L. Miraglia (2006), The December 2002–July 2003 effusive event at Stromboli volcano, Italy: An insight into the shallow plumbing system by petrochemical studies, *J. Volcanol. Geotherm. Res.*, 155, 263–284.
- Métrich, N., A. Bertagnini, P. Landi, and M. Rosi (2001), Crystallization driven by decompression and water loss at Stromboli volcano (Aeolian Islands, Italy), *J. Petrol.*, 42, 1471–1490.
- Métrich, N., A. Bertagnini, P. Landi, M. Rosi, and O. Belhadj (2005), Triggering mechanism at the origin of paroxysms at Stromboli (Aeolian Archipelago, Italy): The 5 April 2003 eruption, *Geophys. Res. Lett.*, 32, L10305, doi:10.1029/2004GL022257.
- Pino, N. A., M. Ripepe, and G. B. Cimini (2004), The Stromboli volcano landslides of December 2002: A seismological description, *Geophys. Res. Lett.*, 31, L02605, doi:10.1029/2003GL018385.
- Ripepe, M., A. J. L. Harris, and R. Carniel (2002), Thermal, seismic and infrasonic insights into conduit process at Stromboli volcano, *J. Volcanol. Geotherm. Res.*, 118, 285–297.
- Rittmann, A. (1931), Der ausbruch des Stromboli am 11 September 1930, *Z. Vulkanol.*, 14, 47–77.
- Rizzo, A., A. Caracausi, R. Favara, M. Martelli, P. M. Nuccio, A. Paonita, A. Roseglio, and M. Paternoster (2006), New insights into magma dynamics during last two eruptions of Mount Etna as inferred by geochemical monitoring from 2002 to 2005, *Geochim. Geophys. Geosyst.*, 7, Q06008, doi:10.1029/2005GC001175.
- Rosi, M., A. Bertagnini, A. J. L. Harris, L. Pioli, M. Pistolesi, and M. Ripepe (2006), A case history of paroxysmal explosion at Stromboli: timing and dynamics of the April 5, 2003 event, *Earth Planet. Sci. Lett.*, 243, 594–606.
- Sano, Y., Y. Nakamura, K. Notsu, and H. Wakita (1988), Influence of volcanic eruptions on helium isotope ratios in hydrothermal systems induced by volcanic eruptions, *Geochim. Cosmochim. Acta*, 52(5), 1305–1308.
- Sano, Y., G. Toshitaka, and S. N. Williams (1997), Secular variations of helium and carbon isotopes at Galeras volcano, Colombia, *J. Volcanol. Geotherm. Res.*, 77, 255–265.
-
- A. Aiuppa, G. Capasso, F. Grassi, S. Inguaggiato, M. Longo, and A. Rizzo, Istituto Nazionale di Geofisica e Vulcanologia—Sezione di Palermo, Via Ugo La Malfa 153, Palermo 90146, Italy. (a.rizzo@pa.ingv.it)
- M. L. Carapezza, Istituto Nazionale di Geofisica e Vulcanologia—Sezione di Roma 1, Via di Vigna Murata 605, 00143 Rome, Italy.

Ground Deformation From Ground-Based SAR Interferometry

Dario Tarchi,¹ Nicola Casagli,² Joaquim Fortuny-Guasch,¹ Letizia Guerri,²
Giuseppe Antonello,¹ and Davide Leva³

An in-depth analysis of the last two images acquired by the ground-based interferometric synthetic aperture radar system installed on Stromboli before the 5 April 2003 explosion allowed us to detect the precursory signals of the explosion related to ground deformation. In particular, it was possible to estimate the exact time of the explosion through the time domain analysis of raw data from the radar acquisition. This was interrupted by a blackout that occurred a few seconds after the event. The explosion onset time corresponds to a clear change in the intensity of the backscattered energy, related to the dense volcanic plume emission from the Crater. In addition, the use of a particular interferometric processing technique for the last two acquisitions, consisting of the selection of synthetic sub-apertures from the main ones and creating with these a sequence of interferograms with a higher temporal resolution, detected precursory deformations starting 2 min before the explosion. These observations indicate the occurrence of an elastic deformation of a centimeter amplitude that affected the volcanic edifice progressively from the Crater down to the Sciara del Fuoco depression.

1. INTRODUCTION

In December 2002, the Stromboli volcano, located in the Mediterranean Sea, erupted triggering a massive landslide that was followed by a destructive tsunami [Pino *et al.*, 2004; Maramai *et al.*, 2005; Bonaccorso *et al.*, 2003]. After

this event, the National Civil Protection Department (DPC) and the National Institute for Geophysics and Volcanology (INGV) set up an extensive monitoring system on Stromboli Island. In particular, the DPC entrust our research group with the installation of an innovative apparatus capable of remote monitoring of ground deformations. This system consists of a ground-based synthetic aperture radar (SAR) interferometer, known as linear SAR (LiSA). It is able to acquire radar images of the observed area every 12 min, with a pixel resolution of about $2 \text{ m} \times 2 \text{ m}$. The interferometric analysis of consecutive radar images allows us to derive the line of sight (LOS) deformation field of the observed area with a millimetric accuracy. Because of its remote sensing character and the possibility of obtaining data in any weather conditions, night and day, the technique is used as an early warning system for civil protection purposes. The LiSA was installed on a stable flank of the Sciara del Fuoco (SdF), the NW steep slope of the volcano, in order to continuously

¹Joint Research Centre, European Commission, Ispra, Italy.

²Department of Earth Sciences, University of Firenze, Firenze, Italy.

³Ellegi s.r.l.-LiSALab, Legnano, Italy.

monitor the displacements on the SdF slope and on the NE Crater (Plate 1).

2. THE INSTRUMENT

The LiSA system was specifically designed for the site conditions on Stromboli. In February 2003, it was installed at an elevation of 400 m above sea level and at an average distance from the target area of about 600 m. The instrument points up toward the NE Crater, with a 25° inclination angle of the radar antennas. This lateral location was chosen due to the logistic impossibility to place the system in front of the unstable slope. The hardware is constituted of a continuous wave step-frequency (CW-SF) radar that creates a synthetic aperture by moving the antennas along a horizontal straight rail, 3.0 m long, at steps of 5 mm. The microwave transmitter produces step-by-step, continuous waves at 1601 discrete frequency values, ranging from 17.0 to 17.1 GHz (average wavelength, 17.6 mm). The receiver acquires both the in-phase and the quadrature components of the microwave signal backscattered by the target. Range and cross-range synthesis of the complex images is obtained by coherently summing the signal contributions relative to different antenna positions and different microwave frequencies. As radar images are obtained through sampling techniques, frequency and spatial steps have to be selected to avoid ambiguity in range and cross-range [Rudolf *et al.*, 1999; Tarchi *et al.*, 2003a, 2003b].

Through these operational parameters, LiSA produces a synthesized radar image of the observed area every 12 min, night and day and in any visibility condition, with a pixel resolution of about 2 m in range and 2 m on average in cross range.

The system is installed within a cabinet, which is connected to the AC power supply line. Data transmission is provided by a HyperLan wireless antenna.

The processing of radar images is based on the radar interferometry technique, well known from satellite applications in the field of Earth observation [Zebker and Goldstein, 1986]. Interferograms are calculated using pairs of sequential images taken at different times exactly from the same position (zero baseline condition). A coherence threshold for the interferograms was chosen equal to 0.8 and pixels with lower coherence rejected. The interferometric analysis of sequences of consecutive images allows us to derive the entire displacement field of the observed portion of the SdF and of the Crater with an accuracy of about 1 mm [Casagli *et al.*, 2003; Antonello *et al.*, 2004].

The procedure for the production of interferograms is shown in Plate 2. The cross correlation of phase between two images taken at different times (T_1 and T_2) gives an interfero-

gram showing, pixel by pixel, the phase difference produced in the time interval $T_2 - T_1$. In the zero baseline condition, this phase difference directly expresses the displacement that has occurred along the LOS in the time interval. Negative values indicate a distance reduction that is a movement toward the observer. The phase values are not unwrapped, and therefore, they are affected by the intrinsic ambiguity of phase measurements: if ground displacement toward the observer exceeds the end of the scale, that is, $-0.25 L = -4.4$ mm, where L is the wavelength, the successive values will restart from the opposite scale end, that is, $+0.25 L = 4.4$ mm. After a ground displacement of $0.5 L = 8.8$ mm, the image pixels are in phase (value = 0) again. The typical effect of phase unwrapped is shown in the interferogram of Plate 2, where five interferometric fringes are evident on the SdF. By counting the number of phase cycles, it is possible to assess the amount of displacement (5×8.8 mm = 44 mm in this case).

Deformation maps are derived by accumulating the displacements from each interferogram and, because of the short time interval (12 min) between measurements, the interferometric displacements are usually smaller than half a wavelength, and unwrapping procedures are not necessary.

3. THE 5 APRIL 2003 PAROXYSM AS MEASURED BY THE LISA SYSTEM

In 5 April 2003, a major explosion from the NE Crater occurred at 0713:35 UT, without any clear precursors from the geophysical instruments [Rosi *et al.*, 2006; Calvari *et al.*, 2006]. The event, classifiable as a paroxysm for its high intensity [Barberi *et al.*, 1993], was comparable in size with the most recent explosion of 1930. It consisted of a major explosion that formed an eruptive column several hundred meters high (Plate 3) accompanied by the ejection of bombs and blocks on the NE and SW sectors of the volcano, reaching the settled areas and causing damage to several buildings located in the Ginostra village and to the monitoring network placed on the summit of the volcanic edifice. The ground-based SAR system was not damaged, even though the data acquisition was interrupted by a blackout caused by the explosion. The system was reactivated 1 h after the event.

In the last 2 h before the event, the deformation field, exposed in the Plate 4, shows a velocity close to zero in the Crater area, and a velocity of 3 mm/h in the SdF, coherently with the trend observed in this period.

The interferometric SAR processing of the images, derived by the last complete SAR acquisition collected before the explosion, and the first available acquisition after the system reactivation, did not reveal any signs from the volcanic event, showing an almost completely decorrelated signal

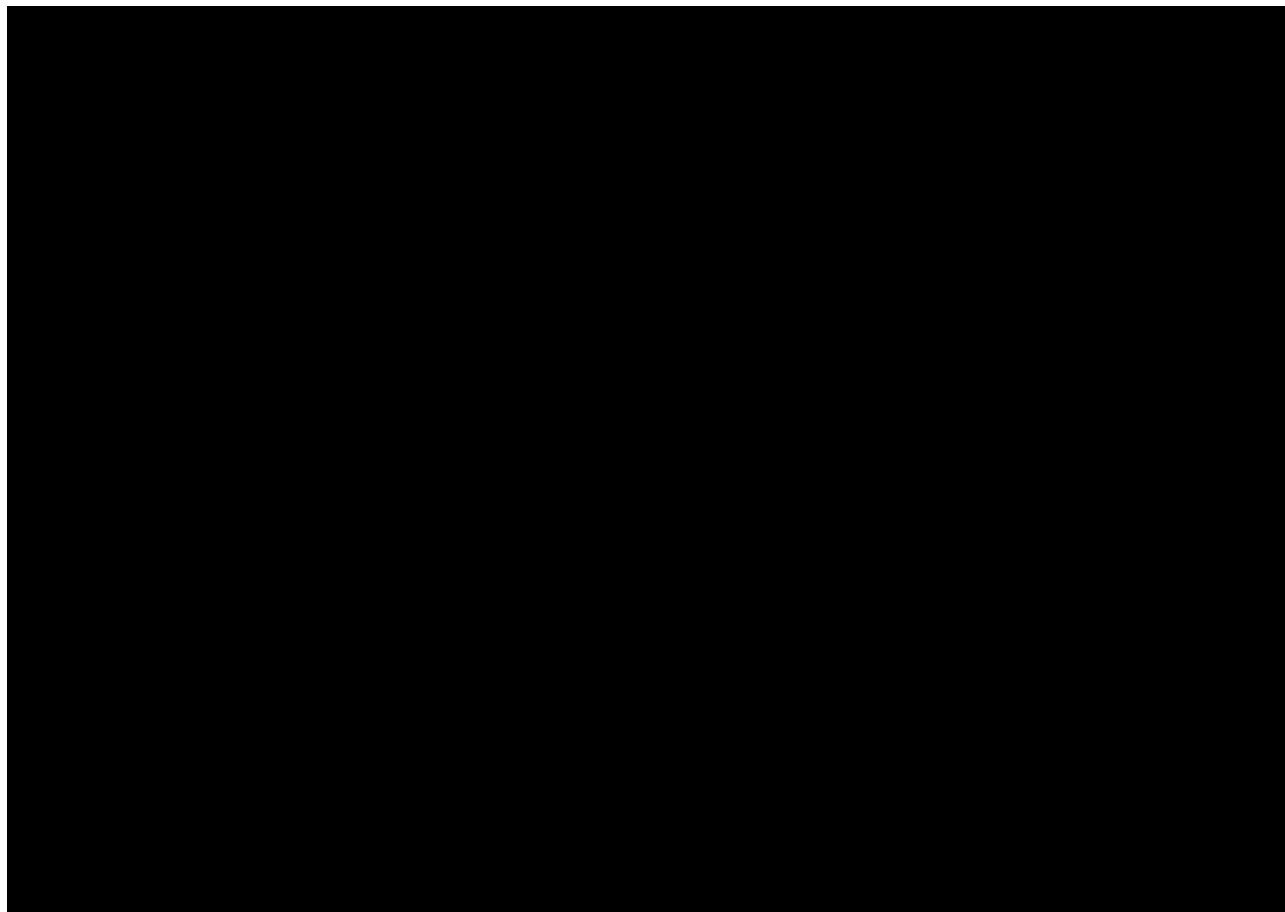


Plate 1. Location map of the Stromboli volcano. (a) Geographical location of the Stromboli volcano, the northernmost island in the Aeolian archipelago. (b) Shaded relief image of the Stromboli volcano projected on a DTM showing the steep NW flank of the island, called Sciara del Fuoco (SdF). The red portion indicates the observed area. The radar location and direction are shown in red.

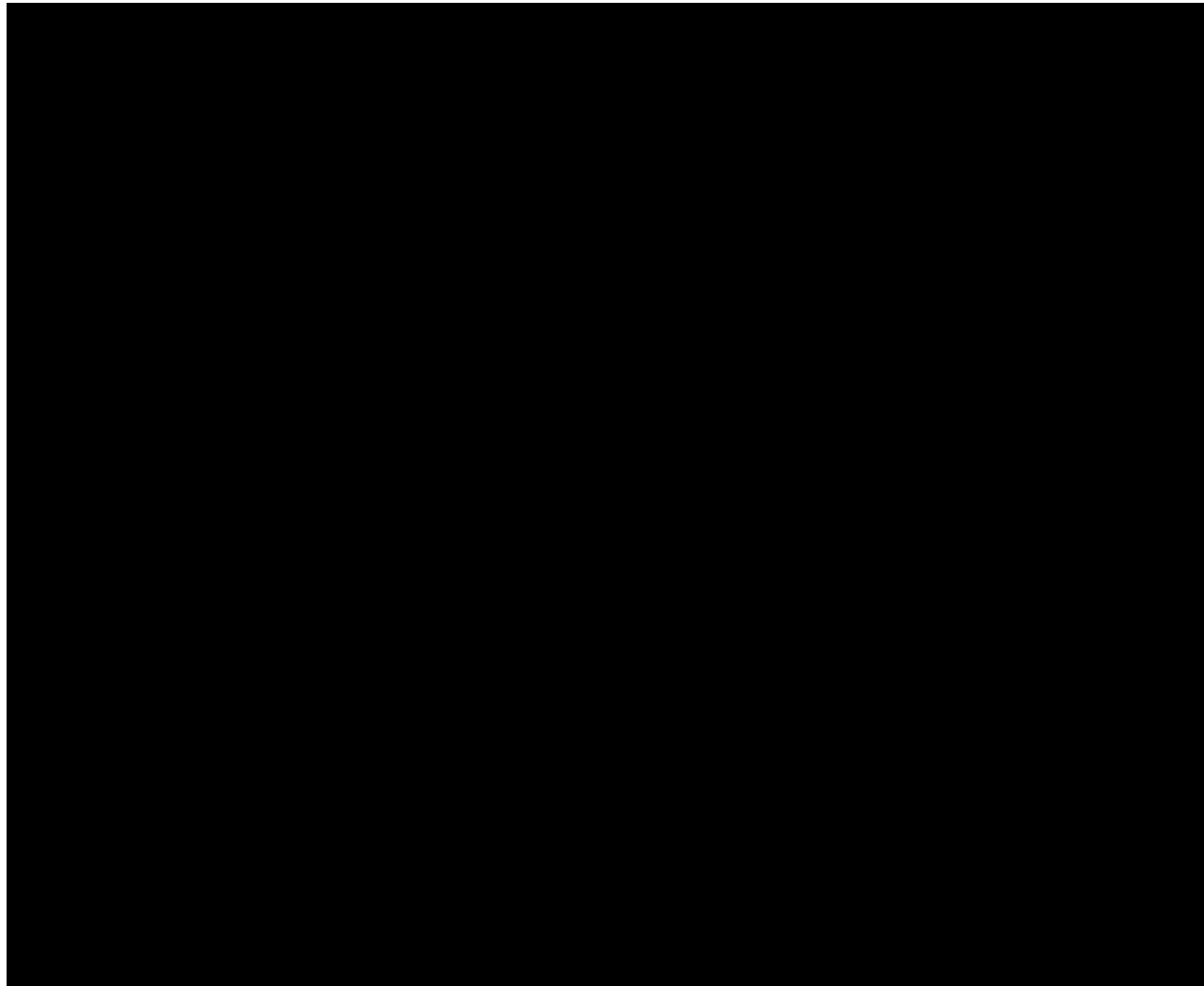


Plate 2. Scheme of the procedure for interferogram production. Interferogram (right) is computed using pairs of sequential images (left) taken at different times exactly from the same position (zero baseline condition). The phase is expressed in millimeters, and it is not unwrapped.

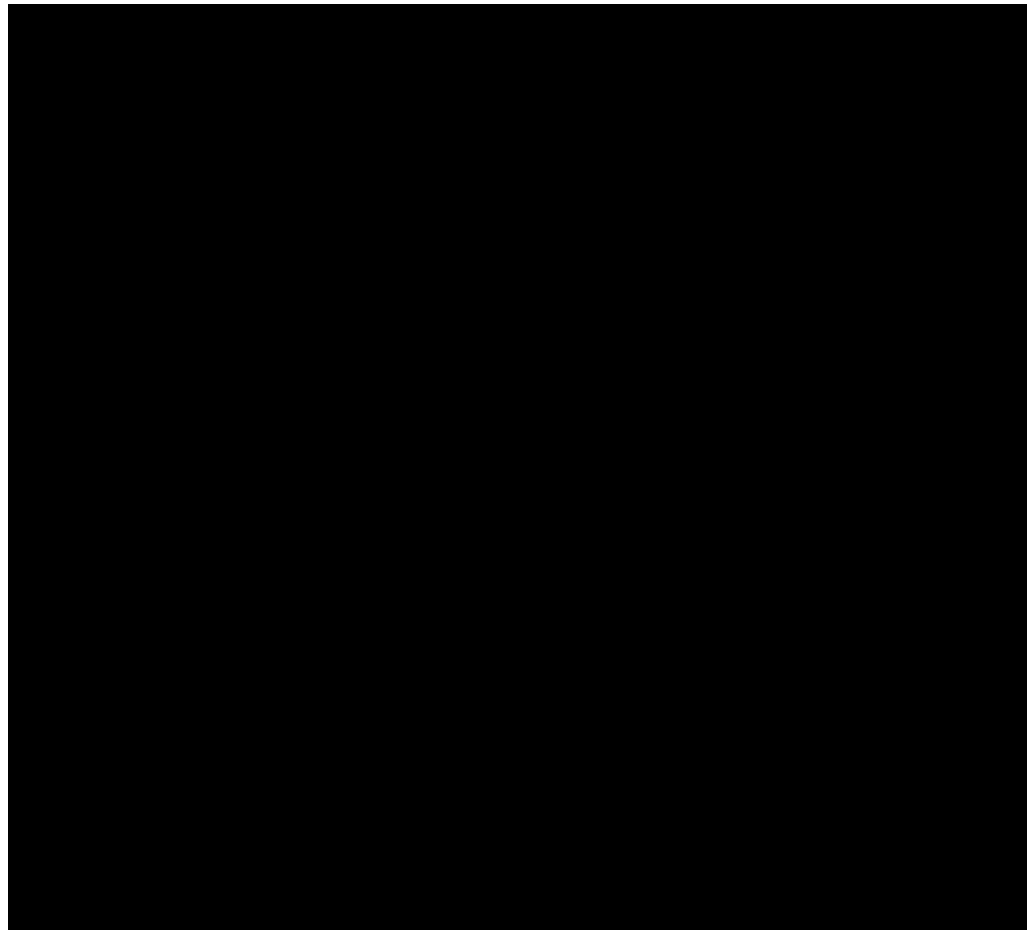


Plate 3. Pictures of the 5 April 2003 eruptive column taken from the San Vincenzo village (left) and from the ground-based SAR system location (right). The frame times (UT) are indicated.

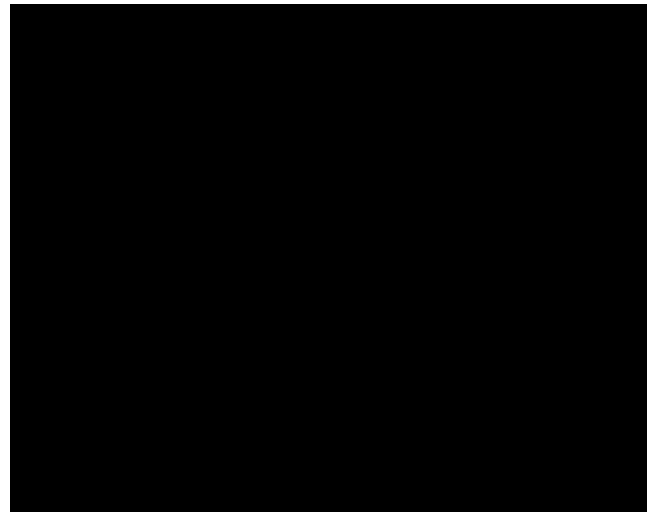


Plate 4. Interferogram covering the temporal interval of 1 h 59 min between 0414 and 0613 UT of 5 April 2003. The data show the stability of the flank of the Crater and a velocity of 2.5 mm/h in the SdF.

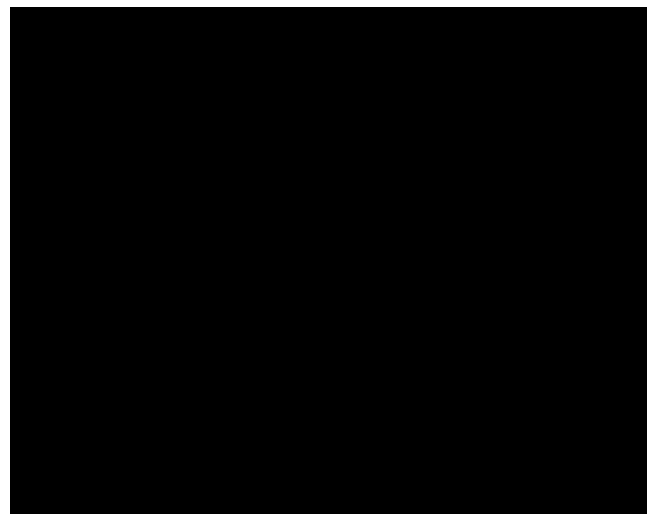


Plate 5. Interferogram covering the temporal interval of 1 h 52 min between 0652 and 0844 UT of 5 April 2003. The data show a decorrelated signal since the interferogram compares the images before and after the explosion, which occurred at 0713 UT.

in the resulting interferogram (Plate 5). Such a decorrelation can be attributed to the abrupt changes in the scattering characteristics caused by the ground shaking and the fall of volcanic material (ashes and blocks) from the plume.

The interferometric analysis of SAR image pairs acquired after the paroxysm registered a sudden acceleration of the ground movements on the NE Crater, where the LOS velocity reached a maximum value of 3 mm/h, an order of magnitude higher than the average value before the explosion (Plate 6). In a few hours, the velocities came back to the pre-event values. The acceleration has been correlated to a transitory dynamic effect, caused by the explosion, on the already unstable upper portion of the NE Crater.

Conversely, the SdF was not affected by the explosive event, since it maintained a constant velocity of 2.5 mm/h, before and after the explosion.

An in-depth analysis of the last two radar acquisitions was performed to discover if the data acquired by the ground-based SAR system before the blackout contained information on the volcanic event dynamics, such as the presence of possible precursors of the explosion, useful to highlight the time scale of preparation of this event. To this end, we have generated a shorter synthetic aperture. In this way, the effect of temporal averages induced by the focusing of the usual 12-min-long scan was removed. As a result of a shorter synthetic aperture, the azimuth spatial resolution of the derived images changed from 2 m to about 10–20 m.

4. EVALUATION OF THE EXPLOSION ONSET TIME

A time domain analysis of the raw data belonging to the acquisition interrupted a few seconds after the explosion was carried out to determine the intrinsic time of the explosion. The last scan (0707 UT) was interrupted by the blackout after 516 out of the 601 positions that correspond to the complete scan along the rail. This partial scan was split into sub-apertures formed by 100 positions, each one corresponding to a temporal interval of about 2 min. Next, a series of SAR amplitude images were obtained by focusing these sub-apertures (Plate 7). The signal processing of the first three sub-apertures has resulted in well-focused images, comparable with the images obtained by focusing a complete scan. Indeed, apart from the lower spatial resolution along the azimuth direction induced by the shorter aperture, all the features present in the usual amplitude images were visible. In contrast, the fourth image (obtained between scan positions 300 and 400) in the upper part, corresponding to the NE Crater, was not well focused. This suggests the occurrence of strong changes to the surface scatterers during the acquisition of this SAR scan portion. By looking at the distribution of backscattered energy as a function of distance

from the radar in the fourth sub-aperture (Plate 8), it is apparent that at position 330, there is an abrupt energy distribution change and a decrease of the relative power in the backscattered signal. From a close-up of that image (Plate 9), it is possible to observe how the power decrease is first recognized at a range distance of 900 m at the 328th scan position (0713:33 UT) and then how such a decrease moves obliquely reaching a distance of 800 m at the 337th position. In Plate 9, the oval indicates the area where the data disturbance is determined, whereas the oblique segment indicates the disturbance delayed with the decreasing of the distance from the instrument. In other words, as indicated by the oblique segment, the disturbance is first generated at major distances and then propagated at lower distances. This analysis, assuming that the disturbance observed in the raw data is due to the effects of the explosion, allows us to date the event. The perturbation of the radar signal could be related to the advance of the volcanic plume which, because of its high optical density, acts as a reflector, backscattering a portion of the signal or at least limiting the portion of the signal able to cross it. This interpretation would explain the absence of the Crater area in the amplitude image of the fourth sub-aperture. Assuming that the decrease in the signal power was induced by the plume advance, it is possible to estimate the onset time of the explosion, which corresponds to the first signal of perturbation in the intensity of the backscattered energy, recorded at the 328th scan position, which corresponds to 0713:33 UT. This time is about the same, which was retrieved from real-time GPS and seismic monitoring [Rosi *et al.*, 2006; D'Auria *et al.*, 2006; Mattia *et al.*, 2004; Ripepe *et al.*, 2008] and to the frames across the event acquired by the video camera installed at the SAR location (Plate 3).

Moreover, an estimation of the propagation velocity of the plume is possible. The signal perturbation covered a distance of about 100 m (from 900 to 800 m range distance) in nine scan positions (corresponding to a temporal interval of 12.5 s) with an average velocity of 7–8 m/s.

5. ANALYSIS OF THE EXPLOSION-INDUCED GROUND DEFORMATION

The presence of ground movements, possible precursors of the paroxysm, was checked by selecting the nonperturbed portion of the scan interrupted by the blackout (the first 300 positions) and by creating an interferogram with the 300-position-long sub-aperture from the last complete scan before the explosion. The obtained interferogram, characterized by a lower azimuth resolution compared to the standard interferograms, showed a general stability of SdF, while some interesting signals are detected in the Crater area (Plate 10),

where ground displacements of 1–2 mm along the system LOS have been recorded. These were probably induced by an expansion of the upper part of the volcanic edifice, with movements toward the radar sensor (negative sign) in the portion of the Crater in front of the radar and movements away from the sensor (positive sign) in the part of the Crater on the opposite side with respect to the radar. This interferogram shows that some minutes before the explosion, a radial expansion of the Crater occurred. It should be stressed that this has to be considered a qualitative indication of the induced deformation pattern, since most of the data acquired during the scan are not affected by the explosion, as visible in Plate 8. This has likely produced a significant underestimation of the displacement values.

To analyze in more depth the effects induced by an event characterized by a fast temporal evolution, the only viable approach was to reduce the SAR aperture length even more, thus minimizing the temporal averaging. From the 12-min-long synthetic aperture (3000 mm), sub-apertures of 250 mm were selected, increasing the temporal resolution of the radar data. A sliding step of 55 mm was defined, similar to the frame rate of a sequence of optical images. The sub-aperture was moved along two scans: the last complete acquisition before the event and the one interrupted by the event, in order to define for every sliding step a corresponding pair of 250-mm-long sub-apertures and, after the focusing, a couple of SAR images.

By coupling the obtained SAR images, an interferogram sequence was then generated to measure the ground displacements (Plate 11). The explosion time, as inferred from the time domain analysis (corresponding to the 328th scan position, at about 0713:33 UT), was considered as the reference time of the sequence. The interferogram sequence, starting about 393 s before the event and ending 226 s after it, shows the external expansion of the NE Crater. In the five interferograms, spanning the time interval from 143 and 77 s before the explosion, the recognizable pattern can be interpreted as an increasing expansion of the Crater area. In fact, the lower portion of the Crater (corresponding to the Crater rim on the side of the observation point) has a negative displacement, namely, a movement toward the system, whereas the upper part, which corresponds to the opposite Crater rim, is moving away from the sensor (positive sign). The values of displacement on the opposite rims of the Crater can be estimated until 77 s before the explosion in about –7 mm (toward the sensor) and about +4 mm (away from the sensor), indicating a dilation of about 10 mm. Afterwards (44 s before the event), the signal on the Crater area has become chaotic, probably due to the increase in the deformation rates not more measurable by the radar system or to an obscuring effect from the volcanic plume emitted just before the major

explosion. No further indication of deformation pattern in the area can be made.

Conversely, in the time span from 44 s before the event to 55 s after the event, we can follow the deformation pattern on the SdF. This starts as a displacement of 1–2 mm toward the system of the upper portion 44 s before the event and increases to a maximum of about 12 mm (22 s after the event) while propagating, with lower values, to the whole SdF. In the interferogram corresponding to 22 s after the event, also a portion of the stable flank of the SdF is affected by the deformation. In the interferogram at 55 s after the event, the measured displacement on the SdF is lower than the previous one, indicating an inversion in the direction of propagation of deformations. This can be interpreted as an elastic rebound of the ground. The series was interrupted by the blackout, which did not permit us to follow the recovery of the deformation field.

In summary, the analysis of the evolution of the deformation pattern in the whole time span covered by the interferograms in Plate 11 indicates the occurrence of an elastic deformation of a centimeter amplitude, affecting the volcanic edifice and started a few minutes before the explosion. Such an interpretation has been confirmed by the analysis of tilt load by seismic station not damaged by the event (M. Ripepe, personal communication, 2008).

6. CONCLUSION

An in-depth analysis of the data acquired just before and after the 5 April 2003 paroxysm by the ground-based SAR system installed on the Stromboli volcano was implemented to obtain information about the ground displacements induced by the explosion. The time domain analysis of the SAR acquisition containing the explosion and showing the disturbance of the radar signal probably caused by the erupted material, allowed us to retrieve the explosion onset time and to estimate the propagation velocity of the plume. In addition, the use of a shorter synthetic aperture was adopted as a possible solution, in order to study the consequences of the volcanic explosion on the ground stability and to carry out an ad hoc procedure for the interferometric processing of the ground-based SAR system, whose acquisition parameters were originally set up for the measurement of slow-moving processes. The procedure revealed the presence of elastic ground deformations, of about 1 cm in magnitude, which started a few minutes before the explosion. The importance of such a result is twofold: First, from a civil protection point of view, the ground-based SAR system could be used to detect precursory ground displacements and the imminent occurrence of a disruptive explosion, thus providing an early warning. Second, the system could detect important signs

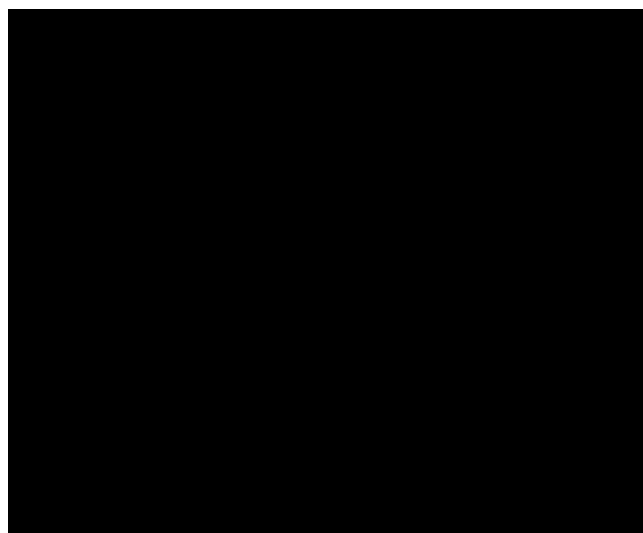


Plate 6. Interferogram covering the temporal interval of 1 h 24 min between 0820 and 0944 UT of 5 April 2003 (after the explosion occurred at 0713 UT). The data show high displacement rates on the Crater area that are related to the acceleration of this sector after the explosion. Displacement rates on the SdF are the same as those recorded before the explosion.

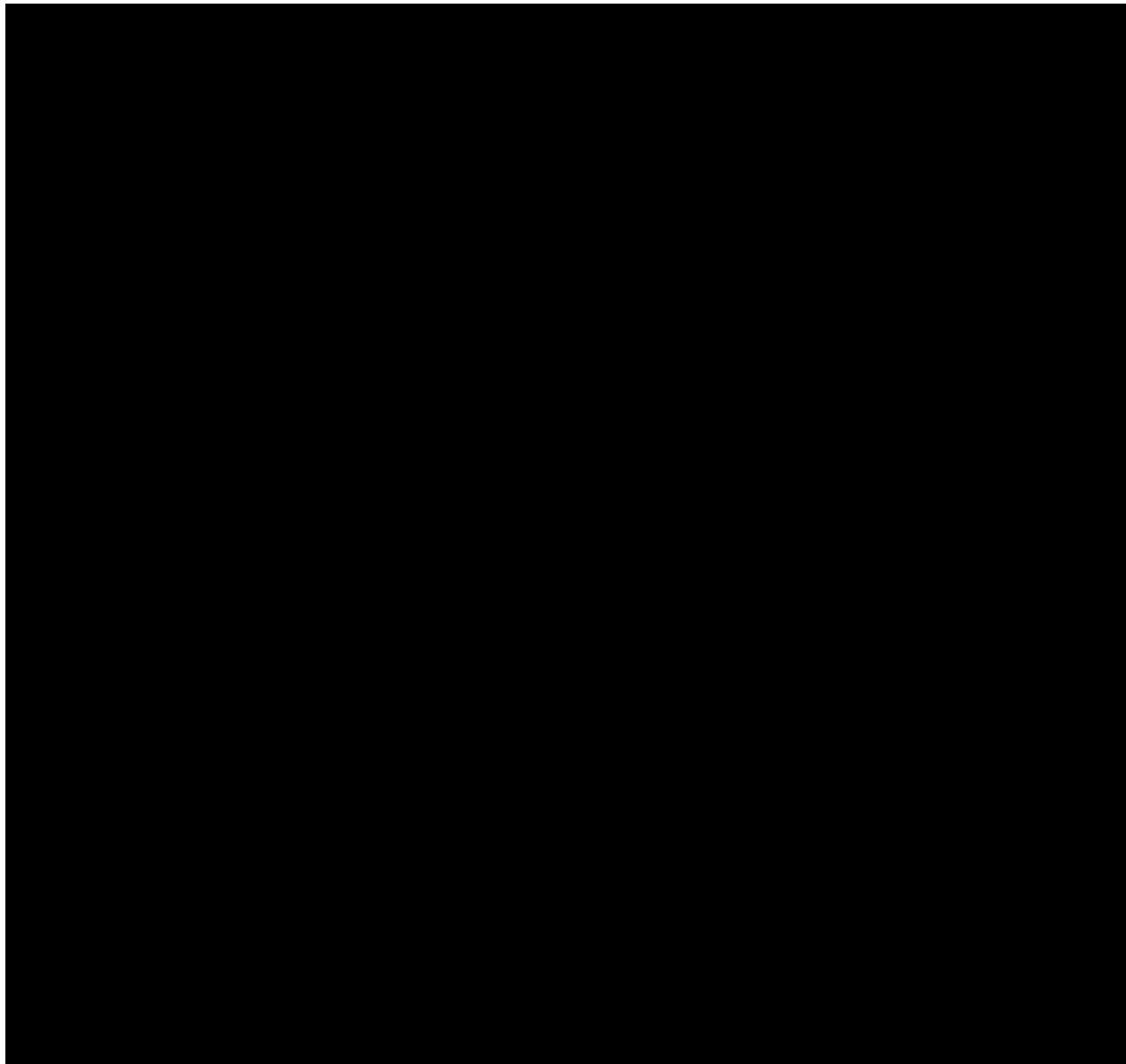


Plate 7. Sequence of amplitude images obtained from the sub-apertures of 100 positions. Every image corresponds to an increment of 2 min, and the sequence begins at 0707 UT. The numbers over the bar indicate the scan positions, and the numbers under the bar correspond to the UT. The black line in the last frame shows the onset time of the explosion, corresponding to the 328th scan position at 0713:33 UT.

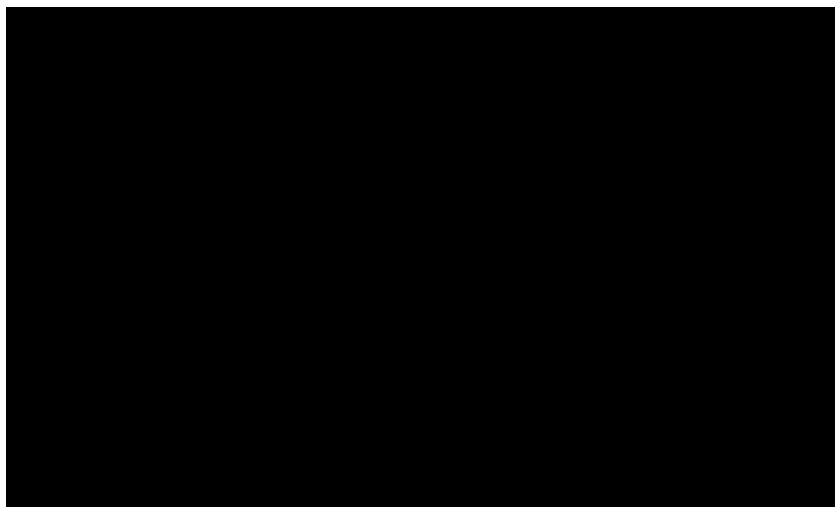


Plate 8. Time domain analysis of the fourth sub-aperture of the SAR acquisition interrupted by the explosion. The NE Crater, characterized by the highest values of backscattered energy, is delimited by the two green vertical lines.

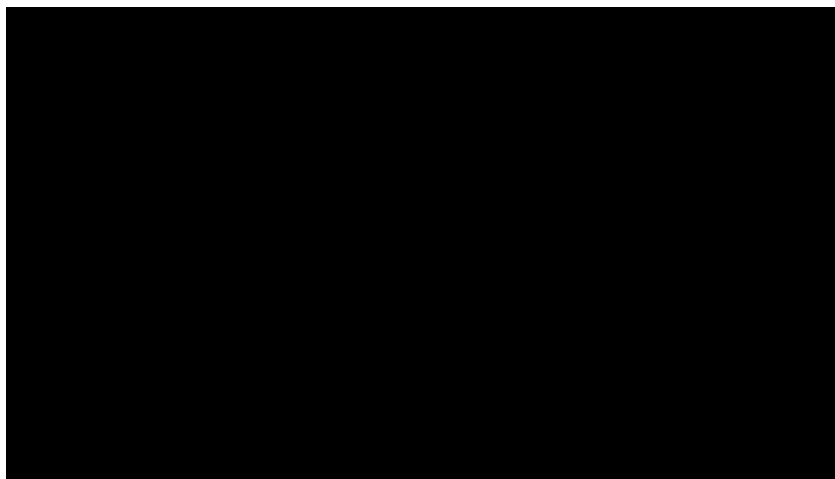


Plate 9. Close-up view of the time domain analysis of the fourth sub-aperture of the SAR acquisition interrupted by the explosion. The oval indicates the area where the data disturbance is determined, whereas the oblique segment indicates the disturbance delayed with the decrease in distance from the instrument.

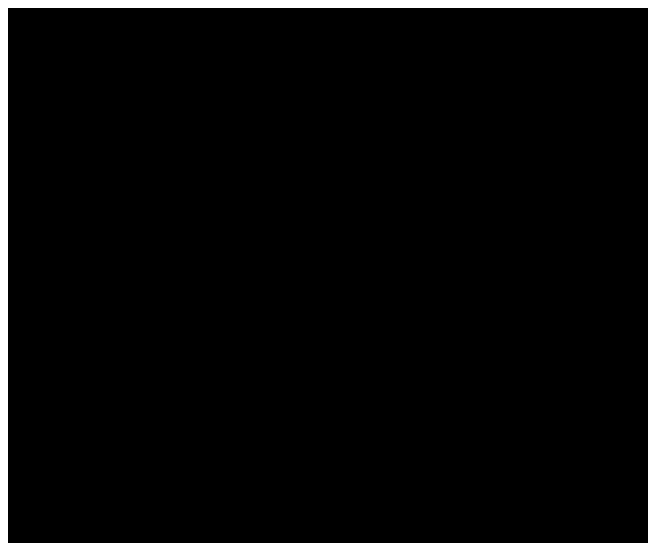


Plate 10. Interferogram obtained coupling the nonperturbed portion of the scan interrupted by the blackout (the first 300 positions) with the 300 position-long sub-aperture from the last complete scan before the event.

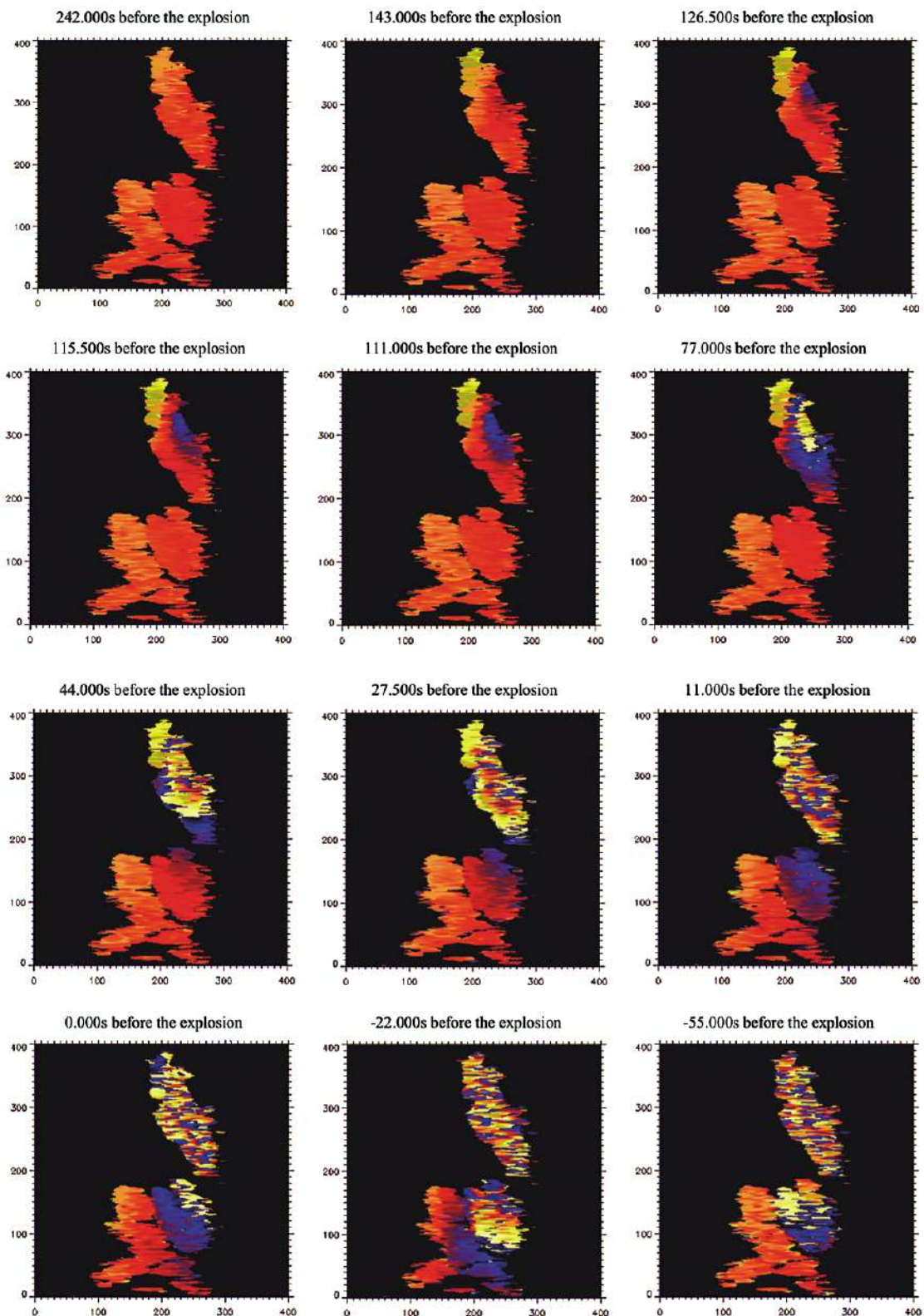


Plate 11. Sequence of interferograms spanning the time interval between 242 s before and 55 s after the explosion onset, as derived from the interferometric analysis of images acquired with a sub-aperture of 250 mm and a sliding step of 55 mm.

into the dynamics of the Stromboli paroxysms, showing how the volcanic Crater acts elastically.

Acknowledgments. This work has been sponsored by the Italian National Civil Protection Department (DPC). The authors wish to acknowledge in particular Bernardo De Bernardinis, Chiara Cardaci, and Antonella Scalzo (DPC).

REFERENCES

- Antonello, G., D. Tarchi, N. Casagli, P. Farina, L. Guerri, and D. Leva (2004), SAR interferometry from satellite and ground-based system for monitoring deformations on the Stromboli volcano, *IGRASS '04, Proceedings. 2004 IEEE International*, 1, 636, doi:10.1109-IGARSS.2004.1369108.
- Barberi, F., M. Rosi, and A. Sodi (1993), Volcanic hazard assessment at Stromboli based on review of historical data, *Acta Vulcanol.*, 3, 173–187.
- Bonaccorso, A., S. Calvari, G. Garfi, L. Lodato, and D. Patanè (2003), Dynamics of the December 2002 flank failure and tsunami at Stromboli volcano inferred by volcanological and geophysical observations, *Geophys. Res. Lett.*, 30(18), 1941, doi:10.1029/2003GL017702.
- Calvari, S., L. Spampinato, and L. Lodato (2005), The 5 April 2003 vulcanian paroxysmal explosion at Stromboli volcano (Italy) from field observations and thermal data, *J. Volcanol. Geotherm. Res.*, 149, 160–175.
- Casagli, N., P. Farina, L. Guerri, D. Tarchi, J. Fortuny, D. Leva, and G. Nico (2003), Preliminary results of SAR monitoring of the Sciara del Fuoco on the Stromboli volcano, Proc. Int. Conf. on Occurrence and Mechanisms of Flow-like Landslides in Natural Slopes and Earthfills, Sorrento, Italy, 14–16 May.
- D'Auria, L., F. Giudicepietro, M. Martini, and R. Peluso (2006), Seismological insight into the kinematics of the 5 April 2003 vulcanian explosion at Stromboli volcano (southern Italy), *Geophys. Res. Lett.*, 33, L08308, doi:10.1029/2006GL026018.
- Maramai, A., L. Graziani, G. Alessio, P. Burrato, L. Colini, L. Cuccia, R. Nappi, A. Nardi, and G. Vilardo (2005), Near- and far-field survey report of the 30 December 2002 Stromboli (Southern Italy) tsunami, *Mar. Geol.*, 215, 93–106.
- Mattia M., M. Rossi, F. Guglielmino, M. Aloisi, and Y. Bock (2004), The shallow plumbing system of Stromboli Island as imaged from 1 Hz instantaneous GPS position, *Geophys. Res. Lett.*, 31, L24610, doi:10.1029/2004GL021281.
- Pino, N. A., M. Ripepe, and G. B. Cimini (2004), The Stromboli Volcano landslides of December 2002: A seismological description, *Geophys. Res. Lett.*, 31, L02605, doi:10.1029/2003GL018385.
- Ripepe, M., and A. J. L. Harris (2008), Dynamics of the 5 April 2003 explosive paroxysm observed at Stromboli by a near-vent thermal, seismic and infrasonic array, *Geophys. Res. Lett.*, 35, L07306, doi:10.1029/2007GL032533.
- Rosi, M., A. Bertagnini, A. J. L. Harris, L. Pioli, M. Pistolesi, and M. Ripepe (2006), A case history of paroxysmal explosion at Stromboli: Timing and dynamics of the 5 April 2003 event, *Earth Planet. Sci. Lett.*, 243, 594–606.
- Rudolf, H., D. Leva, D. Tarchi, and A. J. Sieber (1999), A mobile and versatile SAR system, *IGARSS '99 Proceedings, IEEE 1999 International*, 1, 592–594, doi:10.1109-IGARSS.1999.773575.
- Tarchi, D., N. Casagli, R. Fanti, D. Leva, G. Luzi, A. Pasuto, M. Pieraccini, and S. Silvano (2003a), Landslide monitoring by using ground-based SAR interferometry: An example of application to the Tessina landslide in Italy, *Eng. Geol.*, 68, 15–30.
- Tarchi, D., N. Casagli, S. Moretti, D. Leva, and A. J. Sieber (2003b), Monitoring landslide displacements by using ground-based radar interferometry: Application to the Ruinon landslide in the Italian Alps, *J. Geophys. Res.*, 108(B8), 2387, doi:10.1029/2002JB002204.
- Zebker, H. A., and R. M. Goldstein (1986), Topographic mapping from interferometric synthetic aperture radar observations, *J. Geophys. Res.*, 91, 4993–4999.

G. Antonello, J. Fortuny-Guasch, and D. Tarchi, Joint Research Centre, European Commission, I-21020 Ispra (VA), Italy. (dario.tarchi@jrc.it)

N. Casagli and L. Guerri, Department of Earth Sciences, University of Firenze, Via G. La Pira 4-50121, Firenze, Italy.

D. Leva, Ellegi s.r.l.-LiSALab, I-20025 Legnano (MI), Italy.

Stromboli (2002–2003) Crisis Management and Risk Mitigation Actions

Guido Bertolaso, Bernardo De Bernardinis, Chiara Cardaci, and Antonella Scalzo

Dipartimento Nazionale di Protezione Civile, Rome, Italy

Mauro Rosi

Dipartimento di Scienze della Terra, Università di Pisa, Pisa, Italy

The 2002–2003 eruptive emergency of Stromboli was the most dangerous to have occurred on the island in the past three centuries. Starting from 30 December, the national Department of Civil Protection (DCP), operating under the direct authority of the prime minister, took responsibility for the emergency management. One of the most relevant achievements was the setting up, on the island, of Centro Operativo Avanzato, a permanent scientific/civil protection structure where signals of volcano monitoring are visualized in real time and eventually used by the personnel of the DCP for immediate reactions. Volcanic risk was also structurally reduced by the construction of a new pier to facilitate rapid evacuation of Ginostra village and the planning and implementation of new walking trails and shelters at the top of the mountain. The shelters, six in total, of moderate size, were designed to resist the impact of heavy materials launched by the volcano. The risk mitigation initiatives were completed with the installation of alarm sirens in the two villages, the production and distribution of leaflets, and also by the installation of signs indicating the fastest routes to reach safe waiting areas in case of tsunami. Besides the substantial improvements in the preparedness of the Civil Protection and Stromboli's community to respond effectively to possible future emergencies of the volcano, one of the most important heritages was the elaboration and testing of new protocols and procedures concerning the handling of volcanic emergencies. Although the issues raised during the crisis showed similarities with other volcanic crisis around the world, the role played by the Civil Protection with personnel specifically trained in volcanic problems showed comparatively considerable advantages.

1. INTRODUCTION

Emergency management of natural disasters carried out by civil protection authorities worldwide primarily focuses on relief operations and recovery of ordinary conditions.

The Stromboli Volcano: An Integrated Study of the 2002–2003 Eruption
Geophysical Monograph Series 182
Copyright 2008 by the American Geophysical Union.
10.1029/182GM30

However, volcanic emergencies, usually heralded by warning phases and characterized by prolonged duration, require that crisis management incorporates prevention activities. Prevention activities require, in turn, the collaboration, for a long period and under particularly stressful conditions, of specialists operating in different fields (scientific, administrative, socioeconomic, logistic) who are necessary in providing assistance in making difficult civil protection decisions. Volcanic emergency management represents a new, developing wide-ranging field of interest, because it should take

into consideration different socioeconomic contexts and also by the fact that volcanic systems behave in a wide range of styles. Sharing experiences on an international level, in this specific field, has therefore become of great value in order to best face this new millennium's challenges. The Italian Civil Protection's initiatives carried out at Stromboli since the emergency onset exceeded management and recovery of the emergency, which lasted months, and extended throughout the following years by implementing a series of interventions, organizational infrastructures, and procedures, focused on one final objective, that is, the reduction of risk and learning to live with an active volcano. In this paper, the different actions and activities undertaken by the Civil Protection Department (DCP) during the 2002–2003 crisis are described, and the multiple issues raised by the management of the crisis are discussed.

2. THE ISLAND OF STROMBOLI BEFORE THE CRISIS

The island of Stromboli belongs to the Aeolian archipelago, which is located in the southern Tyrrhenian Sea (Figure 1). On the island, which is just over 12 km² in extension, there are two villages: Stromboli on the NE coast and Ginostra on the SW side with 500 and 40 residents, respectively. In summer, the number of inhabitants grows considerably, reaching 5000 people. Stromboli's administration depends on Lipari's municipality, as do all the archipelago's islands excepting Salina.

At the beginning of the 20th century, Stromboli's economy depended on its own fleet of vessels engaged in trade, vine-growing, and cultivation of olive and fruit groves. The local economy was, however, affected by a serious depression in the years after 1930. During those years, the coincidence of two "calamities" such as the *filossera* (which devastated most of the vine cultivations) and the intense volcanic activity caused a massive exodus of the population. Stromboli's inhabitants decreased from some thousands to just a few hundred people in a very short time.

The island's economy picked up in the early 1950s, thanks to the growth of tourism. The 1949 Rossellini–Bergman film "Stromboli" contributed significantly to the island's popularity in the world. Since the 1950s, tourist activity has been steadily growing. Natural beauties (broad and easily accessed beaches, wildness of the coasts, mountain slopes, and seafloors) as well as the fascinating Mediterranean architecture of the two villages brought to the island an increasing number of people. In addition, a growing number of people visiting the island became captivated by the volcano's explosive activity, which could eventually be enjoyed from a relatively close distance without any apparent risk. All these factors resulted in a rapid expansion of the tourist demand and concurrently to little consideration being paid to the hazards posed by the presence of an active volcano.

3. VOLCANIC ERUPTIONS AND DAMAGE OF THE 20TH CENTURY

Damages caused by the greatest crises of the 20th century are reported in Table 1 [Barberi *et al.*, 1993; Giacomelli and Scandone, 2007]. The total number of fatalities amounted to 12, and approximately 50 people were injured by the eruptive phenomena (launching of eruptive bombs, blocks, and pyroclastic flows). The tsunami caused further casualties. There were eight cases of buildings suffering damage caused mainly by the fallout of heavy material (bombs and blocks) on the settled areas. The eruptions, which caused the highest number of deaths and significant damage, occurred in 1919 and 1930 when four and six casualties, respectively, were reported as well as the collapse of about 20 houses due to the fall of blocks on the village of Stromboli.

After the 1930 eruption, volcanic activity had been mild and the heavy material ejected by the explosive activity did not reach the inhabited areas. This volcanic behavior led people to forget the previous decades of strong eruptions and to consider Stromboli as a spectacular, peaceful volcano, unable to seriously threaten human life. The tradition of behavior based on respect for the volcano's activity, originating from a long familiarity with its more or less harmful nature, and the lessons learned by the population's testimonies were

Figure 1. Map of Stromboli Island. White zone: summit crater area; white star: location of Italian Civil Protection Center (COA).

Table 1. Damages Caused by the Greatest Crises of the 20th Century at Stromboli Volcano

Date	Type of Activity	Number of Dead and Injured	Damages
19 October 1900	Hot avalanches; ash fallout		
16 April 1905	Major explosions		Lapilli fallout up to 4 km; one person injured
27 April 1907	Paroxysm		Ash fallout up the town of Messina (80 km); houses damaged by air shock wave; acid rain
October–November 1912	Opening of a fissure in the SdF		Blocks on the village of Stromboli
13 November 1915	Lava flows, major explosions, hot avalanche		Scoria fallout on inhabited areas
2 July 1916	Paroxysm		
3 July 1916	Lava flows, major explosions		Tsunami
22 May 1919	Paroxysm	4 deaths several injured	1000-kg bomb fell on the village of Stromboli, vegetation fire, ash fallout up to Sicily, tsunami; 20 houses destroyed
11 September 1930	Paroxysm, secondary lava flows	6 deaths and 22 injured	Tsunami, hot avalanches, blocks fallout on Ginostra village; 30-ton blocks destroyed the old Labronzo Navy Observatory; up to 150 kg blocks fell on the village of Stromboli
2 February 1934	Paroxysm		Blocks fallout near Stromboli village; air shock wave caused damages to houses
22 August 1941	Paroxysm, lava fountains 100 m high		Blocks fallout near villages setting fire to vegetation; ash fallout caused little damages to houses
3 December 1943	Paroxysm		Blocks fallout set fire to vegetation; damages to houses
20 August 1944	Paroxysm		Plume 2000 m high, hot avalanche in the Forgia Vecchia, tsunami; one house destroyed
1 February 1954			Ash fallout, hot avalanche, tsunami
December 1972	Two explosions		Lithic fallout on Stromboli village; air shock wave broke a few windows
July 1986		Tourist killed near the craters	
16 October 1993	Major explosion	1 injured	
1 June 1996	Major explosion	4 injured	Tephra fallout set fire to vegetation
4 September 1996	Major explosion	6 injured	Tephra fallout set fire to vegetation
23 August 1998	Major explosion		Tephra fallout set fire to vegetation
26 August 1999	Major explosion	10 injured	Tephra fallout set fire to vegetation
21 October 2001	Major explosion	1 death	
28 December 2002 – 22 July 2003	Lava flow down to the sea; paroxysm 5 April 2003	Several injured	Tsunami 30 December 2002; damages to the edifices along the coast; blocks fallout on Ginostra village causes damages to houses
27 February – 2 April 2007	Lava flow down to the sea; paroxysm 15 March 2007		Tephra fallout set fire to vegetation

then gradually forgotten and lost in the second half of the century when tourism increased dramatically. On December 2002, before the crisis onset, even the residents were only vaguely aware of the potential dangers of the volcano's explosive activities and the risk of tsunamis was almost completely overlooked. In contrast, Stromboli was considered a "nice volcano" to visit and be enjoyed without any particular worries; the rules regulating the access to the volcano, set

out by Lipari's mayor, representing the local civil protection authority on this matter, were not taken seriously enough.

4. EFFECTS OF THE 30 DECEMBER TSUNAMI AND 5 APRIL EXPLOSION

The 2002–2003 eruptive crisis of Stromboli was one of the most intense and dangerous of the past three centuries

and the biggest to have occurred in Italy in the past century after those of 1906 and 1944 eruption of Vesuvius. On 30 December 2002, at 0115 and 0122 LT after the sudden sliding of two portions of the Sciara del Fuoco (SdF), below and above sea level, a series of tsunami waves hit the northern coastline of Stromboli. Minutes later, the tsunami waves, although greatly reduced in amplitude, reached the coast of the other Aeolian islands and the nearby coasts of Sicily and Calabria [Tinti *et al.*, 2003]. Stromboli was by far the most affected island: the maximum height of waves that hit the village of Stromboli was 11 m. Three people were injured, and significant damage to buildings situated close to the shoreline was reported (Figure 2a). As a result of the threat connected with slope failure and tsunami, part of the resident population (330 people) voluntarily left the island. Volcanic hazard climaxed again on April 5 2003 when blocks launched by a sudden explosion of the volcano fell on Ginostra. One house and one rainwater tank were severely damaged by the impact of meter-seized blocks. Some houses also reported broken windowpanes due to the transit of a shock wave. Despite the limited damages, the shower of blocks caused considerable panic among Ginostra's resi-

dents and also concern for a possible further evolution of the volcano activity. The prolonged duration of the crisis (6 months of continuous lava flow emission intercalated to slope failure and paroxysmal explosion) and the fact that the volcano showed in a short period all its potential in terms of dangers were important factors that induced the DCP and the mayor of Lipari to undertake an important project of risk mitigation financed by the national government.

5. THE ITALIAN CIVIL PROTECTION SYSTEM

The expression “civil protection” is intended by the Italian law in a broad sense, i.e., as “a series of actions and activities put forward in order to protect human lives, goods, settlements, and the environment from damages deriving from natural and human-induced calamities.” These actions incorporate the “classical” activity of rescue and recovery of normal conditions but also those related to the “prevention” of disasters.

The prevention activity of civil protection includes, more specifically, the setting up of the “Network of Centres of the Italian Civil Protection System” as well as the development and preparation of evacuation plans. The Network of

Figure 2. (a) House damaged by the tsunami waves; (b) the civil protection and volcano monitoring center (COA); (c) labors for the installation of the ground-based SAR in a difficult access site; and (d) new pier of Ginostra village to facilitate evacuation in case of an emergency.

Centres, based on the prime minister's decree on 27 February 2007, consists of operative units, able to collect, elaborate, and exchange every kind of data (meteorologic, hydrologic, and precipitation data for hydrogeologic and hydraulics risk, volcanic, seismic), thus providing multiple support systems for decision making by the Civil Protection Authorities. The network is coordinated by the DCP, which is under the direct authority of the prime minister of the Italian government.

The DCP is responsible for issuing the guidelines, procedural, and operative standards, as well as coordinating the network during emergencies at a national level. The network includes two types of centers: Centro Funzionale (Centre for Forecasting and Surveillance of Effects [CFSE]) and Centri di Competenza (Centres for Technological and Scientific Services [CTS]). When completed, the CFSE network will include 21 regional centers that will collect observations and run forecast models, the Central Functional Centre, which is already operating, and one at national level, under the control of DCP, which collects regional data, integrates the national picture, and acts as backup when necessary.

The so-called Centri di Competenza (CTS) are national-level institutions that provide services, information, data, elaboration, technical, and scientific contributions for specific topics. With regard to the volcanic risk, the main competence centers involved are all the divisions of Istituto Nazionale di Geofisica e Vulcanologia (INGV), the University of Florence, the Italian Space Agency, and the Air Force Meteorological Service. During emergencies, in addition to the above-mentioned permanent structures, also temporary, coordination structures (Centro Operativo Avanzato [COA] and Mixed Operational Centre [COM]) are eventually activated. The COA at Stromboli eventually became permanent because the volcano has the peculiar characteristic of being permanently active.

6. FIRST RESPONSE TO THE TSUNAMI

Civil protection personnel were alerted immediately after the tsunami event during the afternoon of 30 December 2002. Two DCP teams arrived on the islands of Stromboli and Lipari, which is the archipelago's main island located approximately 40 km SW of Stromboli.

On 30 December, the head of the department (DCP) was appointed by the president of the Council of Ministers as commissioner in charge of coordinating and carrying out all the activities to face the emergency.

A civil protection operational committee was also immediately established in order to guarantee the appropriate coordination of all activities. Two operational centers were set up for the local management of the emergency: the COA in Stromboli and the COM in Lipari.

The 400 Stromboli inhabitants present at the emergency's outbreak were informed about the nature and scale of the phenomena in progress and about the potential danger of eruptive activity and landslides.

On 31 December, about 330 residents decided to evacuate spontaneously. They were accommodated in apartments and hotels made available by the DCP in Sicily and on the other Aeolian islands. About 60 of them moved autonomously to the homes, out of Stromboli, of friends or family offering hospitality. Access to nonresidents was temporarily denied except for experts and authorized personnel (scientists, journalists, TV reporters, and civil protection staff).

In January 2003, only approximately 50 residents were still living on the island, which included alpine and volcanological guides, volcanologists, operators of various sectors, and a small group of young people forming an association in support of civil protection activities.

At the beginning of February, Stromboli's population was returned to the island, and by the month of March access to the island was also granted to nonresidents.

7. EMERGENCY MANAGEMENT

The emergency management was characterized by two main activities: immediate response to the crisis and prevention activities.

The first actions were the setting up of the civil protection operational centers for the emergency management and the planning and setting up of the upgraded volcano monitoring. The latter action had to be carried out in a short period (days to months), with the objective of rapidly improving the volcano's control network.

The civil protection's activities following the initial response can be grouped as follows:

- legislative norms
- management of emergency through the operational centers of Stromboli and Lipari
- support to the monitoring of the volcano
- tsunami alert system

7.1. Legislative Normative

The decrees and laws listed below have granted immediate intervention after the 30 December 2002 tsunami:

- 30 December 2002: Decree issued by the president of the Council of Ministers granting extraordinary powers to the head of the DCP to face emergency situations.
- 2 January 2003: Decree issued by the head of the DCP providing the institution of a COM in Lipari for the

- management and coordination of relief operations carried out on Aeolian islands and of a COA on Stromboli for ensuring the coordination of activities on the island.
- 10 January 2003: Declaration of the “state of emergency” by the national government.
 - 7 March 2003: Ordinance issued by the president of the Council of Ministers containing the regulations and economic measures to adopt in order to implement “the first most urgent relief operations aimed at the reclamation and salvage operations on the Aeolian islands territory.”

A number of legislative decrees set out by Lipari’s mayor, issued throughout the emergency, regulated the access to the island as well as the excursions on Stromboli’s slopes.

7.2. The Operational Centers of Stromboli and Lipari

Emergency management was conducted by the COM of Lipari and the COA of Stromboli.

Lipari’s center managed the temporary evacuation of the Stromboli’s inhabitants at the very outbreak of the emergency and was responsible for air and sea traffic management activities. The use of helicopters (Air Force, Navy, State Police, Carabinieri, and the DCP) during the emergency was necessary for the transportation of personnel involved in relief operations and the transportation of the island’s residents. Significant support to carry out these activities was provided by the Navy and Coast Guard.

Emergency plans pertaining to tsunami risk involving all the Aeolian islands were also outlined at Lipari’s COM, in collaboration with Lipari’s municipality and the region of Sicily. Lipari’s COM was closed on 1 July 2003.

The COA (Figure 2b) of Stromboli was designed to coordinate operations on the island. The principal activities carried out were

- upgrading of monitoring network
- gathering and analysis of monitoring data
- logistic support shipping of material and placement of monitoring instruments/devices; two heliports were built for this purpose
- drafting of the emergency plan for Stromboli against the risk of tsunami
- installation of a radio telecommunications network. The network covers the entire archipelago and the Tyrrhenian side of Messina and the Calabrian coast, including the operational room of the DCP in Rome
- the issue of daily bulletin reporting all the information regarding the activities carried out each day
- daily briefings between the DCP representatives and the scientific community

- information to the population and tourists about the emergency, correct behavior codes, and the volcano’s activity.

7.2.1. Resources and personnel employed in the emergency. The crises management required a great amount of resources and personnel belonging to the central and peripheral state administrations and regional and local institutions and the participation of the civil protection’s voluntary forces.

From January to March 2003, DCP personnel engaged varied daily from 20 to 25 at COA out of a total of 40–45 operating from the COA in Stromboli and the COM in Lipari. The scientific community staff reached daily peaks of 25–30 operators in Stromboli.

The first months of the emergency required the use of four naval units from the Navy and seven units from the Coastal Guard for the transportation of people, equipment, and vehicles. Furthermore, a significant number of helicopters had been used. The data reported in Table 2 refers to the most active period (5 January to 16 February 2003) in terms of each helicopter employed.

7.3. The Improvement of the Monitoring System

The period just after the onset of the eruption was characterized by considerable interaction between DCP and the scientific community for the analysis of the volcanic activity and for the evaluation of future scenarios. This cooperation highlighted the need to substantially improve the surveillance of volcanic and gravitational phenomena along the SdF. By early January, the DCP approved and financially supported, the plan submitted by the scientific committee to improve the Stromboli’s monitoring activity. In the meantime, DCP installed two optical TV cameras at the altitudes of 190 and 400 m above sea level (asl), which allowed for the observation of the activity along the SdF slope.

The upgrading of the geophysical, geochemical, and volcanological monitoring was largely accomplished in about a month, requiring the use of extraordinary means. Due to access difficulties to the middle and high parts of the volcano, the deployment of the delicate instruments required in particular the extensive use of suitable helicopters provided by the DCP (Figure 2c). In a few cases, specialized personnel working in the civil protection system was also involved to speed up operations and carry out specific labor tasks.

Devices installed by INGV and University of Florence included seismic, seismic-acoustic, geochemical, and ground deformation (electronic distance measurement, GPS, clinometers), devices, magnetic and gravimetric instruments,

and optical and thermal cameras. A ground-based synthetic aperture radar interferometer (SAR) and two wave meters were also installed to monitor landslides and tsunamis. All the monitoring signals were transmitted, via radio and optic fiber in real time, to the COA and, in some case, to the scientific research centers involved in the monitoring process.

Installation of the ground-based SAR system and three continuous GPS stations, called SCiaradat, required the greatest effort on behalf of the DCP.

The site for the placement of the ground-based SAR and the cameras was chosen on the side of SdF, about halfway up the volcanic summit, at an altitude of 400 m asl. The ground-based SAR was positioned in a small, reinforced concrete shelter on a concrete base. The Fire Brigade's Special Units carried out much of the work necessary for the installation of the system, whereas the Army's Sapper Corps arranged for the building of the nearby helicopter landing pad.

The ground-based SAR installed in Stromboli was conceived in the framework of common projects of the University of Florence and the European Committee's Common Research Center at Ispra. Although the SAR system had been already successfully tested to control landslides before, this was the first time it was installed on an active volcano.

By the time most monitoring instruments had been positioned, DCP began to work on deformation monitoring of the volcano's higher part, by activating the SCiaradat network. This network (three GPS stations) was designed by the Catania INGV section and consisted of three continuous GPS devices able to work autonomously without the specialized personnel's support and in an unfriendly environment. Because of their location on the dangerous volcanic slope, the three stations, completely assembled before their final realization, were located by the DCP helicopters.

Due to Stromboli's volcanic activity, the SCiaradat network transmitted data for only a short time: one station was reached and covered by a lava flow on 20 February 2003, while the other two stations were destroyed by the explosion of 5 April 2003.

The setting up of a reliable monitoring system in a short time was strategic in order to gain a good control of the ongoing phenomena and thus allow for the return to normality in a short time, after the events of 30 December 2002. The population came back to the island on early February, and the access to nonresidents was granted at the end of the next month.

7.4. Tsunami Alert System

The tsunami warning system at the beginning of the 2003 was based on a combination of cameras, seismic signals, and wave meter monitoring. As scientists, in the early stage of

the emergency, had not discarded the possibility of a large-scale collapse of the SdF during the early phase of the crisis, the DCP had installed a communication system based on the use of the telephone (SMS, fax, and e-mails) to alert communities living close to the coastline on the other Aeolian Islands, Calabria, and Sicily. In addition, a series of alarm sirens were installed near the coast of the village of Stromboli. Directive signposts were meanwhile set up to identify the escape routes from the coast to the waiting areas.

After the emergency was over the warning system was improved, and slightly changed. The current alert system primarily relies on the control and monitoring activities of the volcano focused on the possibility of anticipating potentially critical situations. The island's alarm sirens, previously utilized in case of sudden and unpredictable events, are now used for preventive alert, as occurred during the last eruption on 27 February 2007.

8. INTEGRATION OF CIVIL PROTECTION AND THE SCIENTIFIC COMMUNITY

The Stromboli emergency came after a series of crises that involved other Italian volcanoes. In July 2001 and in October 2002 to January 2003, Etna volcano produced major lava flows on three sides of the volcano, strong seismic activity (a $M = 4.4$ magnitude quake occurred on 29 October 2002 on Etna's eastern flank), and quasi-sustained emissions of ash that lasted for months. In November 2002, a site close to the volcanic island of Panarea (only a few kilometers SW of Stromboli) was affected by sudden and strong gas emissions offshore that generated concern for a possible volcanic reactivation.

During these events, the DCP was in charge of managing the emergencies (assisting the homeless population and reinstating the transportation conditions) and carrying out activities aimed at risk mitigation (diversion of lava flows in the summit part of Etna). The scientific support to the DCP was provided through the High Risks Committee (CGR), more specifically by the Volcanic Risk Sector, constituted by 10 members, whose opinion was granted upon request. During the first phase of Stromboli emergency, the High Risk Committee, in addition to providing its own evaluation on the ongoing phenomena, also recommended consultation with Prof. Barry Voight (University of Pennsylvania, USA) for an evaluation of the slope instability of the SdF. After having visited the island from 23 to 29 January, Prof. Voight presented his evaluation on January 30.

The Stromboli crisis, however, from the very beginning proved to be too complicated logically to be handled by a committee of 10 people. For this reason, the head of the department, by virtue of his extraordinary role as chief

commissioner in charge, decided to appoint a technical scientific committee (CTS), constituted by five experts belonging to both academic and monitoring institutions.

The cooperation between the Civil Protection and the scientific community has benefited from Stromboli's crisis, which lasted for a considerable length of time, and the opportunity to work side by side with the COA. Both components were actually quite satisfied with the COA experience. The scientific community entrusted with monitoring functions (INGV, University of Florence, and University of Rome) has benefited considerably from the recognition of its supporting role in the emergency management, besides having the chance to perform monitoring activities efficiently and making use of extraordinary logistic support. The DCP functionaries had, on the other hand, the chance to interact in real time with scientists, increase their experience, and perfect their scientific skills.

The most significant aspect emerging from the collaborative spirit within the COA was the daily evening briefing that brought together all DCP functionaries and researchers to comment and discuss the outcome of the monitoring data and analyze the ongoing phenomena. In this way, the volcanology experts, supported by the CTS, provided scientific information on a daily basis, which the civil protection could access instantly and in real time.

The COA, with its operational rooms, the seat for the collection and discussion of data emerging from the various scientific components' monitoring activity, became the premises for the national Central Functional Centre, the sector dedicated by the DCP to volcanic risk, where information and data regarding the most important Italian active volcanoes are collected (decree by Italian prime minister on 27 February 2004).

The Stromboli experience also contributed greatly to defining a commonly shared separation of roles and responsibilities between the scientific community and the DCP in terms of volcanic emergency management. The scientific community has become accustomed to focusing on daily evaluations, hazards, and civil protection in transforming hazard probability data in an evaluation of the potential "short-term risk" for people, which can eventually be reduced or eliminated by taking proper counter measures.

However, the two points of view have, at times, different evaluations, reflecting the fact that the scientific approach tends to be more cautious (when dealing with the subject of volcanoes, it is inherently difficult to exclude particularly dangerous scenarios completely), while the DCP must focus its decisions on people's safety and as much as possible on the reduction of the potential social and economic damage in order to minimize the crisis' negative effects on the country's economy.

9. OTHER MEASURES FOR THE VOLCANIC RISK MITIGATION

Following the Stromboli events of 30 December 2002, the DCP set up various projects to mitigate the volcanic risk for the resident population and tourists eventually present on the island during the summer season. The projects consisted of the construction of a new pier at Ginostra and the planning and implementation of new trails and volcano shelters at the top of the mountain.

9.1. Pier at Ginostra Village

The tsunami of 30 December 2002 stressed the need to provide the hamlet of Ginostra with a secure pier that would allow the rapid evacuation of the local inhabitants in case of an emergency.

The pier project (Figure 2d) was made by the University of Aquila, taking meteomarine parameters into proper consideration in order to minimize the environmental impact. The construction took 18 months of labor and was completed in April 2005. The pier serves to provide protective measures for the existing pier at Pertuso, which works both as a waiting area and boarding zone during evacuations and also as a port of call for other ships traveling from the mainland to and from the other islands. The work consisted of producing large prefabricated tanks of reinforced concrete built on the mainland, then transported to the site and sunken into the water to provide a stable foundation for the dock area. The dock is protected from the sea waves from the west by blocks of lava weighing up to 10 tonnes each. The total pier length is circa 60 m and is connected to the shore by a stone and concrete walkway (also circa 60 m in length).

9.2. Walking Trails

In order to provide the island with good accesses to the mountain, the DCP designed new walking trails and incorporated a few already present (Figure 3). The new and restored trails cross areas that have proven in the past to be less exposed to falling pyroclastic material.

The project was carried out by the Sicilian Public Company for forests under the supervision of the DCP. Furthermore, given that the island of Stromboli is a natural reserve, the works were executed according to existing norms concerning interventions in protected areas and using naturalistic engineering techniques.

Although the new walking trails cannot ensure risk-free conditions, they nevertheless significantly reduce risk exposure to researchers carrying out surveillance and monitoring tasks, as well as to excursionists climbing the volcano to

Figure 3. New walking trail to reach the volcano summit on the northeast side of the mountain. Stromboli village in the background.

watch the explosive activity. Excursionists, however, must be accompanied by volcanic guides and should be fully informed of the risks involved before commencing the climb.

9.3. Shelters

The main hazard posed by the volcano to people in the higher part of the mountain is represented by the fallout of heavy blocks and bombs. In order to reduce the risk for scientists and excursionists, it was decided to set up specifically designed shelters (Figure 4) of moderate size and with limited environmental impact. Each structure was designed to hold 20 people.

The University of Basilicata (Potenza, Italy) was entrusted by the DCP to design a shelter prototype capable of resisting the impact of heavy materials launched by the sudden and violent explosions of the volcano. Each shelter was specifically designed to respond to the following requisites: capacity to resist the impact of a block measuring 0.50 m in diameter and weighing 150 kg hitting the shelter at a speed faster than 200 km/h. Each shelter also has foundations capable of resisting the impact's force and avoiding the shelter's movements and rotations.

Each structure is made of reinforced concrete and metal parts and consists of three sections: (a) the foundation (Figure 4a), (b) the rigid inner shell (Figure 4b), and (c) the outer shield (Figure 4b). The most important component is the

outer shield. The shield, besides being the most resistant part, also works as a shock absorber, thanks to its connection to the inner shell with two rubber-made connectors located on the sides of the structure between the inner shelter and the shield.

The shelter's metal structures were screened from atmospheric discharge. Each shelter was also planned so as to resist adverse weather conditions and chemical agents released by the persistent volcanic activity. Before the final construction and installation, an experimental smaller-scale prototype was subjected to a series of laboratory resistance tests.

The shelters were installed in a short time, thanks to the use of S64 helicopters (Figure 4c), which could carry up to several tons and perform precise maneuvers in order to assemble the various components. Six structures were finally installed in late spring 2006 in strategic positions on the summit area of the volcano (Figure 4d). Three pairs were installed at different azimuth angles to the craters and at points where the craters can be easily visible. One pair is at an altitude of 865 m asl near the helicopter pad, a second pair, at an altitude of 750 m asl southwest of the craters, and the third pair, at an altitude of 790 m asl northeast of the craters.

The external surfaces are of low impact on the environment. The pigment of the cement is similar to the color of volcanic material and the visible steel parts are the same color. Furthermore, each shelter was partially covered by lava stone from the volcano's summit.

Figure 4. (a) Shelter's large foundation slab in concrete [1] provided with a posterior anchorage; (b) the exterior concrete shell [2] provided with two lateral steel walls; the interior shell in concrete provided with two side concrete walls [3]; four devices in rubber and silicone (two per each side) placed between the steel walls of the exterior shell and the interior concrete walls of the inner shell [4]; two steel devices (one per each side) composed of U-shaped elements [5], placed between the steel walls of the exterior shell and the concrete ones of the interior shell; (c) assembling operations of the shelter components using the S64 (sky crane) helicopter; (d) shelters position around the crater area.

10. INFORMATION AND EMERGENCY EXERCISE

The coordination and management of information during an emergency require a rapid evaluation ability, allowing for accurate and fast dissemination of information. Communication in emergency has three levels, i.e., institutions, media, and citizens.

One of the posttsunami reactions was a strong conflict between the local community and the information world. The tsunami phenomenon still quite unknown on a national level, and the volcano's spectacular eruptive activity attracted the TV networks and the press. The media's attention, however, was not positively welcomed by a part of the local community worried about the negative repercussions on the island's economy.

Once the first emergency phase passed, over the following years, the Civil Protection carried out an information policy aimed at spreading information on risks and behavior codes to adopt in case of risk. Every year at the beginning of the tourist season, a leaflet was distributed with information on the volcano and its manifestations and personal safety rules to follow. The most recent version of information leaflets

containing safety rules was planned with the objective of communicating simply understood messages by using the comic strip technique with the deliberate intent of conveying "not alarming" messages related to risk (Figure 5). All the information activity was only partly welcomed by the local community because the leaflets were systematically perceived as potentially scaring tourists.

On 18 April 2005, an exercise simulating a number of eruptive scenarios was carried out in Stromboli. The exercise served the purpose of testing procedures, and the relief systems were tested by rescuing an injured person in a mountainous environment by helicopter during an emergency. The coordination activities were carried out by the Italian Navy's *S. Giorgio* ship taking part in the exercise.

11. DISCUSSION

During the 2002–2003 crisis, the Civil Protection has interacted profoundly and for a long period with the scientific community and with the local community taking the responsibility of making decisions based on the "acceptable risk"

Figure 5. Information leaflet.

and playing a fundamental role of “buffering” tensions due to the long-lasting stress conditions posed by the crisis.

The collaboration and synergy between the scientific community and the staff of the department resulted in the achievement of two types of objectives: (a) contributing to the realization of a monitoring instrumental network able to ensure an effective protection of inhabitants and tourists and (b) creation of protocols and resources for DCP—scientific community consultation and putting the DCP in the position to make operational decisions in due time.

During the emergency, in the context of decision making by Civil Protection staff, the consultation procedure and the level of integration of the scientific community went through a process of progressive strengthening. The clear assumption of responsibility by the civil protection in the fields of operational decisions, including actions taken for the safety of the population as well as the management of relations with the media, puts the scientific community in the position to act in the best possible way, excluding negative interferences from the local communities and the media.

Communities subject to restrictive measures have very often protested, even vividly against the scientists, when decision makers have acted in a very conservative way, i.e., giving excessive weight to scientific evaluations that were not excluding unpleasant, although low-probability, eruptive scenarios. This had, for instance, occurred during the crisis of St. Helens (1980) and Long Valley (1982–2000) [Thompson, 2000], Monserrat (1994–2007) [Aspinall *et al.*, 2002], and Tungurahua (1999–2006) [Aguilera Ortiz and Dueñas Marín, 2007]. In fact, communities often perceive these measures as the result of an anxious scientific community excessively preoccupied with not excluding the worst development of a crisis. It is, for instance, known that in a few cases, some pessimistic evaluations by scientists have resulted in a collapse of their credibility, resulting in a loss of control of the management of the crisis. In Stromboli’s case, this did not occur because the Civil Protection assumed the full responsibility for these actions.

One of the worthiest efforts spent by the Civil Protection in terms of optimizing the contribution offered by the

scientific community lies within its very role; in fact, the Civil Protection is the financing body of scientific research and the “end user” of its results, strengthening the synergy between the Civil Protection and the scientific community, thanks to the constant sharing of data and evaluations of critical situations.

This procedure has been carried out on a daily basis during the crisis (briefing at the COA), on a regular basis at the restricted Scientific Committee level, and rarely at the Commission of High Risks level (volcanic session). The level of sharing and interaction between scientists reached extraordinary levels. This led to significant results even from a strictly scientific point of view. It is indeed common knowledge that in the sector of volcanic observatories, the sharing of monitoring data is far from a perfect mechanism; there is, in fact, a wiggling competition among scientists, who are afraid that their data could be used by other scientists for the publication of scientific articles. In the Stromboli experience, the role played by the Civil Protection greatly contributed to overcome those difficulties.

Another relevant feature of the Civil Protection role was the optimization of the scientific work by integrating all the available expert opinions. Evaluation of monitoring data was, in fact, made during meetings at which representatives of different institutions (experts of the Stromboli volcanic system, experts of volcanic processes, and modelers) all took part in the discussion freely.

The level of integration between the interventions carried out by the Civil Protection and the local community experienced alternate phases even though, over all, it is to be considered satisfactory. Tension rose when awareness-raising initiatives targeting the population and tourists were perceived as an excessive emphasis on the risks, which could heavily affect the island’s tourism.

12. CONCLUSIVE REMARKS

The intervention of the DCP during and after the 2002–2003 crises was substantial both in terms of coordination and logistic support during the aftermath and also in terms of structural initiatives for the mitigation of the volcanic risks.

Immediately after the tsunami, the department provided assistance to the population by carrying out rescue operations and temporary lodging for displaced people. In the following months, the DCP, in collaboration with the local civil protection authority (the mayor of Lipari), coordinated the partial refunding of the economic losses caused by the tsunami.

The most relevant feature of the intervention of the DCP, however, is the profound reshaping of the conditions of co-habitation with the volcano, accomplished by undertaking

a number of actions for the mitigation of the volcanic risks. On the whole, the realized interventions led to a substantial upgrading of the safety standards. A further important aspect of the crisis management was to designate Stromboli as a “laboratory” for the setting up and testing of civil protection procedures to be eventually applied to other volcanic risk realities of Italy.

The COA of Stromboli represents the most important permanent heritage of the process of integration between the scientific component and the DCP. The COA is the “common house” where, even in noncrisis periods, the volcano monitoring and Civil Protection activities are carried out, side by side, and where signals of volcano monitoring are eventually used by the personnel of DCP to activate ready-to-respond procedures. During noncrisis periods, COA gives support to the volcanological guides leading groups of excursionists to the volcano summit by providing, via radio, real-time information on the state of the volcano.

It is a difficult task to evaluate the actual effectiveness and success of the undertaken initiatives in terms of reducing the risk and establishing the proper synergy among the population, economical activities, and use of the resource “volcano.” Only through experience will we gain definite answers. It is indeed true that the Stromboli experience, and what has been done there, represents the basis, in terms of know-how, for a better response to possible and plausible future crises.

In contrast with the management of recent volcanic crisis around the world (St. Helens, 1980; Nevado del Ruiz, 1985; Rabaul, 1994; Monserrat, 1995; Tungurahua, 1999, to name a few), the management of the Stromboli’s crisis was characterized by a prominent role played by the Civil Protection authority. The strength of the role was dictated by the particular nature of the Italian Civil Protection system with personnel specifically trained in volcanic disaster prevention. This resulted in a series of advantages such as (a) offering prompt financial and logistic support to volcanologists and scientific institutions involved in the volcano monitoring activities, (b) taking the full responsibility of handling the relations with the media structurally solving the problem of the “single voice,” and (c) taking full responsibility in making preventive decisions (i.e., evaluating both the scientific and socioeconomic issues), eventually ensuring refunding to the population for induced, undesired, economic losses.

In short, the experience of Stromboli has illustrated, once more, all the inherent difficulties of searching the best cost (induced economic losses)/benefit (people safety) balance. Indeed, the role of civil defense staff personnel with background in volcanological issues and the collaboration with the volcanological community was of strategic importance in order to make decisions that combine all the factors entering

in the cost/benefit analysis. Many eruptive crises around the world have, in fact, extensively demonstrated that the direct interaction of scientists with decision makers without any elemental background in volcanological problems (poorly trained decision makers: administrators, or politicians) has often resulted in serious difficulties and misunderstandings and in some cases have led to catastrophic consequences. The difficulties have been primarily those of communication (misunderstanding the nature of the hazards posed by the volcanic activity and of the probabilistic evaluation of different scenarios), an excessive dependence of the mitigation action on the conservative attitude of scientists and on the lack of an efficient chain of command in responding to critical issues. The Armero's tragedy of 1985 with its 23,000 victims has been, in this regard, a tremendous worldwide lesson [Voight, 1990].

It is in this sense, it is hopeful that management of volcanic crises around the world will see a growing role of well-organized civil protection authorities with training in prevention and, above all, in interacting with the scientific component.

The effort made by the DCP is fully sympathetic with the economic development of the Stromboli's tourism and the creation of a "volcano park" where active volcanism is used to attract people to the island. The volcano/economy synergy is made possible, thanks to the presence of an integrated, scientific, and civil protection system capable of promptly taking, on site, actions for the protection of people if necessary and also by proper information given to tourists. From this point of view, Stromboli could become an interesting and innovative worldwide example to be mimed by other realities.

Acknowledgments. We wish to thank the personnel of the office "Pianificazione, Valutazione e Prevenzione dei Rischi" of DCP

for the collaboration offered for the preparation of the manuscript. Costanza Bonadonna is acknowledged for generously providing comments to earlier version of the manuscript. Vivien Anceschi kindly revised the English form.

REFERENCES

- Aguilera Ortiz, E., and W. Dueñas Marín (2007), Las erupciones del volcán Tungurahua de Julio y Agosto de 2006, *Proyecto de descentralización y desarrollo local-PDDL*, 52 pp., Quito.
- Aspinall, W. P., S. C. Loughlin, F. V. Michael, A. D. Miller, G. E. Norton, K. C. Rowley, R. S. J. Sparks, and S. R. Young (2002), The Montserrat Volcano Observatory: Its evolution, organization, role and activities, in *The Eruption of Soufrière Hills Volcano, Montserrat, from 1995 to 1999*, *Geol. Soc. Lond. Mem.*, vol. 21, edited by T. H. Druitt, and B. P. Kokelaar, pp. 71–91.
- Barberi, F., M. Rosi, and A. Sodi (1993), Volcanic hazard assessment at Stromboli volcano based on review of historical data, *Acta Vulcanol.*, 3, 173–187.
- Giacomelli, L., and R. Scandone (2007), *Vulcani d'Italia*, 320 pp., Liguori, Napoli, Italy.
- Thompson, D. (2000), *Volcano Cowboys: The Rocky Evolution of a Dangerous Science*, 326 pp., St. Martin's Griffin, New York.
- Tinti, S., G. Pagnoni, and F. Zaniboni (2003), Tsunami generation in Stromboli Island and impact on the south-east Tyrrhenian coasts, *Nat. Hazards Earth Syst. Sci.*, 3, 299–309.
- Voight, B. (1990), The 1985 Nevado del Ruiz volcano catastrophe: Anatomy and retrospection, *J. Volcanol. Geotherm. Res.*, 44, 349–386.

G. Bertolaso, C. Cardaci, B. De Bernardinis, and A. Scalzo, Dipartimento Nazionale di Protezione Civile, Rome, Italy. (guido.bertolaso@protezionecivile.it)

M. Rosi, Dipartimento di Scienze della Terra, Università di Pisa, Via Santa Maria, 56126 Pisa, Italy.

Scientific Community and Civil Protection Synergy During the Stromboli 2002–2003 Eruption

G. Bertolaso

Dipartimento della Protezione Civile, Presidenza del Consiglio dei Ministri, Rome, Italy

A. Bonaccorso and E. Boschi

Istituto Nazionale di Geofisica e Vulcanologia, Catania, Italy

The eruption of Stromboli 2002–2003, thanks to its complex scenario (flank instability, tsunami, necessity to rapidly upgrade monitoring networks), has provided an important opportunity to verify the response of the national system of civil protection to volcanic emergencies. In particular, it has tested and validated the model of collaboration, in use by Italian law, between the Department of Civil Protection and the National Institute of Geophysics and Volcanology. This synergy has enabled a better understanding and ability to tackle the eruptive crisis from its first stages, as well as implement monitoring systems both dependably and swiftly. In this work, the numerous first monitoring tasks carried out during the critical initial stages of the eruption are described, and the activities and planned action are reported over the course of the eruption that has made Stromboli one of the best monitored volcanoes not only in Italy but throughout the world.

1. INTRODUCTION

In Italy, the national service for the emergency management, known as Civil Protection, was instituted with the aim of protecting the integrity of life, heritage, inhabited settlements, and the environment from damage or the threat of damage caused by natural calamities, catastrophes or other disastrous events (State Decree 225, 1992). This national service is under the control of the presidency of the Council of Ministers that promotes and coordinates the activities of the administration of the State and all government bodies. To carry out these objectives, the Presidency of the Council relies upon the Department of Civil Protection, Dipartimento

di Protezione Civile (DPC), which is thus responsible for co-ordinating all the activities carried out in an emergency.

Until the end of the 1990s, there were various research groups in Italy that maintained permanent seismic monitoring systems in different areas of the country and at the active Italian volcanoes. The National Institute of Geophysics and Volcanology, Istituto Nazionale di Geofisica e Vulcanologia (INGV) was founded in 1999 (Decree 381, 1999) to officially carry out seismic and volcanic surveillance of the national territory and to coordinate regional and local seismic networks. A number of already existing research and monitoring institutions, such as the National Institute of Geophysics (Rome), the Vesuvian Observatory (Naples), and the National Research Council Institutes of Volcanology (Catania), Geochemistry (Palermo), and Seismic Risk (Milan) were then united within the INGV. The INGV thus represents a combined force of various existing structures whose objective is to carry out geophysical and volcanological research, also for civil protection purposes through its

collaboration with the DPC. A highly important and innovative aspect in the volcanological field is that the INGV is by law a component of the national service of civil protection. Moreover, study and monitoring activities, concerning the assessment of hazard and danger, are carried out jointly by agreement with the DPC.

After the beginning of the joint operation in 2000–2001, the first emergency in which the DPC–INGV coupling actually worked in complete integration was during the eruption of Etna in 2002–2003. This very complex eruption engaged the two agencies in synergy on various aspects. In a framework of active collaboration, the INGV used the continuous multidisciplinary monitoring to update and interpret the evolution of the phenomena underway (fracture propagation, evaluate seismicity, update lava field development, simulations to forecast the routes of lava flows, geophysical and volcanological parameters to monitor the activity, surveys of seismic damage). The INGV and DPC then jointly tackled various problems and critical events associated with the eruption. Many actions were focused on mitigating the risk and directed toward decision making for civil protection purposes and for the safety of the population. In particular, the continuous thermal monitoring of the lava flows from aircraft made available by the DPC allowed following the evolution of the lava flows with constancy, and the simulations enabled predicting the routes of the flows. These aspects enabled the DPC to quickly and aptly intervene in positioning the diversion barriers of the flow on 20–22 November 2002 to protect the tourist center on the high southern slope.

The full collaboration of the INGV then continued in other very important aspects, such as seismic zoning to evaluate areas at greatest risk with the aim of allowing the DPC to best plan the legislative procedures on behalf of damaged towns and the appraisal of the studies that followed and actions to be undertaken to improve monitoring volcanic clouds. In particular, during the 2002–2003 eruption, this latter aspect proved to be a prime critical hazard, in so far as it caused major problems to infrastructures in Catania including the repeated, sometimes extended, closure of the international airport.

While the eruption at Etna was fully underway, there was also the sudden emergency of the eruption at Stromboli, compelling the scientific community and the DPC to face a maximum limit scenario that had never taken place in previous decades, namely, two contemporary eruptions, both particularly complex, occurring at two different volcanic edifices.

The eruption of Stromboli, as explored in several other chapters of this monograph, raised important new issues (flank instability and tsunami, summit crater area surveillance, necessity to rapidly upgrade the entire monitoring

network) that further strengthened the collaboration and understanding between the DPC and INGV.

In this work, the crucial moments of the beginning of the eruption with the first important stages of appraising the phenomenon are outlined; then, the main actions rapidly undertaken to upgrade the monitoring and volcanic surveillance are described; lastly, the scientific activities planned and conducted in the successive months are illustrated that, through the profitable collaboration between DPC and INGV, have led Stromboli to become one of the best monitored volcanoes in Italy and indeed the world.

2. ONSET OF THE ERUPTIVE ACTIVITY AND THE ASSOCIATED EMERGENCY

Ordinary activity of Stromboli is characterized by persistent explosive activity of Strombolian type with an average of three to five events per hour. The explosive activity is characterized by unexpected major events that generally occur a couple of times a year. Much more energetic and violent explosive phenomena, defined as paroxysms, occur every 5–15 years on average [Barberi *et al.*, 1993]. The historical lava flows come from craters and effusive vents in the Sciara del Fuoco (SdF) depression, and therefore, the lava flows remain confined to this area (Figure 1).

In 2002, the permanent monitoring at Stromboli managed by the INGV comprised a number of seismic stations of the regional network of the Aeolian islands, four permanent GPS stations, two borehole tiltmeters, and a video camera installed on the top of the volcano about 100 m above the crater area (Figure 1). Geochemical monitoring of the fluids emitted from the soil and craters was carried out periodically.

In the first part of 2002, Stromboli showed alternating stages of greater and minor ordinary explosive activity that was interrupted by two major events on 23 January and 24 July. In the next months, the ordinary explosive activity underwent large fluctuations, both in hourly frequency as well as intensity (height reached by clasts) with an increase in October (8–10 events per hour) and a peak in the second week of November, when a continuous emission of spatter was recorded from the northern crater with numerous explosions that exceeded 150 m in height (internal reports, <http://www.ct.ingv.it/>).

Following this increase in explosive activity in November, thermal surveys were carried out from the helicopter provided by the DPC, which revealed a significant increment in the temperature inside the craters and confirmed the very high level of magma close to the crater rim with small overflow from crater 2 (central vent) that had produced flows limited to a few tens of meters inside the depression of the SdF.

Figure 1. Island of Stromboli. Map of the permanent monitoring devices in 2002.

The seismic stations, which recorded tremor with the normal fluctuations in amplitude during 2002, showed maximum values on 14–17 November at the same time as strong explosive activity. Permanent tilt networks and GPS did not detect any particularly anomalous trends (internal reports, <http://www.ct.ingv.it>).

Therefore, in November, the assumed picture was that of a possible effusive eruption with spillage of lava from the northern crater, which, owing to the summit morphology, might produce a lava flow inside the SdF depression (Figure 1). This scenario, which would not have led to any great risk, was the phenomenon that indeed happened on 28 and 29 December when a lava flow occurred in the SdF, a week after highly anomalous CO₂ flux values were recorded at the crater rim [Carapezza *et al.*, 2004] and 4 d after an abrupt increase in the explosive activity comparable to the peak values of mid-November [internal reports, <http://www.ct.ingv.it>; Calvari *et al.*, 2005].

In the first days of the eruption, although the complex eruption of Etna was fully underway, the INGV organized various activities for further evaluation of the phenomenon in progress at Stromboli. In particular, with the support of the helicopter of the DPC, many overflights for the visual and thermal surveillance of the activity were undertaken everyday, with consequent mapping and updating of the extent of the lava field. From the first day, the INGV set up a Web site dedicated to the eruption, releasing official notices, the first reports, images, maps, and description of the monitoring networks.

More or less without warning, in an unexpected and unforeseeable way given the data in hand, on 30 December, the effusive phenomenon was outstripped by the landslide of the SdF into the sea. This landslide, triggered by the movement begun in the submerged lower part of the SdF [Tommasi *et al.*, 2005], caused a tsunami that mainly affected the northern part of the island. There was damage to various structures

[*Tinti et al.*, 2005] but fortunately no loss of life, thanks also to the fact that the island has few tourists in the winter.

In the days/hours preceding the landslide, no particular seismic activity or any increase in amplitude of the tremor was detected. No significant variations in the permanent devices of ground deformation (GPS and tilt) were recorded either, although indeed all are located outside the SdF [*Bonaccorso et al.*, 2003].

What then proved to be the true prelude to the phenomenon, although not provoking anomalies in the existing geophysical networks, was observable only in the images obtained from the helicopter approximately an hour before. These showed the first trace of the edges of the landslide scars (Figure 2a). In the early afternoon of 30 December, just after the landslide occurred, another overflight was made (Figure 2b), and then another one on 31 December, when the dust and landslides had ended and the collapse sectors were very clear [Figure 2c; *Bonaccorso et al.*, 2003; *Calvari et al.*, 2005].

Between 30 and 31 December, the INGV produced a broad multidisciplinary report for the DPC [INGV-CT, 2002] that gave a picture of the events underway with specific reference to the landslide phenomenon of the SdF and consigned it to the Chief of the DPC who was in Stromboli from 30 December to coordinate the first interventions of civil protection. The report contained the interpretation and description of the phenomenon, established that it involved two landslide bod-

ies, determined the exact times of the event, provided the estimate of the volumes involved, and traced the probable scenario. In the following days, the group called “Emergeo” for the survey and quantifying of the effects of the tsunami also entered into action.

From 30 December, the phenomenon of the flank landslide of the SdF and the tsunami changed the expected scenario, and consequently, the hazard level rose. In the reports of the next days, the INGV indicated to the DPC the further actions to be undertaken for integrating the already existing monitoring as described in the next paragraph. In these first critical days, the Web site of the INGV became a fundamental instrument for the transmission of correct information. The main data acquired was shared with the DPC and successively selected and issued on appropriate Web pages. This became a key aspect for the diffusion of scientifically correct news and support for the DPC in regulating reports with the media, an important link with the population. An instrument, among other things, to counteract speculation and unwarranted alarmism, ever present on the occasion of natural events like those associated with an eruption.

In general, for a range of scientific aspects, the INGV support became essential. It soon played a vital role for the DPC in the successive briefings on the state of activity of the volcano and for the further planning of monitoring actions to be undertaken. Many of these meetings then took place in presence of the Commission of Great Risks, a consultant organ

Figure 2. Sciara del Fuoco (SdF) taken from the north: (a) 30 December 2002, 1200 UT, 1 h before the landslide, with the opened fractures highlighted in red and the traces of the successive landslide scars in yellow; (b) early afternoon 30 December 2002, right after the landslide in the SdF; (c) 31 December, after the landslide with scars and dimensions of collapsed bodies highlighted in yellow.

of the National Service of Civil Protection for the activities aimed at appraising the various hazard hypotheses, which has always approved the lines proposed by the INGV.

From the beginning of the eruption, the DPC promptly took on, as its duty by law, the general coordination of the activities of civil protection, involving the support of air and naval craft, and staff from various military bodies (Police, Carabinieri, Fire Department, Forestry Corps, Coast Guard, and Alpine Guides of the Finance Police). In particular, the DPC regulated the activities and flow of people to the island that were restricted to the staff of civil protection, and authorized research agencies provided helicopter support and guides for the reconnaissance of the lava flow and the stable and landslide areas. Moreover, an operational center of civil protection that also acted as an observatory for monitoring, called Advanced Operational Centre (COA), was quickly set up in the San Vincenzo locality (Figure 3) and was quickly undertaken. In a few days, this observatory was to become the advanced center of the DPC for the coordination of all the activities of civil protection. It would also host the acquisition, intentionally centralized here, of the permanent geophysical and volcanological monitoring systems on the island.

The COA became the base shared by the DPC and scientific community for the daily briefings, usually in the afternoon, which provided the latest on the volcano's state of activity, on the recorded measurements, and the activities in progress. This center was also open to researchers from the various Italian universities that collaborate in different areas to integrate the existing monitoring (photogrammetry, bathymetric, and marine measurements, infrasonic signals, synthetic aperture radar (SAR) measurements). All this allowed the broad-based circulation and sharing of information and research in the course, which in the successive weeks became a unique occasion to look in depth into the eruptive activity, the interpretations of the phenomenon, and actions to be taken in a continuous and permanent way.

3. MAIN IMMEDIATE INTERVENTIONS

Following the eruption, numerous activities were rapidly begun for the immediate evaluation of the recent phenomena and in progress. The DPC immediately made some helicopters available to the scientific community for thermal and visual monitoring, repair of out-of-order stations, and ordinary maintenance of the existing observation systems.

Figure 3. Island of Stromboli from above with view of the location of COA, which was to become the center shared by DPC and scientific community to coordinate and monitor the activities undertaken for monitoring and surveillance.

Table 1. Outline of the Disciplinary Fields of the INGV for the Monitoring and Surveillance of Stromboli

Seismology	Volcanology	Deformation	Geochemistry
• Permanent seismic network	• Geological and structural investigations	• Permanent GPS network	• Gas sampling from soil, water, and fumaroles
• Upgrading and installation of broadband stations	• Mobile thermal camera helicopter survey	• High-frequency summit permanent GPS network	• Gas and temperature permanent stations
• Real-time analysis of the mechanisms and parameters of the seismicity	• Volcano products sampling	• Permanent tilt stations	• SO ₂ /HCl plume Fourier transform infrared measurements
• H24 surveillance in the Operation Room	• Products laboratory analysis (petrology, mineralogy, XRF)	• Electronic distance measurement (summit and unstable areas)	• SO ₂ plume UV scanner permanent network
	• Permanent camera network	• Automatic geodetic station	

Moreover, the DPC quickly started the restructuring of the COA, upgraded the information and calculation systems, set up spaces to allot permanent rooms for the acquisition and visualization of various data, and boosted the networks dedicated to data transmission. In particular, with the aim of optimizing the transmission and information connections, various activities like the installation of connections to the Internet, activation of wireless networks and dedicated fiber-optic links for the connection of different sites and monitoring stations to the COA were carried out.

The data of the permanent seismic networks and the video camera images are transmitted to the COA and then sent on to the INGV operation rooms of Catania and Naples, which work 24 h a day and thus contribute to the surveillance at a distance.

To operate effectively, the INGV was subdivided into four disciplinary fields: volcanology, seismology, deformation, and geochemistry (Table 1), each coordinated by respective research supervisors and the directors of the INGV structures involved in the emergency (Catania, Naples, and Palermo). The supervisors of these four fields, or their substitutes, then participated at the daily briefings at the COA and drew up official notices everyday and periodic reports on the activities being undertaken. A synthetic picture of the various disciplinary activities performed by the INGV is shown in Table 1.

The very first action, following the information from the already existing permanent networks (seismic, GPS, tilt, geochemistry, and video camera), concerned an immediate contribution to the control of the different elements, such as the

Table 2. Main Immediate Scientific Activities of the INGV Supporting Already Operating Systems

Type	Activity	DPC Support
Thermal survey	Monitoring and thermal mapping of the summit crater areas, the flow and the SdF with aerial coverage	Helicopter
Seismology	Installation of first permanent broad-band stations to update the existing network	Helicopter
Deformation	Electronic distance measurement for the control of the stability of the summit area and movements of the SdF	Helicopter and guides
Investigations on tsunami effects on the coast	Survey, monitoring, and appraisal of the effects of the tsunami on the coast	Boat and guides
Structural “analysis”	Analysis of the structural field and fractures associated with the eruption and evaluation of the stability of the crater area	Helicopter and guides
Petrological analysis	Analysis of emitted ash for the characterization of the explosive process	Guides
Fluid geochemistry	Intensification of the sampling of ground degassing around inhabited areas and in summit crater	Helicopter and guides
Remote sensing geochemistry	Fourier transform infrared measurements for the control of the HCl/SO ₂ ratio from the plume	Helicopter
Remote sensing geochemistry	Measurements with COSPEC technique to control SO ₂ release from the plume	Boat

state of activity of the crater area and its stability, the monitoring of the SdF and the unstable landslide area, as well as the surveillance of internal sources. A general picture of the first interventions realized by the INGV is given in Table 2.

The use of the thermal cameras, in frequent daily flyovers, soon proved indispensable, since they enabled detection of morphologic variations in the craters even in conditions of abundant gaseous emissions [Calvari *et al.*, 2006], which usually encircle the craters with an impenetrable cloud and, moreover, allowed monitoring of the depth of the magmatic column in the conduits. Surveillance of the SdF and the related lava flow with the thermal cameras allowed to monitor the opening of new fractures, highlighted by their permeability to high temperature magmatic gases, and the shifting of effusive vents and calculation of the effusion rate [Calvari *et al.*, 2005, 2006; Harris *et al.*, 2005; Lodato *et al.*, 2007].

On 30 December, we collected ash samples at two different localities on Stromboli. We carried out grain size and morphological (by scanning electron microscope) analyses on these samples. Overall, the characteristics previously described did not supply indications of a fragmentation of a magmatic type, caused by the increase and breakage of the vesicles, but they could be imputed to other processes such as mechanical abrasion and/or interaction of the magma with water. However, monitoring the gaseous emissions of the summit conduits became fundamental, and Fourier transform infrared measurements were undertaken to determine the SO₂/HCl relationship that, to combine safety and speed, were made from the helicopter supplied by the DPC. The measurements showed a minimal variation between September 2002 and January 2003, indicating that the eruptive activity was not due to a strong increase in the input rate of magma in the system. The study of the main chemical parameters was intensified by monitoring the degassing on the ground near the inhabited areas as well as in the summit crater zone [Carapezza *et al.*, 2004; Brusca *et al.*, 2004] and through Cospec remote measurements (also with the aid of boats made available by the DPC) of SO₂ emission from the plume [Ripepe *et al.*, 2005].

Following the landslide events, evaluation of the fracture field inside the SdF and the stability of the crater area still remained to be done. To this end, a structural survey was carried out that highlighted fractures that could be differentiated and described separately by their genesis, kinematics, and evolution. In particular, it was confirmed that the crater area was collapsing but not subject to gravitational sliding [Acocella *et al.*, 2006]. This aspect proved very important as it allowed excluding a broader sliding with the possible involvement of the craters, which could have led to explosive activity triggered by rapid decompression. For the evaluation of the movements of the crater area and the SdF, with

the aid of the alpine guides provided by the DPC, geodetic reflectors were installed in the crater area (measured from the upper rim of the crater area) and in the upper part of the SdF (measured from the low southern rim of the SdF). The measurements were repeated daily, in the summit area with the support of the helicopter and the guides, and allowed obtaining a first picture of the movements that confirmed the summit stability and defined the slip rates of the SdF [Puglisi *et al.*, 2005].

The first phase was completed with the installation of broadband seismic stations, to be boosted in the successive weeks to configure a new network for the real-time monitoring of fundamental parameters associated with explosive activity [VLP events, localization and mechanism of the seismic source; Auger *et al.*, 2006].

4. MAIN SCIENTIFIC ACTIONS PLANNED AND UNDERTAKEN IN THE COURSE OF 2003

In the successive weeks after the beginning of the eruption, together with the immediate tasks, the INGV planned various scientific projects to further implement the monitoring of the volcanic activity and the unstable flank of the SdF. The proposals were discussed during the daily briefings at the COA and also officially presented in the meetings that the DPC held in the presence of the Commission of Great Risks. The projects were approved by the DPC and then backed both by logistic support as well as funding regulated by an appropriate agreement between the DPC and INGV.

The program of the planned and undertaken activities was particularly wide in scope and tasking and included multiple activities (Table 3) made possible by the logistic and operating support (communications, boats, helicopters, guides) made available by the DPC.

A high-density broadband permanent seismic network, composed of 15 stations, was installed with the precise objective of locating in real time the superficial and deep volumes involved in the mechanism of accumulation and release of explosive energy, identifying in real time the mechanisms of release and volumetric variations of sources of the single explosive phenomena, localising and defining the geometry of the conduits of the rising fluids, by monitoring variations with time.

Geochemical monitoring was upgraded, both in the number of sites and the frequency of sampling, for the evaluation of the gas emissions. In particular, the program and activities included the discontinuous monitoring of the thermal aquifers and the diffuse degassing from the ground (areas of the inhabited center) and fumarole gases, as well as profiles of spontaneous potential and radon in the summit area [Brusca *et al.*, 2004].

Table 3. Main Scientific Interventions Planned and Realized in 2003

Type	Activity
Seismic network	Broadband network installation
Webcam network	Set up of network of two sites, each with two webcams (visible and thermal) to monitor summit and the SdF
Geochemistry of fluids (periodical measurements and permanent instruments)	Upgrading of the discontinuous monitoring of the thermal aquifer, the degassing from ground and fumarole gases, measurements of potential and radon in summit area
Geochemical remote sensing (permanent array)	Installation network of four permanent stations for the continuous telesurveying and monitoring of the SO ₂ flow
GPS real-time network	Installation of permanent GPS real-time array (one data per second)
Automatic theodolite	Installation
Gravimetric and magnetic permanent network	Installation of a permanent gravimeter and an array of permanent magnetic stations

Moreover, permanent stations for the continuous monitoring of the chemical–physical parameters of the aquifers and of the emission of the CO₂ from the ground (inhabited centers and crater zone) were installed [Inguaggiato *et al.*, 2004; Capasso *et al.*, 2005]. Special attention was given to the flows emitted from the central conduits by the installation of a network composed of four permanent stations equipped with “mini-DOAS” geochemical sensors for the continuous detection and monitoring of the SO₂ flow from the craters.

Particular attention was given to the problem of the evaluation of the activity and movements of the summit area and the SdF. The visible video camera on the upper rim of the crater was integrated with another permanent infrared video camera, and two more permanent video cameras were installed (thermal and visible) on the northern rim of the SdF to monitor the effusive activity in the SdF.

A new aspect, very difficult to achieve, was monitoring the movements of the SdF, which, owing to its harsh morphology, did not allow easy access and made the installation of permanent stations difficult. It was decided to proceed with a dual control provided both with GPS stations installed inside the SdF by the aid of the helicopter, as well as an automatic geodetic station situated at a distance. In particular, a real-time GPS array, for the continuous monitoring of movements, acquisition rate data, has been installed in the summit crater area and high SdF [Puglisi *et al.*, 2005]. Therefore, the GPS summit network continuously monitored a few points installed in key positions. For a greater density of check points inside the landslide area of the SdF, which proved difficult and dangerous to access, it was decided to install simple reflecting geodetic prisms with the aid of specialist guides. These were measured daily in the first weeks by electronic distance measurement measurements, and then, in the successive months, it was envisaged to permanently in-

stall an integrated theodolite (automatic measurement of angles and distances, remote controlled) positioned on the low northern rim of the SdF. In addition to monitoring the slip of the landslide area, the deformation measurements have had a fundamental role in real-time evaluation of the processes of migration of the effusive vents in mid-February, as well as understanding the mechanisms and effects associated with the paroxysmic explosion of 5 April 2003 [Mattia *et al.*, 2004; Calvari *et al.*, 2006].

Finally, for complete geophysical monitoring, the INGV carried out the installation of a continuous gravimeter to control mass movements and an array of three permanent magnetic stations.

The final picture with the map of the permanent devices installed in 2003, following the planned activities is shown in Figure 4.

To complete the monitoring picture with the integration of specific disciplines that are not fully of INGV competence, the DPC also started and financed collaboration with university institutes. Various activities in full synergy with the activities planned by the DPC–INGV included the bathymetric surveys around the island [Tommasi *et al.*, 2005], the interpretation of repeated aerial photogrammetry [Baldu *et al.*, 2005, 2007], the installation of a synthetic aperture radar (SAR) device on the ground located on the northern rim of the SdF to measure the movements of the upper part of the landslide [Casagli *et al.*, 2003a, 2003b], and the upgrading of a permanent network of infrasonic sensors [Ripepe, 2007].

The two dramatic phenomena during the eruption course were the SdF flank failure with the associated tsunami and the paroxysm explosion during the effusive activity. The learned conclusion was that the first was an unexpected event, although in the future, it could be better surveyed,

Figure 4. Island of Stromboli. Map of the permanent devices set up following the actions in 2003. The comparison with the former situation until 2002 (Figure 1) shows the vast and complete development of the observation systems installed and working in a very short time.

while the second was an unpredictable event, and more effort is needed to try to detect possible valid precursors.

As described above, the permanent integrated theodolite, automated and remote controlled, and the ground-based SAR device were installed for the control of the movements of the SdF. Moreover, an automatic procedure of detection and reckoning of the seismic events provoked by small landslides was implemented.

These instrumentations and techniques should allow monitoring of the stability of the flank and its possible accelerations.

A more difficult issue, and also an open challenge, is the detecting of possible valid precursors associated with the paroxistic explosions. Significant chemical changes from the main craters emission were observed a few days before the paroxysm [Aiuppa and Federico, 2004; Carapezza et al., 2004]. These changes were detected only because the sampling frequency was increased from week/months to daily,

this indicating the need to use automatic continuous stations in future monitoring.

The continuous GPS and seismic station showed near co-explosive signals, which are important to study the source mechanisms, but did not show a valid precursor signal. An important planned intervention is the installation of instrumentation with high sensitivity and precision such as deep strainmeters, installed at 150–200 m depth, and borehole tilt, installed in the summit crater area to verify the possibility of detecting precursor signals.

5. CONCLUDING REMARKS

The eruption of Stromboli prompted an enormous effort in various monitoring activities. For the first time in Italy, and in such a brief time, there was an immense and complete development and upgrading of the observation systems on a volcano during an eruption. This effort was characterized

by the capacity of the joint DPC–INGV both to respond in a short time with immediate interventions as well as plan further multiple scientific activities over the medium term.

This commitment to optimize the monitoring was in complete harmony with numerous research joint projects started in the DPC–INGV agreement on Stromboli and then continued in a further agreement in the 3 years from 2004 to 2006 when, in addition to the maintenance of the monitoring systems, part of the research plans with objectives for civil protection purposes was started. In this part of the agreement dedicated to the research projects, a particular session was foreseen for Stromboli, and numerous studies involving many other institutes of research and university departments have been carried out.

Therefore, the eruption of Stromboli has also instigated a commendable process of feedback between monitoring and research, which reinforces these two elements and lays the groundwork for a modern and effective enactment of the service of civil protection.

In particular, the vision of the system of civil protection envisaged by Italian law, in which the DPC promotes and coordinates with the administrations of the state during emergencies and the INGV supplies scientific support, has proved valid and functional. The eruption of Stromboli has therefore completed and at the same time validated this model of collaboration and has highlighted the aspects of mutual synergy, demonstrating that the Italian system of civil protection has a unity and effectiveness in the management of volcanic hazard.

Acknowledgments. Warm and heartfelt thanks are owed to all the staff of the scientific community and to the National Service of Civil Protection who, with the highest professionalism and self-sacrifice, made possible all the numerous and important activities carried out during the crisis of Stromboli in 2002–2003. We thank A. L. Martin del Pozzo, P. Dellino, and an anonymous referee for their reviews that led to improvements in the manuscript. We thank Stephen Conway for correcting the English of the manuscript.

REFERENCES

- Acocella, V., M. Neri, and P. Scarlato (2006), Understanding shallow magma emplacement at volcanoes: Orthogonal feeder dikes during the 2002–2003 Stromboli (Italy) eruption, *Geophys. Res. Lett.*, 33, L17310, doi:10.1029/2006GL026862.
- Aiuppa, A., and C. Federico (2004), Anomalous magmatic degassing prior to the 5th April 2003 paroxysm on Stromboli, *Geophys. Res. Lett.*, 31, L14607, doi:10.1029/2004GL020458.
- Auger, E., L. D'Auria, M. Martini, B. Chouet, and P. Dawson (2006), Real-time monitoring and massive inversion of source parameters of very long period seismic signals: An application to Stromboli Volcano, Italy, *Geophys. Res. Lett.*, 33, L04301, doi:10.1029/2005GL024703.
- Baldi, P., M. Fabris, M. Marsella, and R. Monticelli (2005), Monitoring the morphological evolution of the Sciara del Fuoco during the 2002–2003 Stromboli eruption using multi-temporal photogrammetry, *ISPRS J. Photogramm. Remote Sens.*, 2005(59), 199–211.
- Baldi, P., M. Coltellini, M. Fabris, M. Marsella, and P. Tommasi (2007), High precision photogrammetry for monitoring the evolution of the NW flank of Stromboli volcano during and after the 2002–2003 eruption, *Bull. Volcanol.*, in print, doi:10.1007/s0044500701621.
- Barberi, F., M. Rosi, and A. Soda (1993), Volcanic hazard assessment at Stromboli based on review of historical data, *Acta Vulcanol.*, 3, 173, 187.
- Bonaccorso, A., S. Calvari, G. Garfi, L. Lodato, and D. Patané (2003), Dynamics of the December 2002 flank failure and tsunami at Stromboli volcano inferred by volcanological and geophysical observations, *Geophys. Res. Lett.*, 30(18), 1941, doi:10.1029/2003GL017702.
- Brusca, L., S. Inguaggiato, M. Longo, P. Madonia, and R. Maugeri (2004), The 2002–2003 eruption of Stromboli (Italy): Evaluation of the volcanic activity by means of continuous monitoring of soil temperature, CO₂ flux, and meteorological parameters, *Geochem. Geophys. Geosyst.*, 5, Q12001, doi:10.1029/2004GC000732.
- Calvari, S., L. Spampinato, L. Lodato, A. J. L. Harris, M. R. Patrick, J. Dehn, M. R. Burton, and D. Andronico (2005), Chronology and complex volcanic processes during the 2002–2003 flank eruption at Stromboli volcano (Italy) reconstructed from direct observations and surveys with a hand-held thermal camera, *J. Geophys. Res.*, 110, B02201, doi:10.1029/2004JB003129.
- Calvari, S., L. Spampinato, and L. Lodato (2006), The 5 April 2003 vulcanian paroxysmal explosion at Stromboli volcano (Italy) from field observations and thermal data, *J. Volcanol. Geotherm. Res.*, 149, 160–175.
- Capasso, G., M. L. Carapezza, C. Federico, S. Inguaggiato, and A. Rizzo (2005), Geochemical monitoring of the 2002–2003 eruption at Stromboli volcano (Italy): Precursory changes in the carbon and helium isotopic composition of fumarole gases and thermal waters, *Bull. Volcanol.*, 68, 118–134, doi:10.1007/s0044500504275.
- Carapezza, M. L., S. Inguaggiato, L. Brusca, and M. Longo (2004), Geochemical precursors of the activity of an open-conduit volcano: The Stromboli 2002–2003 eruptive events, *Geophys. Res. Lett.*, 31, L07620, doi:10.1029/2004GL019614.
- Casagli, N., P. Farina, D. Leva, G. Nico, and D. Tarchi (2003a), Landslide monitoring on a short and long time scale by using ground-based SAR interferometry, *Proc. SPIE*, 4886, 322–329.
- Casagli, N., P. Farina, L. Guerri, D. Tarchi, J. Fortuny, D. Leva, and G. Nico (2003b), Preliminary results of SAR monitoring of the Sciara del Fuoco on the Stromboli volcano, in *Occurrence and Mechanisms of Flow-like Landslides in Natural Slopes and Earthfills, Sorrento, Italy, May 14–16, 2003*, edited by L. Picarelli, 2, pp. 291–295, Patron Editore, Bologna.
- Harris, A. J. L., J. Dehn, M. R. Patrick, S. Calvari, M. Ripepe, and L. Lodato (2005), Lava effusion rates from hand-held thermal

- infrared imagery: An example from the June 2003 effusive activity at Stromboli, *Bull. Volcanol.*, 68, 107–117.
- Inguaggiato, S., and A. Rizzo (2004), Dissolved helium isotope ratios in ground-waters: A new technique based on gas–water re-equilibration and its application to Stromboli volcanic system, *Appl. Geochem.*, 19, 665–673.
- INGV-CT (2002), Rapporto stato attività Stromboli 2° semestre 2002 con particolare riferimento agli eventi effusivi e di frana del 28–31 Dicembre, *Internal Report for DPC*, 31 December 2002.
- Lodato, L., L. Spampinato, A. J. L. Harris, S. Calvari, J. Dehn, and M. R. Patrick (2007), The morphology and evolution of the Stromboli 2002–03 lava flow field: An example of a basaltic flow field emplaced on a steep slope, *Bull. Volcanol.*, 69, 661–679.
- Mattia, M., M. Rossi, F. Guglielmino, M. Aloisi, and Y. Bock (2004), The shallow plumbing system of Stromboli Island as imaged from 1 Hz instantaneous GPS positions, *Geophys. Res. Lett.*, 31, L24610, doi:10.1029/2004GL021281.
- Puglisi, G., A. Bonaccorso, M. Mattia, M. Aloisi, A. Bonforte, O. Campisi, M. Cantarero, G. Falzone, B. Puglisi, and M. Rossi (2005), New integrated geodetic monitoring system at Stromboli volcano (Italy), *Eng. Geol.*, 79, 13–31.
- Ripepe, M., E. Marchetti, G. Ulivieri, A. Harris, J. Dehn, M. Burton, T. Caltabiano, and G. Salerno (2005), Effusive to explosive transition during the 2003 eruption of Stromboli volcano, *Geology*, 33(5), 341–344.
- Ripepe, M., E. Marchetti, and G. Ulivieri (2007), Infrasonic monitoring at Stromboli volcano during the 2003 effusive eruption: Insights on the explosive and degassing process of an open conduit system, *J. Geophys. Res.*, 112, B09207, doi:10.1029/2006JB004613.
- Tinti, S., A. Maramai, A. Armigliato, L. Graziani, A. Manucci, G. Pagnoni, and F. Zaniboni (2006), Observations of physical effects from tsunamis of December 30, 2002 at Stromboli volcano, southern Italy, *Bull. Volcanol.*, 68, 450–461, doi:10.1007/s00445-005-0021-x.
- Tommasi, P., P. Baldi, F. Chiocci, M. Coltelli, M. Marsella, M. Pompilio, and C. Romagnoli (2005), The Landslide sequence induced by the 2002 eruption at Stromboli volcano, in *Landslide—Risk Analysis and Sustainable Disaster Management*, edited by K. Sassa, H. Fukuoka, F. W. Wang, and G. Wang, pp. 251–258, Springer, New York.
-
- G. Bertolaso, Dipartimento della Protezione Civile, Presidenza del Consiglio dei Ministri, Via Ulpiano 11, 00187 Rome, Italy.
 A. Bonaccorso and E. Boschi, Istituto Nazionale di Geofisica e Vulcanologia, Sezione di Catania, Piazza Roma 2, 95125 Catania, Italy.

Index

atmospheric effects, 269
back-arc basin processes, 157
computational seismology, 81
control surveys, 229, 247
debris flow and landslides, 129, 171
decision making under uncertainty, 373
effusive volcanism, 93, 201, 213
eruption mechanisms and flow emplacement, 39, 81, 105, 201, 229, 259, 317
explosive volcanism, 19, 39, 65, 81, 93, 105, 259, 305, 317, 331
field relationships, 269, 305
fluid and melt inclusion geochemistry, 19
geochemical modeling, 49, 65
hydrothermal systems, 49, 117, 347
image processing, 229
instruments and techniques, 183, 247, 279, 359, 387
integrations of techniques, 183
magma migration and fragmentation, 39, 105
magnetic and electrical methods, 287
major and trace element geochemistry, 19, 213, 331

marine sediments: processes and transport, 157
mineral and crystal chemistry, 19, 213, 331
numerical modeling, 147
radiogenic isotope geochemistry, 213, 331
remote sensing of volcanoes, 65, 93, 171, 201, 305, 359, 387
seafloor morphology, geology, and geophysics, 157, 171
stable isotope geochemistry, 117
stresses: general, 5
submarine landslides, 129, 147, 157
system operation and management, 373
tectonics and magmatism, 5
tsunamis and storm surges, 147
volcanic arcs, 5
volcanic gases, 49, 65, 117, 259, 269, 287, 347
volcanic hazards and risks, 5, 39, 105, 129, 147, 247, 287, 317, 347, 373, 387
volcano monitoring, 49, 93, 117, 171, 183, 201, 229, 247, 259, 269, 279, 287, 347, 359, 373, 387
volcano seismology, 81, 279
volcanoclastic deposits, 129, 317
volcanology, 305